INTERNATIONAL COUNCIL FOR RESEARCH AND INNOVATION
IN BUILDING AND CONSTRUCTION

WORKING COMMISSION W18 - TIMBER STRUCTURES

CIB - W18

MEETING THIRTY-THREE

DELFT

THE NETHERLANDS

AUGUST 2000

Lehrstuhl für Ingenieurholzbau und Baukonstruktionen
Universität Karlsruhe
Germany
Compiled by Rainer Görlacher
2000

ISSN 0945-6996

CONTENTS

CIB-W18 Papers 33-1-1 up to 33-102-1

0 List of Participants

INTERNATIONAL COUNCIL FOR RESEARCH AND INNOVATION
IN BUILDING AND CONSTRUCTION
WORKING COMMISSION W18 - TIMBER STRUCTURES

MEETING THIRTY-THREE
DELFT, THE NETHERLANDS 28-30 AUGUST 2000

LIST OF PARTICIPANTS

CANADA

E Karacabeyli	Forintek, Vancouver
F Lam	University of British Columbia

CZECH REPUBLIK

P Kuklik	Czech Technical University

DENMARK

P Ellegaard	Aalborg University
H J Larsen	Danish Building Research Institute, Hørsholm
J Nielsen	Aalborg University, Aalborg

FINLAND

M Kairi	Finforst Oy, Kerto
J Kangas	VTT Building Technology, Espoo
A Ranta-Maunus	VTT Building Technology, Espoo

FRANCE

J P Biger	Bureau Veritas; Paris
T Lamadon	Bureau Veritas, Saint Quentin en Yvelines Cedex
P Racher	C.U.S.T. Aubiere Cedex
F Rouger	CTBA, Bordeaux

GERMANY

H J Blaß	University of Karlsruhe
J Ehlbeck	University of Karlsruhe
R Görlacher	University of Karlsruhe
V Krämer	University of Karlsruhe
B Laskewitz	University of Karlsruhe
K Rautenstrauch	Bauhaus University, Weimar

ISRAEL

U Korin	National Building Research Institute, Haifa

ITALY

A Ceccotti	Universities of Florence and Venice
M Ballerini	University of Trento

JAPAN

N Kawai	Building Research Institute, Tsukuba
M Yasumura	Shizuoka University, Shizuoka

NETHERLANDS

J Janssen	INBAR, TU Eindhoven
A Jorissen	TU Delft
J Kuipers	TU Delft
A D Leijten	TU Delft
J W van de Kuilen	TU Delft
L A G Wagemans	TU Delft

POLAND

B Szyperska	ITB, Warszawa

SWEDEN

C Bengtsson	Swedish National Testing and Research Institute
H Johansson	Lulea University of Technology, Lulea
B Källsner	Swedish Institute for Wood Technology Research, Stockholm
J König	Swedish Institute for Wood Technology Research, Stockholm
L Stehn	Lulea University of Technology, Lulea
S Svensson	Lund University
S Thelandersson	Lund University

UK

M P Ansell	University of Bath
R Bainbridge	TRADA Technology LTD, Buckinghamshire
R F Marsh	Consultant, London
C J Mettem	TRADA Technology LTD, Buckinghamshire

USA

B Yeh	American Plywood Association

1. Chairman's Introduction
2. Co-operation With Other Organisations
3. Limit State Design
4. Timber Joints and Fasteners
5. Laminated Members
6. Trussed Rafters
7. Structural Stability
8. Fire
9. Structural Design Codes
10. Any Other Business
11. Venue for Next Meeting
12. Close

INTERNATIONAL COUNCIL FOR RESEARCH AND INNOVATION
IN BUILDING AND CONSTRUCTION

WORKING COMMISSION W18 - TIMBER STRUCTURES

MEETING THIRTY-THREE

DELFT, THE NETHERLANDS 28-30 AUGUST 2000

MINUTES
(F Lam)

1. CHAIRMAN'S INTRODUCTION

H. Blass opened the meeting and welcomed the participants to the 33rd meeting of CIB W18, working commission 18 "Timber Structures of the International Council for Research and Innovation in Building and Construction.

Delft University of Technology, represented by A. Leijten and J. Kuipers, was thanked for hosting and organizing the meeting. H. Blass is also pleased with the venue because of the time he spent in Delft from 1991 to 1995. He also mentioned that he took over the task as coordinator of CIB W18 from Chris Stieda in 1991 and still enjoys the task and will continue as coordinator as long as CIB W18 members agree. H. Blass stated that a CIBW18 meeting was held in Delft 1974. Three participants from the 1974 meeting are again with us in the 33rd meeting.

Papers bought directly to the meeting will not be accepted for presentation, discussions, or publication. There are fewer papers than last year, as some authors did not submit full paper although their abstracts were accepted. This problem will have to be solved in the future. All papers were distributed electronically via the Internet. A revised version of paper 33-7-7 by T.A.C.M. van der Put and A. Leijten is distributed directly in the meeting.

The minutes for last meeting were prepared by Frank Lam who has agreed to take over this task again this year.

2. CO-OPERATION WITH OTHER ORGANISATIONS

(a) RILEM

J. Ehlbeck reported on activities of RILEM TC 169 "Test methods for load transferring metal works for use in timber structures". There was no meeting since last CIB W18 meeting. A progress report was presented at Sept 1999 in RILEM meeting in Stockholm. It also appeared in Materials and Structures in March 2000. There are cooperation activities with EOTA to establish guidelines/rules for calibration and verification of models of 3-dimensional nail plates. This includes test arrangements, specimen selection, test details etc.

The second RILEM group working on Historical Timber Structures has not met in two years.

(b) CEN

H.J. Larsen stated that TC124 deals with material for timber structures with the exception of wood based panels. It focuses primarily with test methods and standards for products. There are approximately 20 test methods based on the work done by CIB W18. Test standard on the Performance of fasteners for cyclic loading is almost ready for inclusion. The TC will be working on the Method for MOE Measurements and expect interesting discussions. It will also work on implementation of product directives issues (Quality assurance) on built-up beams, LVL, etc.

J. König reported on TC 250 Subcommittee 5 activities. Although Eurocode 5 is based on the work done by CIB W18, the official work done for Eurocode 5 is via TC 250 SC5. Timetable for the various activities is as follows:

General Part 1-1:	
First draft	July 1999
Second draft	Oct 2000
Final draft	May 2001
To CEN for final vote	Nov 2001
Implementation:	
Date of availability	May 2002
Date of publishing	May 2004 (with national Annexes)
Date of withdrawal of non-conforming items	May 2006 (2 years of co-existence with national standards)
Fire Part 1-2:	
First draft	Oct 2000
Final draft	Oct 2001
Bridge Part 2:	
First draft	Oct 2001
Final draft	Jan 2003

(c) IABSE

IABSE - Report was not available although there is meeting scheduled for end of August 2001 in Helsinki.

(d) IUFRO S5.02

F. Rouger reported that during last CIB W18 meeting it was agreed that IUFRO 5.02 meeting would be intended for a small group of 40 to 50 people to present and discuss basic timber engineering and scientific issues. There were no activities since the CIB W18 meeting. A proposal to join the next CIB W18 meeting with an IUFRO 5.02 meeting in a 4 day meeting to be held in Venice 2001 will be discussed with our next host A. Ceccotti on the possibilities.

(e) COST

F. Rouger also reported that a new COST group on Reliability of Timber Structures has been approved. The work will start end of the year. Collaborations are welcomed.

(f) ISO

ISO TC165 Standard for cyclic testing of joints

E. Karacabeyli reported that a Standard for Cyclic Testing of Joints has been under development. He suggested that this standard be considered in future European code revisions.

3. LIMIT STATE DESIGN

Paper 33-1-1 *Aspects on Reliability Calibration of Safety Factors for Timber Structures* - ***S. Svensson, S. Thelandersson***

Presented by: S. Thelandersson

· H. Blass questioned whether high quality information on the tails of distributions would be available.
· S. Thelandersson responded that it is very difficult therefore the method must be used with care.
· H. Blass asked could we expect engineers to correctly apply the method given the fact that younger people are without the background knowledge?
· S. Thelandersson answered that the equations in the code are in a form that can be used by practicing engineers although practicing Engineers are not using this method yet.
· J. Ehlbeck questioned which is better Normal or Gumbel distribution.
· S. Thelandersson answered that Gumbel distribution is better because it is of the extreme type. In general, there is too much calibration without consideration of consequences. E.g. High partial coefficient for permanent loads in Eurocode
· J. Ehlbeck questioned whether the dependency of γ_n on safety class (low, normal, high) should be part of the Eurocode also.
· S. Thelandersson answered that this is a consistent description for all materials and is general for design basis. It is in use in Nordic countries.
· H.J. Larsen stated that discussion about one philosophy is important. More important structures should have better quality and quality control and therefore do not need higher β or γ_n.
In national codes and Eurocode, the γ values should be decided by people with knowledge of material behaviour and failures. An example is the damage of the recent storm in Denmark (100 year return wind storm) in which some one or two storey timber houses suffered damage. In one site of 100 houses there were 3 failures while not one of the failed houses was designed correctly. This recent experience on reality should be considered.
· M. Ansell asked for more information on Gumbel distribution.
· S. Svensson answered that the Gumbel distribution fitted the upper tail very well.
· H.J. Larsen stated that one should agree on a distribution and calibrate against it rather than focusing on a particular β level.
· S. Svensson agreed that β values are not universal parameters.
· F. Rouger stated that the influence of resistance distribution type could be reduced by

fitting to lower tails of resistance distribution as demonstrated by R.Foschi.
· E. Karacabeyli asked about the resistance side of the failure function.
· S. Thelandersson responded that constant lognormal distribution was used.

Paper 33-1-2 *Sensitivity studies on the reliability of timber structures* – ***A. Ranta-Maunus, M. Fonselius, J. Kurkela, T. Toratti***

Presented by: A. Ranta-Maunus

· H. Blass asked whether the results would be reported to the Eurocode project team.
· A. Ranta-Maunus responded yes.
· S. Thelandersson asked for clarification on the conclusion that safety was independent of COV for the Gumbel distribution.
· A. Ranta-Maunus clarified that the characteristic values were fixed while distribution mean and COV were varied.
· F. Lam commented that system effect should be considered when γ values were sought for a given target β level.
· A. Ranta-Maunus stated that the plan was to start with the simple cases and look into the sensitivity issue and what are the important issues. He will look into the details in the future.
· J.W. van der Kuilen asked whether time effects were considered.
· A. Ranta-Maunus stated that it would be interesting to look into this issue. He felt that a simple approach would be to adjust the resistance distribution on the basis of DOL information.
· S. Thelandersson stated this type of work has been initiated. A paper on DOL effect was presented at 32nd CIB W18. The choice of damage model was critical.

4. TIMBER JOINTS AND FASTENERS

Paper 33-7-1 *Determination of Yield Strength and Ultimate Strength of Dowel-Type Timber Joints* - ***M. Yasumura, K. Sawata.***

Presented by: M. Yasumura

· H.J. Larsen commented that it could be misleading to use a standard for nails to be applied to bolts. The definition of yield point as the departure point from elastic zone or the entry point to yield was also questioned. He also asked whether the minimum edge distance for the splitting case should be beam depth dependent or bolt diameter dependent.
· M. Yasumura responded that based on fracture mechanics analysis mix mode of failure was present; therefore, minimum edge distance should be beam depth dependent.
· H.J. Larsen further pointed a case where if the design were already safe to start off, further increase in beam depth should not lead to a less safe situation.
· M. Yasumura would look into this further.
· H. Blass asked whether bending angles of dowels were examined in the joint tests.
· M. Yasumura answered that this was not an issue for the perpendicular to grain case.

Paper 33-7-2 *Lateral Shear Capacity of Nailed Joints* - ***U. Korin***

Presented by: U. Korin

· H. Blass asked for clarification on the definition of failure load at 5 mm deformation.

· U. Korin responded that the failure load was taken as the load at 5 mm deformation if the peak load was not reached; otherwise, the maximum load would be used as the failure load.
· H. Blass asked why 5 mm deformation was chosen.
· U. Korin responded that the choice was based on embedment strength information.
· J. Ehlbeck commented that the procedures comparing theoretical values with test results were incorrect because conservative yield moments of nails (design values) in Eurocode 5 were used in the procedures. The code referred to minimum nail strength of 600 MPa.
· U. Korin responded that only wire strength information was collected during the test.

Paper 33-7-3 *Height-Adjustable Connector for Composite Beams* – ***Y.V. Piskunov, E.G. Stern***

Not Presented.

· A letter of regret (health issue) was received from E.G. Stern and read to the members. Transparencies were also provided by E.G. Stern and made available for distribution and discussions. H. Blass will provide a letter of reply.

Paper 33-7-4 *Engineering Ductility Assessment for a Nailed Slotted-In Steel Connection in Glulam* - ***L. Stehn, H. Johansson***

Presented by: L. Stehn

· H.J. Larsen questioned the research philosophy because codes should penalize brittle joints by assigning larger γ values relative to those for ductile joints. The evaluated joints in this study were already ductile because they were defined under the Johansen yield theory. He also questioned the need to jump to a new definition of ductility measures. Finally H.J. Larsen commented that there should be no need to conclude with more testing.
· H. Blass asked for the reasoning behind definition of engineering ductility.
· L. Stehn responded that there was a need to show the degree of ductility even with ductile connectors. The engineering ductility definition was reasoned to relate to effective thickness of the wood needed to be mobilized for ductile behaviour.

Paper 33-7-5 *Effective Bending Capacity of Dowel-Type Fasteners* - ***H.J. Blass, A. Bienhaus, V. Krämer***

Presented by: V. Krämer

· A. Leijten pointed out in the moment rotation graphs, the moment corresponding to 20° was 90% of the moment corresponding to 45°. This difference was relatively minor.
· H. Blass responded that the differences for cases of 4° to 6° were significant.
· H.J. Larsen commented that in many cases the d=15 mm limit for a test would not be reached. The joint strength was diameter dependent. May be change the original criteria to 10° would be a simple alternative.
· H. Blass responded that engineering judgment was uesed to choose d=15 mm as a starting point. There was conservatism in other part of the procedures to allow for reasonable results at the end.

· C. Mettem asked about the wood species differences.
· H. Blass responded that if there was no splitting the procedure would be appropriate.
· H.J. Larsen suggested that an editorial change to the statement: "The plastic bending capacity is partially used..." be changed to "Reserve capacity can only be partially used..."
· H. Blass agreed

Paper 33-7-6 *Load-Carrying Capacity of Joints with Dowel-Type fasteners and Interlayers* - ***H.J. Blass, B. Laskewitz***

Presented by: B. Laskewitz

· S. Svensson asked for and received clarification on tensile test set up.
· M. Ansell questioned the role of OSB as the interlayer.
· H. Blass responded that this would be a typical application of hangers on shear walls. This study provided the information needed by designers.
· M. Ansell questioned why OSB.
· B. Laskewitz responded that OSB is commonly used as sheathing for walls.

Paper 33-7-7 *Evaluation of Perpendicular to Grain Failure of Beams caused by Concentrated Loads of Joints* - ***A.J.M. Leijten, T.A.C.M. van der Put***

Presented by: A.J.M. Leijten

· H. Blass commented that M_1 and M_2 values as depicted in Figure 2 were incorrect as normal forces were ignored.
· A. Leijten responded that the influence was minor and the data fitted the model well.
· H. Blass commented that with incorrect basic assumptions the theory would be questionable.
· H.J. Larsen commented that as in the case of notched beams, the moments might not be as important as the crack length and shear forces.
· H. Blass commented that the notch beam analogy would be different.
· M. Ballerini stated his disagreement with some of the statements in this paper. He provided detailed critic and rebuttal to the points raised in section 4.1 of this paper. He pointed out that there were numerous misinterpretation of his own work presented previously in CIB W18 paper 32-7-2. M. Ballerini also pointed out that a factor of 2 seemed to be omitted in the current study. Finally, M. Ballerini made available videotapes of his tests and pictures of the failed specimen.
· A. Leijten responded that the calculations were carefully checked. Further discussions took place.
· H. Blass suggested that A. Leijten, M. Ballerini, and T.A.C.M. van der Put meet and sort out their differences and provide written comments.

Paper 33-7-8 *Test Methods for Glued-In-Rods for Timber Structures* – ***C. Bengtsson, C.J. Johansson***

Presented by: C. Bengtsson

· J. Kangas asked whether there were failures during proof loading.
· C. Bengtsson responded that there were few failures and their failure load values were included in the analysis.
· M. Ansell asked whether thick epoxy glueline (5 mm) was tried.

· C. Bengtsson responded no.
· M. Ansell suggested that thick epoxy glueline (5 mm) could lead to higher strength values. He also asked whether wood or glueline failures were observed.
· C. Bengtsson responded that wood failure was observed with the epoxy.
· S. Svensson asked why was beech wood used.
· C. Bengtsson responded that beech was specified in the test standard.
· H.J. Larsen questioned the findings that only epoxy passed and stated that the test method may not be suitable to address different type of adhesives.
· C. Bengtsson agreed that the requirements might not be suitable.
· J. Kuipers commented on the glue type dependency of test methods.
· C. Bengtsson agreed.
· F. Lam asked whether the observed differences were statistically significant.
· C. Bengtsson answered yes.

Paper 33-7-9 *Stiffness Analysis of Nail Plates* – ***P. Ellegaard***

Presented by: P. Ellegaard

· S. Thelandersson asked and received clarification on the beam analogy in the truss plate model such that along the main axis of the truss plate the "link zone" was modeled with small beams. The number and size of the beams were determined according to the actual geometric parameters of the truss plate with respect to the joint.
· J. Kangas asked how were the Eurocode values obtained.
· P. Ellegaard responded that they were obtained via basic tests.
· J. Kangas stated that correction factors should be used; otherwise, the wrong Eurocode values would be obtained. It was subsequently clarified that the correction factors refer to information only available in the current existing draft.
· B. Källsner asked whether the large gap of 5 mm in the test exceeded the values specified in the test standard.
· P. Ellegaard responded that the minimum gaps specified in the standard compression and tension tests were 4 mm and 2 mm, respectively.
· S. Thelandersson asked how to deal with another type of plate with the verification based on one type of nail plate.
· P. Ellegaard responded that he would try another type of plate soon with the 6 basic tests.
· B. Källsner stated that the interaction formula might cause problems for another type of plate.
· P. Ellegaard responded that hopefully the yield surface approach would be better.

Paper 33-7-10 *Capacity, Fire Resistance and Gluing Pattern of the Rods in V-Connections* – ***J. Kangas***

Presented by: J. Kangas

· J. Ehlbeck asked whether slip modulus between timber/concrete connections was available.
· J. Kangas responded that there are test results from VTT available from past reports.
· J. Ehlbeck asked about the influence of α on connection strength
· J. Kangas responded that 30 degree gave higher values
· M. Ansell asked whether repair and reinforcement of existing structure could be considered with reinforcement rods.
· J. Kangas responded that it could be done. There were some repairs already made.

Reinforcement also increases shear capacity.
· H. Blass questioned the dowel effect on design.
· J. Kangas responded that it was considered in the model. Deformation of the tensile dowel would cause the other rod to act as a dowel.
· H. Blass commented the dowel effect should be in both rods.
· J. Kangas responded that the rods moved together at their connection point; therefore, only one rod would act as a dowel.
· H. Blass agreed.
· B.J. Yeh asked and received clarification on beam versus joint failure.

Paper 33-7-11 *Bonded-In Pultrusions for Moment-Resisting Timber Connections* – ***K. Harvey, M.P. Ansell, C.J. Mettem, and R.J. Bainbridge***

Presented by: M.P. Ansell

· J. Ehlbeck asked how to provide input to national or international design code.
· M. Ansell stated that the coauthors are experienced in transferring scientific results and engineering data to code format. It will however be a slow process.
· S. Svensson stated that saturated timber would have reduced strength and asked whether strains were measured.
· M. Ansell responded that the connections were not instrumented for strains.
· S. Svensson further questioned the compression stress transfer of the member in Fig 15.
· M. Ansell responded that rod would take most of the load although the wood members did have contact.
· A. Ceccotti clarified that the load displacement curves were not ductile.
· M. Ansell commented that Acoustic Emission tests indicated that there was substantial micro-damage during loading which would dissipate energy.
· J. Kuipers asked about the long-term behaviour of the joints.
· M. Ansell responded that DOL tests were underway and there were no early failures.
· S. Thelandersson asked for clarification of the claim of excellent fire resistance.
· M. Ansell responded that the timber would protect the bonded in connector.

Paper 33-7-12 *Fatigue Performance of Bonded-In Rods in Glulam, Using Three Adhesive Types* – ***R.J. Bainbridge, K. Harvey, C.J. Mettem, and M.P. Ansell***

Presented by: C.J. Mettem

· U. Korin asked about the low tensile stress in the timber during test.
· M. Ansell responded that the interface between rod and timber would be important. One could plot shear force versus N_f as an alternative.

5. LAMINATED MEMBERS

Paper 33-12-1 *Internal Stresses in the Cross-Grain Direction of Wood Induced by Climate Variation* – ***J.Jönsson, S. Svensson***

Presented by: S. Svensson

· A. Ranta-Maunus commented that the test results could be compared to numerical values from VTT.

· M. Ansell asked for more details on the image analysis techniques.
· S. Svensson responded that the University of Lund software was used to detect the mean intensity values of the markers to achieve a gray scale number. Photo image results and image analysis results were similar. Micro-strain resolution was approximately -4 to -5.
· R. Görlacher asked why 30% difference was found between dynamic and static E.
· S. Svensson stated that the reason was not known and wanted to use only the dynamic E results.
· R. Görlacher stated that dynamic E values should be more reliable because of geometry effect of the small specimens.

6. TRUSSED RAFTERS

Paper 33-14-1 *Moment capacity of Timber Beams Loaded in Four Point Bending and Reinforced with Punched Metal Plate Fasteners* – ***J. Nielsen***

Presented by: J. Nielsen

· M. Ansell suggested that using bonded plates (full depth) on both sides with adhesive as solution.
· J.Nielsen stated that economic might not allow for this solution.
· S. Thelandersson asked whether there was the economic thinking on what can be gained through impact analysis of more pay (value added) for high strength.
· J. Nielsen responded that intention was to decrease the required depth with reinforcement to arrive at a safe and efficient solution.
· L. Stehn stated that in Swedish analysis in economic gains would be available.
· S. Svensson suggested that the increase in stiffness via reinforcement might prove to be important for beam and joist applications.

7. STRUCTURAL STABILITY

Paper 33-15-1 *Lateral Load Capacities of Horizontal Sheathed Unblocked Shear Walls* – ***C. Ni, E. Karacabeyli, A. Ceccotti***

Presented by: E. Karacabeyli

· H. Blass asked about the rationale of horizontally sheathed shear walls and whether the same rationale for plywood would apply to OSB.
· E. Karacabeyli stated that 3-layer 9.5 mm OSB would be similar to plywood in terms of orientation; therefore, the same rationale would also apply. This is also important for industrial building with unblocked high walls in low seismic zones.
· M. Yasumura stated that from FEM analysis significant bending in the studs are observed in unblocked shear walls. Vertical loads will be more important for these walls.
· E. Karacabeyli responded that vertical loads would be important for cases without holddowns.
· M. Yasumura stated that large bending deformation of the studs would lead to second order effects from vertical loads.
· E. Karacabeyli responded that he would check whether vertical loads were applied in the tests.

Paper 33-15-2 *Prediction of Earthquake Response of Timber Houses Considering Shear Deformation of Horizontal Frames* - ***N. Kawai***

Presented by: N. Kawai

· A. Ceccotti commented that it was a good paper combining the evaluation of diaphragm flexibility with torsional response. He questioned the rationale of adding 20% more forces for static calculations based on torsional moment.
· N. Kawai responded that the procedures give better solution.
· A. Ceccotti asked about the planned future work.
· N. Kawai responded that much work needed to be done. Some examples included multistory model, evaluation of force modification rules, more realistic houses with many vertical frames.
· M. Yasumura stated that the procedures that used heq_I would depend on load protocol therefore, one would need to be careful with it.
· N. Kawai agreed and stated that ISO load protocol was used.
·E. Karacabeyli asked 0.8 heq_I was used.
· N. Kawai responded that 100% heq_I would under-predict the response and overestimate the performance.

Paper 33-15-3 *Eurocode 5 Rules for bracing* - ***H.J. Larsen***

Presenter: H.J. Larsen

· H. Blass asked which MOE would one use in the design equation.
· H.J. Larsen said the MOE with the γ factor could be used although steel design used the unfactored MOE values.
· H. Blass commented that a factored MOE would lead to reduction in design requirements.
· H.J. Larsen agreed and will have to look into the details. Nevertheless, the design format has been formulated.

8. FIRE

Paper 33-16-1 *A Design Model for Load-carrying Timber Frame Members in Walls and Floors Exposed to Fire* - ***J. König***

Presented by: J. König

· H. Blass commented on the important influence of joints in gypsum boards on the charring rate and suggested that considering the joints be distributed everywhere would be easier. Load sharing of members during a fire was also discussed. H. Blass also asked whether gypsum boards would act as additional bracing for the wall.
· J. König answered that the gypsum on the fireside would not contribute.
· S. Thelandersson commented on the empirical based approach of the research in terms of what is the experimental background; how can the results be generalized; and how to handle the randomness and uncertainties of the parameters?
· J. König responded that information on material properties would be presented in another paper. Also no statistical data is currently available. He only used the average values; e.g., the average charring rate. In future additional factors might be introduced to take uncertainties into consideration.
· S. Thelandersson commented fire-rating information could be in the range of 65

minutes (+ or – 20 minutes); therefore, doubtful in principle that using average values would be appropriate. He also suggested that direct fire test on wall assembly should be considered.
· J. König responded that fire test results might also be doubtful. The current approach was to developed empirical model on the basis of testing of difference parameters; e.g., thermal properties. Model these properties and fit to model factors and perform critically analysis of the information. However, one could not really guarantee the outcome. Another example would be simplification with linearity of charring rate as a practical choice.
· S. Svensson questioned why design values could be given in the paper but not characteristic value information.
· J. König continued that too limited information is available to allow characteristic value information be given.
· S. Svensson asked about the factors used in the analysis.
· J. König responded that effect of temperature on strength and stiffness as material properties was determined.
· S. Svensson asked about where is the time term in Equation 15.
· J. König responded that in the Equation terms were related to engineering properties and heating. It is an indirect but easiest way.
· S. Svensson asked whether this approach gave good correspondence to strength reduction.
· J. König responded yes.
· E. Karacabeyli commented that the weight of gypsum on the ceiling would make a difference.
· J. König agreed but commented that data was not available therefore could not generalize. In these situation, code format should say failure time should be determined by testing.

Paper 33-16-2 *A Review of Component Additive Methods Used for the Determination of Fire Resistance of Separating Light Timber Frame Construction* - ***J. König, T. Oksanen, K. Towler***

Presented by: J. König

No discussion.

Paper 33-16-3 *Thermal and Mechanical Properties of Timber and Some Other Materials Used in Light Timber Frame Construction* - ***B. Källsner, J. König***

Presented by: B. Källsner

· S. Thelandersson stated that the title was misleading and it was not clear where the properties came from. Also the thermal and mechanical properties should be measurable. In the paper some of these parameters were obtained via back calculations; therefore, one would need to be careful to put information in code as material properties.
· B. Källsner agreed. The information in the paper was apparent properties not test values and would make clear in code.
· S. Thelandersson stated that the scope of application should be limited.
· B. Källsner agreed that the scope should be limited to this type of walls that are normally used.
· J. Nielsen stated that the insulation and timber had perfect fit in the model. In reality I

to 2 cm gap might exist. How would the results be influenced?
· B. Källsner answered the model used apparent values through calibration.
· S. Svensson commented that the influence on mechanical properties would be more sensitive to moisture rather than heat. In model, mass transfer was ignored. This type of information would be available from numerical results on wood drying.
· J. König agreed that moisture and temperature would have major influence. 100°c is a critical point below which moisture and temperature softening would be huge. Therefore, simplified approach with bi-linear relationship was adopted with the transition point at 100°c.
· S. Svensson commented that fire takes 1 hour and drying takes longer time.
· J. König agreed but said. Drying and burning are different. Moisture continuous change information with time is available. This may be supported via experiment of others.

9. STRUCTURAL DESIGN CODES

Paper 33-102-1 International Standards for Bamboo - ***J.J.A. Janssen***

Presented by: J.J.A. Janssen

· H. Blass asked about the availability of the document for design, testing, etc.
· J.J.A. Janssen answered that ISO document would be available in 4 yrs. He will check with ISO TC 165 for permission to release the draft information.
· A. Jorissen asked about the connection and commented that a structure such as the Pavilion in Expo 2000 could not be designed from standards.
· J.J.A. Janssen agreed and it would take time. The standard deals with how to perform tests on joints with reference to other standards.
· Marsh asked about friction/bounded joints.
· J.J.A. Janssen answered that loss of strength of bamboo will result because friction/bound joints would be the weakness.
· E. Karacabeyli commented that the working drafts of ISO TC 165 could be obtained from representatives of individual countries.

10. ANY OTHER BUSINESS

Visit to Timber Engineering Laboratory at TU Delft will be available after lunch.

11. VENUE AND PROGRAM FOR NEXT MEETING

Venice Italy will be the venue for the 34th CIBW18 meeting during August 22, 2001 to August 24, 2001.
The venue for the 35th CIBW18 meeting is set for September 16 to 19, 2002 in Kyoto, Japan. It will be a four-day meeting with a full day excursion.
Tentatively IUFRO S5.02 will have either a meeting or workshop in Venice Italy August 27 to 28 2001. It was not possible to have a 4-day combined CIBW18 and IUFRO S5.02 meeting because of logistics of the venue.
IABSE conference on Innovative Wooden Structure and Bridges will be held in Lahti, Finland August 29 to 31, 2001

12. CLOSE

H. Blass again thanked TU Delft, A. Leijten, and other colleagues for successfully hosting the 33rd CIBW18 meeting.

13. List of CIB-W18 Papers, Delft, The Netherlands 2000

List of CIB-W18 Papers, Delft, The Netherlands 2000

33-1-1	Aspects on Reliability Calibration of Safety Factors for Timber Structures – S Svensson, S Thelandersson
33-1-2	Sensitivity studies on the reliability of timber structures – A Ranta-Maunus, M Fonselius, J Kurkela, T Toratti
33-7-1	Determination of Yield Strength and Ultimate Strength of Dowel-Type Timber Joints – M Yasumura, K Sawata
33-7-2	Lateral Shear Capacity of Nailed Joints – U Korin
33-7-3	Height-Adjustable Connector for Composite Beams – Y V Piskunov, E G Stern
33-7-4	Engineering Ductility Assessment for a Nailed Slotted-In Steel Connection in Glulam– L Stehn, H Johansson
33-7-5	Effective Bending Capacity of Dowel-Type Fasteners - H J Blaß, A Bienhaus, V Krämer
33-7-6	Load-Carrying Capacity of Joints with Dowel-Type Fasteners and Interlayers - H J Blaß, B Laskewitz
33-7-7	Evaluation of Perpendicular to Grain Failure of Beams caused by Concentrated Loads of Joints – A J M Leijten, T A C M van der Put
33-7-8	Test Methods for Glued-In Rods for Timber Structures – C Bengtsson, C J Johansson
33-7-9	Stiffness Analysis of Nail Plates – P Ellegaard
33-7-10	Capacity, Fire Resistance and Gluing Pattern of the Rods in V-Connections – J Kangas
33-7-11	Bonded-In Pultrusions for Moment-Resisting Timber Connections – K Harvey, M P Ansell, C J Mettem, R J Bainbridge, N Alexandre
33-7-12	Fatigue Performance of Bonded-In Rods in Glulam, Using Three Adhesive Types - R J Bainbridge, K Harvey, C J Mettem, M P Ansell

33-12-1 Internal Stresses in the Cross-Grain Direction of Wood Induced by Climate Variation – J Jönsson, S Svensson

33-14-1 Moment Capacity of Timber Beams Loaded in Four-Point Bending and Reinforced with Punched Metal Plate Fasteners – J Nielsen

33-15-1 Lateral Load Capacities of Horizontally Sheathed Unblocked Shear Walls – C Ni, E Karacabeyli, A Ceccotti

33-15-2 Prediction of Earthquake Response of Timber Houses Considering Shear Deformation of Horizontal Frames – N Kawai

33-15-3 Eurocode 5 Rules for Bracing – H J Larsen

33-16-1 A Design Model for Load-carrying Timber Frame Members in Walls and Floors Exposed to Fire - J König

33-16-2 A Review of Component Additive Methods Used for the Determination of Fire Resistance of Separating Light Timber Frame Construction - J König, T Oksanen, K Towler

33-16-3 Thermal and Mechanical Properties of Timber and Some Other Materials Used in Light Timber Frame Construction - B Källsner, J König

33-102-1 International Standards for Bamboo – J J A Janssen

14. Current List of CIB-W18(A) Papers

CURRENT LIST OF CIB-W18(A) PAPERS

Technical papers presented to CIB-W18(A) are identified by a code CIB-W18(A)/a-b-c, where:

a denotes the meeting at which the paper was presented. Meetings are classified in chronological order:

1 Princes Risborough, England; March 1973
2 Copenhagen, Denmark; October 1973
3 Delft, Netherlands; June 1974
4 Paris, France; February 1975
5 Karlsruhe, Federal Republic of Germany; October 1975
6 Aalborg, Denmark; June 1976
7 Stockholm, Sweden; February/March 1977
8 Brussels, Belgium; October 1977
9 Perth, Scotland; June 1978
10 Vancouver, Canada; August 1978
11 Vienna, Austria; March 1979
12 Bordeaux, France; October 1979
13 Otaniemi, Finland; June 1980
14 Warsaw, Poland; May 1981
15 Karlsruhe, Federal Republic of Germany; June 1982
16 Lillehammer, Norway; May/June 1983
17 Rapperswil, Switzerland; May 1984
18 Beit Oren, Israel; June 1985
19 Florence, Italy; September 1986
20 Dublin, Ireland; September 1987
21 Parksville, Canada; September 1988
22 Berlin, German Democratic Republic; September 1989
23 Lisbon, Portugal; September 1990
24 Oxford, United Kingdom; September 1991
25 Åhus, Sweden; August 1992
26 Athens, USA; August 1993
27 Sydney, Australia; July 1994
28 Copenhagen, Denmark, April 1995
29 Bordeaux, France, August 1996
30 Vancouver, Canada, August 1997
31 Savonlinna, Finland, August 1998
32 Graz, Austria, August 1999
33 Delft, The Netherlands, August 2000

b denotes the subject:

1 Limit State Design
2 Timber Columns
3 Symbols
4 Plywood
5 Stress Grading
6 Stresses for Solid Timber
7 Timber Joints and Fasteners
8 Load Sharing
9 Duration of Load
10 Timber Beams
11 Environmental Conditions
12 Laminated Members
13 Particle and Fibre Building Boards
14 Trussed Rafters
15 Structural Stability
16 Fire
17 Statistics and Data Analysis
18 Glued Joints
19 Fracture Mechanics
20 Serviceability
21 Test Methods
100 CIB Timber Code
101 Loading Codes
102 Structural Design Codes
103 International Standards Organisation
104 Joint Committee on Structural Safety
105 CIB Programme, Policy and Meetings
106 International Union of Forestry Research Organisations

c is simply a number given to the papers in the order in which they appear:

Example: CIB-W18/4-102-5 refers to paper 5 on subject 102 presented at the fourth meeting of W18.

Listed below, by subjects, are all papers that have to date been presented to W18. When appropriate some papers are listed under more than one subject heading.

LIMIT STATE DESIGN

1-1-1	Limit State Design - H J Larsen
1-1-2	The Use of Partial Safety Factors in the New Norwegian Design Code for Timber Structures - O Brynildsen
1-1-3	Swedish Code Revision Concerning Timber Structures - B Noren
1-1-4	Working Stresses Report to British Standards Institution Committee BLCP/17/2
6-1-1	On the Application of the Uncertainty Theoretical Methods for the Definition of the Fundamental Concepts of Structural Safety - K Skov and O Ditlevsen
11-1-1	Safety Design of Timber Structures - H J Larsen
18-1-1	Notes on the Development of a UK Limit States Design Code for Timber - A R Fewell and C B Pierce
18-1-2	Eurocode 5, Timber Structures - H J Larsen
19-1-1	Duration of Load Effects and Reliability Based Design (Single Member) - R O Foschi and Z C Yao
21-102-1	Research Activities Towards a New GDR Timber Design Code Based on Limit States Design - W Rug and M Badstube
22-1-1	Reliability-Theoretical Investigation into Timber Components Proposal for a Supplement of the Design Concept - M Badstube, W Rug and R Plessow
23-1-1	Some Remarks about the Safety of Timber Structures - J Kuipers
23-1-2	Reliability of Wood Structural Elements: A Probabilistic Method to Eurocode 5 Calibration - F Rouger, N Lheritier, P Racher and M Fogli
31-1-1	A Limit States Design Approach to Timber Framed Walls - C J Mettem, R Bainbridge and J A Gordon
32 -1-1	Determination of Partial Coefficients and Modification Factors- H J Larsen, S Svensson and S Thelandersson
32 -1-2	Design by Testing of Structural Timber Components - V Enjily and L Whale
33-1-1	Aspects on Reliability Calibration of Safety Factors for Timber Structures – S Svensson and S Thelandersson
33-1-2	Sensitivity studies on the reliability of timber structures – A Ranta-Maunus, M Fonselius, J Kurkela and T Toratti

TIMBER COLUMNS

2-2-1	The Design of Solid Timber Columns - H J Larsen
3-2-1	The Design of Built-Up Timber Columns - H J Larsen
4-2-1	Tests with Centrally Loaded Timber Columns - H J Larsen and S S Pedersen
4-2-2	Lateral-Torsional Buckling of Eccentrically Loaded Timber Columns- B Johansson
5-9-1	Strength of a Wood Column in Combined Compression and Bending with Respect to Creep - B Källsner and B Norén
5-100-1	Design of Solid Timber Columns (First Draft) - H J Larsen
6-100-1	Comments on Document 5-100-1, Design of Solid Timber Columns - H J Larsen and E Theilgaard
6-2-1	Lattice Columns - H J Larsen
6-2-2	A Mathematical Basis for Design Aids for Timber Columns - H J Burgess

6-2-3	Comparison of Larsen and Perry Formulas for Solid Timber Columns- H J Burgess
7-2-1	Lateral Bracing of Timber Struts - J A Simon
8-15-1	Laterally Loaded Timber Columns: Tests and Theory - H J Larsen
17-2-1	Model for Timber Strength under Axial Load and Moment - T Poutanen
18-2-1	Column Design Methods for Timber Engineering - A H Buchanan, K C Johns, B Madsen
19-2-1	Creep Buckling Strength of Timber Beams and Columns - R H Leicester
19-12-2	Strength Model for Glulam Columns - H J Blaß
20-2-1	Lateral Buckling Theory for Rectangular Section Deep Beam-Columns- H J Burgess
20-2-2	Design of Timber Columns - H J Blaß
21-2-1	Format for Buckling Strength - R H Leicester
21-2-2	Beam-Column Formulae for Design Codes - R H Leicester
21-15-1	Rectangular Section Deep Beam - Columns with Continuous Lateral Restraint - H J Burgess
21-15-2	Buckling Modes and Permissible Axial Loads for Continuously Braced Columns - H J Burgess
21-15-3	Simple Approaches for Column Bracing Calculations - H J Burgess
21-15-4	Calculations for Discrete Column Restraints - H J Burgess
22-2-1	Buckling and Reliability Checking of Timber Columns - S Huang, P M Yu and J Y Hong
22-2-2	Proposal for the Design of Compressed Timber Members by Adopting the Second-Order Stress Theory - P Kaiser
30-2-1	Beam-Column Formula for Specific Truss Applications - W Lau, F Lam and J D Barrett
31-2-1	Deformation and Stability of Columns of Viscoelastic Material Wood - P Becker and K Rautenstrauch

SYMBOLS

3-3-1	Symbols for Structural Timber Design - J Kuipers and B Norén
4-3-1	Symbols for Timber Structure Design - J Kuipers and B Norén
28-3-1	Symbols for Timber and Wood-Based Materials - J Kuipers and B Noren
1	Symbols for Use in Structural Timber Design

PLYWOOD

2-4-1	The Presentation of Structural Design Data for Plywood - L G Booth
3-4-1	Standard Methods of Testing for the Determination of Mechanical Properties of Plywood - J Kuipers
3-4-2	Bending Strength and Stiffness of Multiple Species Plywood - C K A Stieda
4-4-4	Standard Methods of Testing for the Determination of Mechanical Properties of Plywood - Council of Forest Industries, B.C.
5-4-1	The Determination of Design Stresses for Plywood in the Revision of CP 112 - L G Booth

5-4-2	Veneer Plywood for Construction - Quality Specifications - ISO/TC 139. Plywood, Working Group 6
6-4-1	The Determination of the Mechanical Properties of Plywood Containing Defects - L G Booth
6-4-2	Comparsion of the Size and Type of Specimen and Type of Test on Plywood Bending Strength and Stiffness - C R Wilson and P Eng
6-4-3	Buckling Strength of Plywood: Results of Tests and Recommendations for Calculations - J Kuipers and H Ploos van Amstel
7-4-1	Methods of Test for the Determination of Mechanical Properties of Plywood - L G Booth, J Kuipers, B Norén, C R Wilson
7-4-2	Comments Received on Paper 7-4-1
7-4-3	The Effect of Rate of Testing Speed on the Ultimate Tensile Stress of Plywood - C R Wilson and A V Parasin
7-4-4	Comparison of the Effect of Specimen Size on the Flexural Properties of Plywood Using the Pure Moment Test - C R Wilson and A V Parasin
8-4-1	Sampling Plywood and the Evaluation of Test Results - B Norén
9-4-1	Shear and Torsional Rigidity of Plywood - H J Larsen
9-4-2	The Evaluation of Test Data on the Strength Properties of Plywood - L G Booth
9-4-3	The Sampling of Plywood and the Derivation of Strength Values (Second Draft) - B Norén
9-4-4	On the Use of the CIB/RILEM Plywood Plate Twisting Test: a progress report - L G Booth
10-4-1	Buckling Strength of Plywood - J Dekker, J Kuipers and H Ploos van Amstel
11-4-1	Analysis of Plywood Stressed Skin Panels with Rigid or Semi-Rigid Connections- I Smith
11-4-2	A Comparison of Plywood Modulus of Rigidity Determined by the ASTM and RILEM CIB/3-TT Test Methods - C R Wilson and A V Parasin
11-4-3	Sampling of Plywood for Testing Strength - B Norén
12-4-1	Procedures for Analysis of Plywood Test Data and Determination of Characteristic Values Suitable for Code Presentation - C R Wilson
14-4-1	An Introduction to Performance Standards for Wood-base Panel Products - D H Brown
14-4-2	Proposal for Presenting Data on the Properties of Structural Panels - T Schmidt
16-4-1	Planar Shear Capacity of Plywood in Bending - C K A Stieda
17-4-1	Determination of Panel Shear Strength and Panel Shear Modulus of Beech-Plywood in Structural Sizes - J Ehlbeck and F Colling
17-4-2	Ultimate Strength of Plywood Webs - R H Leicester and L Pham
20-4-1	Considerations of Reliability - Based Design for Structural Composite Products - M R O'Halloran, J A Johnson, E G Elias and T P Cunningham
21-4-1	Modelling for Prediction of Strength of Veneer Having Knots - Y Hirashima
22-4-1	Scientific Research into Plywood and Plywood Building Constructions the Results and Findings of which are Incorporated into Construction Standard Specifications of the USSR - I M Guskov
22-4-2	Evaluation of Characteristic values for Wood-Based Sheet Materials - E G Elias
24-4-1	APA Structural-Use Design Values: An Update to Panel Design Capacities - A L Kuchar, E G Elias, B Yeh and M R O'Halloran

STRESS GRADING

1-5-1 Quality Specifications for Sawn Timber and Precision Timber - Norwegian Standard NS 3080

1-5-2 Specification for Timber Grades for Structural Use - British Standard BS 4978

4-5-1 Draft Proposal for an International Standard for Stress Grading Coniferous Sawn Softwood - ECE Timber Committee

16-5-1 Grading Errors in Practice - B Thunell

16-5-2 On the Effect of Measurement Errors when Grading Structural Timber- L Nordberg and B Thunell

19-5-1 Stress-Grading by ECE Standards of Italian-Grown Douglas-Fir Dimension Lumber from Young Thinnings - L Uzielli

19-5-2 Structural Softwood from Afforestation Regions in Western Norway - R Lackner

21-5-1 Non-Destructive Test by Frequency of Full Size Timber for Grading - T Nakai

22-5-1 Fundamental Vibration Frequency as a Parameter for Grading Sawn Timber - T Nakai, T Tanaka and H Nagao

24-5-1 Influence of Stress Grading System on Length Effect Factors for Lumber Loaded in Compression - A Campos and I Smith

26-5-1 Structural Properties of French Grown Timber According to Various Grading Methods - F Rouger, C De Lafond and A El Quadrani

28-5-1 Grading Methods for Structural Timber - Principles for Approval - S Ohlsson

28-5-2 Relationship of Moduli of Elasticity in Tension and in Bending of Solid Timber - N Burger and P Glos

29-5-1 The Effect of Edge Knots on the Strength of SPF MSR Lumber - T Courchene, F Lam and J D Barrett

29-5-2 Determination of Moment Configuration Factors using Grading Machine Readings - T D G Canisius and T Isaksson

31-5-1 Influence of Varying Growth Characteristics on Stiffness Grading of Structural Timber - S Ormarsson, H Petersson, O Dahlblom and K Persson

31-5-2 A Comparison of In-Grade Test Procedures - R H Leicester, H Breitinger and H Fordham

32-5-1 Actual Possibilities of the Machine Grading of Timber - K Frühwald and A Bernasconi

32-5-2 Detection of Severe Timber Defects by Machine Grading - A Bernasconi, L Boström and B Schacht

STRESSES FOR SOLID TIMBER

4-6-1 Derivation of Grade Stresses for Timber in the UK - W T Curry

5-6-1 Standard Methods of Test for Determining some Physical and Mechanical Properties of Timber in Structural Sizes - W T Curry

5-6-2 The Description of Timber Strength Data - J R Tory

5-6-3 Stresses for EC1 and EC2 Stress Grades - J R Tory

6-6-1 Standard Methods of Test for the Determination of some Physical and Mechanical Properties of Timber in Structural Sizes (third draft) - W T Curry

7-6-1 Strength and Long-term Behaviour of Lumber and Glued Laminated Timber under Torsion Loads - K Möhler

9-6-1	Classification of Structural Timber - H J Larsen
9-6-2	Code Rules for Tension Perpendicular to Grain - H J Larsen
9-6-3	Tension at an Angle to the Grain - K Möhler
9-6-4	Consideration of Combined Stresses for Lumber and Glued Laminated Timber - K Möhler
11-6-1	Evaluation of Lumber Properties in the United States - W L Galligan and J H Haskell
11-6-2	Stresses Perpendicular to Grain - K Möhler
11-6-3	Consideration of Combined Stresses for Lumber and Glued Laminated Timber (addition to Paper CIB-W18/9-6-4) - K Möhler
12-6-1	Strength Classifications for Timber Engineering Codes - R H Leicester and W G Keating
12-6-2	Strength Classes for British Standard BS 5268 - J R Tory
13-6-1	Strength Classes for the CIB Code - J R Tory
13-6-2	Consideration of Size Effects and Longitudinal Shear Strength for Uncracked Beams - R O Foschi and J D Barrett
13-6-3	Consideration of Shear Strength on End-Cracked Beams - J D Barrett and R O Foschi
15-6-1	Characteristic Strength Values for the ECE Standard for Timber - J G Sunley
16-6-1	Size Factors for Timber Bending and Tension Stresses - A R Fewell
16-6-2	Strength Classes for International Codes - A R Fewell and J G Sunley
17-6-1	The Determination of Grade Stresses from Characteristic Stresses for BS 5268: Part 2 - A R Fewell
17-6-2	The Determination of Softwood Strength Properties for Grades, Strength Classes and Laminated Timber for BS 5268: Part 2 - A R Fewell
18-6-1	Comment on Papers: 18-6-2 and 18-6-3 - R H Leicester
18-6-2	Configuration Factors for the Bending Strength of Timber - R H Leicester
18-6-3	Notes on Sampling Factors for Characteristic Values - R H Leicester
18-6-4	Size Effects in Timber Explained by a Modified Weakest Link Theory- B Madsen and A H Buchanan
18-6-5	Placement and Selection of Growth Defects in Test Specimens - H Riberholt
18-6-6	Partial Safety-Coefficients for the Load-Carrying Capacity of Timber Structures - B Norén and J-0 Nylander
19-6-1	Effect of Age and/or Load on Timber Strength - J Kuipers
19-6-2	Confidence in Estimates of Characteristic Values - R H Leicester
19-6-3	Fracture Toughness of Wood - Mode I - K Wright and M Fonselius
19-6-4	Fracture Toughness of Pine - Mode II - K Wright
19-6-5	Drying Stresses in Round Timber - A Ranta-Maunus
19-6-6	A Dynamic Method for Determining Elastic Properties of Wood - R Görlacher
20-6-1	A Comparative Investigation of the Engineering Properties of "Whitewoods" Imported to Israel from Various Origins - U Korin
20-6-2	Effects of Yield Class, Tree Section, Forest and Size on Strength of Home Grown Sitka Spruce - V Picardo
20-6-3	Determination of Shear Strength and Strength Perpendicular to Grain - H J Larsen

21-6-1	Draft Australian Standard: Methods for Evaluation of Strength and Stiffness of Graded Timber - R H Leicester
21-6-2	The Determination of Characteristic Strength Values for Stress Grades of Structural Timber. Part 1 - A R Fewell and P Glos
21-6-3	Shear Strength in Bending of Timber - U Korin
22-6-1	Size Effects and Property Relationships for Canadian 2-inch Dimension Lumber - J D Barrett and H Griffin
22-6-2	Moisture Content Adjustements for In-Grade Data - J D Barrett and W Lau
22-6-3	A Discussion of Lumber Property Relationships in Eurocode 5 - D W Green and D E Kretschmann
22-6-4	Effect of Wood Preservatives on the Strength Properties of Wood - F Ronai
23-6-1	Timber in Compression Perpendicular to Grain - U Korin
24-6-1	Discussion of the Failure Criterion for Combined Bending and Compression - T A C M van der Put
24-6-3	Effect of Within Member Variability on Bending Strength of Structural Timber - I Czmoch, S Thelandersson and H J Larsen
24-6-4	Protection of Structural Timber Against Fungal Attack Requirements and Testing- K Jaworska, M Rylko and W Nozynski
24-6-5	Derivation of the Characteristic Bending Strength of Solid Timber According to CEN-Document prEN 384 - A J M Leijten
25-6-1	Moment Configuration Factors for Simple Beams- T D G Canisius
25-6-3	Bearing Capacity of Timber - U Korin
25-6-4	On Design Criteria for Tension Perpendicular to Grain - H Petersson
25-6-5	Size Effects in Visually Graded Softwood Structural Lumber - J D Barrett, F Lam and W Lau
26-6-1	Discussion and Proposal of a General Failure Criterion for Wood - T A C M van der Put
27-6-1	Development of the "Critical Bearing": Design Clause in CSA-086.1 - C Lum and E Karacabeyli
27-6-2	Size Effects in Timber: Novelty Never Ends - F Rouger and T Fewell
27-6-3	Comparison of Full-Size Sugi (Cryptomeria japonica D.Don) Structural Performance in Bending of Round Timber, Two Surfaces Sawn Timber and Square Sawn Timber - T Nakai, H Nagao and T Tanaka
28-6-1	Shear Strength of Canadian Softwood Structural Lumber - F Lam, H Yee and J D Barrett
28-6-2	Shear Strength of Douglas Fir Timbers - B Madsen
28-6-3	On the Influence of the Loading Head Profiles on Determined Bending Strength - L Muszyñsky and R Szukala
28-6-4	Effect of Test Standard, Length and Load Configuration on Bending Strength of Structural Timber- T Isaksson and S Thelandersson
28-6-5	Grading Machine Readings and their Use in the Calculation of Moment Configuration Factors - T Canisius, T Isaksson and S Thelandersson
28-6-6	End Conditions for Tension Testing of Solid Timber Perpendicular to Grain - T Canisius
29-6-1	Effect of Size on Tensile Strength of Timber - N Burger and P Glos

29-6-2 Equivalence of In-Grade Testing Standards - R H Leicester, H O Breitinger and H F Fordham

30-6-1 Strength Relationships in Structural Timber Subjected to Bending and Tension - N Burger and P Glos

30-6-2 Characteristic Design Stresses in Tension for Radiata Pine Grown in Canterbury - A Tsehaye, J C F Walker and A H Buchanan

30-6-3 Timber as a Natural Composite: Explanation of Some Peculiarities in the Mechanical Behaviour - E Gehri

31-6-1 Length and Moment Configuration Factors - T Isaksson

31-6-2 Tensile Strength Perpendicular to Grain According to EN 1193 - H J Blaß and M Schmid

31-6-3 Strength of Small Diameter Round Timber - A Ranta-Maunus, U Saarelainen and H Boren

31-6-4 Compression Strength Perpendicular to Grain of Structural Timber and Glulam - L Damkilde, P Hoffmeyer and T N Pedersen

31-6-5 Bearing Strength of Timber Beams - R H Leicester, H Fordham and H Breitinger

32-6-1 Development of High-Resistance Glued Robinia Products and an Attempt to Assign Such Products to the European System of Strength Classes - G Schickhofer and B Obermayr

32-6-2 Length and Load Configuration Effects in the Code Format - T Isaksson

32-6-3 Length Effect on the Tensile Strength of Truss Chord Members - F Lam

32-6-4 Tensile Strength Perpendicular to Grain of Glued Laminated Timber - H J Blaß and M Schmid

32-6-5 On the Reliability-based Strength Adjustment Factors for Timber Design - T D G Canisius

TIMBER JOINTS AND FASTENERS

1-7-1 Mechanical Fasteners and Fastenings in Timber Structures - E G Stern

4-7-1 Proposal for a Basic Test Method for the Evaluation of Structural Timber Joints with Mechanical Fasteners and Connectors - RILEM 3TT Committee

4-7-2 Test Methods for Wood Fasteners - K Möhler

5-7-1 Influence of Loading Procedure on Strength and Slip-Behaviour in Testing Timber Joints - K Möhler

5-7-2 Recommendations for Testing Methods for Joints with Mechanical Fasteners and Connectors in Load-Bearing Timber Structures - RILEM 3 TT Committee

5-7-3 CIB-Recommendations for the Evaluation of Results of Tests on Joints with Mechanical Fasteners and Connectors used in Load-Bearing Timber Structures - J Kuipers

6-7-1 Recommendations for Testing Methods for Joints with Mechanical Fasteners and Connectors in Load-Bearing Timber Structures (seventh draft) - RILEM 3 TT Committee

6-7-2 Proposal for Testing Integral Nail Plates as Timber Joints - K Möhler

6-7-3 Rules for Evaluation of Values of Strength and Deformation from Test Results - Mechanical Timber Joints - M Johansen, J Kuipers, B Norén

6-7-4 Comments to Rules for Testing Timber Joints and Derivation of Characteristic Values for Rigidity and Strength - B Norén

7-7-1	Testing of Integral Nail Plates as Timber Joints - K Möhler
7-7-2	Long Duration Tests on Timber Joints - J Kuipers
7-7-3	Tests with Mechanically Jointed Beams with a Varying Spacing of Fasteners - K Möhler
7-100-1	CIB-Timber Code Chapter 5.3 Mechanical Fasteners;CIB-Timber Standard 06 and 07 - H J Larsen
9-7-1	Design of Truss Plate Joints - F J Keenan
9-7-2	Staples - K Möhler
11-7-1	A Draft Proposal for International Standard: ISO Document ISO/TC 165N 38E
12-7-1	Load-Carrying Capacity and Deformation Characteristics of Nailed Joints - J Ehlbeck
12-7-2	Design of Bolted Joints - H J Larsen
12-7-3	Design of Joints with Nail Plates - B Norén
13-7-1	Polish Standard BN-80/7159-04: Parts 00-01-02-03-04-05. "Structures from Wood and Wood-based Materials. Methods of Test and Strength Criteria for Joints with Mechanical Fasteners"
13-7-2	Investigation of the Effect of Number of Nails in a Joint on its Load Carrying Ability - W Nozynski
13-7-3	International Acceptance of Manufacture, Marking and Control of Finger-jointed Structural Timber - B Norén
13-7-4	Design of Joints with Nail Plates - Calculation of Slip - B Norén
13-7-5	Design of Joints with Nail Plates - The Heel Joint - B Källsner
13-7-6	Nail Deflection Data for Design - H J Burgess
13-7-7	Test on Bolted Joints - P Vermeyden
13-7-8	Comments to paper CIB-W18/12-7-3 "Design of Joints with Nail Plates"- B Norén
13-7-9	Strength of Finger Joints - H J Larsen
13-100-4	CIB Structural Timber Design Code. Proposal for Section 6.1.5 Nail Plates - N I Bovim
14-7-1	Design of Joints with Nail Plates (second edition) - B Norén
14-7-2	Method of Testing Nails in Wood (second draft, August 1980) - B Norén
14-7-3	Load-Slip Relationship of Nailed Joints - J Ehlbeck and H J Larsen
14-7-4	Wood Failure in Joints with Nail Plates - B Norén
14-7-5	The Effect of Support Eccentricity on the Design of W- and WW-Trussed with Nail Plate Connectors - B Källsner
14-7-6	Derivation of the Allowable Load in Case of Nail Plate Joints Perpendicular to Grain - K Möhler
14-7-7	Comments on CIB-W18/14-7-1 - T A C M van der Put
15-7-1	Final Recommendation TT-1A: Testing Methods for Joints with Mechanical Fasteners in Load-Bearing Timber Structures. Annex A Punched Metal Plate Fasteners - Joint Committee RILEM/CIB-3TT
16-7-1	Load Carrying Capacity of Dowels - E Gehri
16-7-2	Bolted Timber Joints: A Literature Survey - N Harding

16-7-3	Bolted Timber Joints: Practical Aspects of Construction and Design; a Survey - N Harding
16-7-4	Bolted Timber Joints: Draft Experimental Work Plan - Building Research Association of New Zealand
17-7-1	Mechanical Properties of Nails and their Influence on Mechanical Properties of Nailed Timber Joints Subjected to Lateral Loads - I Smith, L R J Whale, C Anderson and L Held
17-7-2	Notes on the Effective Number of Dowels and Nails in Timber Joints - G Steck
18-7-1	Model Specification for Driven Fasteners for Assembly of Pallets and Related Structures - E G Stern and W B Wallin
18-7-2	The Influence of the Orientation of Mechanical Joints on their Mechanical Properties - I Smith and L R J Whale
18-7-3	Influence of Number of Rows of Fasteners or Connectors upon the Ultimate Capacity of Axially Loaded Timber Joints - I Smith and G Steck
18-7-4	A Detailed Testing Method for Nailplate Joints - J Kangas
18-7-5	Principles for Design Values of Nailplates in Finland - J Kangas
18-7-6	The Strength of Nailplates - N I Bovim and E Aasheim
19-7-1	Behaviour of Nailed and Bolted Joints under Short-Term Lateral Load - Conclusions from Some Recent Research - L R J Whale, I Smith and B O Hilson
19-7-2	Glued Bolts in Glulam - H Riberholt
19-7-3	Effectiveness of Multiple Fastener Joints According to National Codes and Eurocode 5 (Draft) - G Steck
19-7-4	The Prediction of the Long-Term Load Carrying Capacity of Joints in Wood Structures - Y M Ivanov and Y Y Slavic
19-7-5	Slip in Joints under Long-Term Loading - T Feldborg and M Johansen
19-7-6	The Derivation of Design Clauses for Nailed and Bolted Joints in Eurocode 5 - L R J Whale and I Smith
19-7-7	Design of Joints with Nail Plates - Principles - B Norén
19-7-8	Shear Tests for Nail Plates - B Norén
19-7-9	Advances in Technology of Joints for Laminated Timber - Analyses of the Structural Behaviour - M Piazza and G Turrini
19-15-1	Connections Deformability in Timber Structures: A Theoretical Evaluation of its Influence on Seismic Effects - A Ceccotti and A Vignoli
20-7-1	Design of Nailed and Bolted Joints-Proposals for the Revision of Existing Formulae in Draft Eurocode 5 and the CIB Code - L R J Whale, I Smith and H J Larsen
20-7-2	Slip in Joints under Long Term Loading - T Feldborg and M Johansen
20-7-3	Ultimate Properties of Bolted Joints in Glued-Laminated Timber - M Yasumura, T Murota and H Sakai
20-7-4	Modelling the Load-Deformation Behaviour of Connections with Pin-Type Fasteners under Combined Moment, Thrust and Shear Forces - I Smith
21-7-1	Nails under Long-Term Withdrawal Loading - T Feldborg and M Johansen
21-7-2	Glued Bolts in Glulam-Proposals for CIB Code - H Riberholt
21-7-3	Nail Plate Joint Behaviour under Shear Loading - T Poutanen

21-7-4	Design of Joints with Laterally Loaded Dowels. Proposals for Improving the Design Rules in the CIB Code and the Draft Eurocode 5 - J Ehlbeck and H Werner
21-7-5	Axially Loaded Nails: Proposals for a Supplement to the CIB Code - J Ehlbeck and W Siebert
22-7-1	End Grain Connections with Laterally Loaded Steel Bolts A draft proposal for design rules in the CIB Code - J Ehlbeck and M Gerold
22-7-2	Determination of Perpendicular-to-Grain Tensile Stresses in Joints with Dowel-Type Fasteners - A draft proposal for design rules - J Ehlbeck, R Görlacher and H Werner
22-7-3	Design of Double-Shear Joints with Non-Metallic Dowels A proposal for a supplement of the design concept - J Ehlbeck and O Eberhart
22-7-4	The Effect of Load on Strength of Timber Joints at high Working Load Level - A J M Leijten
22-7-5	Plasticity Requirements for Portal Frame Corners - R Gunnewijk and A J M Leijten
22-7-6	Background Information on Design of Glulam Rivet Connections in CSA/CAN3-086.1-M89 - A proposal for a supplement of the design concept - E Karacabeyli and D P Janssens
22-7-7	Mechanical Properties of Joints in Glued-Laminated Beams under Reversed Cyclic Loading - M Yasumura
22-7-8	Strength of Glued Lap Timber Joints - P Glos and H Horstmann
22-7-9	Toothed Rings Type Bistyp 075 at the Joints of Fir Wood - J Kerste
22-7-10	Calculation of Joints and Fastenings as Compared with the International State - K Zimmer and K Lissner
22-7-11	Joints on Glued-in Steel Bars Present Relatively New and Progressive Solution in Terms of Timber Structure Design - G N Zubarev, F A Boitemirov and V M Golovina
22-7-12	The Development of Design Codes for Timber Structures made of Compositive Bars with Plate Joints based on Cyclindrical Nails - Y V Piskunov
22-7-13	Designing of Glued Wood Structures Joints on Glued-in Bars - S B Turkovsky
23-7-1	Proposal for a Design Code for Nail Plates - E Aasheim and K H Solli
23-7-2	Load Distribution in Nailed Joints - H J Blass
24-7-1	Theoretical and Experimental Tension and Shear Capacity of Nail Plate Connections - B Källsner and J Kangas
24-7-2	Testing Method and Determination of Basic Working Loads for Timber Joints with Mechanical Fasteners - Y Hirashima and F Kamiya
24-7-3	Anchorage Capacity of Nail Plate - J Kangas
25-7-2	Softwood and Hardwood Embedding Strength for Dowel type Fasteners - J Ehlbeck and H Werner
25-7-4	A Guide for Application of Quality Indexes for Driven Fasteners Used in Connections in Wood Structures - E G Stern
25-7-5	35 Years of Experience with Certain Types of Connectors and Connector Plates Used for the Assembly of Wood Structures and their Components- E G Stern
25-7-6	Characteristic Strength of Split-ring and Shear-plate Connections - H J Blass, J Ehlbeck and M Schlager

25-7-7	Characteristic Strength of Tooth-plate Connector Joints - H J Blass, J Ehlbeck and M Schlager
25-7-8	Extending Yield Theory to Screw Connections - T E McLain
25-7-9	Determination of k_{def} for Nailed Joints - J W G van de Kuilen
25-7-10	Characteristic Strength of UK Timber Connectors - A V Page and C J Mettem
25-7-11	Multiple-fastener Dowel-type Joints, a Selected Review of Research and Codes - C J Mettem and A V Page
25-7-12	Load Distributions in Multiple-fastener Bolted Joints in European Whitewood Glulam, with Steel Side Plates - C J Mettem and A V Page
26-7-1	Proposed Test Method for Dynamic Properties of Connections Assembled with Mechanical Fasteners - J D Dolan
26-7-2	Validatory Tests and Proposed Design Formulae for the Load-Carrying Capacity of Toothed-Plate Connectored Joints - C J Mettem, A V Page and G Davis
26-7-3	Definitions of Terms and Multi-Language Terminology Pertaining to Metal Connector Plates - E G Stern
26-7-4	Design of Joints Based on in V-Shape Glued-in Rods - J Kangas
26-7-5	Tests on Timber Concrete Composite Structural Elements (TCCs) - A U Meierhofer
27-7-1	Glulam Arch Bridge and Design of it's Moment-Resisting Joints - K Komatsu and S Usuku
27-7-2	Characteristic Load - Carrying Capacity of Joints with Dowel - type Fasteners in Regard to the System Properties - H Werner
27-7-3	Steel Failure Design in Truss Plate Joints - T Poutanen
28-7-1	Expanded Tube Joint in Locally DP Reinforced Timber - A J M Leijten, P Ragupathy and K S Virdi
28-7-2	A Strength and Stiffness Model for the Expanded Tube Joint - A J M Leijten
28-7-3	Load-carrying Capacity of Steel-to Timber Joints with Annular Ring Shanked Nails. A Comparison with the EC5 Design Method - R Görlacher
28-7-4	Dynamic Effects on Metal-Plate Connected Wood Truss Joints - S Kent, R Gupta and T Miller
28-7-5	Failure of the Timber Bolted Joints Subjected to Lateral Load Perpendicular to Grain - M Yasumura and L Daudeville
28-7-6	Design Procedure for Locally Reinforced Joints with Dowel-type Fasteners - H Werner
28-7-7	Variability and Effects of Moisture Content on the Withdrawal Characteristics for Lumber as Opposed to Clear Wood - J D Dolan and J W Stelmokas
28-7-8	Nail Plate Capacity in Joint Line - A Kevarinmäki and J Kangas
28-7-9	Axial Strength of Glued-In Bolts - Calculation Model Based on Non-Linear Fracture Mechanics - A Preliminary Study - C J Johansson, E Serrano, P J Gustafsson and B Enquist
28-7-10	Cyclic Lateral Dowel Connection Tests for seismic and Wind Evaluation - J D Dolan
29-7-1	A Simple Method for Lateral Load-Carrying Capacity of Dowel-Type Fasteners - J Kangas and J Kurkela
29-7-2	Nail Plate Joint Behaviour at Low Versus High Load Level - T Poutanen

32-7-7	Concentric Loading Tests on Girder Truss Components - T N Reynolds, A Reffold, V Enjily and L Whale
32-7-8	Dowel Type Connections with Slotted-In Steel Plates - M U Pedersen, C O Clorius, L Damkilde, P Hoffmeyer and L Esklidsen
32-7-9	Creep of Nail Plate Reinforced Bolt Joints - J Vesa and A Kevarinmäki
32-7-10	The Behaviour of Timber Joints with Ring Connectors - E Gehri and A Mischler
32-7-11	Non-Metallic, Adhesiveless Joints for Timber Structures - R D Drake, M P Ansell, C J Mettem and R Bainbridge
32-7-12	Effect of Spacing and Edge Distance on the Axial Strength of Glued-in Rods - H J Blaß and B Laskewitz
32-7-13	Evaluation of Material Combinations for Bonded in Rods to Achieve Improved Timber Connections - C J Mettem, R J Bainbridge, K Harvey, M P Ansell, J G Broughton and A R Hutchinson
33-7-1	Determination of Yield Strength and Ultimate Strength of Dowel-Type Timber Joints – M Yasumura and K Sawata
33-7-2	Lateral Shear Capacity of Nailed Joints – U Korin
33-7-3	Height-Adjustable Connector for Composite Beams – Y V Piskunov and E G Stern
33-7-4	Engineering Ductility Assessment for a Nailed Slotted-In Steel Connection in Glulam– L Stehn and H Johansson
33-7-5	Effective Bending Capacity of Dowel-Type Fasteners - H J Blaß, A Bienhaus and V Krämer
33-7-6	Load-Carrying Capacity of Joints with Dowel-Type Fasteners and Interlayers - H J Blaß and B Laskewitz
33-7-7	Evaluation of Perpendicular to Grain Failure of Beams caused by Concentrated Loads of Joints – A J M Leijten and T A C M van der Put
33-7-8	Test Methods for Glued-In Rods for Timber Structures – C Bengtsson and C J Johansson
33-7-9	Stiffness Analysis of Nail Plates – P Ellegaard
33-7-10	Capacity, Fire Resistance and Gluing Pattern of the Rods in V-Connections – J Kangas
33-7-11	Bonded-In Pultrusions for Moment-Resisting Timber Connections – K Harvey, M P Ansell, C J Mettem, R J Bainbridge and N Alexandre
33-7-12	Fatigue Performance of Bonded-In Rods in Glulam, Using Three Adhesive Types - R J Bainbridge, K Harvey, C J Mettem and M P Ansell

LOAD SHARING

3-8-1	Load Sharing - An Investigation on the State of Research and Development of Design Criteria - E Levin
4-8-1	A Review of Load-Sharing in Theory and Practice - E Levin
4-8-2	Load Sharing - B Norén
19-8-1	Predicting the Natural Frequencies of Light-Weight Wooden Floors - I Smith and Y H Chui
20-8-1	Proposed Code Requirements for Vibrational Serviceability of Timber Floors - Y H Chui and I Smith

21-8-1 An Addendum to Paper 20-8-1 - Proposed Code Requirements for Vibrational Serviceability of Timber Floors - Y H Chui and I Smith

21-8-2 Floor Vibrational Serviceability and the CIB Model Code - S Ohlsson

22-8-1 Reliability Analysis of Viscoelastic Floors - F Rouger, J D Barrett and R O Foschi

24-8-1 On the Possibility of Applying Neutral Vibrational Serviceability Criteria to Joisted Wood Floors - I Smith and Y H Chui

25-8-1 Analysis of Glulam Semi-rigid Portal Frames under Long-term Load - K Komatsu and N Kawamoto

DURATION OF LOAD

3-9-1 Definitions of Long Term Loading for the Code of Practice - B Norén

4-9-1 Long Term Loading of Trussed Rafters with Different Connection Systems - T Feldborg and M Johansen

5-9-1 Strength of a Wood Column in Combined Compression and Bending with Respect to Creep - B Källsner and B Norén

6-9-1 Long Term Loading for the Code of Practice (Part 2) - B Norén

6-9-2 Long Term Loading - K Möhler

6-9-3 Deflection of Trussed Rafters under Alternating Loading during a Year - T Feldborg and M Johansen

7-6-1 Strength and Long Term Behaviour of Lumber and Glued-Laminated Timber under Torsion Loads - K Möhler

7-9-1 Code Rules Concerning Strength and Loading Time - H J Larsen and E Theilgaard

17-9-1 On the Long-Term Carrying Capacity of Wood Structures - Y M Ivanov and Y Y Slavic

18-9-1 Prediction of Creep Deformations of Joints - J Kuipers

19-9-1 Another Look at Three Duration of Load Models - R O Foschi and Z C Yao

19-9-2 Duration of Load Effects for Spruce Timber with Special Reference to Moisture Influence - A Status Report - P Hoffmeyer

19-9-3 A Model of Deformation and Damage Processes Based on the Reaction Kinetics of Bond Exchange - T A C M van der Put

19-9-4 Non-Linear Creep Superposition - U Korin

19-9-5 Determination of Creep Data for the Component Parts of Stressed-Skin Panels - R Kliger

19-9-6 Creep an Lifetime of Timber Loaded in Tension and Compression - P Glos

19-1-1 Duration of Load Effects and Reliability Based Design (Single Member) - R O Foschi and Z C Yao

19-6-1 Effect of Age and/or Load on Timber Strength - J Kuipers

19-7-4 The Prediction of the Long-Term Load Carrying Capacity of Joints in Wood Structures - Y M Ivanov and Y Y Slavic

19-7-5 Slip in Joints under Long-Term Loading - T Feldborg and M Johansen

20-7-2 Slip in Joints under Long-Term Loading - T Feldborg and M Johansen

22-9-1 Long-Term Tests with Glued Laminated Timber Girders - M Badstube, W Rug and W Schöne

22-9-2 Strength of One-Layer solid and Lengthways Glued Elements of Wood Structures and its Alteration from Sustained Load - L M Kovaltchuk, I N Boitemirova and G B Uspenskaya

24-9-1 Long Term Bending Creep of Wood - T Toratti

24-9-2 Collection of Creep Data of Timber - A Ranta-Maunus

24-9-3 Deformation Modification Factors for Calculating Built-up Wood-Based Structures - I R Kliger

25-9-2 DVM Analysis of Wood. Lifetime, Residual Strength and Quality - L F Nielsen

26-9-1 Long Term Deformations in Wood Based Panels under Natural Climate Conditions. A Comparative Study - S Thelandersson, J Nordh, T Nordh and S Sandahl

28-9-1 Evaluation of Creep Behavior of Structural Lumber in Natural Environment - R Gupta and R Shen

30-9-1 DOL Effect in Tension Perpendicular to the Grain of Glulam Depending on Service Classes and Volume - S Aicher and G Dill-Langer

30-9-2 Damage Modelling of Glulam in Tension Perpendicular to Grain in Variable Climate - G Dill-Langer and S Aicher

31-9-1 Duration of Load Effect in Tension Perpendicular to Grain in Curved Glulam - A Ranta-Maunus

32-9-1 Bending-Stress-Redistribution Caused by Different Creep in Tension and Compression and Resulting DOL-Effect - P Becker and K Rautenstrauch

32-9-2 The Long Term Performance of Ply-Web Beams - R Grantham and V Enjily

TIMBER BEAMS

4-10-1 The Design of Simple Beams - H J Burgess

4-10-2 Calculation of Timber Beams Subjected to Bending and Normal Force - H J Larsen

5-10-1 The Design of Timber Beams - H J Larsen

9-10-1 The Distribution of Shear Stresses in Timber Beams - F J Keenan

9-10-2 Beams Notched at the Ends - K Möhler

11-10-1 Tapered Timber Beams - H Riberholt

13-6-2 Consideration of Size Effects in Longitudinal Shear Strength for Uncracked Beams - R O Foschi and J D Barrett

13-6-3 Consideration of Shear Strength on End-Cracked Beams - J D Barrett and R O Foschi

18-10-1 Submission to the CIB-W18 Committee on the Design of Ply Web Beams by Consideration of the Type of Stress in the Flanges - J A Baird

18-10-2 Longitudinal Shear Design of Glued Laminated Beams - R O Foschi

19-10-1 Possible Code Approaches to Lateral Buckling in Beams - H J Burgess

19-2-1 Creep Buckling Strength of Timber Beams and Columns - R H Leicester

20-2-1 Lateral Buckling Theory for Rectangular Section Deep Beam-Columns - H J Burgess

20-10-1 Draft Clause for CIB Code for Beams with Initial Imperfections - H J Burgess

20-10-2 Space Joists in Irish Timber - W J Robinson

20-10-3 Composite Structure of Timber Joists and Concrete Slab - T Poutanen

21-10-1 A Study of Strength of Notched Beams - P J Gustafsson

22-10-1 Design of Endnotched Beams - H J Larsen and P J Gustafsson

22-10-2 Dimensions of Wooden Flexural Members under Constant Loads - A Pozgai

22-10-3 Thin-Walled Wood-Based Flanges in Composite Beams - J König

22-10-4 The Calculation of Wooden Bars with flexible Joints in Accordance with the Polish Standart Code and Strict Theoretical Methods - Z Mielczarek

23-10-1 Tension Perpendicular to the Grain at Notches and Joints - T A C M van der Put

23-10-2 Dimensioning of Beams with Cracks, Notches and Holes. An Application of Fracture Mechanics - K Riipola

23-10-3 Size Factors for the Bending and Tension Strength of Structural Timber - J D Barret and A R Fewell

23-12-1 Bending Strength of Glulam Beams, a Design Proposal - J Ehlbeck and F Colling

23-12-3 Glulam Beams, Bending Strength in Relation to the Bending Strength of the Finger Joints - H Riberholt

24-10-1 Shear Strength of Continuous Beams - R H Leicester and F G Young

25-10-1 The Strength of Norwegian Glued Laminated Beams - K Solli, E Aasheim and R H Falk

25-10-2 The Influence of the Elastic Modulus on the Simulated Bending Strength of Hyperstatic Timber Beams - T D G Canisius

27-10-1 Determination of Shear Modulus - R Görlacher and J Kürth

29-10-1 Time Dependent Lateral Buckling of Timber Beams - F Rouger

29-10-2 Determination of Modulus of Elasticity in Bending According to EN 408 - K H Solli

29-10-3 On Determination of Modulus of Elasticity in Bending - L Boström, S Ormarsson and O Dahlblom

29-10-4 Relation of Moduli of Elasticity in Flatwise and Edgewise Bending of Solid Timber - C J Johansson, A Steffen and E W Wormuth

30-10-1 Nondestructive Evaluation of Wood-based Members and Structures with the Help of Modal Analysis - P Kuklik

30-10-2 Measurement of Modulus of Elasticity in Bending - L Boström

30-10-3 A Weak Zone Model for Timber in Bending - B Källsner, K Salmela and O Ditlevsen

30-10-4 Load Carrying Capacity of Timber Beams with Narrow Moment Peaks - T Isaksson and J Freysoldt

ENVIRONMENTAL CONDITIONS

5-11-1 Climate Grading for the Code of Practice - B Norén

6-11-1 Climate Grading (2) - B Norén

9-11-1 Climate Classes for Timber Design - F J Keenan

19-11-1 Experimental Analysis on Ancient Downgraded Timber Structures - B Leggeri and L Paolini

19-6-5 Drying Stresses in Round Timber - A Ranta-Maunus

22-11-1 Corrosion and Adaptation Factors for Chemically Aggressive Media with Timber Structures - K Erler

29-11-1 Load Duration Effect on Structural Beams under Varying Climate Influence of Size and Shape - P Galimard and P Morlier

30-11-1 Probabilistic Design Models for the Durability of Timber Constructions - R H Leicester

LAMINATED MEMBERS

6-12-1 Directives for the Fabrication of Load-Bearing Structures of Glued Timber - A van der Velden and J Kuipers

8-12-1 Testing of Big Glulam Timber Beams - H Kolb and P Frech

8-12-2 Instruction for the Reinforcement of Apertures in Glulam Beams - H Kolb and P Frech

8-12-3 Glulam Standard Part 1: Glued Timber Structures; Requirements for Timber (Second Draft)

9-12-1 Experiments to Provide for Elevated Forces at the Supports of Wooden Beams with Particular Regard to Shearing Stresses and Long-Term Loadings - F Wassipaul and R Lackner

9-12-2 Two Laminated Timber Arch Railway Bridges Built in Perth in 1849 - L G Booth

9-6-4 Consideration of Combined Stresses for Lumber and Glued Laminated Timber - K Möhler

11-6-3 Consideration of Combined Stresses for Lumber and Glued Laminated Timber (addition to Paper CIB-W18/9-6-4) - K Möhler

12-12-1 Glulam Standard Part 2: Glued Timber Structures; Rating (3rd draft)

12-12-2 Glulam Standard Part 3: Glued Timber Structures; Performance (3 rd draft)

13-12-1 Glulam Standard Part 3: Glued Timber Structures; Performance (4th draft)

14-12-1 Proposals for CEI-Bois/CIB-W18 Glulam Standards - H J Larsen

14-12-2 Guidelines for the Manufacturing of Glued Load-Bearing Timber Structures - Stevin Laboratory

14-12-3 Double Tapered Curved Glulam Beams - H Riberholt

14-12-4 Comment on CIB-W18/14-12-3 - E Gehri

18-12-1 Report on European Glulam Control and Production Standard - H Riberholt

18-10-2 Longitudinal Shear Design of Glued Laminated Beams - R O Foschi

19-12-1 Strength of Glued Laminated Timber - J Ehlbeck and F Colling

19-12-2 Strength Model for Glulam Columns - H J Blaß

19-12-3 Influence of Volume and Stress Distribution on the Shear Strength and Tensile Strength Perpendicular to Grain - F Colling

19-12-4 Time-Dependent Behaviour of Glued-Laminated Beams - F Zaupa

21-12-1 Modulus of Rupture of Glulam Beam Composed of Arbitrary Laminae - K Komatsu and N Kawamoto

21-12-2 An Appraisal of the Young's Modulus Values Specified for Glulam in Eurocode 5- L R J Whale, B O Hilson and P D Rodd

21-12-3 The Strength of Glued Laminated Timber (Glulam): Influence of Lamination Qualities and Strength of Finger Joints - J Ehlbeck and F Colling

21-12-4 Comparison of a Shear Strength Design Method in Eurocode 5 and a More Traditional One - H Riberholt

22-12-1	The Dependence of the Bending Strength on the Glued Laminated Timber Girder Depth - M Badstube, W Rug and W Schöne
22-12-2	Acid Deterioration of Glulam Beams in Buildings from the Early Half of the 1960s - Prelimination summary of the research project; Overhead pictures - B A Hedlund
22-12-3	Experimental Investigation of normal Stress Distribution in Glue Laminated Wooden Arches - Z Mielczarek and W Chanaj
22-12-4	Ultimate Strength of Wooden Beams with Tension Reinforcement as a Function of Random Material Properties - R Candowicz and T Dziuba
23-12-1	Bending Strength of Glulam Beams, a Design Proposal - J Ehlbeck and F Colling
23-12-2	Probability Based Design Method for Glued Laminated Timber - M F Stone
23-12-3	Glulam Beams, Bending Strength in Relation to the Bending Strength of the Finger Joints - H Riberholt
23-12-4	Glued Laminated Timber - Strength Classes and Determination of Characteristic Properties - H Riberholt, J Ehlbeck and A Fewell
24-12-1	Contribution to the Determination of the Bending Strength of Glulam Beams - F Colling, J Ehlbeck and R Görlacher
24-12-2	Influence of Perpendicular-to-Grain Stressed Volume on the Load-Carrying Capacity of Curved and Tapered Glulam Beams - J Ehlbeck and J Kürth
25-12-1	Determination of Characteristic Bending Values of Glued Laminated Timber. EN-Approach and Reality - E Gehri
26-12-1	Norwegian Bending Tests with Glued Laminated Beams-Comparative Calculations with the "Karlsruhe Calculation Model" - E Aasheim, K Solli, F Colling, R H Falk, J Ehlbeck and R Görlacher
26-12-2	Simulation Analysis of Norwegian Spruce Glued-Laminated Timber - R Hernandez and R H Falk
26-12-3	Investigation of Laminating Effects in Glued-Laminated Timber - F Colling and R H Falk
26-12-4	Comparing Design Results for Glulam Beams According to Eurocode 5 and to the French Working Stress Design Code (CB71) - F Rouger
27-12-1	State of the Art Report: Glulam Timber Bridge Design in the U.S. - M A Ritter and T G Williamson
27-12-2	Common Design Practice for Timber Bridges in the United Kingdom - C J Mettem, J P Marcroft and G Davis
27-12-3	Influence of Weak Zones on Stress Distribution in Glulam Beams - E Serrano and H J Larsen
28-12-1	Determination of Characteristic Bending Strength of Glued Laminated Timber - E Gehri
28-12-2	Size Factor of Norwegian Glued Laminated Beams - E Aasheim and K H Solli
28-12-3	Design of Glulam Beams with Holes - K Riipola
28-12-4	Compression Resistance of Glued Laminated Timber Short Columns- U Korin
29-12-1	Development of Efficient Glued Laminated Timber - G Schickhofer
30-12-1	Experimental Investigation and Analysis of Reinforced Glulam Beams - K Oiger
31-12-1	Depth Factor for Glued Laminated Timber-Discussion of the Eurocode 5 Approach - B Källsner, O Carling and C J Johansson
32-12-1	The bending stiffness of nail-laminated timber elements in transverse direction- T Wolf and O Schäfer

33-12-1 Internal Stresses in the Cross-Grain Direction of Wood Induced by Climate Variation – J Jönsson and S Svensson

PARTICLE AND FIBRE BUILDING BOARDS

7-13-1 Fibre Building Boards for CIB Timber Code (First Draft)- O Brynildsen

9-13-1 Determination of the Bearing Strength and the Load-Deformation Characteristics of Particleboard - K Möhler, T Budianto and J Ehlbeck

9-13-2 The Structural Use of Tempered Hardboard - W W L Chan

11-13-1 Tests on Laminated Beams from Hardboard under Short- and Longterm Load - W Nozynski

11-13-2 Determination of Deformation of Special Densified Hardboard under Long-term Load and Varying Temperature and Humidity Conditions - W Halfar

11-13-3 Determination of Deformation of Hardboard under Long-term Load in Changing Climate - W Halfar

14-4-1 An Introduction to Performance Standards for Wood-Base Panel Products - D H Brown

14-4-2 Proposal for Presenting Data on the Properties of Structural Panels - T Schmidt

16-13-1 Effect of Test Piece Size on Panel Bending Properties - P W Post

20-4-1 Considerations of Reliability - Based Design for Structural Composite Products - M R O'Halloran, J A Johnson, E G Elias and T P Cunningham

20-13-1 Classification Systems for Structural Wood-Based Sheet Materials - V C Kearley and A R Abbott

21-13-1 Design Values for Nailed Chipboard - Timber Joints - A R Abbott

25-13-1 Bending Strength and Stiffness of Izopanel Plates - Z Mielczarek

28-13-1 Background Information for "Design Rated Oriented Strand Board (OSB)" in CSA Standards - Summary of Short-term Test Results - E Karacabeyli, P Lau, C R Henderson, F V Meakes and W Deacon

28-13-2 Torsional Stiffness of Wood-Hardboard Composed I-Beam - P Olejniczak

TRUSSED RAFTERS

4-9-1 Long-term Loading of Trussed Rafters with Different Connection Systems - T Feldborg and M Johansen

6-9-3 Deflection of Trussed Rafters under Alternating Loading During a Year - T Feldborg and M Johansen

7-2-1 Lateral Bracing of Timber Struts - J A Simon

9-14-1 Timber Trusses - Code Related Problems - T F Williams

9-7-1 Design of Truss Plate Joints - F J Keenan

10-14-1 Design of Roof Bracing - The State of the Art in South Africa - P A V Bryant and J A Simon

11-14-1 Design of Metal Plate Connected Wood Trusses - A R Egerup

12-14-1 A Simple Design Method for Standard Trusses - A R Egerup

13-14-1 Truss Design Method for CIB Timber Code - A R Egerup

13-14-2 Trussed Rafters, Static Models - H Riberholt

13-14-3	Comparison of 3 Truss Models Designed by Different Assumptions for Slip and E-Modulus - K Möhler
14-14-1	Wood Trussed Rafter Design - T Feldborg and M Johansen
14-14-2	Truss-Plate Modelling in the Analysis of Trusses - R O Foschi
14-14-3	Cantilevered Timber Trusses - A R Egerup
14-7-5	The Effect of Support Eccentricity on the Design of W- and WW-Trusses with Nail Plate Connectors - B Källsner
15-14-1	Guidelines for Static Models of Trussed Rafters - H Riberholt
15-14-2	The Influence of Various Factors on the Accuracy of the Structural Analysis of Timber Roof Trusses - F R P Pienaar
15-14-3	Bracing Calculations for Trussed Rafter Roofs - H J Burgess
15-14-4	The Design of Continuous Members in Timber Trussed Rafters with Punched Metal Connector Plates - P O Reece
15-14-5	A Rafter Design Method Matching U.K. Test Results for Trussed Rafters - H J Burgess
16-14-1	Full-Scale Tests on Timber Fink Trusses Made from Irish Grown Sitka Spruce - V Picardo
17-14-1	Data from Full Scale Tests on Prefabricated Trussed Rafters - V Picardo
17-14-2	Simplified Static Analysis and Dimensioning of Trussed Rafters - H Riberholt
17-14-3	Simplified Calculation Method for W-Trusses - B Källsner
18-14-1	Simplified Calculation Method for W-Trusses (Part 2) - B Källsner
18-14-2	Model for Trussed Rafter Design - T Poutanen
19-14-1	Annex on Simplified Design of W-Trusses - H J Larsen
19-14-2	Simplified Static Analysis and Dimensioning of Trussed Rafters - Part 2 - H Riberholt
19-14-3	Joint Eccentricity in Trussed Rafters - T Poutanen
20-14-1	Some Notes about Testing Nail Plates Subjected to Moment Load - T Poutanen
20-14-2	Moment Distribution in Trussed Rafters - T Poutanen
20-14-3	Practical Design Methods for Trussed Rafters - A R Egerup
22-14-1	Guidelines for Design of Timber Trussed Rafters - H Riberholt
23-14-1	Analyses of Timber Trussed Rafters of the W-Type - H Riberholt
23-14-2	Proposal for Eurocode 5 Text on Timber Trussed Rafters - H Riberholt
24-14-1	Capacity of Support Areas Reinforced with Nail Plates in Trussed Rafters - A Kevarinmäki
25-14-1	Moment Anchorage Capacity of Nail Plates in Shear Tests - A Kevarinmaki and J. Kangas
25-14-2	Design Values of Anchorage Strength of Nail Plate Joints by 2-curve Method and Interpolation - J Kangas and A Kevarinmaki
26-14-1	Test of Nail Plates Subjected to Moment - E Aasheim
26-14-2	Moment Anchorage Capacity of Nail Plates - A Kevarinmäki and J Kangas
26-14-3	Rotational Stiffness of Nail Plates in Moment Anchorage - A Kevarinmäki and J Kangas
26-14-4	Solution of Plastic Moment Anchorage Stress in Nail Plates - A Kevarinmäki

26-14-5 Testing of Metal-Plate-Connected Wood-Truss Joints - R Gupta

26-14-6 Simulated Accidental Events on a Trussed Rafter Roofed Building - C J Mettem and J P Marcroft

30-14-1 The Stability Behaviour of Timber Trussed Rafter Roofs - Studies Based on Eurocode 5 and Full Scale Testing - R J Bainbridge, C J Mettern, A Reffold and T Studer

32-14-1 Analysis of Timber Reinforced with Punched Metal Plate Fasteners- J Nielsen

33-14-1 Moment Capacity of Timber Beams Loaded in Four-Point Bending and Reinforced with Punched Metal Plate Fasteners – J Nielsen

STRUCTURAL STABILITY

8-15-1 Laterally Loaded Timber Columns: Tests and Theory - H J Larsen

13-15-1 Timber and Wood-Based Products Structures. Panels for Roof Coverings. Methods of Testing and Strength Assessment Criteria. Polish Standard BN-78/7159-03

16-15-1 Determination of Bracing Structures for Compression Members and Beams - H Brüninghoff

17-15-1 Proposal for Chapter 7.4 Bracing - H Brüninghoff

17-15-2 Seismic Design of Small Wood Framed Houses - K F Hansen

18-15-1 Full-Scale Structures in Glued Laminated Timber, Dynamic Tests: Theoretical and Experimental Studies - A Ceccotti and A Vignoli

18-15-2 Stabilizing Bracings - H Brüninghoff

19-15-1 Connections Deformability in Timber Structures: a Theoretical Evaluation of its Influence on Seismic Effects - A Ceccotti and A Vignoli

19-15-2 The Bracing of Trussed Beams - M H Kessel and J Natterer

19-15-3 Racking Resistance of Wooden Frame Walls with Various Openings - M Yasumura

19-15-4 Some Experiences of Restoration of Timber Structures for Country Buildings - G Cardinale and P Spinelli

19-15-5 Non-Destructive Vibration Tests on Existing Wooden Dwellings - Y Hirashima

20-15-1 Behaviour Factor of Timber Structures in Seismic Zones. - A Ceccotti and A Vignoli

21-15-1 Rectangular Section Deep Beam - Columns with Continuous Lateral Restraint - H J Burgess

21-15-2 Buckling Modes and Permissible Axial Loads for Continuously Braced Columns- H J Burgess

21-15-3 Simple Approaches for Column Bracing Calculations - H J Burgess

21-15-4 Calculations for Discrete Column Restraints - H J Burgess

21-15-5 Behaviour Factor of Timber Structures in Seismic Zones (Part Two) - A Ceccotti and A Vignoli

22-15-1 Suggested Changes in Code Bracing Recommendations for Beams and Columns - H J Burgess

22-15-2 Research and Development of Timber Frame Structures for Agriculture in Poland- S Kus and J Kerste

22-15-3	Ensuring of Three-Dimensional Stiffness of Buildings with Wood Structures - A K Shenghelia
22-15-5	Seismic Behavior of Arched Frames in Timber Construction - M Yasumura
22-15-6	The Robustness of Timber Structures - C J Mettem and J P Marcroft
22-15-7	Influence of Geometrical and Structural Imperfections on the Limit Load of Wood Columns - P Dutko
23-15-1	Calculation of a Wind Girder Loaded also by Discretely Spaced Braces for Roof Members - H J Burgess
23-15-2	Stability Design and Code Rules for Straight Timber Beams - T A C M van der Put
23-15-3	A Brief Description of Formula of Beam-Columns in China Code - S Y Huang
23-15-4	Seismic Behavior of Braced Frames in Timber Construction - M Yasumara
23-15-5	On a Better Evaluation of the Seismic Behavior Factor of Low-Dissipative Timber Structures - A Ceccotti and A Vignoli
23-15-6	Disproportionate Collapse of Timber Structures - C J Mettem and J P Marcroft
23-15-7	Performance of Timber Frame Structures During the Loma Prieta California Earthquake - M R O'Halloran and E G Elias
24-15-2	Discussion About the Description of Timber Beam-Column Formula - S Y Huang
24-15-3	Seismic Behavior of Wood-Framed Shear Walls - M Yasumura
25-15-1	Structural Assessment of Timber Framed Building Systems - U Korin
25-15-3	Mechanical Properties of Wood-framed Shear Walls Subjected to Reversed Cyclic Lateral Loading - M Yasumura
26-15-1	Bracing Requirements to Prevent Lateral Buckling in Trussed Rafters - C J Mettem and P J Moss
26-15-2	Eurocode 8 - Part 1.3 - Chapter 5 - Specific Rules for Timber Buildings in Seismic Regions - K Becker, A Ceccotti, H Charlier, E Katsaragakis, H J Larsen and H Zeitter
26-15-3	Hurricane Andrew - Structural Performance of Buildings in South Florida - M R O'Halloran, E L Keith, J D Rose and T P Cunningham
29-15-1	Lateral Resistance of Wood Based Shear Walls with Oversized Sheathing Panels - F Lam, H G L Prion and M He
29-15-2	Damage of Wooden Buildings Caused by the 1995 Hyogo-Ken Nanbu Earthquake - M Yasumura, N Kawai, N Yamaguchi and S Nakajima
29-15-3	The Racking Resistance of Timber Frame Walls: Design by Test and Calculation - D R Griffiths, C J Mettem, V Enjily, P J Steer
29-15-4	Current Developments in Medium-Rise Timber Frame Buildings in the UK - C J Mettem, G C Pitts, P J Steer, V Enjily
29-15-5	Natural Frequency Prediction for Timber Floors - R J Bainbridge, and C J Mettem
30-15-1	Cyclic Performance of Perforated Wood Shear Walls with Oversize Oriented Strand Board Panels - Ming He, H Magnusson, F Lam, and H G L Prion
30-15-2	A Numerical Analysis of Shear Walls Structural Performances - L Davenne, L Daudeville, N Kawai and M Yasumura
30-15-3	Seismic Force Modification Factors for the Design of Multi-Storey Wood-Frame Platform Construction - E Karacabeyli and A Ceccotti
30-15-4	Evaluation of Wood Framed Shear Walls Subjected to Lateral Load - M Yasumura and N Kawai

31-15-1 Seismic Performance Testing On Wood-Framed Shear Wall - N Kawai

31-15-2 Robustness Principles in the Design of Medium-Rise Timber-Framed Buildings - C J Mettem, M W Milner, R J Bainbridge and V. Enjily

31-15-3 Numerical Simulation of Pseudo-Dynamic Tests Performed to Shear Walls - L Daudeville, L Davenne, N Richard, N Kawai and M Yasumura

31-15-4 Force Modification Factors for Braced Timber Frames - H G L Prion, M Popovski and E Karacabeyli

32-15-1 Three-Dimensional Interaction in Stabilisation of Multi-Storey Timber Frame Buildings - S Andreasson

32-15-2 Application of Capacity Spectrum Method to Timber Houses - N Kawai

32-15-3 Design Methods for Shear Walls with Openings - C Ni, E Karacabeyli and A Ceccotti

32-15-4 Static Cyclic Lateral Loading Tests on Nailed Plywood Shear Walls - K Komatsu, K H Hwang and Y Itou

33-15-1 Lateral Load Capacities of Horizontally Sheathed Unblocked Shear Walls – C Ni, E Karacabeyli and A Ceccotti

33-15-2 Prediction of Earthquake Response of Timber Houses Considering Shear Deformation of Horizontal Frames – N Kawai

33-15-3 Eurocode 5 Rules for Bracing – H J Larsen

FIRE

12-16-1 British Standard BS 5268 the Structural Use of Timber: Part 4 Fire Resistance of Timber Structures

13-100-2 CIB Structural Timber Design Code. Chapter 9. Performance in Fire

19-16-1 Simulation of Fire in Tests of Axially Loaded Wood Wall Studs - J König

24-16-1 Modelling the Effective Cross Section of Timber Frame Members Exposed to Fire - J König

25-16-1 The Effect of Density on Charring and Loss of Bending Strength in Fire - J König

25-16-2 Tests on Glued-Laminated Beams in Bending Exposed to Natural Fires - F Bolonius Olesen and J König

26-16-1 Structural Fire Design According to Eurocode 5, Part 1.2 - J König

31-16-1 Revision of ENV 1995-1-2: Charring and Degradation of Strength and Stiffness - J König

33-16-1 A Design Model for Load-carrying Timber Frame Members in Walls and Floors Exposed to Fire - J König

33-16-2 A Review of Component Additive Methods Used for the Determination of Fire Resistance of Separating Light Timber Frame Construction - J König, T Oksanen and K Towler

33-16-3 Thermal and Mechanical Properties of Timber and Some Other Materials Used in Light Timber Frame Construction - B Källsner and J König

STATISTICS AND DATA ANALYSIS

13-17-1 On Testing Whether a Prescribed Exclusion Limit is Attained - W G Warren

16-17-1 Notes on Sampling and Strength Prediction of Stress Graded Structural Timber - P Glos

16-17-2 Sampling to Predict by Testing the Capacity of Joints, Components and Structures - B Norén

16-17-3 Discussion of Sampling and Analysis Procedures - P W Post

17-17-1 Sampling of Wood for Joint Tests on the Basis of Density - I Smith, L R J Whale

17-17-2 Sampling Strategy for Physical and Mechanical Properties of Irish Grown Sitka Spruce - V Picardo

18-17-1 Sampling of Timber in Structural Sizes - P Glos

18-6-3 Notes on Sampling Factors for Characteristic Values - R H Leicester

19-17-1 Load Factors for Proof and Prototype Testing - R H Leicester

19-6-2 Confidence in Estimates of Characteristic Values - R H Leicester

21-6-1 Draft Australian Standard: Methods for Evaluation of Strength and Stiffness of Graded Timber - R H Leicester

21-6-2 The Determination of Characteristic Strength Values for Stress Grades of Structural Timber. Part 1 - A R Fewell and P Glos

22-17-1 Comment on the Strength Classes in Eurocode 5 by an Analysis of a Stochastic Model of Grading - A proposal for a supplement of the design concept - M Kiesel

24-17-1 Use of Small Samples for In-Service Strength Measurement - R H Leicester and F G Young

24-17-2 Equivalence of Characteristic Values - R H Leicester and F G Young

24-17-3 Effect of Sampling Size on Accuracy of Characteristic Values of Machine Grades - Y H Chui, R Turner and I Smith

24-17-4 Harmonisation of LSD Codes - R H Leicester

25-17-2 A Body for Confirming the Declaration of Characteristic Values - J Sunley

25-17-3 Moisture Content Adjustment Procedures for Engineering Standards - D W Green and J W Evans

27-17-1 Statistical Control of Timber Strength - R H Leicester and H O Breitinger

30-17-1 A New Statistical Method for the Establishment of Machine Settings - F Rouger

GLUED JOINTS

20-18-1 Wood Materials under Combined Mechanical and Hygral Loading - A Martensson and S Thelandersson

20-18-2 Analysis of Generalized Volkersen - Joints in Terms of Linear Fracture Mechanics - P J Gustafsson

20-18-3 The Complete Stress-Slip Curve of Wood-Adhesives in Pure Shear - H Wernersson and P J Gustafsson

22-18-1 Perspective Adhesives and Protective Coatings for Wood Structures - A S Freidin

FRACTURE MECHANICS

21-10-1 A Study of Strength of Notched Beams - P J Gustafsson

22-10-1 Design of Endnotched Beams - H J Larsen and P J Gustafsson

23-10-1 Tension Perpendicular to the Grain at Notches and Joints - T A C M van der Put

23-10-2 Dimensioning of Beams with Cracks, Notches and Holes. An Application of Fracture Mechanics - K Riipola

23-19-1 Determination of the Fracture Energie of Wood for Tension Perpendicular to the Grain - W Rug, M Badstube and W Schöne

23-19-2 The Fracture Energy of Wood in Tension Perpendicular to the Grain. Results from a Joint Testing Project - H J Larsen and P J Gustafsson

23-19-3 Application of Fracture Mechanics to Timber Structures - A Ranta-Maunus

24-19-1 The Fracture Energy of Wood in Tension Perpendicular to the Grain - H J Larsen and P J Gustafsson

28-19-1 Fracture of Wood in Tension Perpendicular to the Grain: Experiment and Numerical Simulation by Damage Mechanics - L Daudeville, M Yasumura and J D Lanvin

28-19-2 A New Method of Determining Fracture Energy in Forward Shear along the Grain - H D Mansfield-Williams

28-19-3 Fracture Design Analysis of Wooden Beams with Holes and Notches. Finite Element Analysis based on Energy Release Rate Approach - H Petersson

28-19-4 Design of Timber Beams with Holes by Means of Fracture Mechanics - S Aicher, J Schmidt and S Brunold

30-19-1 Failure Analysis of Single-Bolt Joints - L Daudeville, L Davenne and M Yasumura

SERVICEABILITY

27-20-1 Codification of Serviceability Criteria - R H Leicester

27-20-2 On the Experimental Determination of Factor k_{def} and Slip Modulus k_{ser} from Short- and Long-Term Tests on a Timber-Concrete Composite (TCC) Beam - S Capretti and A Ceccotti

27-20-3 Serviceability Limit States: A Proposal for Updating Eurocode 5 with Respect to Eurocode 1 - P Racher and F Rouger

27-20-4 Creep Behavior of Timber under External Conditions - C Le Govic, F Rouger, T Toratti and P Morlier

30-20-1 Design Principles for Timber in Compression Perpendicular to Grain - S Thelandersson and A Mårtensson

30-20-2 Serviceability Performance of Timber Floors - Eurocode 5 and Full Scale Testing - R J Bainbridge and C J Mettem

32-20-1 Floor Vibrations - B Mohr

TEST METHODS

31-21-1 Development of an Optimised Test Configuration to Determine Shear Strength of Glued Laminated Timber - G Schickhofer and B Obermayr

31-21-2 An Impact Strength Test Method for Structural Timber. The Theory and a Preliminary Study - T D G Canisius

CIB TIMBER CODE

2-100-1 A Framework for the Production of an International Code of Practice for the Structural Use of Timber - W T Curry

5-100-1 Design of Solid Timber Columns (First Draft) - H J Larsen

5-100-2 A Draft Outline of a Code for Timber Structures - L G Booth

6-100-1	Comments on Document 5-100-1; Design of Solid Timber Columns - H J Larsen and E Theilgaard
6-100-2	CIB Timber Code: CIB Timber Standards - H J Larsen and E Theilgaard
7-100-1	CIB Timber Code Chapter 5.3 Mechanical Fasteners; CIB Timber Standard 06 and 07 - H J Larsen
8-100-1	CIB Timber Code - List of Contents (Second Draft) - H J Larsen
9-100-1	The CIB Timber Code (Second Draft)
11-100-1	CIB Structural Timber Design Code (Third Draft)
11-100-2	Comments Received on the CIB Code a U Saarelainen b Y M Ivanov c R H Leicester d W Nozynski e W R A Meyer f P Beckmann; R Marsh g W R A Meyer h W R A Meyer
11-100-3	CIB Structural Timber Design Code; Chapter 3 - H J Larsen
12-100-1	Comment on the CIB Code - Sous-Commission Glulam
12-100-2	Comment on the CIB Code - R H Leicester
12-100-3	CIB Structural Timber Design Code (Fourth Draft)
13-100-1	Agreed Changes to CIB Structural Timber Design Code
13-100-2	CIB Structural Timber Design Code. Chapter 9: Performance in Fire
13-100-3a	Comments on CIB Structural Timber Design Code
13-100-3b	Comments on CIB Structural Timber Design Code - W R A Meyer
13-100-3c	Comments on CIB Structural Timber Design Code - British Standards Institution
13-100-4	CIB Structural Timber Design Code. Proposal for Section 6.1.5 Nail Plates - N I Bovim
14-103-2	Comments on the CIB Structural Timber Design Code - R H Leicester
15-103-1	Resolutions of TC 165-meeting in Athens 1981-10-12/13
21-100-1	CIB Structural Timber Design Code. Proposed Changes of Sections on Lateral Instability, Columns and Nails - H J Larsen
22-100-1	Proposal for Including an Updated Design Method for Bearing Stresses in CIB W18 - Structural Timber Design Code - B Madsen
22-100-2	Proposal for Including Size Effects in CIB W18A Timber Design Code - B Madsen
22-100-3	CIB Structural Timber Design Code - Proposed Changes of Section on Thin-Flanged Beams - J König
22-100-4	Modification Factor for "Aggressive Media" - a Proposal for a Supplement to the CIB Model Code - K Erler and W Rug
22-100-5	Timber Design Code in Czechoslovakia and Comparison with CIB Model Code - P Dutko and B Kozelouh

LOADING CODES

4-101-1	Loading Regulations - Nordic Committee for Building Regulations
4-101-2	Comments on the Loading Regulations - Nordic Committee for Building Regulations

STRUCTURAL DESIGN CODES

1-102-1	Survey of Status of Building Codes, Specifications etc., in USA - E G Stern
1-102-2	Australian Codes for Use of Timber in Structures - R H Leicester
1-102-3	Contemporary Concepts for Structural Timber Codes - R H Leicester
1-102-4	Revision of CP 112 - First Draft, July 1972 - British Standards Institution
4-102-1	Comparsion of Codes and Safety Requirements for Timber Structures in EEC Countries - Timber Research and Development Association
4-102-2	Nordic Proposals for Safety Code for Structures and Loading Code for Design of Structures - O A Brynildsen
4-102-3	Proposal for Safety Codes for Load-Carrying Structures - Nordic Committee for Building Regulations
4-102-4	Comments to Proposal for Safety Codes for Load-Carrying Structures - Nordic Committee for Building Regulations
4-102-5	Extract from Norwegian Standard NS 3470 "Timber Structures"
4-102-6	Draft for Revision of CP 112 "The Structural Use of Timber" - W T Curry
8-102-1	Polish Standard PN-73/B-03150: Timber Structures; Statistical Calculations and Designing
8-102-2	The Russian Timber Code: Summary of Contents
9-102-1	Svensk Byggnorm 1975 (2nd Edition); Chapter 27: Timber Construction
11-102-1	Eurocodes - H J Larsen
13-102-1	Program of Standardisation Work Involving Timber Structures and Wood-Based Products in Poland
17-102-1	Safety Principles - H J Larsen and H Riberholt
17-102-2	Partial Coefficients Limit States Design Codes for Structural Timberwork - I Smith
18-102-1	Antiseismic Rules for Timber Structures: an Italian Proposal - G Augusti and A Ceccotti
18-1-2	Eurocode 5, Timber Structures - H J Larsen
19-102-1	Eurocode 5 - Requirements to Timber - Drafting Panel Eurocode 5
19-102-2	Eurocode 5 and CIB Structural Timber Design Code - H J Larsen
19-102-3	Comments on the Format of Eurocode 5 - A R Fewell
19-102-4	New Developments of Limit States Design for the New GDR Timber Design Code - W Rug and M Badstube
19-7-3	Effectiveness of Multiple Fastener Joints According to National Codes and Eurocode 5 (Draft) - G Steck
19-7-6	The Derivation of Design Clauses for Nailed and Bolted Joints in Eurocode5 - L R J Whale and I Smith
19-14-1	Annex on Simplified Design of W-Trusses - H J Larsen

20-102-1	Development of a GDR Limit States Design Code for Timber Structures - W Rug and M Badstube
21-102-1	Research Activities Towards a New GDR Timber Design Code Based on Limit States Design - W Rug and M Badstube
22-102-1	New GDR Timber Design Code, State and Development - W Rug, M Badstube and W Kofent
22-102-2	Timber Strength Parameters for the New USSR Design Code and its Comparison with International Code - Y Y Slavik, N D Denesh and E B Ryumina
22-102-3	Norwegian Timber Design Code - Extract from a New Version - E Aasheim and K H Solli
23-7-1	Proposal for a Design Code for Nail Plates - E Aasheim and K H Solli
24-102-2	Timber Footbridges: A Comparison Between Static and Dynamic Design Criteria - A Ceccotti and N de Robertis
25-102-1	Latest Development of Eurocode 5 - H J Larsen
25-102-1A	Annex to Paper CIB-W18/25-102-1. Eurocode 5 - Design of Notched Beams - H J Larsen, H Riberholt and P J Gustafsson
25-102-2	Control of Deflections in Timber Structures with Reference to Eurocode 5 - A Martensson and S Thelandersson
28-102-1	Eurocode 5 - Design of Timber Structures - Part 2: Bridges - D Bajolet, E Gehri, J König, H Kreuzinger, H J Larsen, R Mäkipuro and C Mettem
28-102-2	Racking Strength of Wall Diaphragms - Discussion of the Eurocode 5 Approach - B Källsner
29-102-1	Model Code for the Probabilistic Design of Timber Structures - H J Larsen, T Isaksson and S Thelandersson
30-102-1	Concepts for Drafting International Codes and Standards for Timber Constructions - R H Leicester
33-102-1	International Standards for Bamboo – J J A Janssen

INTERNATIONAL STANDARDS ORGANISATION

3-103-1	Method for the Preparation of Standards Concerning the Safety of Structures (ISO/DIS 3250) - International Standards Organisation ISO/TC98
4-103-1	A Proposal for Undertaking the Preparation of an International Standard on Timber Structures - International Standards Organisation
5-103-1	Comments on the Report of the Consultion with Member Bodies Concerning ISO/TC/P129 - Timber Structures - Dansk Ingeniorforening
7-103-1	ISO Technical Committees and Membership of ISO/TC 165
8-103-1	Draft Resolutions of ISO/TC 165
12-103-1	ISO/TC 165 Ottawa, September 1979
13-103-1	Report from ISO/TC 165 - A Sorensen
14-103-1	Comments on ISO/TC 165 N52 "Timber Structures; Solid Timber in Structural Sizes; Determination of Some Physical and Mechanical Properties"
14-103-2	Comments on the CIB Structural Timber Design Code - R H Leicester
21-103-1	Concept of a Complete Set of Standards - R H Leicester

JOINT COMMITTEE ON STRUCTURAL SAFETY

3-104-1 International System on Unified Standard Codes of Practice for Structures - Comité Européen du Béton (CEB)

7-104-1 Volume 1: Common Unified Rules for Different Types of Construction and Material - CEB

CIB PROGRAMME, POLICY AND MEETINGS

1-105-1 A Note on International Organisations Active in the Field of Utilisation of Timber - P Sonnemans

5-105-1 The Work and Objectives of CIB-W18-Timber Structures - J G Sunley

10-105-1 The Work of CIB-W18 Timber Structures - J G Sunley

15-105-1 Terms of Reference for Timber - Framed Housing Sub-Group of CIB-W18

19-105-1 Tropical and Hardwood Timbers Structures - R H Leicester

21-105-1 First Conference of CIB-W18B, Tropical and Hardwood Timber Structures Singapore, 26 - 28 October 1987 - R H Leicester

INTERNATIONAL UNION OF FORESTRY RESEARCH ORGANISATIONS

7-106-1 Time and Moisture Effects - CIB W18/IUFRO 55.02-03 Working Party

INTERNATIONAL COUNCIL FOR RESEARCH AND INNOVATION
IN BUILDING AND CONSTRUCTION

WORKING COMMISSION W18 - TIMBER STRUCTURES

ASPECTS ON RELIABILITY CALIBRATION OF SAFETY FACTORS FOR TIMBER STRUCTURES

by

S Svensson

S Thelandersson

Department of Structural Engineering

Lund University

SWEDEN

MEETING THIRTY-THREE
DELFT
THE NETHERLANDS
AUGUST 2000

Presented by: S. Thelandersson

· H. Blass questioned whether high quality information on the tails of distributions would be available.

· S. Thelandersson responded that it is very difficult therefore the method must be used with care.

· H. Blass asked could we expect engineers to correctly apply the method given the fact that younger people are without the background knowledge?

· S. Thelandersson answered that the equations in the code are in a form that can be used by practicing engineers although practicing Engineers are not using this method yet.

· J. Ehlbeck questioned which is better Normal or Gumbel distribution.

· S. Thelandersson answered that Gumbel distribution is better because it is of the extreme type. In general, there is too much calibration without consideration of consequences. E.g. High partial coefficient for permanent loads in Eurocode

· J. Ehlbeck questioned whether the dependency of γ_n on safety class (low, normal, high) should be part of the Eurocode also.

· S. Thelandersson answered that this is a consistent description for all materials and is general for design basis. It is in use in Nordic countries.

· H.J. Larsen stated that discussion about one philosophy is important. More important structures should have better quality and quality control and therefore do not need higher β or γ_n.

In national codes and Eurocode, the γ values should be decided by people with knowledge of material behaviour and failures. An example is the damage of the recent storm in Denmark (100 year return wind storm) in which some one or two storey timber houses suffered damage. In one site of 100 houses there were 3 failures while not one of the failed houses was designed correctly. This recent experience on reality should be considered.

· M. Ansell asked for more information on Gumbel distribution.

· S. Svensson answered that the Gumbel distribution fitted the upper tail very well.

· H.J. Larsen stated that one should agree on a distribution and calibrate against it rather than focusing on a particular β level.

· S. Svensson agreed that β values are not universal parameters.

· F. Rouger stated that the influence of resistance distribution type could be reduced by fitting to lower tails of resistance distribution as demonstrated by R.Foschi.

· E. Karacabeyli asked about the resistance side of the failure function.

· S. Thelandersson responded that constant lognormal distribution was used.

Aspects on reliability calibration of safety factors for timber structures

Staffan Svensson and Sven Thelandersson
Structural Engineering, Lund University, Sweden

1 Introduction

From time to time national structural codes are revised. The safety coefficients for actions as well as strengths for different materials are then often calibrated in reliability studies and different structural materials are benchmarked against each other.

In structural reliability analysis an important aspect is how to describe the random variables governing the problem. It is often forgotten that the target safety index β_{target} and the required probability of failure were once determined under certain circumstances. In the Scandinavian countries target safety indices were determined more than 25 years ago by calibration against existing simple structures with proven performance. For the sake of simplicity, it was then assumed that loads were normal distributed and that parameters related to the load carrying capacity were log-normal distributed. However, for time variable actions such as snow and wind, Gumbel or Gamma distributions give better fitting to data. In recent studies it is, therefore, not surprising that evaluation of structural reliability is made using Gumbel distributed variable load, together with the safety index, β_{target}, given in building codes. The problem is, however, that the values of β_{target} are based on calibration to earlier proved practice under other assumptions, as mentioned above. A reliability based design will then give larger dimensions or higher required strength for load bearing elements compared to earlier practice. If the evaluations are used for code calibration it will lead to proposals to increase the partial coefficients, γ, to ensure structural reliability. The change of variable load description, from a normal to a Gumbel distribution, with fixed β_{target} affects structures with low portion of permanent load (dead weight) such as timber structures more severely than heavy structures. The reason for this is misinterpretation of safety indices, and failure probability, as absolute values of reliability.

The effects of using Gumbel distributions instead of normal distribution for variable load in code calibration of material partial coefficients for timber will be demonstrated. The calibration of target safety index is repeated as it was done when probabilistic theory was introduced in the building codes, but with new assumptions of load description, and it is shown that the target safety index is not an absolute value but should depend on the assumptions used in the calibration. The direct consequences of this approach for code calibrations related to design of timber structures are illustrated.

2 Partial safety factor code format

The national building codes, here focusing on the Swedish code, state rules of structural design in a deterministic format. Most commonly, the design equations require that a design value of the load, S_d, never exceeds the design value of a structural member's load carrying capacity, R_d. If a partial safety factor code format is used, the design values (in its simplest form) consist of characteristic values and partial coefficients, γ. The deterministic expression found in the Swedish code is given in equation (1) for the case with one permanent load, G, and one time-variable load, Q.

$$R_d = \frac{R_k}{\gamma_R} \geq (G_k \cdot \gamma_G + Q_k \cdot \gamma_Q) = S_d \qquad (1)$$

where index k denotes characteristic value.

For the case with more than one variable load action equation (1) will be a sum of all loads in combination with so called load reduction factors, not considered for the simple case herein.

The load carrying capacity is a function of material strength, f, and geometric quantities, a. For the case with pure bending of beams, considered here, the geometric quantities are the member's section modulus and length, whereas the material strength is the bending strength f_m.

It may be convenient to use partial coefficients connected to assessable safety aspects such as severity of failure, variability of material strength, quality control, uncertainty of design model, etc. Two partial coefficients related to bearing capacity of timber structures are used in the Swedish code. To consider the consequence of failure, the members of a building structure are assigned to safety classes. For members in high safety class, implying severe failure consequences, a larger partial coefficient is used compared to the normal or low safety classes. The other partial coefficient used is connected to the uncertainties of material strength. Equation (2) gives the design load carrying capacity for a simple case, such as pure bending.

$$R_d = \frac{R_k}{\gamma_R} = a_k \frac{f_k}{\gamma_1 \gamma_2} \qquad (2)$$

For cases where load carrying capacity depends on member volume, ambient climate, load duration, etc. modification factors are introduced in the design equation. However, in the present study it has been considered important to work with the design equation on its simplest form, disregarding such modification parameters. This simplification will not affect the conclusions from the present work.

The partial safety code format is visually not different from any other code format when it comes to the design equation. Codes using the partial safety format are, however, connected to a reliability method, usually a first order reliability method (FORM). The partial coefficients are usually calibrated against the solution of a probabilistic evaluation taking into account known or assumed statistical variations of loads and load carrying capacity. Another important element of the safety system is that the characteristic values are assigned to specific percentiles of the corresponding random parameters. Table 1 lists the random parameters, their corresponding partial coefficient and the definitions of characteristic values as percentiles according to the Swedish codes. The coefficient of variations for the variables used in the analyses performed in this study are also presented in Table 1.

Table 1. Coefficient of variation, characteristic values and partial coefficients for parameters used in this study.

Parameter	Coef. of Var. %	Char. Value, %-tile	Part. Coef, γ
Bending strength, f	20	5	1.25
Section modulus, a	2	50	-
Permanent load, G	5	50	1.00
Snow load, Q	40	98	1.30
Model uncertainty	10	-	-

3 Probabilistic format

The reliability format, used to calibrate the code format, is based on the following definition.

$$P(R-S \leq 0) = p_f \tag{3}$$

This equation states that the probability, P(), of the load exceeding the capacity is equal to the probability of failure, p_f. It is not considered important here to advance deep into the probabilistic theories, but rather briefly describe the way the problem was solved in this study. For more information concerning probabilistic methods, standard textbooks within the field are recommended, e.g. Thoft-Christiansen and Baker (1982) and Ditlevsen and Madsen (1996).

It is convenient to replace the probability of failure with safety index, β, defined as

$$p_f = \Phi(-\beta) \leftrightarrow \beta = -\Phi^{-1}(p_f). \tag{4}$$

This is often the case in building codes where failure probabilities are seldom presented directly and instead presented in terms safety indices. The target β -values given in the Swedish code for the ultimate limit state are given in table 2.

Table 2. β- values for different safety classes according to Swedish code, BKR 99

Safety class	β-Value	Part. Coef, γ_n
Low	3.7	1.0
Normal	4.3	1.1
High	4.8	1.2

The starting point in reliability analysis is a failure condition on the form

$$g(x_1, x_2, .. x_n) = 0 \tag{5}$$

where $\mathbf{X}=(x_1, x_2, ...x_n)$ are the set of random variables governing the problem. The variables x_i are here assumed to be independent.

The first order reliability method (FORM) is based on the transformation of random variables, **X**, into normal distributed, standardised random variables, **Z**, see Hasofer and Lind (1973 and 1974). For a random variable x_i, with cumulative distribution function F_{X_i} the transformation from the design point, x_i^*, to the corresponding design point, z_i^*, for the standardised random variable z_i is given by

$$F_{X_i}(x_i^*) = \Phi(z_i^*) \tag{6}$$

where Φ is the standardised normal distribution function. The failure condition (5) can be interpreted as a surface in the n-dimensional space defined by the variables **X** or **Z,** separating non-failure regions from failure regions. The design point is the point on this surface which determines the failure probability, p_f.

In the standardised normal co-ordinate system the co-ordinates z_i^* of the design point may also be expressed as $\beta\alpha_i$, where β is the safety index. It follows from equation (6) that

$$x_i^* = F_X^{-1}(\Phi(\beta\alpha_i)). \tag{7}$$

The safety index, β, is the shortest distance to the failure function from the origin and $\alpha = (\alpha_1, \alpha_2 \ldots \alpha_n)$ is a unit vector in the standardised normal co-ordinate system. α_i is given by

$$\alpha_i = \frac{-\frac{\partial g}{\partial x_i}\frac{\partial x_i}{\partial z_i}}{\sqrt{\sum_{k=1}^{n}\left(\frac{\partial g}{\partial x_k}\frac{\partial x_k}{\partial z_k}\right)^2}}; \; i = 1..n. \tag{8}$$

The failure function g in equation (5) corresponds through the transformation (6) to a failure function, f, in the standardised normal co-ordinate system. For the common distributions used later in this study, the transformation (7) results in the following expressions based on mean value, μ, and coefficient of variation, V for a random variable x.

$$x^* = \mu(1+\beta\alpha V) \qquad \text{Normal distribution} \tag{9}$$

$$x^* = \mu e^{\beta\alpha V} \;;\; V < 0.25 \qquad \text{Log-normal distribution} \tag{10}$$

$$x^* = \mu\left(1 - \frac{\sqrt{6}}{\pi} V\left[0.5772 + \ln(-\ln\Phi(\beta\alpha))\right]\right) \qquad \text{Gumbel distribution} \tag{11}$$

3.1 Load bearing capacity

Material strength, f, is here considered log-normal distributed. Other distributions may fit as well as the log-normal for example the Weibull distribution. The load carrying capacity, R, is here determined as R=afC, where a is a geometric factor and C is a random variable describing model uncertainty. All these random variables are assumed log-normal distributed. The following relation is valid for the design point

$$R^* = \mu_R \, e^{\beta\alpha_R V_R} \tag{12}$$

where the mean value is

$$\mu_R = \mu_a \, \mu_f \, \mu_C. \tag{13}$$

The coefficient of variation can be expressed as

$$V_R = \sqrt{V_a^2 + V_f^2 + V_C^2}. \tag{14}$$

The values used for the different random parameters related to load carrying capacity are presented in table 1.

3.2 Load

The random parameter load is often a sum of loads of different nature, e.g. dead weight, snow load, imposed load, etc. When probabilistic methods were introduced as a tool for code calibration all loads were assumed normal distributed. This enables probabilistic evaluations by hand. It should also be pointed out that even though distributions of the extreme type (e.g. the Gumbel distribution) are preferable when describing natural loads such as wind and snow loads, a truncated or censored normal distribution might be just as adequate describing a certain range of the loads, e.g. the upper tail. For the case with one permanent load G and one variable load Q, both normal distributed, the total load at the design point may be expressed as;

$$S^* = \mu_S (1 + \beta\alpha_S V_S) \tag{15}$$

where the mean of the total load is,

$$\mu_S = \mu_G + \mu_Q = ((1-\nu) + \nu)\, \mu_S \tag{16}$$

The load ratio, ν, is defined as,

$$\nu = \frac{\mu_Q}{\mu_S} = \frac{\mu_Q}{\mu_Q + \mu_G}. \tag{17}$$

The coefficient of variation for total load, V_s, can be expressed as,

$$V_S = \sqrt{V_G^2 (1-\nu)^2 + V_Q^2 \nu^2}\ . \tag{18}$$

If the loads are described with other distributions the total load has to be evaluated with each load as a random parameter. By using (9) and (11) the total load at the design point for normal distributed permanent load and Gumbel distributed variable load is,

$$S^* = \mu_G (1 + \beta\alpha_G V_G) + \mu_Q \left(1 - \frac{\sqrt{6}}{\pi} V_Q \left[0.5772 + \ln(-\ln \Phi(\beta\alpha_Q))\right]\right). \tag{19}$$

3.3 Effect of load description in probabilistic design

As previously discussed it is recommended to use for example Gumbel distribution when describing some time variable loads. It is then of interest to show the consequences when changing from one load description (15), originally used in code calibration, to another (19) for a given target safety index, β_{target}.

A probabilistic design is made for a beam with rectangular cross-section subjected to pure bending. The load carrying capacity of the beam is described by Equations (12-14) using the parameters in table 1. The probabilistic design was made with two alternative descriptions of the variable load Q, normal distribution (15) and Gumbel distribution (19). Changing the load description from normal to Gumbel distribution results in larger required dimension of the beam to achieve the same target safety index. Figure 1 shows the relative increase in beam height for load combinations ranging from 20% variable load to only variable load. For each load combination all parameters are held constant except cross-section height. The calculations are accomplished for normal safety class and high safety class with target β-values of 4.3 and 4.8 respectively. It is seen that the effect on dimensions is quite significant when the variable load is dominating, as is the usual case for timber structures.

Since the partial coefficients are calibrated to give the code format (1) the same safety level as that obtained from a probabilistic analysis a change of load description also leads to a change of partial coefficients. Furthermore, the target safety index nowadays prescribed in many codes has been evaluated through a calibration against older practice. As will be shown in the next section the assumptions behind the evaluation of the target safety index is very important for the result and for the future use of probabilistic based analyses.

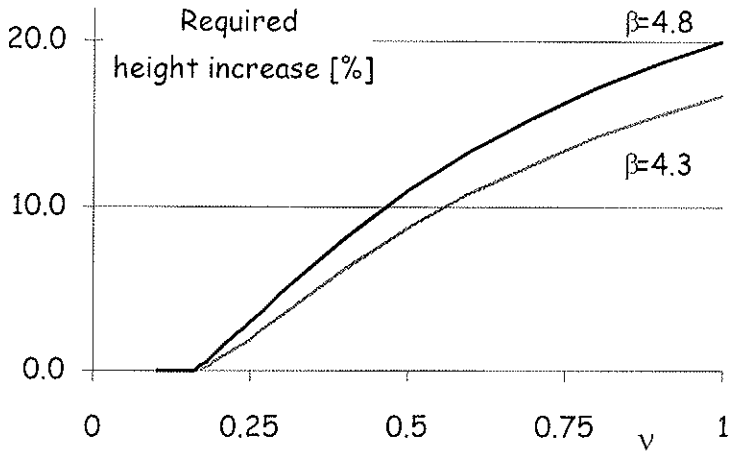

Figure 1. Required height increase due to change of variable load description. Comparison of Normal distributed variable load and Gumbel distributed variable load for target safety indices $\beta = 4.3$ and 4.8.

4 Derivation of safety levels for structural members based on former practice

When the Swedish code was revised to a partial safety factor code format, the existing code, at that time, was used to determine the reliability of buildings (Östlund 2000). Statistical data were collected for random quantities entering the design equations. Representative structural members were selected for calculation of the reliability levels in terms of safety index β, valid for earlier practice. A flow chart of this procedure is shown in figure 2.

The Swedish code format existing before 1979 was based on safety factors. The design criteria can formally be written as

$$R_c - G_c - Q_c = 0 \tag{20}$$

where R, G, and Q represents load bearing capacity, permanent load and variable load respectively. Index c stands for prescribed code value.

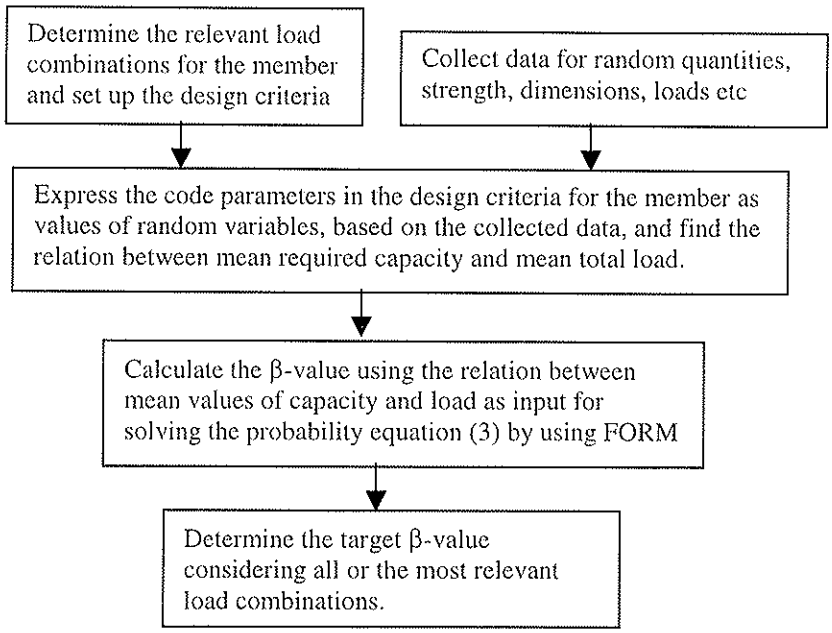

Figure 2. Flow chart for deriving safety levels from existing codes for a specific structural member.

4.1 Load bearing capacity

For pure bending the capacity R_c was expressed as,

$$R_c = a_c \sigma = a_c \frac{f_c}{s} \tag{21}$$

where a is a geometry factor, σ is the allowable stress which is derived from the nominal material strength, f_c, (here bending strength of sawn timber) and a safety factor, s. For structural members of sawn timber the safety factor was 1.8 according to the former code, SBN 1980, under the conditions of exceptional variable load. The load case of exceptional or dominating variable load is normally decisive for the design of timber structures in the ultimate limit state.

The allowable stress, σ, for sawn timber graded according to grading class T30 in bending was prescribed to 15.4 MPa for exceptional load. This corresponds to a nominal code value for bending strength, f_c, of 27.7 MPa. This deterministic code value may be evaluated as a fractile value of the random parameter bending strength, f. Assuming that the bending stress is log-normal distributed with mean μ_f, and coefficient of variation, V_f, the following relation is valid,

$$f_c = \mu_f e^{\Phi^{-1}(p_c)V_f} \tag{22}$$

where p_c is the fractile corresponding to f_c. The value of p_c can be evaluated from bending strength data. Such data were produced by Foslie and Moen (1968) in an extensive test series of structural timber. Some of the data from this study is summarised in table 3. Bending strength of Scandinavian timber has been investigated in many other studies, but the one presented by Foslie and Moen (1968) was chosen here.

Table 3. Values for bending strength (Foslie and Moen 1968). COV = coefficient of variation.

Grade	Dimension	Number of tests	Mean, μ_f	COV: V_f	$p_c = P(f \leq f_c)$
T30	3"x 8"	215	43 MPa	19 %	1.0 %
T30	2"x 4"	202	55 MPa	20 %	0.03 %
No grade	3"x 8"	593	43 MPa	23 %	2.0 %
No grade	2"x 4"	758	53 MPa	23 %	0.2 %

It is seen from table 3 that the value of fractile p_c corresponding to the nominal code value varies between different test series and different dimensions. For the purpose of this study the highest value value p_c = 2 % is chosen on the safe side. The geometry factor a_c used in codified design is assumed to be equal the mean value μ_a of a random variable a, also log-normal distributed. Using equations (21) and (22) the relation between the allowable capacity R_c and the stochastic parameters μ_f, V_f and μ_a is given as,

$$R_c = \mu_a \frac{\mu_f e^{\Phi^{-1}(0.02)V_f}}{s} = \frac{\mu_a \mu_f}{s \cdot e^{2.05 V_f}}. \qquad (23)$$

4.2 Loads

In the same way as shown for capacity the load values prescribed in the code may be written as fractiles of random variables. Data from investigations of loads have to be used in the same fashion as shown for bending strength.

Permanent loads, G, are usually considered normal distributed and the code values represent their mean value, see e.g. CIB (1989).

The variable load Q considered in this study, is snow load. Originally, variable loads were considered normal distributed when the partial safety code format was introduced in Sweden (Östlund 2000). The snow load values prescribed in the old code was compared to extensive data (Nord and Taesler 1973). It was then concluded that they correspond to the 98th percentile in the normal distribution. The code values for a load combination, S_c, of permanent load and snow load is then written as follows,

$$S_c = G_c + Q_c = \mu_G + \mu_Q(1 + \Phi^{-1}(0.98)\, V_Q) = \mu_S\, ((1-\nu) + \nu(1 + 2.05\, V_Q)) \qquad (24)$$

Where ν is the ratio between variable and total load defined in (17).

If the snow load is described with a Gumbel distribution instead of a normal distribution, then the code values will correspond to the 96th percentile when compared to the same data as above. Under these new circumstances the load according to code may be expressed as:

$$S_c = G_c + Q_c = \mu_G + \mu_Q\left(1 - \frac{\sqrt{6}}{\pi} V_Q\left[0.5772 + \ln(-\ln(0.96))\right]\right) =$$
$$= \mu_S\, ((1-\nu) + \nu(1 + 2.05\, V_Q)) \qquad (25)$$

Thus, the relation between the deterministic value prescribed in the code and the mean and coefficient of variation of the corresponding random variable does not depend on the distribution used to describe the random variable.

4.3 Evaluation of safety level.

By inserting equations (23) and (24) alternatively (25) into the design criterion (20), with known values of the coefficients of variation of the random variables the relation between mean capacity and mean values of Q and G can be calculated. Based on this relation, a probabilistic analysis can be performed giving the safety index corresponding to the design format expressed in the code. This operation was performed for different values of the load ratio v, and for alternative assumptions regarding the distribution assumed for the variable load Q. The results from these analyses are shown in figure 3.

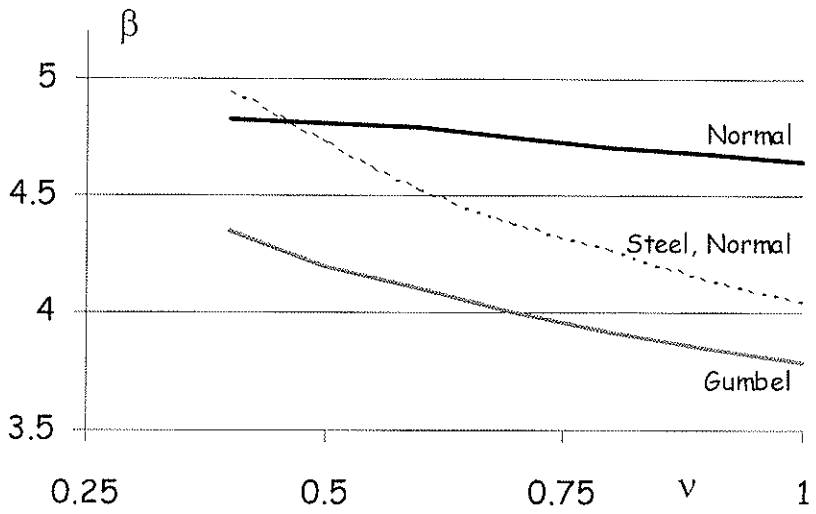

Figure 3. Safety level, β, for different statistical description of variable load.

The results in figure 3 show that the safety indices evaluated from the old code depend significantly on the statistical distribution assumed for the variable load. A structural member of sawn timber in pure bending, designed according to the former Swedish code SBN 1980, have a safety level of 4.65 – 4.8 in the range $0.5<v<1$, under the condition that both the permanent and the variable load are assumed normal distributed. Changing only this condition by assuming that the variable load is Gumbel distributed gives the same structural member a much lower safety level, $\beta = 3.8 - 4.2$. This shows that the target safety indices, e.g. in the present Swedish code table 2, are not universal values but rather variables dependent on the conditions under which they were once derived. In code calibration where partial safety coefficients are determined so that a certain prescribed target index is achieved, it is very important to use the same statistical assumptions for the random parameters as those used when the target safety index was determined. When determining the target safety levels included in the current Swedish code the random parameters related to capacity were assumed log-normal distributed and the random variables related to loads were assumed normal distributed. If the description of variable load is assumed Gumbel distributed instead of normal, partial coefficients should be calibrated against target safety levels derived from the lower curve in figure 3.

It should be pointed out that when the safety levels of the present Swedish code was determined this was done using structural members of steel as reference. The variability of structural steel is much lower than that for wood, which results in quite a different shape of the curve representing safety level vs. load ratio. The dotted line in figure 3 represents the safety level for a steel structure design under assumption of elastic stress distribution and in accordance with the former Swedish code. The loads acting on this structural member were considered normal distributed based on the parameters shown in table 1.

The same evaluation of safety levels as conducted for the former code may of course be carried out for the present code. Figure 4 shows the results of such an evaluation. The continuous curves represent the safety levels for the present code with the design equation (1) and characteristic values, partial coefficients according to tables 1 and 2. The variability of the random parameters used in the FORM calculation were those presented in table 1. The safety levels of the present code are compared with the former code, shown as a dotted curve in figure 4. It is seen that the current code gives a higher level of safety for structural members of sawn timber with dominating variable load ($\nu > 0.7$).

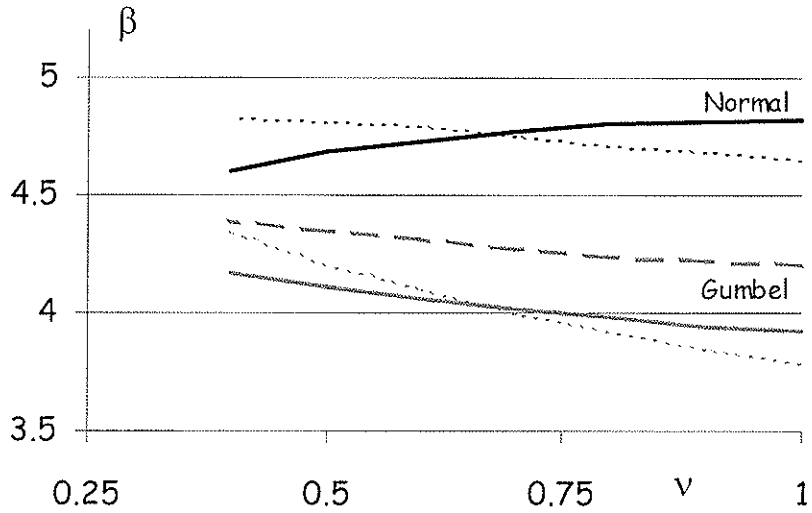

Figure 4. Safety levels evaluated for the present Swedish code (continuous curves) and old code (dotted curves). The two upper curves were derived for normal distributed variable load. The lower three curves were derived for gumbel distributed variable load. The dashed curve is based on the misinterpretation that the characteristic value for variable load given in the code is the 98 % also when the load is gumbel distributed.

The dashed line in figure 4 indicate the safety levels of a member of sawn timber when the characteristic value for variable load given by the code as 98 %-tile is believed to originate from the Gumbel distribution. This is a consequence of considering the fractile connected to the characteristic values, given in the code, independent of the description of the random parameters from which they originate. The characteristic values are of course very dependent on their origin and if this is not considered it will influence the safety levels and therefore also the partial coefficients in a code calibration. If the characteristic value given in the Swedish code is believed to come from a Gumbel distribution instead of the normal distribution this will still result in increasing cost in the same way as for a misinterpretation of the safety levels, however, the cost increase will be smaller.

5 Conclusions

The main aim of this study is to demonstrate the consequences of changing the statistical description of random parameters in reliability based code format without considering how the rules in the code once were derived. These consequences were not discovered in this study, they were already pointed out when the concept of invariant safety index was first introduced (Hasofer and Lind 1973). Results presented herein, however, are thought to give clear picture of the consequences for timber structures. The study discusses the common issue of changing the statistical description for natural (snow) loads from Normal to Gumbel distribution. Similar consequences will result if the statistical description of any other random parameter is changed. The message of this study can be concluded as:

- Target safety levels, β, presented in codes are not universal values. They will vary depending on the circumstances they were derived.
- Changing the statistical description of a random parameter without considering the origin of the safety levels given in codes will lead to wrong conclusions.
- Light weight structures, such as timber structures, are more affected by a incorrect change of variable load description from normal to Gumbel distribution, i.e. when the change of description is done without considering the origin of the safety levels.
- The definition of characteristic value must be consistent with the statistical description used in the reliability analysis.

6 References

BKR99, Boverkets konstruktionsregler (1999), ISBN 91-7147-455-2.

CIB (1989); Action on Structures Self-Weight Loads, CIB Commission W81, CIB Publication No. 115.

Ditlevsen, O., and H. O. Madsen (1996); Structural Reliability Methods, Wilsey & Sons.

Foslie, M., and K. Moen (1968); Strength Properties of Norwegian Spruce, Meddelelse nr. 33, The Norwegian Inst. of Wood Working and Wood Techn.

Hasofer, A. M., and N. C. Lind (1973); An exact and invariant first-order reliability format, Paper No. 119, Solid Mechanics Division, University of Waterloo, Ontario, Canada.

Hasofer, A. M., and N. C. Lind (1974); Exact and invariant second-moment code format, ASCE Journal of the Engineering Mechanics Division, vol. 100 pp111-121.

Nord, M., and R. Taesler (1973); Snötäckets densitet och massa i Sverige, National Swedish Building Research, Rapport R21

SBN 1980 Svensk Bygg Norm (1980) Statens planverks författningssamling 1980:1. ISBN 91-38-05209-1.

Toft-Christiansen, P., and M. J. Baker (1982); Structural Reliability Theory and Its Applications, Springer-Verlag.

Östlund, L., (2000), Personal communications.

INTERNATIONAL COUNCIL FOR RESEARCH AND INNOVATION
IN BUILDING AND CONSTRUCTION

WORKING COMMISSION W18 - TIMBER STRUCTURES

SENSITIVITY STUDIES ON THE RELIABILITY OF TIMBER STRUCTURES

by

A Ranta-Maunus
M Fonselius
J Kurkela
T Toratti
VTT Building Technology

FINLAND

MEETING THIRTY-THREE
DELFT
THE NETHERLANDS
AUGUST 2000

Presented by: A. Ranta-Maunus

· H. Blass asked whether the results would be reported to the Eurocode project team.
· A. Ranta-Maunus responded yes.
· S. Thelandersson asked for clarification on the conclusion that safety was independent of COV for the Gumbel distribution.
· A. Ranta-Maunus clarified that the characteristic values were fixed while distribution mean and COV were varied.
· F. Lam commented that system effect should be considered when γ values were sought for a given target β level.
· A. Ranta-Maunus stated that the plan was to start with the simple cases and look into the sensitivity issue and what are the important issues. He will look into the details in the future.
· J.W. van der Kuilen asked whether time effects were considered.
· A. Ranta-Maunus stated that it would be interesting to look into this issue. He felt that a simple approach would be to adjust the resistance distribution on the basis of DOL information.
· S. Thelandersson stated this type of work has been initiated. A paper on DOL effect was presented at 32nd CIB W18. The choice of damage model was critical.

Sensitivity studies on the reliability of timber structures

Alpo Ranta-Maunus, Mikael Fonselius, Juha Kurkela, Tomi Toratti
VTT Building Technology, Finland

1 Introduction

Reliability analysis has been used to assess structural safety for about half a century. In the early works the distributions of variables were limited to only Normal distributions to enable closed form solutions. Development of the methods was active in 1970´s when modern computers enabled wider range of methods to be used and textbooks were written on the subject (Leporati 1979). The role of reliability analysis was discussed also in the CIB-W18 meetings (Skov et al 1976). A comprehensive study on the reliability based design of wood structures was published by Foschi (1989).

Numerical methods enable today fairly easy computation of structural safety parameters for comparison or calibration of safety coefficients of different materials and loads. These kind of studies have been recently made related to Eurocode preparations (SAKO group 1998, Larsen et al 1999, Thelandersson et al 1999).

The failure probability P_f, or safety index β, is sensitive to the load and strength distributions selected. Eurocode (Draft prEN 1990, Basis of design, Annex C) gives advise on how to make the structural safety assessment. For instance, extreme distributions have been named for imposed and natural loads and Lognormal or Weibull distributions for material strength. Indicative values are given also for target safety level as shown in Table 1.

Table 1. Target reliability index β *for normal structural members (prEN 1990).*

Limit state	Target reliability index	
	1 year	50 year
Ultimate	4.7	3.8
Fatigue		1.5 to 3.8 [2)]
Serviceability (irreversible)	2.9	1.5
[2)] Depends on degree of inspectability, reparability and damage tolerance.		

The objective of this paper is to analyse, how sensitive the calculated safety parameters are to the selection of the types of distributions and to the values of coefficient of variation

(COV). Concerning standard distributions, similar studies have been made earlier. Now a numerical procedure is used which allows us to analyse the effect of any numerically given distribution. A more complete report of the research is under work (Ranta-Maunus et al 2000).

2 Method of analysis

Probability of failure is calculated by the use of numerical integration of discrete probability distributions

$$P_f = \int_0^\infty f_S(x) F_R(x) dx \tag{1}$$

where f_S is the probability density function of load effect, and F_R is the cumulative probability function of resistance. The method of using discrete probability distributions was developed some 20 years ago (Ahmed et al 1982) for risk assessments, and has been applied i.e. in safety assessments of nuclear power plants (Ranta-Maunus et al 1985). In this paper, the method is used only in a limited scope as an option for numerical integration.

The calculation was made by programming an Excel macro, for which f_S and F_R are given numerically in columns. Then both distributions are adjusted by a multiplicator:

- k_{mod} for strength, depending on the load duration, and
- another multiplicator is used for load effect. The latter is used to adjust the ratio of resistance and action effect to reach a decided safety factor or probability of failure.

The output of the calculation includes characteristic strength, stress caused by characteristic load, total safety factor γ and P_f. Total safety factor is calculated as

$$\gamma = \frac{k_{\mathrm{mod}} f_{0.05}}{\sigma_k} \tag{2}$$

where $f_{0.05}$ is the 5-percentile of the given strength distribution and σ_k is the stress caused by characteristic load, the percentile being different for different loads and studies. k_{mod} is the factor depending on load duration, adjusting the short term standard test results to correspond the real strength of material under the load of concern.

Failure probabilities can be transferred to safety indices β by the use of relation

$$P_f = \Phi(-\beta) \tag{3}$$

where Φ is the cumulative distribution function of the standardised Normal distribution. The relation between Φ and β is given in Table 2.

Table 2. Relation between β *and* P_f

P_f	10^{-1}	10^{-2}	10^{-3}	10^{-4}	10^{-5}	10^{-6}	10^{-7}
β	1,28	2,32	3,09	3,72	4,27	4,75	5,20

Until now our calculation has been made only in case of the action of a single load.

Different forms of cumulative standard strength distributions are illustrated in Figure 1 on a relative scale when 5-percentile values are denoted by 1. Small values, below 5-percentile, are shown separately on logarithmic scale. The lower tail shapes are quite different: the Lognormal distribution is decreasing faster than the Normal distribution, most unfavourable of these three distributions being the 2-parameter Weibull. 3-parameter Weibull is not included in this comparison, because any form of tail can be described by it, depending on the threshold value parameter. Similarly, density functions of Gumbel and Normal distributed load effects are shown in Figure 2 when the characteristic value is 20 in all cases. An obvious difference between Normal and Gumbel distributions is observed: high loads above the characteristic value have a clearly higher probability of occurrence in case of a Gumbel distribution than in case of a Normal distribution.

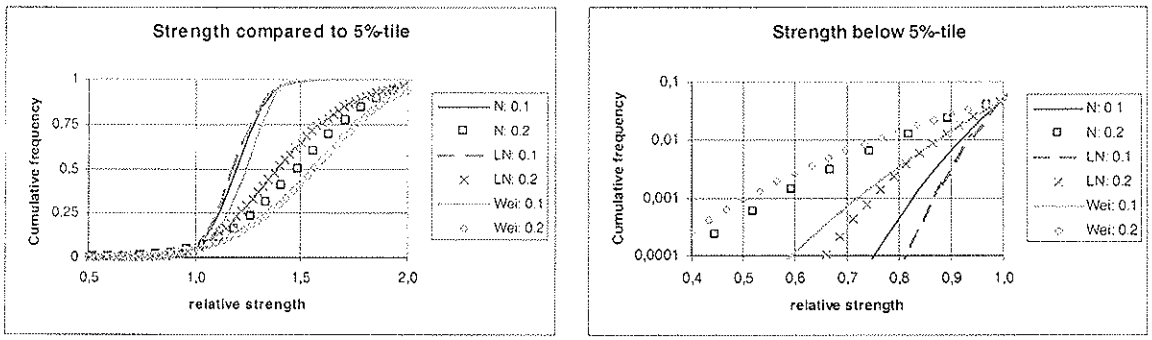

Figure 1. Comparison of Normal (N), Lognormal (LN) and 2-parametric Weibull (Wei) distributions when coefficient of variation is 10 or 20%, the number following N, LN or Wei is the coefficient of variation.

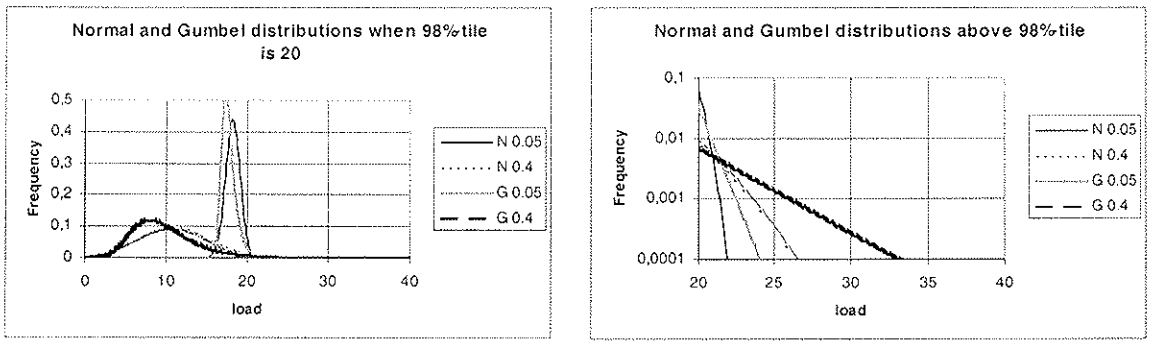

Figure 2. Comparison of loads following Normal and Gumbel distributions when the 98 percentile value is 20. N means Normal and G Gumbel distribution, number following N or G is the coefficient of variation.

3 Sensitivity studies

This study uses the following basic variables if not otherwise stated:

- Gumbel distribution with COV = 0.4 for a variable load. As an alternative Normal distribution with COV = 0.4 is also used.
- Lognormal distribution with COV = 0.1 or 0.2 for resistance. As a reference Normal distribution is also used.

Characteristic values of loads are 98%-tiles and those of strength 5%-tiles. Safety levels expressed in terms of P_f or β (per year) are calculated for different total safety factors (ratio of the characteristic resistance and the characteristic action effect). No other factors than material strength and load are included in this calculation.

3.1 Effect of load distribution type

The calculated results are illustrated in Figure 3. For Gumbel load distribution with COV = 0.4 the calculated safety is insensitive to material strength variation, when the strength distribution is Lognormal: practically same results are obtained for COV = 0.1 and 0.2, namely $\gamma = 2$ corresponds to $P_f = 10^{-5}$ and $\gamma = 2.3$ corresponds to $P_f = 10^{-6}$. Same result is obtained when strength distribution is Normal with COV = 0.1, whereas Normal distribution with COV = 0.2 results in much lower safety level: $\gamma = 3$ needed for $P_f = 10^{-5}$.

When the load follows a Normal distribution with the same COV = 0.4, safety levels obtained in the calculation are much higher. The qualitative difference is that now the safety level is more sensitive to COV of material strength. In all cases the use of Normal strength distribution with COV = 0.2 leads to unacceptable safety levels.

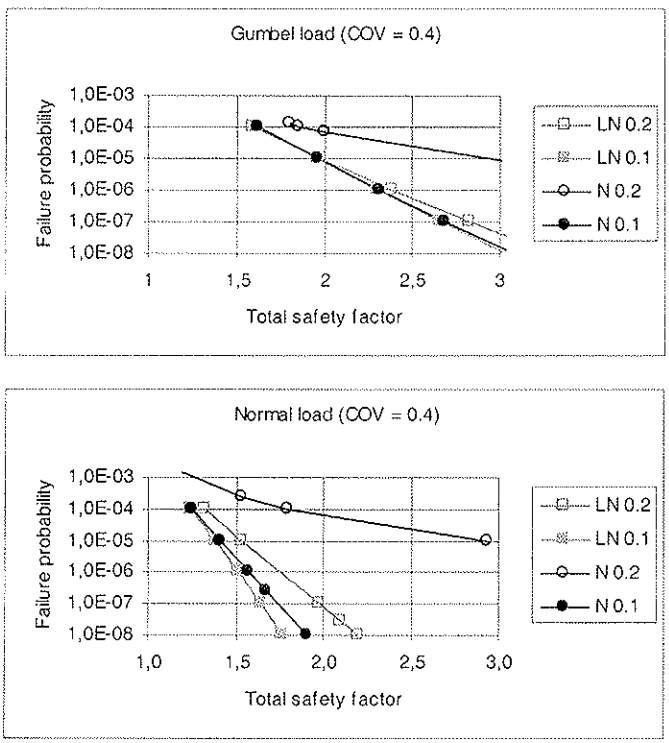

Figure 3. Calculated correspondence of P_f and γ. COV of strength is given after symbol of distribution.

3.2 Effect of strength distribution approximations

As a case study, different distribution functions fitted to the same material data are used in reliability calculation. The material is spruce, machine sorted to C30, and parameters of fitted Normal and Lognormal distributions are given in Table 3. Separate fittings are made to all data and to the lower tail, below 5 percentile. These distribution functions with the test data are illustrated in Figure 4 in the lower tail area. It is obvious that both functions fitted to the tail area seem to fit well to the observations, whereas Normal distribution fitted to all data is conservative and Lognormal distribution fitted to all data is unconservative in the tail area of this data.

Table 3. The modelled distribution functions for spruce with a depth of 150 mm machine sorted to C30. Number of sorted specimens 500.

Distribution function	Data	Parameters in the distribution function	
		μ	σ
Normal	All	47.48	10.27
Normal	Tail	41.8	6.9
Lognormal	All	3.836	0.226
Lognormal	Tail	3.85	0.26

The effect of different fitted distributions to material strength data is analysed when the load distribution is Gumbel or Normal (COV=0.4). The fitted distributions to be analysed are:

- Normal distribution fitted to all data (N all), Normal fitted to the lowest 5% of the data (N tail) and combination of the two: different Normal distribution functions below and above 5%-tile (N+N).

- Lognormal distribution fitted to all data (LN all), Lognormal fitted to the lowest 5% of the data (LN tail), and combination of Lognormal distribution below and Normal distribution above 5%-tile (LN+N).

- Nonparametric distribution based on direct use of test data, where two alternatives are analysed: test data only indicating that there are no weaker specimens than the lowest value tested (test), and the combination of nonparametric distribution and Lognormal distribution fitted to the lowest 5%-tile so that Lognormal distribution is used below the lowest test value (LN+test).

The results indicate that Normal distribution fitted to all test data gives the lowest safety level ($\beta = 3.64$) and Lognormal fitted to all data the highest ($\beta = 4.34$ with Gumbel and $\beta = 5.16$ with Normal load distribution), the other combinations being fairly close to each other ($\beta = 4.1$ to 4.2 for Gumbel loads, and 4.4 to 4.8 for Normal loads). The combined distributions fit very closely to the test data and are obviously the most correct ones. We can also conclude that the distributions fitted to the lowest 5 percentile of test data give practically the same reliability as combined distributions. Results are shown in Table 4 in terms of failure probability and in Table 5 in terms of beta index.

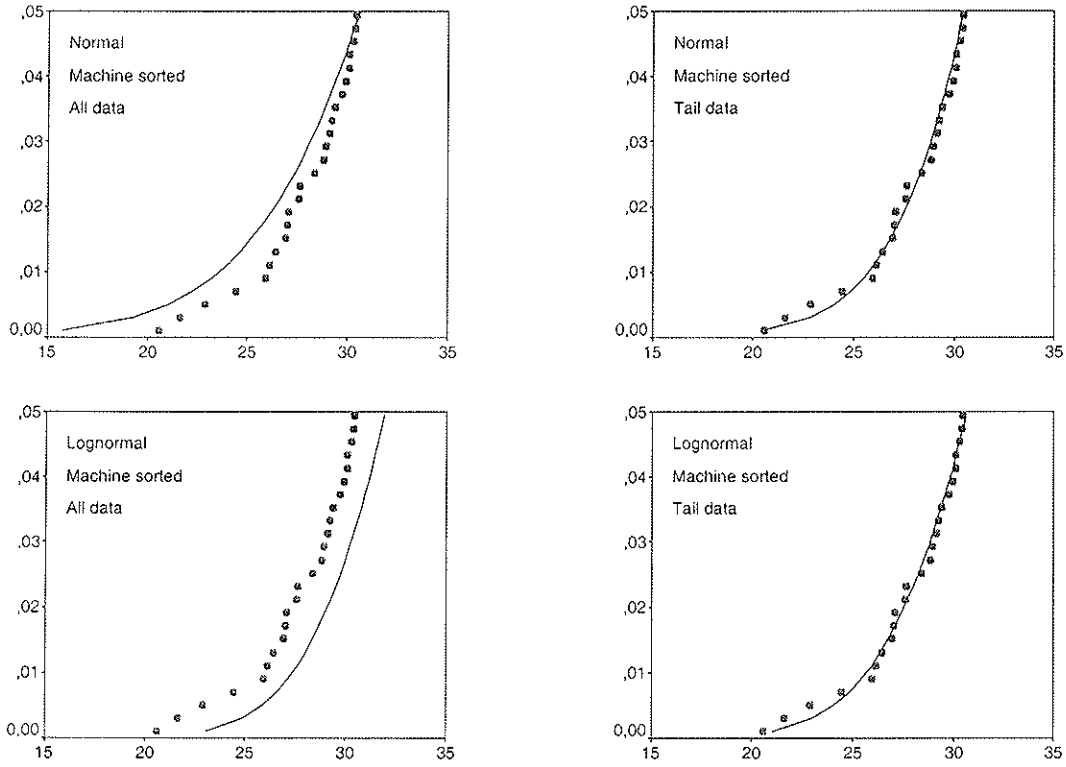

Figure 4. Cumulative distributions of bending strength for machine sorted spruce of dimensions 42 x 146 mm. The spruce was sorted by Raute Timgrader to the European strength class C30.

The ranked test data of 500 specimens, gives the same safety level as the best fitted functions when load is Gumbel distributed, in spite of the fact that no lower values than the lowest test result were assumed to exist. Instead, when nonparametric distribution was calculated with Normal distributed load, safety level was the highest and the lack of data below 0.1 percentile had a clear influence on the safety level. When the tail fitted Lognormal distribution is added to test data below 0.1 percentile, β index is decreased by 0.4, and P_f increased by factor of 7. The nonparametric cumulative distribution combined with Lognormal tail is illustrated together with load density distribution in Figure 5.

Table 4. Probability of failure $x10^{-6}$ when load distribution is Gumbel or Normal with COV=0.4, total safety factor 1,3x1,5=1,95 and material is C30 as given in table 3.

Load distribution	Strength distribution							
	N all	N tail	N+N	LN all	LN tail	LN+N	test	LN+test
Normal	135	5.5	5.5	0.12	0.92	0.92	0.14	0.95
Gumbel	137	20	19	7	15	14	13	15

Table 5. Beta index when load distribution is Gumbel or Normal with COV=0.4, total safety factor 1,3x1,5=1,95 and material is C30 as given in table 3.

Load distribution	Strength distribution							
	N all	N tail	N+N	LN all	LN tail	LN+N	test	LN+test
Normal	3.64	4.41	4.40	5.16	4.77	4.77	5.14	4.76
Gumbel	3.64	4.11	4.12	4.34	4.18	4.18	4.21	4.17

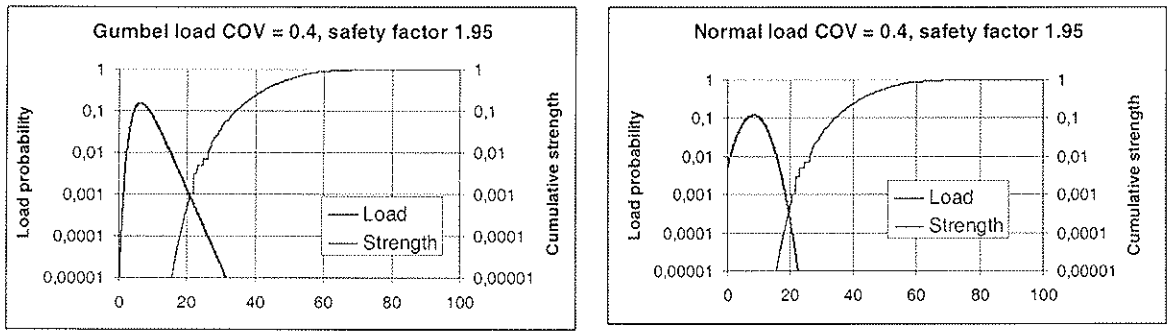

Figure 5. Illustration of load density distributions used in analysis with a cumulative material strength distribution (LN+test).

4 Conclusions

These simple calculations indicate that the present level of safety coefficients in Eurocode 5 (γ_m = 1.3 and γ_Q = 1.5 for variable loads: total safety factor γ = 1.95) results in safety level β = 4.2 in case of Gumbel load (COV = 0.4), and β = 4.8 in case of Normal load (COV = 0.4). The result with Gumbel load suggests that instructions given in Eurocode, Basis of Design, Annex C are inconsistent: the use of Gumbel distribution for variable loads together with target safety level of $P_f = 10^{-6}$ or $\beta = 4.75$ leads to requirement of so high safety coefficients which cannot be supported by practical experience. In the history of timber structures such failures can hardly be identified, which should be counteracted by the rise of general safety level in design.

Sensitivity analysis reveals that quite different conclusions can be made depending on the load distribution type used:

1. in case of Gumbel distribution the structural safety seems not to depend much on deviation of strength values, especially if Lognormal distribution is used for strength. Also, truncation of the lower tail by good quality control gives only a small advantage in terms of safety coefficient.
2. in case of Normal distribution the safety level depends more strongly on COV of material strength: Lognormal distribution with COV = 0.2 needs 16% higher safety coefficient than material with COV = 0.1 to achieve the same safety. In case of Gumbel load, the same difference is only 1%.

Acknowledgement

This work is part of a study on reliability of timber structures financed by TEKES, Finnish Wood Research Ltd., Finnish wood hall producers and VTT which is gratefully acknowledged.

References

Ahmed S., Clark R.D., Metcalf D.R., 1982, A method for propagating uncertainty in probabilistic risk assessment. Nuclear Technology 59, 238-245.

Foschi R.O., Folz B.R., Yao F.Z., 1989, Reliability-Based Design of Wood Structures. Structural research series, Report 34. Department of Civil Engineering, University of British Columbia, Vancouver, Canada.

Larsen H.J., Svensson S., Thelandersson S., 1999, Determination of partial coefficients and modification factors. CIB W18 Meeting in Graz, August 1999, Paper 32-1-1, 10 p.

Leporati E., 1979, The assessment of structural safety. Research studies press. 133 p.

prEN 1990 Eurocode : Basis of design, CEN, Draft 4.2.2000

Ranta-Maunus A., Hietanen O., Reponen H., Saari H., Valkeajärvi, Virolainen R., 1985, A systematic evaluation of the coverage of pressure vessel inspection. SMiRT-8 Conference, Brussels, Paper M11/5.

Ranta-Maunus A., Fonselius M., Kortesmaa M., Kurkela J., Toratti T., 2000, Manuscript for VTT Research Notes.

SAKO Joint Nordic Group for Structural Matters, 1998, Proposal for modification of partial safety factors in Eurocodes. Draft Dec. 1998.

Skov K., Ditlevsen O., 1976, On the application of the uncertainty theoretical methods for the definition of the fundamental concepts of structural safety. CIB-W18 meeting in Aalborg. Paper 6-1-1.

Thelandersson S., Larsen H.J., Östlund L., Isaksson T., Svensson S., 1999, Säkerhetsnivåer för trä och träproducter i konstruktioner. Lund Universitet. Rapport TVBK-3039. 37 p. + app.

INTERNATIONAL COUNCIL FOR RESEARCH AND INNOVATION
IN BUILDING AND CONSTRUCTION

WORKING COMMISSION W18 - TIMBER STRUCTURES

DETERMINATION OF YIELD STRENGTH AND ULTIMATE STRENGTH OF DOWEL-TYPE TIMBER JOINTS

by

M Yasumura
K Sawata
Department of Forest Resources Science
Shizuoka University

JAPAN

MEETING THIRTY-THREE
DELFT
THE NETHERLANDS
AUGUST 2000

Presented by: M. Yasumura

· H.J. Larsen commented that it could be misleading to use a standard for nails to be applied to bolts. The definition of yield point as the departure point from elastic zone or the entry point to yield was also questioned. He also asked whether the minimum edge distance for the splitting case should be beam depth dependent or bolt diameter dependent.
· M. Yasumura responded that based on fracture mechanics analysis mix mode of failure was present; therefore, minimum edge distance should be beam depth dependent.
· H.J. Larsen further pointed a case where if the design were already safe to start off, further increase in beam depth should not lead to a less safe situation.
· M. Yasumura would look into this further.
· H. Blass asked whether bending angles of dowels were examined in the joint tests.
· M. Yasumura answered that this was not an issue for the perpendicular to grain case.

Determination of Yield Strength and Ultimate Strength of Dowel –type Timber Joints

Motoi YASUMURA and Kei SAWATA
Department of Forest Resources Science, Shizuoka University, Japan

1. Introduction

Japanese new building codes enforced in June 2000 stipulate the design method based on the damage limit and safety limit of building structures. Damage limit is the limit where no structural elements are damaged by the actions that may occur during the life of the building, and safety limit is the limit where the safety of structure is ensured during the extreme actions.

Dowel-type joints are designed by the yield theory (1949) based on the embedding strength of wood and yield moment of dowels. European standards EN383 (1993) and prEN409 (1991) stipulate the test methods for determining the embedding strength of wood and yield moment of dowels, respectively. Embedding strength is determined by the maximum stress up to 5mm displacement in EN383, and yield moment is determined by the maximum moment up to 45 degree of bending angle in prEN409. This is applied only to nails whose diameters are not larger than 8mm, and Eurocode 5 (1993) describes to take 80% of the ultimate tensile strength to obtain yield moment of dowels.

In this paper, yield and ultimate strengths of bolted joints were calculated from the embedding tests of one thousand specimens and bending and tensile tests of dowels from different manufacturers to compare with the experimental results of bolted joints subjected to lateral forces parallel and perpendicular to the grain (1998,1999,2000). From these results, the calculating methods to determine the yield strength and ultimate strength were proposed to design the damage limit and safety limit of timber structures.

2. Embedding tests

2.1 Specimen

Embedding tests were conducted on Ezomatsu (Picea jezonensis CARRIERE) laminae graded into four grades according to JAS (Japanese Agricultural Standard). The dowel diameters were 8, 12, 16 and 20mm. The width and length of specimens were respectively six and fourteen times dowel diameter as shown in Fig.1. The thickness of specimen was kept to 32mm for all specimens regardless of dowel diameters. Number of specimens and density of each grade laminae are shown in Table 1.

2.2 Test method

Twelve millimeters thick steel plates were attached to both sides of wood and connected with a dowel as shown in Fig.1. In the case of loading parallel to the grain, embedding stress of 10 to 30 MPa/min. was applied, and the tests were terminated either when the displacement attained to the dowel diameter or when the load decreased to a half of maximum load. In the case of loading perpendicular to the grain, embedding stress of 5 to 15 MPa/min. was applied, and tests were terminated when the displacements were equal to the dowel diameter or the crack reached the ends

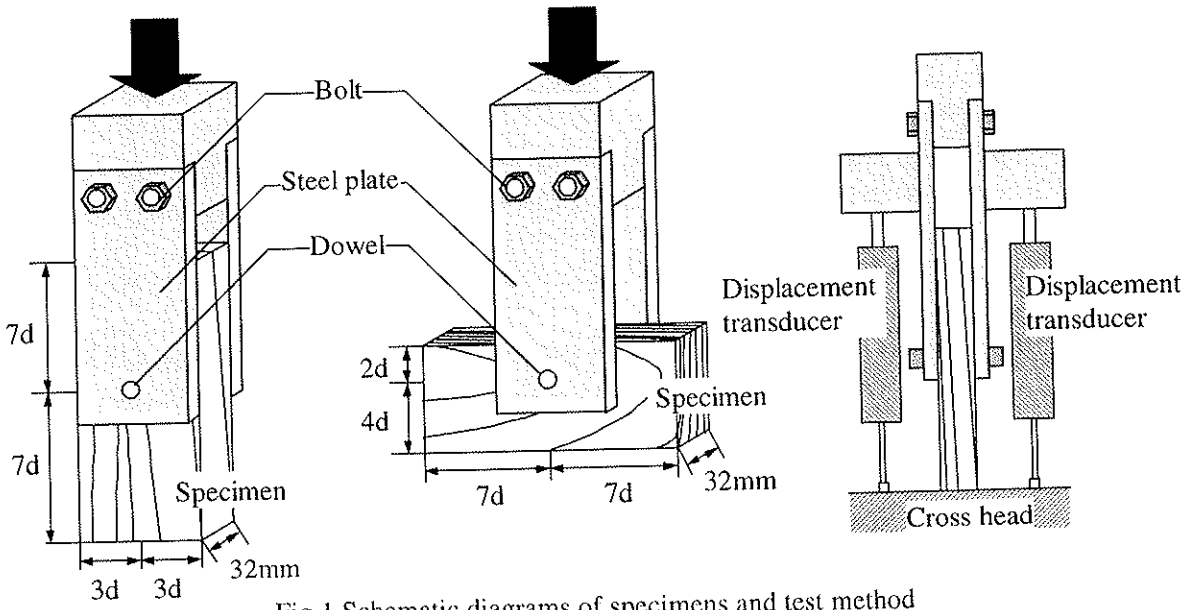

Fig.1 Schematic diagrams of specimens and test method

Table 1 Density and number of specimens

Grade		//			·口		
		n	Density		n	Density	
			mean(kg/m^3)	c.o.v(%)		mean(kg/m^3)	c.o.v(%)
WP-8	total	57	390.9	11.38	57	387.1	10.94
	L90	14	381.0	10.97	14	372.9	9.57
	L100	14	368.7	8.36	14	364.3	7.10
	L110	15	398.9	9.58	15	398.5	9.13
	L125	14	414.4	12.26	14	412.0	12.04
WP-12	total	117	393.5	10.23	119	389.4	10.31
	L90	30	359.4	6.47	30	350.7	5.05
	L100	30	393.0	11.96	30	383.4	9.36
	L110	30	394.5	6.05	30	401.0	9.87
	L125	27	422.2	8.26	29	419.7	6.89
WP-16	total	212	399.5	11.15	212	402.8	11.07
	L90	50	350.1	10.23	50	357.0	7.64
	L100	56	388.9	4.99	56	391.8	4.45
	L110	56	410.8	7.52	56	404.0	7.73
	L125	50	448.1	5.33	50	459.8	6.08
WP-20	total	117	403.0	10.74	118	401.5	12.23
	L90	29	371.7	7.05	30	361.5	6.26
	L100	30	381.5	9.65	30	371.7	8.50
	L110	30	418.8	5.63	30	418.3	5.68
	L125	28	441.4	9.67	28	450.4	11.06

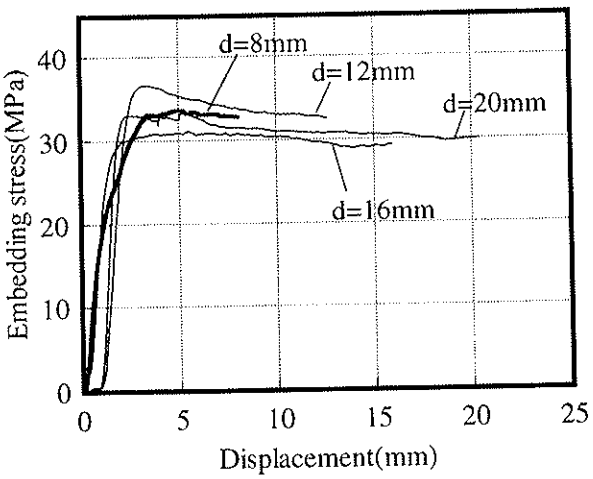

Fig.2 Stress-displacement relationship Loading Parallel to the grain

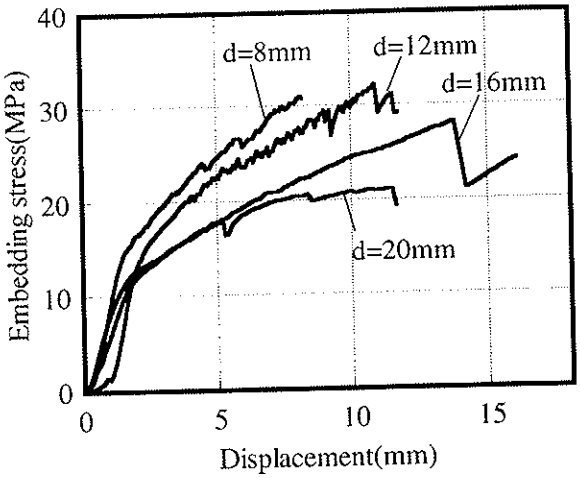

Fig.3 Stress-displacement relationship Loading Perpendicular to the grain

of wood.

2.3 Test results

Figs.2 and 3 show typical load-deformation curves in the case of loading parallel and perpendicular to the grain, respectively. The embedding stress parallel to the grain showed almost constant values after yielding, while that perpendicular to the grain continued to increase after yielding. Embedding strengths were evaluated by following two methods from load-deformation relationships. One was determined by 5% off-set method as shown in Fig.4, and the other was the maximum load up to 5mm displacement as described in EN383. In the case of loading parallel to the grain, the embedding strength determined by EN383 showed close values to those evaluated by 5% off-set method except for those with dowel diameter of 8mm. As the wooden thickness was comparatively thick (4d) in the specimens with dowel diameter of 8mm, the embedding strength evaluated by 5% off-set tended to show smaller values than other specimens because of the bending of dowels. In the case of loading perpendicular to the grain, the embedding strength determined by EN383 showed higher values than those evaluated by 5% off-set method.

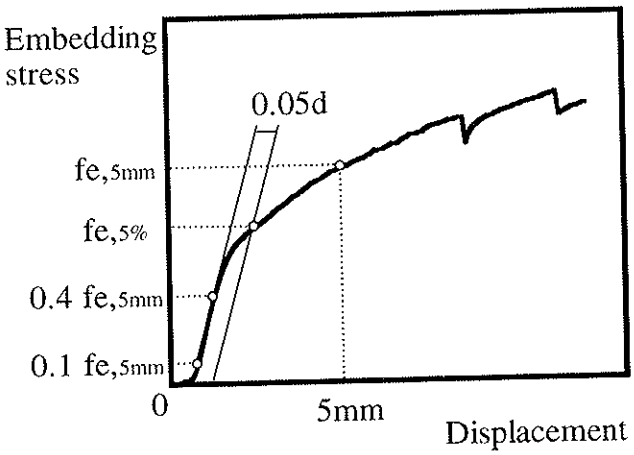

Fig.4 Definition of embedding strength

Figs. 5 and 6 show the relationships between density (D) and embedding strength evaluated by 5% off-set method (fe,5%) and EN383 (fe,5mm), and Fig. 7 shows those between dowel diameter and embedding strengths evaluated by the former and the later. The embedding strength parallel to the grain decreased slightly as the increase of dowel diameter and showed similar values between those evaluated by 5% off-set and EN383. However, embedding strength perpendicular to the grain determined by EN383 showed a significant decrease according to the increase of dowel diameter, while that evaluated by 5% off-set method was not influenced much by dowel diameter. Fig.8 compares the design values in EC5 with those obtained by dividing the yield strength by the density in each specimen. The value (fe,5%/D) decreased slightly as the dowel diameter increased

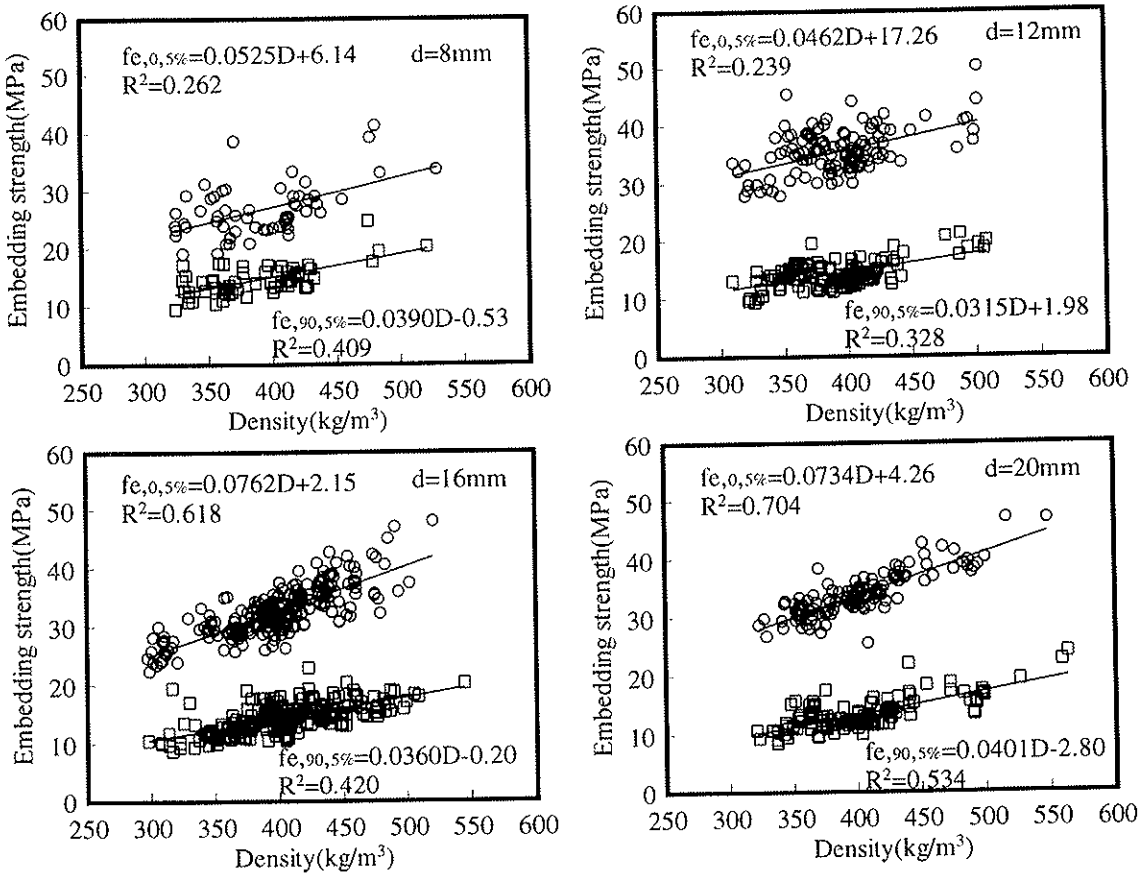

Fig.5 Relation between embedding strength and density (parallel to the grain)

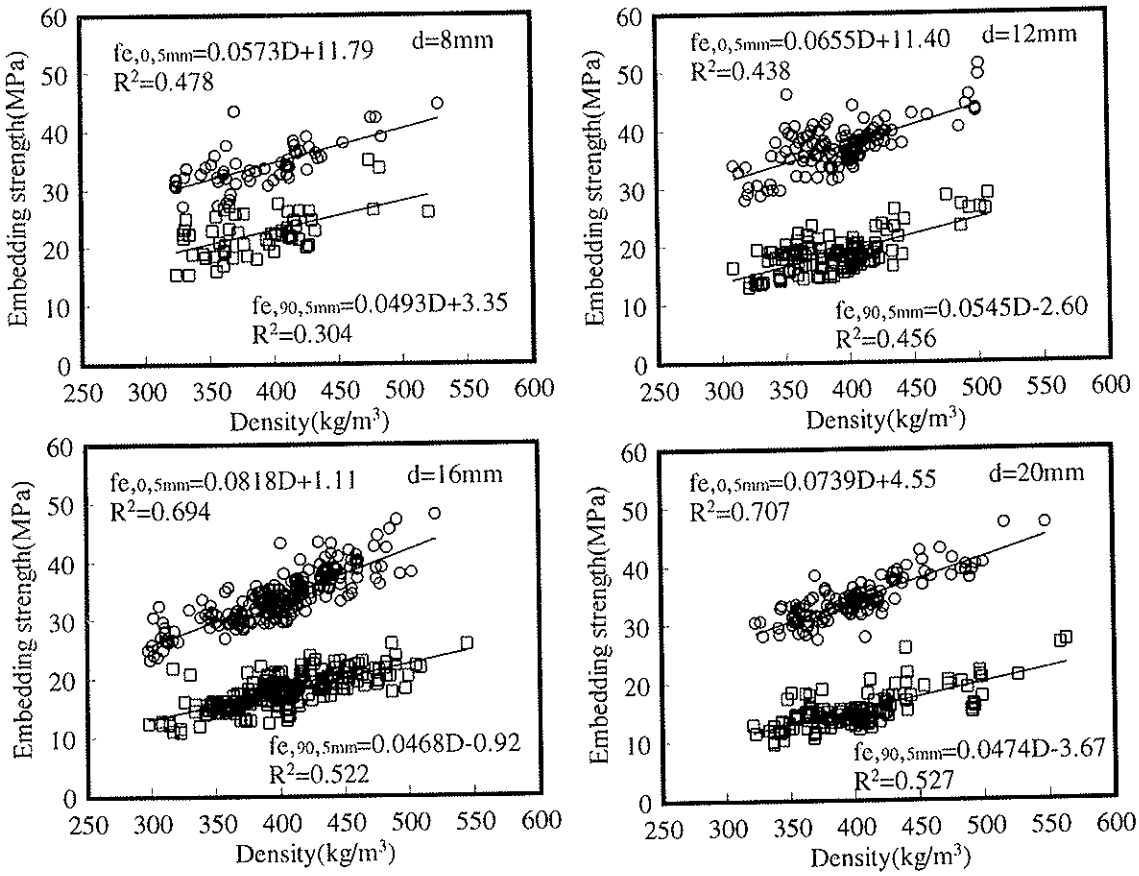

Fig.6 Relation between embedding strength and density (perpendicular to the grain)

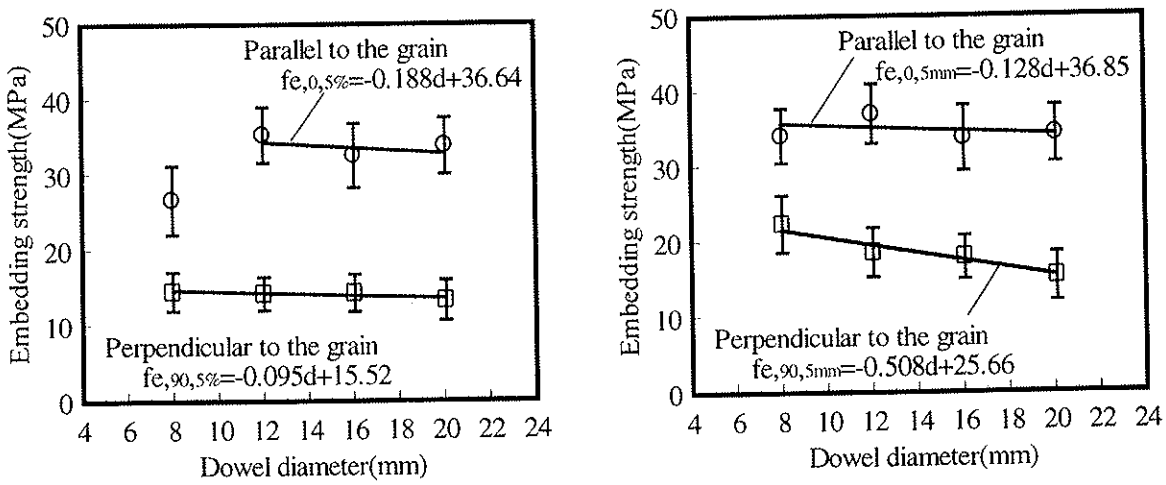

Fig.7 Relation between embedding strength and dowel diameter

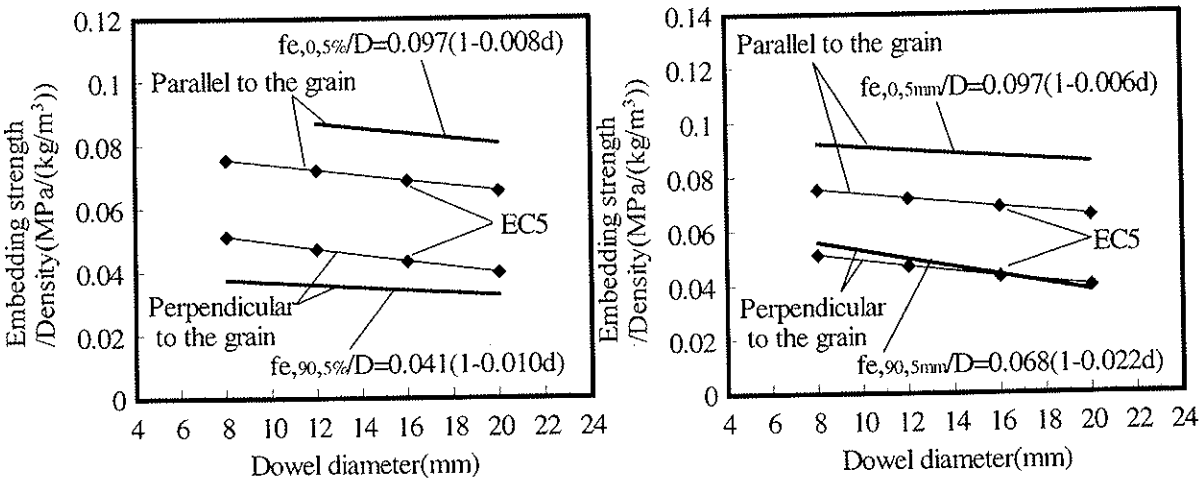

Fig.8 Comparison with design values in EC5

in both cases of loading parallel and perpendicular to the grain. The slope of the regression equation of (fe,5%/D) of EC5 was almost the same as that of the experiments, however the experimental values parallel to the grain were approximately 10% higher and that perpendicular to the grain were approximately 10% lower than the design values. The experimental values of (fe,5mm/D) were also approximately 10% higher than the design values in the case of loading parallel to the grain, and showed good agreement with the design values in the case of loading perpendicular to the grain.

3. Bending and tensile tests of dowels

3.1 Specimens

Bending and tensile tests were conducted on six steel rods of 8, 12, 16 and 20mm diameters, respectively. Steel rods for bolted timber joints were obtained from twelve different manufacturers.

3.2 Test methods

Bending tests were conducted on six rods from each lot according to prEN409 as shown in Fig.9. Tensile tests were also carried out on six rods from each lot according to JIS Z2241.

3.3 Results

Bending moment was evaluated by two methods. One was that according to prEN409. Maximum

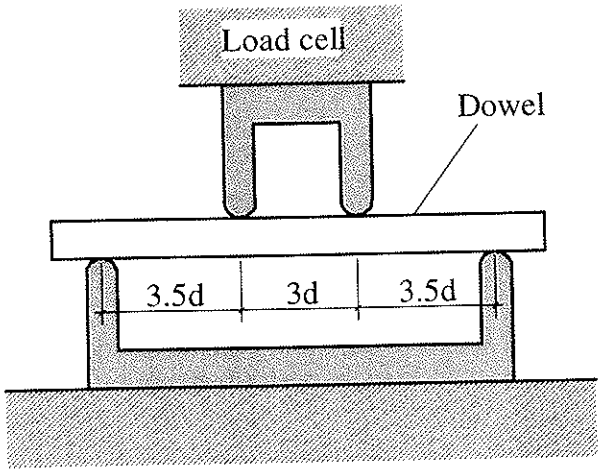

Fig.9 Bending test of dowels

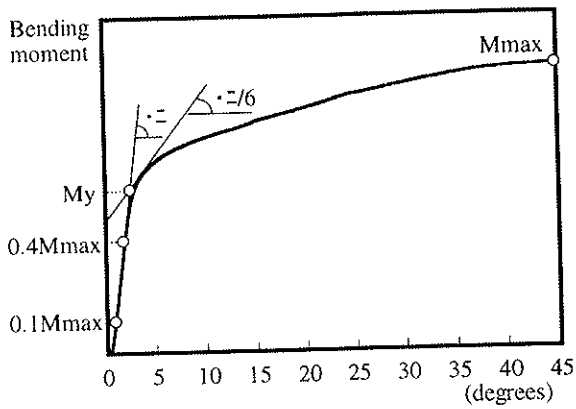

Fig.10 Definition of yield and ultimate moment

bending moment up to 45 degree of bending angle was taken. The other was one-sixth method as shown in Fig.10. We call the former as "yield moment" and the later as "ultimate moment" in this paper.

The relationships between yield strength and ultimate strength by bending test and tensile tests are shown in Figs.11 to 14. The yield and ultimate strengths of dowels were obtained from the following formula.

$$F_y = \frac{6}{d^3} M_y \quad : \quad F_u = \frac{6}{d^3} M_u$$

These figures show that the strength obtained by prEN409 (45 degree bending angle) was almost the same as the ultimate strength obtained by tensile test, and the yield strength obtained by 1/6 method was 10% lower than that obtained by tensile test. In consequence, the yield strength obtained by bending and tensile tests of dowels was 72% and 82% of the ultimate strength obtained by the tensile tests. These results indicate that the "ultimate moment" obtained from 45 degree bending angle in bending test of dowels corresponds to the "ultimate strength" in tensile tests, and 70 to 80% of the "ultimate moment" should be taken for the "yield moment".

4. Discussion

4.1 Yield and ultimate strengths of bolted joints subjected to lateral force parallel to the grain

Figs.15 and 16 show the comparison of the calculated yield strength with the experimental results of bolted joints with steel side plates and a steel center web, respectively. The yield strength of bolted joints were calculated by the yield theory with the embedding strength obtained by 5% off-set method and yield moment obtained by 1/6 method. Yield strength of bolted joints was obtained by 5% off-set method. The calculated yield strength of bolted joints showed comparatively good agreement with the experimental results, and it was proved that the calculation with the embedding strength obtained by 5% off-set method and yield moment obtained by 1/6 method predicts well the yield strength of dowel-type joints.

Figs.17 and 18 show the comparison of the calculated ultimate strength with the experimental results

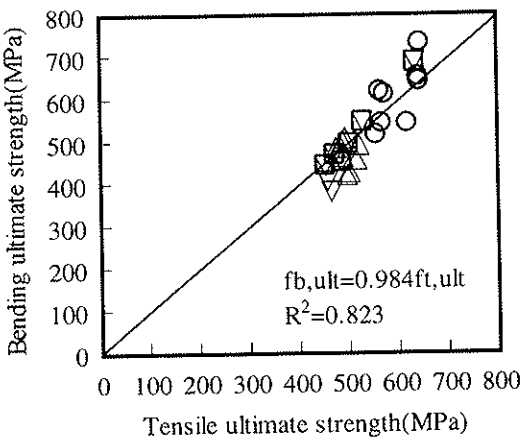

Fig.11 Bending ultimate strength and tensile ultimate strength

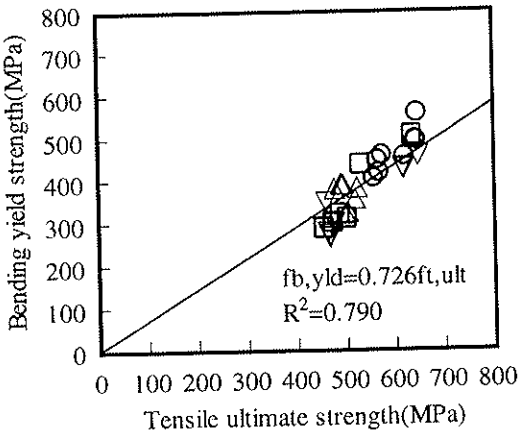

Fig.12 Bending yield strength and tensile ultimate strength

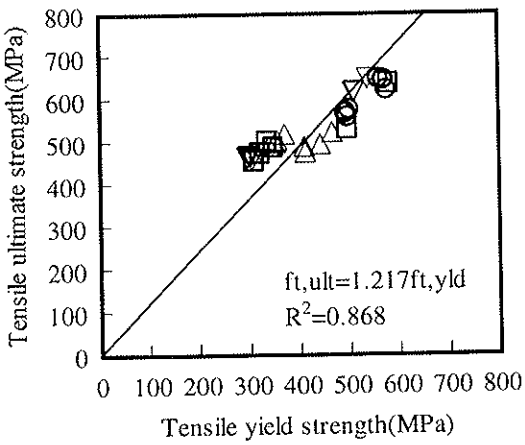

Fig.13 Tensile ultimate strength and tensile yield strength

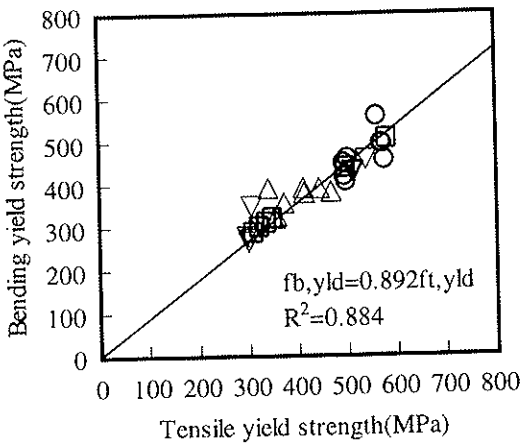

Fig.14 Bending yield strength and tensile yield strength

of bolted joints with steel side plates and a steel center web, respectively. The ultimate strength of bolted joints was calculated by the yield theory with the embedding strength obtained by EN383 and ultimate moment obtained by prEN409. The calculated values showed comparatively good agreement with the experimental results except for the joints whose slenderness ratio was comparatively large. For the joints whose slenderness ratio was comparatively large, the experimental results tended to exceed the calculation because the friction caused by rope effects. It was proved that the calculation with the embedding strength obtained by EN383 and ultimate moment obtained by prEN409 predicts well the ultimate strength of dowel-type joints.

4.2 Ultimate strengths of bolted joints subjected to lateral force perpendicular to the grain

Fig.20 shows the comparison of the calculated yield strength with ultimate strengths of bolted joints with steel side plates as shown in Fig.19 subjected to lateral force perpendicular to the grain. The yield strengths of bolted joints were calculated by the yield theory with the embedding strength obtained by EN383. As the slenderness ratio of joints was small, the yield strength was determined only by the embedding strength. Different from the case of loading parallel to the grain, the experimental values of ultimate strength of joints differed much from the strength calculated with the em-

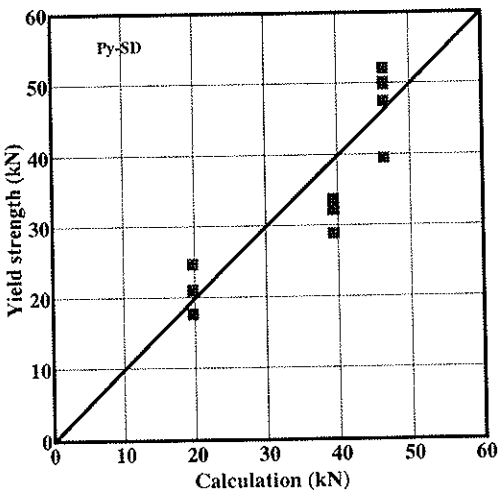

Fig.15 Comparison of calculated yield strength with experimental results in steel side plates joints

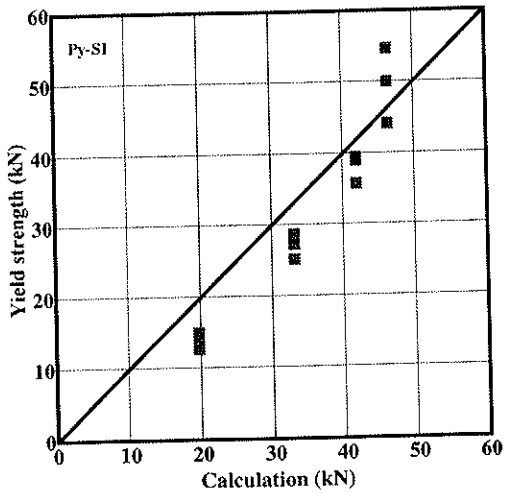

Fig.16 Comparison of calculated yield strength with experimental results in steel center web joints

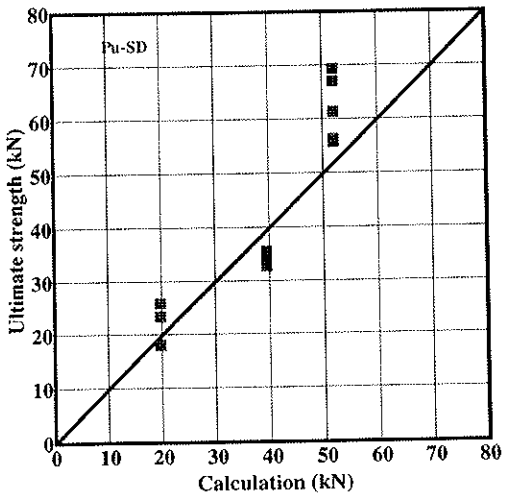

Fig.17 Comparison of calculated ultimate strength with experimental results in steel side plates joints

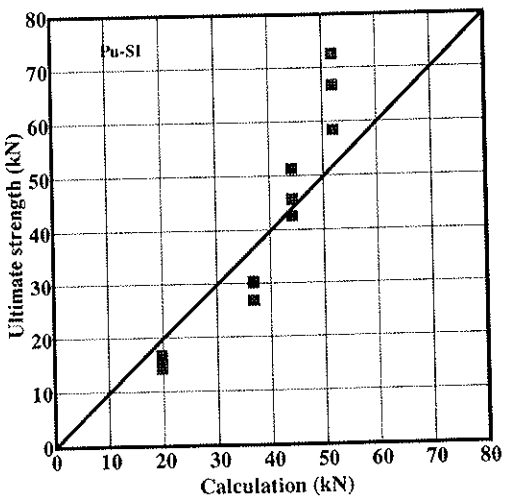

Fig.18 Comparison of calculated ultimate strength with experimental results in steel center web joints

bedding strength. This is because the embedding stress continued to increase after 5mm displacement when the edge distance was sufficiently large, while the joints failed according to the fracture of wood when the edge distance was comparatively small.

These results indicate that the ultimate strength of bolted joints subjected to lateral force perpendicular to the grain should be determined by considering the fracture of wood, and the edge distance should be larger than one third to a half of beam height in order that the joints do not fail by the fracture of wood before the embedding of dowels.

5. Conclusions

Summarizing the results mentioned above, the following conclusions are led.

1) The embedding stress parallel to the grain shows almost constant values after yielding, while that perpendicular to the grain continues to increase after yielding.
2) In the case of loading parallel to the grain, the embedding strength determined by EN383 shows close values to those evaluated by 5% off-set method except for those with dowel diameter of 8mm. In the case of loading perpendicular to the grain, the embedding strength determined by

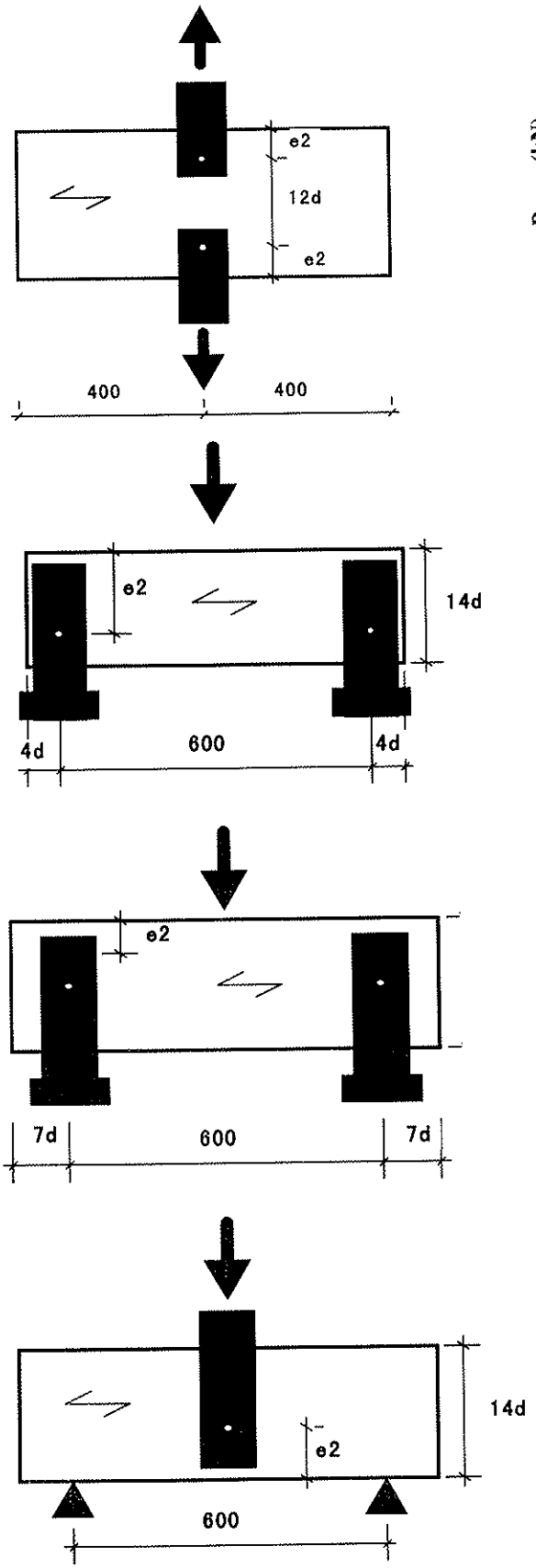

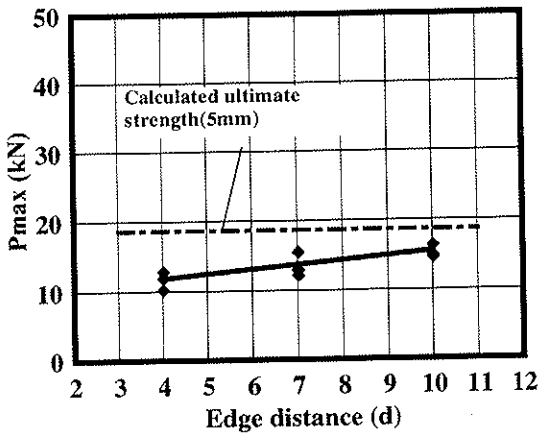

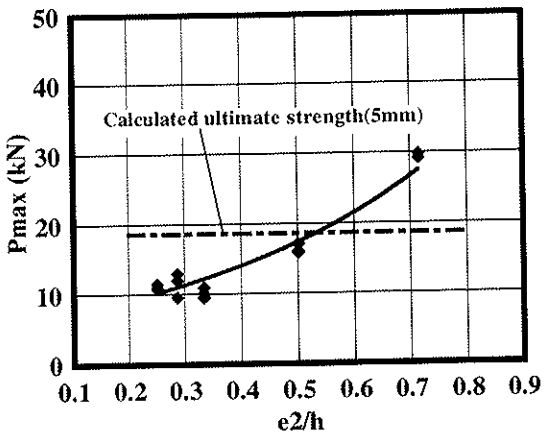

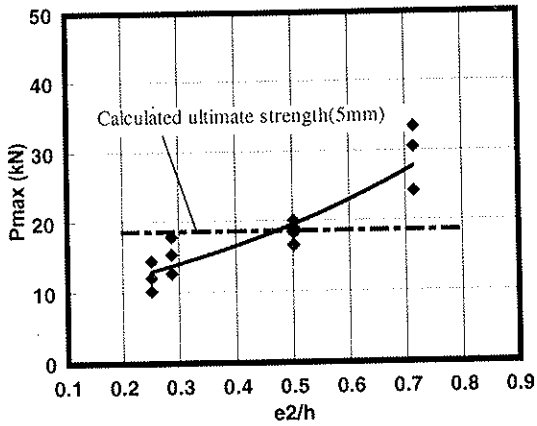

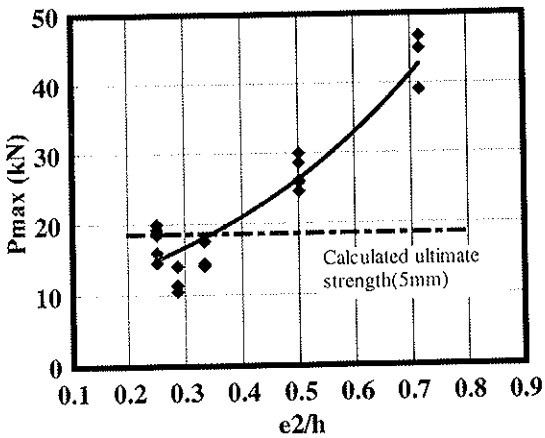

Fig.19 Schematic diagrams of specimen (t=4d, d=16mm)

Fig.20 Comparison of experimental results with calculated ultimate strength by embedding

EN383 shows higher values than those evaluated by 5% off-set method.

3) Strength obtained by bending test of dowel according to prEN409 (45 degree bending angle) is almost the same as the ultimate strength obtained by the tensile test, and yield strength obtained by 1/6 method is 10% lower than that obtained by tensile test. This indicates that the "ultimate moment" obtained from 45 degree bending angle corresponds to the "ultimate strength" in tensile test, and 70 to 80% of the "ultimate moment" should be taken for the "yield moment".
4) Calculation with the embedding strength obtained by 5% off-set method and yield moment obtained by 1/6 method predicts well the yield strength of dowel-type joints.
5) Calculation with the embedding strength obtained by EN383 and ultimate moment obtained by prEN409 predicts well the ultimate strength of dowel-type joints.
6) Ultimate strength of bolted joints subjected to lateral force perpendicular to the grain should be determined by considering the fracture of wood, and the edge distance should be larger than one-thirds to a half of beam height in order that the joints do not fail by the fracture of wood before the embedding of dowels.

6. References

Ministry of Construction: Building Standard Law: Enforcement Order

EN383: 1993: "Timber structures – Test methods – Determination of Embedding Strength and Foundation Values for Dowel Type Fasteners"

PrEN409: 1991: "Timber structures – Test methods – Determination of the Yield Moment for Dowel Type Fasteners – Nails"

Eurocode 5: 1993: Design of Timber structures. Part 1-1: General rules and rules for buildings.

Johansen.K.W., "Theory of Timber Connections", IABSE Publications 9:249-262,1949

Sawata,K. and Yasumura,M. ,"Evaluation of Yield Strength of Bolted Timber Joints by Monte-Carlo Simulation", Proceedings of WCTE2000, 2000.

Yasumura,M., "Mechanical Properties of Dowel Type Joints under Reversed Cyclic Lateral Loading", Proceeding of CIB-W18, paper 31-7-1, 1998.

Yasumura,M. and Daudeville,L., "Design and Analysis of Bolted Timber Joints under Lateral Force Perpendicular to Grain", Proceeding of CIB-W18, paper 32-7-3, 1999

INTERNATIONAL COUNCIL FOR RESEARCH AND INNOVATION
IN BUILDING AND CONSTRUCTION

WORKING COMMISSION W18 - TIMBER STRUCTURES

LATERAL SHEAR CAPACITY OF NAILED CONNECTORS

by

U Korin
National Building Research Institute
The Technion, Haifa

ISRAEL

MEETING THIRTY-THREE
DELFT
THE NETHERLANDS
AUGUST 2000

Presented by: U. Korin

· H. Blass asked for clarification on the definition of failure load at 5 mm deformation.
· U. Korin responded that the failure load was taken as the load at 5 mm deformation if the peak load was not reached; otherwise, the maximum load would be used as the failure load.
· H. Blass asked why 5 mm deformation was chosen.
· U. Korin responded that the choice was based on embedment strength information.
· J. Ehlbeck commented that the procedures comparing theoretical values with test results were incorrect because conservative yield moments of nails (design values) in Eurocode 5 were used in the procedures. The code referred to minimum nail strength of 600 MPa.
· U. Korin responded that only wire strength information was collected during the test.

Lateral Shear Capacity of Nailed Connectors

Dr. Uri Korin

National Building Research Institute, The Technion, Haifa, Israel

Abstract

The paper reports the results of an investigation of the lateral shear capacity of nailed joints made with Israeli manufactured plain wire nails and whitewood from European origin, used in Israel for construction purposes.

The parameters of the study were nail size(60 mm, 75 mm, and 90 mm nails), loading directions (ingrain and perpendicular to grain), and number of nails in the connector (two nails, four nails, six nails, eight nails and ten nails).

The results were compared with the design values given in Eurocode 5, and good agreement was found.

The results of the study will be included in the local standards and specifications for design of timber structures.

1 Introduction

The purpose of the reported investigation was to establish design values for nailed timber connectors, made with the most common timber used by the construction industry in Israel (European whitewood), and locally fabricated plain drawn wire nails. The data and the information obtained through this work, will eventually be used in the revision of the Israeli standard for timber structures [1], and the Israeli standards for scaffoldings [2,3]. The shear capacity values obtained in the study were compared with the design values for wood connectors proposed by the European Standard Eurocode 5: Design of Timber Structures[4].

2 The Geometry of the Investigated Joints

The joints investigated during the study were of the "Timber to Timber" type fasteners, in single shear corresponding to equation 6.2.1 f [4]:

$$R_d = 1.1\sqrt{\frac{2\beta}{1+\beta}}\sqrt{2M_{y,d}f_{h,1,d}d} \qquad (1)$$

The experiments were conducted with the angles α between the applied force F and the grain direction of the wood at the nail head side (nailing component "1") of the specimens were 0° or 90° (ingrain direction or perpendicular to grain direction). Components "2" of the joints, the penetration component, for all the nail sizes investigated, were made of 44 mm thick lumber (44 mm x 100 mm).

Lumber or boards of various thickness were used for the nailing side components (components "1") of the joints as shown in table 1.

Table 1- Joints Geometry

Nail type	Nail diameter "d" (mm)	Nail length (mm)	Nominal thickness of nailing side,t1 (mm)	Nominal penetration depth ,t2 (mm)	Nominal penetration slenderness
16/60	2.83	60	22	38	13d>8d
18/75	3.4	75	38	37	10.9d>8d
20/90	4.5	90	44	46	9.8d> 8d

3 The Nails

The tested connectors were prepared with two, four, six, eight or ten nails in each connector. The nails used for the investigation, were manufactured and donated by the Hod Corporation, which is the largest steel transformer in Israel. Some samples of the drawn wires, used for the fabrication of the nails, were provided together with the nails, and were eventually tested to determine the mechanical properties of the cold worked steel from which the nails were made.

Three sizes of nails were used in the study: 16/60, 18/75, and 20/90. The measured diameters of the nails and the mechanical properties of the wires from which the nails were produced are given in table 2.

Table 2 – Sizes and Mechanical Properties of the Nails

Diameter (mm)and designation of nail	Yield strength (MPa)	Ultimate strength (Mpa)	Fracture elongation (%)	
			over 10 d	over 200 mm
2.83 mm	731	854	9.0	2.3
16/60	738	846	8.3	2.3
	746	854	7.7	2.5
3.40 mm	596	639	8.5	2.8
18/75	596	639	9.3	2.6
	596	645	9.3	2.4
4.50 mm	656	711	8.0	3.0
20/90	671	720	7.6	3.5
	656	714	7.8	2.8

Equation 6.3.1.2 c from reference [4] was used for the calculation of the yield moment of the nails:

$$M_y = 180\, d^{2.6} \qquad (2)$$

4 The Timber

Whitewood, which is in common use in Israel for construction purposes was used to produce the test pieces required for the study. The 22 x 100 mm boards and the 44 x 100 mm lumber, were imported from Sweden and the 35 x 100 mm wood was from Austrian origin.

The bulk density of each one of the test pieces used in the study was determined from its individual air dry weight and its individual bulk volume as calculated from its external measurements. The moisture content of all the test pieces was measured by the use of an electrical resistance moisture meter. The bending properties of some representative samples of the timber were determined according to the International Standard ISO 8375-1985 [5]. The test data for the timber properties are presented in table 3.

Table 3 –Timber Properties

Designation	Moisture content (%)	Dimensions (mm)	Bulk density (kg/m³)	Bending strength (MPa)	Modulus of elasticity (MPa)
22/101	10	23.0x99.5	443	55.7	11,230
22/102	10	22.6x98.7	449	57.2	13,990
35/101	10	38.4x97.2	421	61.0	13,690
35/102	10	38.0x97.6	449	46.9	11,710
44/101	10	43.8x99.9	489	62.7	15,210
44/102	10	43.6x100.0	491	66.4	16,640

5 The Lateral Shear Experiments

The lateral shear experiments were conducted in a special loading rig assembled for the study. The loading rig comprised a steel frame, an hollowed hydraulic ram, and an Instron electrical resistance load cell. The hydraulic pressure for the hydraulic ram was created by an adjacent Amsler Universal Testing Machine. The load cell output and the displacements of the joints measured by a L.V.D.T. extensiometer , were recorded by the use of computerized data collecting system at 3 seconds intervals during each operation.

The rig enabled to perform the connector shear tests in the grain direction and across the grain direction. The lumber at the penetration side of the connectors was always placed in the grain direction. During the ingrain direction tests, the free ends of the two wood pieces of the connector, were fixed to the testing rig by the use of shear bolts. For the across grain direction tests, the penetration side was held in the testing rig in a similar mode to the ingrain direction tests. Special fixing housing was prepared for the purpose of holding the nailing side in position in perpendicular orientation to the penetration side. The details of the fixing arrangements are shown in Fig.1. The fixing arrangement enabled the conduction of single shear experiments without eccentricity, and with freedom of rotation of the ends of the tested samples. The loading tests of the various specimens continued until reaching total joint displacements of about 20 mm.

The values considered as the shear resistance of the specimens, were worked out from the shear load – displacement charts provided by the data retrieving system. Where a

maximum value was observed on the curve at displacement smaller than 5 mm, it was considered as the shear resistance of the sample. The shear loads at 5 mm displacements, were regarded as the shear resistance of all the other samples. A typical load-displacement curve is shown in figure 2.

6 The Nailing of the Connectors

The nailing of the 22 mm boards by the use of the 16/60 nails, and the nailing of the 38 mm lumber by the use of the 18/75 nails, were carried out without pre-drilling (no splitting of the wood was observed). The embedding strength of the wood was predicted by the use of equation 6.3.1.2a of reference [4]:

$$f_h=0.082\rho d^{-0.3} \ N/mm^2 \qquad (3)$$

It was observed that the nailing of the 44 mm lumber by the use of the 20/90 nails without pre-drilling resulted splitting of some of the lumber pieces. Thus, 3.5 mm holes were pre-drilled, and the most of the 44 mm lumber test pieces prepared for the study, were of the predrilled type. Equation (3) was used for the calculation of the embedding strengths of the specimens prepared without pre-drilling. The embedding strengths of the wood of the pre-drilled pieces were calculated according the equation presented in reference [4] (6.3.1.2b):

$$f_h=0.082(1-0.01d)\rho \ N/mm^2 \qquad (4)$$

The nailing of all the nails in this study was carried out manually with a hammer. The spacing of the nails, and the distances of the nails from the ends and the edges of the timber, were within the recommendation of Eurocode 5 [4].

7 The Tested Population

The boards and the lumber used for the experiments were cut into short lengths required for the preparation of the nailed connectors. Each of the sawn pieces was marked, measured and weighed. Then the mass volume density of each wood piece, ρ, was calculated. A set of 10 mm holes at a standard pattern, was prepared at the free end of the wood cuttings for the purpose of fixing in the test rig. The test pieces were assembled by nailing the nailing side (1) (22 mm, 38 mm, and 44 mm) over the penetration side (44 mm) of the connector.

The lengths of the wood cuttings sawn for the study, enabled multiple use of most of the cuttings, for preparation of new test connectors, after sawing away the nailed zone of the wood. Damaged or split wood pieces were not re-used.

Six assembled connectors were tested for each combination of the test parameters (nail size, number of nails in the connector, and grain direction of the nailing side), and thus, the total number of the tested assembled connectors was 180.

8 Prediction of the Shear Resistance of the Connectors

The following values were used to predict the shear resistance of the connectors:

Nails bending moment-

$M_{yk} = 180\ d^{2.6}$ (2)

2.83 mm nails – $M_{y,k}$=2691 Nmm
3.40 mm nails – $M_{y,k}$=4336 Nmm
4.50 mm nails – $M_{y,k}$=8987 Nmm

Wood embedding strengths (without pre-drilling):

$f_h = 0.082\rho d^{-0.3}$ N/mm² (3)

2.83 mm nails – $f_{h,k} = 0.0600\rho_k$ N/mm²
3.40 mm nails – $f_{h,k} = 0.0568\rho_k$ N/mm²
4.50 mm nails – $f_{h,k} = 0.0522\rho_k$ N/mm²

Wood embedding strengths (pre-drilled):

$f_h = 0.082(1-0.01d)\rho$ N/mm² (4)

4.50 mm nails – $f_{h,k} = 0.0783\rho_k$ N/mm²

Thus, the predicted shear capacity for each of the tested assemblies was calculated taking in account the particular density of the two cuttings forming the connector, the embedding strengths of the two members, the ratio $\beta = f_{h,2,d}/f_{h,1,d}$, and the nails bending moment.

Table 4 :Average ultimate shear capacities (2.83 mm nails)

Direction of nail side and nail diameter	Nail number	Predicted value per nail (N)	Predicted value per connector (N)	Resulted value per connector (N)	Resulted value per nail (N)	Resulted/ predicted ratio
2.83 mm	2	743	1486	1759	880	1.184
(a-in grain)	4	736	2943	3568	892	1.212
	6	682	4094	4662	777	1.139
	8	702	5615	6733	842	1.199
	10	666	6661	8270	827	1.242
Average a	-	706	-	-	844	1.195
2.83 mm	2	741	1481	1859	929	1.245
(b-across	4	696	2785	3581	895	1.286
Grain)	6	682	4089	5250	875	1.283
	8	741	5929	7852	982	1.325
	10	738	7383	9065	907	1.228
Average b	-	720	-	-	918	1.273
Average a+b	-	713	-	-	881	1.234

Table 5 :Average ultimate shear capacities (3.40 mm nails)

Direction of nail side and nail diameter	Nail number	Predicted value per nail (N)	Predicted value per connector (N)	Resulted value per connector (N)	Resulted value per nail (N)	Resulted/ predicted ratio
3.40 mm	2	982	1963	2065	1033	1.052
(a-ingrain)	4	975	3902	3839	960	0.984
	6	980	5879	5756	959	0.979
	8	985	7877	8171	1021	1.037
	10	973	9725	10132	1013	1.041
Average a	-	979	-	-	996	1.019
3.40 mm	2	957	1913	2170	1086	1.133
(b-across	4	963	3852	4272	1068	1.109
Grain)	6	965	5792	5882	980	1.016
	8	956	7646	8711	1089	1.139
	10	955	9545	11134	1113	1.166
Average b	-	959	-	-	1067	1.113
Average a+b	-	969	-	-	1032	1.065

Table 6 :Average ultimate shear capacities (4.50 mm nails)

Direction of nail side and nail diameter	Nail number	Predicted value per nail (N)	Predicted value per connector (N)	Resulted value per connector (N)	Resulted value per nail (N)	Resulted/ predicted ratio
4.50 mm	2	1518	3035	3447	1724	1.136
	2-predrilled	1852	3705	3728	1864	1.006
(a-ingrain)	4	1555	6220	6383	1596	1.026
	4-predrilled	1847	7388	6784	1696	0.918
	6	1554	9321	9877	1646	1.059
	6-predrilled	1891	11346	10559	1760	0.931
	8-predrilled	1910	15281	15402	1925	1.008
	10-predrilled	1928	19280	18445	1845	0.957
Average a	Non-drilled	1542	-	-	1655	1.074
	Pre-drilled	1886	-	-	1818	0.964
4.50 mm	2-predrilled	1911	3823	3895	1947	1.019
(b-across	4-predrilled	1927	7708	7723	1931	1.002
Grain)	6-predrilled	1923	11539	11372	1895	0.986
	8-predrilled	1954	15633	15437	1930	0.988
	10-predrilled	1885	18850	18599	1860	0.987
Average b	-	1920	-	-	1913	0.996
Average a+b	Predrilled	1903	-	-	1866	0.980

8 Design Recommendations

The following parameters were taken in account for the preparation of the design recommendations for construction of single shear nailed joints: the results of the study for the behavior of the connectors, a characteristic density of 400 kg/m^3 for the timber,

Table 7- Design Recommendation for Single Shear Nailed Connectors

Nail designation	16/60	18/75	20/90
Nail diameter (mm)	2.83	3.40	4.50
Characteristic bending moment $M_{y,k}$(Nmm)	2691	4336	8987
Design bending moment $M_{y,d}$(Nmm)	2446	3942	8170
Embedding strength of timber			
Non predrilled –characteristic $f_{h,1,k}$	24.1	22.7	20.9
Predrilled –characteristic $f_{h,1,k}$			31.3
Non predrilled- design $f_{h,1,d}$	13.0	12.3	11.3
Predrilled –design $f_{h,1,d}$			16.9
Design value for nail shear capacity R_d			
Non predrilled (N)	467	632	1003
Predrilled (N)			1226

γ_m=1.1 for the nails, γ_m=1.3 for the timber and K_{mod}=0.7 for the timber. The design recommendations are summarized in table 7.

9 Discussion and Conclusions

The results of the study demonstrate a good agreement between the lateral shear capacity of nailed, single shear connectors, calculated according to equation 6.2.1 f of Erocode 5, and the lateral shear capacity determined from the experimental investigation. The values obtained for non predrilled specimens were higher than the calculated values (ratios of 1.234 for the 2.8/60 nails, 1.065 for the 3.4/75 nails and 1.074 for the 4.5/90 nails, between experimental and predicted values). However, the ratio obtained for specimens with predrilled 4.5/90 nails, was only 0.980.

Each one of the investigated connectors comprised two, four, six, eight, or ten nails. The experimental shear capacity for a single nail in that range of nail numbers, for each of the nail sizes, was practically independent of the number of the nails in the connector. No bias of the results was observed with the growing number of nails in the connectors.

Two types of connectors were investigated in the study: a- "ingrain connectors" where the two timber cuttings forming the connector (the nailing side and the penetration side), both were loaded along the direction of the grain of the wood (longitudinal connectors); and b- "across grain connectors" where the penetration side of the connector was loaded in the direction of the grain, and the nailing side of the connector was positioned perpendicular to the penetration side and loaded across the grain direction of the wood. The standard does not allow any priority to any of the loading directions in the nailed connectors. However, the experimental results clearly show that the lateral shear capacity of the unites loaded across grain was higher than the lateral shear capacity of the unites loaded along grain. The ratios between the average capacities of the "across grain" and the "ingrain" specimens were 1.065 for the 2.8/60 nails, 1.092 for the 3.4/75 nails, and 1.033 for the 4.5/90 (predrilled) nails.

The study employed nails of standard sizes, and lumber of standard sizes. Thus, the penetration slenderness was maintained for all the cases higher than the minimum value specified in the Eurocode 5 (8d), but was not kept constant for all the nail sizes (13.0d, 10.9d, and 9.8d for 2.8/60, 3.4/75, and 4.5/90 nails respectively). The opinion of the author is that the differences between the experimental and predicted results, may be influenced by the increased penetration slenderness above the required minimum slenderness. The penetration length of the 2.8/60 nails was 1.625 of the required minimum penetration. The

ratio between the average experimental shear capacities and the predicted ones was 1.234. With 3.4/75 nails, the penetration length was 1.3625 of the recommended minimum, and the ratio between the experimental and predicted values was 1.065. Similar results were obtained for the 4.5/90 nails with penetration length of 1.225 of the required minimum, and experimental/ predicted shear ratio of 1.075.

Predrilling was needed to enable safe nailing of the 4.5/90 nails. The calculated shear capacity of the predrilled connectors yielded shear values 1.22 times the calculated values of the non-predrilled connectors. But comparison of the experimental results for the two types of the connectors, shows that the advantage of the predrilled connector was smaller than the expected. The experimental results for the non-predrilled connectors were 1.075 of the predicted. The experimental results for the predrilled connectors were only 0.980 of the predicted. Thus, the advantage of the predrilled connector over the non-predrilled connector was reduced to 1.112. It is suggested by the author, to proceed with further verification of the equations suggested for the prediction of the lateral shear capacity of predrilled nails.

Acknowledgements

The author wishes to thank all the parties who were involved and who assisted him in this study and particularly to the "National Building Research Institute", which enabled him to use the Institute laboratories for the experimental part of this work, to Mr Elhanan Itshak for his assistance in the experiments and data retrieving , and to the "Hod Corporation Ltd", for the funding of part of this work and the supply of the nails and wires used in the research.

References:

[1] Israeli Institution of Standards- Institute specification No 270- "Roofs made from timber trusses", 1990.

[2] Israeli Institution of Standards- Israeli Standard SI 904- "Formwork for concrete", 1995.

[3] Israeli Institution of Standards- Israeli Standard SI 1139- "Scafoldings", 1995.

[4] Eurocode 5: "Design of Timber structures", Part 1.1, DD ENV 1985-1-1 :1994 , General rules and rules for buildings.

[5] International Standard ISO 8375- "Solid timber in structural sizes- Determination of Some physical and mechanical properties, 1985.

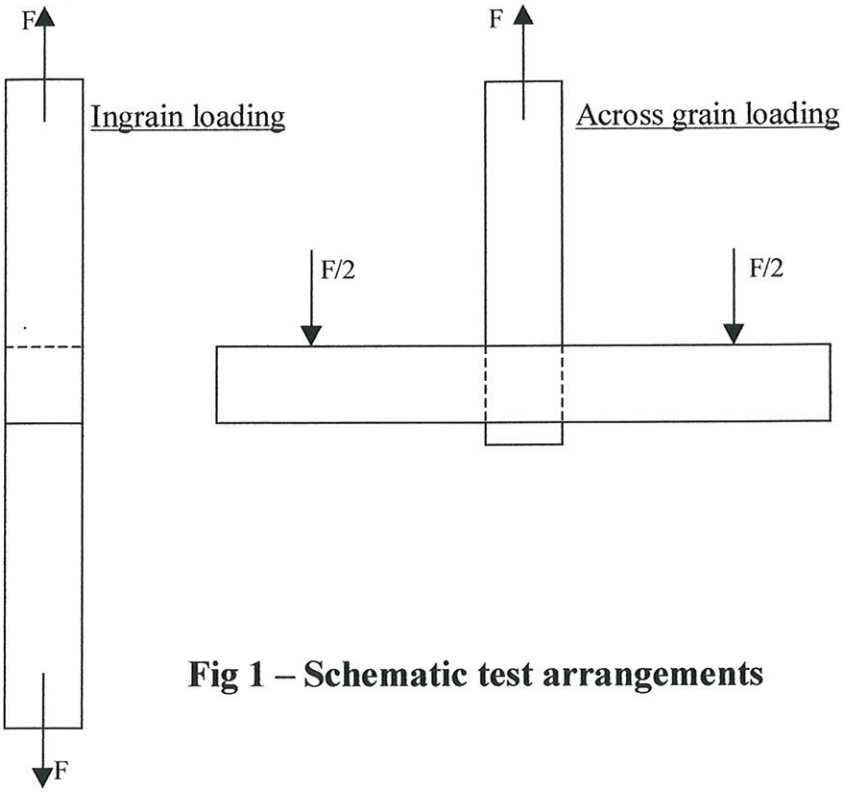

Fig 1 – Schematic test arrangements

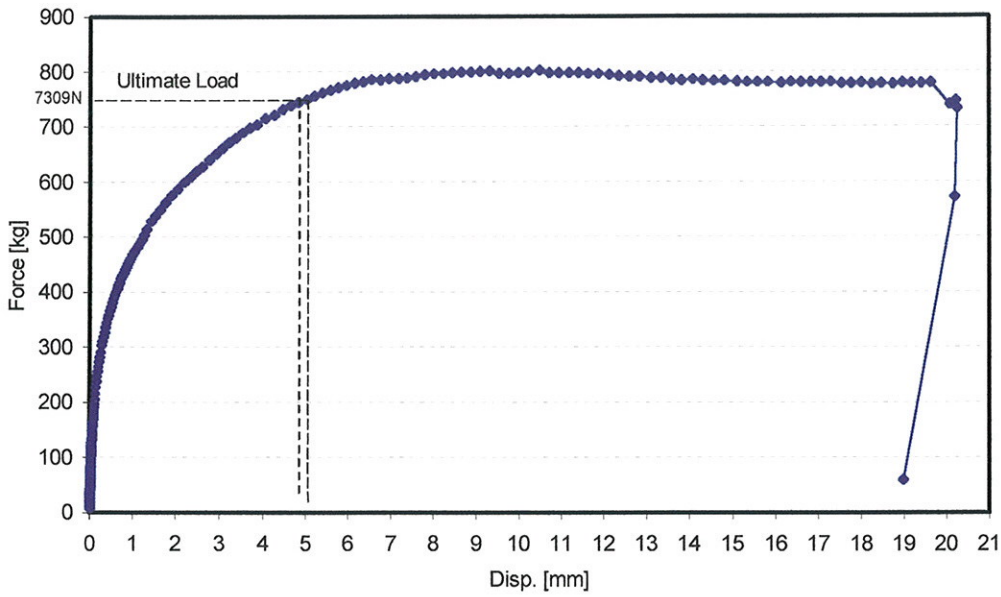

Fig 2- Typical load-displacement curve
(specimen 22102- 8 number , 16/60 nails, in grain)

INTERNATIONAL COUNCIL FOR RESEARCH AND INNOVATION IN BUILDING AND CONSTRUCTION

WORKING COMMISSION W18 - TIMBER STRUCTURES

HEIGHT-ADJUSTABLE CONNECTOR FOR BUILT-UP BEAMS (WITH TIMBERS OR LOGS SERVING AS SPACED LOWER AND UPPER CHORD MEMBERS)

by

Y V Piskunov
Center for Research, Engineering, and Manufacture of Building Structures
Vyatka State Technical University, Kirov

RUSSIA

E G Stern
Department of Wood Science and Forest Products
Virginia Polytechnic Institute and State University, Blacksburg, VA

USA

MEETING THIRTY-THREE
DELFT
THE NETHERLANDS
AUGUST 2000

Not Presented.

· A letter of regret (health issue) was received from E.G. Stern and read to the members. Transparencies were also provided by E.G. Stern and made available for distribution and discussions. H. Blass will provide a letter of reply.

Height-Adjustable Connector for Built-Up Beams (With Timbers or Logs Serving as Spaced Lower and Upper Chord Members)

By
Yurij V. Piskunov
Center for Research, Engineering, and Manufacture of Building Structures
Vyatka State Technical University, Kirov, Russia
and
E. George Stern
Department of Wood Science and Forest Products
Virginia Polytechnic Institute and State University, Blacksburg, VA, USA

Abstract

Because solid timbers and logs of very large cross-section are no longer readily available, the use of composite structural members has become more and more attractive. Where glue-laminated and bonded wood-particle members are not available, mechanically built-up timbers and logs can provide the answer to fulfill local needs and to meet specific requirements.

Built-up composite timber-beam and log assemblies can be parallel-chord beams. Height-adjustable connectors can be used to increase the load-carrying capacity and stiffness of these assemblies by increasing the space between the chord members and, thereby, the height of the beams. These structural assemblies can be used in new structures as well as in reinforcing and repairing existing timber and log structures, particularly where exposure to detrimental environmental conditions resulted in physical deterioration of individual elements or in wall buckling.

Individual elements of built-up beam and log structures can be connected with devices consisting of spacers of given heights attached to flat or curved steel bearing plates, as indicated in Fig. 1. Fasteners are inserted into predrilled holes to connect these devices to the timbers. Short connectors have been known and used for a variety of applications. They serve at times as anchors with fixed or adjustable heights, as shown in the catalogues of building hardware manufacturers and distributors (see Fig. 2). These devices are mainly used to attach timbers to concrete. The benefits of these devices are often limited by their relatively small load-carrying and anchoring capacity and the limited stiffness and rigidity of the assembled structural elements. Furthermore, any decrease in their effective cross-sectional area, resulting from any predrilled holes, often required for fastener insertion, decreases the member strength.

Improved connectors of this type are "nail-plate connectors" (1-10) with flat or curved steel plates with integral pointed nails, spikes, or pins, welded to the plates or driven into tightly fitting plate holes. These fasteners, which cantilever from both plate sides (see Fig. 3), are pressed into the timbers or logs to be connected by these devices to result in mechanically laminated elements. These nail-plate connectors have relatively high load-carrying capacity and stiffness.

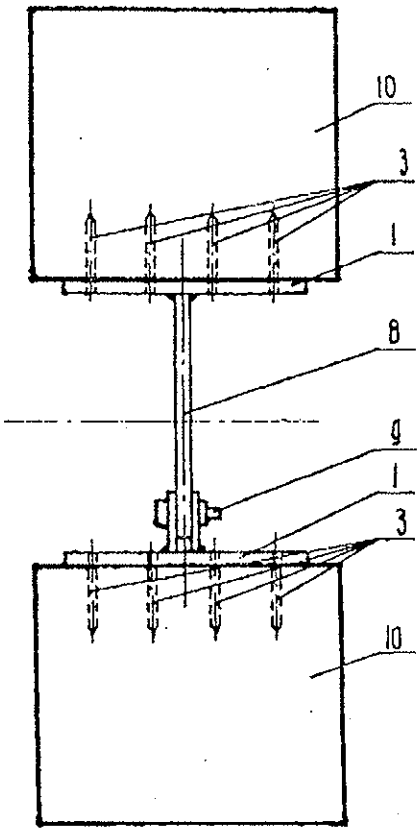

Fig. 1.- Connector for spacing upper and lower chords of built-up timber beam.

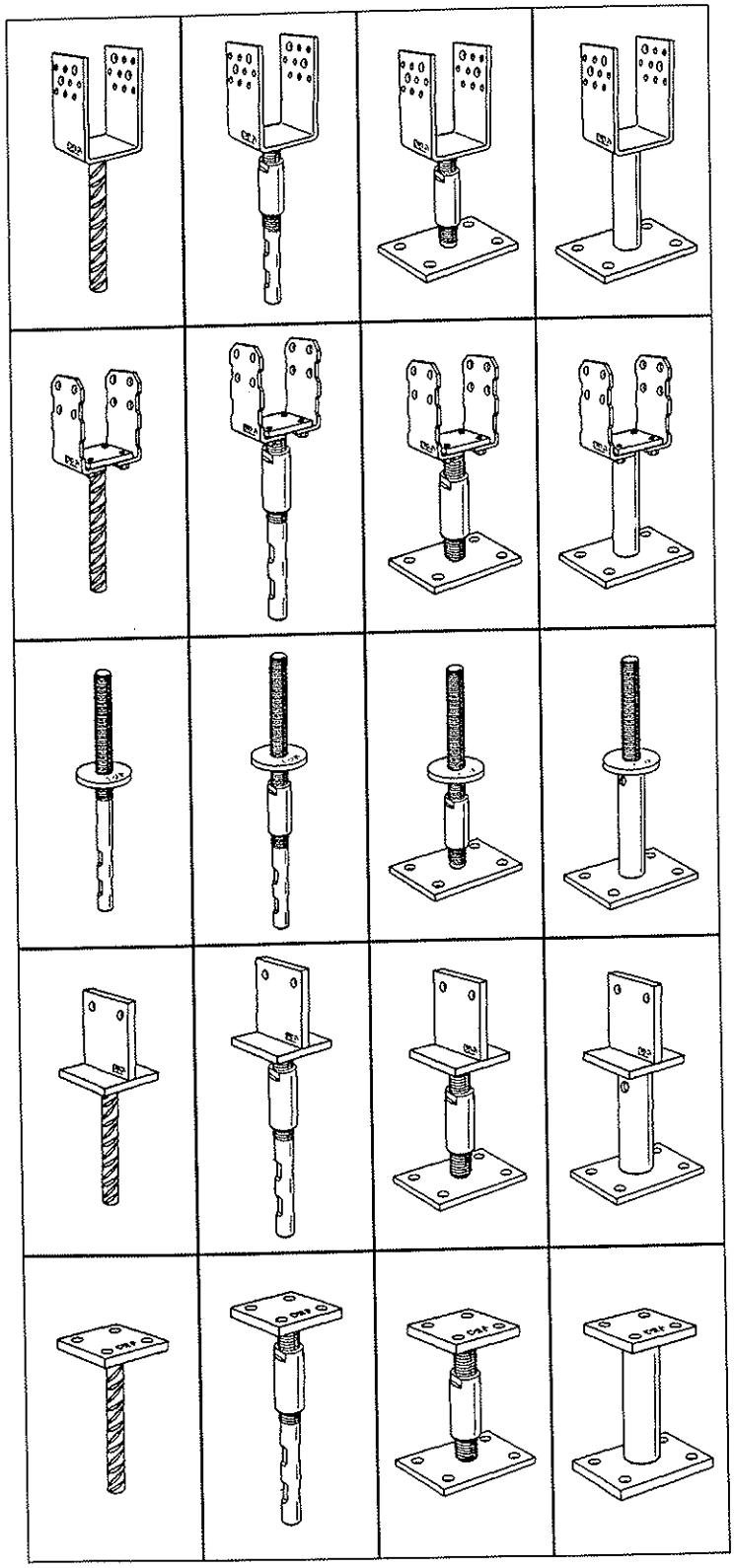

Fig. 2.- Anchors of fixed and adjustable heights for wood structures, as provided by German manufacturer and distributor of building hardware.

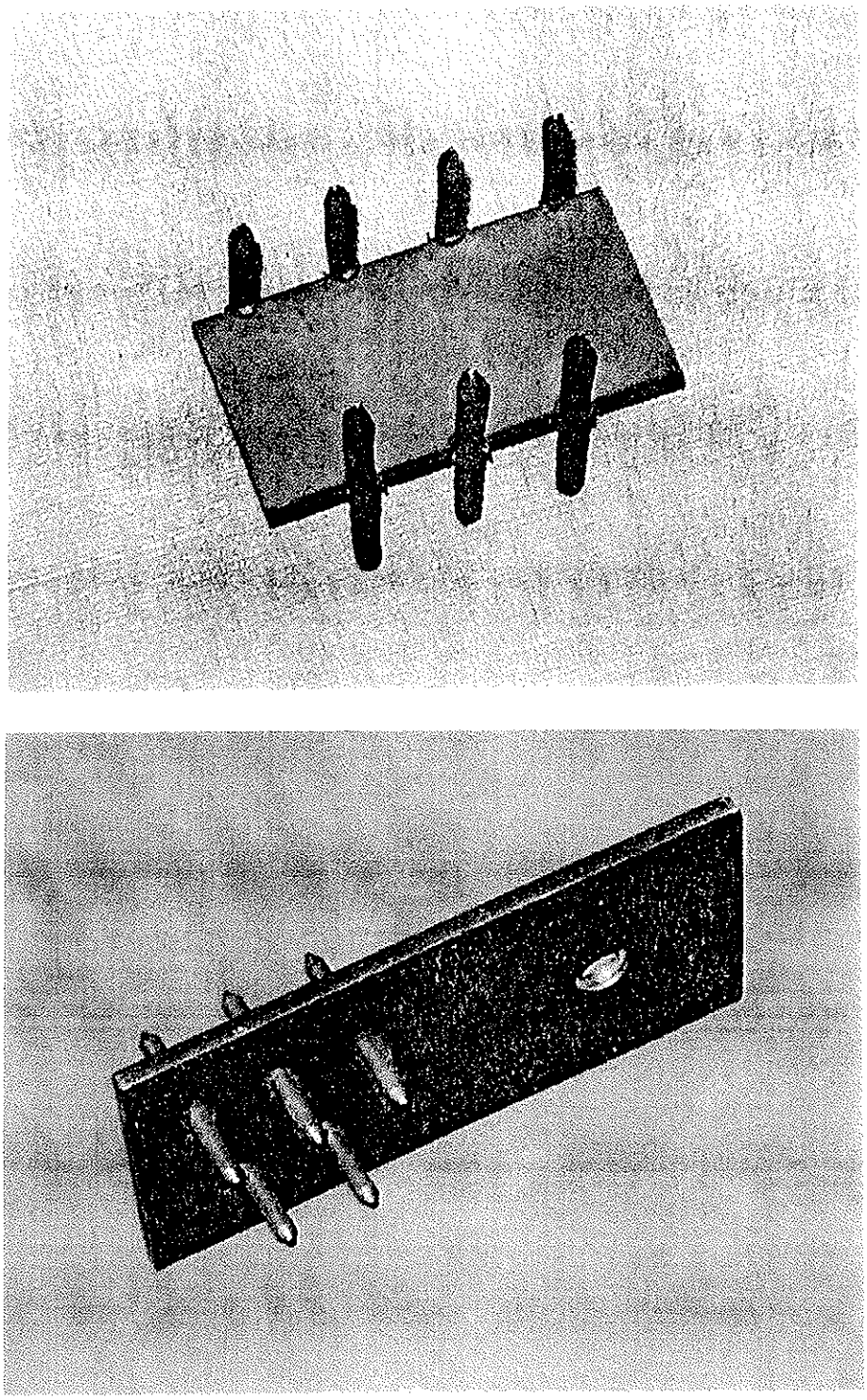

Fig. 3.- "Nail-Plate Connector" with pins welded to the edges of the plate (top) and pressed into tightly fitting plate holes (bottom), cantilevering from both plate sides.

They can be used to produce spaced beams, columns, and log assemblies of high performance. These connectors do not facilitate adjustment to local situations which require exact spacing of the upper and lower chord members of the structural assembly to resist prevailing or potential forces.

The purpose of the novel height-adjusting connecting devices is to provide, in addition to the benefits previously described for nail-plate connectors, adjustability to prevailing local situations by introducing a variable height adjustment (see Fig. 4). This is accomplished by providing the steel bearing plates, which are to be fastened to the timbers or logs, with integral steel screws threaded at their ends in opposite directions and/or with threaded steel couplings. Thus, the space between the timbers or logs can be increased or decreased as required by turning the screws or the couplings in one or the other direction. Variations of the systems involved are depicted in Fig. 5. An application of this system to provide or restore the required structural support to a buckled log wall is shown in Fig. 6.

The reference numbers in Figs. 1, 5, and 6 refer to the individual elements of the connecting devices and connections, as described below:

1 – flat or curved steel bearing plate
2 – integral pointed nails, spikes, or pins cantilevering from both sides of the bearing plates
3 – supplementary nails or spikes
4 –screws threaded at both ends in opposite directions
5 – device or coupling for turning screws
6 – screws cantilevering from bearing plates
7 – elongating or shortening threaded coupling for screws
8 – simulated web members connecting lower and upper chord members, slotted to allow adjustment during installation
9 – bolt for fastening web member to bearing plate
10 – lower and upper chord members spaced by height-adjustable connectors
11 – existing logs or buckled log wall securely attached to newly installed composite structural timber assembly

During assembly of the timber or log structure, the integral nails or spikes are pressed into the timbers or logs by expanding screws being inherent parts of the connectors or by using special-purpose presses. The purpose of these pins is to fix the location of the timbers or logs during the pressing operation as well as to resist shear forces in the assemblies. Supplementary nails, spikes, or pins, as may be needed, can be driven to provide for the transfer of additional forces.

During repair work, the height-adjustable connector ensures that sufficient initial clearance is provided to allow placement of the composite-beam assembly between adjacent elements of the original structure, as is indicated in Fig. 6.

Effectiveness of Height-Adjustable Connector

Tests on the effectiveness of the height-adjustable connectors and built-up Russian pine beams of 7 to 9% moisture content and moduli of elasticity of 800 and 1050 kgf/mm^2 and assembled with these connectors were performed at the Center for Research, Engineering, and Manufacture of Building Structures (CREMBS) at Vyatka State Technical University in Kirov, Russia. The experimental studies, based on the shear-deformation model presented in Fig. 7, included three types of static shear tests described in Figs. 8, 9, and 10. In addition, a full-size built-up pine

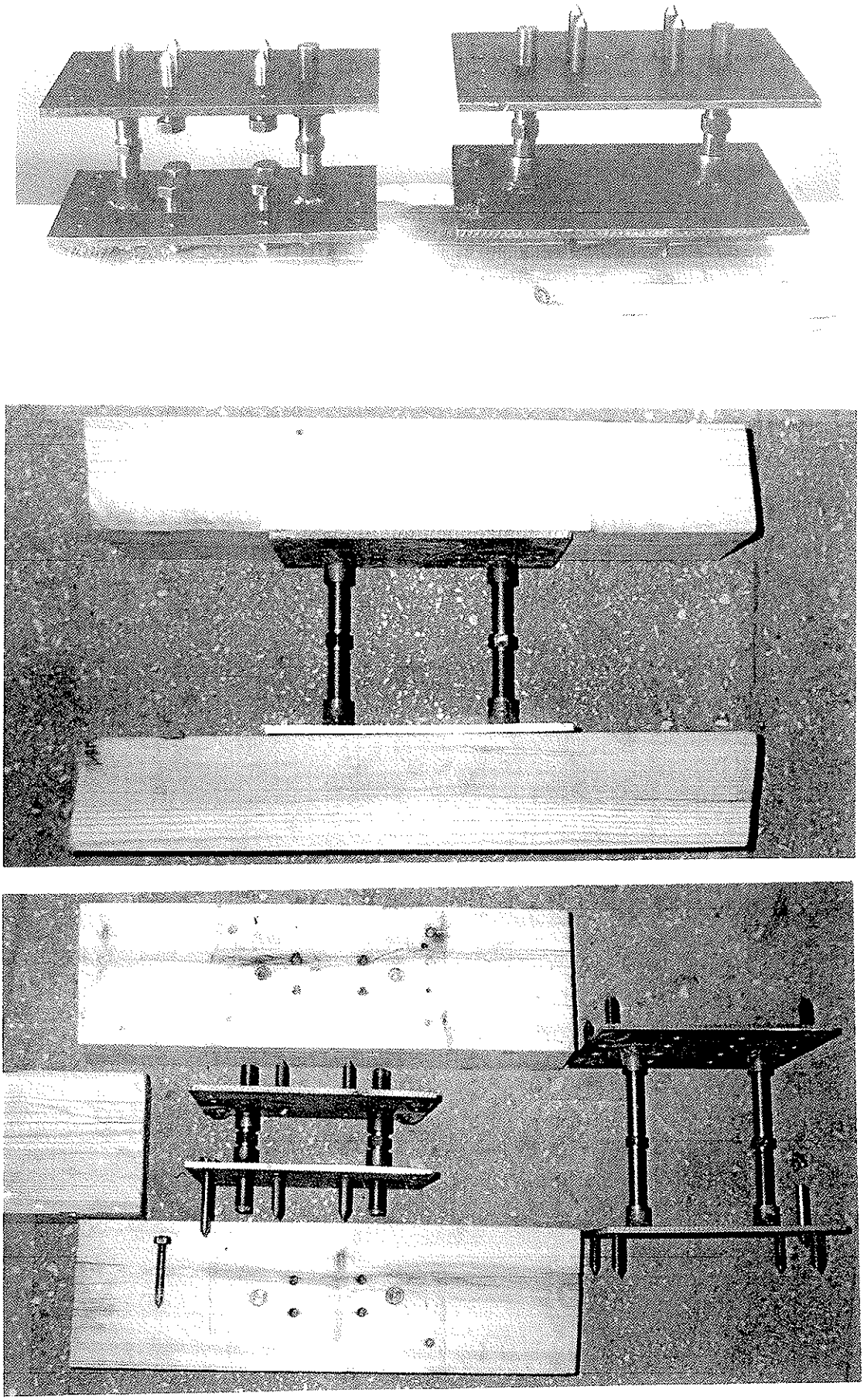

Fig. 4.- Top: Height-adjustable fastener connecting upper and lower chords of built-up beam, with lagscrews (top left) and pointed pins (top right) to fasten connector to chord members. Center: Assembled connection. Bottom: Connection disassembled after testing for deflection of built-up beam.

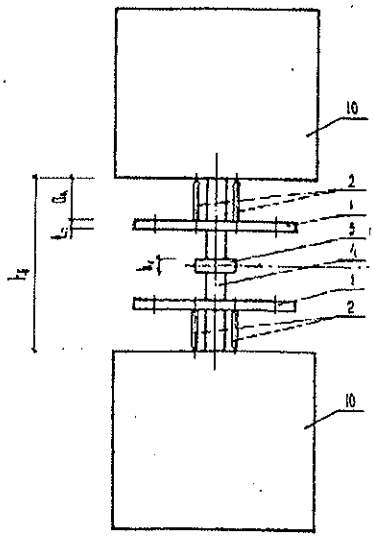

Fig. 5a.- Side view prior to press-assembly.

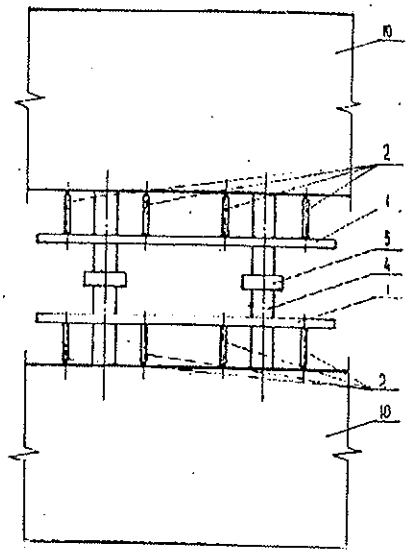

Fig. 5b.- Front view prior to press-assembly.

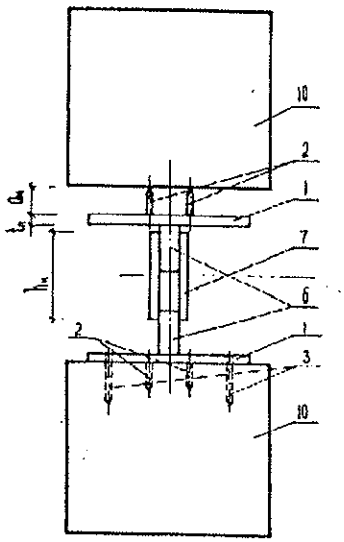

Fig. 5e.- Side view of assembled beam with chords separated by connector provided with threaded coupling to facilitate adjusting of beam height.

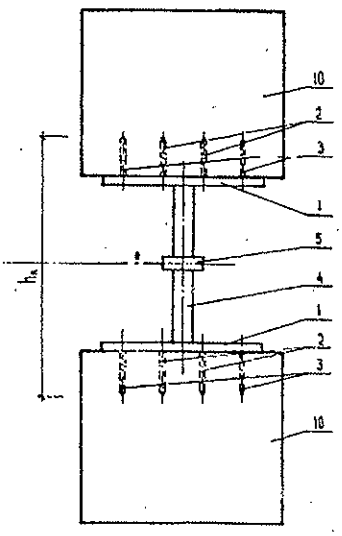

Fig. 5c.- Side view after press-assembly.

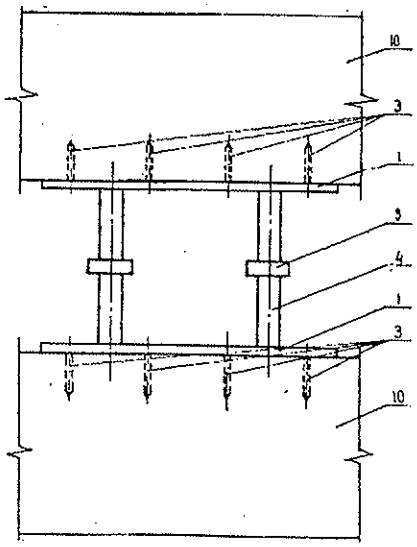

Fig. 5d.- Front view after press assembly.

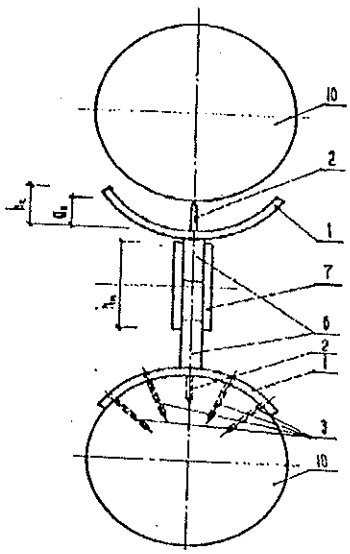

Fig. 5f.- Side view prior to assembly of top and after assembly of bottom part of log-beam element, with logs supported by curved bearing plates.

Fig. 5.- Height-adjustable connectors spacing upper and lower timber chords of built-up beams.

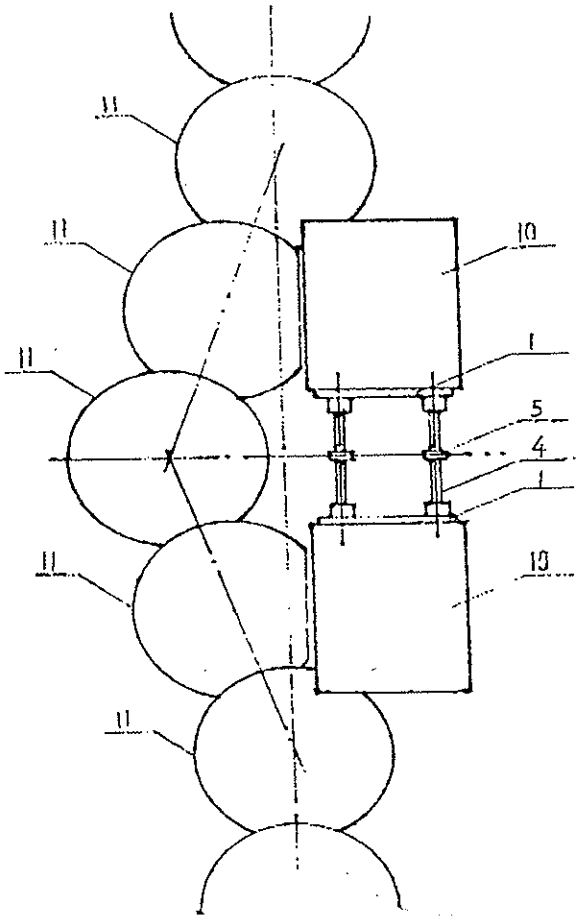

Fig. 6.- Use of built-up beam, with height-adjustable connector spacing upper and lower chords as required, to reinforce buckled log wall during restoration of the Church of The Transfiguration on Kizhi Island, Karelia, Russia.

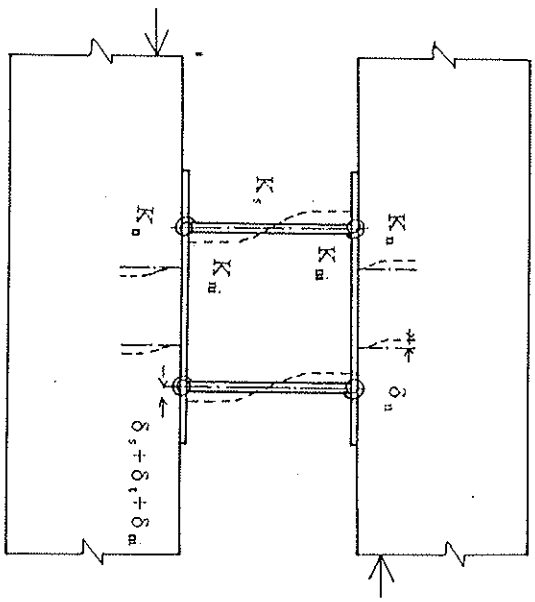

Fig. 7.- Shear-deformation model for connection spacing upper and lower chord members of built-up timber beam.

beam assembled with these connectors was tested statically in flexure. The test results are summarized below:

Shear resistance of fasteners attaching the height-adjustable connector to the pine chord members (Fig. 8).- The total displacements observed for the connections, assembled with five types of fasteners, fully described in Fig. 8 and inserted into predrilled holes, are listed in Table I.

Table I.- Influence of type of fasteners attaching connector to timbers on shear resistance of connection.-

Connector No.	Pin Type	Number of Pins	Pin Diameter mm	Pin Length mm	Test Load kgf	Total Displacement mm, after First Loading	Total Displacement mm, after 3 Subsequent Loadings
1	1	4	12	55+10	500	0.000	0.000
					3000	0.420	0.280
					500	0.220	0.280
2	2	4	14	90+0	500	0.000	0.000
					2500	0.197	0.137
					500	0.135	0.137
3	3	4	14	55+10	500	0.000	0.000
					3000	0.145	0.058
					500	0.070	0.035
4	2+3	8	14	90+0	1000	0.000	0.000
				55+10	6000	0.185	0.097
					1000	0.082	0.092
5	4	4	12	55+10	500	0.000	0.000
					3000	0.260	0.195
					500	0.167	0.187
6	5	4	12	55+10	500	0.000	0.000
					3000	0.180	0.120
					500	0.110	0.120

Additional quadruple cyclic loading tests within the 400 to 1600-kgf loading range were performed on connections with the Type 5 fasteners. The observed average displacements are listed in Table II, with grand-average displacements after 32 loadings and unloadings amounting to 0.082 and 0.074 mm, respectively.

Table II.- Influence of repetitive loading in shear resistance of connection.-

Loading kgf	Averages of Four Readings After Eight Loadings and Unloadings mm							
400-1600	0.106	0.079	0.080	0.077	0.079	0.082	0.077	0.075
1600-400	0.079	0.074	0.078	0.071	0.073	0.074	0.072	0.070

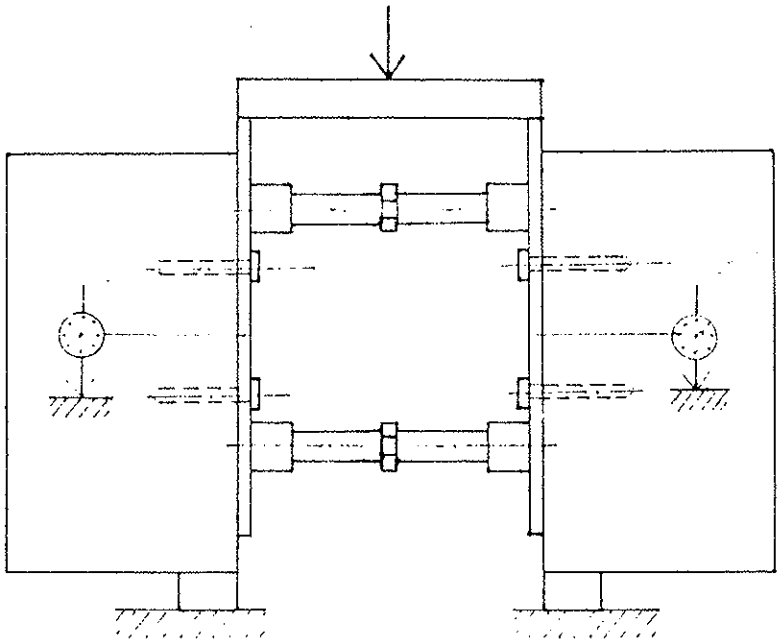

Fasteners Used:

No.	Type	Diameter mm	Length* mm	Shank	Point	Head	Fastened to Bearing Plate
1	1	12	55&10	Plain	Yes	No	In plain holes
2	2	14	90&0	Threaded	No	Yes	In threaded holes
3	3	14	55&0	Threaded	Yes	Yes	In threaded holes
4	2 (50%) 3 (50%)	14	90&0 55&10	Threaded Threaded	No Yes	Yes Yes	In threaded holes
5	4	12	55&10	Threaded	Yes	Yes	In threaded holes **
6	5	12	55&10	Lagscrew	Yes	Yes	In plain holes

* First number: Length of thread. ** in nuts welded to plates.
Second number: length of point and head.

Fig. 8.- Diagrammatic test set-up for determination of shear resistance of fasteners used for attaching the height-adjustable connector to the chord members of the built-up timber beam.

Supplementary shear tests on the ultimate load-carrying capacity were performed on connections assembled with Type 1, 4, and 5 pins. The maximum test loads amounted to 9,000, 9,800, and 9,700 kgf, respectively.

Shear resistance of height-adjustable connectors (Fig. 9).- The total displacements observed for connectors with two adjusting screws of 20-mm diameter and 180 and 130-mm lengths are listed in Table III.

Table III.- Shear resistance of connectors.-

Test No.	Screw Length mm	Loading kgf	Total Deformation During First Loading mm	Total Deformation During Subsequent Loadings mm	Deformation of Screws mm
1	180	400-1600	2.86	2.37	1.86
		1600-400	2.45	2.16	1.86
2	180	400-1600	2.96	2.43	1.86
		1600-400	2.45	2.40	1.86
3	130	400-1600	1.76	1.58	0.70
		1600-400	1.53	1.54	0.70
4	130	600-2600	2.92	2.39	1.17
		2600-600	2.20	2.29	1.17

Shear resistance of height-adjustable connection (Fig. 10).- The total displacements observed for connections consisting of connectors with two integral adjusting screws of 20-mm diameter and 180-mm length and with a total of four fasteners of 12-mm diameter attaching the plates to the timbers, after repetitive loading to 1600 kgf and unloading to 400 kgf, are listed in Table IV.

Table IV.- Shear resistance of connections as indicated by total connection deformation, in mm, and connection rigidity, in kgf/mm, for given loading and unloading cycles.-

Property	Loading and Unloading Cycles											
	1		2		3		4		5		6	
	Def.	Rig.	Def.	Rig.	Def.	Rig.	Deg	Rig.	Def.	Rig.	Def.	Rig.
After Loading	4.42	271.5	3.86	310.9	3.44	348.8	3.25	269.2	3.24	370.4	3.18	377.4
After Unloading	2.80	428.6	2.95	406.8	2.46	487.8	2.44	491.8	2.72	441.2	2.69	446.1

Effectiveness of a built-up timber beam assembled with height-adjustable connectors (Figs. 11 and 12).- According to preliminary tests performed on 165 x 140-mm beams, to serve as chords for the built-up beam, spanning 4.0 m and loaded at mid-point, the top and bottom chords exhibited moduli of elasticity of 800 and 1050 kgf/mm^2. The total deflections at the center of the built-up beam, spanning 4.0 m and loaded at mid-point, with height-adjustable connectors and Type 5 fasteners placed 600 mm from the beam supports and at the beam center, as shown in Fig. 11, are given in Table V for the first loading up to 1000 kgf and subsequent loadings up to 800 kgf. The grand-average deflections after the first loading amounted to 11.6 mm and that after the subsequent loadings amounted to 9.1 mm.

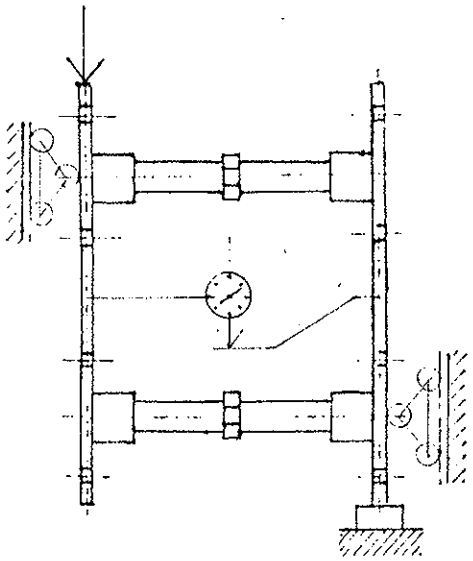

Fig. 9.- Diagrammatic test set-up for determination of shear resistance of two screws used for adjusting distance between upper and lower chord members of built-up timber beam.

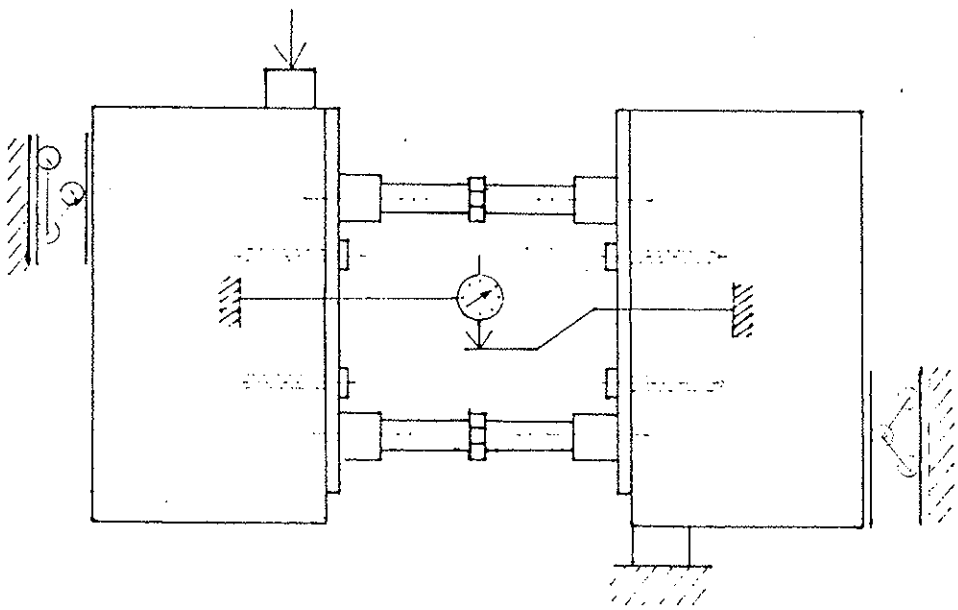

Fig. 10.- Diagrammatic test set-up for determination of shear resistance of height-adjustable connection spacing upper and lower chord members of built-up timber beam.

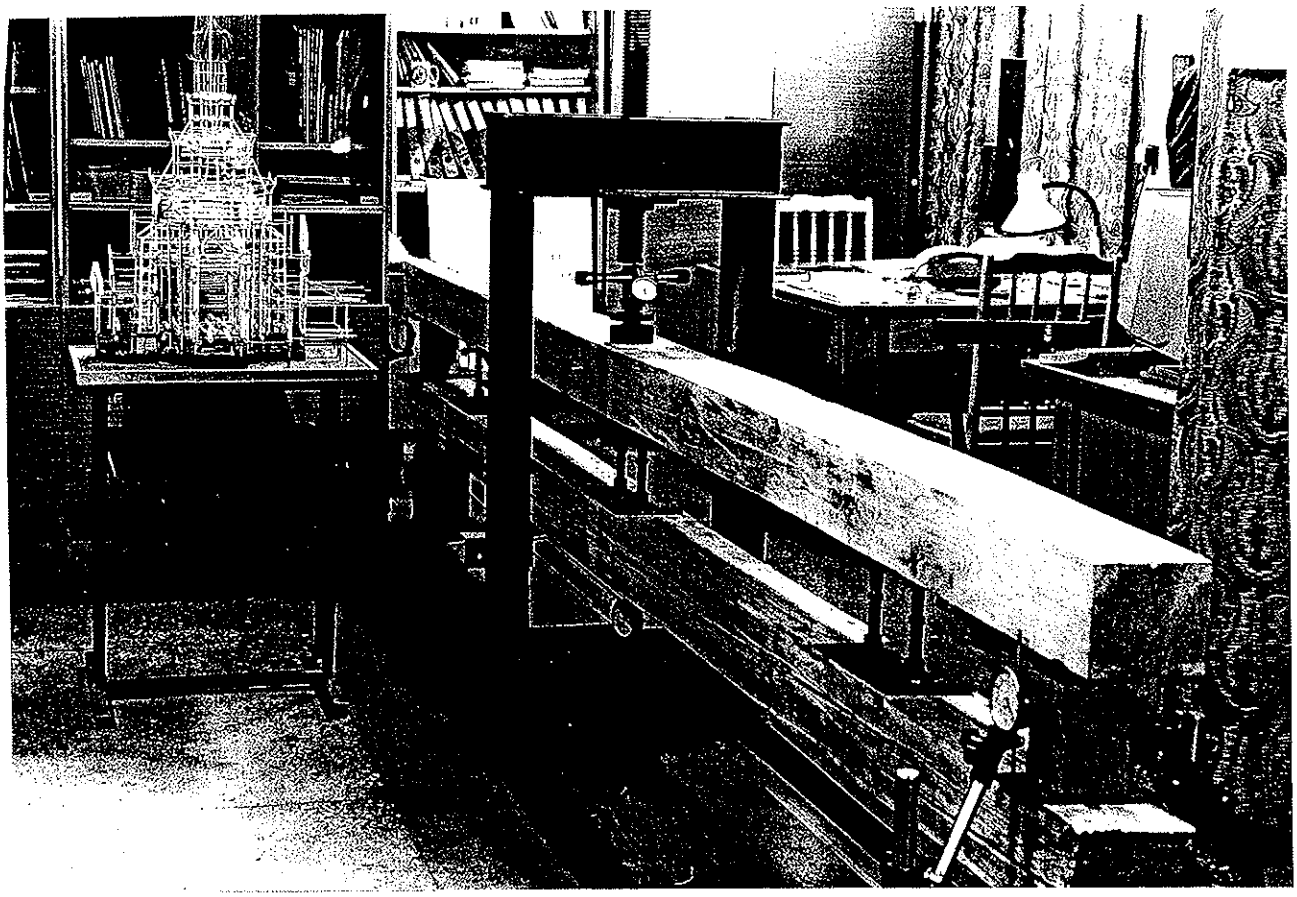

Fig. 11.- Test set-up for determination of effectiveness of built-up beam with upper and lower timber chords spaced by height-adjustable connectors located at intermediate points.

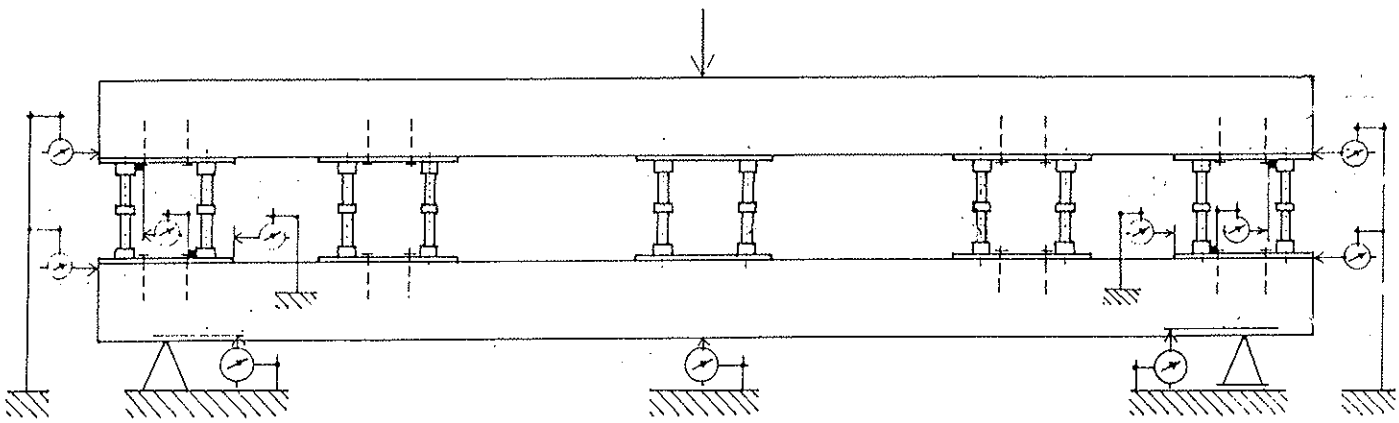

Fig. 12.- Diagrammatic test set-up for determination of effectiveness of built-up beam with upper and lower timber chords spaced by height-adjustable connectors throughout length of beam.

Table V.- Shear resistance of built-up beam as indicated by its deflection, in mm, after loading and unloading.-

	Loading and Unloading Cycles					
	1	2	3	4	5	6
After Loading	12.35	11.14	11.15	11.95	11.09	12.02
After Unloading	8.9	9.2	9.0	9.2	8.9	9.3

During a subsequent test on the same built-up beam with height-adjustable connectors placed between the chord members also above the beam supports, as shown in Fig. 12 (instead of the blocks shown in Fig. 11), the deflections of the center of the beam during repetitive loading from 250 to 1000 kgf were observed and are listed in Table VI. The grand-average deflections during the nine loading cycles amounted to 7.5 mm.

Table VI.- Shear resistance of built-up beam as indicated by its deflection, in mm, during nine loading cycles.-

	Loading Cycles								
	1	2	3	4	5	6	7	8	9
After Loading	7.28	7.57	7.85	7.84	7.65	7.65	7.68	7.35	7.51

Summary.- Design of Built-Up Beams Assembled with Height-Adjustable Connectors

To facilitate the preliminary design of the height-adjustable connectors located between the upper- and lower-chord members of the built-up beam, the following dimensions can serve as a basis for the initial calculations:

(1) For height-adjustable screws: 24-mm diameter.
(2) For pointed pins attaching the connectors to solid wood: 6-mm diameter.
(3) For threaded pins inserted into predrilled holes in the timbers and logs: 12-mm diameter.

When designing the height-adjustable connectors, determine:

(1) The number of fasteners to attach connectors to timbers and logs by giving consideration to the shear-load transmission capacity of the fasteners in the chord members and that of the height-adjustable screws;
(2) The required distance between the chord members and the length of the height-adjustable screws;
(3) The size of the flat or curved bearing plates by giving consideration to
   a) the minimum distance in the wood between the fasteners attaching the connectors to the timbers and logs (in the direction parallel to the wood grain, use 12 diameters for fasteners driven into solid wood and 6 diameters for fasteners driven into predrilled holes; in the direction perpendicular to the wood grain, use 4 and 3 diameters, respectively);
   b) the minimum edge distances in the wood (same as above);
   c) the load-bearing capacity of the wood in contact with the plate;
   d) the width of the chord members (if their width is smaller than that required according to previous calculations, fasteners of smaller diameters may have to be selected).

Ultimately, in all instances, local code requirements are governing and need to be met.

References Cited

(1) Piskunov, Yurij V. 1988. Recommendations for the Design and Manufacture of Wood Construction Elements with Fasteners of Plates with Cylindrical Dowels (in Russian), 77 pages. Vyatka State Technical University, Kirov, Russia.

(2) Piskunov, Yurij V. 1993. Fastening Element and Its Modifications. SU Patent No. 1201449A (in Russian). Also, Device for Fixing Nails to Connect Timber Elements and Methods of Connecting. SU Patent No. 1689540A1 (in Russian). Also, Timber Building Element. SU Patent No. 1705522A1 (in Russian).

(3) Piskunov, Yurij V. 1993. Scientific and Technical Problems of the Nail-Plate Usage for Manufacturing Building Timber Structures. Proceedings of International Council for Building Research Studies and Documentation (CIB) Conference on Design and Construction of Timber Structures Assembled with Metal Connector Plates and Nail Connectors, Kirov, Russia, pp 36-47; 187-204 (in English: Dept. of Wood Science and Forest Products, VPI&SU, Blacksburg, VA, USA; and in Russian: Center for Research, Engineering, and Manufacture of Building Structures, Vyatka State Technical University, Kirov, Russia.

(4) Kovalchuck, L.M., S.B. Turkowski, Y.V. Piskunov, Y.A. Varfolomeer, and S.L. Kovaltchuck. 1995. Timber Structures in Building Construction (in Russian), 246 pages. Stroyizdat (Building Construction Publisher), Moscow, Russia.

(5) DeGroot, Klaas W. 1995. Nail Element and Method for Its Manufacture. US Patent No. 5,391,114.

(6) Piskunov, Yurij V. 1995. Some Aspects of Nail-Plate Connector Applications in Building Construction. Proceedings of CIB-W18-TG6 International Workshop on Significant Research on Structural Wood Connections, Delft, The Netherlands, pp 142-153. Dept. of Engineered Wood Construction and Building Construction, University of Karlsruhe, Karlsruhe, Germany.

(7) Platt, R. Terry, and Joseph R. Loferski. 1995. Preliminary Examination of a Nail-Plate Connector for a Ready-to-Assemble Housing System. Ibidem, pp 154-162.

(8) Platt, R. Terry. 1997. Ready-to-Assemble Wood Construction System. U.S. Patent Application Serial No. 08-788, 990 of January 27, 1997.

(9) Piskunov, Yurij V. 1997. Concepts of Repair, Restoration, and Reinforcement Systems of the Church of The Transfiguration on Kizhi Island, Karelia, Russia. Proceedings of Workshop and Conference on Preservation of Russian Antiquities, Its Impact on Russia's Rejuvenation, St. Petersburg-Moscow, Russia, pp 47-55. Dept. of Wood Science & Forest Products, VPI&SU, Blacksburg, VA, USA.

(10) Platt, R. Terry. 1998. The Development of Ready-to-Assemble Construction System, 210pp, Ph.D. Dissertation, Dept. of Wood Science & Forest Products, VPI&SU, Blacksburg, VA, USA.

INTERNATIONAL COUNCIL FOR RESEARCH AND INNOVATION
IN BUILDING AND CONSTRUCTION

WORKING COMMISSION W18 - TIMBER STRUCTURES

ENGINEERING DUCTILITY ASSESSMENT FOR A NAILED SLOTTED-IN STEEL CONNECTION IN GLULAM

by

L Stehn

H Johansson

Division of Timber Structures, Luleå University of Technology

SWEDEN

MEETING THIRTY-THREE
DELFT
THE NETHERLANDS
AUGUST 2000

Presented by: L. Stehn

· H.J. Larsen questioned the research philosophy because codes should penalize brittle joints by assigning larger γ values relative to those for ductile joints. The evaluated joints in this study were already ductile because they were defined under the Johansen yield theory. He also questioned the need to jump to a new definition of ductility measures. Finally H.J. Larsen commented that there should be no need to conclude with more testing.
· H. Blass asked for the reasoning behind definition of engineering ductility.
· L. Stehn responded that there was a need to show the degree of ductility even with ductile connectors. The engineering ductility definition was reasoned to relate to effective thickness of the wood needed to be mobilized for ductile behaviour.

Engineering ductility assessment for a nailed slotted-in steel connection in glulam

Lars Stehn and Helena Johansson
Division of Timber Structures, Luleå University of Technology, Sweden

Abstract

The aim with the paper is to characterize a suitable ductility measure based on the displacement of a timber joint. The ductility measure should be convenient for an engineer allowing for a direct comparison between different types of joints. If possible, this approach might later be useful when incorporating safety reasoning for ductile failure modes through adapted γ_m factors. Based on the plasticity theory for dowel type fasteners, theoretical reasoning and experimental results, an engineering ductility model of a slotted-in steel plate type connection is proposed. The connection consists of two 2 mm slotted-in steel plates with 97 x 3.7 mm^2 shot-through nails in glulam. The model is based on "engineering" parameters and estimates the relative ductility, D_e, from the slenderness ratio, $\lambda = t/d$, timber density, ρ_k, and the fastener yield strength in bending, $f_{y,k}$: $D_e = \lambda\,[\rho_k/(4.1\ f_{y,k})]^{1/2}$.The analytical model predicts reasonably well available experimental results for comparable joints.

1 Introduction

Steel truss and concrete frame systems for industrial buildings, indoor sport arenas, and warehouses etc. dominate the Swedish market. Timber frame systems have a market share of only 5%. A research and development project was initiated as a joint industrial-university initiative. The project is founded on the thought to develop a complete glulam truss system for buildings with a span ≈ 25-30 m. No such system exists in Sweden today but several types are available on the European market.

The starting point for the development of the building system is a methodical investigation of an effective connection system. For this purpose, a joint with slotted-in steel plates and shot through nails was investigated. Systems considerations and capacity tests were performed on glulam medium size specimens, Johansson and Stehn (2000). The aim of this paper is to evaluate the test results from the viewpoint of an engineering characterisation of ductility. A suitable ductility measure based on the displacement of the joint, without direct information of the load-displacement behaviour, will be useful to an engineer for a direct comparison between different types of joints.

1.1 Concurrent connection design

The glulam manufacturer/supplier production costs were major decision constraints for the connection design. The connection design must allow accurate manufacturing methods where the connections can be fabricated using tools and methods that justify the investments necessary for the manufacturer. For instance, fast manufacturing points to a solution where connections needing precision should be avoided. This means that bolts/dowels are not chosen since they need a high degree of precision to mobilise the necessary load-bearing capacity, Mischler (1998).

A nailed connection solution yields constraints on the load carrying capacity. The aim is systems with a span 25-30 m that for a medium-term snow load on the roof of 2.5 kN/m^2 leads to a possible tension force of 700 kN. For nailed connections this might lead to problems with premature brittle shear-plug failures, Kangas and Vesa (1998), if too many nails must be used to transfer that load.

The reasoning above leads to the following connection design: a joint with slotted-in steel plates and shot through nails using customary tools (nailer and production machinery) and inexpensive and production tolerant nails and steel plates.

2 Ductile connection design

2.1 Ductility considerations

The design equations for dowel-type fasteners in section 6.2 in Eurocode 5 (EC5) are based on the plastic theory in Johansen (1949). The load-carrying capacity, R_k, per shear plane of a dowel-type fastener in a timber-to-steel joint with inner thin or thick steel plates is determined by:

$$R_k = \min\begin{cases} f_{h,k} dt_{eff} & t_{eff} = t \cdot 1 & \text{mode I} \\ f_{h,k} dt_{eff} & t_{eff} = t \cdot \left(\sqrt{2 + 4\frac{M_{y,k}}{f_{h,k} dt^2}} - 1 \right) & \text{mode II} \\ f_{h,k} dt_{teff} & t_{eff} = 2\sqrt{\frac{M_{y,k}}{f_{h,k} d}} & \text{mode III} \end{cases} \quad (1)$$

here t is the minimum of timber member thickness and fastener embedded length, $f_{h,k}$ the embedding strength, d the diameter and $M_{y,k}$ the yield moment (plastic bending resistance) and t_{eff} the effective thickness (minimum embedded length with constant embedding stresses).

During the years, various experimental investigations have shown the applicability of the plasticity theory, recent investigations on slotted-in steel plate joints are Pedersen et al. (1999) and Siem (1999), and the limitations of the plasticity approach e.g. brittle failure modes and multiple fastener joints of stout dowels Blass and Ehlbeck (1998).

A premature brittle failure reduces the load-carrying capacity of the joint why a ductile failure of the joint must be preferred. Still, the fasteners reach their ultimate resistance only after significant plastic deformations of the dowel that may exceed the embedding capacity. An increased ductility will result in a semi-rigid behaviour and a lower probability for premature brittle failures to occur (higher level of safety).

Methods to promote the design of more ductile connections are found in Blass et al. (1999). Several joint design approaches are possible to achieve a type III failure mode

- **Dowel geometry**. High λ ratios, slender fasteners, should be used to reduce the tendency of premature splitting. Dowels with a rougher surface increase the ductility through a more developed friction, Siem (1999). Increased friction allows a higher degree of plasticity that contradicts the splitting tendency perpendicular to the grain.
- **Dowel spacing.** Minimum requirements for spacing among the fasteners and the timber member thickness/fastener embedding length has (at least) to be met and also be *adapted* to the combined effect of the timber properties, the strength of the dowels and also the type of connection used, Mischler (1998) and Haller (1998).

However, promoting ductile connections will probably both lead to a decrease in load-carrying capacity and an increase in total deflections of the structural system. Both effects must be regarded as negative for practical design using the current codes. So to reach the target of a strong and ductile connection, ductility should be rewarded in the codes. An interesting approach could therefore be to require larger safety for brittle failures and less for ductile failure modes, i.e., adapted γ_m factors in combination with a k_{mod} factor, as presented by Blass et al. (1999).

2.2 Engineering ductility assessment

Despite the fact that a failure is characterised as ductile or brittle no accepted definition of ductility is available. In Racher (1995) the ductility is defined as the relative deformation capacity associated with the maximum load (load-bearing capacity):

$$D_u = \frac{u_u}{u_y} \tag{2}$$

Here u_u is the deformation corresponding to the maximum load and u_y the "elastic" deformation, see definitions in figure 4a. Racher (1995) also proposes that ductility affects the structure reliability in a positive way and proposes a linearly decreasing γ_m value with increasing D_u values. In Mischler (1999) a similar expression is used where u_f, the deformation associated with the final failure, is used instead of u_u.

Siem (1999) investigates, in an extensive study of joints with slotted-in steel plates and dowels, the statistical validity of different interpretations of ductility. For inner thick steel plates Siem found, using a probabilistic analysis, that the definition of D_u was statistically significant and increasing when the slenderness ratio increased from $\lambda = 2.1$ to $\lambda = 8.3$ (increasing t from 25 to 100 mm).

The "engineering" ductility is proposed, in accordance with D_u, as the ratio of actual timber member thickness to the effective thickness t_y.

$$D_e = \frac{t}{t_y} \tag{3}$$

Let t_{eff} required for mode II failure to occur represent the "elastic" deformation u_y. This corresponds to mode I failure on the limit to mode II failure where the "elastic" embedding strength $f_{h,k}$ is evaluated. The effective thickness can be derived by equalling the load-carrying capacities for mode I and II in equation (1)

$$t_y = \sqrt{\frac{2M_{y,k}}{df_{h,k}}} \tag{4}$$

A motivation for equation (3) is expressed by the following example. Consider a case with two geometrically similar connections (A and B). Both has the same timber properties and

same timber member thickness t_D, but the fastener yield strength in bending for connection B is 50% of connection *A*. With the exception of an initial elastic ductility it can be noted that the ductile behaviour starts when the failure mode changes from I to II, i.e., at t_y. From this definition it can be seen that connection *B* has to be more ductile since it "enters" the ductility regime (mode II and III) "earlier" than connection *A* since $t_{y,B} < t_{y,A}$. The ductility representative for connection B should be larger than connection *A* which it is by using equation (3): $D_{eB} = t_D/t_{y,B} > D_{eA} = t_D/t_{y,A}$.

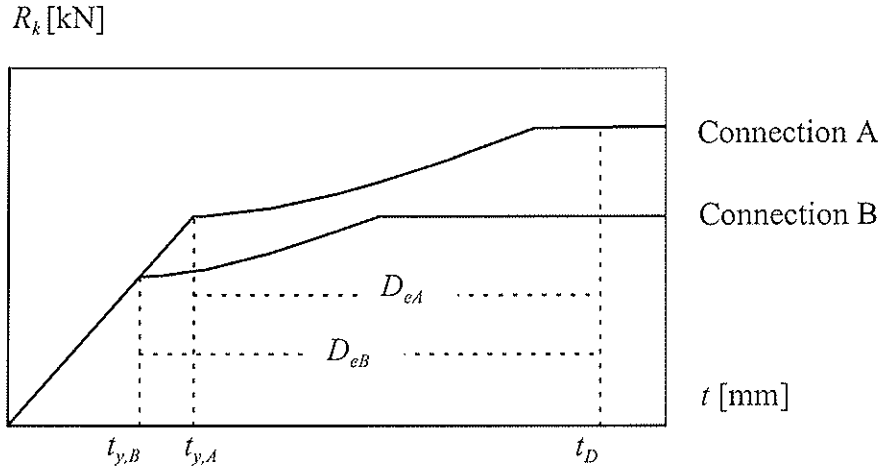

Figure 1: Proposed interpretation of ductility viewed in a R_k, versus t plot.

A lower minimum value, D_0 (initial elastic ductility), and upper maximum value (above which u_u is constant) sets the limit for D_u. Using equation (3) and (1) a mode I failure is obtained for $D_e \leq 1$ and a mode III failure for $D_e \geq 2.82$. This is theoretically displayed in figure 2.

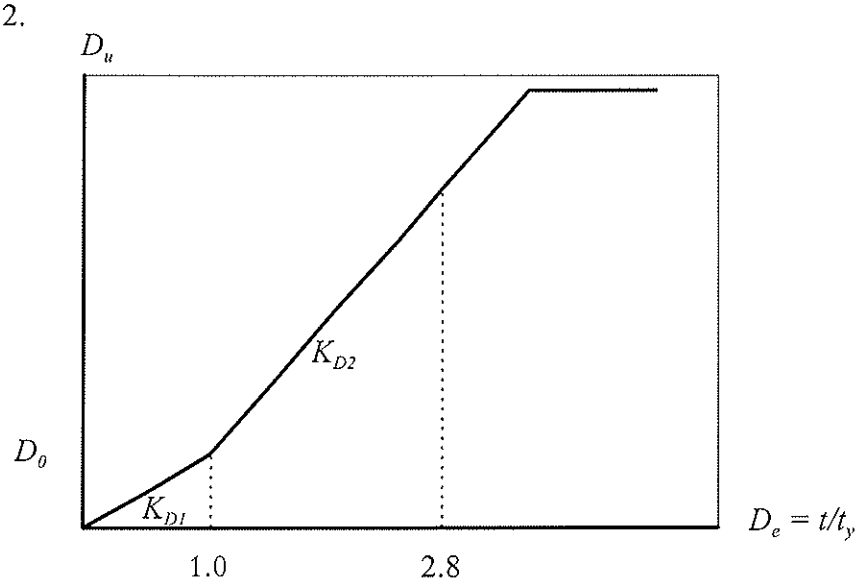

Figure 2: Proposed ductility model for joints with slotted-in steel plates.

The ductility can thus be expressed as:

$$D_u = D_0 + K_{D2} \cdot D_e \tag{5}$$

The values for D_0 and K_{D2} are dependent on the type of connection and must be experimentally validated. If proper statistical and structure reliability investigations are performed D_0 and K_{D2} could be associated to a safety level and used in combination with γ_m and k_{mod} factors as discussed above.

Using the definitions of embedding strength, without predrilled holes and the yield moment in EC5 in equation (4) gives:

$$t_y = 2.02\sqrt{\frac{f_{y,k}}{\rho_k}} \cdot d \tag{6}$$

Included in equation (6) is an assumption of a required minimum steel wire strength $f_{y,k}$ = 600 MPa in bending with a strain hardening effect that is reduced with increased nail diameter as $f_{y,k}(1-\alpha d)$. Incorporated in the parameter α is the strain hardening and, in a more arbitrary way, the effect of the large variability in wire strength since the quality control in practice is minimal. In equation (6) an estimation is made for nails with $3 < d < 5$ mm (relevant for this study) and $0.05 < \alpha < 0.09$, with α interpreted from Larsen and Riberholt (1999) and Ehlbeck et al. (1990). Using equation (6) in equation (3) yields

$$D_e = \frac{t}{2.02d} \cdot \sqrt{\frac{\rho_k}{f_{y,k}}} = \lambda\sqrt{\frac{\rho_k}{4.1 f_{y,k}}} \tag{7}$$

In practise, an optimisation model is necessary to design ductile connections with as high capacity as possible. This model should at least take the two items on page 3 into account.

3 Experimental study

3.1 Test set-up and specimens

Medium size joints in glulam (spruce) were tested in tension parallel to the grain according to figure 3. The joint consisted of two steel plates 2 mm thick in 2.2 mm slots with nails d = 3.7 mm and length 97 mm driven through the wood and the steel plates with a pneumatic nailer. The investigation comprised one series of fifteen specimens with 10 nails in each specimen. The nail pattern shown in figure 3 was chosen to avoid shear plug failure and end distance effects. The timber member cross section was 90 × 180 mm^2 from glulam of the Swedish strength class L40 (corresponding to GL32 in EC5). The steel plates were 2 × 180 × 400 mm^3 with $f_{y,k}$ = 355 MPa reported by the steel manufacturer.

The specimens were tested in a moisture condition resembling actual manufacturing conditions for the joints. The joints were assembled and tested immediately after the glulam was taken from manufacturing plant. The tests were conducted according to ISO 6891 with a time to failure between 8 and 15 minutes. The servohydraulic testing machine was a DARTEC system with a maximum load of 600 kN and a maximum error of 1 % over the entire range. Displacements were measured during the tests by transducers (LVDT, 0 - 50 mm, Vishay) placed centrally in the joint region. Data was sampled with a frequency of 2 Hz.

The yield moment was determined according to EN 409 and the yield limit according to EN 10002. The sample size was 20 nails and the tests were performed at Karlsruhe University. The yield moment, $M_{y,k}$, of the nails was determined to 18.7 Nm with a standard deviation of 0.335 Nm

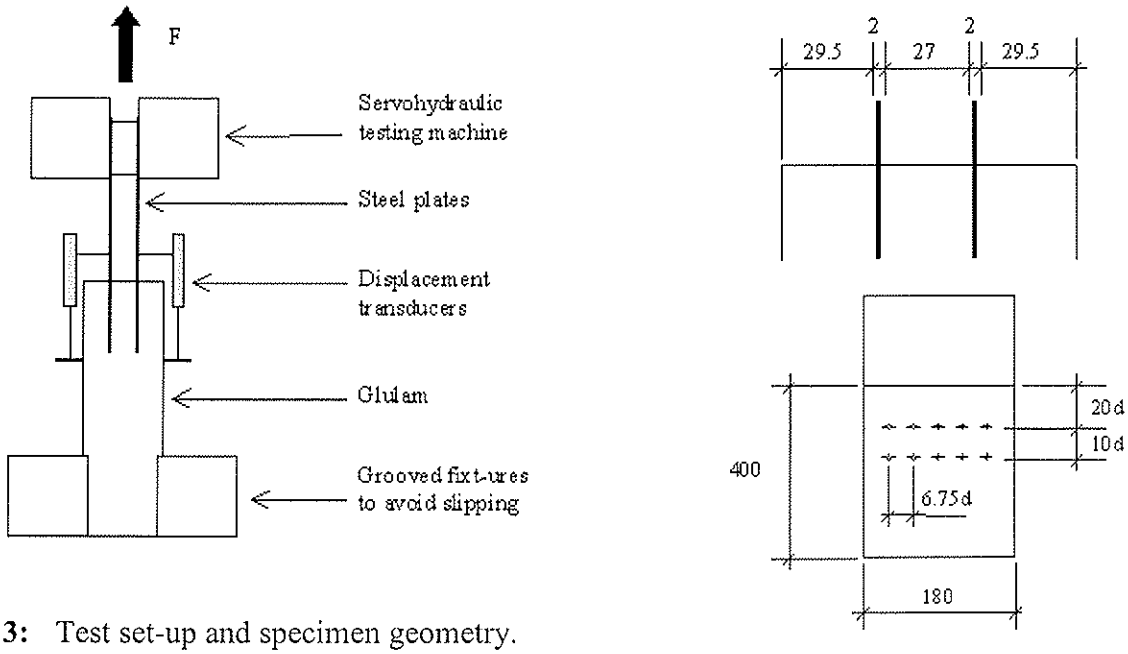

Figure 3: Test set-up and specimen geometry.

3.2 Results and analysis

Table 1 presents the resistance and deformation values for the test series where F_u (kN/nail) is the maximum load and u_u is the corresponding deformation. The final displacement u_f is defined as the displacement where splitting in the wood occurs. In all specimens yielding of the nails occurred prior to splitting and thus $u_f > u_u$. The stiffness K_1 and K_2 were determined by linear regression to the linear parts of the load-displacement curve. D_u is the ductility according to equation (2). The definitions of these values are found in figure 4.

The conventional density and the moisture content of the wood were determined according to ISO 3131 and ISO 3130 immediate after the joints were tested. Measurements were made on four samples from each of the joints, one sample from each lamella, a grand total of 48 samples. The size of the samples were 40 × 40 × 40 mm^3.

Table 1: Results from medium-scale tests.

No.	Capacity, F_u [kN/nail]	Density, ρ [kg/m^3]	u_y [mm]	u_u [mm]	u_f [mm]	Ductility D_u	Moisture content [%]	Pith distance [mm]
1	8.84	-	-	-	-	-	-	-
2	8.99	403	0.54	4.2	15	10	11	24
3	8.34	418	0.36	5.2	5.6	15	11	23
4	9.97	441	0.31	8.3	9.9	-	11	25
5	8.41	426	0.42	2.2	5.0	6	11	23
6	8.35	434	0.34	5.8	6.5	20	10	24
7	8.52	421	0.32	5.3	8.8	21	10	22
8	8.43	-	-	-	-	-	-	-
9	7.95	440	0.26	3.3	5.0	13	11	29
10	8.43	410	0.34	3.8	5.8	12	10	27
11	8.17	444	0.35	3.7	6.4	12	11	24
12	7.64	424	0.40	5.5	7.2	21	11	25
13	8.22	411	0.31	4.1	5.4	13	10	24
14	8.08	421	0.42	6.2	12	20	11	24
15	9.15	421	0.42	9.4	12	26	11	26
Mean	**8.35**	**423**	**0.37**	**4.9**	**7.9**	**17**	**11**	**25**
Std.dev.	0.41	30	0.07	1.8	3.3	5.7	0.5	1.8

The deformation values in table 1 are the average from the two displacement transducers. Density and moisture content is taken as the average of values from four specimens. The distance from pith was evaluated by averaging values within the nail region. The annual ring width was about 1.5 mm.

Specimen no. 1 was not loaded according to ISO 6891, but used a linearly increasing load ramp of 3 mm/min. Therefore this specimen is to be regarded as an exploratory experiment. Specimen no. 8 had just passed the ultimate load when a power cut ended the experiment. Specimen no. 4 must also be disregarded since the specimen was severely damaged by the nailer during manufacturing of the joint. The data were treated statistically with linear regression to examine the supposed relationship between density – capacity and between pith distance – capacity. None of these relationships were found to be significant on the 5% significance level. This is probably due to the fact that these joints were produced with the aim to be as similar as possible and thus the result is that density, pith distance and capacity does not vary enough to produce any tendencies in the relationships.

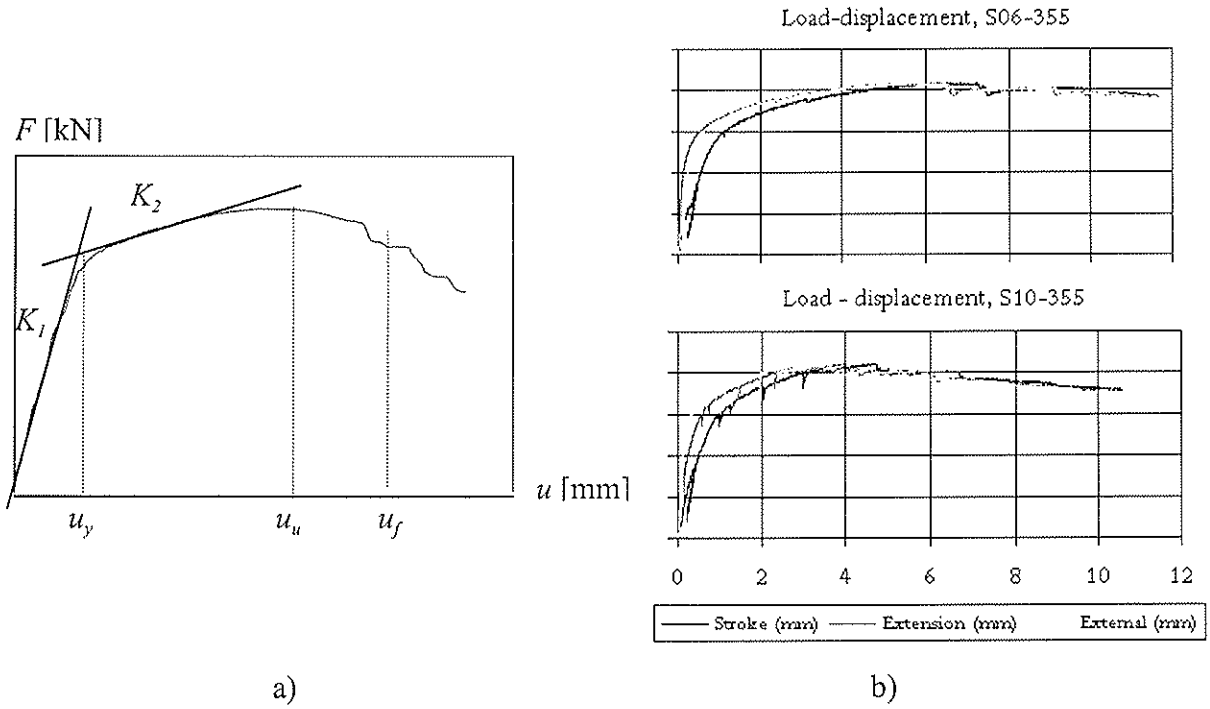

Figure 4: a) Definition of parameters. b) Load-displacement measurements for specimens no. 10 and 6.

The final failure was defined as the splitting of the wood member. Generally the crack propagated from one of the outer nails and occurred in the timber section the nail first passed through during manufacturing, see figure 5a.

As seen in figure 5b the failure was in mode II. The photo was taken after a displacement of 30 mm. At this moment the rotation angle is 20° for all nail parts except the upper right in figure 5b where the rotation angle is 45°. None of the specimens experienced a shear plug failure since the size of the joint was too small.

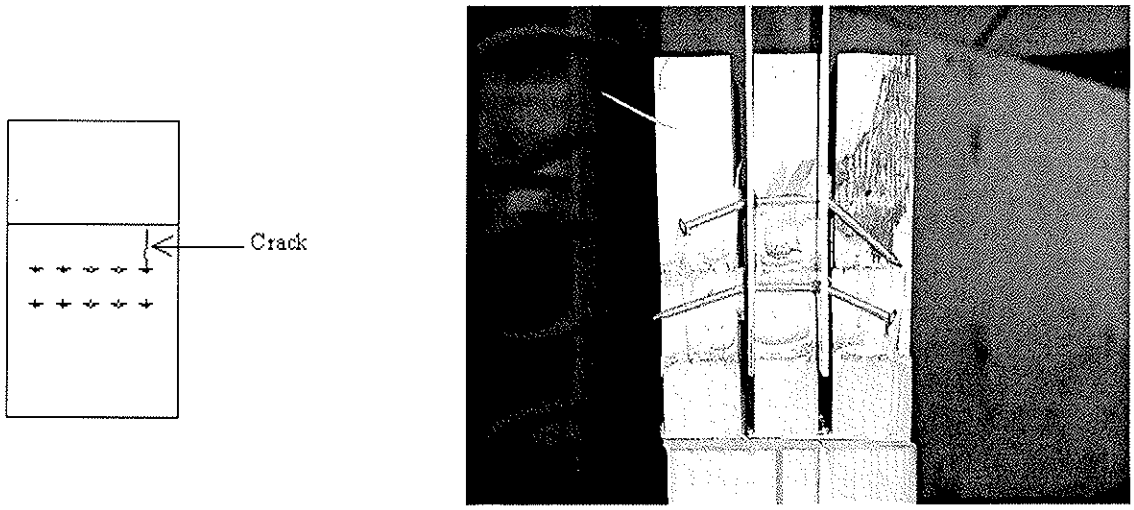

a) b)

Figure 5: a) Crack propagation and b) failure mode.

4 Discussion

Figure 6 depicts ductility results for different types of slotted-in or "internal" joint designs presented in the literature, Siem (1999), Pedersen et al. (1999) and Burstrand and Salmonsson (1996), together with the results from this study. The data for the experimentally observed ductility $D_u = u_t/u_y$ is plotted against $D_e = t/t_y$. Dowels are not produced from wire why no strain hardening effect is expected. Hence, for dowels, equation (6) must be multiplied with $d^{0.15}$. This was performed on the data in Siem and Pedersen et al.

The average value of D_e in this study is 1.42. Concerning the boundaries presented in figure 2, $D_e > 1$, a mode II failure is expected. Evidences of mode II failure were likewise found when examining the fractured specimens, se above and figure 5b.

From figure 6 it is possible to extract $D_0 = 9$ and $K_{D2} = 5.5$, albeit with low statistical validity. Without knowledge about acceptable values for D_u, D_0 and K_{D2} the use of equations (6) and (7) is limited. However, to demonstrate the usefulness of the approach D_e is applied to calculate the minimum thickness to achieve mode II and mode III failures. This implies that $D_e = 1$ for mode II failure and $D_e = 2.82$ for mode III failure. Using values for $\rho_k = 423 \pm 30$ kgm^{-3} from table 1 and $f_{y,k} = 2216 \pm 46$ MPa from the yield moment tests of the nails gives:

$$t_{II} \geq 1 \cdot d \cdot \sqrt{\frac{4.1 f_{y,k}}{\rho_k}} = 4.9d \qquad (8)$$

$$t_{III} \geq 2.82 \cdot d \cdot \sqrt{\frac{4.1 f_{y,k}}{\rho_k}} = 13.7d$$

With acceptable D_u values 1 and 2.82 in equation (7) above changes to $(D_u\text{-}D_0)/K_{D2}$ implying that larger D_0 and K_{D2} values, i.e., more ductile behaviour, requires smaller timber member or embedding lengths.

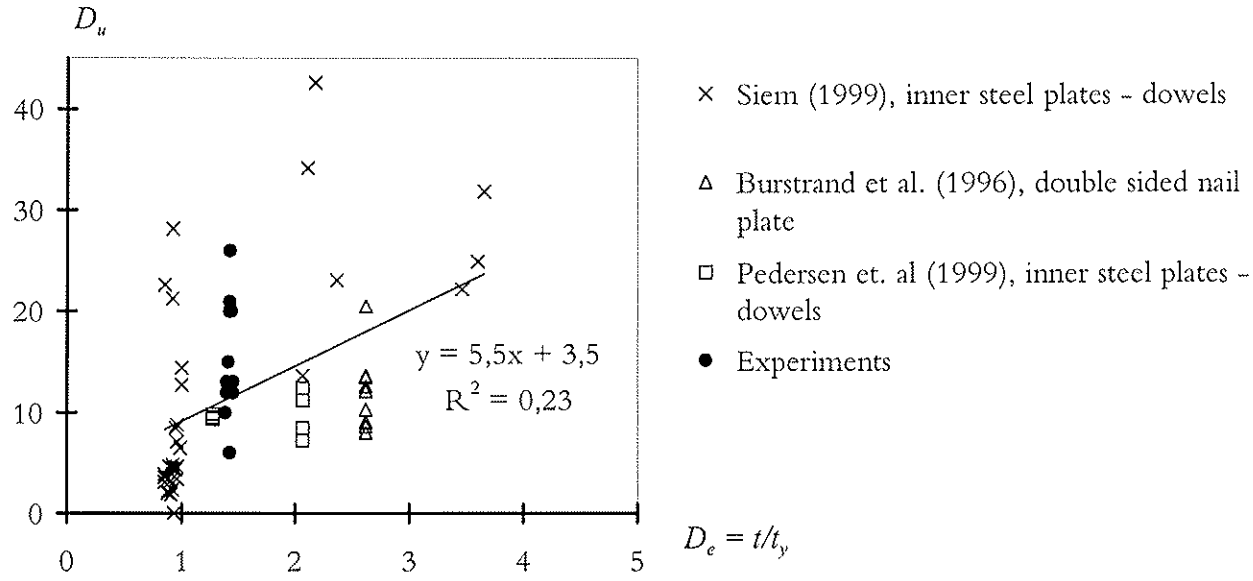

Figure 6: D_u versus D_e plot from literature and experiments.

5 Conclusions

Based on the plasticity theory for dowel type fasteners, theoretical reasoning and experimental results, a model is proposed describing the ductility behaviour of mechanical joints. The model is exemplified and verified for a slotted-in steel plate type connection. For other types of mechanical connections with different behaviour a modified version of D_e is needed. The D_e philosophy might give engineers tools to assess ductility in the same manner as different models are used for different types of connections.

It is recognised that due to the large scatter (variability) in the results, too few specimens and a limited number of comparable experiments in the literature this investigation is not sufficient to state that D_u can be described by D_e. The least-square fit line in figure 6, that could be used to predict the ductility based on available engineering parameters, has a low correlation coefficient (R^2 = 0.23). Hence a statistically strong enough proof of the validity of the engineering ductility model is not yet achieved.

For the proposed model to be further developed, both within the continuation of this project and as an accepted ductility assessment tool, a more comprehensive study must be performed:

- So that a larger regime of $D_e = t/t_y$ is covered that might give support to the proposed model. Effects from an expanded geometry design (end and side distances, timber member thickness etc.), timber and nail properties and grain angle effects must be considered.
- If adapted γ_m factors in combination with a k_{mod} factor based on this model are to be introduced. This work includes that acceptable levels of (mode II and III type) ductility $D_u = 1.82 \cdot K_{D2} + D_0$ associated to safety limits and structural reliability are verified for the ultimate limit state

6 Acknowledgements

This research was in part supported by Ljungan Trä AB (glulam supplier/manufacturer) and in part by NUTEK. We want to thank Martin Pedersen and his co-workers at DTU for the load-displacement data from their experiments on slotted-in dowels and Dr.-Ing. Rainer Görlacher and his staff at the University of Karlsruhe for yield moment testing of the nails.

References

Blass H.J. and Ehlbeck J. (1998). "Simplified design of connections with dowel-type fasteners", in proceedings from CIB-W18 meeting 31, Savolinna, Finland, August 1998, ISSN 0945-6996.

Blass H.J., Ehlbeck J. and Rouger F. (1999). "Simplified design of joints with dowel-type fasteners", in proceedings from Pacific timber engineering conference, ed. G.B. Walford and D.J. Gaunt, Rotorua, New Zealand, 14-18 March, 1999, pp. 275 – 279.

Burstrand H. and Salmonsson J. (1996). "Utformning av spikförband till stora fackverk av limträ" (in Swedish), Diploma work 1996:197E, Luleå university of technology, Division of Steel structures, Luleå, Sweden.

Ehlbeck J., Siebert W. and Werner H. (1990). "Nail and nail wire bending tests", report, Dept. Timber Engineering, University Fridericiana Karlsruhe, November 1990, 9p.

Haller P. (1998). "Progress in timber joint development and modelling", in proceedings from 5th world conference on timber engineering, ed. J. Natterer and J.-L. Sandoz, Montreqaux, Switzerland, August 17-20, 1998, pp. 337-344.

Johansen K.W. (1949). "Theory of timber connections", International Association of Bridge and Structural Engineering, Publication 9, pp. 249-262.

Johansson H. and Stehn L. (2000). "Systematic glulam truss design with nailed connections", Submitted for publication in Civil Engineering and Environmental systems.

Kangas J. and Vesa J. (1998). "Design on timber capacity in nailed steel-to-timber joints", in proceedings from CIB-W18 meeting 31, Savolina , Finland, August 1998, ISSN 0945-6996.

Larsen H.J. and Riberholt H. (1999). "Trækonstruktioner – forbindelser" (in Danish), SBI-anvisning 194, Statens Byggeforskningsinstitut, Hørsholm, Denmark, ISBN 87-563-1014-5.

Mischler A. (1998). "Design of joints with laterally loaded dowels", in proceedings from CIB-W18 meeting 31, Savolina, Finland, August 1998, ISSN 0945-6996.

Mischler A. (1999). "Doweled timber connections with high efficiency", in proceedings from 1st RILEM symposium on Timber engineering, ed. L. Boström, Stockholm, Sweden, September 13-15, 1999, pp 99-108, ISBN 2-912143-10-1.

Pedersen M.U., Clorius C.O., Damklide L., Hoffmeyer P. and Eskildsen L. (1999). "Dowel type connections with slotted-in steel plates", in proceedings from CIB-W18 meeting 32, Graz, Austria, August 1999, ISSN 0945-6996.

Racher P. (1995). "Mechanical timber joints – general, Timber Engineering STEP1", Centrum Hout, The Netherlands, ISBN 90-5645-001-8.

Siem J. (1999). "Kapasitet og duktilitet av dybelförbindelser I trekonstruktioner" (in Norwegian), Ph.D. Thesis 1999:46, NTH, Div. of Structural Engineering, Trondheim, Norway, ISBN 82-471-0414-8.

INTERNATIONAL COUNCIL FOR RESEARCH AND INNOVATION
IN BUILDING AND CONSTRUCTION

WORKING COMMISSION W18 - TIMBER STRUCTURES

EFFECTIVE BENDING CAPACITY OF DOWEL-TYPE FASTENERS

by

H J Blaß
A. Bienhaus
V Krämer

University of Karlsruhe
GERMANY

MEETING THIRTY-THREE
DELFT
THE NETHERLANDS
AUGUST 2000

Presented by: V. Krämer

· A. Leijten pointed out in the moment rotation graphs, the moment corresponding to 20° was 90% of the moment corresponding to 45°. This difference was relatively minor.
· H. Blass responded that the differences for cases of 4° to 6° were significant.
· H.J. Larsen commented that in many cases the d=15 mm limit for a test would not be reached. The joint strength was diameter dependent. May be change the original criteria to 10° would be a simple alternative.
· H. Blass responded that engineering judgment was uesed to choose d=15 mm as a starting point. There was conservatism in other part of the procedures to allow for reasonable results at the end.
· C. Mettem asked about the wood species differences.
· H. Blass responded that if there was no splitting the procedure would be appropriate.
· H.J. Larsen suggested that an editorial change to the statement: "The plastic bending capacity is partially used..." be changed to "Reserve capacity can only be partially used..."
· H. Blass agreed

Effective Bending Capacity of Dowel-Type Fasteners

H. J. Blass, A. Bienhaus, V. Krämer
Lehrstuhl für Ingenieurholzbau und Baukonstruktionen
Universität Karlsruhe
Germany

1 Introduction

The load-carrying capacity of connections with dowel-type fasteners like bolts, dowels or nails may be determined on the basis of Johansen [2]. According to Johansen the load-carrying capacity depends on the geometry of the connection, the bending resistance of the dowel and the embedding strength of the timber or wood-based material. For the bending resistance of the dowel, Johansen assumed the elastic moment capacity of the dowel's cross-section, the possible increase due to plastic deformations was disregarded. The design equations in Eurocode 5 [3], which are derived from Johansen's work, are based on a rigid-plastic behaviour of both, the dowel under bending moments and the wood under embedding stresses and take into account the plastic moment capacity of the dowel.

According to Johansen, three different failure modes are possible for timber-timber-connections in double shear (see **figure 1**). Failure mode 1 corresponds to the embedding failure of the middle or side member, respectively, where the embedding strength according to EN 383 [5] is defined as „an average compressive stress at maximum load in a specimen of timber or wood-based sheet product under the action of a stiff linear fastener". In failure modes 2 and 3, apart from the embedding strength of the wood the bending capacity of the fastener is reached. Failure modes 2 and 3 of dowels loaded in double shear correspond to identical failure modes of dowels loaded in single shear.

According to EN 409 [6] the yield moment of a nail is determined at a bending angle of 45°. For such a large bending angle, the whole cross-section of the fastener is assumed to be under plastic strain. In [7] results of fastener bending tests are published where the bending capacity of fasteners with d > 8mm is also determined on the basis of EN 409.

For bending angles below 45° only the outer areas of the cross-section of a fastener are deformed plastically. In this case, the reserve capacity can only be partially used and the fastener bending moment lies between the elastic and plastic bending capacity of the often circular dowel cross-section.

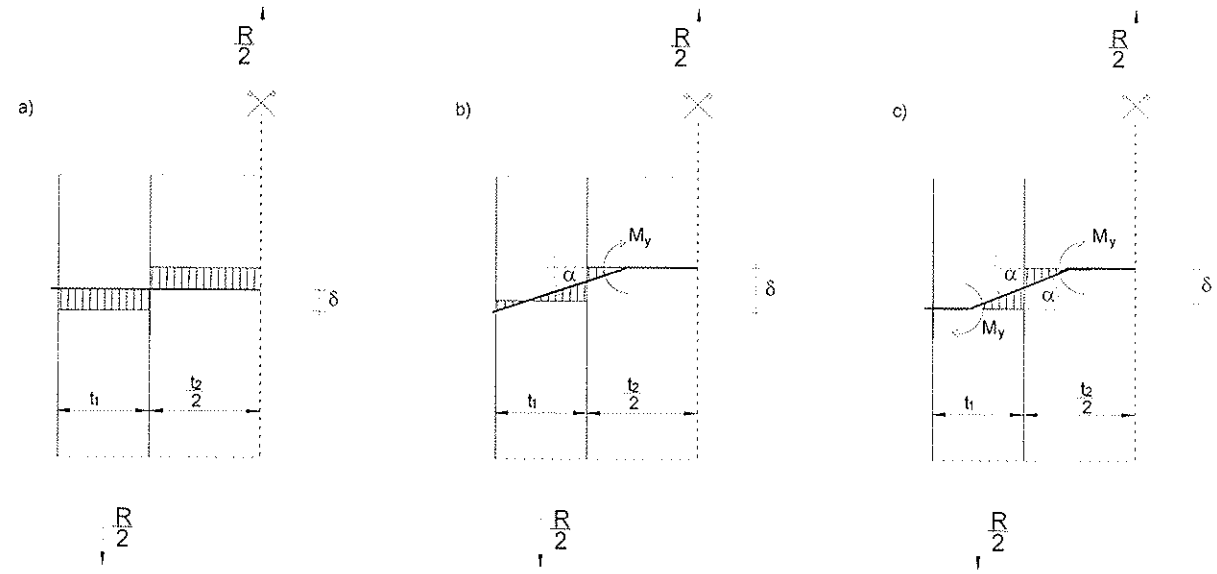

Figure 1 Failure modes of a double shear timber-to-timber connection

2 Deformation behaviour of dowel-type fasteners

If the load-carrying capacity and the deformation behaviour of connections with dowel-type fasteners is determined by tests according to EN 26891 [8], the connection strength is defined as the maximum load before a deformation of $\delta = 15$ mm parallel to the load direction is reached.

For a large number of connections tested at Delft University of Technology, Jorissen [7, 9] measured the bending angles α of dowels after the connection had reached the maximum load. In most cases where failure modes 2 or 3 occurred, the bending angles were significantly below $\alpha = 45°$. This means that the plastic hinge was not fully developed and the plastic moment capacity of the dowel was not attained in the connection. (see **Figure 2**).

Since the fastener's cross-sections were only partially plasticised, their bending capacity was lower than according to EN 409. This lower bending capacity influences the load-carrying capacity of the connection for failure modes 2 and 3 and results in lower connection strength values. For a realistic connection design the actually reached bending moment is therefore important. If a deformation limit of 15 mm is assumed for the connection, the

effective bending capacity depends on the yield strength of the fastener material, the fastener diameter and the shape of the moment-angle-diagram of the fastener.

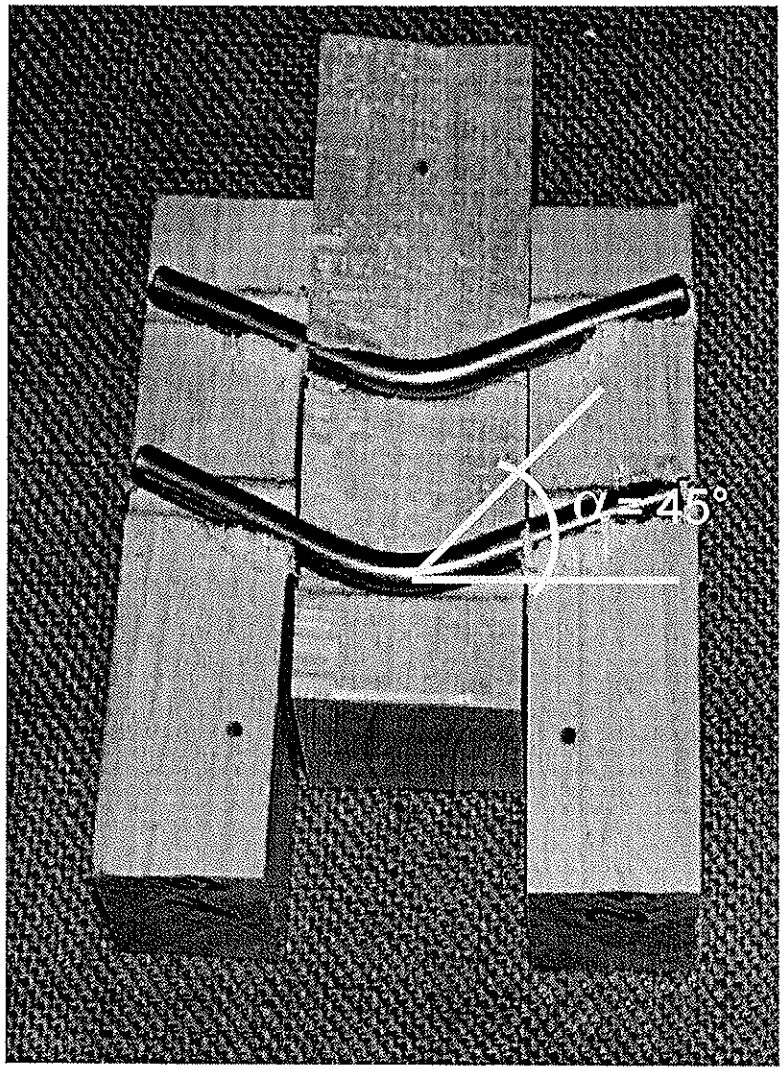

Figure 2 Test specimen opened after reaching maximum load

In order to determine the moment-angle-diagrams of the fasteners bending tests with different fasteners were evaluated. Since different steel grades and different fastener diameters lead to large differences in absolute moment values, the moment-angle-diagrams were normalised by dividing the moment values by the moment capacity corresponding to a bending angle of $\alpha = 45°$ (see **Figure 3**):

$$\overline{M}(\alpha, d) = \frac{M(\alpha, d)}{M(\alpha = 45°, d)} \quad (1)$$

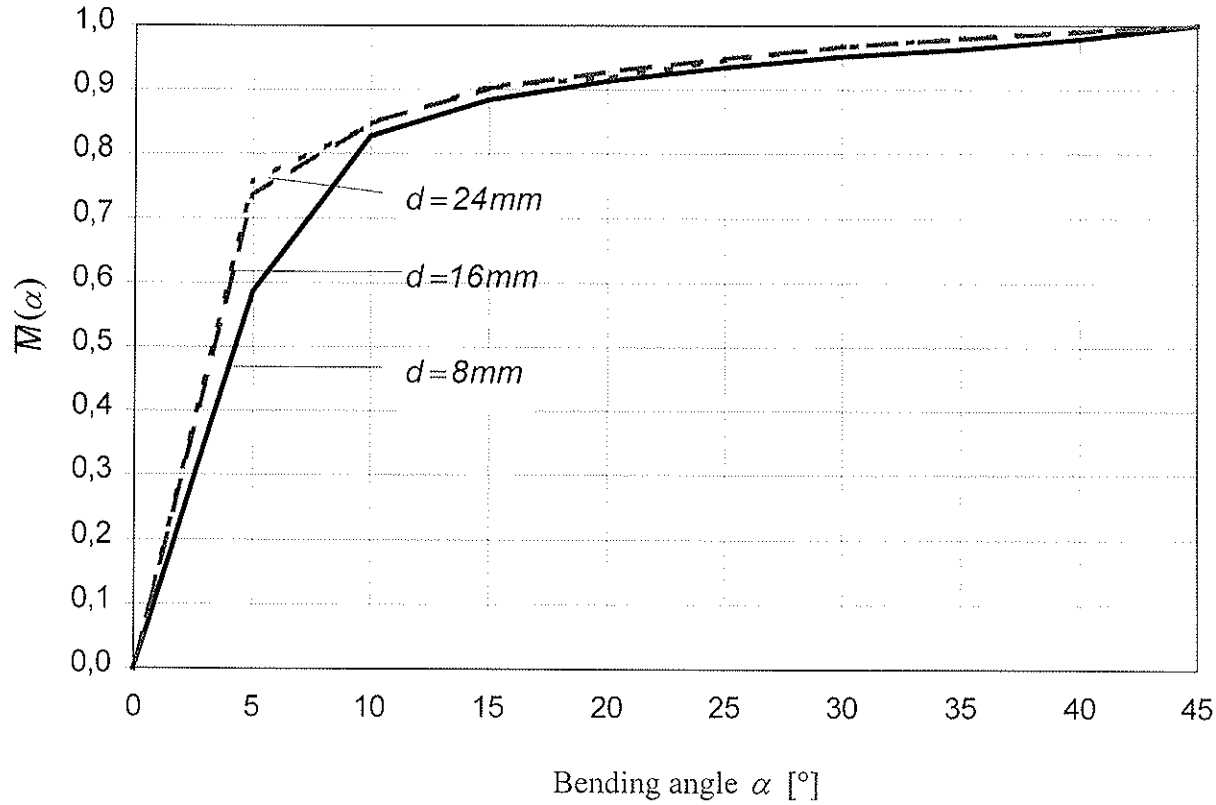

Figure 3 Normalised moment-angle-diagrams of dowel-type fasteners of different diameter *d*.

Since the shape of $\overline{M}(\alpha, d)$ is very similar for different fastener diameters d, a mean curve $\overline{M}(\alpha)$ was determined. This relation neither depends on the fastener diameter d nor on the fastener material properties and may be approximated by an exponential function (see **Figure 4**).

$$\overline{M}(\alpha) = (0{,}866 + 0{,}00295 \cdot \alpha) \cdot \left(1 - e^{\left(\frac{-0{,}248 \cdot \alpha}{0{,}866}\right)}\right) \qquad (2)$$

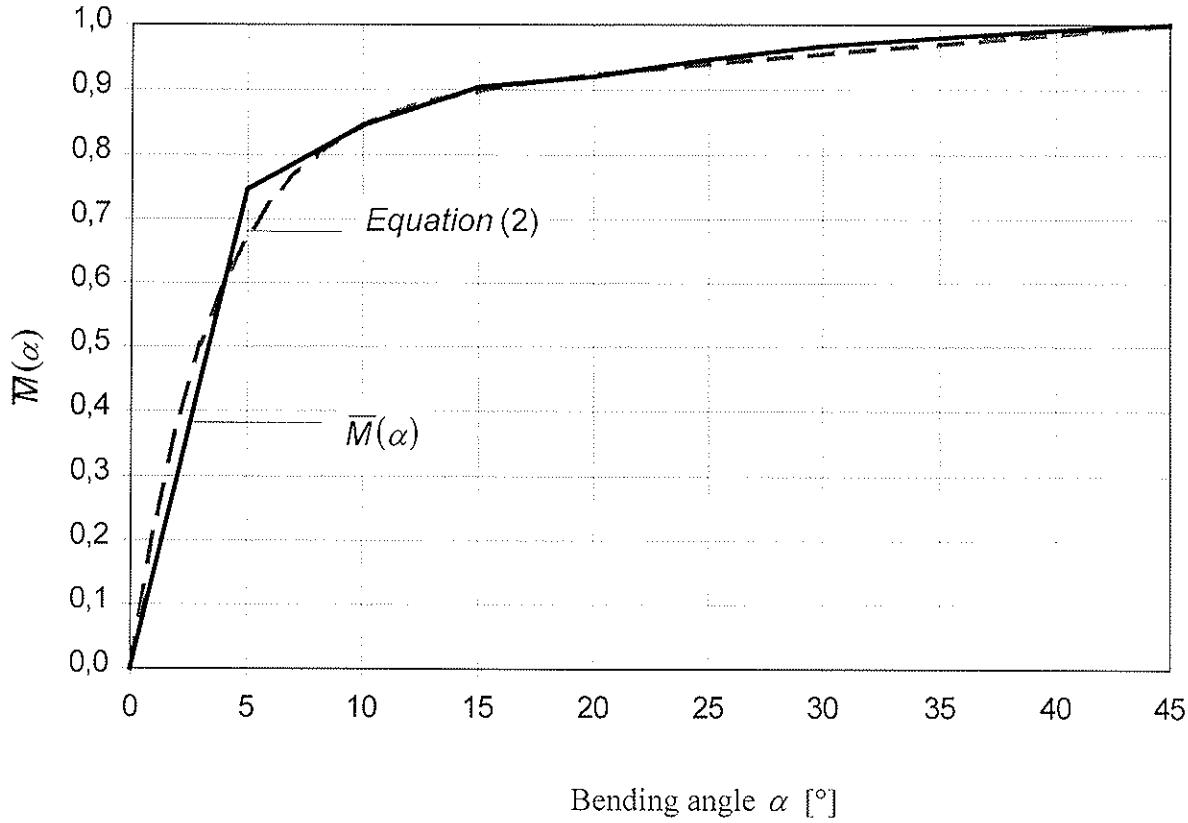

Figure 4 Mean normalised moment-angle-diagram of dowel-type fasteners and approximation

3 Theoretical bending angles in connections

Figure 5 shows the failure modes 2 and 3, where the angle α is defined as

$$\alpha = arctan\left(\frac{\delta}{\ell}\right) \tag{3}$$

Here, δ is the maximum deformation of δ = 15 mm parallel to the load direction. The length ℓ corresponds to the length of the wood or wood-based material where the embedding strength is reached. For failure mode 2 the length ℓ results as

$$\ell = a_2 + b_1 + b_2 \tag{4.1}$$

and failure mode 3 as

$$\ell = b_1 + b_2 . \tag{4.2}$$

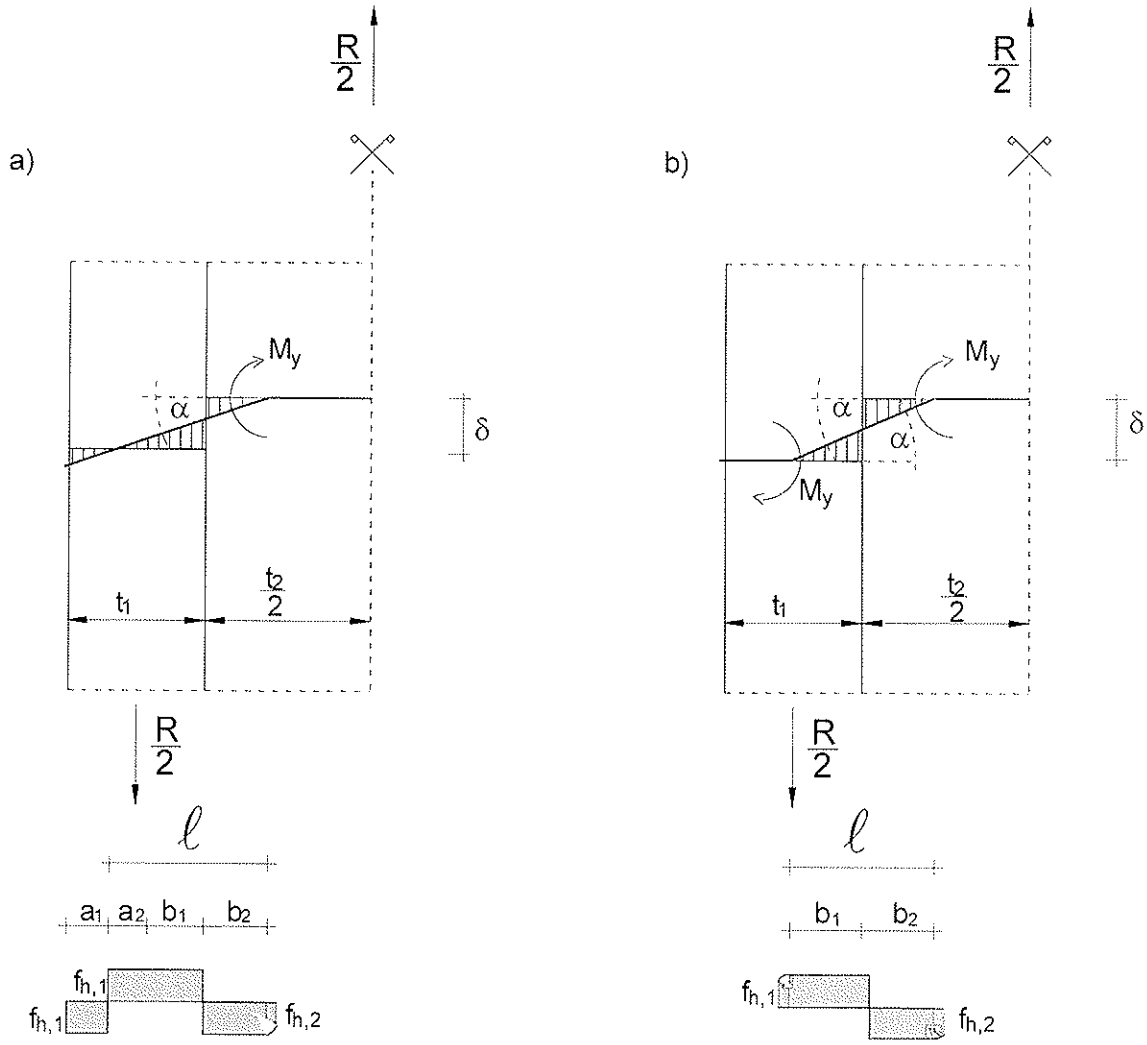

Figure 5 Failure mode 2 (left) and 3 (right) for a fastener in single or double shear

In both cases ℓ depends on the fastener diameter d, the embedding strength f_h and the yield moment M_y. The fastener yield moment itself depends on the fastener diameter d and the yield strength f_y of the fastener material, the embedding strength also is a function of d and of the density ρ.

Subsequently the derivation of α as a function of the fastener diameter d is shown as an example for failure mode 3. For a load-grain angle of 0° and for the same densities ρ of the middle and side member the embedding strength f_h is constant and the connection is symmetrical. Consequently $b_1 = b_2 = b$ and $\ell = 2 \cdot b$. The dimension b may now be determined from the equilibrium of forces (see **figure 5**) and results as

$$b = \sqrt{\frac{2 \cdot M_y}{f_h \cdot d}} . \qquad (5)$$

The bending angle α consequently is calculated as

$$\alpha = \arctan\left(\frac{\delta}{2\cdot\sqrt{\frac{2\cdot M_y}{f_h\cdot d}}}\right). \tag{6}$$

α depends on the fastener bending moment M_y. Since in general at maximum load $\alpha < 45°$, the full plastic bending capacity is not reached. Using equation (7), the dependence between the bending moment M_y and the bending angle α may be taken into account by an iterative procedure. $\alpha = 45°$ is taken as a first value. In the next step the normalised moment according to equation (2) is calculated and inserted in equation (7). After three iteration steps the difference $\Delta\alpha$ is less than 1°.

$$\alpha_{i+1} = \arctan\left(\frac{\delta}{2\cdot\sqrt{\frac{2\cdot M_{y,k}\cdot\overline{M}(\alpha)}{f_{h,k}\cdot d}}}\right) \tag{7}$$

The parameters influencing $\alpha(d)$ depend on the fastener material and the embedding strength and therefore require a different determination of the effective bending capacity for different types of fastener. For bolts, dowels and nails in predrilled holes the embedding strength is determined as

$$f_{h,k} = 0{,}082\cdot(1-0{,}01\cdot d)\cdot\rho_k \tag{8}$$

The corresponding equation to calculate the embedding strength for nails in non predrilled members is:

$$f_{h,k} = 0{,}082\cdot d^{-0{,}3}\cdot\rho_k\,. \tag{9}$$

The yield strength in bending f_y according to Eurocode 5 is 80% of the tensile strength $f_{u,k}$ of the steel grade used.

Scheer, Peil and Nölle (1988) have published the results of bending tests with bolts 4.6 and 5.6 and give a 5-percentile value of the yield strength in bending of 67% of the actual tensile strength. The value of 67% includes the strain hardening due to large strains in the outer areas of the circular cross-section and relates to a bending angle $\alpha = 10°$. The plastic bending moment for $\alpha = 45°$ is 19% higher than for $\alpha = 10°$ (see **figure 4**). Consequently,

for $\alpha = 45°$ a value for the yield strength in bending of $67\% \cdot 1{,}19 = 80\%$ of $f_{u,k}$ results. This confirms the equation for the fastener yield moment for bolts and dowels given in Eurocode 5 independently of the steel grade:

$$M_{y,k} = 0{,}8 \cdot f_{u,k} \cdot \frac{d^3}{6}. \tag{10}$$

The yield moment of nails with circular cross-section with a minimum wire tensile strength of 600 N/mm^2 is according to Eurocode 5:

$$M_{y,k} = 180 \cdot d^{2,6}. \tag{11}$$

Figure 6 shows as an example the bending angle α depending on the fastener diameter d for failure modes 2 (fm2) and 3 (fm3) according to Johansen. The parameters tensile strength $f_{u,k}$ and characteristic density ρ_k were chosen as 1000 N/mm^2 and 350 kg/m^3, respectively. A large value of the tensile strength and a low value of the density lead to comparatively low values of the bending angle α and are therefore conservative.

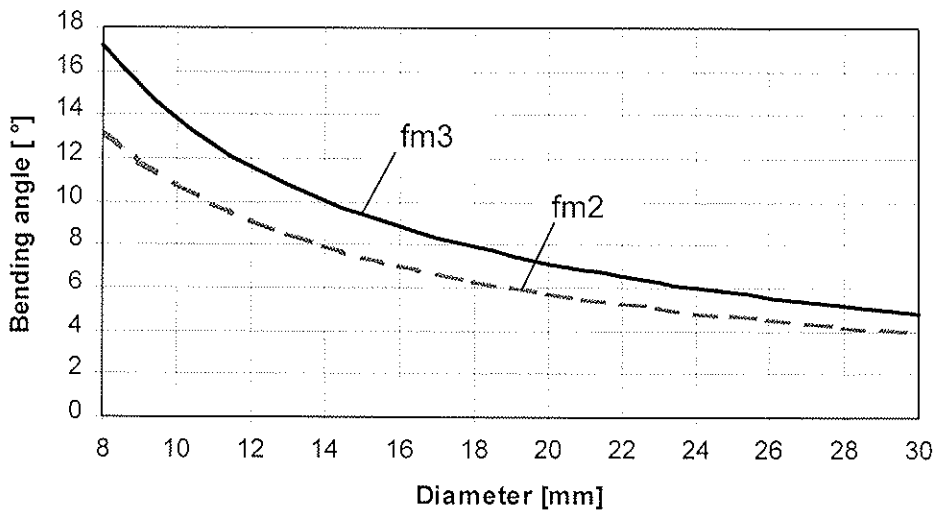

Figure 6 Bending angle α depending on fastener diameter d for failure modes 2 and 3.

4 Effective bending capacity of dowel-type fasteners

For the different types of fastener the function $\alpha(d)$ was determined, resulting in minimum values of the bending angle α. For this purpose, the governing parameters were conservatively chosen, resulting in maximum values for the steel tensile strength and minimum values for the characteristic density. For connections with bolts or dowels, the tensile strength $f_{u,k}$ was chosen as 1000 N/mm^2 and the characteristic density ρ_k as 350 kg/m^3. Inserting these values in equation (2) results in a relation between the normalised moment and the fastener diameter d. Multiplying $\overline{M}(\alpha(d))$ and the yield moment according to equation (10), a simplified approximate expression for the effective bending capacity of bolts and dowels for a deformation δ = 15 mm results:

$$M_{y,k} = 0{,}24 \cdot f_{u,k} \cdot d^{2,7} \quad \text{Nmm} \tag{12}$$

where

$f_{u,k}$ fastener tensile strength in N/mm^2

d fastener diameter in mm

Using equation (12) instead of equation (10) for the bending capacity of bolts or dowels, the decreasing bending angle with increasing fastener diameter is implicitly taken into account.

A similar evaluation for nailed connections leads to a relation for the effective bending capacity of nails which is very close to equation (11). Consequently, the determination of the bending capacity of nails in Eurocode 5 should not be altered, whereas equation (10) should be replaced by equation (12). When determining fastener bending capacities by tests, the evaluation of the moment-angle-diagrams should take into account the reduced bending angles depending on the fastener diameter according to figure 6.

5 Conclusion

The design of connections with dowel-type fasteners according to Eurocode 5 is based on Johansen's theory. Here, the bending capacity of the fastener is an important parameter. Tests with timber connections with dowel-type fasteners show plastic deformations of fasteners in failure modes 2 and 3. The plastic hinge, however, is in most cases not fully developed and consequently the full plastic fastener bending moment is not reached. Depending on the moment-angle relation of fasteners in bending a modified equation was derived to determine the fastener bending capacity. The bending capacity of bolts and dowels according to the proposed modified equation leads to significantly lower bending capacities especially for large fastener diameters. Using the modified equation results in a better agreement between test results and theoretically determined connection capacities.

References

[1] Bienhaus, A.: Die Ermittlung des Fließmomentes stiftförmiger Verbindungsmittel. Vertieferarbeit am Lehrstuhl für Ingenieurholzbau und Baukonstruktionen, Universität Karlsruhe, 1999

[2] Johansen, K. W.: Theory of Timber Connections. In: International Association of Bridge and Structural Engineering, 1949

[3] DIN V ENV 1995-1 Teil1-1 Eurocode 5 : Design of timber structures; Part 1-1 : General rules and rules for buildings; German version ENV 1995-1-1 : 1993

[4] E DIN 1052. Entwurf, Berechnung und Bemessung von Holzbauwerken. November 1999

[5] EN 383, Timber structures; Test methods; Determination of embedding strength and foundation values for dowel type fasteners; German version EN 383 : 1993

[6] EN 409, Timber structures; Test methods; Determination of the yield moment of dowel type fasteners; Nails; German version EN 409 : 1993

[7] Jorissen, A.; Blaß, H.J.: The fastener yield strength in bending. Paper 31-7-6, Proceedings CIB-W18 meeting, Savonlinna, Finnland, 1998

[8] EN 26891 Timber structures; Joints made with mechanical fasteners; General Principles for the determination of strength and deformation characteristics (ISO 6891 : 1983); German version EN 26891 : 1991

[9] Jorrisen, A.: Double Shear Timber Connections with Dowel Type Fasteners, Dissertation, TU Delft, Niederlande, 1998

[10] Scheer, J.; Peil, U.; Nölle, H.: Schrauben mit planmäßiger Biegebeanspruchung. Stahlbau 57, 1988, S. 237-245

INTERNATIONAL COUNCIL FOR RESEARCH AND INNOVATION
IN BUILDING AND CONSTRUCTION

WORKING COMMISSION W18 - TIMBER STRUCTURES

LOAD-CARRYING CAPACITY OF JOINTS WITH DOWEL-TYPE FASTENERS AND INTERLAYERS

by

H J Blaß
B Laskewitz
University of Karlsruhe

GERMANY

MEETING THIRTY-THREE
DELFT
THE NETHERLANDS
AUGUST 2000

Presented by: B. Laskewitz

· S. Svensson asked for and received clarification on tensile test set up.
· M. Ansell questioned the role of OSB as the interlayer.
· H. Blass responded that this would be a typical application of hangers on shear walls. This study provided the information needed by designers.
· M. Ansell questioned why OSB.
· B. Laskewitz responded that OSB is commonly used as sheathing for walls.

Load-Carrying Capacity of Joints with Dowel-Type Fasteners and Interlayers

H.J. Blaß, B. Laskewitz

University of Karlsruhe, Germany

1 Introduction

The design rules in Eurocode 5 for joints with dowel-type fasteners loaded perpendicular to their axis do not take into account an interlayer or a distance between the members to be connected although this may significantly influence the load-carrying capacity of the joint.

One example of a connection with an interlayer is a joist hanger attached at a shear wall. In this case, the load is transferred from the steel plate through the wood-based panel into the studs. In these cases not considered by the design rules the structural engineers and the building authorities are uncertain about the joint's load-carrying capacity.

The load-carrying capacity of timber-to-timber- or steel-to-timber-joints with an interlayer may be derived according to the theory of Johansen which forms the basis of the design rules for dowel-type fasteners in Eurocode 5. A condition for this is the knowledge of the embedding strength of the different materials and the moment capacity of the dowel-type fasteners.

Within a research project supported by Deutsche Gesellschaft für Holzforschung e.V. the load-carrying capacity of single-shear timber-to-timber- and steel-to-timber-joints with an interlayer were derived according to the theory of Johansen. The theoretical values were verified by tests.

2 Experimental Study

2.1 Shear tests with timber-to-timber joints

The load-carrying capacity and the deformation behaviour of single shear timber-to-timber joints were determined by tests. An interlayer consisting of 12 mm OSB panels was placed between the timber members. The OSB interlayer was stapled to the timber. The timber members were connected either with smooth or ringed shank nails. Figure 1 shows the test set-up and table 1 the testing programme. Table A1 (Enclosure 1) contains the values of the density and the moisture content of the timber. During the tests the force and the relative displacements of the timber members were measured.

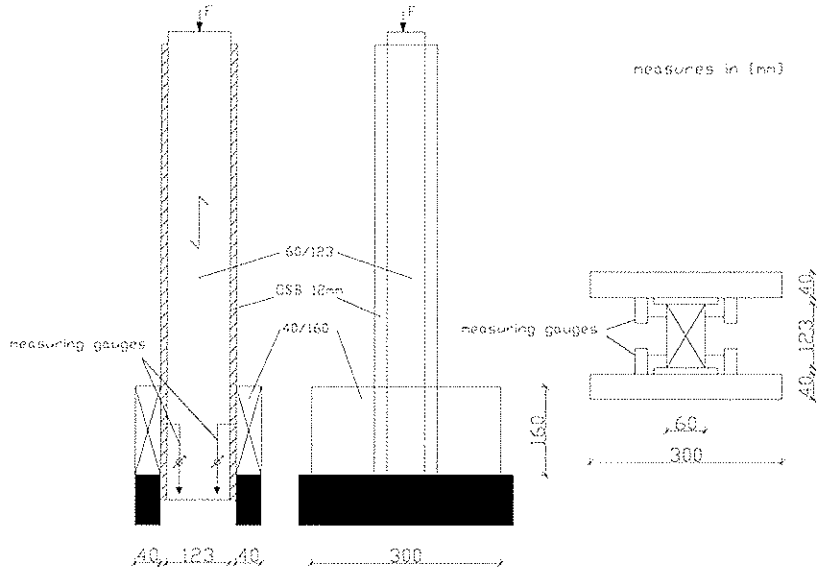

Figure 1: Test set-up of the single shear timber-to-timber joints

Table 1: Testing programme of the single shear timber-to-timber joints

Test series	Timber-to-timber connection	OSB-to-timber connection	Number of tests
A1	2x14 smooth nails 38x100 pre-drilled	2x20 staples 1.88x44	3
A2	2x14 ringed shank nails 40x100 pre-drilled	2x20 staples 1.88x44	3

All test specimens showed a similar failure mechanism. The fasteners to connect the timber members were loaded in shear. With increasing displacement two plastic hinges in the nails were formed and the embedding strength of the timber was reached. The staples were also deformed plastically. Compared to the total displacement the relative displacement between the OSB and the stud was not significant. As expected the tests with ringed shank nails showed higher load-carrying capacities because of a distinctive chord effect. The results of both test series are summarised in table A2 (Enclosure 1). Typical load-displacement curves are shown in figures A1 and A2 (Enclosure 2). The deformed nails of one test specimen are shown in figure A3 (Enclosure 3).

2.2 Shear tests with steel-to-timber joints

The tensile tests simulate typical situations in timber frame construction. Table A3 (Enclosure 3) contains the timber density and moisture content. The 12 mm OSB panels were placed on the stud by means of staples or adhesive (polyurethane). Two perforated steel plates per test specimen were nailed to the stud by means of ringed shank nails.

Figure 2 shows the test set-up and table 2 contains the test programme. During the tests the force and the relative displacements between the steel plates and the stud were measured.

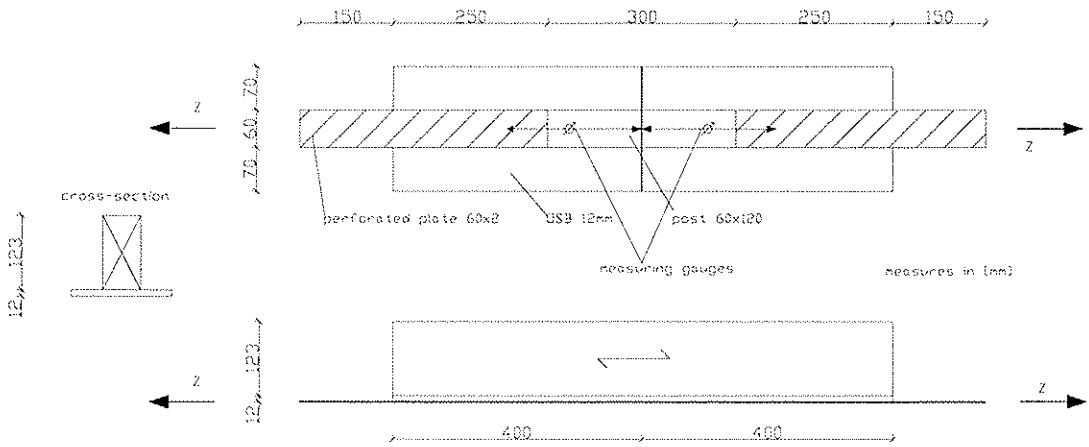

Figure 2: Test set-up of the tensile tests

Table 2: Testing programme of the tension tests

Test series	Steel-to-timber connection	OSB-to-timber connection	Number of tests
A	2x12 ringed shank nails 4.0x50 not pre-drilled	2x15 staples 1.88x44	3
B	2x12 ringed shank nails 4.0x50 not pre-drilled	Adhesive (polyurethane)	3

The failure mechanisms of the two test series were different. The tests with a stapled connection between OSB and stud showed large deformations accompanied by two plastic hinges in the nails. The nail heads were clamped in the steel plates. In every staple leg one plastic hinge was formed. The tests with bonded OSB panels showed a more rigid behaviour. One plastic hinge occurred in every nail. Only the beginning of a second plastic hinge close to the steel plate was noticeable. Despite the different stiffness the load-carrying capacities were hardly different.

The results of the two test series are summarised in table A4 (Enclosure 4). Two typical load-displacement curves are shown in figures A4 and A5 (Enclosures 4). A x-ray of a test specimen is shown in figure A6 (Enclosure 5).

2.3 Additional tests

For the verification of the test results the yield moment of the nails was determined according to DIN EN 409. The mean value of the yield moment for the smooth nails was 7.4 Nm, for the ringed shank nails with a length of 100 mm 7.1 Nm and for the ringed shank nails with a length of 50 mm 8.1 Nm.

The embedding strength of the OSB was determined according to DIN EN 383. Tensile as well as compressive tests with different orientations of the outer strands relative to the load direction were performed. The smooth nails had a diameter of 3.8 mm and were pre-drilled with a diameter of 3.4 mm. The mean value of the embedding strength parallel to the outer strands was 37.7 N/mm² (tensile tests) and perpendicular to the outer strands 45.2 N/mm² (compressive tests) and 45.9 N/mm² (tensile tests).

3 Theoretical models

According to the theory of Johansen [1] the load-carrying capacity of single-shear timber-to-timber- and steel-to-timber-joints with an interlayer were derived. Because of the semi-rigid stapled connection between OSB and stud the load-carrying capacity was derived for two cases: no connection and rigid connection between OSB and timber stud, respectively.

3.1 Theoretical models for timber-to-timber joints

3.1.1 No connection between interlayer and timber

Failure mechanism 1aozw:

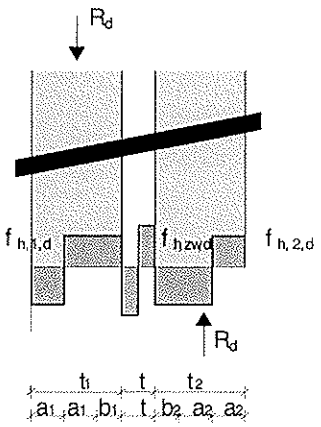

Load-carrying capacity:

$$R_d = f_{h,1,d} \cdot b_1 \cdot d \qquad (1)$$

with $\beta = \frac{f_{h,2,d}}{f_{h,1,d}}$ and $\delta = \frac{f_{h,zw,d}}{f_{h,1,d}}$

and the condition $b_1 = \beta \cdot b_2$

b_1 follows as:

$$b_1 = \frac{\beta}{1+\beta} \cdot \left(-2t - t_1 - t_2 + \sqrt{(4+\delta+\frac{\delta}{\beta}) \cdot t^2 + (2+\frac{1}{\beta})t_1^2 + (2+\beta)t_2^2 + 4tt_1 + 4tt_2 + 2t_1t_2} \right) \qquad (2)$$

Failure mechanism 1bozw:

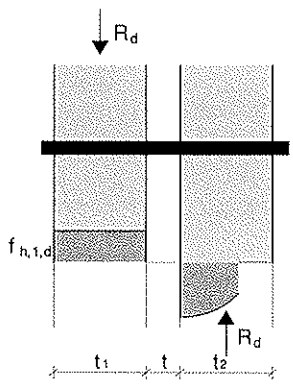

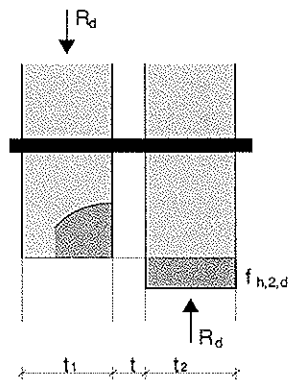

Load-carrying capacity

$$R_d = f_{h,1,d} \cdot d \cdot t_1 \qquad (3)$$

$$R_d = f_{h,2,d} \cdot d \cdot t_2 \qquad (4)$$

Failure mechanism 2aozw:

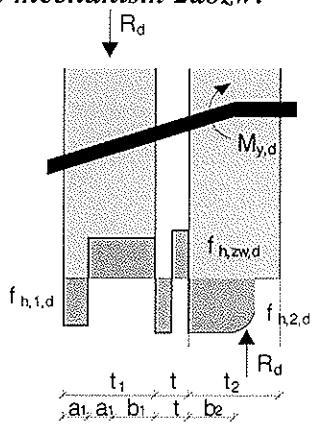

Load-carrying capacity:

$$R_d = f_{h,1,d} \cdot b_1 \cdot d \tag{5}$$

with $\beta = \dfrac{f_{h,2,d}}{f_{h,1,d}}$

and the condition $b_1 = \beta \cdot b_2$

b_1 follows as:

$$b_1 = \frac{1}{\frac{1}{\beta}+\frac{1}{2}}\left(-2t - t_1 + \sqrt{t^2 + tt_1 + \frac{t_1^2}{2} + \frac{f_{h,zw,d}t^2}{2f_{h,1,d}\beta} + \frac{t_1^2}{2\beta} + \frac{2M_y}{f_{h,1,d}\beta d} + \frac{f_{h,zw,d}t^2}{f_{h,1,d}4} + \frac{M_y}{f_{h,1,d}d}}\right) \tag{6}$$

Failure mechanism 2bozw:

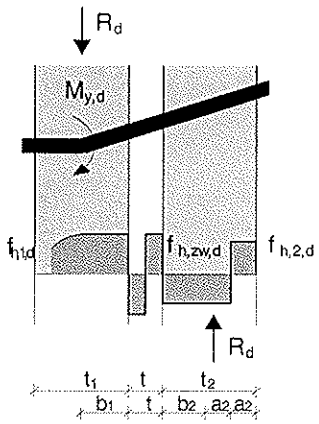

Load-carrying capacity:

$$R_d = f_{h,1,d} \cdot b_1 \cdot d \tag{7}$$

with $\beta = \dfrac{f_{h,2,d}}{f_{h,1,d}}$ and $\delta = \dfrac{f_{h,zw,d}}{f_{h,1,d}}$

and the condition $b_1 = \beta \cdot b_2$

b_1 follows as:

$$b_1 = \frac{\beta}{\frac{1}{2}+\beta}\left(-t - \frac{t_2}{2} + \sqrt{\left(1 + \frac{\delta}{4\beta} + \frac{\delta}{2}\right)t^2 + \left(\frac{1}{2} + \frac{1}{2}\beta\right)t_2^2 + tt_2 + \frac{M_{y,d}}{f_{h,1,d}d\beta} + \frac{2M_{y,d}}{f_{h,1,d}d}}\right) \tag{8}$$

Failure mechanism 3bozw:

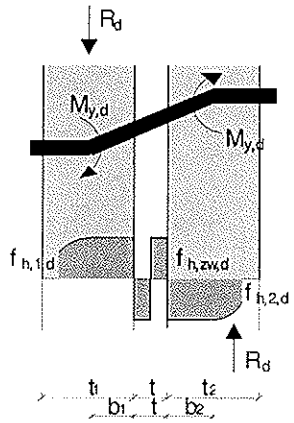

Load-carrying capacity:

$$R_d = f_{h,1,d} \cdot b_1 \cdot d \tag{9}$$

with $\beta = \dfrac{f_{h,2,d}}{f_{h,1,d}}$ and $\delta = \dfrac{f_{h,zw,d}}{f_{h,1,d}}$

and the condition $b_1 = \beta \cdot b_2$

b_1 follows as:

$$b_1 = \frac{1}{1+\beta}\left(-\beta t + \sqrt{\beta^2 t^2 + 4\beta(\beta+1)\cdot\frac{M_{y,d}}{f_{h,1,d}d} + \frac{\beta(\beta+1)}{2}\delta t^2}\right) \tag{10}$$

3.1.2 Rigid connection between interlayer and timber

Failure mechanism 1amzw:

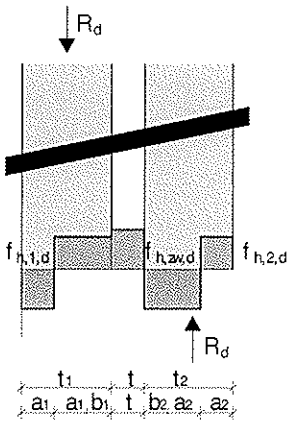

Load-carrying capacity:

$$R_d = f_{h,1,d} \cdot b_1 \cdot d + f_{h,zw,d} \cdot t \cdot d \qquad (11)$$

with $\beta = \frac{f_{h,2,d}}{f_{h,1,d}}$ and $\delta = \frac{f_{h,zw,d}}{f_{h,1,d}}$

and the condition $b_1 = \beta \cdot b_2 - \delta \cdot t$,

b_1 follows as:

$$b_1 = \frac{\beta}{\beta+1}\left(t(\delta-2) - t_1 - t_2 + \sqrt{t^2\left(4 - 2\delta + 2\frac{\delta}{\beta} - \frac{\delta^2}{\beta}\right) + t_1^2\left(2 - \frac{1}{\beta}\right) + t_2^2(2+\beta) + t_1 t\left(4 + 2\frac{\delta}{\beta}\right) + t\, t_2(4-2\delta) + 2t_1\, t_2}\right) - \delta t \qquad (12)$$

Failure mechanism 1bmzw:

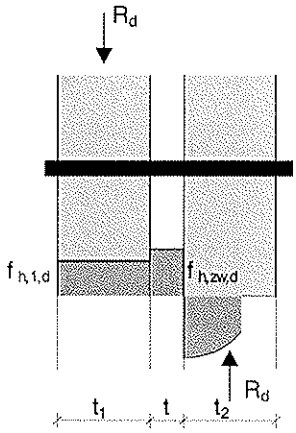

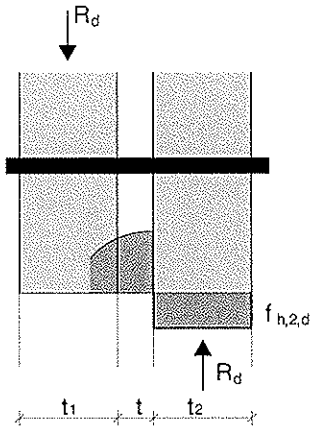

Load-carrying capacity:

$$R_d = f_{h,1,d} \cdot t_1 \cdot d + f_{h,zw} \cdot t \cdot d \qquad (13)$$

$$R_d = f_{h,2,d} \cdot t_2 \cdot d \qquad (14)$$

Failure mechanism 2amzw:

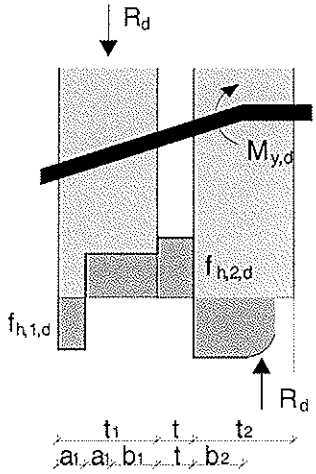

Load-carrying capacity:

$$R_d = f_{h,1,d} \cdot b_1 \cdot d + f_{h,zw,d} \cdot t \cdot d \tag{15}$$

with $\beta = \frac{f_{h,2,d}}{f_{h,1,d}}$ and $\delta = \frac{f_{h,zw,d}}{f_{h,1,d}}$

and the condition $b_1 = \beta \cdot b_2 - \delta \cdot t$,

b_1 follows as:

$$b_1 = \frac{\beta}{\beta+2}\left(t(\delta-2)-t_1\right) + \sqrt{t^2\left(4-2\delta+4\frac{\delta}{\beta}-2\frac{\delta^2}{\beta}\right)+t_1^2\left(2+\frac{2}{\beta}\right)+t\,t_1\left(4+4\frac{\delta}{\beta}\right)+\frac{4M_y}{f_{h,1}d}\left(\frac{2}{\beta}+1\right)} - \delta t \tag{16}$$

Failure mechanism 2bmzw:

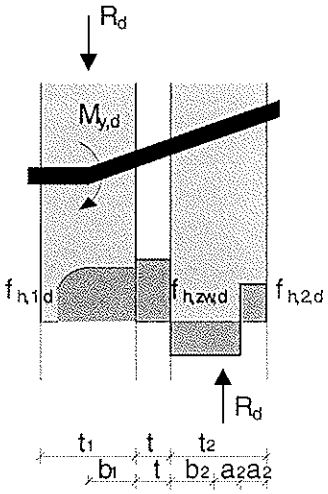

Load-carrying capacity:

$$R_d = f_{h,1,d} \cdot b_1 \cdot d + f_{h,zw,d} \cdot t \cdot d \tag{17}$$

with $\beta = \frac{f_{h,2,d}}{f_{h,1,d}}$ and $\delta = \frac{f_{h,zw,d}}{f_{h,1,d}}$

and the condition $b_1 = \beta \cdot b_2 - \delta \cdot t$,

b_1 follows as:

$$b_1 = \frac{\beta}{2\beta+1}\left(t(2\delta-2)-t_2\right) + \sqrt{t^2\left(4-4\delta-\frac{2\delta^2}{\beta}+\frac{2\delta}{\beta}\right)+t_2^2(2+2\beta)+t\,t_2(4-4\delta)+\frac{4M_y}{f_{h,1}d}\left(2+\frac{1}{\beta}\right)} - \delta t \tag{18}$$

Failure mechanism 3mzw:

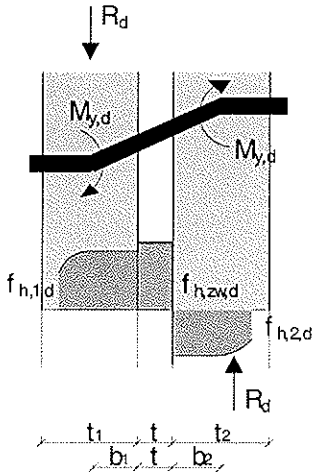

Load-carrying capacity:

$$R_d = f_{h,1,d} \cdot b_1 \cdot d + f_{h,zw,d} \cdot t \cdot d \tag{19}$$

with $\beta = \frac{f_{h,2,d}}{f_{h,1,d}}$ and $\delta = \frac{f_{h,zw,d}}{f_{h,1,d}}$

and the condition $b_1 = \beta \cdot b_2 - \delta \cdot t$,

b_1 follows as:

$$b_1 = \frac{\beta}{\beta+1}\left(t(\delta-1) + \sqrt{t^2\left(1-\delta+\frac{\delta}{\beta}-\frac{\delta^2}{\beta}\right)+\frac{4M_{y,d}}{f_{h,1,d}d}\left(1+\frac{1}{\beta}\right)}\right) - \delta t \tag{20}$$

3.2 Theoretical models for steel-to-timber joints

3.2.1 No connection between interlayer and timber

Failure mechanism 1ozw - thick steel plate:

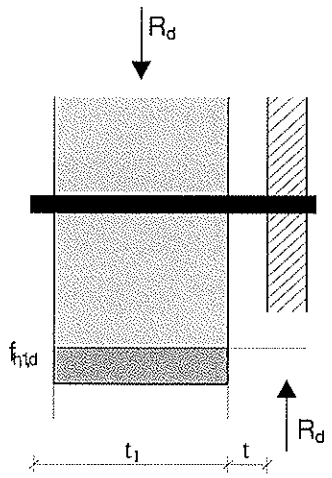

Load-carrying capacity:

$$R_d = f_{h,1,d} \cdot t_1 \cdot d \tag{21}$$

Failure mechanism 2ozw - thick steel plate:

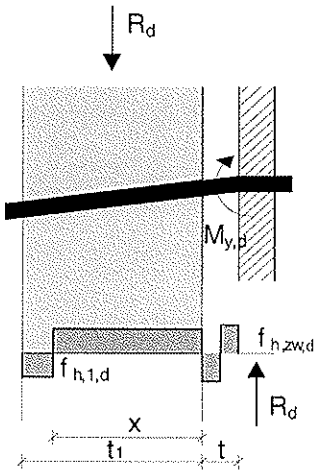

Load-carrying capacity:

$$R_d = 2 \cdot f_{h,1,d} \cdot x \cdot d - f_{h,1,d} \cdot t_1 \cdot d \tag{22}$$

$$x = -t + \sqrt{t^2 + \frac{M_{y,d}}{f_{h,1,d} d} + \frac{f_{h,zw,d} t^2}{4 f_{h,1,d}} + t_1 t + \frac{t_1^2}{2}} \tag{23}$$

Failure mechanism 3ozw - thick steel plate:

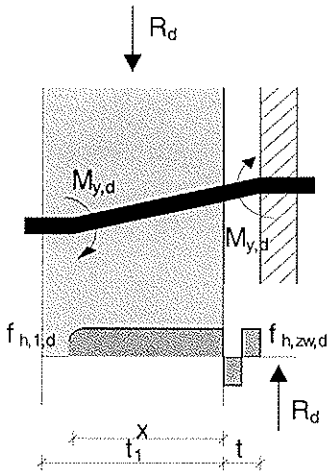

Load-carrying capacity:

$$R_d = f_{h,1,d} \cdot x \cdot d \tag{24}$$

$$x = -t + \sqrt{t^2 + \frac{4 M_{y,d}}{f_{h,1,d} d} + \frac{f_{h,zw,d} t^2}{2 f_{h,1,d}}} \tag{25}$$

Failure mechanism 1aozw - thin steel plate:

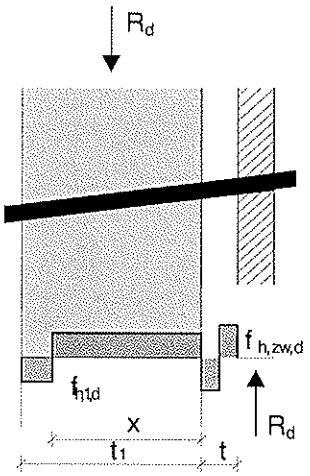

Load-carrying capacity:

$$R_d = 2 \cdot f_{h,1,d} \cdot x \cdot d - f_{h,1,d} \cdot t_1 \cdot d \tag{26}$$

$$x = -t + \sqrt{t^2 + \frac{f_{h,zw,d} t^2}{4 f_{h,1,d}} + t_1 t + \frac{t_1^2}{2}} \tag{27}$$

Failure mechanism 2ozw - thin steel plate:

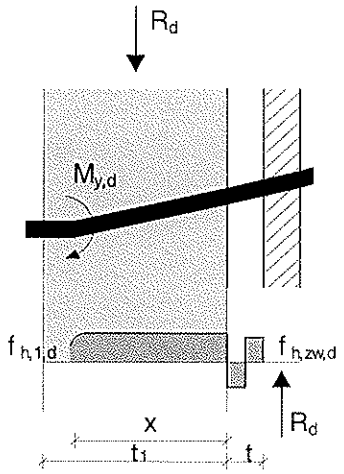

Load-carrying capacity:

$$R_d = f_{h,1,d} \cdot x \cdot d \tag{28}$$

$$x = -t + \sqrt{t^2 + \frac{2M_{y,d}}{f_{h,1,d} d} + \frac{f_{h,zw,d} t^2}{2 f_{h,1,d}}} \tag{29}$$

3.2.2 Rigid-connected interlayer to the timber

Failure mechanism 1mzw - thick steel plate:

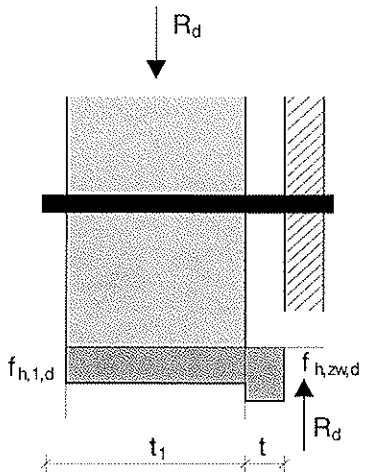

Load-carrying capacity:

$$R_d = f_{h,1,d} \cdot t_1 \cdot d + f_{h,zw,d} \cdot t \cdot d \tag{30}$$

Failure mechanism 2mzw - thick steel plate:

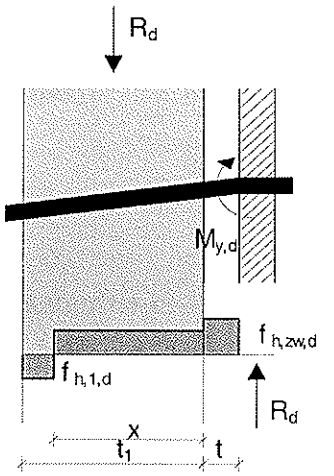

Load-carrying capacity:

$$R_d = 2 \cdot f_{h,1,d} \cdot x \cdot d - f_{h,1,d} \cdot t_1 \cdot d + f_{h,zw,d} \cdot t \cdot d \tag{31}$$

$$x = -t + \sqrt{t^2 + \frac{M_{y,d}}{f_{h,1,d} d} - \frac{f_{h,zw,d} t^2}{2 f_{h,1,d}} + t_1 t + \frac{t_1^2}{2}} \tag{32}$$

Failure mechanism 3mzw - thick steel plate:

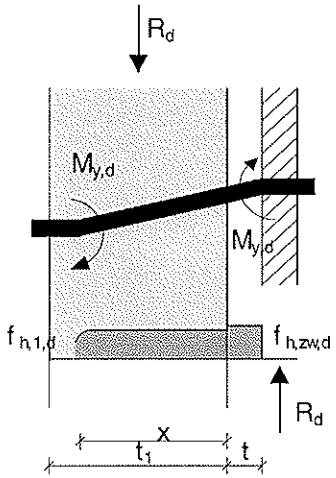

Load-carrying capacity:

$$R_d = f_{h,1,d} \cdot x \cdot d + f_{h,zw,d} \cdot t \cdot d \tag{33}$$

$$x = -t + \sqrt{t^2 + \frac{4M_{y,d}}{f_{h,1,d} d} - \frac{f_{h,zw,d} t^2}{f_{h,1,d}}} \tag{34}$$

Failure mechanism 1amzw - thin steel plate:

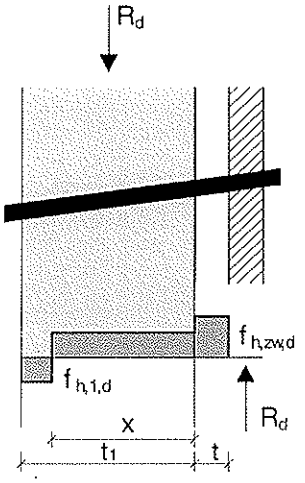

Load-carrying capacity:

$$R_d = 2 \cdot f_{h,1,d} \cdot x \cdot d - f_{h,1,d} \cdot t_1 \cdot d + f_{h,zw,d} \cdot t \cdot d \tag{35}$$

$$x = -t + \sqrt{t^2 - \frac{f_{h,zw,d} t^2}{2 f_{h,1,d}} + t_1 t + \frac{t_1^2}{2}} \tag{36}$$

Failure mechanism 2mzw - thin steel plate:

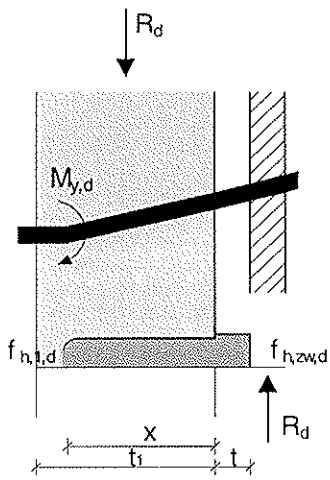

Load-carrying capacity:

$$R_d = 2 \cdot f_{h,1,d} \cdot x \cdot d - f_{h,1,d} \cdot t_1 \cdot d \tag{37}$$

$$x = -t + \sqrt{t^2 + \frac{f_{h,zw,d} t^2}{4 f_{h,1,d}} + t_1 t + \frac{t_1^2}{2}} \tag{38}$$

4 Verification of the theoretical models

The test results are compared with the theoretical load-carrying capacities. The theoretical values were determined using the average values of the embedding strength and yield moment, respectively, determined by tests. Because the slip between OSB panels and timber studs was not measured during the tests, the two extreme cases are considered in the comparison: one case with no connection between OSB and stud and the case with a rigid connection.

Because of the formation of two plastic hinges per fastener, equations (9) and (19), respectively were at first evaluated for the timber-to-timber connections. The chord effect causing tensile forces in the nails and thereby increasing the load-carrying capacity was not taken into account. Since one plastic hinge occurred in the OSB-layer in test series A1 and A2, equation (19) does not apply. In this case, the connection acted as a usual timber-to-wood-based-panel connection with two plastic hinges per shear plane. Consequently, the corresponding Johansen equation was evaluated leading to the respective values in the last column of Table 3.

For the steel-to-timber connections equations (24) and (33) were used. A rigid connection between OSB and the timber stud was assumed in test series B. Although a 'thin' steel plate was used a clamped support of the nails in the steel plate was observed, leading to two plastic hinges per shear plane.

Table 3: Verification of the theoretical models

Test	test result [kN]	Theoretical model without connection [kN]	theoretical model with connection [kN]
A1-1	20.3	14.1	20.0
A1-2	23.3	14.4	20.3
A1-3	20.0	13.9	19.7
A2-1	34.0	15.0	20.8
A2-2	33.0	14.2	20.3
A2-3	34.6	14.5	20.4
A-1	32.7	14.9	26.4
A-2	33.7	15.0	26.5
A-3	32.2	13.8	26.3
B-1	32.4	14.9	26.4
B-2	34.4	14.8	26.4
B-3	34.8	14.8	26.4

Generally, the theoretical model disregarding a slip between OSB and timber stud predict the test results better than the model without a connection between OSB and timber. The calculated load-carrying capacities for the tests with smooth nails (series A1) agree very well with the test results. The load-carrying capacities of the tests with ringed shank nails (series A2) are higher than the calculated values because the cord effect was not taken into account in the calculation. The same applies for the steel-to-timber connections (series A and B), regardless whether the OSB was bonded or stapled to the timber studs.

5 Conclusions

Because of the lack of knowledge about the load-carrying capacity of connections with dowel-type fasteners, where a wood-based panel is put between the members to be connected, the theoretical values of the load-carrying capacity based on the Johansen theory were derived and verified by a small number of tests. Two cases were considered in the theoretical models: one with a rigid connection between interlayer and one timber member and another case without a connection. For the case with connection, tests were performed with rigid and semi-rigid connections, respectively.

The slip between the timber member and the attached interlayer did not influence the load-carrying capacity of the connection. This statement is true, if the connection between interlayer and timber member is designed to carry the load introduced into the wood-based panel. In this case, the theoretical model based on a rigid connection may be used to calculate the load-carrying capacity of the connection. In all other cases, the conservative model disregarding a load transfer between wood-based panel and timber member should be used.

6 References

[1] Johansen, K.W.: Theory of timber connections. International Association for Bridge and Structural Engineering, Vol.9, p.249-262, 1949

[2] Werner, H.: Tragfähigkeit von Holz-Verbindungen mit stiftförmigen Verbindungsmitteln unter Berücksichtigung streuender Einflußgrößen, 1993

[3] Blaß, H.J. and Laskewitz, B.: Tragfähigkeit von Verbindungen an Holztafelelementen, research report of Versuchsanstalt für Stahl, Holz und Steine, Abt. Ingenieurholzbau, University of Karlsruhe, 2000

Table A1: Density and moisture content of the timber-to-timber shear joints tests

test	component	density [g/cm³]	Moisture content [%]
A1-1	post	0.411	12.5
	edge beam 1	0.450	14.0
	edge beam 2	0.434	13.8
A1-2	post	0.457	12.4
	edge beam 1	0.432	13.4
	edge beam 2	0.509	13.7
A1-3	post	0.403	12.4
	edge beam 1	0.424	13.4
	edge beam 2	0.409	13.6
A2-1	post	0.569	12.5
	edge beam 1	0.507	13.6
	edge beam 2	0.505	13.6
A2-2	post	0.417	12.3
	edge beam 1	0.403	13.7
	edge beam 2	0.517	13.5
A2-3	post	0.469	12.5
	edge beam 1	0.507	13.7
	edge beam 2	0.425	13.6

Table A2: Results of the timber-to-timber shear joint tests according to DIN EN 26891

test	F_{max} [kN]	v_{max} [mm]	v_{01} [mm]	v_{04} [mm]	$v_{i,mod}$ [mm]	k_i [kN/mm]	k_s [kN/mm]
A1-1/1	40.6	12.04	0.024	0.317	0.391	56.78	46.04
A1-1/2	40.6	14.33	0.084	0.894	1.080	20.13	16.67
A1-2/1	46.5	10.82	0.064	0.694	0.840	25.94	21.43
A1-2/2	46.5	11.15	0.016	0.368	0.469	48.91	38.38
A1-3/1	39.9	11.90	0.097	0.656	0.745	27.44	24.16
A1-3/2	39.9	13.19	0.054	0.995	1.255	18.09	14.34
mean	42.3	-	-	-	-	32.88	26.84
COV [%]	8.6	-	-	-	-	48.8	47.07
A2-1/1	67.9	12.61	0.071	1.101	1.373	21.80	17.48
A2-1/2	67.9	15.00	0.333	2.250	2.556	10.67	9.39
A2-2/1	66.0	13.30	0.161	1.353	1.589	17.74	15.10
A2-2/2	66.0	15.00	0.094	1.380	1.715	17.39	13.99
A2-3/1	69.1	15.00	0.106	1.508	1.869	15.92	12.84
A2-3/2	69.1	14.80	0.286	1.723	1.916	13.93	12.53
mean	67.7	-	-	-	-	16.24	13.6
COV [%]	2.3	-	-	-	-	23.2	20.0

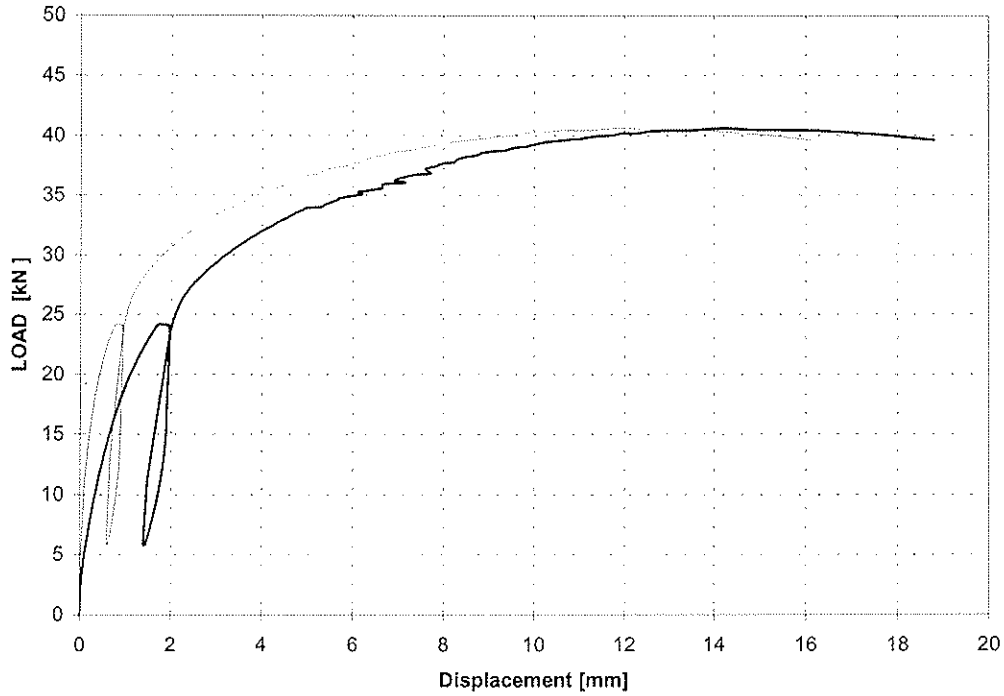

Figure A1: Load-displacement curves of a test specimen with smooth nails

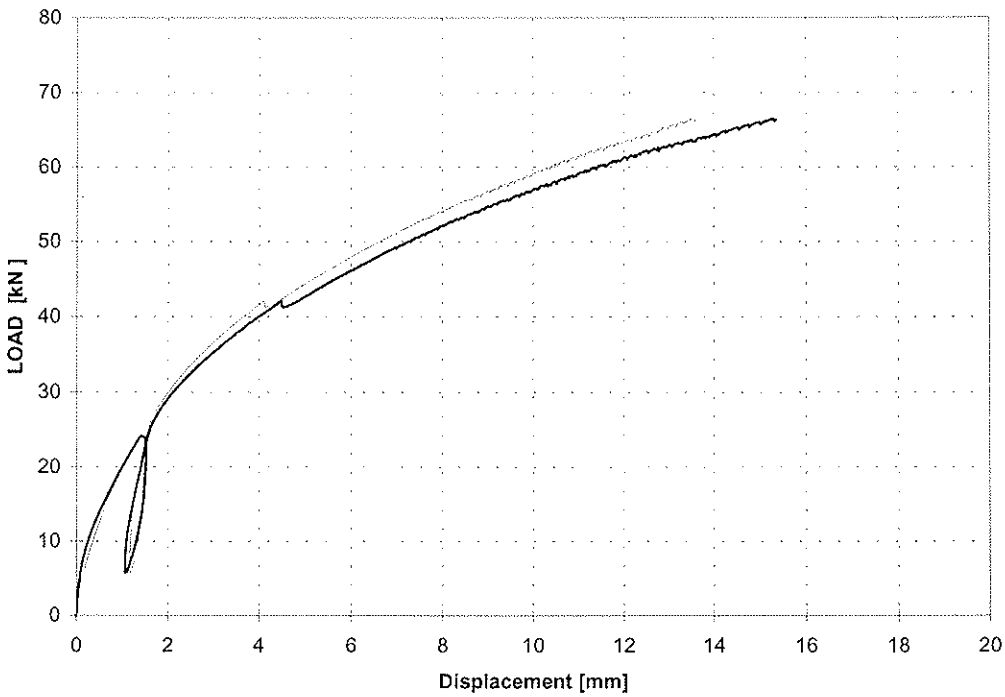

Figure A2: Load-displacement curves of a test specimen with ringed shank nails

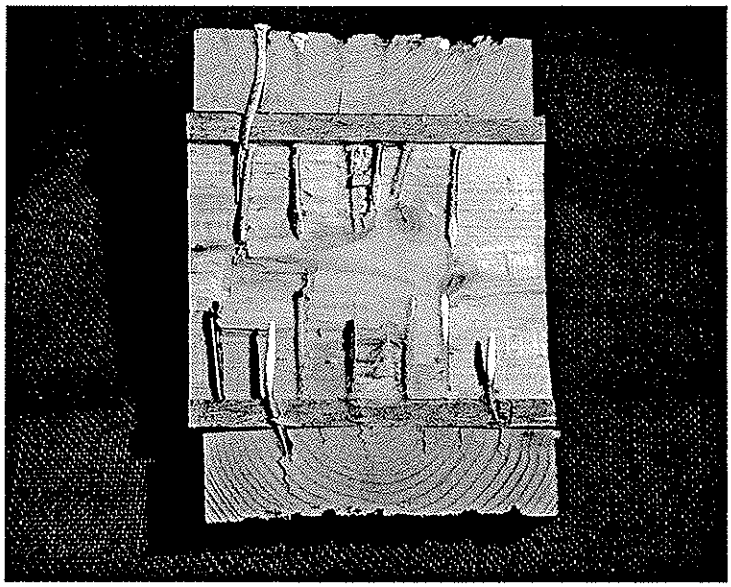

Figure A3: Opened specimen after the test

Table A3: Density and moisture content of the steel-to-timber shear joint tests

test	density [g/m³]	moisture content [%]
A-1	0.527	12.9
A-2	0.543	12.7
A-3	0.389	12.5
B-1	0.530	12.7
B-2	0.510	12.9
B-3	0.511	12.7

Table A4: Results of the tension tests according to DIN EN 26891

Versuch	F_{max} [kN]	v_{max} [mm]	v_{01} [mm]	v_{04} [mm]	$v_{i,mod}$ [mm]	k_i [kN/mm]	k_s [kN/mm]
A-1/1	32.7	15.00	0.104	1.380	1.701	10.14	8.23
A-1/2	32.7	11.66	0.078	1.359	1.708	10.30	8.20
A-2/1	33.7	15.00	0.188	1.774	2.115	7.89	6.62
A-2/2	33.7	11.36	0.093	1.318	1.633	10.62	8.57
A-3/1	32.2	15.00	0.197	2.561	3.152	5.47	4.44
A-3/2	32.2	11.86	0.167	1.864	2.263	7.51	6.19
mean	32.9	-	-	-	-	8.66	7.04
COV [%]	2.3	-	-	-	-	23.6	22.7
B-1/1	32.4	3.97	0.086	1.032	1.261	13.57	17.65
B-1/2	32.4	5.23	0.133	1.284	1.535	10.90	9.12
B-2/1	34.4	7.86	0.099	0.975	1.168	14.36	11.99
B-2/2	34.4	-	0.090	1.135	1.393	12.33	10.05
B-3/1	34.8	5.94	0.109	0.923	1.085	15.17	12.90
B-3/2	34.8	-	-	-	-	-	-
mean	33.9	-	-	-	-	13.27	12.3
COV[%]	3.8	-	-	-	-	12.7	26.95

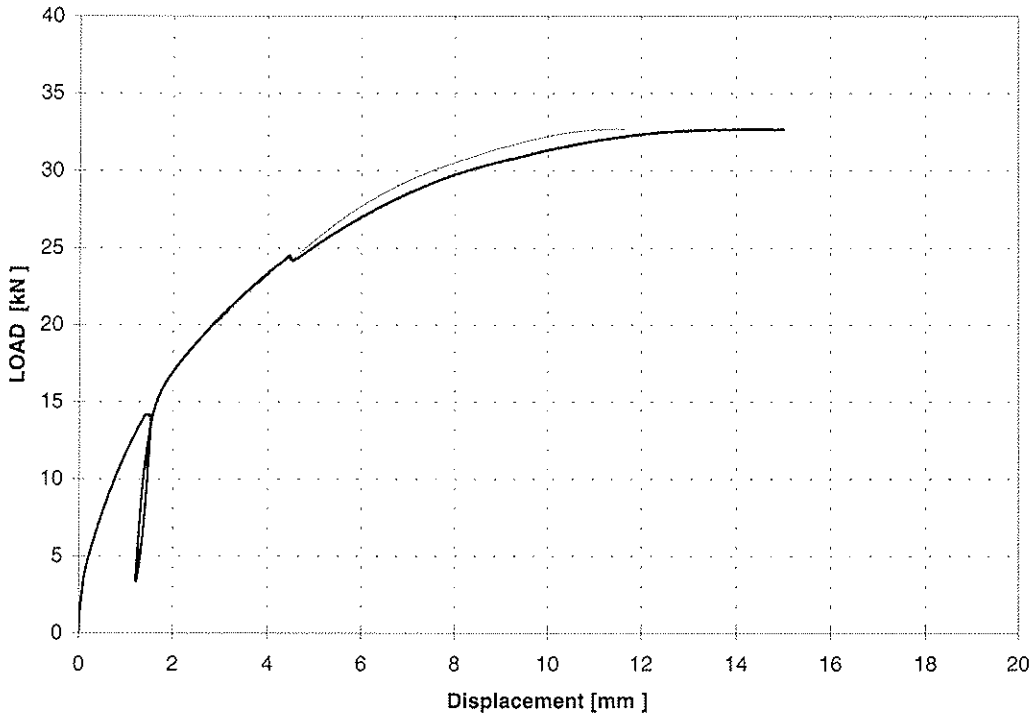

Figure A4: Load-displacement curves of a tension test specimen with a stapled connection between OSB and timber

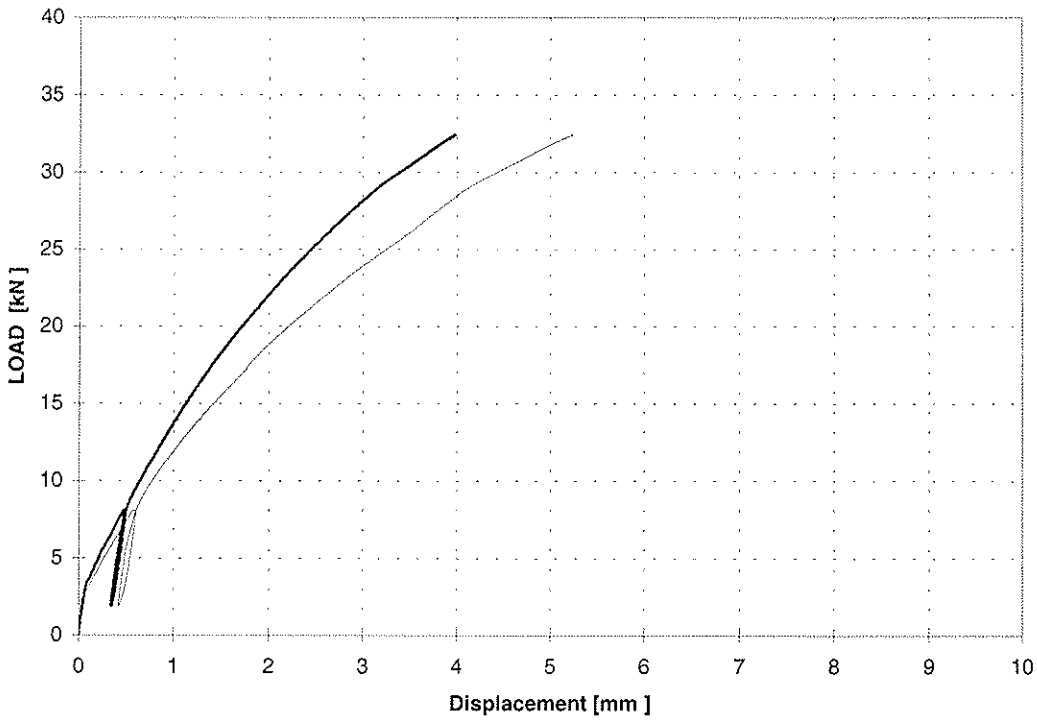

Figure A5: Load-displacement curves of a tension test specimen with a bonded connection between OSB and timber

Figure A6: X-ray of a specimen of series A-1

INTERNATIONAL COUNCIL FOR RESEARCH AND INNOVATION
IN BUILDING AND CONSTRUCTION

WORKING COMMISSION W18 - TIMBER STRUCTURES

EVALUATION OF PERPENDICULAR TO GRAIN FAILURE OF BEAMS CAUSED BY CONCENTRATED LOADS OF JOINTS

by

T A C M van der Put
A J M Leijten
Delft University of Technology

THE NETHERLANDS

MEETING THIRTY-THREE
DELFT
THE NETHERLANDS
AUGUST 2000

Presented by: A.J.M. Leijten

· H. Blass commented that M_1 and M_2 values as depicted in Figure 2 were incorrect as normal forces were ignored.
· A. Leijten responded that the influence was minor and the data fitted the model well.
· H. Blass commented that with incorrect basic assumptions the theory would be questionable.
· H.J. Larsen commented that as in the case of notched beams, the moments might not be as important as the crack length and shear forces.
· H. Blass commented that the notch beam analogy would be different.
· M. Ballerini stated his disagreement with some of the statements in this paper. He provided detailed critic and rebuttal to the points raised in section 4.1 of this paper. He pointed out that there were numerous misinterpretation of his own work presented previously in CIB W18 paper 32-7-2. M. Ballerini also pointed out that a factor of 2 seemed to be omitted in the current study. Finally, M. Ballerini made available videotapes of his tests and pictures of the failed specimen.
· A. Leijten responded that the calculations were carefully checked. Further discussions took place.
· H. Blass suggested that A. Leijten, M. Ballerini, and T.A.C.M. van der Put meet and sort out their differences and provide written comments.

Comments to paper 33-7-7 "Evaluation of perpendicular to grain failure of beams caused by concentrated loads of joints"

M. Ballerini, University of Trento - Italy

The authors have revised the paper reported in these proceedings after the presentation at the conference. Although some changes have been done, questionable assumptions and conclusions are still present in this last release of the contribution.
The major debatable points, mainly related to my research results, are commented below. In the following, text from the paper is written in italics while comments are in roman.

Chapter 1

Fourth, the joint is under-designed and splitting may still occur but probably not sooner than after the elongated holes have damaged the cross-section considerable.

As I already told to the authors, this sentence is not true since in my research there were a lot of specimens that didn't show the large plastic deformations and consequently the considerable damage of cross-section the authors think. This can be noticed easily by the comparison between the values of f_s reported in Table 1 and the value of the average embedding strength perpendicular to grain (beams in my research have an average density of about 430 kg/m^3, than the average embedding strength perpendicular to the grain can be estimated of about 21 MPa).

Chapter 3

For higher values of η (L/h ratio of a simply supported beam) not tested in [5], for instance $\eta \geq 5$ the splitting strength will not be determining over bending or shear failure and other failure mechanisms depending on the loading.

I tested specimens with 2η of about 17 and 8.5. For both slenderness values, I recorded a lot of splitting failures at load levels well below the bending and the shear strengths of beams. With regard to the *"other failure mechanisms depending on the loading"*, Table 1 shows clearly that some failure loads were lower than the average embedding strength of the timber (21 MPa).

Chapter 4.1

It was reported in [4] that in all tests plastic deformation of the wood occurred prior to splitting.

To be exactly in [4] I wrote: "With regard to the perpendicular-to-grain plastic deformations under dowel's contact area, it is necessary to highlight that all tests, with the only exception of those characterised by very low α values, have shown more or less plastic deformations before failure."

The embedment stresses calculated as F_u / bd are high compared to the compression strength perpendicular to the grain, Table 1. This so-called hardening is due to confined dilatation perpendicular to the grain and depends on the deformation and thus the ability to spread the concentrated load as shown in Figure 3.

Usually stresses beneath dowels are compared with the embedding strength and not with the compression strength perpendicular to grain. Since the formula for the embedding strength has been derived experimentally, I think that it already includes the effect of confined dilatation as well as other effects.

In tests with two dowels the spacing is small, 3d. It appears from this data and also from other investigations that the spacing between the two dowels being less than 4d result in reduction of strength by early local failure. This explains the reduction of 4.4/5.1 in the table above.

The spacing of 3d is the minimum required by ENV 1995-1-1:1993.

The reduction simply comes from the fact that the increasing in strength of S2 specimens were lower than those predicted by the theory given in Appendix II.

The $f_{c,90}$ data reported in Table 1 comes from eq. (13). Unfortunately, the derivation of eq. (13) is not clear since it is not possible to understand the origin of n in the square root of eq. (11b) (Chapter 5).

Lastly, it is not possible to understand why from the low values of f_s and $f_{c,90}$ reported in Table 1 for S2 specimens the authors derive *"early local failure"*, while from the same low values of $f'_{c,90}$ in Table 3 (chapter 6) they derive *"that splitting of the beam is the determining failure mechanism and not the joint"*.

When full bearing is activated at about 1.5d deformation only 1.5d of spacing is left.

As I already told to the authors, the "plastic deformation" of about 15mm (1.5d) they mention in this sentence was recorded for specimen S1-4050-2 which has only 1 dowel ([4], figure 6 right). Since for specimens with 2 dowels (the only ones for which spacing has a meaning), the stresses induced by dowels were lower, also the deformations were lower and the final spacing larger.

In Figure 4 it is shown that with eq.(13), derived later, the results with one dowels can be explained. The same appears for the tests with two dowels (no figure given). It can be concluded that all test results of [4] can be explained by the spreading effect of compression perpendicular to grain theory as given above although finally all tests ended by splitting of the beam.

Since the structure of eq. (13) doesn't differ from that of eq. (7) derived by Van der Put for the splitting strength of beams, in my opinion the authors cannot conclude that they have explained the test results. Indeed, also eq. (7) gives a good prediction of test results with a simple reduction of the value of $\sqrt{GG_c}$ of about 30% ($\sqrt{GG_c} \cong 9$ N/mm$^{1.5}$).

As the yielding opens up the cracks at the shear plane of the joint these tests are not particularly suited to study the perpendicular to grain splitting. The upper value for the local strength when the spreading is more than adequate could not be determined as those values were omitted [4].

The opinion of the writer is that the authors simply don't want to take into account these test results. This conclusion comes from the fact that, as I shown above, it is easy to find in my research tests that fail at loads lower than the connection strength.

With regard to the latter sentence, I already told to the authors that the test results of specimens failed by embedding were not reported because, as I wrote in [4], of not interest for the research. If authors are interested they can found these data on my paper of Montreux (WCTE'98).

Chapter 5.1

The bearing strength of fasteners close to the loaded edge is smaller than the embedment strength as calculated in designing joints by the timber design code. The model that takes this phenomenon into account is as follows:

If the above sentence is true, the check of the strength of connections loaded perpendicular to grain should be modified. This can be done only in two ways: (1) modifying the formulas for the embedding strength derived experimentally; (2) introducing a new check for *"the spreading effect of compression perpendicular to grain"*. Is this the proposal of the authors?

Chapter 6

From Table 2 it follows that the mean f_c value of Series C is 6.2 N/mm^2 (c.o.v. 0.09). This value can easily be explained by the volume effect. The mean f_c value in [4] was 5.1 for dowels of 10 mm diameter. In Series C the nails are 3.8 mm diameter so: ... In this case the fit indicates n = 0.18.

It is not clear why the authors need the Weibull theory to explain these test results since they have a formula that already takes into account the different volumes involved by means of a, a_r, and d. Moreover, it is not clear why they take into account the different volumes simply by means of the different values of the fasteners diameter.

The influence of the row length a_r is examined by the Series G1.1 to G1.4, Table 4, having the same geometric parameters except the row length a_r. Figure 5. The strength is again governed by eq.(13). This Series is taken because it can be expected to follow the theory better than Series C where joints are very high loaded at fracture.

Since the authors write that the values of $f'_{c,90}$ can be used to recognise if failures are joint failures or splitting failures, it is not possible to understand why the authors save all the test results of Ehlbeck & Görlacher. Indeed, the values of $f'_{c,90}$ reported in Table 4 are of the same order of the values of $f'_{c,90}$ reported in Table 2 for series C whose results are discarded.

Figure 7: Failure of the joint, test Series G

$$y = \frac{F_u}{b\sqrt{h}}\sqrt{\frac{n_c}{n}}\sqrt{\frac{1+60/300}{1+a_r/3a}}\sqrt{\frac{b}{100}} = \frac{F_u}{b\sqrt{h}}\sqrt{\frac{8}{n}}\sqrt{\frac{1.2}{1+a_r/3a}}\sqrt{\frac{b}{100}} = f_c'\sqrt{\frac{d}{b}}\sqrt{d3\alpha 1.2*8} = 43.36\sqrt{\alpha}$$

On the vertical axes the normalised value of $F_u/b\sqrt{h}$ to the value at $n=n_c=8$; $a_r=60$; $a=100$mm; $b=100$ mm

The formula for y, developed to normalise the failure loads of Ehlbeck & Görlacher tests, is not correct since it doesn't agree the prediction formula developed by same authors (eq.(7) or eq.(15)). Particularly, it is not correct the introduction of the term $\sqrt{b/100}$. With this term the failure load it is not more a linear function of b!

EVALUATION OF PERPENDICULAR TO GRAIN FAILURE OF BEAMS CAUSED BY CONCENTRATED LOADS OF JOINTS

T.A.C.M. van der Put,
Delft Wood Science Foundation
A.J.M. Leijten
Delft University of Technology, the Netherlands

1. Introduction

This paper reviews test data and a fracture mechanical model designed for beams loaded perpendicular to grain by joints, see Figure 5. The aim is to show the capabilities of the model and to give a guideline for Eurocode 5. Splitting of beams loaded perpendicular to the grain by joints, was explained by fracture mechanics by Van der Put, [1] and [2]. An effort is made to make the theory more transparent and to show how well the method explains the test results of [3] and [4].

1.1 Summary

Splitting of beams loaded perpendicular to the grain by joints is explained by fracture mechanics by Van der Put as shown earlier [1] and [2]. Test data of two sources are being considered [3] and [4]. The test data can be divided into four groups. First, the joint is over-designed compared to the splitting strength. Second, the joint start to yield at the moment of splitting. Third, the joint yields followed by hardening and finally splitting of the beam. Fourth, the joint is under-designed and splitting may still occur but probably not sooner than after the elongated holes have damaged the cross-section considerable. An important parameter to distinguish between the cases is the apparent value of $\sqrt{GG_c}$.
In addition a model is presented to predict the capacity of fasteners located near the loaded edge based on the compression strength perpendicular to grain. The theory is given in Appendix II. It is shown that all the available test data can be explained. Simple design equations that derived to be considered by code writers.

2 Fracture mechanic approach

As several modes of crack propagation in two directions are expected to occur the energy approach is convenient to obtain solutions for splitting of beams. As mentioned in the RILEM State of the Art Report on fracture Mechanics (RC-110-TFM, Research Notes 1263, ESPOO 1991) that the energy approach does not show good results, a better concept is derived and verified in [2] and applied for notched beams. This derivation is also given in appendix I. As the behaviour of beams loaded perpendicular to grain by joints is comparable with notched beams the same method is applied, [1] and [2]. The derivation with slightly different constants is given in the following.

3. Fracture of the beam caused by joints.

The same principle and superposition method as given in [2] for notched beams is applied when joints load the beam perpendicular to the grain near the loaded edge. The difference of beam deformation in case of the not-cracked situation and the cracked state is calculated as follows:

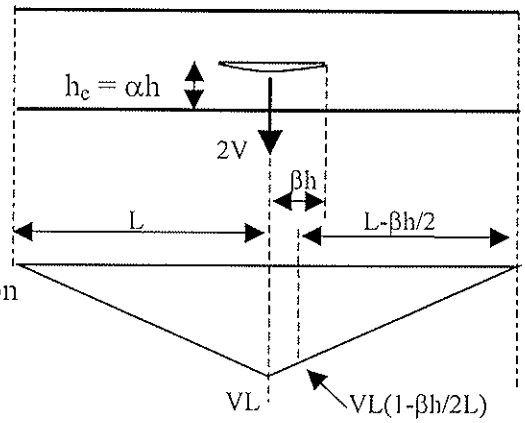

Beam with crack caused by a shear force

Schematic representation of the bending moment diagram

Figure 1: Joint loaded the beam perpendicular at grain at lower part

For a connection as shown in Figure 1 the following applies after a stable split occurs. The crack separated parts divide the bending moment of the initially not-cracked cross-section. A bending moment M is divided into two parts, M_2 is taken by the upper part of the beam (stiffness I_2) and M_1 and the shear force (V) is taken by the lower part (stiffness I_1). Normal forces can be neglected as they are of second order influence. The total crack length is set to $2\lambda=2\beta h$. The rotation φ at the end of crack length $\lambda=\beta h$ can be determined for both part by:

$$\varphi = \frac{M_2\,\lambda}{EI_2} = \frac{(M - M_1)\,\lambda}{EI_2} = \frac{M_1\lambda}{EI_1} + \frac{V\lambda^2}{2EI_1} \qquad (1)$$

with $M = M_1 + M_2$

being the moment at the end of the crack or:

$$M_1\left(1+\frac{I_2}{I_1}\right) = M - \frac{V\lambda I_2}{2I_1} \text{ and } \varphi = \frac{\overline{M}\lambda}{E(I_1+I_2)} \qquad (2)$$

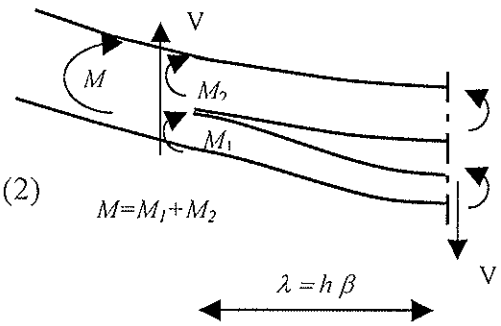

Figure 2: Static of half the crack

where:

$$\overline{M} = M + V\lambda/2$$

which is the mean bending moment over half the crack length $\lambda = \beta h$ which corresponds to a bending moment of:

$$\overline{M} = VL(1-\beta h/2L)$$

The relative deflection consisting of a shear and bending component is:

$$\delta = \delta_v + \varphi(L - \beta h/2)$$

$$\delta = \frac{1.2}{G}\left(\frac{\beta h}{b\alpha h} - \frac{\beta h}{bh}\right)V + \varphi(L - \beta h/2)$$

and with $\varphi = \dfrac{\overline{M}\lambda}{E(I_1 + I_2)}$ and $\overline{M} = VL(1 - \beta h/2L)$ it follows

$$\delta = \frac{1.2}{G}\left(\frac{\beta h}{b\alpha h} - \frac{\beta h}{bh}\right)V + VL\left(1 - \frac{\beta h}{2L}\right)\frac{\beta h}{E}\left(L - \frac{\beta h}{2}\right)\left(\frac{1}{I_1 + I_2}\right)$$

Furthermore:

$$\frac{\delta}{V} = \frac{1.2}{Gb}\beta\left(\frac{1}{\alpha} - 1\right) + L\left(1 - \frac{\beta h}{2L}\right)\frac{\beta h}{E}\left(L - \frac{\beta h}{2}\right)\left(\frac{1}{I_1 + I_2}\right) \qquad (3)$$

and

$$\frac{\partial\delta}{\partial\beta V} = \frac{1.2}{Gb}\left(\frac{1}{\alpha} - 1\right) + \frac{12\eta^2}{Eb}\left(1 - \frac{\beta}{2\eta}\right)\left(1 - \frac{3\beta}{2\eta}\right)\left(\frac{3\alpha(1-\alpha)}{1 - 3\alpha(1-\alpha)}\right) \qquad (4)$$

Where η is the L/h ratio

Substitution of $\gamma = 2\eta/3 - \beta$ in

$$\left(1 - \frac{\beta}{2\eta}\right)\left(1 - \frac{3\beta}{2\eta}\right) = \left(\frac{\gamma}{\eta}\right)\left(1 + \frac{3\gamma}{4\eta}\right) \approx \frac{\gamma}{\eta}$$

The potential energy of the symmetrical half of the beam is $W = V\,\delta/2$ were δ is the deflection in the middle. When V is constant the increase of the crack length Δx will increase the deflection with $\Delta\delta$. When the loss of potential energy ΔW becomes equal to the energy of the crack formation, crack propagation occurs, with $\Delta x = h\,\Delta\beta$. According to the principle [1] is

$$\int V\,\mathrm{d}\delta = \int G_f bh\,\mathrm{d}\beta = bh\int G_f\,\mathrm{d}\beta = G_{f,m}bh\beta$$

$$\int V\,\mathrm{d}\delta = \int V\frac{\partial\delta}{\partial V}\mathrm{d}V = \frac{\partial\delta}{\partial V}\int \mathrm{d}\left(\frac{V^2}{2}\right) = \frac{\partial\delta}{\partial V}\frac{V_f^{\,2}}{2}$$

where $\dfrac{\partial\delta}{\partial V} = \dfrac{\delta}{V}$ independent of V

At the constant maximal value of the shear force V fracture occurs when

$$\frac{\partial(\partial\delta/\partial V)}{\partial\beta}\cdot\frac{V_f^2}{2} = \int\frac{\partial G_f}{\partial\beta}\mathrm{d}\beta = \int^{C} dG_f = G_c$$

$$or\ V_f = \sqrt{\frac{2G_c}{\dfrac{\partial(\delta/V)}{\partial\beta}}} \qquad (5)$$

At the start of crack propagation G_f should be high enough to propagate also in width direction. When G_l and G_w are both the energy release rates in length and width direction it follows:

$$G_f bh\Delta\beta + G_w bh\Delta\xi = G_f bh\Delta\beta(1+\frac{G_w}{G_f}\frac{d\xi}{d\beta}) = G_f' bh\Delta\beta$$

Both G's are assumed to be covered by the apparent value of G_f'. Determining for total fracture is the combined mode I and II in length direction, see appendix I.

Substitution of the above in eq.(5) and for small values of β and E/G=18 it follows:

$$\frac{V_f}{b\alpha h} = \frac{\sqrt{GG_c/h}}{\sqrt{0.6\alpha(1-\alpha)+\eta\alpha^3(1-\alpha)\gamma/(1-3\alpha+3\alpha^3)}} \qquad (6)$$

The second term in the denominator appears to have a small influence for small values of α and η in the available test data. Also for increasing (stable) crack extension (or increase of β) the eq.(6) becomes eq.(7) for $\beta \approx 2\eta/3$, or $\gamma \approx 0$ giving an upper limit for failure.

$$\frac{V}{b\alpha h} = \frac{\sqrt{GG_c/h}}{\sqrt{0.6\alpha(1-\alpha)}} \quad or \quad \frac{V_f}{b\sqrt{h}} = \sqrt{GG_c}\sqrt{\frac{\alpha}{0.6(1-\alpha)}} \qquad (7)$$

For higher values of η (L/h ratio of a simply supported beam) not tested in [5], for instance $\eta \geq 5$ the splitting strength will not be determining over bending or shear failure and other failure mechanisms depending on the loading.

4. Failure caused by joints [4]

This chapter comprises a reaction on CIB/W18 paper 32-7-2 [4] to explain the test results. The dowels used can be regarded as rigid dowels as the slenderness ratio was b/d = 4 where b is the middle member thickness.
The configuration of the joint considered in the next chapters is shown in Figure 5.

4.1 Explanation of the test results of paper CIB/W18/32-7-2

It was reported in [4] that in all tests plastic deformation of the wood occurred prior to splitting. Figure 6 of the paper [4] shows plastic deformations from 4 up to 12mm. Obviously, one dowel of 10 mm diameter used as bearing plate is unable to force bending failure of the whole beam. The embedment stresses calculated as F_v/bd are high compared to the compression strength perpendicular to the grain, Table 1. This so-called hardening is due to confined dilatation perpendicular to the grain and depends on the deformation and thus the ability to spread the concentrated load as shown

$$f_s = c\, f_{c.90}\sqrt{L_s/d} \approx f_{c.90}\sqrt{3a/d}$$

in Figure 3. This can be explained by the equilibrium method of constructing a stress field in the specimen that satisfies the equilibrium and boundary conditions and that nowhere surmounts the failure criterion. As shown in appendix II it can be derived that the bearing strength can be expressed as:

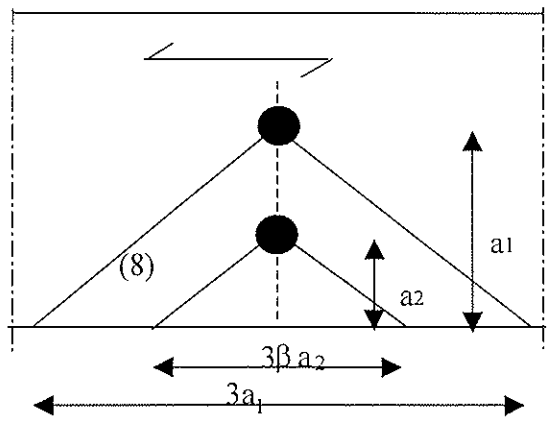

Figure 3: Spreading effect of two dowels

with $c \approx 1$ and a spreading slope 1:1.5 Where $L_s = 3a = 3h_e$ is the spreading length and a the loaded edge distance. In Table 1 the bearing stress f_s and compression stress perpendicular to grain $f_{c,90}$ are derived from the experimental values with eq.(8). In [4] test are performed with a single and with two dowels as shown in Figure 3. According to the theory of Appendix II two dowels in load direction, perpendicular to grain, can build equal resistance only if they have the same spreading surface. The spreading is equal when:

$3a_1 - 3\beta a_2 = 3\beta a_2$ or $\beta a_2 = a_1 / 2$

and both pins have a spreading length of $3a_1/2$

Table 1: Test data of [4]

Specimen	No.of	d	a	Spacing	a/h	$F_u=2V$	$f_s=F_u/db$	√3a/d	$f_{c,90}$
	test	mm	mm	mm		kN	Mpa		Mpa
	beam: b.h=40.196mm 1 dowel								Eq.(8)
S1-2020	2	10	40	0	0.20	7.6	19.0	3.46	5.5
2025	2	10	50	0	0.26	7.7	19.3	3.87	5
2030	2	10	60	0	0.31	8.3	20.8	4.24	4.9
2035	2	10	70	0	0.36	9.3	23.3	4.58	5.1
2040	2	10	80	0	0.41	10.3	25.8	4.9	5.3
2050	2	10	100	0	0.51	10.6	26.5	5.48	4.8
2060	2	10	120	0	0.61	15.5	38.8	6	6.4
2070	2	24	140	0	0.71	14.7	15.3	4.18	3.7
								mean	**5.1**
	beam: b.h = 40.196 mm 2 dowels							c.o.v	0.15
S2-2035	1	10	70	30	0.36	9.9	12.4	3.24	3.8
2040	1	10	80	30	0.41	12.2	15.3	3.46	4.4
2050	1	10	100	30	0.51	14.7	18.4	3.87	4.8
2060	1	10	120	30	0.61	14.9	18.6	4.24	4.4
2070	2	10	140	30	0.71	13.2	16.5	4.58	3.6
								mean	**4.1**
	beam: b.h = 40.397mm 1 dowels							c.o.v.	0.12
S1-4010	3	10	40	0	0.10	7.2	18	3.46	5.2
4015	2	10	60	0	0.15	7.8	19.5	4.24	4.6
4020	2	10	80	0	0.20	9.4	23.5	4.9	4.8
4025	2	10	100	0	0.25	10.4	26	5.48	4.7
4030	3	10	120	0	0.30	12.9	32.25	6	5.4
4035	1	10	140	0	0.35	12	30	6.48	4.6
4040	2	10/24	160	0	0.40	16.5/18.3	41.3/19.0	6.93/4.47	6.0/4.3
4050	2	10	200	0	0.50	14.8	37	7.75	4.8
4060	2	10/24	240	0	0.60	18.9/20.1	47.3/20.9	8.49/5.48	5.6/3.8
							d=10mm	**mean**	**5.1**
	beam: b.h = 40.397mm 2 dowels							c.o.v.	0.09
S2-4018	1	10	70	30	0.18	9.8	12.3	3.24	3.8
4020	1	10	80	30	0.20	10.6	13.3	3.46	3.8
4030	1	10	120	30	0.30	19.6	24.5	4.24	5.8
4040	1	10	160	30	0.40	17.1	21.4	4.9	4.4
4043	1	10	170	30	0.43	19.6	24.5	5.05	4.9
4050	1	10	200	30	0.50	18.1	22.6	5.48	4.1
4060	1	10	240	30	0.60	24.8	31	6	5.2
4070	1	24	280	30	0.71	35.6	18.5	4.18	4.4
							d=10mm	**mean**	**4.6**
								c.o.v	0.15

S1 – tests with one dowel

S2 – test with two dowels

Mean $f_{c.90}$ values of Table 1.

Series	Per dowel $f_{c.90}$ [Mpa]	Mean
S1-200	5.1	5.1
S1-400	5.1	
S2-200	4.1	4.4
S2-400	4.6	

S1 refers to tests with one dowel,
S2 refers to tests with two dowels.

In tests with two dowels the spacing is small, $3d$. It appears from this data and also from other investigations that the spacing between the two dowels being less than $4d$ result in reduction of strength by early local failure. This explains the reduction of 4.4/5.1 in the table above. When full bearing is activated at about $1.5d$ deformation only $1.5d$ of spacing is left. The Eurocode5 code should therefore specify 4d as the minimum distance to avoid this effect instead of 3d. The mean strength $f_{c.90} = 4.1$ MPa for the (three) tests with dowels of 24 mm diameter compared to 5.1 MPa for the 10 mm diameter dowels can be explained by the volume effect.

$$f_{c.90} = f_{c.90,1}\left(\frac{d_1}{d}\right)^n = 5.1\left(\frac{10}{24}\right)^{0.25} = 4.1\,\text{MPa}$$

where $n = 3v/1.2 = 2.5v$ and v is the coefficient of variation of the sample in question. In this case $n = 0.25$

In Figure 4 it is shown that with eq.(13), derived later, the results with one dowels can be explained. The same appears for the tests with two dowels (no figure given).

It can be concluded that all test results of [4] can be explained by the spreading effect of

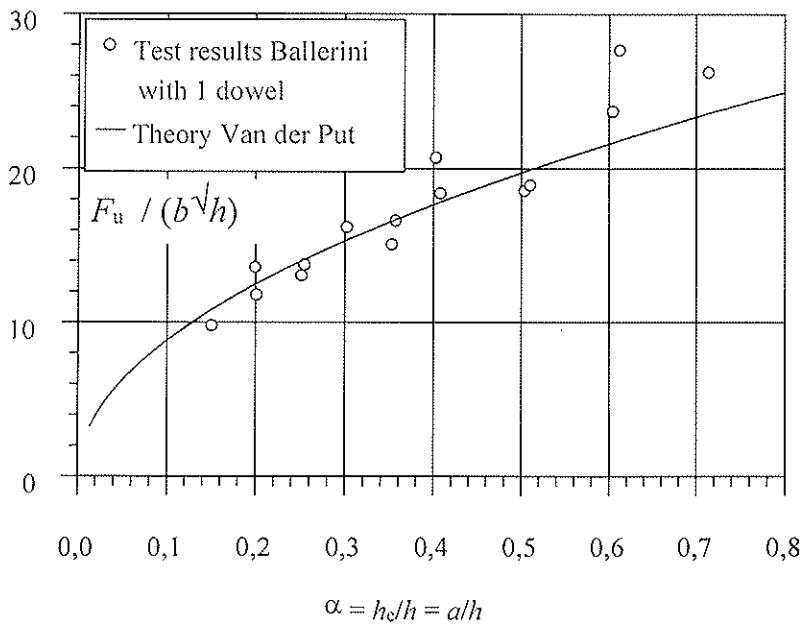

$$\frac{F_u}{b\sqrt{h}} = f_c\sqrt{n.3\alpha d} = 5.1\sqrt{3.10.\alpha} = 27.9\sqrt{\alpha}$$

Figure 4: Explanation of the test data of [4] with eq.(13) with $L_s = 3a = 3\alpha h$

compression perpendicular to grain theory as given above although finally all tests ended by splitting of the beam. It means that actually yielding of the joint started followed by hardening and ending with splitting. As the yielding opens up the cracks at the shear plane of the joint these tests are not particularly suited to study the perpendicular to grain splitting. The upper value for the local strength when the spreading is more than adequate could not be determined as those values were omitted [4].

5 Final state of failure of connections with dowels type fasteners

The previous chapter dealt with a special case of rigid dowels where the spreading of the compression stresses could be considered uniform in beam depth. In this chapter a more general approach is given dependent of dowel slenderness.

After the fastener starts to yield in bending, the resistance of joints with long fasteners still increases, showing only flow or hardening at increasing deformation. As shown in [6] and [7] this is due to the deformed shape of the fastener particularly for nails. The shape of the deformed nail compares well with a logarithmic spiral, where at the final stage the nail is bend over a large angle even up to nearly 90^0. The nails acts as a thin shell showing equilibrium of the embedment stresses with the normal forces in the shank and even yielding of the steel shank may occurs, for instance in the situation shown in Figure 5. In that case only the effective length of the shank takes part in the bearing. The spreading effect mentioned in the previous chapter can no longer be considered in one plane as with rigid dowels. The limited effectiveness of the shank length in spreading should be taken into account as far as it's smaller than half the beam thickness. For slender dowels full bearing across the whole middle beam is possible when sufficient deformation is able to develop. Another fastener type where the effective length is smaller than half the middle member thickness is the punched metal plate. For those cases eq. (8) is transformed into:

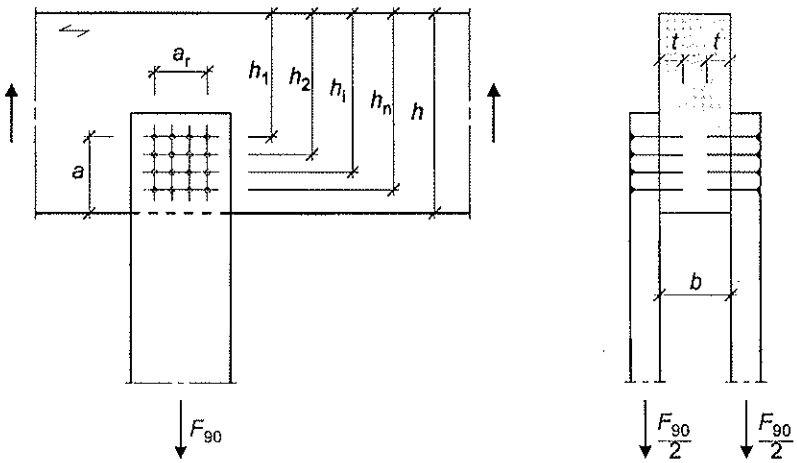

Figure 5: Parameters of a connection perpendicular to grain

$$f_{emb} = f_{c,90}\sqrt{\frac{A_1}{A_0}} = f_{c,90}\sqrt{\frac{L_s\, t}{d\ \lambda d}} \qquad (9)$$

where:

A_1 and A_0 are the spreading and loaded surfaces, respectively.

L_s is the spreading length along the grain

t half the middle member thickness, $b/2$, of the three member joint assuming the loaded edge distance is such that spreading across half the member depth is assured.

λd is the effective length of the fastener

d is the fastener diameter

If the fastener ends in the middle beam as shown in Figure 5. The load per shear plane of the joint per fastener becomes:

$$F/2 = f_{emb} d\, l = f_{emb} d\,(\lambda\, d) = f_{emb} \lambda\, d^2 \qquad (10)$$

Thus total for n fasteners per shear plane

where L_s/n is actually the spreading length per fastener, so with eq.(9) it becomes.

$$F = 2n\, f_{c.90} \sqrt{(L_s t)/(\lambda d^2)}\ \ \lambda\, d^2 \qquad (11)$$

$$F = n\, f_{c.90}\, d \sqrt{2\lambda}\, \sqrt{b\, L_s / n}$$

$$F = f_{c.90}\, d \sqrt{2\lambda} \sqrt{n L_s\, b} = f'_{c,90} d \sqrt{n\, L_s\, b} \qquad (12)$$

When the bearing length is half the member thickness $\lambda\, d = b/2$ as was the case in [4], eq.(12) becomes:

$$F = f_{c.90} b \sqrt{n\, L_s d} \qquad (13)$$

When $\lambda < b/2$, the penetration depth of the fastener ends within the middle member. For long nails with a penetration length of 12d then 3d at the point is needed for clamping, 3d for the anchoring (withdrawal capacity) leaving 6d for bearing. In that case $2\lambda d = 12d$ for two nails in both shear planes of the three member joints and eq.(12) becomes

$$F = f_{c.90} d \sqrt{2\lambda} \sqrt{n\, L_s b}\ = 3.5 f_{c.90} d \sqrt{n L_s b} \qquad (14)$$

In eq.(10) to eq.(14) the spreading length $L_s = a_r + 3a$ where a_r is the width of the fastener pattern, see Figure 5.

5.1 Summarising:

The bearing strength of fasteners close to the loaded edge is smaller than the embedment strength as calculated in designing joints by the timber design code. The model that takes this phenomenon into account is as follows:

For nails with penetration depth of more than $12d$:

$$F = f_{c.90} b \sqrt{n\, L_s d}$$

for $b \leq 12\, d$

$$F = 3.5 f_{c.90} d \sqrt{n\, L_s d}$$

with

$$L_s = 3a + a_r$$

and

$$f_{c.90} = 5.1 \left(\frac{10}{d} \right)^{0.25}$$

where:

F	is the ultimate load of the middle beam
b	width of the beam (middle member)
n	the number of fasteners/ shear plane
d	fastener diameter, in mm
L_s	is the
a	greatest distance to the loaded edge, Figure 5
a_r	the row length of the fastener pattern

Table 2: TU-Karlsruhe test data No.1: Joint with nails

Type	No.of	d	rows	Col.	$a=\alpha h$	a_r	$F_{u=2V}$	c.o.v.	f_c	f_c	$\sqrt{GG_c}$	$\eta=L/h$	$F/b\alpha h$
Test	tests		m	N			Mean		Eq(12)	Eq.(13)	Eq.(7)		
NAILS		[mm]			[mm]	[mm]	[kN]		[MPa]	{MPa]	[N/mm$^{1.5}$]		[MPa]
	beam: b.h = 40.180 mm												
L+A1	8	3.8	5	1	28	76	8.25	0.16	12.1	3.7	13.9	2.37	7.37
L7+A2	4	3.8	5	1	47	76	10.94	0.21	13.8	4.3	13.3	2.37	5.82
A3	3	3.8	5	1	66	76	11.93	0.04	13.4	4.2	11.3	2.37	4.52
A4	3	3.8	5	1	85	76	13.40	0.07	13.7	4.2	10.2	2.37	3.94
A5	3	3.8	5	1	104	76	18.90	0.21	17.8	5.5	11.7	2.37	4.54
	beam: b.h = 40.180 mm							**mean**	**14.2**	**4.4**	**12.1**		
L6+B1	4	3.8	5	2	28	76	12.73	0.05	11.4	3.5	15.5	2.37	6.77
B2	3	3.8	5	3	28	76	18.87	0.24	12.2	3.8	17.9	2.37	7.15
B3	3	3.8	5	4	28	76	21.13	0.26	10.8	3.3	16.1	2.37	6.21
B4	3	3.8	5	5	28	76	27.83	0.12	11.8	3.6	17.2	2.37	6.69
	beam: b.h = 40.120 mm							**mean**	**11.6**	**3.6**	**16.7**		
C1	3	3.8	2	1	28	76	9.53	0.12	22.1	6.8	15.3	2.18	8.51
C2	3	3.8	2	1	28	57	8.07	0.05	20.0	6.2	13.0	2.26	7.21
C3	3	3.8	2	1	28	38	6.80	0.02	18.1	5.6	10.9	2.34	6.07
C4	3	3.8	2	1	28	19	6.42	0.12	18.6	5.7	10.3	2.42	5.73
C5	3	3.8	1	1	28	0	6.95	0.20	22.3	6.9	11.2	2.50	6.21
C6	3	8	1	1	28	0	6.05	0.13	13.2	5.8	9.7	2.50	5.40
	beam: b.h = 40.180 mm							**mean**	**19.1**	**6.2**	**11.7**		
L8	1	8	1	1	28	0	5.20	-	11.2	5.0	8.8	2.50	4.64

6 Analyses of TU-Karlsruhe testdata

The test data is given in Tables 2 to 4. The parameters correspond to Figure 5. The ultimate load is given for two shear planes and therefore represent the total load on the middle beam loaded perpendicular to the grain. First a distinction has to be made to what category Series belong. Are the joints "over-designed" or "under-designed" compared to the splitting strength?

In Series B the nails are still loaded to a low level when splitting occurs, indicated by low f_c and f_c' values compared to Series A and C, Table 2. Apparently the joints are "over-designed". Despite the variation in number of nails from 10 to 25 the parameter $\sqrt{GG_c}$ =16.7 N/mm$^{1.5}$ (c.o.v. is 0.07) remains at the same level. The other Series A and C show lower values for $\sqrt{GG_c}$ which is a indication of a different behaviour.

For series C, with long nails, the working or effective length, λd according to eq.(12), of the spiral shape of the deformed nail, becomes larger than half the middle member thickness and thus λd is limited to $b/2$ and eq.(13) applies. From Table 2 it follows that the mean f_c value of Series C is 6.2 N/mm^2 (c.o.v. 0.09). This value can easily be explained by the volume effect. The mean f_c value in [4] was 5.1 for dowels of 10 mm diameter. In Series C the nails are 3.8 mm diameter so:

$$f_{emb} = f_{emb,1}\left(\frac{d_1}{d}\right)^n = 5.1\left(\frac{10}{3.8}\right)^{0.18} = 6.1\,\text{Mpa}$$

In this case the fit indicates n = 0.18.

The influence of the row length a_r is examined by the Series $G_{1.1}$ to $G_{1.4}$, Table 4, having the same geometric parameters except the row length a_r Figure 5. The strength is again governed

by eq.(13). This Series is taken because it can be expected to follow the theory better than Series C where joints are very high loaded at fracture. The influence given in Figure 6 and compared to the provision in the draft German design standard for row length.

Series A and Series V_5 to V_{10} of Table 3, also show a low value for the $\sqrt{GG_c}$ parameter that probably is caused by the number of nails being below the critical number as will be explained later. Confirmation by tests with more nails is necessary to estimate this critical number for Series V.

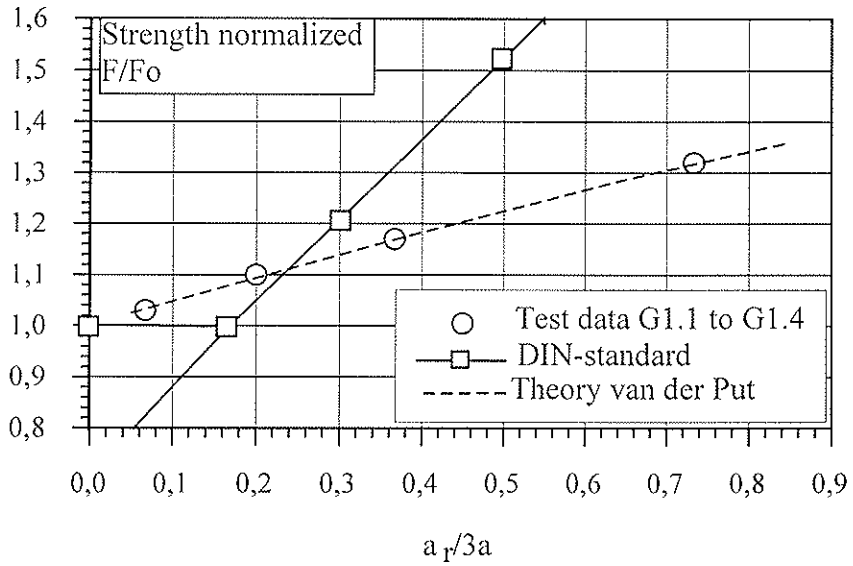

$$y = \frac{F}{F_0} = \sqrt{1 + \frac{a_r}{3a}} \qquad \text{DIN} \quad y = \frac{F}{F_0} = \max\left\{ \begin{array}{l} 1.0 \\ 0.7 + 1.4\dfrac{a_r}{h} \end{array} \right. = 0.7 + \frac{1.4 a_r\, 3a}{3a\ \ h} = 0.7 + \frac{a_r}{3a}\frac{4.2\ \ 100}{250} = 0.7 + 1.68\frac{a_r}{3a}$$

Figure 6: Influence of row length of fastener pattern a_r

As mentioned earlier low values of $f_c^{'}$ in Table 3 indicate that splitting of the beam is the determining failure mechanism and not the joint. This will be discussed below.

Table 3: TU-Karlsruhe test data No.2

Type	Fastener	No.of	d	Rows	col	$a=\alpha h$	a_r	$F_u=2V$	$F/b\alpha h$	$f_c^{'}$	$\sqrt{GG_c}$	$\eta=L/h$	$\sqrt{GG_m}$
	type	Tests		m	n			mean		Eq(12)	Eq.(7)		
			[mm]			[mm]	[mm]	[kN]	[Mpa]	[Mpa]	[N/mm$^{1.5}$]		
	beam:b.h = 100.1200mm												
V5	nails	1	4.2	10	4	300	205	75	2.48	8.44	14.4	1.42	39.7
V10	nails	1	4.2	10	4	600	205	119	1.98	9.96	13.3	1.42	31.7
	beam: b.h = 100.1200 mm								**mean**	**9.2**	**13.9**		
V2	dowels	1	16	3	2	300	205	90	3	6.91	17.5	1.43	48.2
V23	dowels	1	16	3	2	900	205	190	2.11	8.99	12.3	1.43	33.7
V3	dowels	1	16	3	4	300	205	112	3.73	6.08	21.7	1.43	59.9
V9	dowels	1	16	3	6	600	205	179	2.99	5.91	20.1	1.43	48.0
V4	dowels	1	16	2	2	300	205	65	2.17	6.11	12.6	1.37	34.1

	beam: b.h = 100.600 mm								mean	6.8	16.8		
V11/12	dowels	2	16	3	4	300	205	127	4.23	6.89	20.1	0.94	38.9
V13/14	dowels	2	16	3	2	450	205	190	4.22	12.3	17.4	0.94	38.8
V26	dowels	1	16	3	2	450	205	220	4.89	14.2	20.1	1.4	54.9
V24	dowels	1	16	3	2	150	205	70	4.63	6.93	19.0	1.4	54.7
V27	dowels	1	16	3	2	150	205	63	4.17	6.23	17.2	0.44	26.3
V25	dowels	1	16	3	2	300	205	103	3.43	7.91	16.3	1.4	38.5
V28	dowels	1	16	2	2	150	205	56	3.73	6.8	15.3	0.83	32.3
	beam: b.h = 100.1200 mm								mean	8.8	17.9		
V15/16	split-ring	2	65	2	2	300	205	135	4.49		21.3		
V17/18	split-ring	2	65	2	2	450	205	180	4.00		16.5		
V6	split-ring	1	65	1	4	600	0	184	3.06		20.6		
V7	split-ring	1	65	2	2	600	205	117	1.95		13.1		
V8	split-ring	1	65	2	2	300	300	89	2.98		17.3		
V1	split-ring	1	65	2	2	300	205	113	3.76		21.9		
									mean		18.4		

In Table 4 all Series show $\sqrt{GG_c}$ values smaller than the critical value of 17 N/mm$^{1.5}$ The strength values F_u are higher than according to the Johanson equations. This also can be

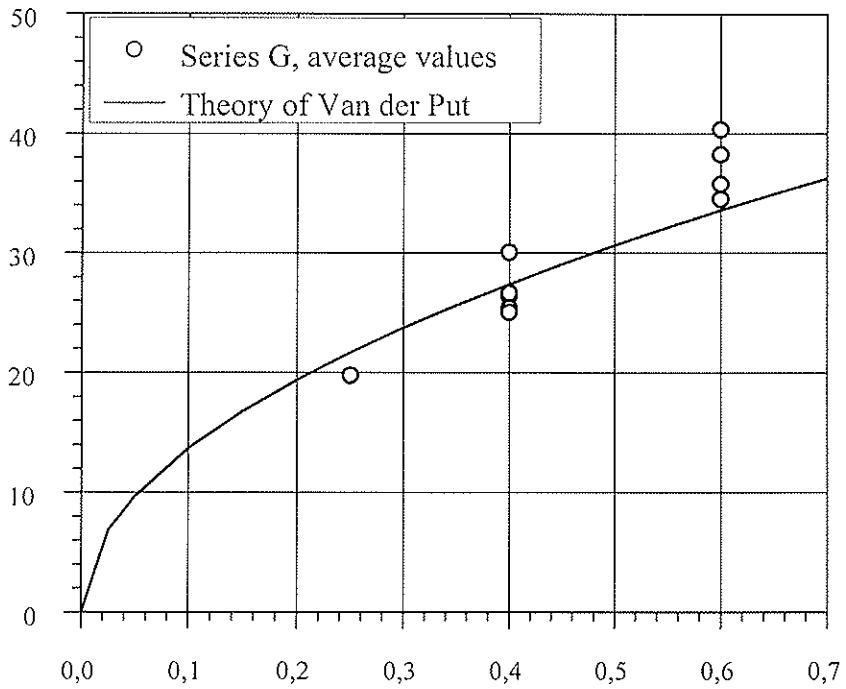

On the vertical axes the normalised value of $F_u/b\sqrt{h}$ to the value at $n = n_c = 8$
$a_r = 60$
$a = 100$mm
$b = 100$ mm

$$y = \frac{\frac{F}{b\sqrt{h}}}{\frac{F_u}{b\sqrt{h}}}$$

$$y = \frac{F_u}{b\sqrt{h}}\sqrt{\frac{n_c}{n}}\sqrt{\frac{1+60/300}{1+a_r/3a}}\sqrt{\frac{b}{100}} = \frac{F_u}{b\sqrt{h}}\sqrt{\frac{8}{n}}\sqrt{\frac{1.2}{1+a_r/3a}}\sqrt{\frac{b}{100}} = f_c'\sqrt{\frac{d}{b}}\sqrt{d3\alpha 1.2*8} = 43.36\sqrt{\alpha}$$

Figure 7: Failure of the joint, test Series G

expected by the under dimensioned joints and by possible hardening. Series $G_{5.1}$ with only 4 nails per shear plane is 0.85 times as strong as other Series with a comparable beam and 8 nails. For a "small" number of high loaded nails yielding of the nails causes not direct splitting of the beam probably because the crack opening is not yet critical. With a "small"

number of nails splitting becomes finally determining and apparently independent of the number of nails at a value for the apparent parameter $\sqrt{GG_c}$ = 12.2 N/mm$^{1.5}$ as will be discussed in the next chapter. Series G6, joints at the end of a cantilevered beam, has against the rules a nail distance of 7mm or 1.75 *d*, in stead of 4*d*. This obviously reduces the strength, as the hardening effect can't fully develop at the weakest nail.

Table 4: TU-Karlsruhe test data No.3

Type	Fastener	No.of	*d*	rows	col.	*a*=*αh*	a_r	F_u=2*V*	c.o.v.	*f*'c	$\sqrt{GG_c}$	*η*	*F*/*bαh*
	Type	tests		m	n			mean		Eq(12)	Eq.(7)		
			[mm]			[mm]	[mm]	[kN]		[Mpa]	[N/mm$^{1.5}$]		[Mpa]
		beam: b.h = 100.250 mm											
G1.1	Nails*	3	4.0	2	4	100	20	37.3	0.07	18.4	11.2	2.60	3.73
G1.2	Nails*	3	4.0	2	4	100	60	41.7	0.15	19.4	12.5	2.53	4.17
G1.3	Nails*	3	4.0	2	4	100	110	42.9	0.12	18.7	12.9	2.40	4.29
G1.4	Nails*	3	4.0	2	4	100	220	48.0	0.08	18.6	14.4	2.12	4.8
G1.5	Nails*	3	4.0	2	4	150	60	53.0	0.09	20.7	10.6	2.53	3.53
G1.6	Nails*	3	4.0	2	4	150	110	57.6	0.18	21.5	11.5	2.40	3.84
G1.7	Nails*	3	4.0	2	4	150	220	71.1	0.07	24.3	14.2	2.12	4.74
G2.1	Nails*	2	4.0	2	4	100	20	35.7	-	17.6	10.7	2.00	3.57
G2.2	Nails*	2	4.0	2	4	100	60	39.0	-	18.2	11.7	1.50	3.90
		beam: b.h = 80.250 mm							**mean**	**19.7**	**12.2**		
G3.1	Nails*	3	4.0	2	4	100	60	34.9	0.13	18.2	13.1	2.53	4.36
		beam: b.h = 120.250 mm							mean	19.9	11.6		
G3.2	Nails*	3	4.0	2	4	100	60	46.2	0.09	19.6	11.6	2.53	3.85
G3.3	Nails*	3	4.0	2	4	100	60	46.7	0.04	19.8	11.6	2.53	3.89
		beam: b.h = 100.250 mm							**mean**	**19.9**	**11.6**		
G3.4	Nails*	3	6.0	2	4	100	60	44.3	0.05	13.8	13.3	2.53	4.43
		beam: b.h = 100.400 mm											
G4.1	Nails*	3	4.0	2	4	100	60	39.6	0.05	18.4	13.3	1.95	3.95
G4.2	Nails*	3	4.0	2	4	160	60	51.7	0.20	19.7	12.3	1.95	3.23
		beam: b.h = 100.150 mm							**mean**	**19.1**	**12.8**		
G4.3	Nails*	1	4.0	2	4	90	60	47.3	-	23.0	12.2	2.53	5.26
		beam: b.h = 100.250 mm											
G5.1	Nails*	3	4.0	2	2	100	60	35.6	0.22	23.4	10.7	2.52	3.56
G5.2	Nails*	3	4.0	2	2	100	60	33.6	0.18	22.1	10.1	2.52	3.36
G5.3	Nails*	3	4.0	2	4	100	60	42.2	0.09	19.7	12.7	2.52	4.22
									mean	**21.7**	**11.2**		
G6.1	Nails*	2	4.0	2	4	100	20	18.8	-	9.3	11.3	2.48	3.77
G6.2	Nails*	2	4.0	2	4	100	20	23.5	-	11.6	14.1	2.16	4.71
	*) ring shanked nails with steel side members								**mean**	**10.5**	**12.7**		

7. Splitting of the beam

The derived formulas predict stable crack propagation until only shear deformation becomes determining, mode II fracture, resulting in unstable crack propagation. This results in a simple formula given by eq.(7). This equation exactly applies for joints as end supports (and notched beams).

For over-designed, thus "low" loaded joints the splitting strength of the beam, expressed in $\sqrt{GG_c}$, is determining as primary failure mechanism. Series B_2 to B_4 of Table 2 are examples

where the joints are loaded to a low degree and the number of nails have no influence on the splitting capacity, the mean value of $\sqrt{GG_c}$ = 17.1 N/mm$^{1.5}$
However, when the joint is designed less strong the fasteners are higher loaded and yielding may occur at the time of splitting.. For even further under designed joints compared to the splitting strength of the beam the joints may become very high loaded and yielding and/or hardening occur prior to splitting.

Assume that a force V_n leads to the plastic flow of one fastener and with n fasteners the total shear force of eq.(5) becomes $V = n\,V_n$. If V_c is the critical shear force obtained with a critical number of fasteners n_c. That means that splitting of the beam and first flow of the fasteners occur simultaneously, than $V_c = n_c\,V_n$ so $V = n\,V_n / n_c$ and eq.(5) changes into eq.(15). In

$$V_f = \sqrt{\frac{2G_c bh}{\frac{\partial\delta / V_c}{\partial\beta}}}\sqrt{\frac{n}{n_c}} \qquad (15)$$

case the number of fasteners is lower than the critical number, until a certain minimum, there is a decrease of the apparent parameter $\sqrt{GG_c}$ in proportion to $\sqrt{(n/n_c)}$. This applies until a minimum value of n because of the low loading of the beam and the relatively small "initial" crack length. For n values below that minimum also splitting is determining independently of the number of fasteners and may occur after the flow or hardening behaviour of the joint when cracks are sufficiently opened.

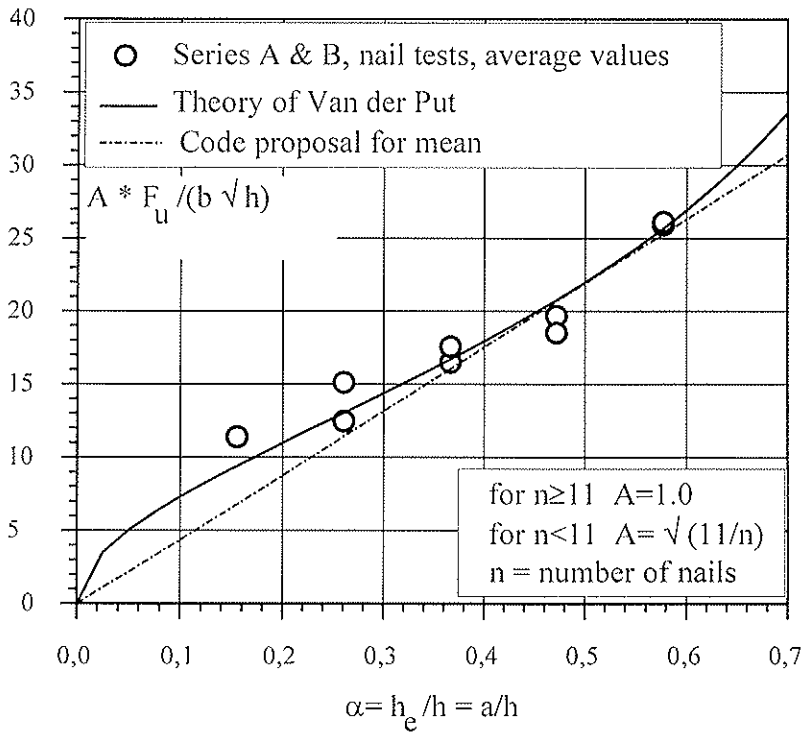

$$y = \frac{F_u}{b\sqrt{h}} = \frac{2V}{b\sqrt{h}} = 22\sqrt{\frac{\alpha}{1-\alpha}}$$

Figure 8: Splitting of the beam, test Series A and B and Equation (7)

For Series B_1, with n = 10 the value of $\sqrt{GG_c}$ = 15.5 N/mm$^{1.5}$ was calculated. The difference 17.0/15.5 = 1.10 equals the factor $\sqrt{n_c}/n$ = $\sqrt{(12.2/10)}$= 1.1 where the critical number of fasteners n_c is taken as 12.2.

The reduction of $\sqrt{GG_c}$ in proportion to $\sqrt{n/n_c}$ goes down to values of $n/n_c \approx 0.5$ to 0.4 as for Series A, where 5 dowel fasteners are used and the mean $\sqrt{GG_c}$ = 12.0 N/mm$^{1.5}$. Taking the mean value of $\sqrt{GG_c}$ = 17.1 N/mm$^{1.5}$ of Series B as a starting point the critical number of fasteners is 10 because 17.1/12= 1.43 = $\sqrt{n_c}/n = \sqrt{10}/5$. The critical number of fasteners n_c in series A and B is almost the same, 10.0 and 12.2 respectively. In Figure 8 the mean test values of the test series A and B are presented together with the theoretical prediction based on eq.(7) and on n_c = 11. For less than five dowels, Series C, first yielding of the nail will occur and hardening will start. However, after some hardening the critical crack length (and width) is formed and splitting will occur. For this reason the joints with 2 fasteners, Series C_1, are after strong hardening as strong as the joints with 5 fasteners, Series L+A_1 and L_7+A_2.
The same reduction effect applies for Series V with dowels, Table 3. For Series V_3, V_{11}/V_{12} and V_9, with n =12 and n = 18 fasteners, respectively, the f_c values are rather low compared to the other tests while the mean of $\sqrt{GG_c} \approx 20.5$ N/mm$^{1.5}$ is high. For the other Series V with n = 4 and 6 the $\sqrt{GG_c}$ is reduced to 12.6 and 16.5, respectively. This leads to a assumed critical number of dowels $n_c \approx 8.6$. The result is presented in Figure 9.

Determining in design of the splitting strength are the joints where the fastener yield and hardening finally results in splitting. This applies for all Series G , Series C and A with mean value for $\sqrt{GG_c}$ of 12.1, 11.8 and 12.0 N/mm$^{1.5}$ respectively.

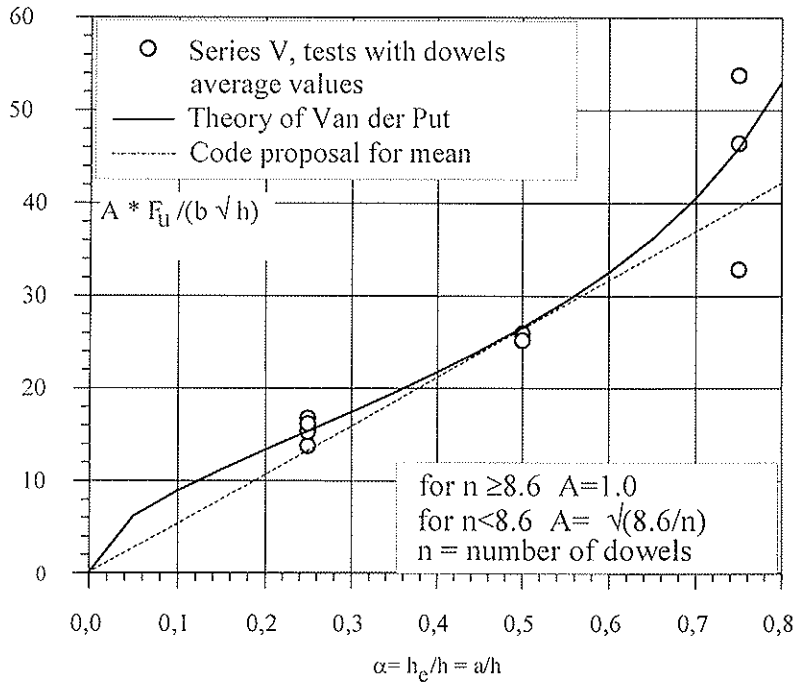

$$y = \frac{F_u}{b\sqrt{h}} = 26.5\sqrt{\frac{\alpha}{1-\alpha}}$$

Figure 9: Splitting of the beam, Series V and Equation (7)

7.1 Design proposals for splitting of the beam

The leading general equation for splitting of the beam is eq.(7), which can be rewritten as:

$$\frac{V_u}{b\sqrt{h}} = \sqrt{\frac{\alpha G G_c}{0.6(1-\alpha)}} = C_1\sqrt{\frac{\alpha}{(1-\alpha)}} \qquad (16)$$

where

$$C_1 = \sqrt{\frac{G G_c}{0.6}}$$

What is the appropriate value for the parameter $\sqrt{GG_c}$. For the test series where the joint do not govern the splitting, Series B, Series V with beam height 1200 and 600 mm (dowels). The weighted mean of $\sqrt{GG_c}$ = 18.5 N/mm$^{1.5}$. This value is about 3 times higher with respect to mode I failure of notched beams indicating a reduced value of the apparent fracture energy of mode II, due to the mixed I-II mode at failure. For the series where the joint were determining, Series A, C and G the weighted mean of factor $\sqrt{GG_c}$ = 12 N/mm$^{1.5}$. The mean lower bound value for C_1 in eq.(16) now becomes $C_1=\sqrt{(GG_c/0.6)}$= 15.5 N/mm$^{1.5}$. Estimation of the characteristic lower bound of C_1= 15.5*2/3 = 10 N/mm$^{1.5}$.

Design proposal 1:

The shear capacity of the middle member is:

for $h_e \leq 0.7\,h$

$$\frac{V_u}{b\sqrt{h}} = 10\sqrt{\frac{\alpha}{(1-\alpha)}} = 10\sqrt{\frac{h_e}{h-h_e}} \qquad (17)$$

To simplify eq.(16) the tangent line can be taken as shown in Figures 8 and 9 by the dotted line. It can be derived that the tangent point is at α = 0.5 and the equation of the dotted line is:

$$\frac{V_u}{b\alpha\sqrt{h}} = 1.7\sqrt{GG_c} \qquad (18)$$

8. Conclusions

- A fracture mechanic model is able to explain the test data related to splitting of the beams loaded perpendicular to grain by joints as given in CIB/W18-22-7-2.

- The fracture mechanics parameter $\sqrt{GG_c}$ plays an important part in the evaluation and interpretation of the test data. The apparent value of $\sqrt{GG_c}$ calculated on the basis of the tests differs for high loaded joints, which show large deformation at splitting and for over-designed low loaded joints, which do not show plastic deformation prior to splitting.
  - When the beam splits and the joints are loaded below their capacity, as in Series B of Table 2, Series V with ring-dowels and joints with more than 6 dowels in Table 3 the apparent value for $\sqrt{GG_c}$ is between 17.1 and 20.5 N/mm$^{1.5}$.
  - When yielding and hardening of the fastener occurs prior to splitting the apparent value for the fracture mechanics parameter becomes $\sqrt{((GG_c)(n/n_c))}$ and changes proportional to $\sqrt{(n/n_c)}$, where n_c is the critical number of fasteners and n the actual number of fasteners. This critical number indicates the boundary between both situations. The lower bound for the apparent $\sqrt{GG_c}$ parameter is probably $\approx$ 12

$N/mm^{1.5}$ as for test Series A, C and G and probably independent of the number of nails.

- When joints are further under-designed with respect to the splitting strength of the beam the joint can show large plastic flow and hardening too. However, splitting may occur finally when the cross-section is badly damaged by the large elongation of the holes.

- The derived formulas predict a stable crack propagation until the work by shear alone becomes determining leading to a simple formulae, eq.(7).

- Design codes guidelines for the splitting strength capacity of beam exposed to perpendicular to grain loads by joints as shown in Figure 5 are given in eq.(17) and a simplified formula in eq.(19)

The high embedment stresses of a dowel loaded perpendicular to the grain can be explained by confined dilatation perpendicular to the loading direction as shown in appendix II. Formulae derived from this approach are given in Chapter 5.1

References:

[1] van de Put, T.C.A.M, 1990: Tension perpendicular to grain at notches and joints , CIB/W18/23-10-1, Lisboa, Portugal

[2] van der Put, T.A.C.M., COST 508, workshop2, papers, Bordeaux, April 1992.

[3] Ehlbeck, J. Görlacher, R., Werner, H. CIB/W1822-7-2, meeting 22, Berlin, Germany, sept.1989.

[4] Ballerini, M., 1999, N new set of experimental tests on beams loaded perpendicular to the grain by dowel type joints, CIB/W18, paper 32-7-2, Graz, Austria.

[5] van de Put, T.C.A.M, 1991: Discussion of the failure criterion for combined bending and compression, CIB/W18/24-6-1, Oxford, U.K.

[6] van de Put, T.C.A.M, 1988: Explanation of the embedment strength of particle board, Stevin report, TU-Delft, 25-88-63/09-HSC6 or Ecproject MA1B-0058-NL

[7] van de Put, T.C.A.M, 1982: Betrachtungen zum Bruchmechanismus von nagelverbindungen, Festschrift K.Möhler, Book:Ingenieurholzbau in forschung und Praxis.

APPENDIX I

Derivation of the fracture- and critical energy release rate equation of wood

Summary

Based on a flat elliptical crack approach it is possible to derive the parabolic mode I - II interaction equation, giving the theoretical basis for this criterion with the extension for combined compression with shear.

The total energy release rate G_c follows $G_c/G_{Ic} = 1$, at micro scale at the crack-surface what may lead to the criterion in macro-stresses eq.(25):

$$\frac{G_c}{G_{IIc}} = \frac{1}{\left(\sqrt{\beta G_{IIc}/G_{Ic}} + \sqrt{1 - \beta}\right)^2}$$

and thus G_c is not equal to the sum $G_{Ic} + G_{IIc}$ of pure mode I and II.

Introduction

In the RILEM state of the art report on fracture mechanics of wood (Espoo, 1991) it is mentioned that there is no theory for mixed mode crack propagation and it is also stated that the energy approach gives no right results. The reason of this omission is the application of the singularity approach, that is now the only theoretical basis of fracture mechanics of all materials, but is not able to give the right general critical stress state of fracture at the crack tip. It is shown here that such a theory exists and for the derivation of the right failure criterion [5], it is sufficient to use the flat elliptical crack approach as theoretical basis for the general "mixed mode" fracture criterion with the extension for combined compression with shear. Because there is no influence on macro-crack propagation of the crack length and geometry and sharpness of the crack-tip of the macro cracks in wood, orthotropic fracture mechanics is not determining. Determining are the small cracks around the macro tip that have to propagate and are determining for the total behaviour. It therefore is necessary to regard micro-crack behaviour in the (quasi) homogeneous isotropic areas as for instance in the lignin (in the middle lamella and around micro-fibrils) and interlayer cracks. Of the random micro-cracks, the worst oriented with respect to the stress field may early propagate but will be arrested or bend off in the neighbourhood of strong layers in wood leading to oriented cracks in the weak direction. The ultimate load then is reached when the oriented cracks in layer direction starts to propagate in that direction.

A classical approach to study this behaviour is to regard flat elliptical cracks and by letting the minor axis approach to zero, a slit occurs, giving the same or equivalent solutions as the, now always applied, ideal mathematical crack of zero thickness (in the region $-c < x < c$), having singularities at the crack tips: $x = c$ or $x = -c$, making comparison of both methods possible. However the mathematical crack approach is concerned with critical states in the neighbourhood of the singularities

while retaining the physical right flat eliptical form for a crack it is possible to regard the highest occuring tensile stress in the material, along the boundary of the crack, giving the determining critical state and a real prediction of the direction of the next crack propagation.

When flow occurs around the crack tip, the boundary condition along the crack-boundary determines the flow stress and to have the same flow stress in the whole flow area the same stress state applies in that area and the same boundary condition as at the crack boundary can be assumed at the elastic-plastic boundary. The amount of flow and of bond-breaking has to be determined in future by deformation kinetics by parameter estimation at different loading pathes and different temperatures.

Basic equations

The classical way of analyzing the elliptic crack problem is to use complex variables, making change of axes very simple, and to use elliptic coordinates.

The Airy stress function can be expressed in terms of two analytic functions of the complex variable z (= x + iy) and the transformation to elliptic coordinates gives:

$z = x + iy = c\cdot\cosh(\xi + i\eta)$ or:

$$x = c\cdot\cosh\xi\cdot\cos\eta, \quad y = c\cdot\sinh\xi\cdot\sin\eta, \tag{1}$$

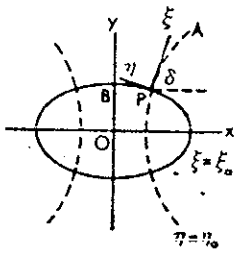

Figure 1 - Elliptic coordinates

showing that when ξ is constant $\xi = \xi_0$ the curve in the x,y plane is the ellipse:
$x^2/a^2 + y^2/b^2 = 1$ of semi-axes: $a = c\cdot\cosh(\xi_0)$, $b = c\cdot\sinh(\xi_0)$.
Similarly, the curves $\eta = \eta_0$, constant, are the hyperbolae:
$x^2/d^2 - y^2/e^2 = 1$, with: $d = c\cdot\cos(\eta_0)$, $e = c\cdot\sin(\eta_0)$.
For this elliptic hole $\xi = \xi_0$ in an infinite region with uniaxial stress p at an infinity in a direction inclined at β to the major axis Ox of the ellipse, the Airy stress function U satisfying $\nabla^2(\nabla^2 U) = 0$, the conditions at infinity and at the surface $\xi = \xi_0$ and showing no discontinuity of displacement, thus being the solution, is:
$U = R\{z\varphi(z) + \chi(z)\}$, with [1]:

$$4\varphi(z) = pce^{2\xi_0}\cos(2\beta)\cdot\cosh(\zeta) + pc(1 - e^{2\xi_0 + 2i\beta})\cdot\sinh(\zeta) \tag{2}$$

$$4\chi'(z) = -pc[\cosh(2\xi_0) - \cos(2\beta) + e^{2\xi_0}\sinh(2\{\zeta - \xi_0 - i\beta\})]\operatorname{cosech}(\zeta) \tag{3}$$

where $\zeta = \xi + i\eta$.

For the stresses, due to a stress p at an angle β to the crack, is:

$$\sigma_\eta - \sigma_\xi + 2i\tau_{\xi\eta} = 2[\bar{z}\varphi''(z) + \chi''(z)]e^{i\delta} \quad \text{and:} \tag{4}$$

$$\sigma_\xi + \sigma_\eta = 2[\varphi'(z) + \overline{\varphi'(z)}] = 4R\{\varphi'(z)\} \tag{5}$$

and the tangential stress σ_t in the surface $\xi = \xi_0$ is simply known from this last equation because here $\sigma_\xi = 0$. Thus:

$$\sigma_t = 2[\varphi'(\xi_0 + i\eta) + \varphi'(\xi_0 - i\eta)] =$$

$$= \frac{p(\sinh(2\xi_0) + \cos(2\beta) - \exp(2\xi_0)\cdot\cos(2\cdot(\beta - \eta))}{\cosh(2\xi_0) - \cos(2\eta)} \tag{6}$$

and the ultimate value is determined by $\varphi(z)$ only while eq.(4) has to vanish at: $\xi = \xi_0$.

This case above can be extended for two mutual perpendicular principal stresses by a simple addition.

Flat crack solutions

For comparison first the flat crack solutions with ξ_0 approaching zero will discussed. For stresses near the tip of a flat crack it is convenient to choose new coordinates X,Y with the origin in the focus of the ellipse and because ξ and η are small, higher powers than the square can be neglected.

$$X = x - c = c(\xi^2 - \eta^2)/2, \qquad Y = y = c\xi\eta \tag{7}$$

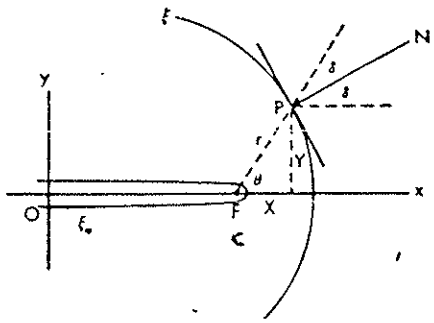

Figure 2 - Confocal coordinates

or in polar coordinates: $r = (X^2 + Y^2)^{0.5}$, $X = r\cos(\vartheta)$, $Y = r\sin(\vartheta)$ (8)

and from eq.(7):

$$\xi^2 + \eta^2 = 2(X^2 + Y^2)^{0.5}/c = 2r/c$$

$$\xi = \sqrt{2r/c}\cdot\cos(\vartheta/2), \qquad \eta = \sqrt{2r/c}\cdot\sin(\vartheta/2) \tag{9}$$

$$\eta/\xi = \tan(\vartheta/2) = \tan(\delta)$$

Using these relations in the solutions of eq.(4) and (5) the following stresses are found in polar coordinates for the loading case of a stress p at infinity at an angle β with the crack:

$$(8r/cp^2)^{0.5}\sigma_r = \sin(\vartheta/2)\cdot(1 - 3\sin^2(\vartheta/2))\cdot\sin(2\beta) + 2\cos(\vartheta/2)\cdot(1 + \sin^2(\vartheta/2))\cdot\sin^2(\beta)$$
$$(8r/cp^2)^{0.5}\sigma_\vartheta = -3\sin(\vartheta/2)\cdot\cos^2(\vartheta/2)\cdot\sin(2\beta) + 2\cos^3(\vartheta/2)\cdot\sin^2(\beta) \quad (10)$$
$$(8r/cp^2)^{0.5}\tau_{r\vartheta} = \cos(\vartheta/2)\cdot(3\cos^2(\vartheta/2) - 2)\cdot\sin(2\beta) + 2\cos^2(\vartheta/2)\cdot\sin(\vartheta/2))\cdot\sin^2(\beta)$$

showing the common stress increase by $1/\sqrt{r}$ when the tip of the crack is approached. Of interest for the same results as according to the singularity method for wood, are the small cracks in the weak direction that only may propagate in this direction. Then $\vartheta = 0$ and the equations (10) become:

$$(8r/cp^2)^{0.5}\sigma_r = 2\cdot\sin^2(\beta) \quad (11)$$
$$(8r/cp^2)^{0.5}\sigma_\vartheta = 2\cdot\sin^2(\beta) \quad (12)$$
$$(8r/cp^2)^{0.5}\tau_{r\vartheta} = 2\cdot\sin(\beta)\cdot\cos(\beta) \quad (13)$$

These equations simply give the Hankinson relation of the strength explained by a maximum strength condition in the main planes. Thus fracture occurs when the tensile strength is reached perpendicular to the grain and/or when the shear strength in this plane is reached (and the same applies in the plane perpendiclur to the grain by p at a slope of $\pi/2 + \beta$). Thus: $K_I \le K_{Ic}$ and $K_{II} \le K_{IIc}$ for all stress states (without interaction). It is known that, although this approximation can be used for uniaxial stress, it does not apply for the general loading case, showing that the, by the singularity method predicted, critical states are not determining for fracture. This also applies for the orthotropic approach, giving the same small crack equations [2]. The definition of the stress intensity implies that the flow stress is reached at $r = r_0$. This however appears to be not a sufficient failure condition in general to represent the critical state as will be shown in the following.

Derivation of the "mode I - II" - interaction equation

A general failure criterion follows from the ultimate stress that occurs at the boundary of the crack. By an extension of eq.(6) (superposition) to $p_1 = \sigma_1$ inclined at an angle $\pi/2 + \beta$ to the ox-axis and $p_2 = \sigma_2$ inclined at an angle β, eq.(6) turns to:

$$\sigma_t = \frac{2\sigma_y\sinh(2\xi_0) + 2\tau_{xy}[(1 + \sinh(2\xi_0))\cdot\cot(2\beta) - \exp(2\xi_0)\cdot\cos(2(\beta - \eta))\cdot\operatorname{cosec}(2\beta)}{\cosh(2\xi_0) - \cos(2\eta)}$$

where the stresses are given in crack coordinates with the x-axis along the crack. For small values of ξ_0 and η, (flat cracks) this equation becomes:

$$\sigma_t = \frac{2(\xi_0\sigma_y - \eta\tau_{xy})}{\xi_0^2 + \eta^2} \quad (14)$$

The maximum (critical) value of the tangential stress σ_t, depending on η, is found by: $d\sigma_t/d\eta = 0$ giving the critical value of η:

$$-2\tau_{xy}/(\xi_0^2 + \eta^2) - \left(2(\xi_0\sigma_y - \eta\tau_{xy})\cdot 2\eta\right)/\left(\xi_0^2 + \eta^2\right)^2 = 0, \text{ or:}$$
$$-\tau_{xy}(\xi_0^2 + \eta^2) = 2\eta(\xi_0\sigma_y - \eta\tau_{xy}) = \eta\sigma_t(\xi_0^2 + \eta^2)$$

where the second equality sign is due to the substitution of eq.(14).

From the first and last term follows that: $\eta\sigma_t = -\tau_{xy}$

and from the first 2 terms:

$$\eta/\xi_0 = [\sigma_y \pm \sqrt{\sigma_y^2 + \tau_{xy}^2}]/\tau_{xy} \tag{15}$$

or with eq.(14):

$$\xi_0\sigma_t = \sigma_y \mp \sqrt{\sigma_y^2 + \tau_{xy}^2} \tag{16}$$

and eq.(16) can be written:

$$1 = \frac{\sigma_y}{\xi_0\sigma_t/2} + \frac{\tau_{xy}^2}{\xi_0^2\sigma_t^2} \tag{17}$$

According to eq.(9) is for a small value of ϑ: $\xi_0 = \sqrt{2r_0/c}$, giving in eq.(17):

$$1 = \frac{\sigma_y\sqrt{\pi c}}{\sigma_t\sqrt{2\pi r_0}/2} + \frac{\left(\tau_{xy}\sqrt{\pi c}\right)^2}{\left(\sigma_t\sqrt{2\pi r_0}\right)^2}$$

what is identical to the emperical parabolic interaction equation of Wu:

$$\frac{K_I}{K_{Ic}} + \frac{\left(K_{II}\right)^2}{\left(K_{IIc}\right)^2} = 1 \tag{18}$$

Eq.(18) thus gives the stress condition that cannot be exceeded because of small crack propagation in the zones ahead of a macro crack (the start of fracture and redistribution of stresses). It is assumed, as usual for a layered structure like wood, that the macro-crack, as well as the larger small cracks, are about in the same (layer) direction. For a real isotropic material, first the worst crack orientation with respect to the given stress state has to be found by equating: $d\sigma_t/d\beta = 0$ in eq.(6). For wood the presence of such cracks will lead to the early formation of small cracks in the weak direction that may act as the initial cracks for failure.

The assumption of isotropy of the matrix with cracks in the weak planes is confirmed by the prediction of eq.(17) and (18) that $K_{IIc} = 2 \cdot K_{Ic}$ for the parabolic interaction equation in accordance with the measurements of Wu on Balsa.

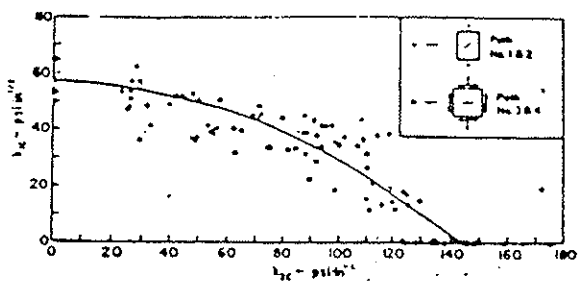

Figure 3 - The Wu - mixed mode interaction equation [3]

Eq.(18) is generally applicable also when σ_y is a compressional stress as also follows from the measurements of figure 4. When the compression is high enough to close

the small cracks ($\sigma_{y,cl} \approx 2G\xi_0$), τ_{xy} has to be replaced by the effective shear stress: $\tau^*_{xy} = \tau_{xy} + \mu(\sigma_y - \sigma_{y,cl})$ in this equation or:

$$1 = \frac{\sigma_{y,cl}}{\xi_0\sigma_t/2} + \frac{(\tau^*_{xy})^2}{\xi_0^2\sigma_t^2}$$

what is fully able to explain fracture by compression perpendicular to the crack.
By multiplying left and right terms of eq.(15) and eq.(16) with each other, again the earlier derived ultimate state condition is found:

$$\sigma_{t,m}\cdot\eta_c = -\tau_{xy}. \tag{19}$$

For most species, with stronger layers than those of Balsa, a much higher value of K_{II} than twice the value of K_I is measured for fracture along the grain. This shows that the propagation direction is not free and the crack may not pass the strong layers. Thus hardening occurs untill the small crack propagation direction is forced to be close to the layer direction. This means that η is smaller than the critical value of eq.(19) giving an apparent higher strength $\sigma_{t,m}$ in the critical direction.
Substitution of $\eta = \alpha\eta_c = -\alpha\tau_{xy}/\sigma_{t,m}$ in eq.(14) gives:

$$\frac{\sigma_y}{\sigma_t\xi_0/2} = 1 - \frac{(2\alpha^2 - \alpha^4)\tau_{xy}^2}{\sigma_t^2\xi_0^2} \tag{20}$$

where $K_{II}/K_I = 2/(\alpha\sqrt{2 - \alpha^2})$

Eq.(20) is parabolic, the same as eq.(17).

For very small values of τ_{xy}, the critical value of η is very small and when $\sigma_y \neq 0$, the ultimate condition eq.(15) applies and eq.(17) is followed at the early start.
A second possibility is the substitution of a maximal value of η, dictated by the possible room for crack propagation between the layers. For instance for bond breaking between two strong layers the equivalent crack tip and stress situation is the same after each breakage of a bond and propagation is the same at every step with the same $\eta = \eta_m = -|\eta|$. For this case, for higher values of τ_{xy} than close to zero, eq.(14) can be written, neglecting $(\eta/\xi_0)^2$:

$$\frac{\sigma_y}{\sigma_t\xi_0/2} = 1 + \frac{\eta^2}{\xi^2} - \frac{\tau_{xy}}{\sigma_t\xi_0^2/(2|\eta|)} \approx 1 - \frac{\tau_{xy}}{\sigma_t\xi_0^2/(2|\eta|)} \tag{20'}$$

where $|\eta|$ is the absolute value of η, being negative. Thus:

$$\frac{K_I}{K_{Ic}} \approx 1 - \frac{K_{II}}{K_{IIc}} \tag{21}$$

as lower bound, giving now: $K_{IIc} = \frac{\xi_0}{|\eta_m|}\cdot K_{Ic}$ (22)

and the maximal value of $\eta = \eta_m$ is found by measuring K_{Ic} and K_{IIc}, giving p.e. a value of about $\xi_0/\eta_m \approx 5$, showing the neglection of $(\eta/\xi_0)^2 = 0.04$ with respect to 1 is right.

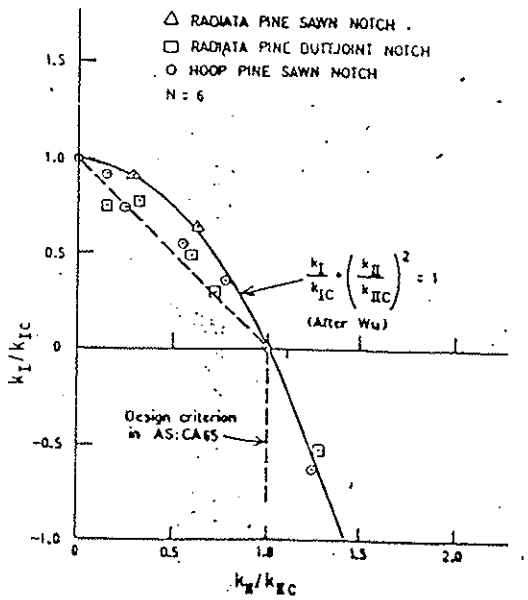

Figure 4 - Fracture strength under combined stresses [4]

An alternative model can be based on the orthotropic ultimate shear condition along the grain that can be applied as approximation because the tangential stress along the crack boundary is uni-axial. According to eq.(19) then is: $|\eta_c| = f_v/\sigma_{t,m}$. Measurements are sometimes between eq.(20) or (20') (the straight and the parabolic line) showing that both criteria may apply depending on the areas of the structure crossed during crack propagation see fig. 4).

Energy principle

It is known that the strain energy due to a crack, W_c, due to stressing is equal to the difference of the strain energy W of a body containing the crack and W_0 of the same body without a crack. Thus: $W_c = W - W_0$

and according to Griffith is, for constant external loading, the failure condition:

$\partial W/\partial c = \partial W_c/\partial c = \partial(G_c 2c)/\partial c$, where G_c is the fracture energy for the formation of the crack surfaces.

As well as for the isotropic and orthotropic cases G_c can be given like:

$$G_{cI} = E_I \cdot K_I^2 \text{ and } G_{cII} = E_{II} \cdot K_{II}^2 \qquad (23)$$

where E_I and E_{II} are equivalent stiffness moduli.

This means that the energy condition for failure is, p.e. according to eq.(21):

$$\frac{K_I}{K_{Ic}} \approx 1 - \frac{K_{II}}{K_{IIc}} \quad \text{or} \quad \frac{\sqrt{G_I}}{\sqrt{G_{Ic}}} = 1 - \frac{\sqrt{G_{II}}}{\sqrt{G_{IIc}}} \qquad (24)$$

or when the critical stress state in the material, that causes tensile failure at the crack boundary, represents $G_I = \beta G$ and $G_{II} = (1 - \beta)G$, the the total energy release rate $G = G_c$ for fracture at combined stresses then is:

$$\frac{G_c}{G_{IIc}} = \frac{1}{\left(\sqrt{\beta G_{IIc}/G_{Ic}} + \sqrt{1-\beta}\right)^2} \qquad (25)$$

what is for instance for $G_{IIc}/G_{Ic} = 5$: $G_c = G_{IIc}/(\sqrt{(5\beta)} + \sqrt{(1-\beta)})^2$
and G_c is not equal to the sum $G_{Ic} + G_{IIc}$ of pure mode I and II (as mostly used).

Conclusions

- Because there is no influence on macro-crack propagation of the crack length and geometry and sharpness of the crack-tip of the macro cracks in wood, orthotropic fracture mechanics is not determining. This also follows from the nearly same fracture toughness and energy release rate for wide and slit notches and the minor influence of rounding the notch. Determining thus is the influence of micro-cracks for the total behaviour, having the same influence at the tip of wide as well as slit notches.
- It is possible to explain the "mixed mode" interaction equation for macro-crack propagation in the weakest plane, by micro-crack propagation at the macro-crack tip, using the ultimate tensile strength criterion for the uniaxial stress along the micro-crack boundary (or elastic plastic boundary).
- When a macro-crack propagates in its own direction, it can be postulated that first micro-cracks, at the macro-crack tip, having the same initial (weakest, worst loaded) direction, have to propagate before macro-cracking occurs. For thick (quasi) isotropic layers at the start, (or when the reinforcement is not able to stop matrix crack propagation as in plastics) this leads to the Wu-interaction equation:

$$\frac{K_I}{K_{Ic}} + \frac{(K_{II})^2}{(K_{IIc})^2} = 1$$

where: $K_{IIc} = 2K_{Ic}$, as is measured by Wu on Balsa. For thin layers, the same equation is obtained with $K_{IIc} >> 2K_{Ic}$, when crack propagation is mainly possible in the weak direction. In general the off axis propagation will be ceased when a strong layer is met and crack propagation may proceed only at a small angle along that layer, causing the high value of K_{II}.
For very thin layers (or interlayer fracture), with a limited small angle of propagation, the linear interaction equation is obtained:

$$\frac{K_I}{K_{Ic}} \approx 1 - \frac{K_{II}}{K_{IIc}}$$

For total failure, probably both criteria apply, depending on all parts of the structure, crossed by the macro-crack propagation, giving the combined criterion:

$$\frac{K_I}{K_{Ic}} + C\cdot\frac{K_{II}}{K_{IIc}} + (1-C)\cdot\frac{(K_{II})^2}{(K_{IIc})^2} = 1 \qquad 0 \le C \le 1$$

being intermediate between straight and parabolic depending on the amount and types of cracking planes.

- The results of the mathematical flat crack approach (singularity approach) are not compatible with the ultimate strength method because a more severe critical state is possible in an other worst direction than given by the singularity approach. Using this concept of initial mathematical flat micro-cracks in the weakest planes, the Hankinson equations are obtained, explained by a maximal stress condition, what is known to be an approximation only possible for uniaxial stress. Further also the by the singularity method predicted two singular stress fields at the crack tip of an orthotropic material are never measured and not shown to exist. There thus is no guaranty that flat crack solutions, as applied in fracture mechanics of wood, provide sufficient solutions for combined stresses.

- The maximal tensile stress criterion along the micro-crack boundary may provide many more explanations of behaviour, what should be investigated. For instance an initial small crack in isotropic lignin at an angle of 30^{0} with the direction of an uniaxial compression stress field may propagate in a zigzag way (with angle of 30^{0} until the critical length 2c is reached, then taking the direction -30^{0} etc.) along this compressional direction, explaning splitting along the grain by compression in the grain direction as may occur by long term loading. In the same way as derived above, the zigzag angle will be much smaller than 30^{0} for interlayer splitting.

References

[1] Timoshenko S. and Goodier J.N., Theory of elasticity, Mcgraw-Hill book comp., N.Y. 1951, 179-204.

[2] Sih G.C. et al, On cracks in rectilinearly anisotropic bodies, Int. J. Fracture mechanics 1, 1977, 189-203.

[3] Wu E.M., Application of fracture mechanics to anisotropic plater, Journ. of applied mechanics Dec. 1967.

[4] Leicester R.H., Fracture strength of wood, First Australian Conf. on Engin. Materials, Univ. of New South Wales, 1974.

[5] van der Put, T.A.C.M., Explanation of the mixed mode interaction equation, COST 508 workshop 2, papers, Bordeaux, April 1992

APPENDIX II

Bearing strength perpendicular to the grain of locally loaded blocks

The local compression strength perpendicular to the grain may increase due to confined dilatation perpendicular to the loading direction. From the figure below it can be seen that the strength increases with the increasing possibility of spreading of the load. Further it can be seen that there is a maximal spreading of about 4 x h. An increase of the strength is then only possible by increasing h.

At plastic flow the increase of strength is about proportional with $\sqrt{L/s}$ (see figure).

$$f_s = c \cdot f_{c,90} \cdot \sqrt{L/s} = 1.08 \cdot f_{c,90} \cdot \sqrt{L/s} \qquad (1)$$

At lower strain this is about proportional to $\sqrt[4]{L/s}$ when the line of the cube strength is not regarded and it is seen that this empirical relation, proposed for the Eurocode, is not right to represent the ultimate state.

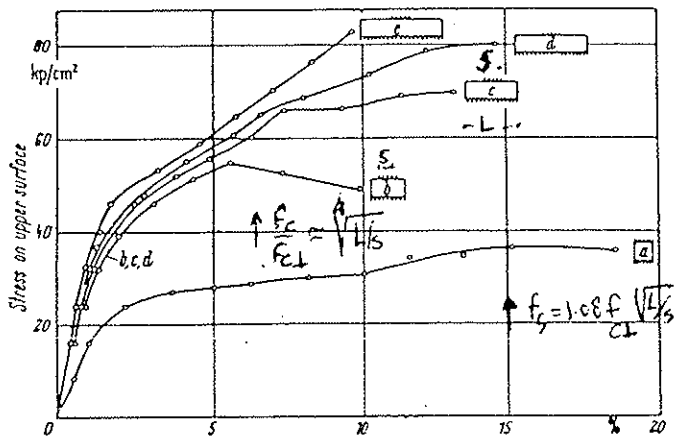

Bearing strength ⊥, specimen 15x15 cm, lengths: 15, 30, 45, 60, 75 cm, of a to e, [1]

The dependence of the strength upon spreading can be explained by the equilibrium method of the theory of plasticity.

In the plastic region, a stress field can be constructed in the specimen that satisfies the equilibrium conditions:

$$\frac{\partial \sigma_x}{\partial x} + \frac{\partial \tau}{\partial y} = 0, \quad \frac{\partial \tau}{\partial x} + \frac{\partial \sigma_y}{\partial y} = 0, \qquad (2)$$

and the boundary conditions and nowhere surmounts the failure criterion.

This failure criterion is of the Mohr-type in the radial plane: $\tau/f_v = \sqrt{1 - \sigma_{c,0}/f_{c,0}}$, [2], or can be approximated by a Coulomb criterion. In the radial plane an inscribed Tresca criterion can be used being a maximum stress criterion:

$$(\sigma_1 - \sigma_2)/2 = k = f_v' \qquad (3)$$

However the result of the derivation does not depend much on the failure criterion used. The Coulomb or the Mohr criterion gives a higher value of c of eq.(1) than the Tresca criterion, the strength $f_{c,90}$ however is related to a prism strength and is lower than the cube strength associated with the Tresca criterion. Both criteria therefore will give comparable values of f_s.

Although "shear-flow" is in the weak direction as in the compression test perpendicular to the grain, the behaviour is simular to a reinforced material (in the strong direction) having the shear strength of the weak direction and confined pressure may build up in all directions when there is friction between bearing plate and specimen in the width direction where the width of the bearing plate is equal to the width of the block. Because failure, according to a shear plane in the weak direction, not affecting the reinforcement, is not determining in this case, the upper stress is determined by the spreading possibility in the strong direction.

Equations (1) to (3) can be written as equations along discontinuity lines (characteristics as for instance Prandtl slip lines) and from the construction of these lines it follows that $\sigma_s = 4k\vartheta + \sigma_0$ and $\vartheta \approx 0.62 \cdot \ln(2H/s)$, see [3], giving:

$$\sigma_s - \sigma_0 = 2.48 \cdot k \cdot \ln(2H/s) \qquad (4)$$

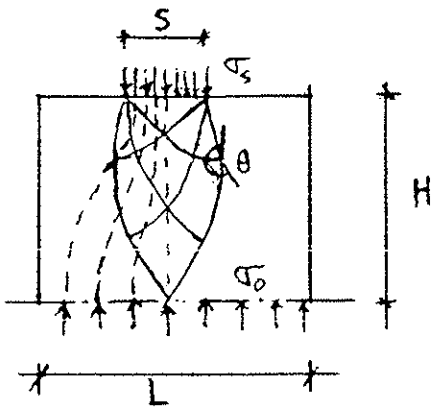

"Slip-lines" determining the direction of the main stresses

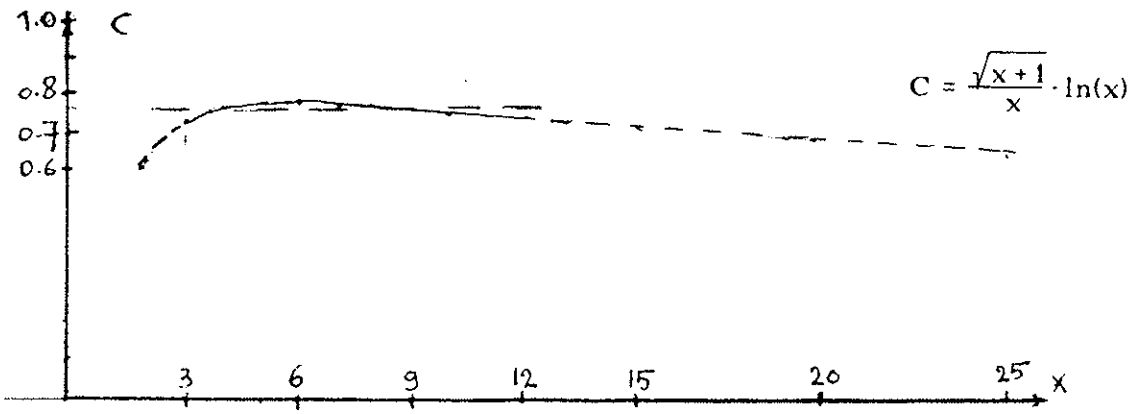

Function C

and because $\sigma_s \cdot s = \sigma_0 \cdot L$ (see figure above) is: $\sigma_s(1 - s/L) = 2.48 \cdot k \cdot \ln(2H/s)$. Further the construction for a finite block gives the indication that the spreading of the stress is below: $L \approx 2H + s$ or: $H \approx (L - s)/2$ when $H > s$, thus: $L/s > 3$ (Below this value the spreading is less strong and finallz failure is simular to the cube test). Substitution of the values for σ_0 and H in eq.(4) gives:

$$\sigma_s = 2.48 \cdot k \cdot \ln\left(\frac{L}{s} - 1\right) \cdot \frac{\sqrt{L/s}}{L/s - 1} \cdot \sqrt{L/s} = 2.48 \cdot k \cdot C \cdot \sqrt{L/s} \qquad (5)$$

where C is a function of L/s only and can be regarded constant of about 0.78. Thus:

$$\sigma_s = 0.97 \cdot 2k \cdot \sqrt{L/s} \qquad (6)$$

The value of k follows from the compression test (cube test) with $\sigma_1 = f_{c,90}$ and $\sigma_2 = 0$, or: $k = f_{c,90}/2$. Thus eq.(6) becomes:

$$f_s = c \cdot f_{c.90} \cdot \sqrt{L/s} \qquad \text{with } c \approx 1 \qquad (7)$$

The higher experimental value of c given in eq.(1) shows the lower bound approach of the chosen method (the real slip-lines must give a higher value). At lower flow strains c also will be lower in experiments. Thus c gives the possibility to adapt the model to test results.

Eq.(7) provides a basis for design rules and is able to explain the different results. As mentioned before the rules of the Eurocode based on $\sqrt[4]{L/s}$ suggest to be based on small deformations (and not the ultimate state) and the dependence on H is omitted in the Code. However for very small values of H there is hardly any spreading and the given rules don't apply. Increase in bearing is then only possible after flow at hardening if the structure remains stable in that state. The given rules seem to apply for a special case: $H \geq (a + l_1)/3 = 250/3 = 84$ mm. This has to be mentioned in the Code.

As discussed in paper CIB-W18/S-10-1, the French rules show the dependence of H and the results are closer to the the ultimate state (see table):

$f_s/f_{c,90}$

s/H	c/H			
	≥ 1.5	1	0.5	0
1	2	1.5	1.25	1
2	1.5	1.25	1.12	1
≥ 3	1	1	1	1

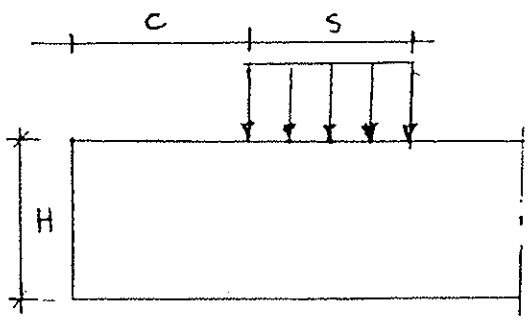

When $c/H = (L - s)/2H \geq 1.5$, thus when $L \geq 3H + s$, the maximal spreading is reached according to the table and to the first figure above of [1]. (This indicates friction

of the plates in the strong direction because without that: $L \approx 2H + s$ is expected). For $s/H \geq 3$, it is assumed that in the middle the same conditions appear as in the cube test. However this is even too low when friction is ignored here and test values will be higher than the table values. The same applies for $c = 0$ when $L > s$, only without friction (and $L = s$) the situation is comparable with the cube test and test values will be higher than 1. The confined pressure may be build up according to the following figure.

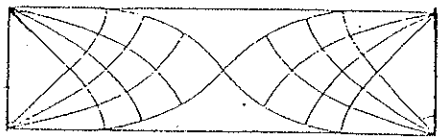

"Failure" between two plates

The influence of no friction along the bearing plate in the strong direction (and thus full friction in the width direction) can be assessed as lower bound by assuming that only symmetrical spreading is possible. Thus $L = 2c + s$. Further $s/H \geq 3$ must comprise $s/H >> 3$. $c/H \geq 1.5$ must be $c/H \geq 1$ and the first column has to be omitted when no friction is assumed. $c = 0$ must comprise $L = s$ giving a value 1.
According to eq.(7) is then:

$f_s/f_{c,90}$

s/H	c/H = (L - s)/2H			
	≥ 1.5	1	0.5	0
1	2	1.7	1.4	1
2	1.6	1.4	1.2	1
≥ 3	1	1	1	1

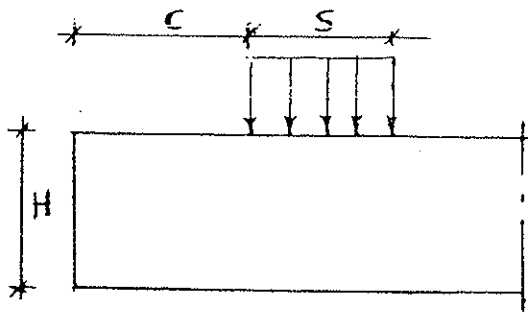

These values are close to the values of the French rules and are comparable when in eq.(7) $c \approx 0.9$ is used indicating that a limited flow is regarded as the ultimate state in the French tests or that safe lower bounds where given.

In paper CIB-W18A/23-6-1 test results are given of bearing in the range where H is not limiting for spreading because: $L < 2H + s$. The determination of $f_{c,90}$ is done on a specimen that is long in the strong direction and the results will be higher than those of the compression test. However the strain chosen as failure strain was lower than the ultimate giving compensating lower strength values. The comparison of this compression test with the ASTM-bearing test in the paper shows that the ASTM

values are about $\sqrt{3}$ times higher according to the theory (L/s = 3 in the ASTM-specimens).

In the following table the test results are compaired with eq.(7) and it is seen that also non-symetrical spreading is possible of end loaded blocks because of the friction between plate and specimen (and the high value of H).

According to the Eurocode a limitting value occurs at $s/L \leq 0.125$ for central loading. The results here show that for end loaded blocks the limit of k_c is about $k_c \approx 2$ for $s/L \leq 0.25$. These limits are due to a local mechanism as for instance given in the figure below. It has to be remembered that the lines are not real slip lines here but means to construct a stress field that satisfies equilibrium, boundary conditions and the failure criterion. The theoretical value of the limit of k_c is higher for central loading and it seems to be possible to obtain higher values by tests.

$f_s/f_{c,90} = k_c$

	measurements			adaption c of eq.(7)	
s/L	central loaded k_c	end loaded k_c	$\sqrt{L/s}$	central loaded $c = k_c/\sqrt{L/s}$	end loaded $k_c/\sqrt{L/s}$
1	1	1	1	1	1
0.875	1.063	1.063	1.069	1	1
0.75	1.188	1.156	1.155	1.03	1
0.625	1.375	1.281	1.265	1.09	1
0.5	1.625	1.438	1.414	1.15	1
0.375	1.969	1.625	1.633	1.2	1
0.25	2.344	1.875	2.0	1.17	0.94 limit
0.125	2.781	2.156	2.83	1 limit	
mean of c:				1.08	1

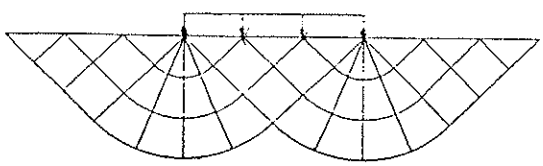

"Local failures"

"slip-lines" when the plate transfers the entire shear stress

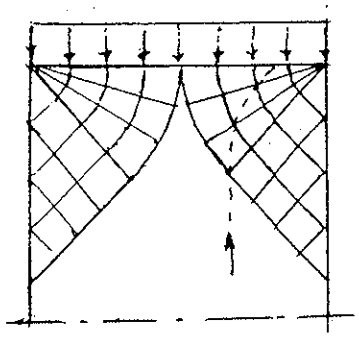

For long blocks with respect to the bearing plates the maximal spreading will occur at both plates according to the figures below.

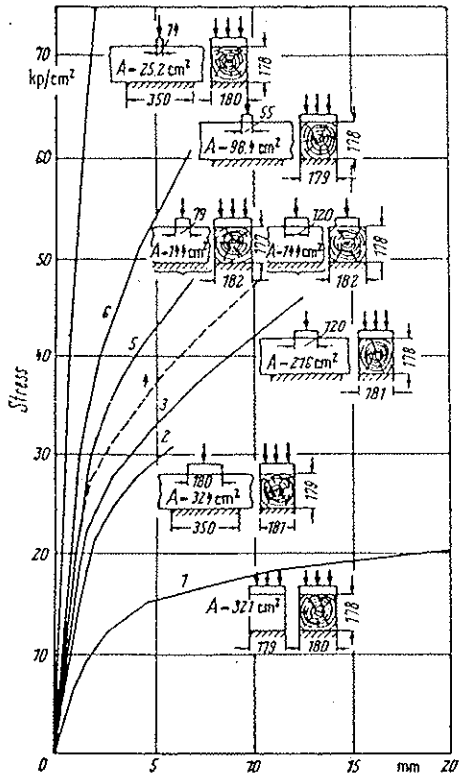

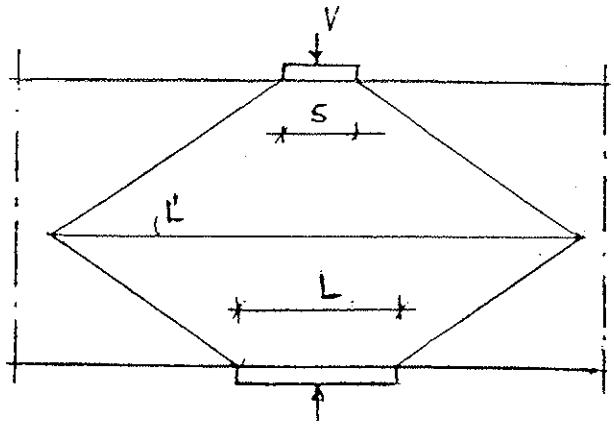

Local loading perp. to the grain [1] Graf Possible spreading

From the figure it follows that: $s + 3\alpha H = L + 3\cdot(1 - \alpha)H$. Thus:

$$\alpha = 0.5 + \frac{L - s}{6H}$$

and thus the equivalent spreading factor (of the strength determining plate) is:

$$\frac{L'}{s} = \frac{s + 3\alpha H}{s} = 1 + \frac{3H}{s}\left(0.5 + \frac{L - s}{6H}\right) = 0.5 + \frac{3H + L}{2s}$$

With H =17.9; L = 35; b = 18.1 cm according to the measurements of O. Graf is:

$$k_{c,90} = c\cdot\sqrt{0.5 + 800/s\cdot b} = 1.1\cdot\sqrt{0.5 + 800/s\cdot b}$$

leading to the values of f_s at 5 mm deformation (see fig.) of the curves:
1: 16 - 2: 30 - 3: 36 - 5: 43 - 6: 52 kgf/cm^2, about the same as the measurements. The highest maximum is not shown (at $f = s\cdot b = 25.2$, see fig.). Predicted according to the last formula is: f_s = 100 kgf/cm^2. However this will be cut off by a local mechanism. Because $f_s \geq 75$ is measured, the maximum value of $k_{c,90}$ is at least 75/16 = 4.7 (close to the theoretical value obtained from a local failure mechanism (giving an upper bound value) of about 5.5 to 6).
The measurements suggest a higher spreading possibility than to: $s + 3\alpha H$. However the model applies for high plastic deformation and after splitting softening may

occur simular to the specimen with 30 cm length in the first figure of this appendix. Because complete curves are not given, rules have to be based on the limited deformation (~ 5 mm here).

It can be concluded that the theory is able to explain all contradictory test results of Suenson, the Eurocode, the French rules, Graf, and of paper CIB-W18A/23-6-1 and design rules should be adapted in the right way as given below.

As proposal for the Eurocode the following rules are possible for bearing blocks:

$$\sigma_{d,90,d} \leq k_{c,90} \cdot f_{c,90,d}$$

where:

$$k_{c,90} = \sqrt{L/s}$$

with: $L \leq a + s + l_1/2$; $L \leq 3H + s$ and:

$k_{c,90} = 2.8$ when $s/L \leq 0.125$ for central loads;

$k_{c,90} = 2$ when $s/L \leq 0.25$ for end loads.

For safe rules (when friction is only in the width direction), the conditions are:

$L \leq 2a + s$; $L \leq s + l_1$; $L \leq 2H + s$,

$k_{c,90} = 2.8$ when $s/L \leq 0.125$

For the bearing strength of a middle section of a beam between two plates of lengths L and s is:

$$k_{c,90} = 1.1 \cdot \sqrt{0.5 + \frac{3H + L}{2s}} \leq 5$$

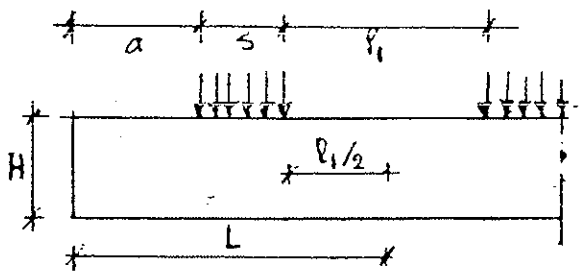

Literature

[1] F. Kollmann, Principles of wood science and technology, vol. I, 1984, Springer-Verlag, Berlin.

[2] T.A.C.M. van der Put, A general failure criterion for wood, Proc. IUFRO S5.02 paper 23, 1982, Boras, Sweden.

[3] H. Schwartz, PhD dissert. Stuttgart, 1969.

[4] P. Vermeijden, P.B.B.J. Kurstjens, Shear strength of close to support loaded beams on 3 supports, report 4-68-13 HE-2, Stevinlab. Delft, 1968 (in Dutch).

INTERNATIONAL COUNCIL FOR RESEARCH AND INNOVATION
IN BUILDING AND CONSTRUCTION

WORKING COMMISSION W18 - TIMBER STRUCTURES

TEST METHODS FOR GLUED-IN RODS FOR TIMBER STRUCTURES

by

C Bengtsson

C-J Johansson

Wood Structures and Materials, Swedish National Testing and Research Institute (SP)

SWEDEN

MEETING THIRTY-THREE
DELFT
THE NETHERLANDS
AUGUST 2000

Presented by: C. Bengtsson

· J. Kangas asked whether there were failures during proof loading.
· C. Bengtsson responded that there were few failures and their failure load values were included in the analysis.
· M. Ansell asked whether thick epoxy glueline (5 mm) was tried.
· C. Bengtsson responded no.
· M. Ansell suggested that thick epoxy glueline (5 mm) could lead to higher strength values. He also asked whether wood or glueline failures were observed.
· C. Bengtsson responded that wood failure was observed with the epoxy.
· S. Svensson asked why was beech wood used.
· C. Bengtsson responded that beech was specified in the test standard.
· H.J. Larsen questioned the findings that only epoxy passed and stated that the test method may not be suitable to address different type of adhesives.
· C. Bengtsson agreed that the requirements might not be suitable.
· J. Kuipers commented on the glue type dependency of test methods.
· C. Bengtsson agreed.
· F. Lam asked whether the observed differences were statistically significant.
· C. Bengtsson answered yes.

Test methods for glued-in rods for timber structures

Charlotte Bengtsson and Carl-Johan Johansson
Wood Structures and Materials, Swedish National Testing and Research Institute (SP), Sweden

1 Introduction

Glued-in rods are being used in several European countries, but the performance requirements and the design rules differ from country to country. In previous work it was concluded that the existing knowledge was insufficient to draft the needed standards. Therefore, a 3-year partly EU-financed project named GIROD (Glued-in Rods for Timber Structures) was started in 1998. The results presented in this paper have been obtained within the GIROD project. The objectives of the work presented in this paper are to develop test methods for:

1. Evaluation of glued-in rods with respect to strength and durability of the adhesive.
2. Production control of glued-in rods for timber structures.

Within the GIROD-project the work is focused on rods glued-in with three adhesives: two-component epoxy (EP), polyurethane (2K PUR) and phenol-resorcinol-formaldehyde (PRF).

2 Experimental work

2.1 Strength and durability of the adhesive

For testing of durability of the adhesive, surrounding the rod, the aim is to develop a test method based on EN 302-1 (determination of bond strength in longitudinal tensile shear for load bearing structures). Only the treatments in EN 302-1 were used. Instead of the wood to wood tensile shear specimens in EN 302-1, small pieces of threaded steel rods bonded into beech blocks were used. Initially, 240 specimens with different rod diameters and different beech wood thicknesses were tested. Based on these results, it was decided to perform further tests by using 16 mm threaded rods bonded into 20 mm thick wooden blocks with a cross section of 40 x 40 mm, see Figure 1a. The hole diameter was 17 mm. This shaping of the test specimens was chosen to simplify the manufacture of the specimens and for making it relatively easy to centre the rod into the beech wood. Also the test set-up was modified for the further tests. A compression test set-up was designed instead of tension tests (according to EN 302-1), see Figure 1b.

The specimens were treated according to A4 (6 hours in boiling water, 2 hours in 20°C water, then testing in the wet state) and A5 in EN 302-1 (6 hours in boiling water, 2 hours in 20°C water, then the specimens were conditioned in 20°C and 65% relative humidity back to 12% moisture content of the wood before the testing). Additionally, a control test series was performed (tested after 7 days in 20°C and 65% relative humidity).

To the three adhesives mainly studied within the GIROD-project, EP, 2K PUR and PRF, four other adhesives were added. These were: melamine-urea-formaldehyde (MUF), one component polyurethane (1K PUR), emulsion-polymer-isocyanate (EPI) and a modified silyl-epoxy (MS). In this way, the suggested test method was applied for a large spectrum of adhesives with differing mechanical and durability properties. For each treatment and adhesive ten specimens were tested, which gave a total amount of 210 specimens.

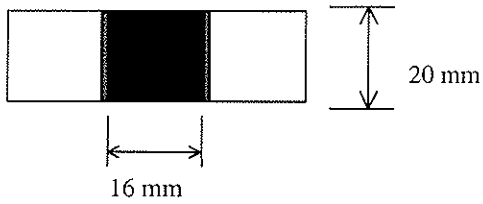

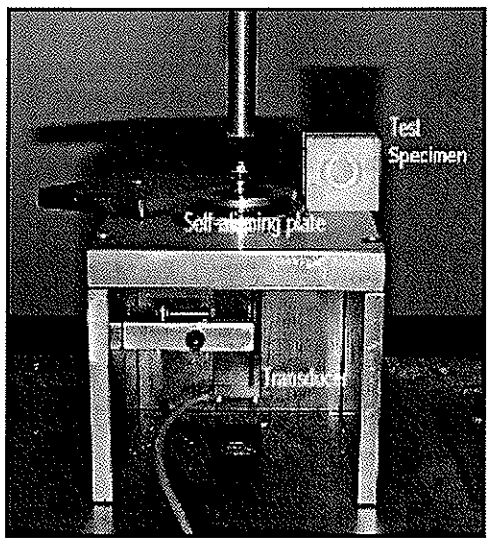

a) b)

Figure 1. a) Geometry of the chosen test specimen.
b) Test set-up for loading in compression.

2.2 Test methods for production control

Two alternative test methods were studied, a proof-loading procedure and destructive tests. The specimens were made of Norway spruce (*Picea abies*) glulam. The cross section consisted of three laminae, visually graded to LT30 (INSTA 142), which corresponds to the C35 strength class (EN 338). All rods (threaded M16, galvanised of quality 8.8) were bonded in centrally, parallel to the grain, into the glulam blocks. A total amount of 804 specimens was tested in this study. The wood blocks were equally divided into groups based on their weights, so that the average weight of the specimens in each of the groups was approximately the same.

2.2.1 Proof-loading

Figure 2 briefly describes the dimensions of the specimens used for the proof-loading tests. Two slenderness ratios ($\lambda=l_g/d_s$), $\lambda=10$ and $\lambda=20$, were studied. The tests were carried out as one-sided pull-compression tests. The test set-up is newly developed and designed with respect to practicality of carrying out the tests. Details about the specimen preparation and the test set-up can be found in (Hausmann and Reil 1999).

2.2.2 Destructive test

Figure 3 briefly describes the dimensions of the specimens used for the destructive tests. The cross sectional dimension of the glulam and the diameter of the rods was the same as for the proof-loading tests. The diameter of the support rod was 24 mm. The destructive tests were performed as, more traditional, two-sided pull-out tests. The length between the

two rods, l_m, was determined as a result of Finite element analysis (Aicher et al. 1998). Details about the specimen preparation and the test set-up can be found in (Hausmann and Reil 1999).

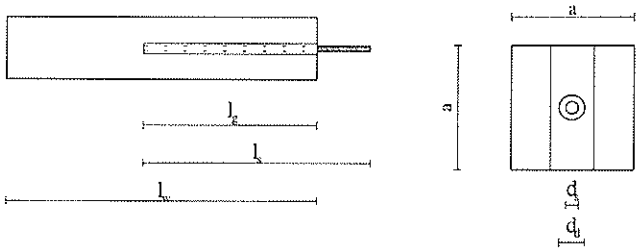

	λ=10	λ=20
d_s [mm]	16	16
d_d [mm]	17/18/20	17/18/20
a [mm]	115	115
l_w [mm]	288	576
l_s [mm]	260	420
l_g [mm]	160	320

b)

gure 2. a) Design of the test specimens for the proof-loading tests.
b) Dimensions of the test specimens.

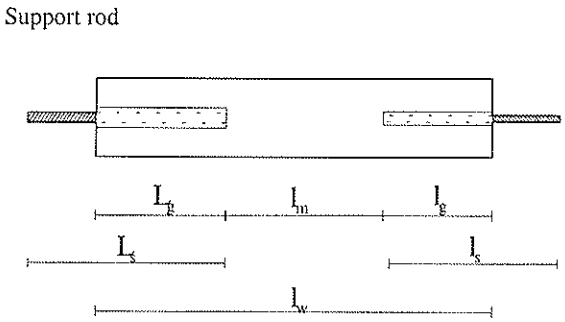

	λ=10	λ=20
l_w [mm]	576	1152
l_s [mm]	280	440
l_g [mm]	160	320
d_d [mm]	17	17
l_m [mm]	226	452
L_s [mm]	310	500
L_g [mm]	190	380
D_d [mm]	25	25

a) b)

Figure 3. a) Design of the test specimens for the destructive tests.
b) Dimensions of the test specimens.

3. Experimental results and discussion

3.1 Strength and durability of the adhesive

The purpose of basing the new test method for durability of the adhesive on EN 302 was to allow comparison with wood-to-wood bonds (pure beech specimens), tested according to this standard, and to apply the requirements (for type I adhesives) set in EN 301 also to glued-in rods. The shear strength requirements according to EN 301 are for thin glue lines: Control: 10 MPa, A4 treatment: 6 MPa, A5 treatment: 8 MPa. For thick glue lines the required values are 80% of the values for thin glue lines. However, the chosen test specimen is very different from standard test pieces according to EN 302. Both the geometry and the thickness of the glue-line differ and the comparison with the

requirements according to EN 301 is therefore questionable. Figures 4-5 and Table 1 show the results of the shear strength tests obtained by the suggested test method.

Anyway, if the requirements according to EN 301 (for thin or thick glue lines) are applied for the glued-in rods tested here only the EP adhesive passes. Whether that is a reasonable result can not be based just on these tests. The A4 treatment (cooking and then testing in wet state) gives very low shear strength values. This verifies that water and high temperatures put strong requirements on the adhesive bonds.

Both treatments, A4 and A5, seem to classify the adhesives in the same order. The shear strength was lower after the A4 treatment as the specimens were tested in the wet state. The EP-bonded specimens clearly display the highest shear strength values. Then, 2K PUR and PRF can be classified as one group. The MUF and 1K PUR control specimens display similar shear strength but MUF-bonded specimens are less cooking resistant. Also the shear strength of EPI-bonded specimens drops dramatically after cooking.

Table 1. Mean shear strength, standard deviation and coefficient of variation (CoV) for each group of ten tested specimens. (The EPI bonded specimens treated according to A4 were not possible to test).

	Control			A4			A5		
	Mean shear [N/mm^2]	St. dev.	CoV [%]	Mean shear [N/mm^2]	St. dev.	CoV [%]	Mean shear [N/mm^2]	St. dev.	CoV [%]
EP	13.57	1.47	11	5.34	1.66	31	11.29	2.41	21
2K PUR	8.97	2.09	23	2.28	0.76	33	7.54	1.57	21
PRF	8.55	0.99	12	1.57	0.36	23	6.26	0.54	9
MUF	7.03	1.38	20	0.76	0.25	33	2.21	0.61	28
1K PUR	6.81	0.56	8	1.54	0.24	15	4.44	0.31	7
EPI	4.27	1.46	34	0	0	0	0.77	0.28	37
MS	1.75	0.2	11	0.37	0.04	12	0.82	0.27	33

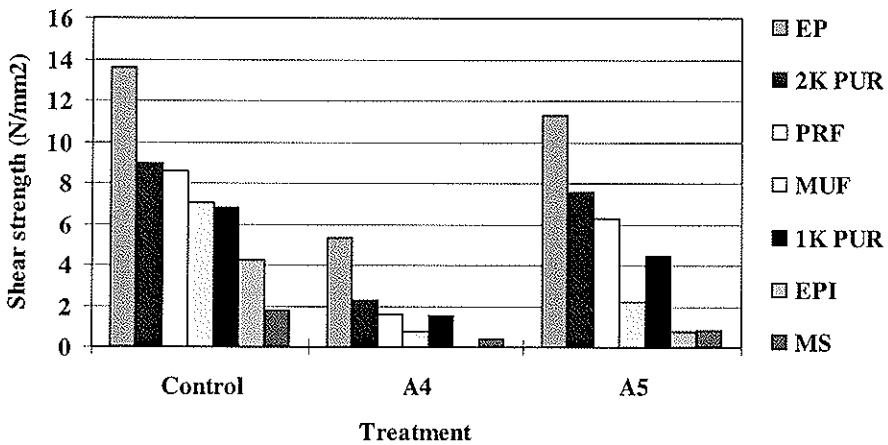

Figure 4. Shear strength (tested in compression). The shown values are average values of the ten specimens in each group.

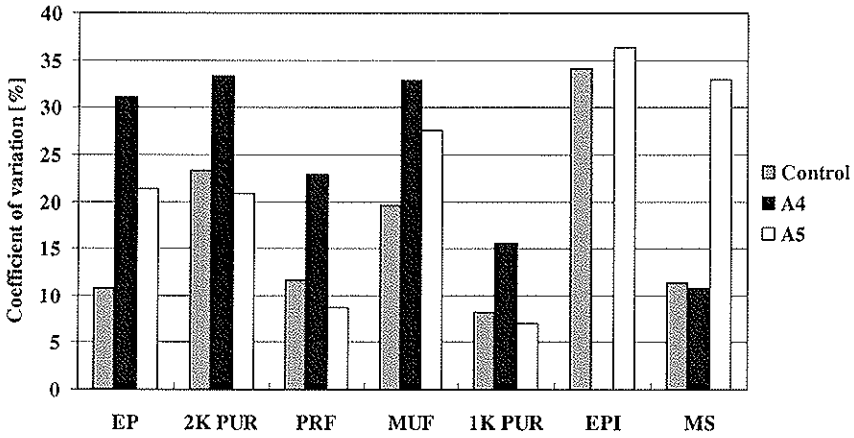

Figure 5. Coefficient of variation for shear strength.

There were large variations (large CoV) in the shear strength test results, see Figure 5. One possible reason for this behaviour can be variation in the beech material. Therefore, all specimens were examined visually. This visual inspection did not point out any clear reasons for the variability in the test results. The different groups of specimens seemed to be similar. However, it appeared that badly centred bolts could be one explanation to the large variation in the test results. The magnitudes of the coefficients of variation were similar for the initial 240 tests as for the here presented tests.

The coefficients of variation are in most cases highest after the A4 treatment. This is probably due to the testing of wet specimens. It is worth to note that also for pure beech specimens tested according to EN 302, the variability in the shear strength test results usually is of the same order as obtained in present tests.

To try to minimise the variability in the test results some more tests, using EP, 2K PUR and PRF will be performed. For these new specimens the variability in the beech material will be minimised and the rods will be carefully centred.

3.2 Test methods for production control

From the large amount of test results available only some results will be presented here. The load-slip curves for the EP- and PUR-bonded specimens were very similar. The failures were brittle and in some cases stress drops preceded the failure. PRF-bonded specimens displayed a different load-slip curve. The curve was non-linear and no stress drops were observed. Examples of load-slip curves were given by Hausmann and Reil (1999).

3.2.1 Comparison between the two test methods

The results obtained by the newly developed one-sided pull-compression test set-up were compared to the results obtained by the two-sided pull-out tests. The comparable tests were performed with a glue line thickness of 0.5 mm, all three adhesives were tested (EP, 2K PUR and PRF) as well as the both slenderness ratios. The pull-out loads shown in Figure 6 are mean values of ten specimens. The two-sided pull-out test specimens bonded with EP and PUR produced higher pull-out loads than the specimens tested one-sided. For EP and PUR specimens with λ=20 the difference in pull-out loads between the two test methods was considerable. This result seems reasonable as EP and PUR are brittle adhesives.

However, this influence of the test method on the pull-out load must be taken into account when requirements are set on the tested glued connections.

The test results obtained at SP by using the two-sided pull-out test set-up are shown in Table 2. The bond shear strength for the different groups of specimens is shown together with coefficients of variation and density of the lamella surrounding the rod. The obtained bond shear strengths are well in accordance with other in the literature published results, see for example Aicher et al. 1999. Also the coefficients of variation are of the same order as other presented results.

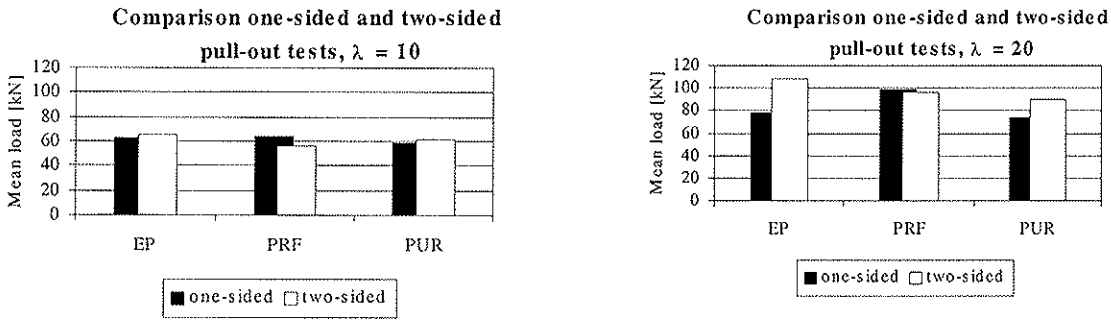

a) b)

Figure 6. Comparison between pull-out loads obtained from one-sided and two-sided pull-out tests. The showed pull-out loads are mean values of ten specimens.
a) Specimens with slenderness, λ=10.
b) Specimens with slenderness, λ=20.

Table 2. Summary of test-results obtained by the two-sided pull-out test set-up.

Slenderness	Adhesive	Bond shear strength		Wood density	
		Mean [MPa]	CoV [%]	Mean [kg/m^3]	CoV [%]
10	EP	7.6	15.9	407.5	6.1
10	PRF	6.5	4.5	407.6	8.8
10	PUR	7.1	11.7	403.2	6.0
20	EP	6.3	8.8	408.2	8.5
20	PRF	5.6	17.4	415.0	5.4
20	PUR	5.3	13.4	420.4	7.6

3.2.2 Influence of glue line thickness on pull-out strength

To investigate how the glue line thickness influences the load bearing capacity of a glued-in rod three different glue line thicknesses were investigated, 0.5 mm, 1 mm and 2 mm. These tests were performed by using the one-sided pull-compression test set-up. The results are shown in Table 3 and in Figure 7. For EP-bonded specimens there is a small increase in bond shear strength for increasing glue line thickness. However not statistically significant. If instead the pull-out loads are considered, as in Figure 7, corresponding increase is significant. For PRF-bonded specimens the pull-out strength decreased drastically with increasing glue line thickness. This decrease is partly caused by shrinkage of the PRF adhesive. PUR-bonded specimens, on the average, display an increased pull-out load when the glue line thickness increases. Expressed as shear strength no such difference is visible.

Table 3. Summary of test results, expressed as shear strength, obtained for different glue line thicknesses. Each group consists of ten specimens.

Slenderness	Adhesive	Thickness	Shear strength [MPa]	CoV [%]
10	EP	0.5	7.3	4.7
10	EP	1.0	7.6	14.2
10	EP	2.0	7.8	18.7
20	EP	0.5	4.5	14.7
20	EP	1.0	5.4	15.7
20	EP	2.0	5.4	10.3
10	PRF	0.5	7.5	7.3
10	PRF	1.0	5.7	7.3
10	PRF	2.0	3.1	17.8
20	PRF	0.5	5.8	6.4
20	PRF	1.0	5.1	8.7
20	PRF	2.0	3.3	4.0
10	PUR	0.5	6.9	16.8
10	PUR	1.0	6.7	10.3
10	PUR	2.0	7.1	9.6
20	PUR	0.5	4.3	13.3
20	PUR	1.0	4.3	14.0
20	PUR	2.0	4.3	12.7

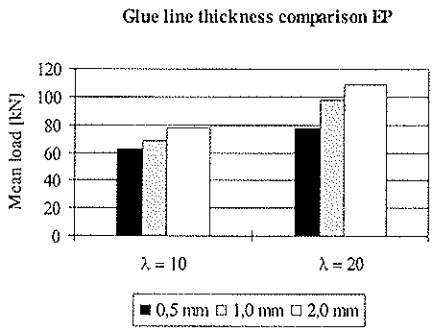

a)

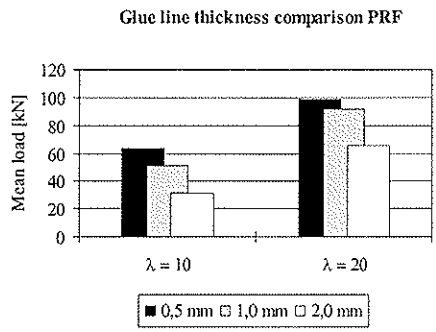

b)

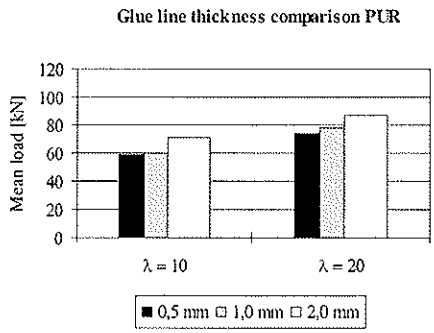

c)

Figure 7. Mean pull-out loads obtained for groups of specimens with different glue line thickness.
a) Specimens bonded with epoxy (EP).
b) Specimens bonded with phenol-resorcinol (PRF).
c) Specimens bonded with polyurethane (2K PUR).

3.2.3 Influence of density on pull-out strength

The correlation between the density of the wood surrounding the glued-in rod and the pull-out strength was examined for the different groups of tested specimens. In some cases there was no correlation at all between density and pull-out strength, see as example Figure 8a. Relationships showing decreased pull-out loads for increased density are not rare within the studied material. However, for a few groups of specimens the correlation between density and pull-out strength was stronger, see for example Figure 8b. In this case the strong correlation was caused by one low density value. In general, no relationship was found between wood density and pull-out strength of the glued-in rod. Poor correlation between pull-out strength of the glued-in rod and density of the surrounding wood was found also in other studies see for example Aicher et al. 1999. Also when testing very small glued-in rod specimens for evaluation of fracture mechanical properties poor correlation between strength and wood density was found, (ULund). The poor correlation is, however, not completely surprising. Generally, the correlation between wood strength and wood density can be poor. For adhesive bonds also the "local" density influences the behaviour of the connection. Both the adhesion to the wood and the stress distribution around the rod are affected.

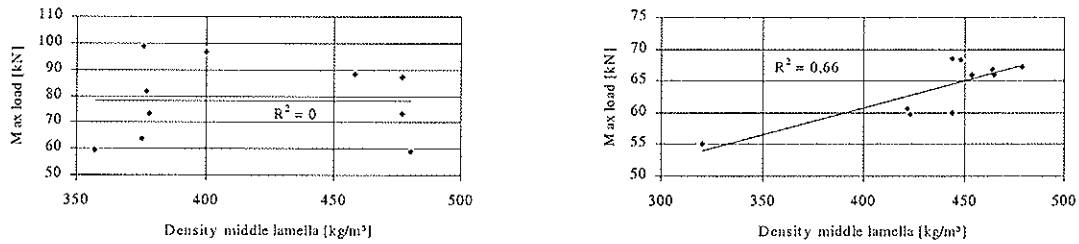

a) b)

Figure 8. Density of the wood surrounding the glued-in rod versus pull-out load for the rod.
a) Specimens bonded with EP, λ=10 and a glue line thickness of 2 mm.
b) Specimens bonded with PRF, λ=10 and a glue line thickness of 0.5 mm.

3.2.4 Proof-loading

Four different proof-load levels (PLL) were tested to try to find the maximum load that does not cause structural damage of the bond line. The levels selected were: 50%, 65%, 80% and 90% of the maximum pull-out loads obtained from the destructive tests. Both slenderness ratios were tested and a glue line thickness of 0.5 mm was used for all cases. Also the destructive tests, for comparison, were performed by the one-sided pull-compression test set-up. Seven test pieces in each group were loaded up to the determined proof-load level (loaded during 30 seconds), then the load was held for 15 seconds. Thereafter, the specimens were unloaded and reloaded until failure within five minutes. Below, in Figure 9 and in Table 4, the mean values of the pull-out loads for each of the tested group of seven specimens are shown together with the mean value of the pull-out loads for the group of ten specimens tested destructively. As glue line thickness and slenderness were the same for the compared groups of specimens pull-out loads are compared instead of shear strength.

For the specimens bonded with EP, it is remarkable that the specimens loaded to the proof-load levels 80% and 90%, on the average, reached higher pull-out loads than the specimens

only tested destructively. The effect was most pronounced for the specimens with the longest glued-in length (λ=20). The pull-out loads were approximately 20% higher for the proof-loaded specimens. Note that also specimens that failed before reaching the proof-load level are included in the mean value of the pull-out loads after proof-loading. Otherwise, the high values were not exceptional. Additional tests with EP-bonded specimens loaded to the proof-load levels 80% and 90% were performed. These new tests confirmed the original effect. The reason for this behaviour is still unknown. One speculation can be that proof-loading to high load levels leads to redistribution of stresses along the glue line. Such a redistribution seems to be advantageous for the pull-out strength of EP-bonded rods.

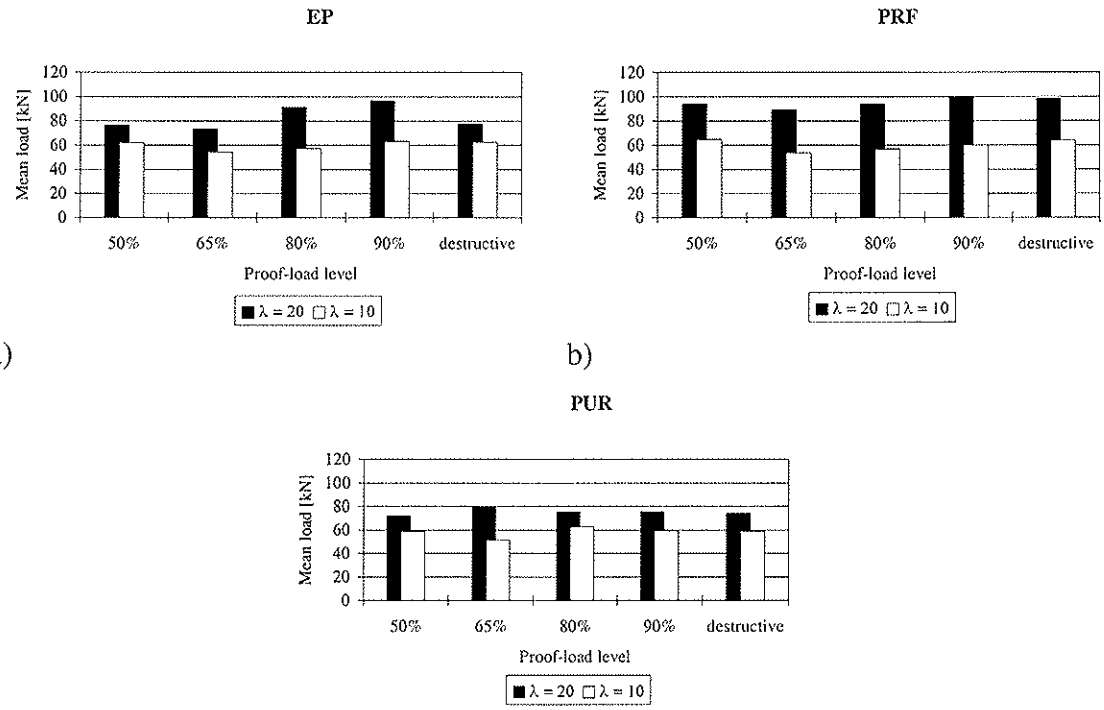

Figure 9. Mean values of the pull-out loads for the groups of specimens tested at different proof-load levels and for the group of specimens tested destructively.
a) Specimens bonded with epoxy.
b) Specimens bonded with phenol-resorcinol.
c) Specimens bonded with polyurethane.

Table 4 shows the mean pull-out loads and the coefficients of variation (CoV) for the destructive tests and for the groups of proof-loaded specimens. For the EP-bonded specimens, the coefficients of variation were largest for the largest slenderness ratio. For the PRF-bonded specimens it was the other way around; the groups of specimens with the smallest slenderness ratio displayed the largest coefficients of variation.

Based on the test results shown above the objective was to determine a proof-load level suitable for production control of glued-in rods. In addition to the results shown above, the density and the moisture content of the wood surrounding the glued-in rod was registered. A total amount of 196 specimens were proof-loaded to the different load levels. Of these specimens, 21 failed before reaching the proof-load level, and approximately ten specimens failed during the re-loading very near the actual proof-load. None of the specimens failed

before reaching the 50% proof-load level and only one specimen failed before reaching the 65% load-level. The amount of failures was equally distributed between the three types of adhesive. Not surprisingly, 16 of the specimens that failed before reaching the proof-load level were loaded at the 90% level. The average middle lamella density for all tested specimens in the study was 419 kg/m^3 (dry density). For some specimens the wood surrounding the glued-in rod was relatively low, around 370 kg/m^3. However, also specimens with high density, around 450 kg/m^3, in the middle lamella failed. Furthermore, as shown above, the correlation between density and pull-out load was poor in present study and therefore it is not possible to draw any conclusions based on the value of the density.

However, for the continuation of the present study it was decided to use 80% as a suitable proof-load level.

Table 4. Mean values and coefficients of variation (CoV) of the pull-out loads for the destructive tests (dest) and the proof-loaded specimens (PLL50 = proof-load level of 50%,...)

	EP, λ=10					**EP, λ=20**				
	dest.	**PLL50**	**PLL65**	**PLL80**	**PLL90**	**dest.**	**PLL50**	**PLL65**	**PLL80**	**PLL90**
Mean [kN]	62.6	62.2	54.3	57.3	63.2	77.4	76.3	73.3	91.2	96.6
CoV [%]	4.7	9.1	15.6	14.2	15.2	14.7	19.5	16.0	19.9	19.8
	PRF, λ=10					**PRF, λ=20**				
Mean [kN]	63.8	64.6	53.8	56.6	59.9	98.4	93.9	88.8	94.0	99.6
CoV [%]	7.3	13.1	14.5	10.5	11.7	6.4	7.9	7.4	6.8	6.3
	PUR, λ=10					**PUR, λ=20**				
Mean [kN]	59.0	58.9	51.4	63.5	59.4	74.1	71.8	78.9	75.4	75.5
CoV [%]	16.8	20.5	9.1	9.3	11.8	13.2	11.0	8.8	13.9	16.5

3.2.5 Error-detection

To ensure that the proof-loading method can detect possible defects of the bonded connection, specimens with six different defects were prepared. The premeditated defects were:

1. Too little adhesive
2. Burnt wood surface in the drilling hole
3. Incorrect mixing proportions of the adhesive components
4. Rod temperature at -10°C
5. Too large drilling diameter
6. Oily rod

In addition, a control series (with no defects) was tested at the same occasion. Each group of specimens consisted of seven specimens and a total amount of 308 specimens was tested. The hardening time for all specimens tested in this test series was seven days.

The results of the proof-loading to 80% of the defect specimens are shown in Figures 10-12. The number of errors detected is marked black. It can be seen that the number of detected errors varies with type of adhesive, slenderness ratio and type of error. In the case of too little adhesive the amount of adhesive was reduced by a factor two. This defect resulted in decreased mean pull-out loads of between 20% and 39% compared to the

control test series. All PRF-bonded specimens and a majority of the EP- and PUR-bonded specimens, with this defect, failed before reaching the 80% proof-load level.

Burnt wood affected the PRF-bonded specimens most seriously. The pull-out loads were decreased by, on the average, 10% to 24%.

The incorrect mixing of the adhesives was detected in all cases. The amount of hardener was strongly reduced (≥ 40%). It is possible that this incorrect mixing was too coarse to act as an indicator for determining whether 80% is a suitable proof-load level. Incorrect mixing of the adhesives components lead to a reduction of the pull-out loads by 31%-55% for PRF- and PUR-bonded specimens. The EP adhesive did not harden and therefore these specimens were not possible to test.

The frozen rod and the oily rod only had a small influence on the pull-out loads for the bonded connections and, consequently, this error was only detected in a few cases.

Producing the hole diameter too large gives the same results as increasing the glue line thickness, i.e. slightly increased pull-out strength for the EP- and the PUR-bonded specimens (by 5% to 29%) and decreased pull-out strength for the PRF-bonded specimens (by 27%-45%).

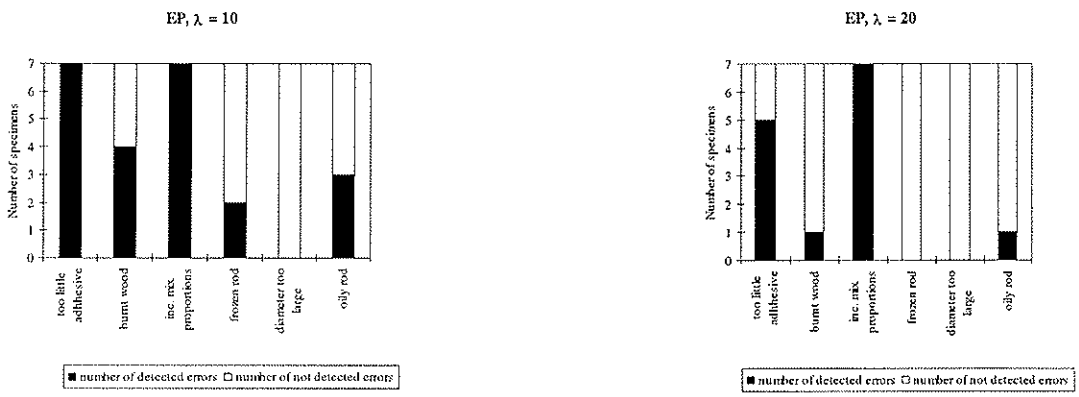

Figure 10. Number of specimens, bonded with EP, with defects found by proof-loading to 80%.

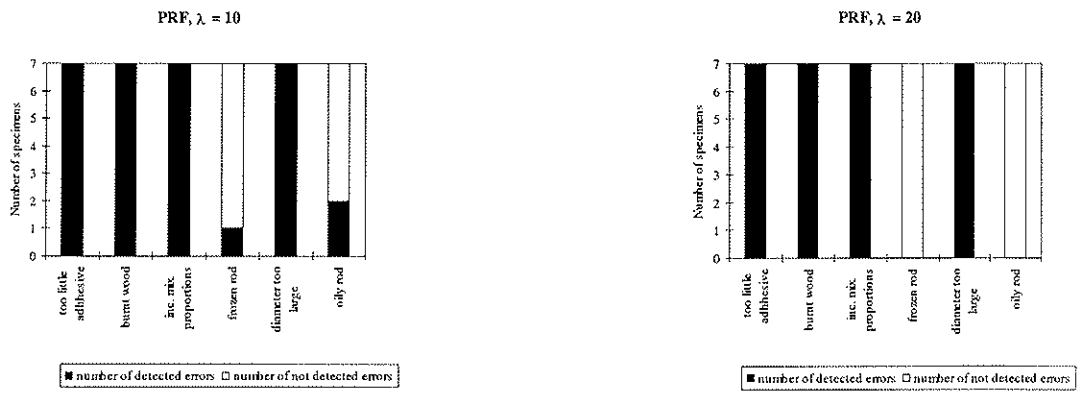

Figure 11. Number of specimens, bonded with PRF, with defects found by proof-loading to 80%.

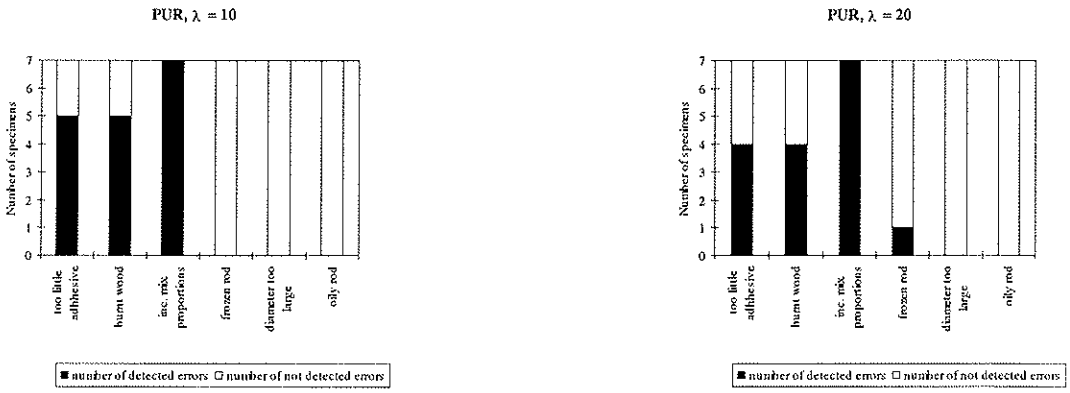

Figure 12. Number of specimens, bonded with PUR, with defects found by proof-loading to 80%.

4. Conclusions

4.1 Strength and durability of the adhesive

A test method for strength and durability of glued-in rods is under development. The suggested method, 40 x 40 x 20 mm beech blocks with glued-in 16 mm threaded rods seems promising. A large variability in the test results was found. This variability will be further evaluated before the test method is finally drafted. Large variability is however also found in other studies where small glued lengths are used.

If present shear strength test results are compared with the requirements according to EN 301 (classification of phenolic and aminoplastic adhesives for load bearing timber) only the EP-bonded connections pass. However, comparison with the requirements according to EN 301 can be questionable as the suggested test specimens are very different from standard specimens prescribed in EN 301. As expected, cooking and testing in the wet state lead to very low shear strength of the glued connection. Bonding steel to wood puts extra strong requirements on the adhesive line as the wood swells while the steel rod is rigid.

Within the GIROD-project also the influence of moisture content on strength of glued-in rods and duration-of-load behaviour of full-sized glued-in rod specimens are investigated. These two aspects are very important for the use of glued-in rods and must be included in testing methods for assessment of glued-in rod connections. It will be examined whether the cooking of small glued-in rod specimens can act as a method for estimating the long-term behaviour of glued-in rod connections.

4.2 Test methods for production control

Based on the results in the present study the method, two-sided pull-out tests, used for destructive testing of glued-in rods worked well. Results obtained at SP agreed with results of similar tests obtained previously. The destructive testing is performed on a specially produced test specimen, hopefully representative for a certain batch of glued-in rods. Therefore this testing does not give a strength value for the actual connection and it is still an uncertainty concerning the reliability of the rod-timber connection in service.

If the more simple test set-up, one-sided pull-compression, is used for destructive testing the difference between the one-sided and the two-sided methods must be taken into

account, primarily for EP- and PUR-bonded specimens which seem to produce lower pull-out loads when tested by the one-sided test set-up.

A proof-loading procedure has the advantage that the actual connection can be tested. The proof-loading test results obtained in the present study are partly confusing. Specimens bonded with EP, on the average, reached higher pull-out loads after proof-loading until 80% and 90% than the specimens tested destructively. None of the tested groups of specimens displayed a decrease in pull-out strength after proof-loading to such high levels as 80% and 90%. The groups of specimens proof-loaded to 65% displayed a decreased pull-out strength. For EP-bonded specimens there was slightly larger variation in the pull-out loads after proof-loading than for the destructive tests. This was not the case for PUR and PRF bonded specimens. It is possible that the evaluation of the test results presented here, based on mean values are misleading. New evaluations will be performed before final conclusions can be drawn.

Error detection was possible for coarse errors by proof-loading up to the 80% level. The induced errors in the present study were sometimes extreme errors. From the results obtained in present study it seems like the most common production errors are detected by proof-loading to 80% of the estimated strength of the connection. It seems also like 80% of the strength is a "safe" level for avoiding permanent damage. It is, however, possible that different proof-load levels should be applied for different adhesives and/or different slenderness of the glued connection. In the present study 80% seemed to be a suitable level for PRF-bonded specimens. For EP and PUR bonded specimens slightly fewer production errors were detected.

Generally, no relationship between density of the wood surrounding the glued-in rod and pull-out strength was found. The same relationship was found in other studies. This fact needs to be further investigated, especially as the density is a parameter included in some design equations.

The GIROD-project results in a large data base with test results for glued-in rods. Present test results together with data for duration-of-load behaviour and moisture dependency will serve as a good base for drafting new test methods.

5. Acknowledgements

This research is sponsored by the European Commission (DG XII) through grant nr SMT 4-CT97-2199 and NUTEK (Swedish National Board for Industrial and Technical Development). The financial support is gratefully acknowledged.

6. References

Aicher, S. Höfflin, L. Wolf, M. 1998. Influence of specimen geometry on stress distributions in pull-out tests of glued-in steel rods in wood, Otto-Graf-Journal, vol.9, FMPA-Otto-Graf-Institute, Stuttgart, 12 pages.

Aicher, S. Gustafsson, P.J. Wolf, M. 1999. Load displacement and bond strength of glued-in rods in timber influenced by adhesive, wood density, rod slenderness and diameter. In proceedings of RILEM symposium on Timber engineering, Stockolm, Sweden, 10 pages.

Hausmann, K. Reil, N. 1999. Test methods for production control of glued-in rods for timber structures. Master´s thesis, Technical University of Karlsruhe, Fakultät für Bauingenieurwesen, 208 pages.
Kemmsies, M. 1999. Comparison of pull-out strengths of 12 adhesives for glued-in rods for timber structures, Swedish National Testing and Research Institute, Building Technology, SP Report 1999:20, 26 pages.
Ulund-PR-3, 2000-02-16, Progress report within the GIROD project (SMT4-CT97-2199) for WP1, Development of a Calculation model, 65 pages.

INTERNATIONAL COUNCIL FOR RESEARCH AND INNOVATION
IN BUILDING AND CONSTRUCTION

WORKING COMMISSION W18 - TIMBER STRUCTURES

STIFFNESS ANALYSIS OF NAIL PLATES

by

P Ellegaard
Department of Building Technology and Structural Engineering
Aalborg University

DENMARK

MEETING THIRTY-THREE
DELFT
THE NETHERLANDS
AUGUST 2000

Presented by: P. Ellegaard

· S. Thelandersson asked and received clarification on the beam analogy in the truss plate model such that along the main axis of the truss plate the "link zone" was modeled with small beams. The number and size of the beams were determined according to the actual geometric parameters of the truss plate with respect to the joint.
· J. Kangas asked how were the Eurocode values obtained.
· P. Ellegaard responded that they were obtained via basic tests.
· J. Kangas stated that correction factors should be used; otherwise, the wrong Eurocode values would be obtained. It was subsequently clarified that the correction factors refer to information only available in the current existing draft.
· B. Källsner asked whether the large gap of 5 mm in the test exceeded the values specified in the test standard.
· P. Ellegaard responded that the minimum gaps specified in the standard compression and tension tests were 4 mm and 2 mm, respectively.
· S. Thelandersson asked how to deal with another type of plate with the verification based on one type of nail plate.
· P. Ellegaard responded that he would try another type of plate soon with the 6 basic tests.
· B. Källsner stated that the interaction formula might cause problems for another type of plate.
· P. Ellegaard responded that hopefully the yield surface approach would be better.

Stiffness Analysis of Nail Plates

Peter Ellegaard

Department of Building Technology and Structural Engineering

Aalborg University, Denmark

E-mail: pe@civil.auc.dk

1. Introduction

An advanced finite element model (TRUSSLAB) for analysis of trusses with nail plates has been developed - see Ellegaard, P., Nielsen, J. (1999). Beam elements are used to model the timber, but the model is special where the joints are concerned. A nail element is used to model the strength and stiffness of a nail group and it connects a beam element with a plate element. The plate element connects two nail groups and describes the strength and stiffness of the nail plate in the joint line between the timber members. The strength and stiffness properties for these special elements are needed as input data in the finite element model.

This paper describes how the stiffness properties of the plate element are determined. In order to obtain these properties, tests with nail plates have been performed for different combinations of the load and plate direction combined with different orientations of the joint line.

The test specimen and results from the tests are presented and the load displacement curves are compared with calculations with the advanced finite element model TRUSSLAB. All tests are carried out for the MITEK GNA20S nail plate with a thickness of 1 mm.

2. Test Description

114 tests have been carried out in order to obtain the strength and stiffness of the nail plate for different combinations of the load and nail plate direction combined with different orientations of the joint line. The test series and the test setup are described in this section.

2.1 Test Series

The specimens are divided into 2 main groups - one group where the members are subjected to tension, see figure 2.1, and one group where the members are subjected to compression, see figure 2.2. The figures illustrate the orientation of the force, the nail plate and the joint line - the figures are not in scale. The plate main direction is represented by the line through the nail plate. The nail plate and the joint line are rotated in steps of 30° so every possible combination is covered.

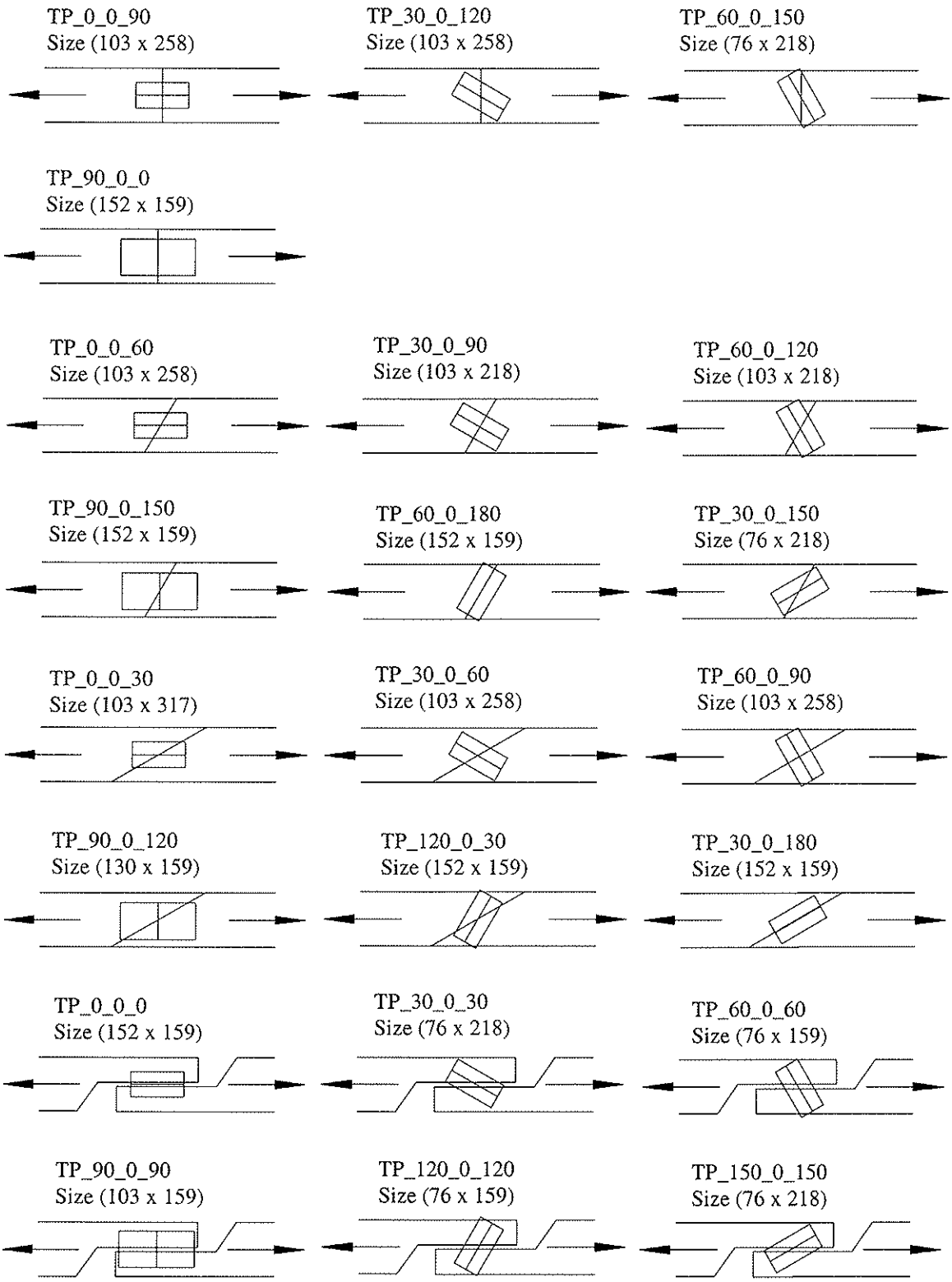

Figure 2.1. Test specimens subjected to tension. Plate sizes in mm (length of the plate main direction x length of the plate perpendicular to the main direction).

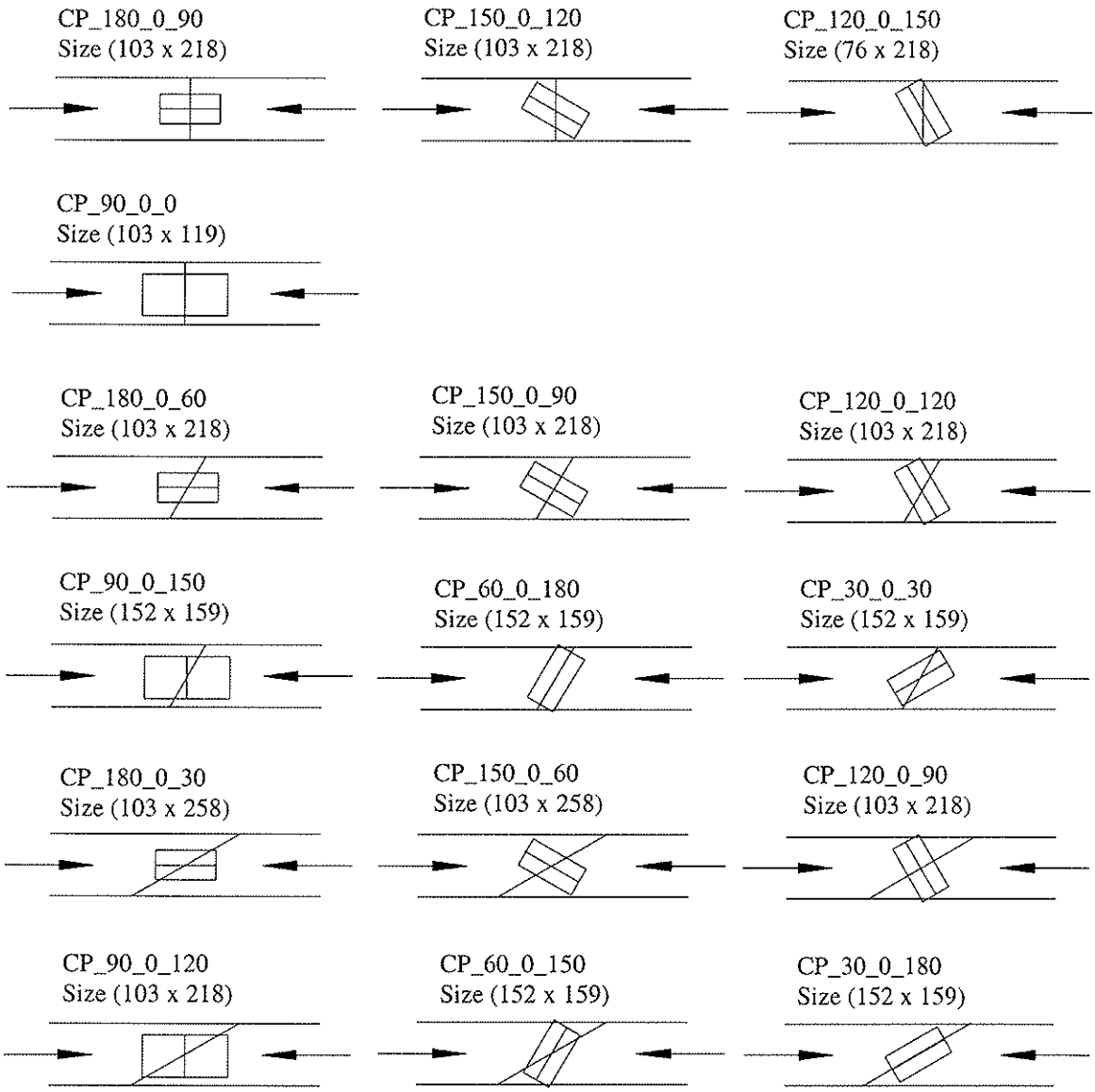

Figure 2.2. Test specimens subjected to compression. Plate sizes in mm (length of the plate main direction x length of the plate perpendicular to the main direction).

The notation of the specimens is TP_α_β_γ (Tension Plate) and CP_α_β_γ (Compression Plate) where:

α: angle between the plate main direction and the force
β: angle between the force and the grain direction
γ: angle between the plate main direction and the joint line

For every specimen 3 copies have been produced and tested.

All the specimens have a gap of 5 mm between the timber parts to avoid that contact forces are transferred. The sizes of the nail plates were chosen in order to achieve plate failure and the nail plates are located so that the centre of the nail plate is placed at the centre of the joint line.

The timber is Swedish spruce of strength class K-24 (S10) with a thickness of 45 mm. The test specimens have been conditioned and manufactured according to prEN 1075.

2.2 Test Setup and Measuring the Deformation of the Plate

The tensile tests were carried out in a test setup, where the timber is clamped at both ends between two jaws. The force is applied to the timber through friction between the jaws and the timber.

The compression specimens were tested in the test setup illustrated in figure 2.3.

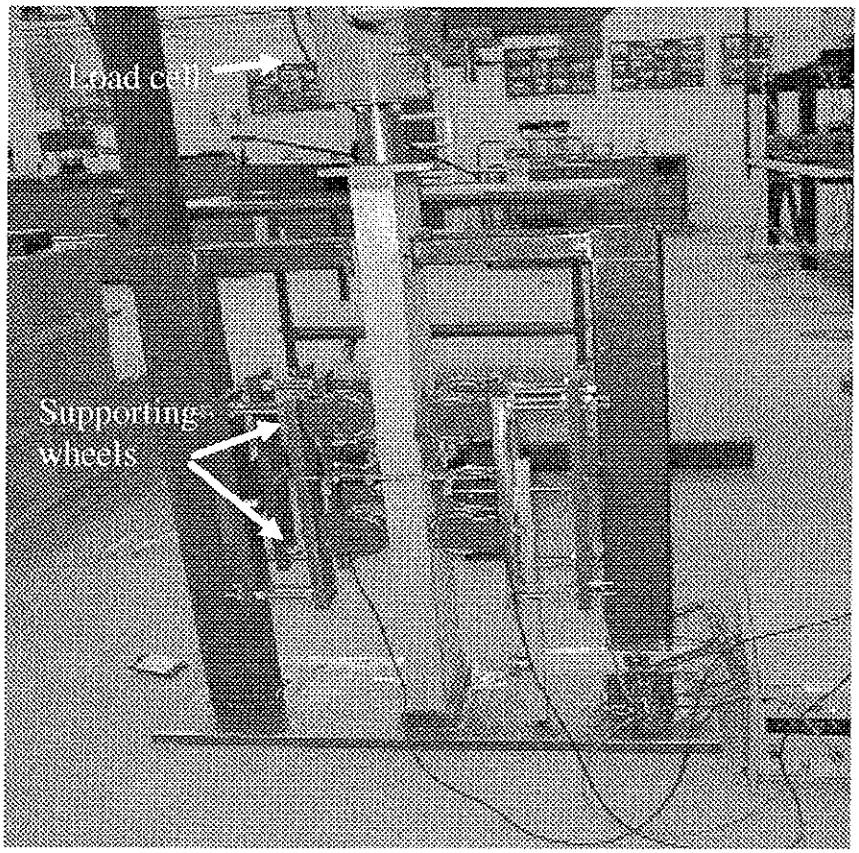

Figure 2.3. Test setup for compression tests.

The 8 supporting wheels were tightened before every test so that they prevented out-of-plane instability. At the bottom the test specimens were simply supported.

For both test setups the load was applied according to EN 26891 and prEN 1075.

The deformation of the nail plates was measured by two HBM DD1 displacement transducers (± 2.5mm) - one on each side, see figure 2.4.

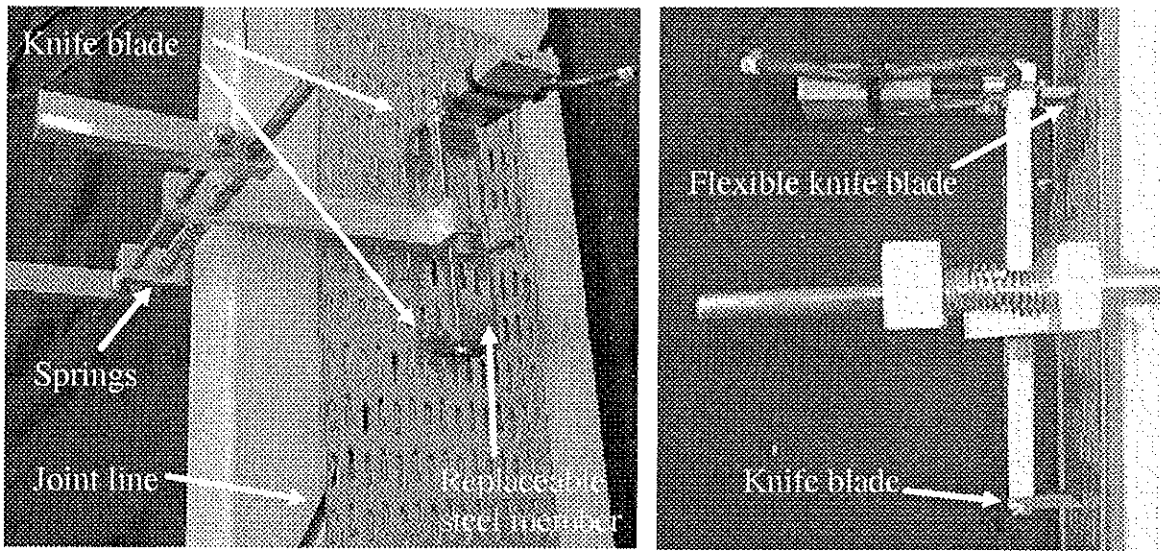

Figure 2.4. Arrangement to measure the deformation of the plate.

The springs press the four knife blades to the nail plates and ensure that the blades are fixed to the points where they are in contact with the nail plates. The displacement between the two blades on each side is measured via a strain gauge that is attached to the flexible knife blade.

The arrangement is always located in such a way that the measured deformation of the nail plate is parallel to the force direction. One of the knife blades on each side is stiffly connected to the steel member that connects the blades. The steel members have a length of 100 mm when the angle between the joint line and the force direction is 60° - otherwise the steel members are replaced so their length is 50 mm.

For the six test series (TP_0_0_0 → TP_X_0_X → TP_150_0_150), where the joint line is parallel to the force direction, two extension steel parts were fastened to two of the blades so that the measured deformation is still the deformation of the nail plate parallel to the force direction.

For some of the tensile test specimens the failures were brittle. This destroyed one DD1 displacement transducer and after this event the tests were stopped after the plates had become plastic, but before the failure load was reached.

The method described above to measure the deformation of the plate was found to be very precise and it was very easy to attach the transducers to the test specimen. The measured deformations of the plate on each side of the specimen are very alike.

In some preliminary compression tests the deformation of the plate was measured as illustrated in figure 2.5. The extension steel bar is attached to the displacement transducer in one end and to the nail plate in the other end (via a small mark on the surface of the nail plate). The arrangement that holds the displacement transducers is fastened to the timber with a screw.

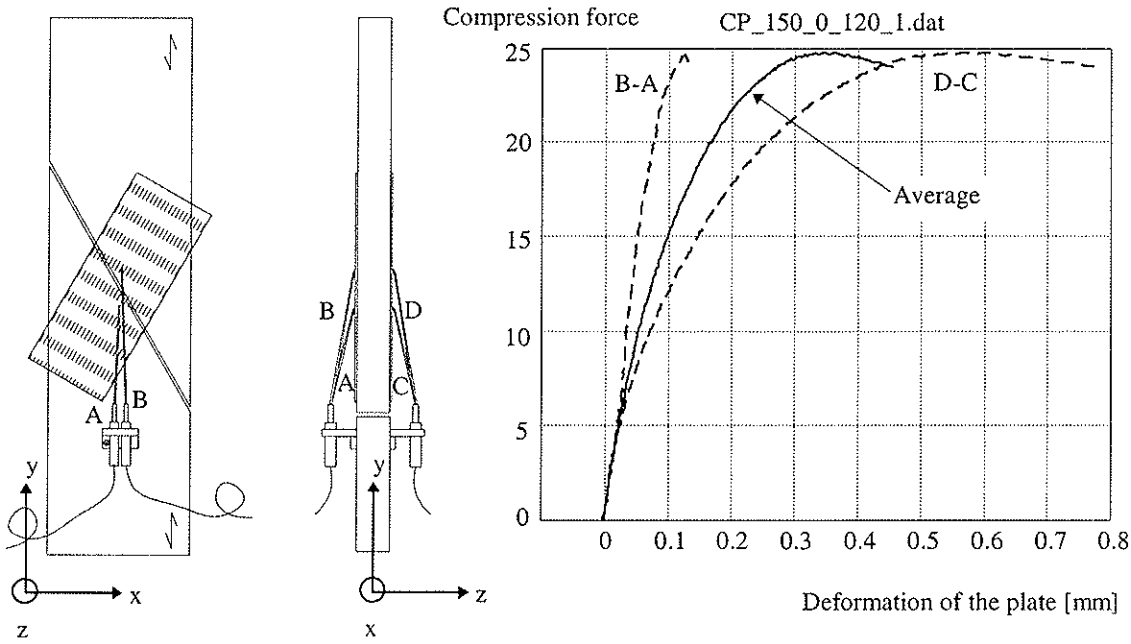

Figure 2.5. One way to measure the deformation that did not perform well. To the right the differences between the displacement transducers on each side are shown.

For some reason this method of measuring the deformation of the plate gave some results that were obviously misleading, see figure 2.5 right. This may be explained by the fact that even a relatively small horizontal movement (bending) at the midpoint of the test specimen in the z-direction will result in a shortening of one of the long displacement transducers and an elongation of the other long displacement transducer. This error of measurement has a value of up to 1/3 of the horizontal movement. The error is caused by the extension steel bars from the displacement transducers that form an angle with the timber. The horizontal movement could be caused by bending around the weak axis of the timber.

The load displacement curve in figure 2.5 is not the worst case - in other cases the difference between the displacement transducers on one side of the specimen gave negative values. This means that the transducer with the short extension bar measures a displacement that is larger than the value measured by the transducer with the long extension bar!

The results from the tests are given in chapter 4.

3. The Advanced Analog TRUSSLAB

The advanced analog TRUSSLAB is set up in the MATLAB environment. For a description of the advanced analog TRUSSLAB see Nielsen J. (1996) or Ellegaard, P., Nielsen, J. (1999). However, the plate element has been further developed since these papers were written so a short description of the theory of the plate element will be given in the following section. It is also shown how the plate parameters needed as input in TRUSSLAB are determined.

3.1 Theory of the Plate Element

A plate element connects two nail elements. The element consists of a number of small Bernoulli beams between two stiff plate regions (nail areas), see figure 3.1.

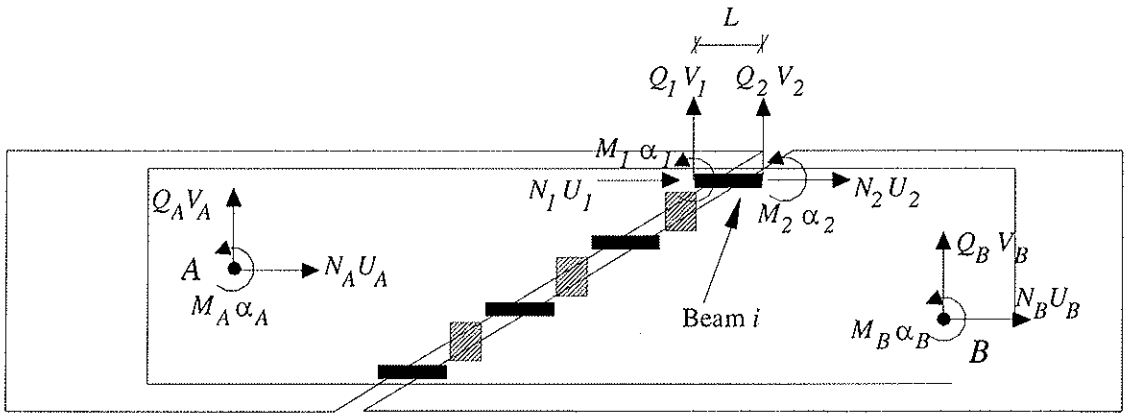

Figure 3.1. Plate element with 4 steel beams in the plate main direction and 3 steel beams perpendicular to the plate main direction.

There are two orientations of the beams. One type is parallel with the plate main direction and the other type is perpendicular to the plate main direction - a simplification of the way a nail plate looks like (GNA20S). The two types of beams have different properties. The number of beams is found from the geometry of the nail plate and the distances between the beams in the plate main direction and perpendicular to this direction are therefore needed as input in TRUSSLAB.

The deformations U_1, V_1, α_1, U_2, V_2 and α_1 of beam i are calculated from the displacements U_A, V_A, α_A, U_B, V_B and α_B of the two plate nodes A and B. The stiffness matrix for the plate element is set up by a summation of the stiffness matrices of the small beams in both directions. Similarly the forces N_A, V_A, M_A, N_B, V_B and M_B at the two plate nodes A and B are calculated by a summation of the forces at the ends of the small beams, see Nielsen (1996).

The small steel beams are assumed to behave bilinearly elastically, see figure 3.2.

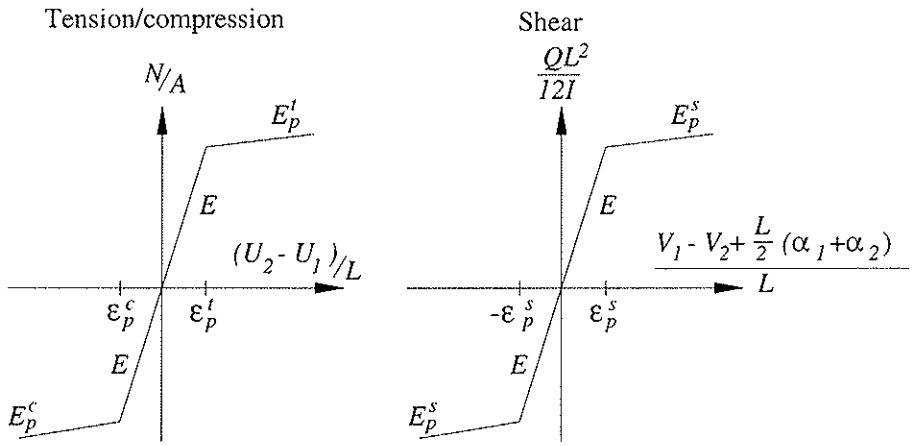

Figure 3.2. Bilinear load displacement curve for the small steel beams.

In compression the tangent stiffness E_p^c is used to model the stiffness of beams in buckling.

Values for the strains ε_p^t, ε_p^c and ε_p^s and values for the modulus of elasticity's E, E_p^t, E_p^c and E_p^s have to be determined from tests. Furthermore, the following parameters are needed as input for the model:

L : Length of the beams

I : Moment of inertia of a beam

A : Cross-sectional area of a beam

The parameters L, I and A are determined from the appearance of the nail plate. All the above-mentioned parameters may have different values for the two different types of beams of the plate element.

In TRUSSLAB the two types of beams try to reflect the real appearance of the plate over the joint line. However the stiffness is overestimated if there is no interaction between the two types of beams. A good approximation of this interaction is found to be given by the factor $\sin^{1.5}(\gamma)$ multiplied by the stiffness of the beams in the plate main direction and the factor $\cos^{1.5}(\gamma)$ multiplied by the stiffness of the beams perpendicular to the plate main direction. γ is the angle between the joint line and the main direction of the plate. Figure 3.3 illustrates this interaction.

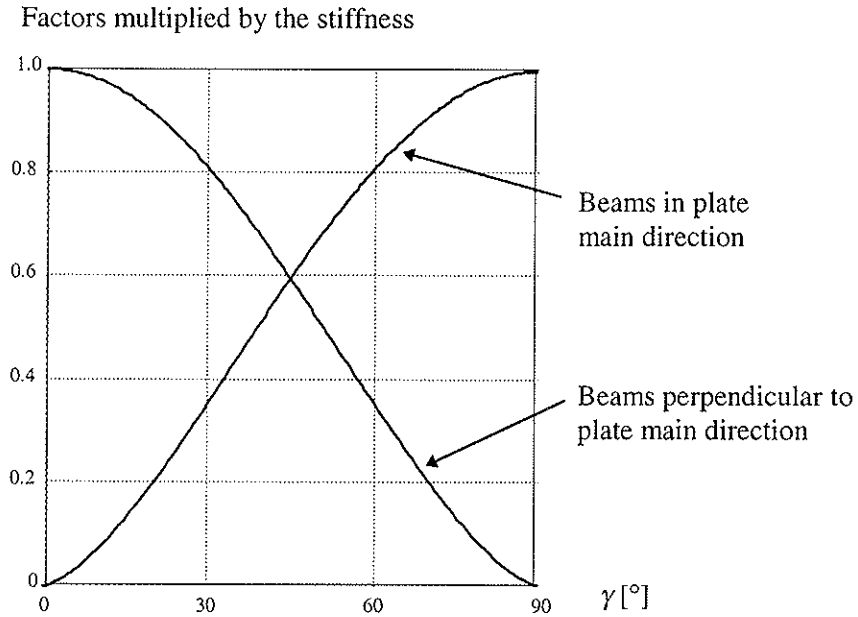

Figure 3.3. Interaction between the two types of beams of the plate element.

3.2 Determination of the Properties of the Plate Element

The properties of the plate element are determined from 6 basic tests (TP_0_0_90, CP_180_0_90, TP_90_0_90, TP_90_0_0, CP_90_0_0 and TP_0_0_0) where the beams in the plate element are subjected to pure tension, compression or a combination of shear and bending. The load displacement curves for these 6 basic tests are shown in figures 4.1 and 4.2.

Beams in the plate main direction:

Using the values L = 12.0 mm, A = 4.0 mm^2, I = 5.3 mm^4, the distance between the beams = 6.9 mm and with the results of the tests TP_0_0_90 (tension), CP_180_0_90 (compression) and TP_90_0_90 (shear/bending) the following values are found:

$$\varepsilon_p^t = 0.010 \quad \varepsilon_p^c = 0.0052 \quad \varepsilon_p^s = 0.025$$

$$E = 45000\,\text{N/mm}^2 \quad E_p^t = 280\,\text{N/mm}^2 \quad E_p^c = 1060\,\text{N/mm}^2 \quad E_p^s = 2000\,\text{N/mm}^2$$

Beams perpendicular to the plate main direction:

Using the values L = 12.0 mm, A = 7.0 mm^2, I = 28.6 mm^4, the distance between the beams = 19.8 mm and with the results of the tests TP_90_0_0 (tension), CP_90_0_0 (compression) and TP_0_0_0 (shear/bending) the following values are found:

$$\varepsilon_p^t = 0.0083 \quad \varepsilon_p^c = 0.0044 \quad \varepsilon_p^s = 0.019$$

$$E = 59000\,\text{N/mm}^2 \quad E_p^t = 780\,\text{N/mm}^2 \quad E_p^c = 3100\,\text{N/mm}^2 \quad E_p^s = 1300\,\text{N/mm}^2$$

The values of E may seem to be low compared with 188000 N/mm^2 which is the value of E for a corresponding steel plate without holes, see Jensen, H., Rasmussen, H. (1993). This is due to the fact that the values of E are calculated on the basis of the values of L and A which are found from the appearance of the nail plate.

4. Comparison of the Test Results with TRUSSLAB

The load displacement curves for the different tensile tests and results from TRUSSLAB calculations are shown in figure 4.1. The series are arranged in the same way as in figure 2.1 that showed the test specimens.

The solid lines represent the test results. Each of the solid lines is an average of the two DD1 displacement transducers. For some of the series there is only one solid line, which means that only one of the three test specimens in the series has been tested. The dashed lines are the corresponding results from calculations in TRUSSLAB.

The length of the nail plate over the joint line for test specimen TP_0_0_0 has been reduced to 80 mm in order to avoid anchorage failure.

As mentioned earlier, the sizes of the nail plates were chosen so plate failure should occur. Anyway, anchorage failure and even timber failure were found for some of the tensile specimens. These failures often developed after the plate had become plastic so the results could be used as usual. However, the series TP_60_0_150, TP_120_0_30, TP_30_0_30 and TP_150_0_150 may show misleading results due to anchorage failure. TRUSSLAB overestimates the strength and stiffness for these four tests, which also indicates that there may have been anchorage failure before the plate in the joint line became plastic. On the other hand, only the load displacement curves from the series TP_30_0_30 are abnormal. For the rest of the tensile tests TRUSSLAB predicts the stiffness well except for the two series TP_60_0_180 and TP_30_0_180 where the stiffness is overestimated by TRUSSLAB.

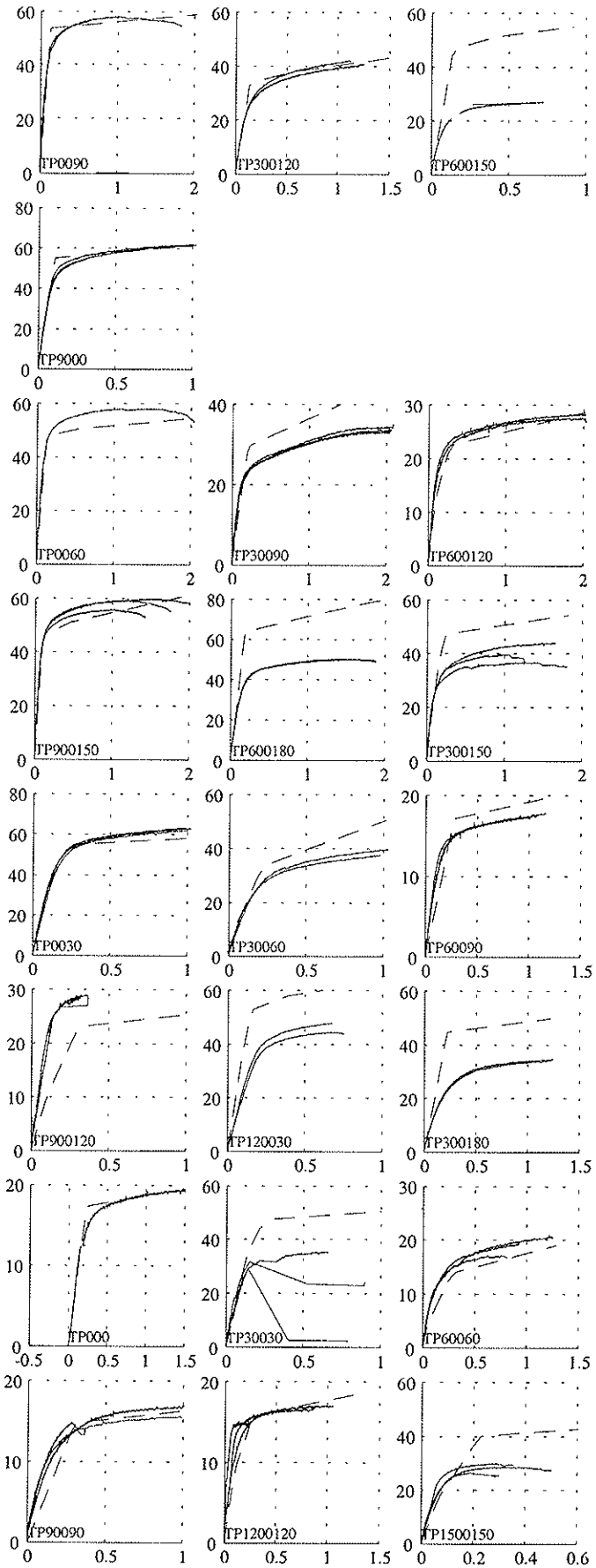

Figure 4.1. Load displacement curves for the tensile tests. The force is shown vertically [kN] and the displacement is shown horizontally [mm].

Figure 4.2 illustrates the load displacement curves for the compression tests and the corresponding results from TRUSSLAB are shown by dashed lines.

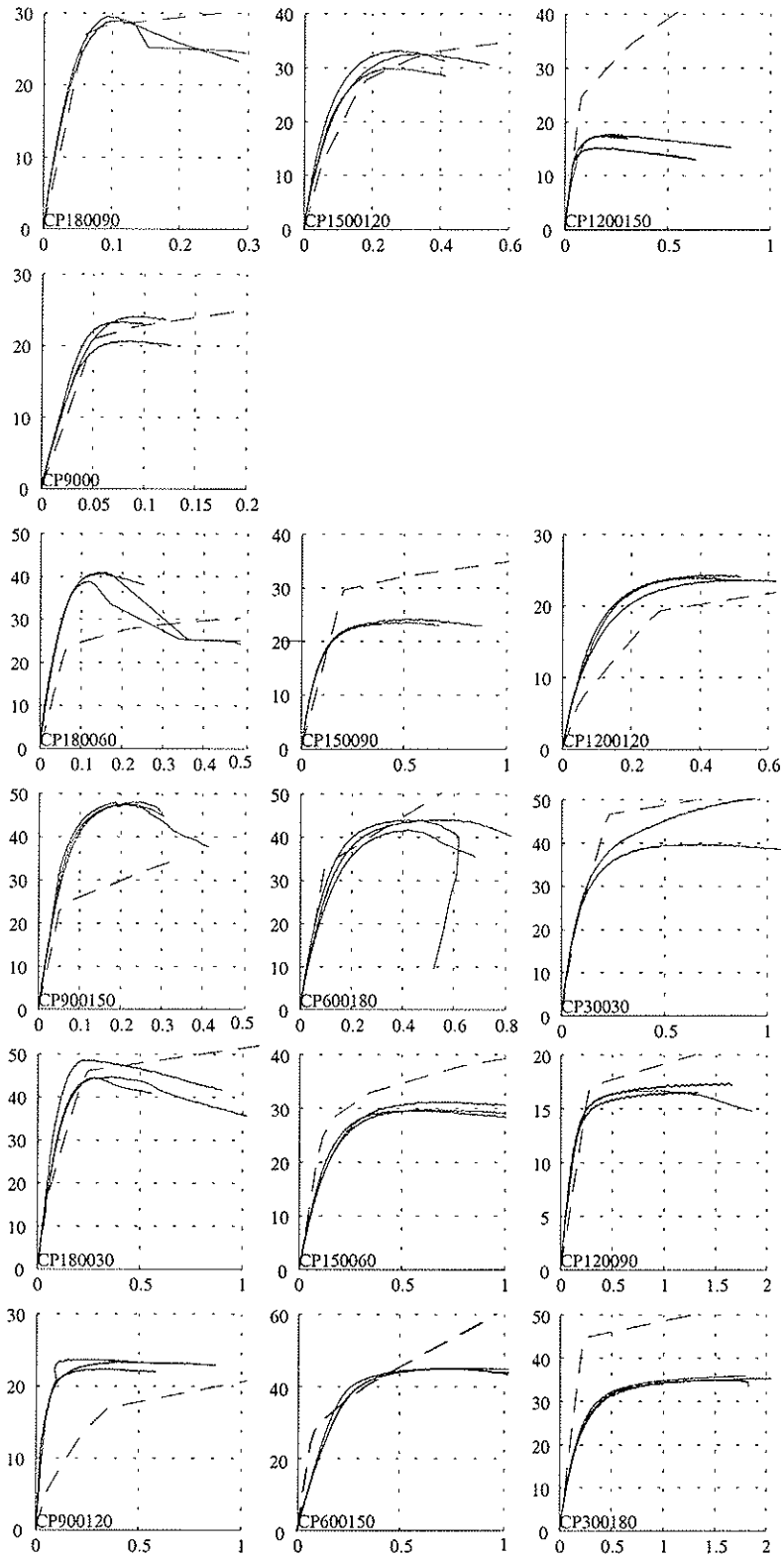

Figure 4.2. Load displacement curves for the compression tests. The force is shown vertically [kN] and the displacement is shown horizontally [mm].

For the compression series the results from the calculations in TRUSSLAB are not quite as close to the test results as they were for the tensile series. This may be caused by the fact

that the load level where the plate starts to buckle is very dependent on the location of the nails near the joint line. In some of the series the nails are located close to the joint line in such a way that the plate can carry more load - compared with the results from TRUSSLAB - before it starts to buckle. In other series the opposite situation may occur. Furthermore, the size of the gab between the timber members has an influence on the load level where the plate starts to buckle.

However, for many of the series TRUSSLAB is able to predict the stiffness and the load level where the plate starts to buckle.

5. Conclusions

TRUSSLAB is able to predict the stiffness quite well for most of the test series. The load level where the plate starts to yield or buckle is also given quite well by TRUSSLAB, even though TRUSSLAB is better in predicting yielding (tension) than in predicting buckling (compression).

When planning the tensile tests (in order to get the plate properties) special care should be taken to avoid anchorage failure before the plate has started to yield. This can be ensured if a larger nail plate is used and if this nail plate is weakened in the joint line by cutting in the plate - see figure 5.3.

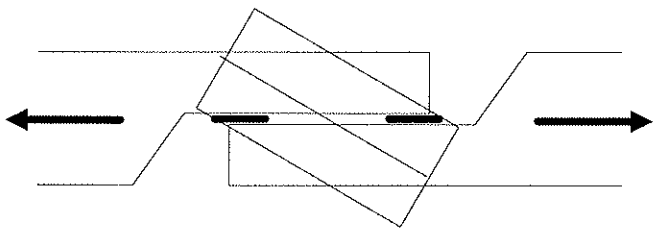

Figure 5.3. Weakening of the nail plate to avoid anchorage failure.

In the nearest future some failure criteria will be implemented in TRUSSLAB so the model can predict failure in the nail plate. Furthermore, tests with the MITEK GNA20S will be carried out to attain the properties for the nail element in TRUSSLAB.

6. References

EN 26891, 'Timber structures - Joints made with mechanical fasteners - General principles for the determination of strength and deformation characteristics', 1991.

Ellegaard, P., Nielsen, J. (1999), 'Advanced Modelling of Trusses with Punched Metal Plate Fastener', Symposium Proceedings, RILEM Symposium on Timber Engineering 1999, Stockholm, Sweden.

Jensen, H., Rasmussen, H. (1993), 'Undersøgelse af tandplader i stødsamlinger' (in Danish) (Analysis of Nail Plates in Tension Splices), University of Aalborg, 1993.

Nielsen, J. (1996), 'Stiffness Analysis of Nail-Plate Joints Subjected to Short-Term Loads', Ph.D.-Thesis, Dept. of Building Technology and Structural Engineering, University of Aalborg, Denmark.

prEN 1075, 'Timber structures - Test methods - Joints made with punched metal plate fasteners', European Standard, CEN May 1999.

INTERNATIONAL COUNCIL FOR RESEARCH AND INNOVATION
IN BUILDING AND CONSTRUCTION

WORKING COMMISSION W18 - TIMBER STRUCTURES

CAPACITY, FIRE RESISTANCE AND GLUING PATTERN OF THE RODS IN V-CONNECTIONS

by

J Kangas
VTT Building Technology

FINLAND

MEETING THIRTY-THREE
DELFT
THE NETHERLANDS
AUGUST 2000

Presented by: J. Kangas

· J. Ehlbeck asked whether slip modulus between timber/concrete connections was available.
· J. Kangas responded that there are test results from VTT available from past reports.
· J. Ehlbeck asked about the influence of α on connection strength
· J. Kangas responded that 30 degree gave higher values
· M. Ansell asked whether repair and reinforcement of existing structure could be considered with reinforcement rods.
· J. Kangas responded that it could be done. There were some repairs already made. Reinforcement also increases shear capacity.
· H. Blass questioned the dowel effect on design.
· J. Kangas responded that it was considered in the model. Deformation of the tensile dowel would cause the other rod to act as a dowel.
· H. Blass commented the dowel effect should be in both rods.
· J. Kangas responded that the rods moved together at their connection point; therefore, only one rod would act as a dowel.
· H. Blass agreed.
· B.J. Yeh asked and received clarification on beam versus joint failure.

Capacity, Fire Resistance and Gluing Pattern of the Rods in V-Connections

Jorma Kangas
VTT Building Technology,

1 Summary

A summary is reported of a large research work on joints of glulam structures based on ribbed steel rods, which have been glued-in at skew angles into the glulam. This paper presents the design of these connections and test results of their loading as well as test results of fire resistance tests under loading. The design method is based on large test series. Model for the design of the moment bearing connection has been developed. To the vector sum of the capacities of the rods forming V-shape also the calculated dowel capacity of the rods with steep direction angle can be added.

Fire resistance tests were carried out with beams under constant bending load with V-connection in the middle span. Fire protection and design is simple. Just 20 mm layer of timber or rock wool is needed to cover the steel rods for each 30 min of fire resistance. Rod distances and spacing have been varied. Minimum values of those in V-connections are proposed.

2 Introduction

The joint technology to be described here has originally been developed in TSNIISK Institute in Moscow (Turkovsky 1989, 1991). Research work had begun already in 1975. The method is based on ribbed steel rods, which have been glued at skew angles into glulam. The rods take forces effectively in their direction up to the tensile capacity of the steel. By welding the rods on to steel members, the forces can be carried forward to next member in the same manner as known in steel structures.

Design of V-connections has been presented earlier in a CIB meeting (Kangas 1993). It was based on new test results, which were later reported (Kangas 1994). A short summary of that experimental research is presented. Since then, fire resistance tests were carried out with three beams with V-connection in the middle span. The constant bending load corresponded to 40% of the loading in normal temperature design. Three thicknesses of fire protection were used (Oksanen, T. and Kangas, J. 2000). Some test specimens with various V-connections were loaded at the end of 1999. Test results of that ongoing project with prefabricated steel elements are shortly reported also .

3 Materials

All connections were made into glulam beams with 45 mm thick lamellae of spruce (Picea abies). Mean density of the beams was ρ_{12} = 430-450 kg/m^3. Moisture content was 9-15%. Various epoxy and polyurethane adhesives were used. All of them gave similar strength values in short term loading. Later only epoxies were used, after we noticed a strong creep deformation in a preliminary duration of load testing with thick glueline of polyurethane.

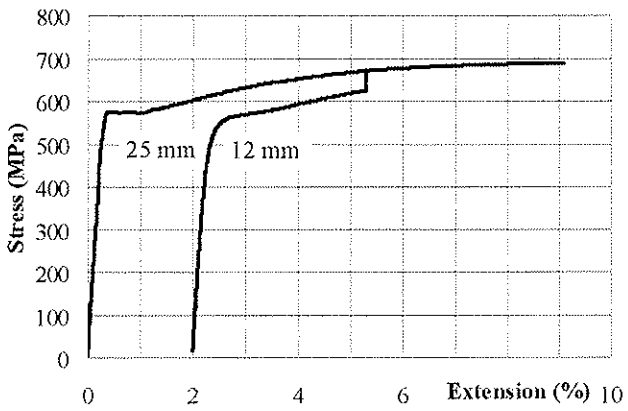

The steel rods were made of hot rolled ribbed reinforcing bars used in concrete structures. Their thickness d in various test series was 12, 16, 20 and 25 mm. Their yield strength f_y was over 500 N/mm^2 and tensile strength f_t over 600 N/mm^2. Their stress-strain curves were according to figure 1.

Figure 1. Stress-strain curves of steel rods.

4 Test series

4.1 Test with one rod

The anchorage strength in the glueline was tested first with joints of two centimetre thick rods, which were glued either with epoxy or polyurethane adhesives into spacious holes drilled into the glulam beams. Their direction angles α with the grain direction were 30°, 45°, 60° and 90°. The rods were loaded in tension or in compression, see Figure 2.

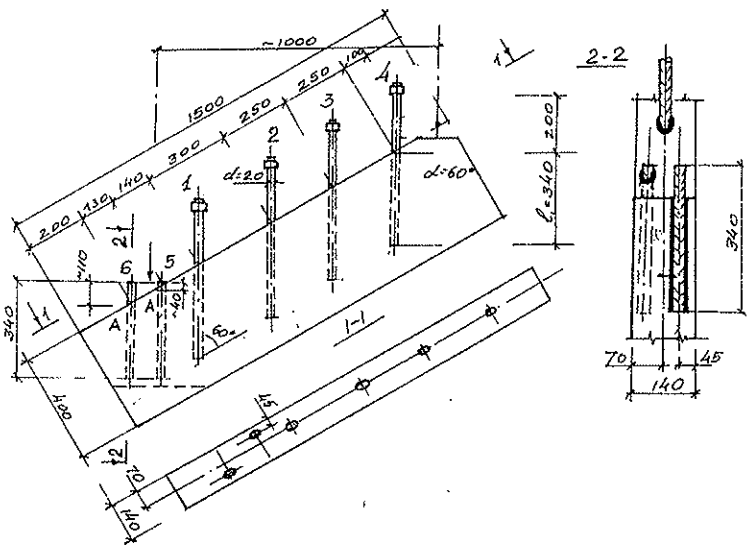

Figure 2. Specimen of tensile test series with α = 60°.

All adhesives gave equal strength values in short term loading. The mean of 96 rods was m{f_a} = 6,4 N/mm^2 and variation coefficient v{f_a} = 0,088, when anchorage length was 340 mm (17d) and the diameter D = 25 mm of the hole was used in calculation of the sheared area. Variation in strength values in different grain and load directions was small.

4.2 Test with V-joints

Different V-anchor joints of two or four rods were loaded in centric tension at skew angles into beam or in shear in the direction of the beam, see Figure 3. The lengths of the rods were chosen so that the anchorage and tensile capacities were close to each other. Breaking of the steel rods often caused the failure with the anchorage length of 25d. Always the yield limits of the rods were exceeded. Tensile strength of the rods was more than 600 N/mm^2. Thickness of the rods was 20 mm or 16 mm. Many combinations of rod and load directions were used. Mean anchorage stress of 32 specimens with anchorage length of $25d$ was $m\{f_a\}$ = 5.44 N/mm^2 and variation coefficient $v\{f_a\}$ = 0.076. The rod force was calculated according to the model and the dowel effect was subtracted from the failure load. Yielding of the rods has had an effect on the failure and on the achieved strength values.

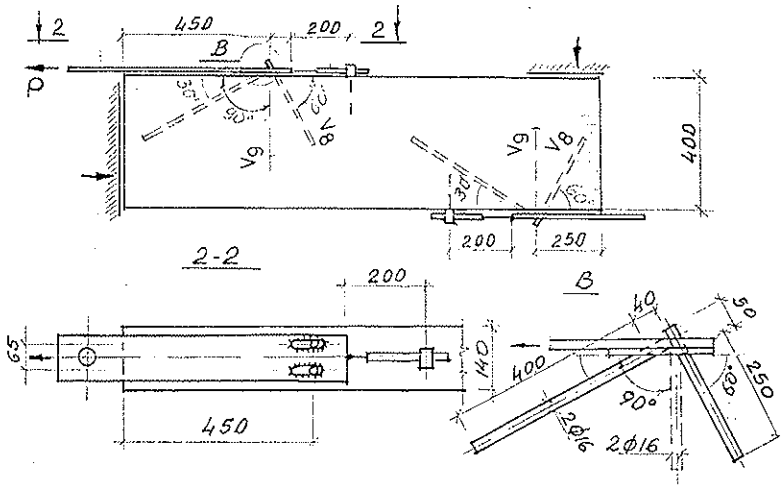

Figure 3. Plans of small joint test series with four 16 mm rods.

4.3 Test with moment bearing connections

4.3.1 Small beam

Two timber members 140x400x1500 mm^3 were connected with V-joints similar to test series V_8 in figure 3. They were loaded by two compression actuators with the span of 2,8 m. Two pairs of V16-joints were welded onto both ends of the steel plates, which crossed the joint of the connection on the tensile and compression sides of the beam. The rod thickness was 16 mm and the anchorage length of the tensile rods 440 mm.

The beam failed in timber member with the external load of 2x157 kN. Calculated bending strength of the beam was 38 N/mm^2 and the tensile force in V-joints 355 kN, which is nearly its tensile capacity and what we reached in the corresponding test series V_8.

4.2.1 Deep beams

Four connections of 1,2 m deep beams were tested. The capacities of timber members and joints were designed to be equal. Two connections of the beams were symmetric, see Figure 4. They broke in a similar way in the tensile joint of the connection with external loads 2F = 560 kN and 548 kN. A piece of timber broke off the beam. Height of it was the same as was held by the anchoring rods. Tensile strength of timber calculated for effective cross section in the connection was f_t = 32,8 N/mm^2 and 32,1 N/mm^2.

Two asymmetric connections were made on the unbroken ends of the loaded symmetric beams. Only the tensile force was taken by V-joints, see Figure 5. The first connection had a shear failure of timber member in the middle depth of the beam with the external load 2F = 610 kN. In the loading of the second connection two farthest rods broke in tension, after the other rods were first one by one torn off from the steel plate due to insufficient welding. Calculated stresses of the rods were equal to material strength. Maximum external load was 2F = 564 kN, which corresponded to lower tensile stress σ_t = 21 N/mm^2 in the timber of the connection due to longer rods with steeper angle. Bending stresses of the beams reached σ_m = 30 N/mm^2. Strain gauges were glued on the steel plates, to which the rods were welded. Relative strains proved with sufficient accuracy that the load was divided evenly between the rods.

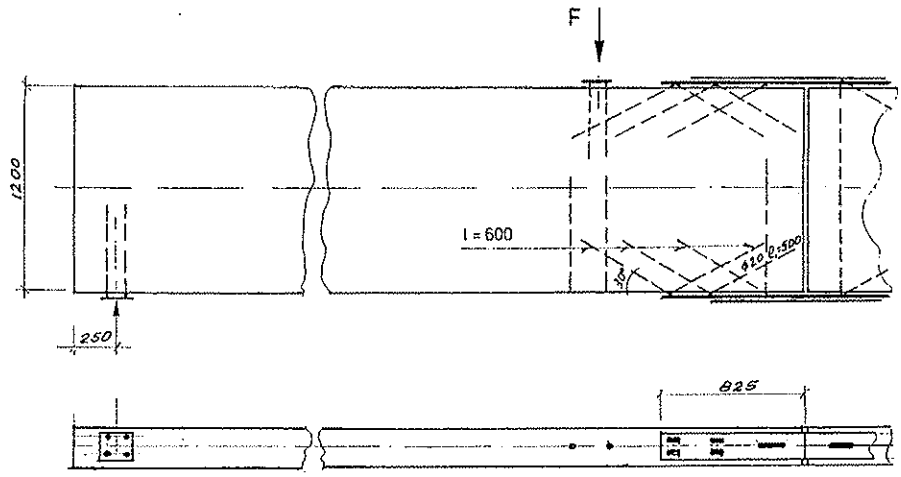

Figure 4. A symmetric connection of 1.2 m deep beam.

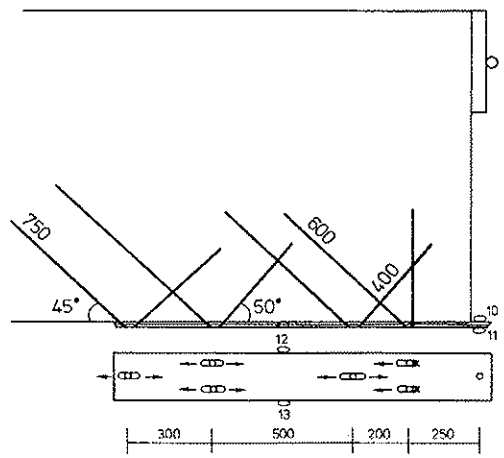

Figure 5. Spacing of the rods in the connections of asymmetric beam 4. Maximum normal force N_{max} in the connection was 1380 kN.

4.4 V-connections with prefabricated steel elements

4.4.1 Background

The connections based on glued-in rods have been made until now by inserting individual rods into the holes and welding them then to other steel elements. It is time consuming and sometimes spoils the timber surface. Also quality control is difficult to carry out. Therefore we have a development project, where we have concentrated on fabricating steel portions to achieve standardised elements and on manufacturing the glulam elements with these V-connections. The means for that are precision drilling and gluing apparatus. For practising the manufacture a group of V-connections were made and loaded.

4.4.2 Test specimens

Two connections were made on the opposite ends of short beams. Their cross sections were 115 mm x 405 mm or 165 mm x 540 mm. V-connections were composed of two steel elements, one for tension and one for compression forces. They were bolted together at the angle of 90°. Direction angle of the tensile element γ_1 was 30° and that of γ_2 of compression element was 120°. A strong steel rod was welded on the tensile element for the purpose of loading, see Figure 6. Connection (25+2D16) was composed of one 25 mm thick tensile rod lengthened for loading and of two 16 mm thick compression rods with direction angle $\gamma_2 = 90°$, see Figure 7.

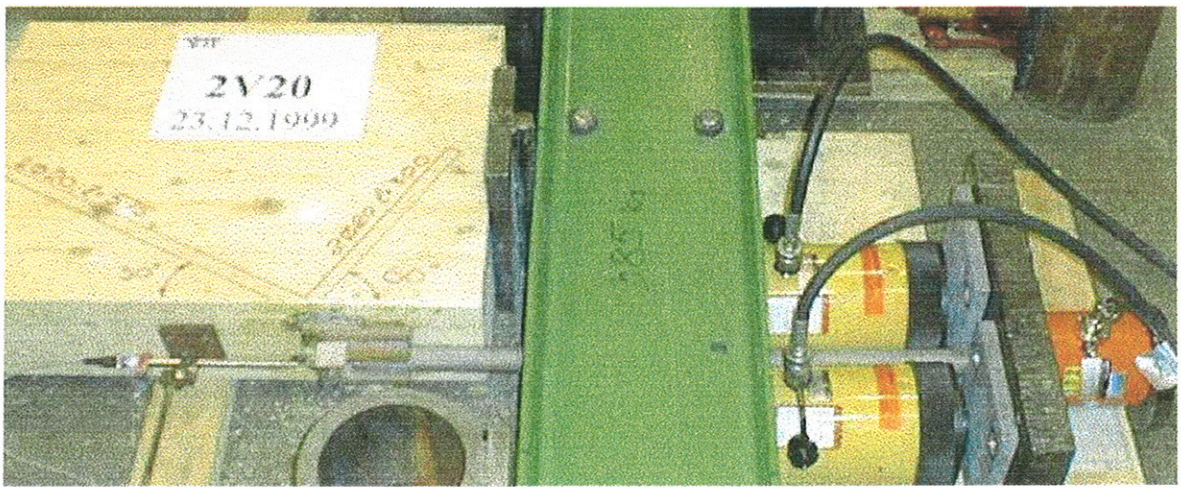

Figure 6. Loading arrangements of double V-joints of 20 mm rods.

4.4.2 Test results

Test results are given in table 1. The first number of the notations of V-connection means number of V-joints and the last one thickness of the rods in mm. R_{est} is the calculated capacity according to the proposed model with the separately measured yield strength f_y of the rods. Relative edge distances a_4 and distances a_2 between the rods varied. The anchorage length l_a of the tensile rods and the relation of the calculated and test capacities R_{test}/R_{est} also are shown. Various failure modes occurred, see Figures7-10. Load-slip curves of V-connections are shown in Figures 11 and 12.

The behaviour of V-connections can be seen from the figures and calculated values in table 1: The tensile rods reached their yield limit and after clear yielding brittle adhesive began to break down locally and the anchorage length was shortened. Finally the rods lost their anchorage capacity when tensile stress was 1,07 times their yield limit. After that the dowel capacity was also exceeded, see Figures 7 and 8. Other failure modes also occurred. The connection with triple V20 joints failed in shear after clear cracks due to tensile stress perpendicular to grain, see Figure 9. In connections with double V20 joints the bolt connecting the tensile and compression elements was cut secondarily.

Rods in V12 joints had no clear yield limit like 16-25 mm thick rods, see Figure 1. Local break down of adhesive did not occur and the connections carried loads up to tensile strength of the rods. Rods in connection 2V12 were glued by hand-mixed cold adhesive, which was not so brittle, and slip was rather big before the rods were broken.

In the connections with double V25 joints the bolt connecting the tensile and compression elements was cut secondarily. Thick rods in 2V25 connections had relatively small clearance in the drilled holes. We did not manage to fit the grooves in the slotted contact surfaces of the tensile and compression elements together while in manufacturing the connections. It can be seen in Figure 10, where the connection is cut open. The grooves are filled with adhesive. Thin slivers were cut from the top of the grooves. V-connection did not work out perfectly. At least the dowel effect was imperfect. The load-slip curves show that the tensile rods were clearly yielding before failure. Higher loads could have been reached with better fitting of the grooves, relatively the same as other connections did.

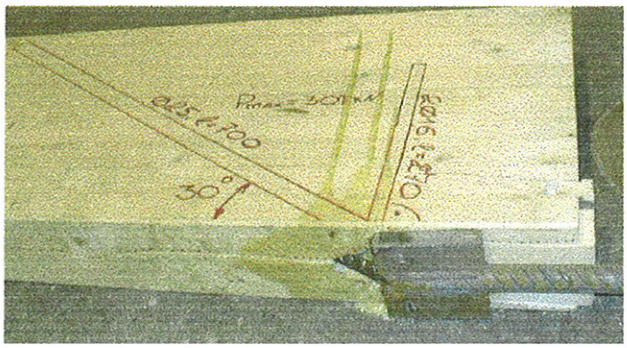

Figure 7. Test specimen 25+2D16 after failure at 302 kN

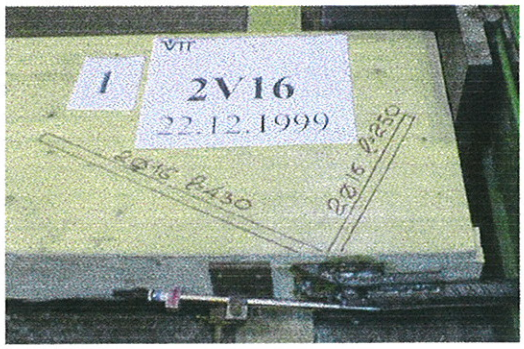

Figure 8. Test specimen 2V16 after failure at 315 kN

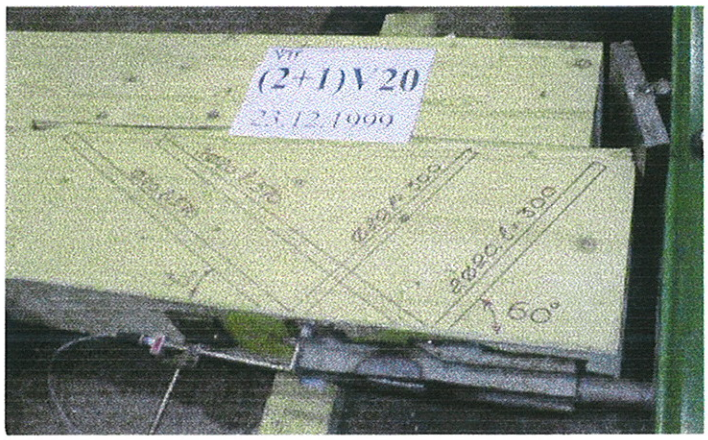

Figure 9. Shear failure at 712 kN following tensile failure perpendicular to grain.

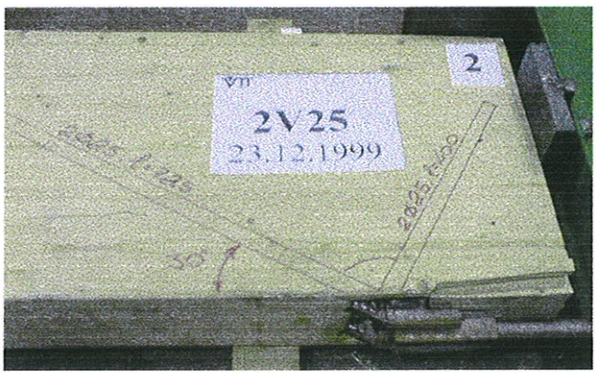

Figure 10. Test specimen 2V25 after failure at 734 kN and cut open.

Table 1. Test results of V-connections with prefabricated steel elements.

connection	b, mm	l_a, mm	a_2, d	a_4, d	f_y, N/mm^2	R_{est}, kN	R_{test},k N	R_{test}
2V12	115	300	4	2,8	549	171	207	1,21[1)]
3V12	160	300	4	2,9	549	256	319	1,24[2)]
2V16	115	400	3,1	2	517	285	315	1,10
2V16	115	400	3,1	2	517	285	294	1,03
2V20	160	530	4	2	519	445	475	1,07[3)]
2V20	160	530	4	2	519	445	478	1,08[3)]
(2+1)V20	160	530	4	2	519	668	712	1,07[4)]
V25	115	725		2,3	593	390	412	1,06
2V25	160	725	3,2	1,6	552	735	707	0,96[3)]
2V25	160	725	3,2	1,6	552	735	734	1,00[3)]
25+2D16	115	700		2,3	538	279	302	1,08

[1)] Tensile failure of the rod with calculated strength f_t = 665 N/mm^2.
[2)] Block of timber was torn off.
[3)] Bolt connecting tension and compression steel elements were cut.
[4)] The beam split due to the tensile force perpendicular to grain.

The gluing apparatus will warm the components of the adhesive to get good batching and mixing of them. The reaction is stronger in high temperature and the adhesive became harder (and more brittle). That is why the tensile failure of the rods did not occur, but the adhesive broke after the rods were yielding. More ductile connections could be reached (and higher capacities) with less brittle adhesive as with testing of V-joints in chapter 4.2 and with 2V12, see Figures 11 and 12. Ductility can also be achieved by yielding of the connecting steel bars outside the V-joints. Connection (25+2D16) with prolonged 25 mm thick tensile rod really yielded about 50 mm before anchorage failure.

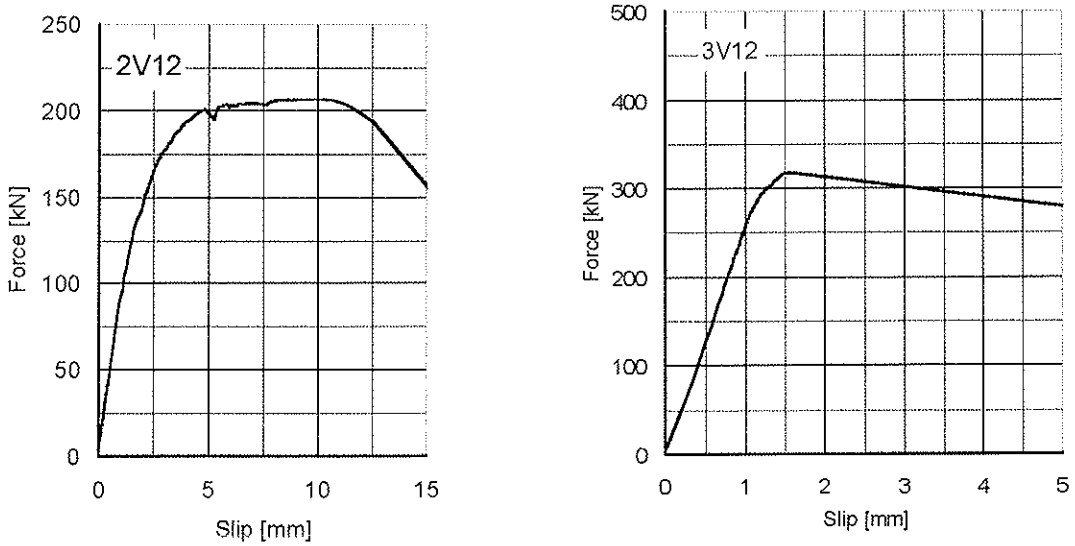

Figure 11. Measured load-slip curves of V-connections with thin rods.

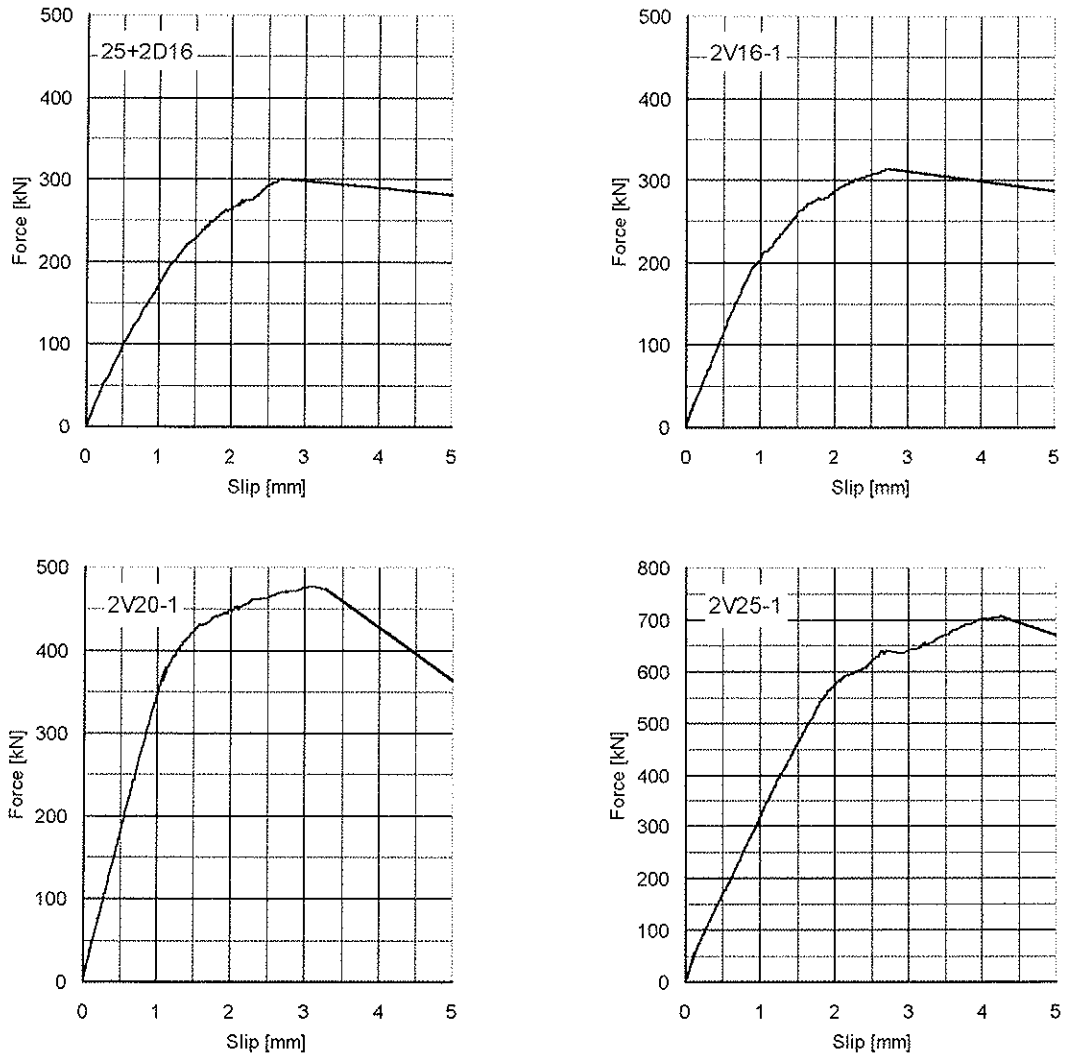

Figure 12. Measured load-slip curves of V-connections with thick rods.

5 Design of the V-connection

5.1 Behaviour of V-joint

Based on the test series described above the behaviour of V-joint has been modelled as follows. Relation of the load F and axial forces in rods S_1 and S_2 is illustrated in Figure 13.

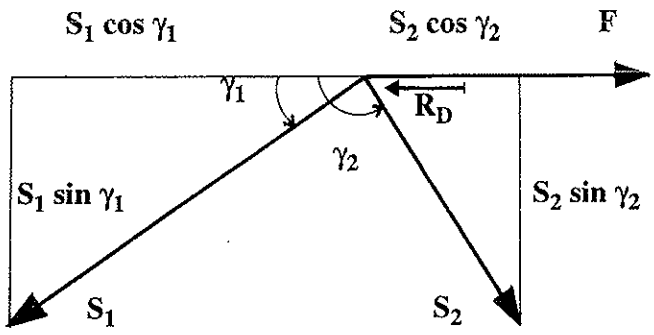

Figure. 13. Modelling of V- joint.

The design model is based on the capacity of the tensile rod. Based on equilibrium of forces the capacity of V-joint in general case is

$$F = S_1 \sin(\gamma_2 - \gamma_1)/\sin\gamma_2 \ (+R_D), \quad (1)$$

where R_D is the dowel effect. The capacities of V-anchors in different distances from the joint line can be summed on the condition that anchorage length allows yielding of the rods. V- shaped joint is quite rigid. Long rods have, however, like mechanical joints some deformation capacity due to yielding of the rod. This lowers possible stress concentrations.

5.1 Anchorage capacity

The rods are presupposed to be situated in several lamellae. Mean anchorage strength f_a is supposed to depend on the size of the rod. Its characteristic value both in compression and tension and in all direction angles $\alpha \geq 15°$ with the grain direction is proposed to be:

$$f_{a,k} = 6{,}5 \cdot (1 - l_a/100d) \cdot \rho_k/440 \ [\mathrm{N/mm^2}]. \quad (2)$$

The Working Draft for Eurocode 5/Revision Date 08/06/99 gives for the shear strength of the wood around the hole in all grain directions:

$$f_{a,k} = 1{,}2 \cdot 10^{-3} D^{-0,2} \rho_k^{1,5} \ [\mathrm{N/mm^2}]. \quad (3)$$

It can be simplified to the formula:

$$f_{a,k} = 11 \cdot D^{-0,2} \cdot \rho_k/440 \ [\mathrm{N/mm^2}]. \quad (4)$$

Anchorage capacity $R_{a,k}$ of the rod is calculated on the outer surface of glued joint, when the diameter of the drilled hole is $D \leq 1.25d$: ·

$$R_{a,k} = \pi D \cdot l_a \cdot f_{a,k}. \quad (5)$$

The tensile rod in V-joint is supposed to yield, when the dowel capacity is also included. Minimum anchorage length $l_{min,k}$ to achieve yielding can be solved by inserting the rod capacity $R_{t,k}$ to formula (5). Nearly equal values will be achieved by anchorage strength formula (2) and the formula (6). Formula (4) gives about 10% shorter anchoring lengths.

$$f_{a,k} = 10 \cdot D^{-0,2} \cdot \rho_k/440 \ [\mathrm{N/mm^2}]. \quad (6)$$

Minimum design anchorage length $l_{min,d}$ for the rod design capacity R_d can be calculated by

$$l_{min,d} = (1{,}3/1{,}1) \cdot l_{min,k}/k_{mod} \quad (7)$$

5.3 Dowel effect

Tensile rods in V-joint can be yielding, while the rods in compression with steep direction angle ($\alpha_2 \geq 50°$ or $\gamma_2 \leq 130°$) are not fully utilised. They will then work also as a dowel, when the load is in grain direction and that capacity can be added to the calculated capacity of V-joint. The capacity of the dowel can be calculated in accordance with Eurocode 5:

$$R_D = 1.5 \cdot (2 \cdot M_y \cdot f_h \cdot d)^{1/2}. \quad (8)$$

If the compression rod has a hinged connection to the main member, The dowel effect is smaller.

5.4 Timber capacity

Some moment connections failed so that a block of timber was torn off from the glulam beam to the depth of the rods. Effective cross section of that block is calculated by reducing the width b of the member by the drilled portion: $b_{ef} = b - n \cdot D$, where n is the number of drilled holes in the farthest cross section. The tensile capacity of the portion of the cross section, which is joined by rods, shall be calculated for the tensile force N in the connection, see Figure 14. The tensile force component perpendicular to the grain shall be designed with separate rods (Blass, H.J. and Steck, G.,1999).

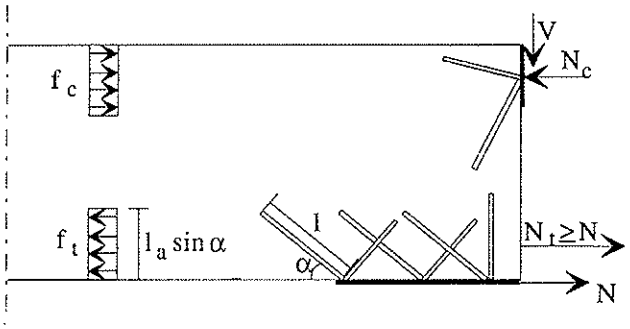

$$b_{ef}\, l \sin\alpha f_t \geq N$$

Figure 14. Diagram about the design of tensile capacity of timber in V-connection.

Bending capacity of the beam will be calculated in the farthest section of the joint. No reduction of effective cross section is needed when the angle between the rods in tension and grain direction is $\alpha \leq 40°$. Moment bearing connections of glulam can then be made without reducing its bending capacity.

5.5 Spacing and distances

The behaviour of V-connection is different from that of individual rods glued in grain direction, where splitting of timber is a common failure mode (Blass & al. 1999). Various spacing and distances have been used in the tested beams and in V-connections with prefabricated steel elements. The only failure mode caused by the arrangements of the rods was a block of timber tearing off the beam. That failure mode can be avoided by designing the tensile capacity of the effective area of timber in the connection, see section 5.4 above. Otherwise it is proposed the following minimum spacing and distances to be used in V-connections:

- spacing parallel to grain $a_1 = 10\ d$,
- spacing perpendicular to grain $a_2 = 3{,}0\ d$,
- end distance parallel to grain $a_3 = 10\ d$ (7d with $\alpha = 90°$),
- edge distance $a_4 = 1{,}5\ d$.

6 Fire resistance test

The aim of fire resistance tests was to determine the fire protection thickness of rock wool and wood needed for V-connections in various fire resistance classes. Three glued laminated timber beams with cross section of 450 x 160 mm^2 and a moment connection in the middle span were tested. Each test specimen had a V-connection in its tensile side and a hinged contact joint in its compression side. Three thicknesses of fire protection were used. The V-joints were glued with epoxy adhesive EA 20. The fire exposed steel parts of the joint

were protected with rock wool PV-PAL (density 140 kg/m^3) and covered with a thin steel sheet fixed by nails with long holes in it to allow the slip in the connection. Thickness of the rock wool at the bottom edge of the beam was varied as well as thickness of the timber boards, which were glued by RF30 on the beam faces.

The fire resistance tests were performed in the model furnace of the VTT Fire Technology Laboratory. The test specimens were simply supported with the concentrated load of 34,5 kN applied at the middle span of 2,4 m. The load corresponded to 40% of the design loading in normal temperature design. Anchorage capacity in glue line was the limiting factor. The beams were free to deflect. The load was kept constant during the test.

Furnace temperature, temperatures of the steel rods and temperatures in timber at various distances from the surface of beams were measured continuously. Furnace temperature was raised according to ISO 834. Measured temperature and deflections are presented in Figures 15 and 16. Deflection rate of beams 2 and 3 increased considerably before failure. The final reason for the failure was the exceeding of the dowel capacity (half of the design load in fire) after the total loss of the anchorage capacity due to softening of the adhesive. Beam 1 failed outside fire protected area. Main results are presented in Table 2.

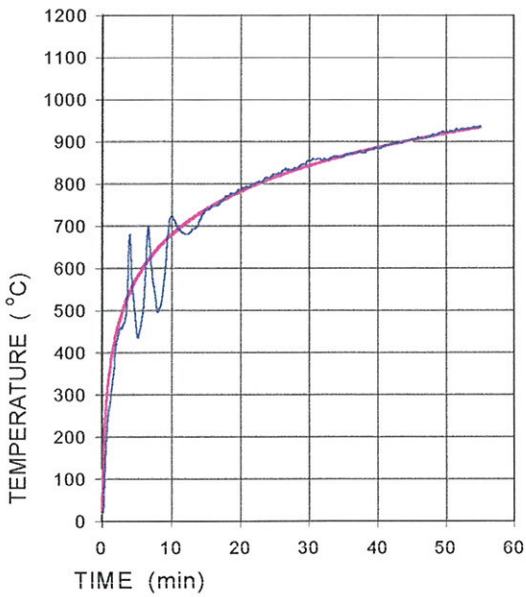

Figure 15. Measured and guiding (ISO 834) temperature of the furnace.

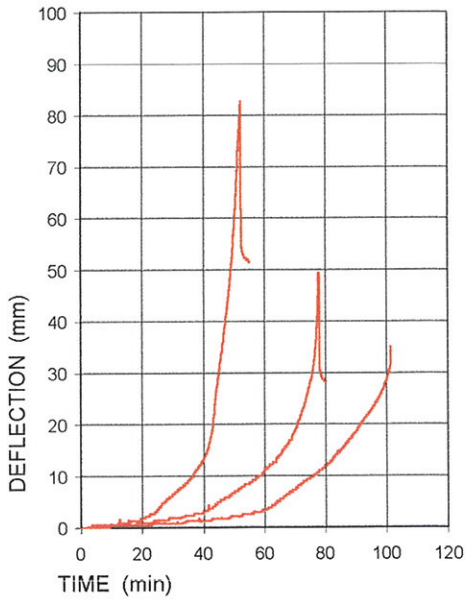

Figure 16. Measured deflections of beams no. 2, 3 and 1 (from left).

The deflection of the beam can be considered to be caused by the slip in the joints and the thermal elongation of the steel parts on the lower edge. That "slip" in the chosen fire class is calculated as an upper limit and given in Table 2. V-joint connections can easily achieve fire resistance classes of R30, R60 and R90, if the thickness of fire protection rock wool (140 kg/m^3) on fire exposed V-joints as well as the edge distances of the rods are 20 mm, 40 mm and 60 mm respectively. In fact 15 minutes higher fire resistance times could be achieved with the proposed fire protection thickness (corresponding "slip" in brackets).

Table 2. Results of fire resistance tests.

	Beam 1	Beam 2	Beam 3
Fire protection (mm)	60	20	40
Loading time (min)	103	52	78
Fire class (min)	90 (105)	30 (45)	60 (75)
"Slip" in the joint (mm)	< 7 (14)	< 2,5 (11)	< 4 (10)
Type of failure	Beam failure	Joint failure	Joint failure

The fire resistance time of V-connections can be given in the formula:

$R_t = 15 \text{ min} + t \cdot 30/20 \text{ min/mm}.$ (8)

The thickness of the fire protection layer, which is needed for the fire resistance time R_t, is:

$t = 2/3 \cdot R_t - 10 \text{ mm},$ (9)

where

R_t is the fire resistance time in minutes

t is the thickness of fire protection layer in mm.

7 Design Proposal

The behaviour of V-joints is illustrated in Figure 13. The capacity of a V-joint is

$F = S_1 \sin(\gamma_2 - \gamma_1)/\sin\gamma_2 (+R_D),$ (1)

where R_D is the dowel effect, which can be summed on the condition that anchorage length allows yielding of the longer rod. Its capacity can be calculated with the formula

$R_D = 1.5 \cdot (2 \cdot M_y \cdot f_h \cdot d)^{1/2}.$ (8)

The anchorage strength f_a in all direction angles $\alpha \geq 15°$ with the grain direction is

$f_{a,k} = 10 \cdot D^{-0,2} \cdot \rho_k/440 \text{ [N/mm}^2\text{]}.$ (6)

Anchorage capacity $R_{a,k}$ of the rod is calculated on the outer surface of glued joint, when the diameter of the drilled hole is $D \leq 1.25d$: ·

$R_{a,k} = \pi \cdot D \cdot l_a \cdot f_{a,k}.$ (5)

Minimum spacing and distances to be used in V-connections are

- spacing parallel to grain $a_1 = 10\ d$,
- spacing perpendicular to grain $a_2 = 3{,}0\ d$,
- end distance on the surface parallel to grain $a_3 = 10\ d$ (7d with $\gamma_2 = 90°$),
- edge distance $a_4 = 1{,}5\ d$.

The tensile capacity of timber in the effective cross section of the connection shall be checked for the tensile force in the connection.

The tensile force component perpendicular to the grain shall be designed with separate rods.

The thickness of the fire protection layer for the fire resistance time R_t, is

$$t = 2/3 \cdot R_t - 10 \text{ mm.} \quad (9)$$

Formula (9) is valid, when the design effect of action on the joint in the fire situation is 40% at the most from the design load carrying capacity for joint at normal temperature:

$$E_{fi,d} \leq 0{,}4 \cdot R_{d,n} \quad (10)$$

8 Concluding Remarks

Design method is proposed for the V-connections, in which the steel rods are glued at skew angles into the glulam. It is based on large test series. The V-connection is not vulnerable to splitting of wood in the anchorage area. Due to limited variation the anchorage strength of the rods can have a high design value in all grain directions bigger than 15°. The calculated dowel capacity of the rods with a steep direction angle also can be added to the vector sum of the capacities of the rods forming V-shape.

V-joint is quite rigid. However, like mechanical joints it has ductile properties due to yielding of the longer rod. The capacities of V-joints can be summed without reduction on the condition that the anchorage length allows yielding of the rods. The connection can carry bending moments up to the capacity of the glulam and is not vulnerable to splitting of wood in the joint area. The tensile capacity of timber shall be checked for the tensile force in the connection. The tensile force perpendicular to grain shall be designed separately. For fire protection a 20 mm layer of timber or rock wool is needed to cover the steel rods for each 30 min of fire resistance.

9 References

Turkovsky, S. B. 1989. Designing of glued wood structures joints on glued-in bars. Proceedings of meeting of international council for building research, studies and documentation. Working commission W18A on timber structures in Berlin DDR, paper 22-7-13. 13p.

Turkowsky, S., Lukyanov, E and Pogoreltsev, A. 1991. Prefabricated joints of timber structures on inclined glued-in bars. Proceedings of the International Timber Engineering Conference, 2-5 September 1991, London, United Kingdom. Pp. 3.212—3.217.

Kangas, J. 1993, Design of joints based on in V-shape glued-in rods. Proceedings of meeting of international council for building research, studies and documentation. Working commission W18A on timber structures in Athens, Georgia, USA, paper 26-7-4. 11p.

Kangas, J. 1994. Joints of glulam structures based on glued-in ribbed steel rods. VTT Publication 196. Espoo, Finland. 61p. + App. 20 p.

Oksanen, T. and Kangas, J. 2000. Strength and fire resistance of connections based on glued-in rods. VTT Research Notes 1970. Espoo, Finland

Eurocode 5. 1999,"Design of timber structures - Part 1-1: General rules, General rules for buildings". First draft EN 1995-1-1. Document CEN/TC250/SC 5: 124. 125 p.

Blass, H.J. and Steck, G., 1999, Perpendicular to the grain tensile reinforcement of timber. Proceedings of Pacific timber engineering conference in Rotorua, New Zealand, 7p.

Blass, H.J. and Laskewitz, B., 1999, Effect of spacing and edge distance on the axial strength of glued-in rods. Proceedings of meeting of international council for building research, studies and documentation. Working commission W18A on timber structures in Graz, Austria, paper 32-7-12. 11p.

INTERNATIONAL COUNCIL FOR RESEARCH AND INNOVATION IN BUILDING AND CONSTRUCTION

WORKING COMMISSION W18 - TIMBER STRUCTURES

BONDED-IN PULTRUSIONS FOR MOMENT-RESISTING TIMBER CONNECTIONS

by

K Harvey
M P Ansell
N Alexandre
University of Bath

C J Mettem
R J Bainbridge
TRADA Technology

UNITED KINGDOM

MEETING THIRTY-THREE
DELFT
THE NETHERLANDS
AUGUST 2000

Presented by: M.P. Ansell

· J. Ehlbeck asked how to provide input to national or international design code.
· M. Ansell stated that the coauthors are experienced in transferring scientific results and engineering data to code format. It will however be a slow process.
· S. Svensson stated that saturated timber would have reduced strength and asked whether strains were measured.
· M. Ansell responded that the connections were not instrumented for strains.
· S. Svensson further questioned the compression stress transfer of the member in Fig 15.
· M. Ansell responded that rod would take most of the load although the wood members did have contact.
· A. Ceccotti clarified that the load displacement curves were not ductile.
· M. Ansell commented that Acoustic Emission tests indicated that there was substantial micro-damage during loading which would dissipate energy.
· J. Kuipers asked about the long-term behaviour of the joints.
· M. Ansell responded that DOL tests were underway and there were no early failures.
· S. Thelandersson asked for clarification of the claim of excellent fire resistance.
· M. Ansell responded that the timber would protect the bonded in connector.

Bonded-In Pultrusions for Moment-Resisting Timber Connections

K Harvey*, M P Ansell*, C J Mettem**, R J Bainbridge** and N Alexandre*

* University of Bath, UK

**TRADA Technology, UK

Abstract

Moment-resisting timber connections were made between laminated veneer lumber (LVL) members using reinforced plastic pultruded rods bonded directly into the LVL. The mechanical performance of the pultruded rods, the rod to LVL interface and the complete jointed structures were evaluated.

The bending and shear performance of pultruded rods was established in three-point bending. The bonded-in strength and shear resistance of connections were evaluated in simple pull-out tests as a function of glue-line thickness, embedment depth, rod diameter, adhesive type and moisture content using LVL as a substrate. Particle-filled epoxy resins and unfilled thixotropic epoxy resins were selected as adhesive systems and surface preparation was optimized by sanding and solvent cleaning. Thick glue lines were found to dissipate localized stresses at the surface of the bonded-in connection and deeper embedment improved joint integrity.

Joints were manufactured and tested in three configurations with and without local reinforcement. The configurations were (a) in-line, moment-resisting, (b) T-piece, moment-resisting and (c) T-piece, shear. In order to prevent splitting of the LVL local reinforcements in the form of small diameter bonded-in rods or wetted-out fabric were included to increase moment resistance. The joints demonstrated a high level of strength and ductility and the local reinforcement improved moment- and shear-resistance. Joint configurations were modelled using FE methods and the advantages of thick glue-lines and local reinforcement were confirmed.

---

1. Introduction

Bonded-in rod connections offer an attractive solution for assembling timber structures, in terms of efficient load transfer, simplicity of design and aesthetic appeal. This paper is concerned with the performance of bonded-in, reinforced plastic, pultruded rods. Most of the relevant literature concerns the performance of steel rods which is reviewed below.

1.1. Bonded-in steel rods

Steel rod is an obvious candidate for bonded-in joints but it requires careful surface preparation before bonding, it is prone to corrosion and its elastic modulus is considerably greater than that of timber, presenting problems of incompatibility. Riberholt and Spoer (1983) investigated solid, conic, grooved and hollow glued-in rods for the root sections of wind turbine blades and found that hollow cylindrical rod gave the best fatigue performance. In the absence of adhesive Eckleman and Cassens (1985) found that plain and spiral groove

dowels gave better face holding strength than multi-grooved dowels. Adhesion difficulties can be overcome by using ribbed steel rods (Ranta-Maunus and Kangas, 1994) or threaded bolts to promote a mechanical bond between the steel and resin adhesive (Johansson, 1995). Uhre Pedersen *et al* (1996) analysed shot blasted hollow tapered rods where the taper caused stress peak levelling to occur. Batchelar and McIntosh (1998) also recommended tapering of the ends of rods to reduce stress concentrations. Using finite element analysis Deng *et al* (1998) found that a hole drilled in the end of the steel rod reduced the stress concentrations there.

1.2. Adhesives and their application

Phenol-resorcinol adhesives have a long history of use in structural applications. However, for bonded-in rods, Riberholt (1988) suggested that phenol-resorcinol should not be used in conjunction with an injection method and for oversized holes, due to the strength reducing effect of the initial hardening shrinkage of the glue. Aicher (1992) found that two component adhesives are sensitive to increases in temperature and should therefore be used with caution, especially when bolts are under high permanent loads and if an injection method is used.

Traditional phenolic adhesives have limited gap-filling qualities and often require the application of pressure to achieve the required strength in the joint. Epoxy resins and polyurethanes have been used as alternatives in certain fields of timber engineering, (Davis, 1997). One example is in the repair of timber structures where better gap-filling qualities are required and the application of pressure is not practicable. Johansson (1995) describes how bolts are bonded-in either by injection of the resin or by screwing the bolt into a hole pre-filled with resin. In the first case the holes are normally 1mm larger than the diameter of the threaded part of the bolt to give sufficient clearance for the injection of resin. In the other case the hole is smaller than the bolt diameter, normally by an amount equal to the depth of the thread. To allow for distribution of the resin, the bolt has a channel cut along its length. Matsui and Nishitani (1987) also used a hole with a diameter 1mm larger than the bolt diameter, and epoxy was poured into the bolt joint. Uhre Pederson *et al* (1996) selected a 2mm diameter oversized hole. In structural repairs (Mettem and Davies, 1996 and Zaboklicki and Gebski, 1997) the pre-drilled holes are typically 4mm in diameter wider than the dowels, and 5mm longer to ensure adequate cover by the epoxy resin adhesive.

1.3. Moisture content and temperature

Gerold (1992), Davis (1997) and Ranta-Maunus and Kangas (1994) indicated that shrinkage and swelling due to changing moisture content may cause considerable shear stresses in the glueline. If the moisture content of timber during bonding is much higher than in service, cracks occur at the ends of the rods. It is best to use timber with moisture content near the equilibrium value for the dry service climate.

Creep and strength properties of adhesives vary depending on temperature and small changes in compound composition, (Ranta-Maunus and Kangas 1994). It is important to be very careful when choosing adhesives especially for structural joints with thick gluelines. Screwed and bonded joints, which at room temperature are considered permanent joints, are readily loosened when heated to temperatures higher than 70°C. Screws, including long screws glued in by using epoxy resin-based and cyanoacrylic adhesives, can be unscrewed without difficulty at 130°C (Kreuger, 1986). Gaunt (1998) discovered that epoxied connections perform best when kept below 50°C.

1.4. Spacing rules

In Eurocode 5 there is an informative annex entitled "Design of timber structures- Part 2: Bridges". The recommendations made in this annex are based on steel rods and do not take in account the thickness of the glueline.

The minimum bonded length for rods, $L_{b,\min} = \max\begin{cases} 0.4d_r^{\,2} \\ 8d_r \end{cases}$,

is the maximum of the two values obtained by the above formula where d_r is the diameter of the rod. Minimum spacings for rods loaded perpendicular and parallel to the grain are represented in Figure 1.

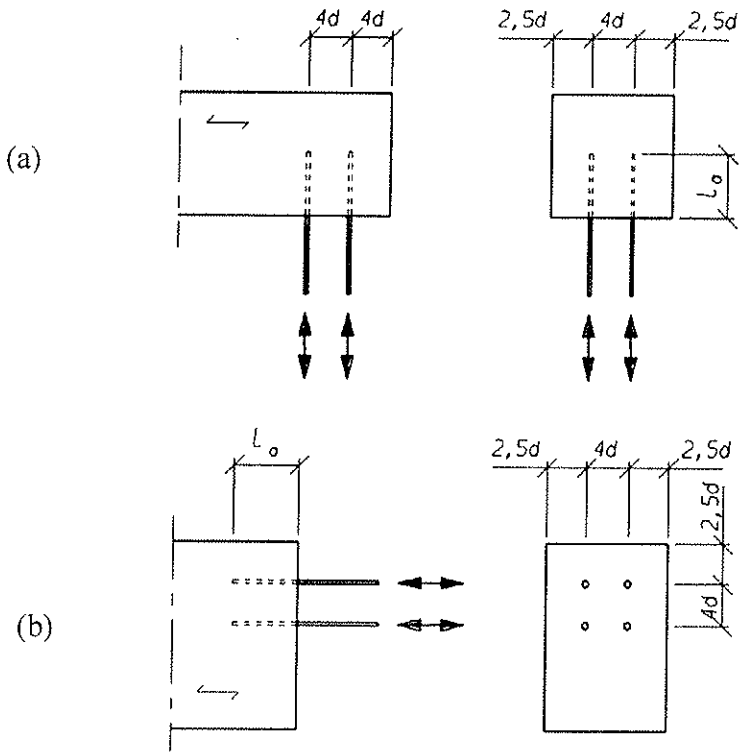

Figure 1. Minimum spacings and distances for axially loaded rods loaded (a) perpendicular to the grain and (b) parallel to the grain, where d is the diameter of the rods (Eurocode 5).

These spacings are specified to reduce splitting of the timber and to maximise the load transfer efficiency of each rod. These spacings may in practice be reduced by the introduction of local reinforcement.

1.5. Reinforced plastic rods

Fibre reinforced plastics (FRP) offer a lightweight, corrosion-resistant, elastically compatible alternative to steel at low cost, with strength greater than that of mild steel. FRP rods consist of unidirectional fibres that are pulled through a resin bath and then through a die to form the shape of the rod in a process called pultrusion (Drake *et al*, 1999). FRPs are more compatible with resin and timber because they are non-metallic. The Young's modulus of glass fibre reinforced plastics (GFRP) is of the order of 45 GPa compared with 210 GPa for

mild steel but the strength of the GFRP is higher. FRPs also offer a high resistance to corrosion, which is useful in a humid or acid environment. The performance of bonded-in FRP rods may be superior due to better resin bonding and connections are lightweight and easy to handle. Drake and Ansell (2000) examined the performance of GFRP dowels for friction-fitted timber joints and Mettem *et al* (1999) evaluated steel and GFRP rods for bonded-in timber connections

1.6. Aims

This paper aims to characterise the performance of bonded-in, pultruded, FRP rods for timber (LVL) connections. The mechanical properties of pultruded GFRP and carbon fibre reinforced plastic (CFRP) rods are compared in three-point bending and the bending strength, modulus and shear strength are assessed as a function of the length to diameter ratio of the rods. The integrity of the rod to LVL interface is established by performing simple tensile pull-out tests. Experimental variables include adhesive type, bondline thickness, embedment length, joint end profiling, moisture content of the timber and properties parallel and perpendicular to the grain. Full scale laboratory tests are performed on three types of moment-resisting joints, including in-line joints, L-shaped joints subjected to a bending moment and L-shaped joints subjected to transverse shear. Local reinforcement in the form of slender bonded-in rods and external fabric reinforcement is added in order to improve the performance of moment-resisting joints by reducing local stress concentrations at the joint interfaces.

2. Selection of materials

2.1. Timber

Kerto S Laminated Veneer Lumber (LVL) was selected, manufactured by Finnforest Oy (Finland). Kerto S is laminated from 3mm thick, rotary cut, scarf jointed, softwood veneers with the grain oriented along the major panel axis. LVL has consistent mechanical properties, essential for this research where the assessment of the performance of the bonded-in connections is the key objective. LVL is rapidly gaining popularity as a materials of construction. Coed Cymru, of Newtown, Wales, supplied green Welsh oak and dried ash.

2.2. Pultrusions

Pultruded GRP rod was manufactured by Tufnol Ltd and by Fibreforce (UK). The volume fraction of unidirectional fibres was of the order of 62%, confirmed by image analysis. Pultrusions can be easily sawn to length using conventional tools. Carbon fibre-reinforced plastic (CFRP) pultrusions were provided by GDP of France. The surfaces of rods were prepared by abrading with sandpaper followed by solvent wiping.

2.3. Adhesives

Ten commercial epoxy and acrylic resins were evaluated to bond in rods. Good results were achieved with Sikadur 31 and Rotafix Timberset epoxy resins, already used in the repair and upgrade of timber structures. All moment-resisting test samples were bonded with Rotafix CB10TSS (Slow Set) adhesive, which is an unfilled, thixotropic, epoxy resin. It has a lubrication capability and surface tension characteristics that enables it to wet the LVL and rods and makes it easier to back fill into drilled holes.

3. Experimental work

3.1. Characterisation of pultrusions

For design and specification purposes, it was necessary to characterise the mechanical properties of GFRP and CFRP rods. Properties were measured in three-point bending for three diameters and span to diameter ratios ranging from 5 to 20. The peak flexural stress

and peak transverse shear stress developed in bending is a function of the ratio between the distance between the outer rollers (L) and the rod diameter (d), where,

Peak flexural stress, $\sigma_{max} = 8FL/\pi d^3$ Peak shear stress, $\tau_{max} = 8F/3\pi d^2$
Ratio, $\sigma_{max} / \tau_{max} = 3L/d$ Flexural modulus, $E = 4FL^3/3\pi d^4\delta$,
where F is the applied force, δ is the centre point deflection.

For GFRP, the peak flexural stress (at failure), Figure 2, is of the order of 0.3 to 0.4 GPa at an L/d ratio equal to 5 and the flexural modulus is ~16 GPa, Figure 3. The peak shear stress (inter-laminar shear strength, ILSS, at L/d = 5) is of the order 25 to 35 MPa, Figure 4. As L/d increases the peak flexural strength increases to a maximum of between 0.79 and 0.92 GPa at L/d = 20, and τ_{max} values fall to between 13 and 16 MPa. This behaviour is expected as the ratio of flexural stress to shear stress increases by a factor of 3 times the L/d ratio. It can be concluded that the flexural strength of pultruded rods is of the order of 0.8 GPa and that the ILSS lies between 25 and 35 MPa.

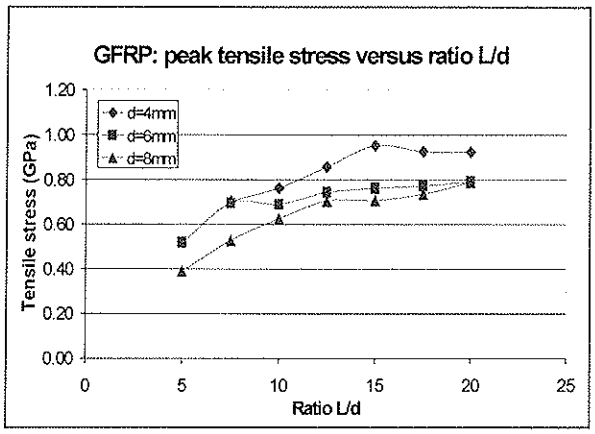

Figure 2. Flexural strength of pultruded GFRP rod versus L/d ratio for d = 4, 6 and 8mm.

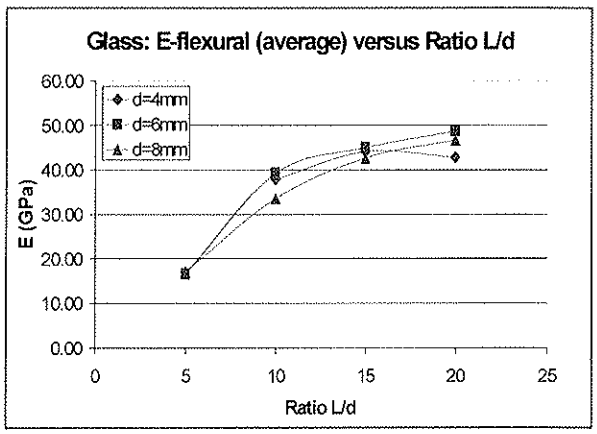

Figure 3. Flexural modulus of pultruded GFRP rod versus L/d ratio for d = 4, 6 and 8mm.

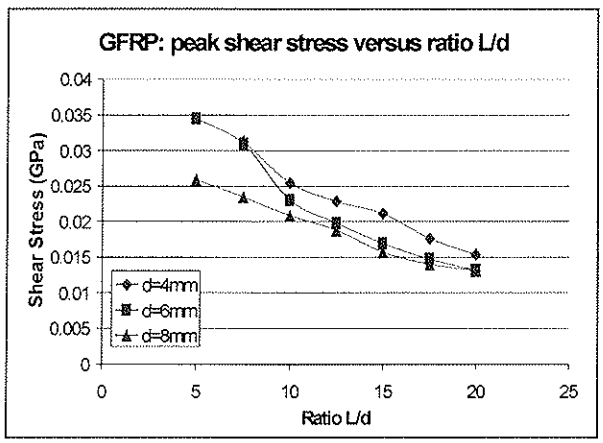

Figure 4. Peak shear stress of pultruded GFRP rod versus L/d ratio for d = 4, 6 and 8mm.

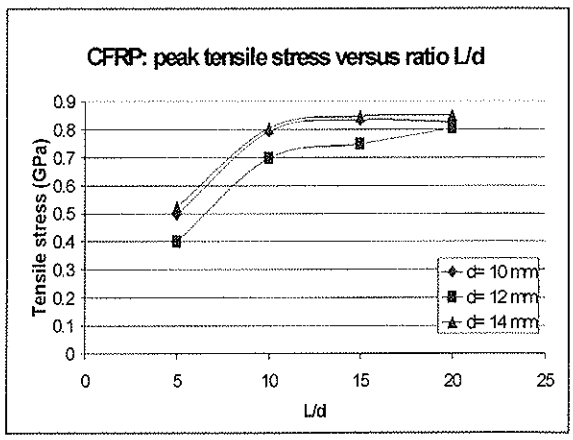

Figure 5. Flexural strength of pultruded CFRP rod versus L/d ratio for d = 10, 12 and 14 mm.

The results for the flexural and shear strengths of CFRP rods are closely similar to those for the GRP rods, although the flexural modulus of CFRP is considerably greater (~110 GPa at L/d = 20) than for GRP rods (~45 GPa at L/d = 20), Figures 5, 6 and 7. In tension the Rule of Mixtures predicts a modulus value of about 115 GPa for CFRP. Overall, GRP is preferred to the much more expensive CFRP because stress transfer, rather than stiffness, is critical.

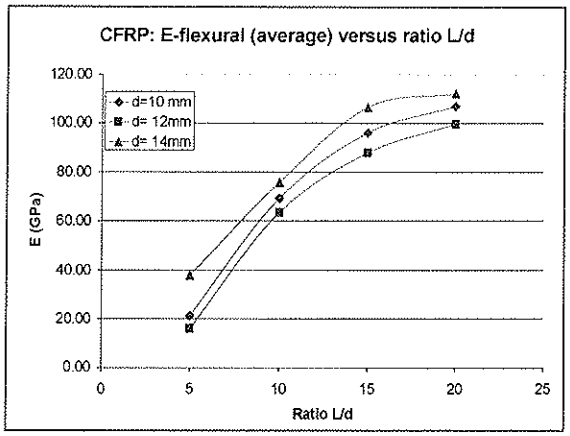

Figure 6. Flexural modulus of pultruded CFRP versus L/d ratio for d = 10, 12 and 14 mm.

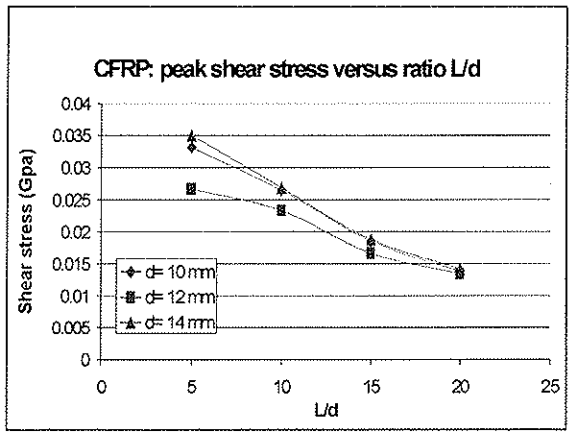

Figure 7. Peak shear stress of pultruded CFRP versus L/d ratio for d = 10, 12 and 14 mm.

3.2. Mechanical performance of pultruded rod bonded into LVL

Several test configurations were investigated, both analytically and experimentally, to assess the performance of bonded-in GRP rods acting in tension. A single-ended pull-through combination, Figure 8, proved to be the most useful in practical terms. Factors which influence pull-out strength include rod surface preparation, bonded-in length, glue-line thickness, adhesive type and joint-end profiling.

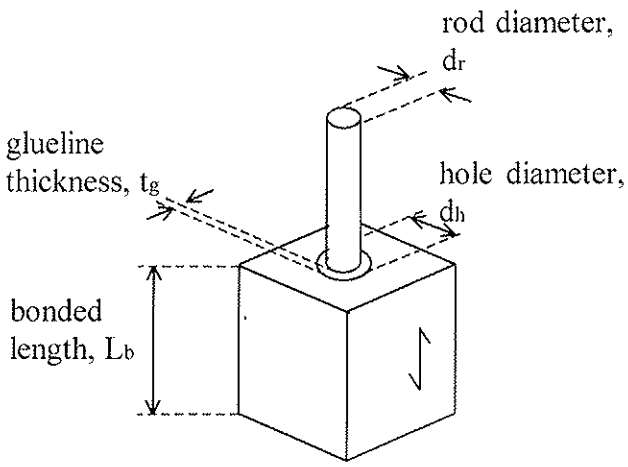

Standard single-ended sample:

bonded length, L_b	63mm
glueline thickness, tg	2mm
rod diameter, d_r	8mm
timber	63*63*63mm
Adhesive	Epoxy

Figure 8. Single-ended test sample.

3.2.1. Effect of adhesive type on pull-out force

All the epoxy adhesives provided good pull-out strengths, Figure 9, irrespective of their moduli, which varied between 0.5 GPa and 7 GPa. Failure of the specimens was invariably

located in the timber close to the adhesive/timber interface (Figure 10) and was due to the failure of the timber, in shear, parallel to the grain.
The average shear stress at failure for these specimens was very consistent, ranging between 4.97 MPa and 6.74 MPa. The shear strength of the LVL is the key material property limiting the pull-out behaviour for these specimens (manufacturer's value is ~5 MPa). Acrylic adhesives failed at half the load of the epoxy adhesives and failure occurred in the adhesive. Epoxy adhesives were selected on the basis of ease of application, gel time and compatibility with the surface of the LVL and the pultruded rods.

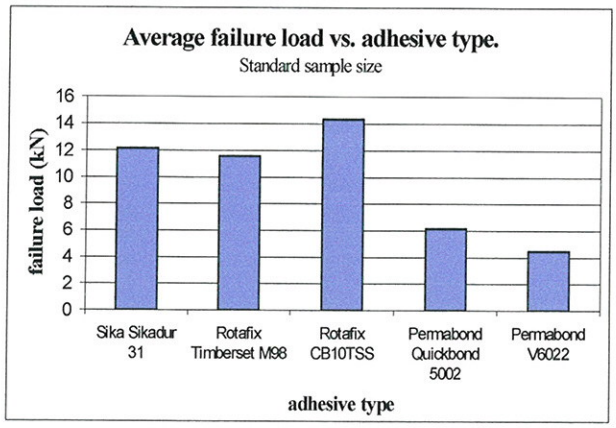

Figure 9. Effect of adhesive type on pull-out force (average of 8 tests for each).

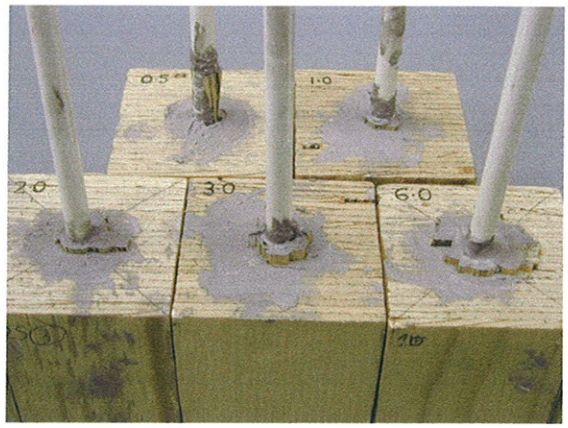

Figure 10. Failure macrograph of bonded-in rods in LVL with glue-line thicknesses of 0.5, 1.0, 2.0, 3.0 and 6.0 mm (Sikadur 31).

3.2.2. Effect of bonded-in length and surface preparation on failure force

Pultruded rods with diameter d_r = 6 mm were bonded into LVL using Sikadur 31 adhesive, with a glue-line thickness of 0.5 mm and with the rod axis parallel to the grain (8 samples). The rods were bonded to depths of between 12 and 60 mm and rod surfaces were either untreated or wiped with ethanol and sandpapered. The ethanol degreases and cleans the rod and the sanding of the rod removes the resin rich surface so the adhesive can bond directly with the uncontaminated resin matrix and fibres. Sandpapering increases the failure load of the joint, Figure 11.

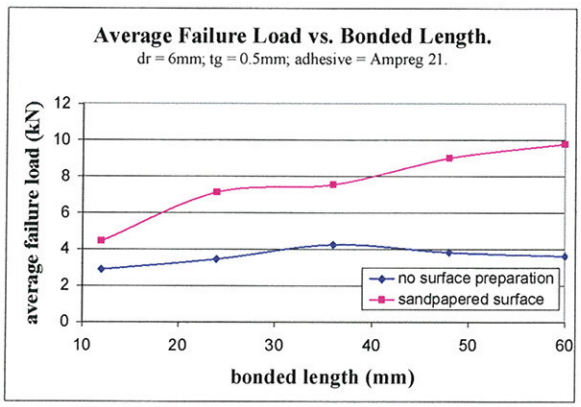

Figure 11. Effect of surface preparation and bonded-in length on push-in force.

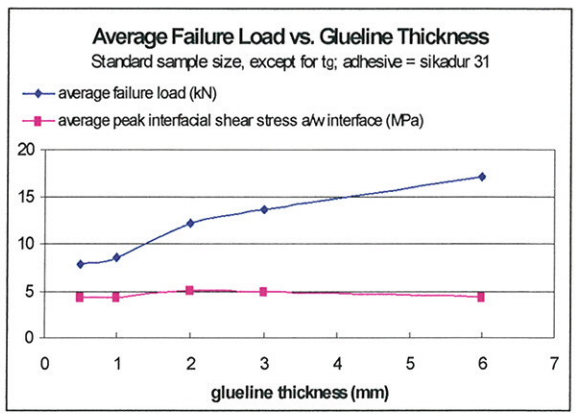

Figure 12. Effect of glue-line thickness on pull-out force and interfacial shear strength.

The load at failure steadily increases as the bonded-in length increases to a maximum failure load of almost 10 kN which equates to a stress of 88 MPa in the rod. The influence of glue-

line thickness on pull-out force and interfacial shear strength is seen in Figure 12. As the glue-line thickness increases the surface area of the cylinder of adhesive increases and the shear strength of this interface remains constant at ~5 MPa. Thick glue lines clearly have a positive effect on increasing the surface area of the LVL failed in shear. European guidance suggests designs based upon 'thin' annular bond lines whereby rods are a close fit in a hole and design guidance for spacing rules is given as a function of rod diameter. Research has shown the clear benefits of 'thick' annular bond lines and the corresponding need to specify designs based in terms of bond diameters. FE analysis confirmed the reduction in bond line stress concentrations.

3.2.3. Pull-out force parallel and perpendicular to the grain.

For an 8mm diameter rod with 2mm thick glue lines the average pull-out force perpendicular to the grain (9.45kN) is almost identical to the pull-out force along the grain (9.66kN) although in the former case the failure topography is confined to the cylindrical zone around the adhesive to LVL interface.

3.2.4. Joint end profile

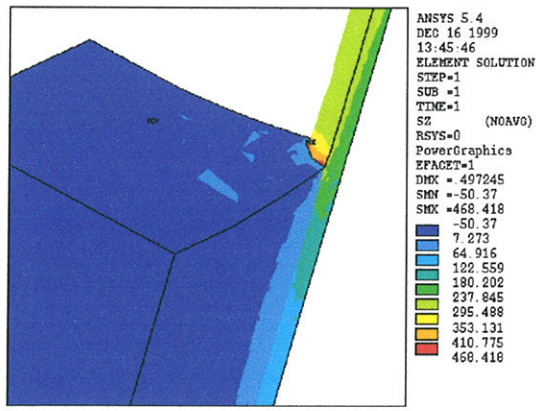

Figure 13. Finite element image of a one quarter element of a pull-out test in tension showing concentrated stress close to the surface.

For pull-out tests, FE analysis (Figure 13) predicts stress concentrations where the rod emerges at the surface. Profiling the end of the joint, where the rod enters the timber, by stepping or conical counter-boring improves the pull-out load. FE analyses clearly predict a reduction in the peak shear stresses up to a depth of 30mm. Beyond this depth the peak shear stress remains unchanged and this trend was verified experimentally. These results confirm the assumption that a non-uniform stress distribution exists along the length of the embedment in which the peak stresses are to be found at the end of the joint at the embedment face.

3.2.5. Timber moisture content.

A number of pull-out specimens using solid ash and oak timber were made using two epoxy adhesives at moisture contents (MCs) ranging between 9% and 38% covering all the various service class conditions. The majority of specimens with MCs in excess of 22% exhibited reduced pull-out strengths irrespective of the epoxy or rod type used. Significant reductions in pull-out strength, of the order of 60-65%, were observed in specimens exhibiting a MC in excess of 25% at the time of bonding. The locus and mode of failure changed as the moisture content of the timber decreased, relocating from within a thin layer of the adhesive close to the rod/adhesive interface, to that of a mixed timber/adhesion failure or an apparent adhesion failure at the adhesive/timber interface. Designing with connections bonded in to green timber is plausible as long as the correct allowances for the reduced strength is included in the design.

3.3. Full-scale laboratory testing of bonded-in joints, pultruded rods

Three types of moment resisting joints, A, B and C, were fabricated with 16mm diameter pultruded GRP connectors in 25mm diameter holes drilled with auger bits, Table 1.

Moment-resisting joint type	**Local reinforcement**	**σ_{max}, M_{max} or F_{max}**
A. In-line, two-component, two bonded-in 200mm long rods (see Figure 14). (subjected to 4-point bending). **A.** 250mm long rods.	(a) Unjointed	49.69 MPa σ_{max}
	(b) Jointed, no local reinforcement	31.75 MPa
	(c) Transverse bonded-in rod.	42.73 MPa
	(d) External fabric reinforcement	38.17 MPa
	(e) Jointed, no local reinforcement	48.37 MPa
B. L-shaped, two-component, bonded-in 170mm long rods (subjected to bending moment)	(a) Jointed, no local reinforcement	1.78 kNm M_{max}
	(b) Transverse bonded-in rod	1.26 kNm
	(c) External fabric reinforcement	1.30 kNm
C. L-shaped, two-component, bonded-in 170mm long rods (subjected to transverse shear)	(a) Jointed, no local reinforcement	20.8 kN F_{max}
	(b) Transverse bonded-in rod	21.79 kN
	(c) External fabric reinforcement	27.71 kN

Table 1. Mean ultimate bending strength (σ_{max}), bending moment (M_{max}) or shear force (F_{max}) values for moment-resisting configurations A, B or C respectively.

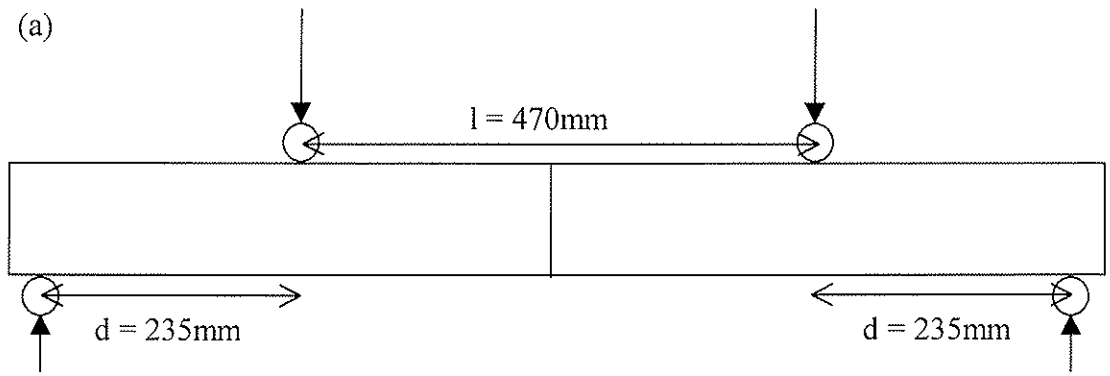

Figure 14. (a) Four-point bend test geometry A;
(b) Position of bonded-in rods.

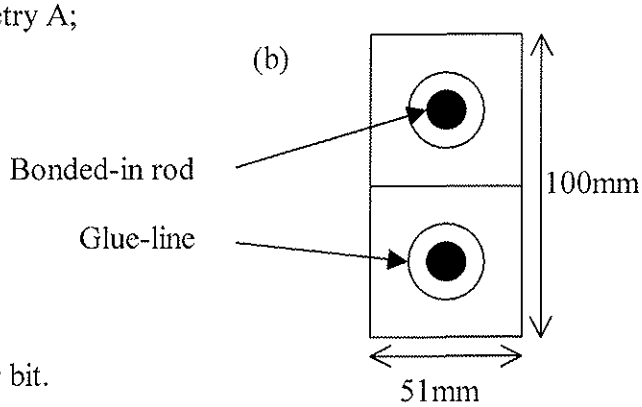

Rods are 16mm in diameter.

Holes are drilled with a 25mm diameter auger bit.

Joint type A (Figure 14) assesses the performance of LVL beams in four-point bending where a pure bending moment exists between the central rollers. Moment-resisting joints were fabricated from straight grained LVL with overall dimensions given in Figure 14. The length of the two rods was restricted to 200mm (100mm embedment) to demonstrate the advantages of local reinforcement to counteract longitudinal splitting of the LVL. Type A joints are designated un-jointed (A(a)), in-line jointed (A(b, e)), jointed with bonded-in transverse local reinforcing rods (A(c)) and external fabric local reinforcement (A(d)).

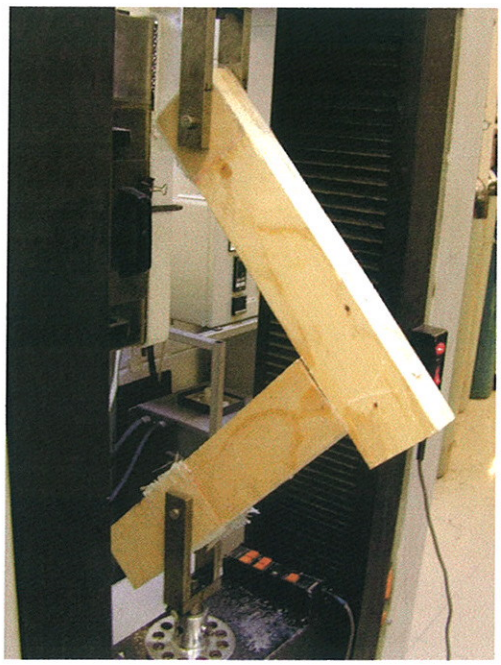

Figure 15. Moment-resisting L-shaped test type B(a) with two bonded-in rods.

The transverse bonded in rods for local reinforcement were GFRP pultrusions, with a diameter of 6 mm, bonded in as pairs across the ends of the members 25 mm from the joint end interface. The external fabric reinforcement was a plain weave glass fabric, weight 280gm^{-2}, bonded with CB10T Slow Set epoxy resin directly onto the faces of the beam at the joint end interface. Joint types B (Figure 15) and C (Figure 16) were L-shaped joints which were subjected to a bending moment (B) and transverse shear load (C) respectively in order to simulate joints found in timber roofs and in post and beam construction. The connecting bonded-in rods are arranged as in Figure 16 but the bonded depth is reduced to 85 mm because of limitations in the width of the LVL. Local reinforcement is again in the form of bonded-in rods and external fabric reinforcement.

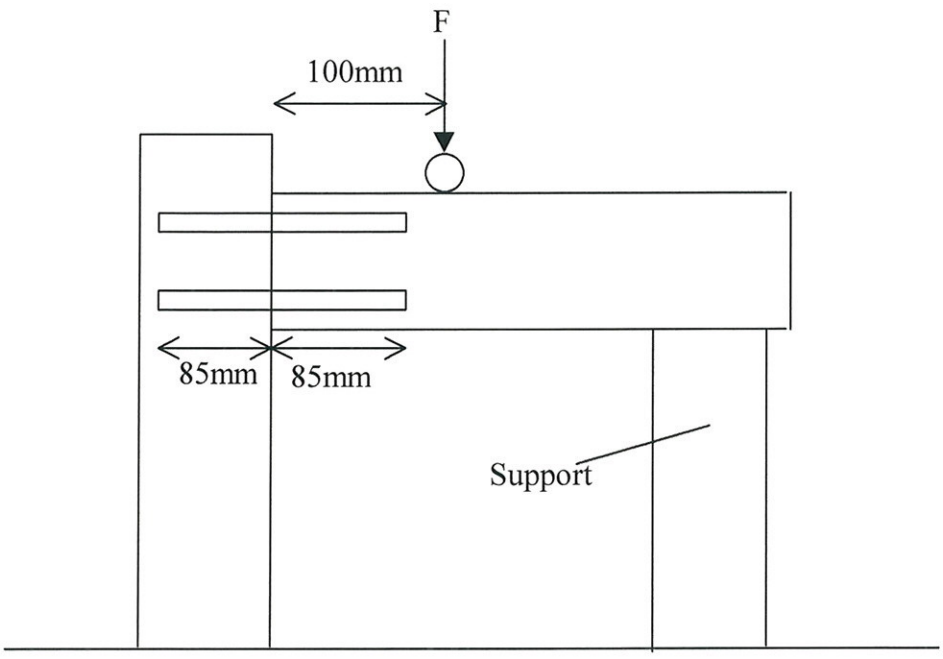

Figure 16. Shear test type C.

Type A tests were performed using a servo-hydraulic Denison-Mayes static/dynamic test machine with a peak load capacity of 200kN, Fig. 17. Load versus displacement was logged for each test to failure and the development of crack propagation was photographed, e.g. Fig. 18. Results for type A(a), un-jointed LVL are summarized in Table 1. The flexural strength averages 50 MPa and this is the control value against which the jointed beams can be compared. The excellent ductility of the joints is gauged from the area under the $\delta = f(F)$ curve, eg. Fig. 19 for test A(d).

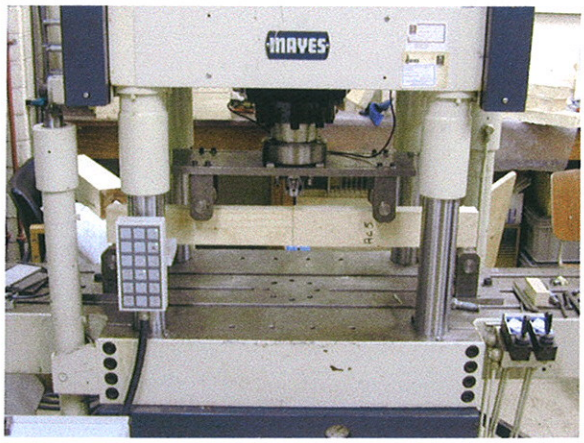

Figure. 17. Four-point bending configuration, in Denison-Mayes 200kN test machine.

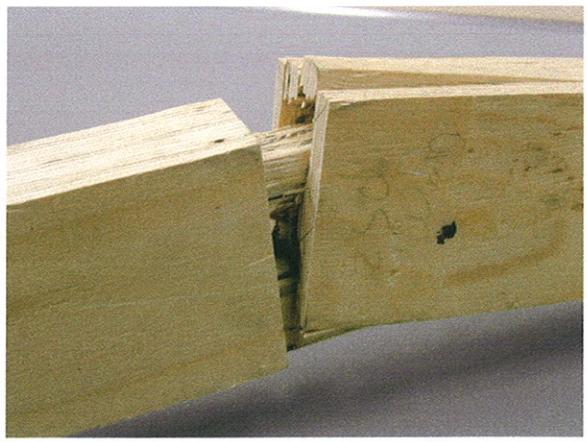

Figure. 18. Fracture of test type A(b) beam with good adhesion between rods and LVL.

The effect of bonded-in length of GRP rod on the flexural strength of type A beams is summarized in Figure 20. Results for bonded-in lengths of 150 mm, 200 mm and 250 mm are also included for tests type A(b), A(c) and A(d). It is clear that flexural strength improves as rod length increases and closely approaches the strength of the unjointed LVL. Local reinforcement has a positive effect on strength, especially for type A (c) joints. One result for bonded-in steel reinforcing bar (200 mm depth) is included for comparison.

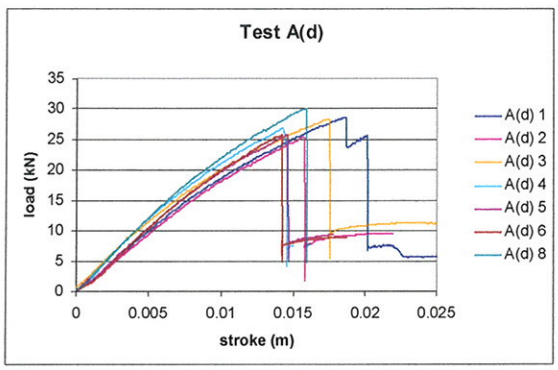

Figure 19. Force versus displacement curves for test type A (d), external fabric reinforcement.

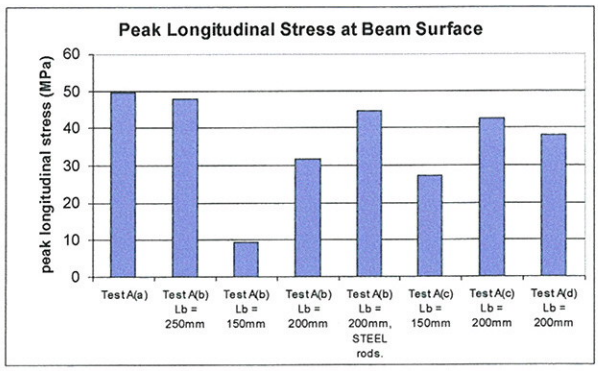

Figure 20. Peak longitudinal stress at beam surface as a function of test type.

In test B a tensile force was applied which acts via two steel pins which pass transversely through the LVL in zones where the surface is reinforced with wetted-out fabric to prevent splitting. The mean peak bending moment (M_{max}) for type B joints was not improved by

local reinforcement in contrast to type A and C tests (Table 1). This loading mode was severe and bonded-in rods were ultimately pulled out of the LVL as the joint rotated.

The mean peak shear force (F_{max}) values for type C tests (Table 1) demonstrate that composite local reinforcement has a beneficial effect on the shear strength of the bonded interface. In these tests heavy crushing of the LVL under the point load occurred with little damage or displacement of the two bonded-in rods.

3.4. FE modelling

Pull-out and moment-resisting tests were extensively FE modelled, for example Figure 13 for pull-out tests, Figure 21 for type A tests and Figure 22 for type B tests. Thermal imaging failed to detect hot spots close to bonded-in rods at the surface, confirmed by FE analysis.

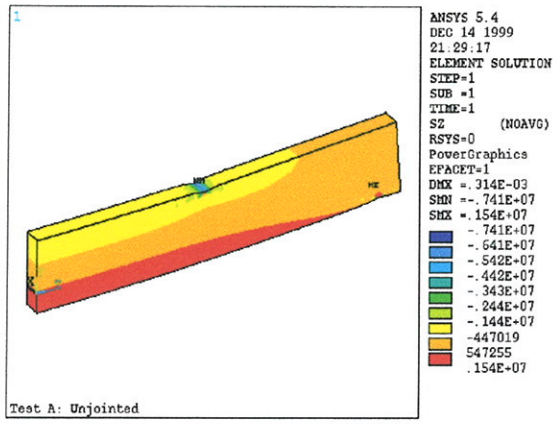

Figure 21. Type A four-point bend test, unjointed, stresses along the beam axis.

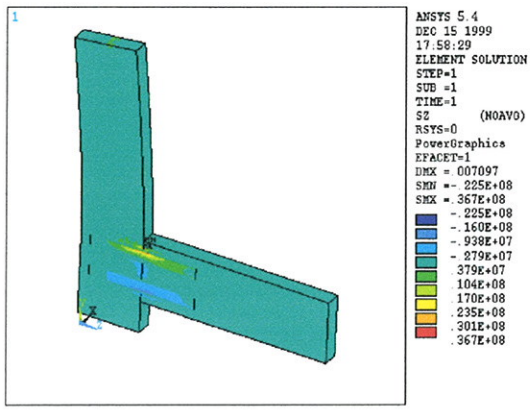

Figure 22. Type B moment-resisting test, stresses along the axis of the rods.

Local reinforcement was seen to reduce stress in the timber adjacent to the primary bonded-in rod connections. This observation will be the subject of a later paper.

3.5. Improvements in environmental impact from using bonded-in joints

The Eco Indicator 95 method indicates high negative environmental scores from the production of steel. The substitution of lighter steel rods or replacement of steel altogether with pultruded rods markedly reduces this negative impact. To a minor extent the use of adhesives for bonding in rods reduces this improvement in environmental rating but it should be noted that the epoxy adhesives used in this research did not contain any solvents or phenols. Life cycle advantages result from replacing heavy, traditional, bolted and plated steel joints with bonded-in steel or pultruded connections.

4. Discussion

The review of the literature examined the performance of bonded-in steel rods for timber connections. This paper has investigated the strength and stiffness of pultruded rods, the practical aspects of bonding smooth GFRP rods into LVL and three types of moment-resisting joints have been tested to destruction. Steps taken by workers such as Uhre Pedersen *et al* (1996) to shot blast steel rod to improve adhesion can be avoided when using FRP pultrusions by substituting abrasion and solvent wiping. The grooving, threading, ribbing or tapering of steel dowels can be avoided by ensuring that glue-line thicknesses are sufficiently high. *A minimum glue-line thickness of 2mm is recommended.* Friction fitting of glued dowels should certainly be avoided and epoxy adhesives appear to offer the best

interfacial strengths at the dowel to timber interface. Increased moisture content of the timber substrate certainly degrades the bonded-in strength.

Spacing rules for steel rods were described in Section 1.4. It is clear that moment-resisting joints, such as type A, break the spacing rules. For a 16mm rod, the rod to edge distance should be 2.5d which equals 40mm. In fact this distance is 25.5mm. The bonded-in depth should be at least 128mm whereas 100mm was selected to gauge the effect of local reinforcement on flexural strength. A major consideration is the strength of the full section of the timber versus the strength of the rods. Taking the tensile strength of a GFRP rod to be 800 MPa and the strength of the LVL to be of the order of 50 MPa it can be seen that the ratio of strengths is equal to 16. Two 16mm diameter rods in a 100mm by 51mm beam have an area ratio of 402mm^2 to 5100mm^2, which is a ratio of 1:13. Hence the rod should, in crude terms, be capable of transferring the applied load. However the spacing rules, developed for steel are transgressed and therefore splitting of the LVL is likely and is, indeed, observed. The likelihood of splitting at design stresses is very much offset by two factors. Firstly, *the bonded-in rods act to reinforce the timber* and secondly, the secondary local reinforcement can prevent splitting and reduce stress concentrations associated with the primary bonded-in rods.

5. Conclusions

Bonded GRP connections for timber buildings offer structural integrity, strong aesthetic appeal, ease of manufacture and low weight, together with excellent ductility, low cost and commercial acceptability. The research has placed these observations in the context of Eurocode 5.

6. Acknowledgements

The authors are pleased to acknowledge funding from the UK Engineering and Physical Sciences Research Council, EPSRC Grant Number GR/L66559, and the European Programme FAIR, Project Reference Number CT98-9548.
We also thank Rotafix Ltd, Cowley Structural Timberwork Ltd, Permabond, Buro Happold Ltd, Ove Arup and Partners, Coed Cymru, Epsilon Composite (France) and Brecon Beacons National Park for making important contributions to the research programmes.

References

Aicher, S., "Testing of adhesives for bonded wood-steel joints," In: Proc. of the IUFRO S 5.02 Meeting, Bordeaux, France, 1992.

Batchelar, M.L., McIntosh, K.A., "Structural joints in glulam," Proceedings of the 5th World Conference on Timber Engineering, Montreux, Switzerland, Vol. 1, pp 289-296, 1998.

Davis, G., " Performance of adhesive systems for structural timbers," Int. J. of Adhesion and Adhesives, Vol. 17, No. 3, pp 247-255, August 1997.

Deng, J.X., Moss, P.J. and Buchanan, A.H., "Glued bolts in glulam – an analysis of stress distribution," Proceedings of the 5th World Conference on Timber Engineering, Montreux, Switzerland, Vol. 2, pp 206-213, 1998.

Drake, R.D., Ansell, M.P., Mettem C.J. and Bainbridge, R., "Non-metallic, adhesiveless joints for timber structures", Proceedings of the 32nd Meeting of Working Commission W18, CIB-W18, Graz, Austria, Paper 32-7-11, August 1999, ISSN 0945-6996.

Drake, R.D., and Ansell, M.P, "Evaluation of joints in timber structures using pultruded GRP dowels and implications for Eurocode 5-based design", The Structural Engineer, June 2000.

Eckleman, C.A., Cassens, D.L., "Withdrawal strength of dowels from wood composites," Forest Products Journal, Vol. 35, No 5, pp 55-60, May 1985.

Gaunt, D.J.,. "Joints in glulam using groups of epoxy grouted steel bars plus an alternative to epoxy bonding," Proceedings of the 5th World Conference on Timber Engineering, Montreux, Switzerland, Vol. 1, pp 281-288, 1998.

Gerold, M., "Verbund von Holz und Gewindestangen aus Stahl", Bautechnik Vol. 69, No. 4, pp 167-178, 1992.

Johansson, C.J., "Glued-in bolts," Structural Timber Education Programme Lecture, Pub. Centrum Hout, C14, Part 1, 1995.

Kreuger, G., "Loosening of screw/bonded joints at higher temperature," Schweisstechnik (Berlin), Vol. 36, No. 8, pp 351-352, 1986.

Matsui, G., Nishitani, A. "Finite element analysis of stresses for orthotropic woods," Waseda Daigaku Rikogatu Kenkyusho Hokoku/Bulletin of Science and Engineering Research Laboratory, No 118, pp 32-39, 1987.

Mettem, C.J., Davies, G., "Resin bonded repair systems for structural timber," Construction Repair, March/April 1996.

Mettem, C.J. Bainbridge, R., Harvey, K., Ansell, M.P., Broughton, J.G. and Hutchinson, A.R., "Evaluation of material combinations for bonded in rods to achieve improved timber connections", Proceedings of the 32nd Meeting of Working Commission W18, CIB-W18, Graz, Austria, Paper 32-7-13, August 1999, ISSN 0945-6996.

Ranta-Maunus, A., Kangas, J., "Glued-in steel rods in V-shape," Pacific Timber Engineering Conference, Gold Coast Australia, July 11-15, 1994.

Riberholt, H.,"Glued bolts in glulam, proposal for CIB Code", in Proceedings of the 21st Meeting of Working Commission W18, CIB-W18, Parksville, Vancouver Island, Canada, Paper 21-7-2, 1988.

Riberholt, H., Spoer, P., "Design of the inglued rods that are used for the wingblade root section on Nibemolle-B," Serie R- Denmarks Tekniske Hojskole, Afdelingen for Baerende Konstructioner, No 167, 1983.

Uhre Pederson, M., Clorius, C.O., Damkilde, L., Hoffmeyer, P., "Residual strength of glued-in bolts after 9 years in situ loading," Proceedings of the 1996 International Conference on Wood Mechanics, COST 508, pp 243-258, 1996.

Zaboklicki, A., Gebski, M., "Continuity of wooden beams as a method of reinforcement and preservation of timber structures at monumental buildings," International Series on Advances in Architecture, Vol. 3, pp 541-546, 1997.

INTERNATIONAL COUNCIL FOR RESEARCH AND INNOVATION
IN BUILDING AND CONSTRUCTION

WORKING COMMISSION W18 - TIMBER STRUCTURES

FATIGUE PERFORMANCE OF BONDED-IN RODS IN GLULAM, USING THREE ADHESIVE TYPES

by

R J Bainbridge
C J Mettem
TRADA Technology

K Harvey
M P Ansell
University of Bath

UNITED KINGDOM

MEETING THIRTY-THREE
DELFT
THE NETHERLANDS
AUGUST 2000

Presented by: C.J. Mettem

· U. Korin asked about the low tensile stress in the timber during test.
· M. Ansell responded that the interface between rod and timber would be important. One could plot shear force versus N_f as an alternative.

CIB-W18/33-7-12
DELFT, THE NETHERLANDS, 28-30 AUGUST 2000

Fatigue Performance Of Bonded-In Rods In Glulam, Using Three Adhesive Types

By R J Bainbridge*, K Harvey**, C J Mettem* and M P Ansell**

** TRADA Technology, UK*
***University of Bath, UK*

Abstract

Bonded-in rods are an economical and architecturally and industrially attractive means of forming connections within a timber structure, and of providing local reinforcement to critical zones of timber members. They also provide an important technology for the repair and upgrading of historically important timber structures that exist throughout Europe.

Structures are subject to variable actions throughout their design lives, which normally result in the repeated development of stresses below the ultimate strength of the material. There is however a theoretical potential for failure to be induced even at low stress levels, due to fatigue[1].

This paper presents the findings of experimental investigations in relation to the use of commercial adhesives to bond threaded steel rods into oversized holes in order to achieve structural timber connections. The work is part of the European Union supported GIROD project, which aims to develop design rules for inclusion in Eurocode 5.

Three types of adhesive are considered – an epoxy, polyurethane and a filled phenol resorcinol formaldehyde, in tests whereby threaded steel rods were axially loaded in a variable tension cycle whilst bonded parallel to the grain of a host glulam member. Fatigue lives are examined for two geometries of test specimen and results from different failure modes are compared to the theoretical performance of the component materials.

Four potential failure modes were identified (timber failure, cohesive failure at timber/adhesive interface, bondline failure and steel rod failure), all of which were observed within a single geometry of specimen. It is demonstrated that the adhesive type has a clear influence upon both the fatigue life and the likely failure mode. The results of tests are also related to the basis of fatigue design in Eurocode 5: Part 2 - Bridges [2].

1. Introduction

Well designed and executed adhesive bonded structural connections can be extremely efficient and may possess many desirable attributes in terms of manufacture, performance, aesthetics and cost. As identified in a recent review of innovative and improved connection methods in timber structures[3], the use of bonded-in rods makes an important contribution to their success. There are a number of recognised advantages achieved through use of bonded-in rods[4], including high local force transfer, high stiffness (especially under axial load) and improved fire performance due to the protective attributes of the timber surrounding the bonded-in rod, which is usually steel.

Structural members are by definition required to adequately resist the effects of actions applied to them throughout their design life. Structural components are normally subjected to a combination of variable (Q) and permanent (G) actions. Permanent actions produce instantaneous effects and also have a further influence over time due to the effects of creep. Variable actions usually result in the development of stresses below the ultimate strength of the material, but their repeated application can induce fatigue damage. The objective of the research described in this paper is to give an indication of whether or not the fatigue behaviour of bonded-in rods may limit their use in certain applications. This paper focuses upon experimental studies developed following theoretical qualification of the potential problem caused by fatigue [5].

The work described in this paper forms part of a 3-year European project titled "GIROD - Glued In Rods For Timber Structures", performed through collaborative activities between partners from UK, Germany and Sweden[6]. At the outset of the project, the fatigue research work package of the project was summarised as follows: "*A minor investigation of the sensitivity to low frequency fatigue will be carried out on full sized glued-in rod specimens.*"

2. Fatigue Test Programme

2.1 Test Specimens

Two sample geometries were tested, based upon 8mm diameter, high tensile steel and 16mm diameter, mild steel test rods. An average bond thickness of 0.5mm was employed across the test series. The specimens were as described in Figure 1 and Table 1.

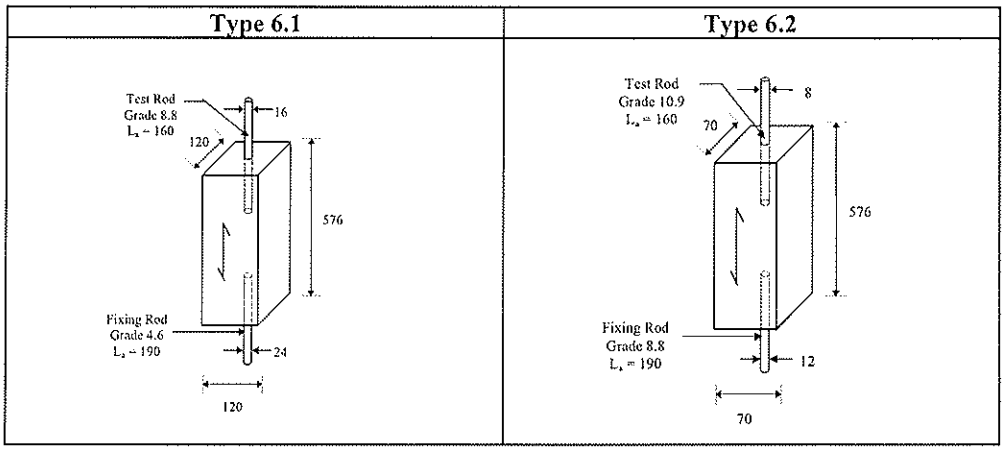

Figure 1 - Fatigue test specimens (all dimensions in mm)

Test Series	6.1 a	6.1 b	6.1 c	6.2 a	6.2 b	6.2 c
Component Laminate Strength Class	C35	C35	C35	C35	C35	C35
Moisture Content (%)	12% ±1%	12% ±1%	12% ±1%	12% ±1%	12% ±1%	12% ±1%
Glued-in Length to Rod Diameter Ratio	10	10	10	20	20	20
Bar Diameter	16mm	16mm	16mm	8mm	8mm	8mm
Bar Grade	8.8	8.8	8.8	10.9	10.9	10.9
Anchorage Length (mm)	160	160	160	160	160	160
Adhesive Type	PRF	PUR	EP	PRF	PUR	EP

Table 1 - Fatigue test specimens

Drilling was carefully performed to avoid burning and compression of sawdust within the hole, the holes being cleared of dust by inverting the blocks after drilling. The bonding was performed within 24 hours of drilling. The adhesives were mixed in accordance with manufacturers' instructions and introduced to the hole through slow injection to the bottom of the hole via a syringe and tube. The steel rods were not cleansed or treated prior to bonding, merely wiped with a clean cloth. The rods were inserted by hand under continuous pressure and rotation until they reached the bottom of the hole. The rotary motion was employed to achieve distribution of the adhesive within the threads. A strip of tape was placed on the glulam block cross-section to protect the surface from overflowing adhesive. The rods were centred visually and left to harden for 24 hours before being handled. The specimens were then left to harden in accordance with the adhesive manufacturer's recommendations prior to test.

2.2 Methodology

Bonded-in steel rod specimens were exposed to low frequency fatigue at fixed stress rates, resulting in test frequencies of approximately 1 Hz. The specimens were tested through application of a sinusoidal varying axial load, as shown in Figure 2. The maximum load levels employed in the cyclic load regimes were defined as fractions of the ultimate strength of samples, as derived from 5-minute ramp load tests performed under other work programmes within the wider project. The tests were performed on three specimens at each of three load levels, resulting in 9 tests per series, hence 54 tests in all. The number of cycles to failure and mode of failure were recorded in each case.

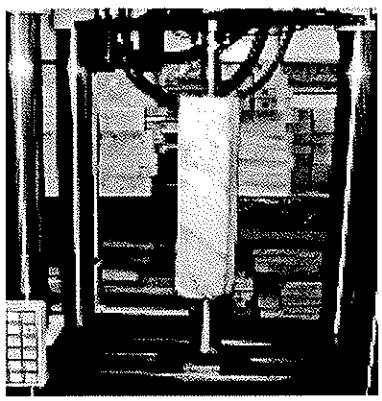

Figure 2 - Fatigue test configuration

3. Results

3.1 Preliminary Tests

To establish the appropriate test method, an initial test was performed at R=-1 (reversed compression-tension loading) at approximately 0.8 $F_{ult,est}$. This is generally the most severe cyclic regime that can be applied in timber structure testing[1]. In this first test, the rod was cut short in an attempt to prevent buckling of the rod through the compressive phase of the load cycle, but it still failed through an unstable compressive mode after four cycles, as shown in Figure 3.

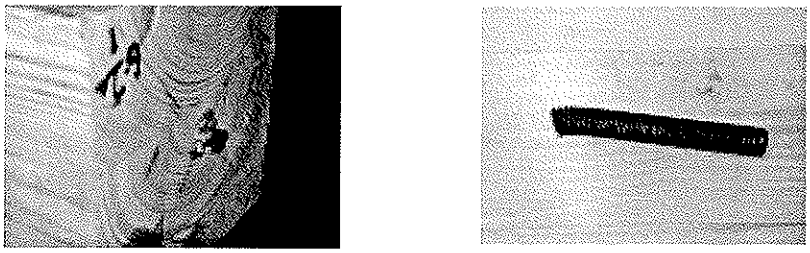

Figure 3 - Test specimen 6.2c (1) - premature failure in rod

The premature failure was believed to be a result of the compression/tension cycling coupled with the brittleness in the high-grade steel rods and slenderness of the rods. This resulted in a susceptibility of the specimens to fatigue damage resulting from the high bending stresses induced in the compressive range of the cycle.

This result led to a rethink of test strategy for this series of specimens, and an exploratory investigation of the performance of the 6.2 series specimens when loaded in tension-tension at R=0.1 (i.e. $\sigma_{t,max} = 10\ \sigma_{t,min}$). Tests were performed at R=0.1 without premature rod failure. was tested and found to be achievable. It is of note that this ratio of stress fluctuation does not produce the worst case, based on the evidence of previous research studies of fatigue performance of structural timber[1] or steel [7].

3.2 16mm Mild Steel Test Rods

3.2.1 PRF Bonded Mild Steel Rod Specimens (Series 6.1a)

The majority of the samples suffered a final failure due to withdrawal of the rod and break-down of the adhesive, with very little of the crumbled adhesive residue intact on the bar. In some cases a small volume of wood fibre immediate to the timber/adhesive interface was also pulled out from the specimen.

In two of the specimens the failure occurred at the larger fixing rod, indicating that the fatigue resistance is not necessarily directly related to the bond area with this adhesive, with variations and faults in the bond-line quality having the potential to become the over-riding influence.

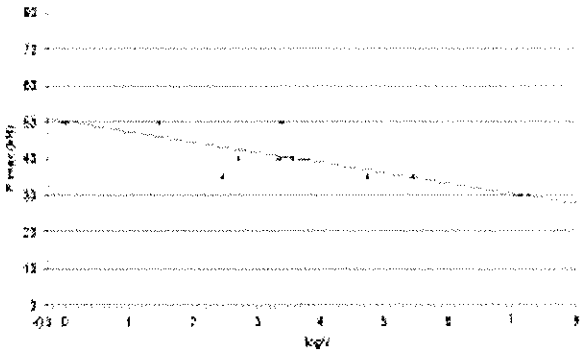

Figure 4 - Specimen series 6.1a results and Load-logN at R=0.1

A summary of results obtained from the complete set of tests is presented in the form of a σ-logN graph as Figure 4. The data is presented in the range from logN = -0.3, as this value relates to a half cycle (analogous to a projected ramp load test performed at the load rate consistent with the fatigue test). Failed test specimens from this series are shown in Figure 5.

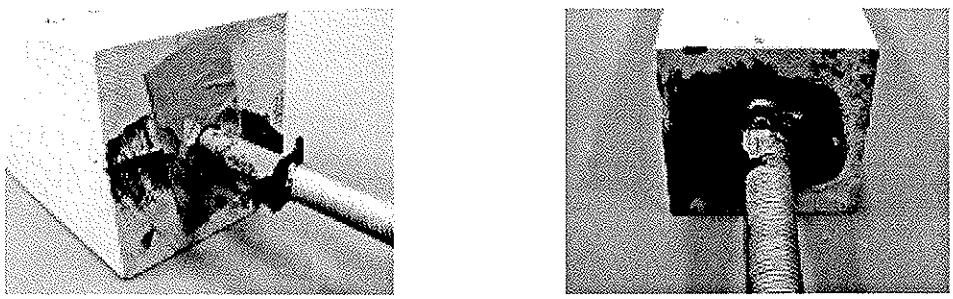

Figure 5 - Specimens from series 6.1a- adhesive failure around test rod

3.2.2 PUR Bonded Mild Steel Rod Specimens (Series 6.1b)

The majority of the samples failed due to pull-out of the test rod with adhesive intact, bringing a small volume of wood fibre with it (as shown in Figure 6). In areas where wood fibre was not intact on the adhesive layer, a profusion of small bubbles could be seen at the adhesive surface. In one case the rod suffered excessive lateral distortion under fatigue loading as the result of poor alignment of the rod during production, and in one

case a failure was experienced in the test rod. A summary of results obtained from the set of tests is presented in the form of a σ-logN graph as Figure 7.

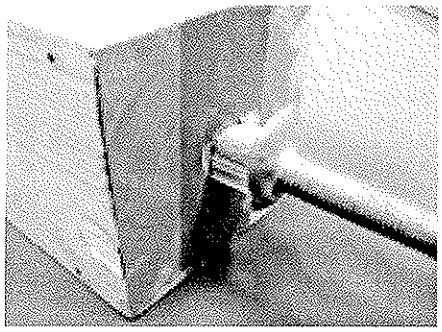

Figure 6 - Typical fatigue failure mode for specimen type 6.1b

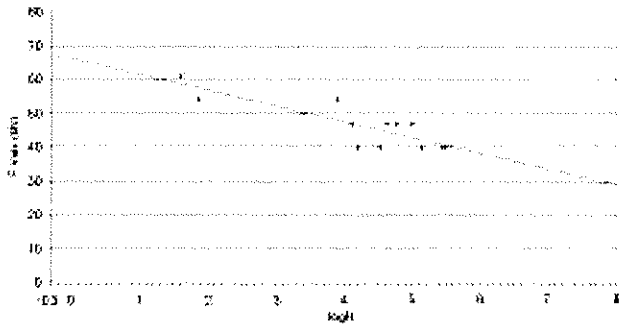

Figure 7 -Load-logN for 6.1b series specimens at R=0.1

3.2.3 Epoxy Bonded Mild Steel Rod Specimens (Series 6.1c)

A summary of results obtained from the set of tests is presented in the form of a σ-logN graph as Figure 8. The majority of the samples failed due to pull-out of a 'plug' of timber around the test rod, with the adhesive and test rod remaining intact. This varied from quite a small volume of timber (as in Figure 9a) to a substantial block following the growth rings in the glulam (Figure 9c). In two cases a failure was experienced in the test rod itself (as shown in Figure 9b). In some cases, the test rod suffered fatigue failure along its exposed length, close to the test machine fixings and in these, the specimen was repositioned and the test continued.

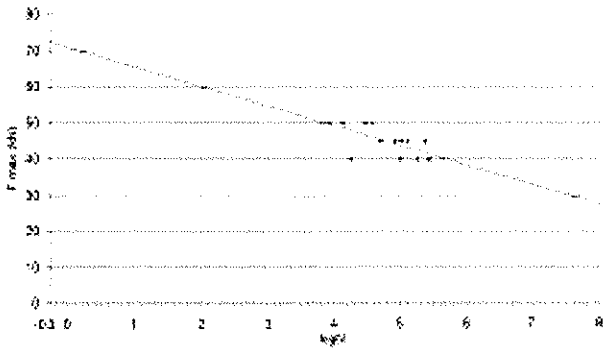

Figure 8 - Load-logN for 6.1c series specimens at R=0.1

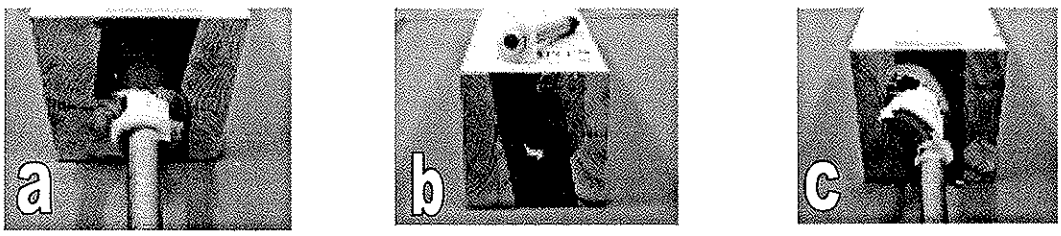

Figure 9 - Failure modes from Specimen Series 6.1c:
a) wood pull-out around test rod
b)test rod failure below timber surface
c) wood pull-out failure around test rod, following growth rings in glulam lamination

3.3 8mm High Tensile Steel Test Rods

3.3.1 PRF Bonded High Tensile Steel Test Rod Specimens (Series 6.2a)

The failures in these samples were of a very similar nature to the PRF bonded specimens tested in series 6.1a. The majority of the samples suffered a final failure due to break-down of the adhesive and withdrawal of the rod and the crumbled residue from the adhesive bondline.

In almost all specimens an audible crack was noted at the start of the tests, indicating that the damage caused by the fatigue was almost instantaneous in its effect, the initial damage being extended along the bond on successive load cycles. A summary of results obtained from the complete set of test is presented in the form of a σ-logN graph as Figure 10.

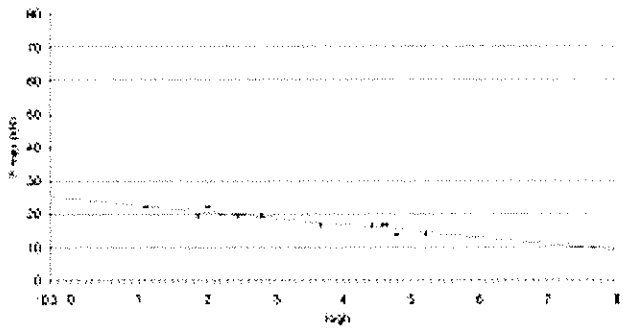

Figure 10 - Specimen series 6.2a Load-logN at R=0.1

3.3.2 PUR Bonded High Tensile Steel Test Rod Specimens (Series 6.2b)

A summary of results obtained from the complete set of tests is presented in the form of a σ-logN graph as Figure 11.

The majority of the samples failed due to pull-out of the test rod with adhesive intact and bringing a small volume of wood fibre with it. Where wood fibre was not intact on the adhesive layer, a profusion of small air bubbles could be seen at the adhesive surface.

In three instances a failure was experienced in the test rod itself at or just below the specimen surface (as shown in Figure 12).

It is also of note that in the majority of cases, the test rod suffered an earlier fatigue failure along its exposed length, close to the test machine fixings. In these, the specimen was repositioned and the test continued in order to obtain data for rod material fatigue modes discussed later in this paper.

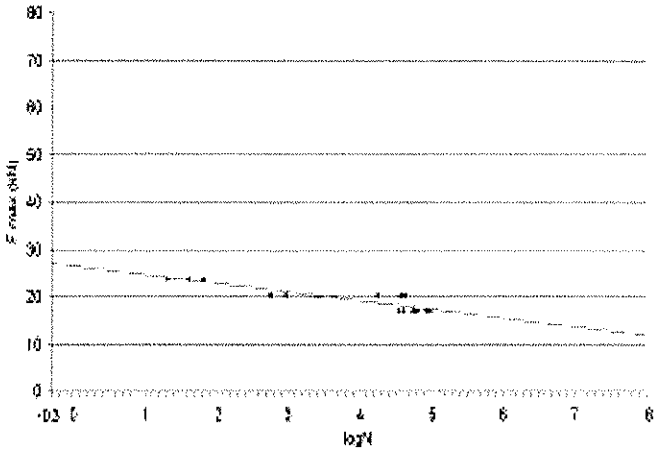

Figure 11 - Specimen series 6.2b results at R=0.1

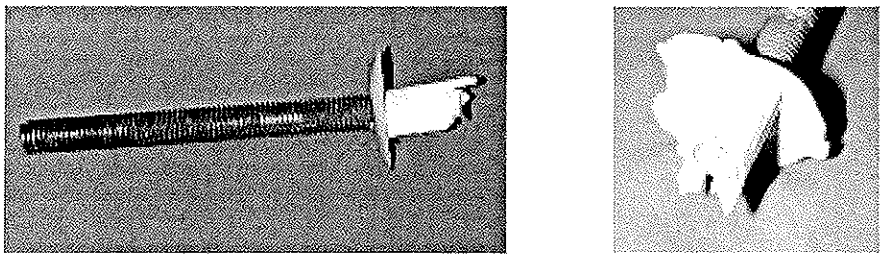

Figure 12 - Rod failure, specimen 6.2b(2)

3.3.3 Epoxy Bonded High Tensile Steel Test Rod Specimens (Series 6.2c)

The majority of the samples failed due to pull-out of a 'plug' of timber around the test rod, with the adhesive and test rod remaining intact.

In some cases, the test rod suffered fatigue failure along its exposed length, normally very close to the test machine fixings. In these, the specimen was repositioned and the test continued, as before.

A summary of results obtained from the complete set of tests, in the form of a σ-logN graph, is presented in Figure 13.

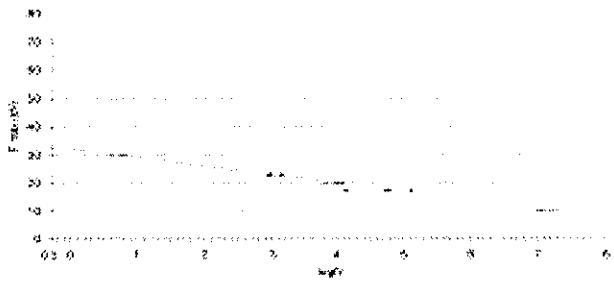

Figure 13 - Results Summary and Load-logN for 6.2c series specimens at R=0.1

4. Discussion

Observations and projected fatigue lives presented herein must be taken in the context of extrapolations based upon a limited data set, lacking confirmatory data at high numbers of load cycle. Despite these limitations, enforced through the cost and practicalities of fatigue testing, it is possible to use the data to draw basic observations of performance in fatigue.

4.1 General Test Observations

Four distinct failure modes were observed through the tests - rod failure, failure in the adhesive (causing breakdown of the material in the bond-line itself), failure in the wood substrate and failure at the interface between timber and adhesive. The incidence of these modes across failed specimens is compiled in Table 2.

The majority of failure modes observed in the tests performed in tension/tension fatigue (R=0.1) were relatively consistent with static test observations.

The features of the most common failure modes are summarised in Table 3 and examples of these are illustrated in Figure 14.

Test Rod Type	Adhesive	Failure Modes Recorded			
		Timber	Steel Rod	Adhesive	Adhesive/ Timber Interface
16mm mild steel	PRF			✓	
16mm mild steel	PUR	✓	✓		✓
16mm mild steel	Epoxy	✓	✓		
8mm HT Steel	PRF			✓	
8mm HT Steel	PUR	✓	✓		✓
8mm HT Steel	Epoxy	✓	✓		

Table 2 - Recorded fatigue failure modes

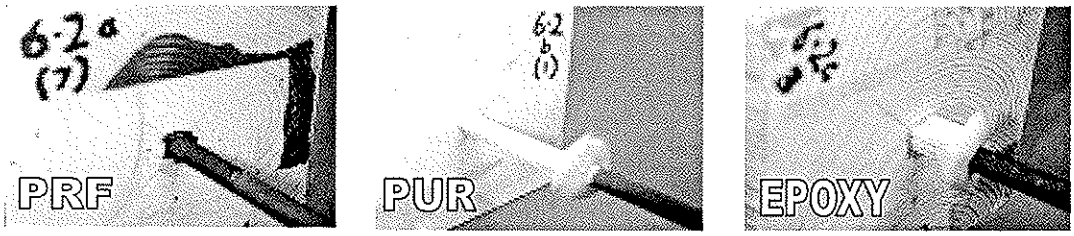

Figure 14 - Typical failed specimens at R=0.1

Adhesive Type	Failure Features
Filled PRF	• Adhesive/rod bond failure • Adhesive disintegrates through loading leaving powder residue and little adhesive intact on bar • Adhesion to timber appears to be retained.
PUR	• Failure at adhesive/timber interface • Pull out draws some timber fibres out • Bubbles visible to naked eye on failed adhesive surface
Epoxy	• Adhesive remains intact on both rod and timber bond lines • Plug of wood drawn out with rod

Table 3 Summary of commonest fatigue failure features

From the results, it is apparent that fatigue does have the potential to cause damage in the tested configurations of bonded-in rods. There is sufficient variation in failure modes to confirm that a fatigue-based failure may take place through damage to any of the component materials (steel rod, adhesive or timber substrate) or breakdown of the timber to adhesive bond interface. Whilst the fatigue lives presented in previous figures illustrate the extrapolated predictions of the performance of the specimens, it is also possible to utilise the data to illustrate failure mode specific aspects of fatigue life. The results in previous sections of this paper relate to number of cycles to failure of a specimen without differentiation between materials that form the bonded-in rod test. The following section addresses the fatigue performance of the component materials.

4.2 Mode Specific Test Observations

4.2.1 Timber Failures

Timber related failures result in pull-out of a plug of wood surrounding an intact bond and test rod. The failure area of timber was non-uniform and variable, generally being about 1-2mm thickness of wood surrounding the adhesive, in some cases more. An attempt has been made to quantify the fatigue behaviour of the timber from experiments where the timber has proved to be the critical material leading to fatigue failure.

Figure 15 collates data from such failures in the form of F_{max} against log-N, for the two geometries of test specimen in the investigation. F_{max} is plotted here in preference to σ due to the variability in failure surface area and hence shear stress equated to the test load. From these plots it is apparent that in both test sets there is a reasonably close fit to the linear relationship anticipated for timber behaviour in fatigue[1].

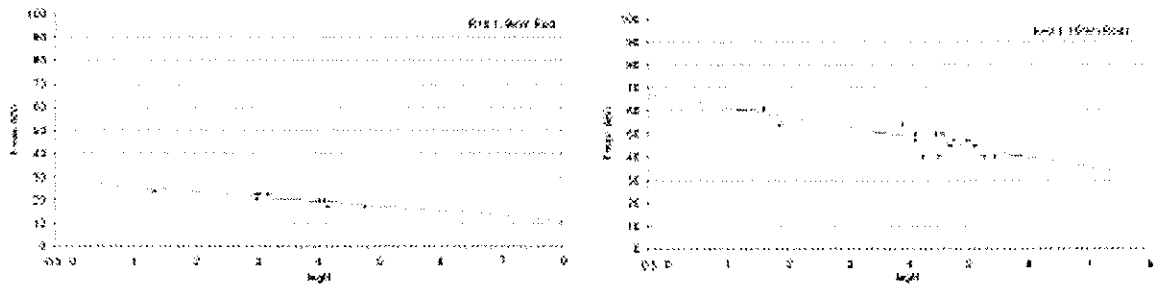

Figure 15 - Fatigue performance associated with timber failure modes in the series 6.2 (8mm ∅ bars) and series 6.1 (16mm ∅ bars) GIROD specimens at R=0.1 (combined epoxy and PUR sample data)

Through comparing load levels in each test to the one half cycle (logN =-0.3) value produced from the graph (i.e. the equivalent ramp load predicted ultimate strength at fatigue test load rate), it is possible to combine the data from the tests performed with both rod diameters. Figure 16 presents the combined data set from all tests where timber is the critical fatigue failure mode.

In cases where the timber fatigue has determined the GIROD sample fatigue performance, the extrapolated strength at 10^7 cycles (with R=0.1) as compared to the first half cycle strength in tension represents a 55% reduction. This is of the order that would be expected from variable tension tests at R=0.1, based upon evidence such as that illustrated in Figure 17 from tests performed on clear unidirectional laminated timber.

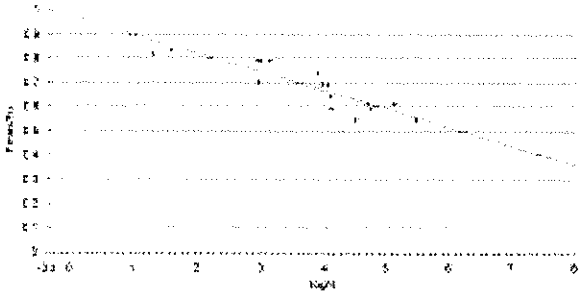

Figure 16 - Fatigue performance associated with timber failure modes in the GIROD fatigue specimens at R=0.1

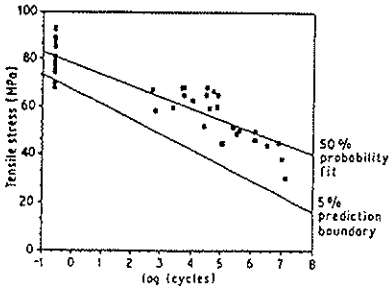

Figure 17 - σ-logN data for Khaya (Khaya ivorensis) at R=0.1 from studies by Bonfield et al.[8]

4.2.2 Steel Rod Failures

Steel does not have the same general linear σ-logN trend as timber, as illustrated in the compilation of construction material fatigue performance shown in Figure 18 [9].

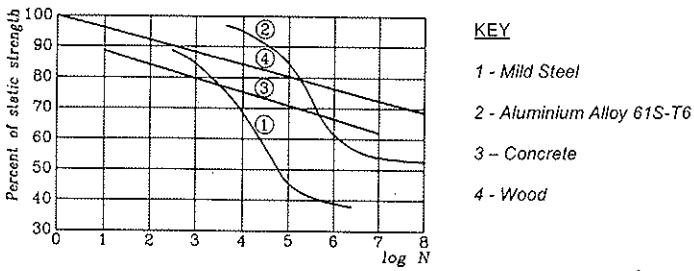

Figure 18 - Fatigue diagrams for various construction materials (R=0.1) [9]

Data abstracted from the steel rod failures experienced is compiled in Figure 19, together with a curve showing typical anticipated performance of mild steel through fatigue at R=0.1. There is clearly a potential risk of fatigue failure in the bonded-in rod used to form the connection.

Whilst the higher strength steel out-performs the mild steel in terms of the percentage of its stress range that can be utilised at a high number of cycles, a higher number of failures were recorded in the higher strength steel rods. The rod failures observed in the specimens indicate that the fatigue performance can be determined by classic fatigue failure in steel rods.

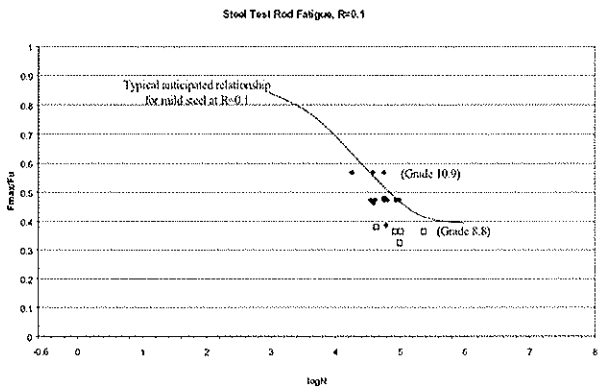

Figure 19 - Fatigue performance associated with steel rod failure modes in the GIROD fatigue specimens

Recorded failures in the mild steel (Grade 8.8) rods are observed at a lower numbers of cycles (or alternatively in a lower stress range) than the basic material data would suggest. The explanation for this can be attributed to the threaded surface on the rod acts as a series of stress raising notches. This has a recognised impact upon fatigue damage development, the feature often being much more important than the steel composition when determining fatigue resistance [10,11].

The higher grade steels have a higher fatigue resistance in terms of the average stress causing failure in the data set obtained between 10^5 and 10^4 cycles, but it is of note that a greater number of samples suffered rod

failure with the higher grade steel. In addition to the thread effect, contributory factors defining the rod mode of failure include brittleness in the rods coupled with minor flaws and eccentricities in the test specimens resulting in combined bending and tension stress development. This may explain in part, the increased incidence of failure in the more slender and more brittle high-grade rods.

4.2.3 Adhesive Breakdown Across Bondline

Failures within the bond-line were only encountered with the filled PRF adhesive. σ-logN relationships for the PRF bonded specimens from series 6.1 and 6.2 are shown in Figure 20.

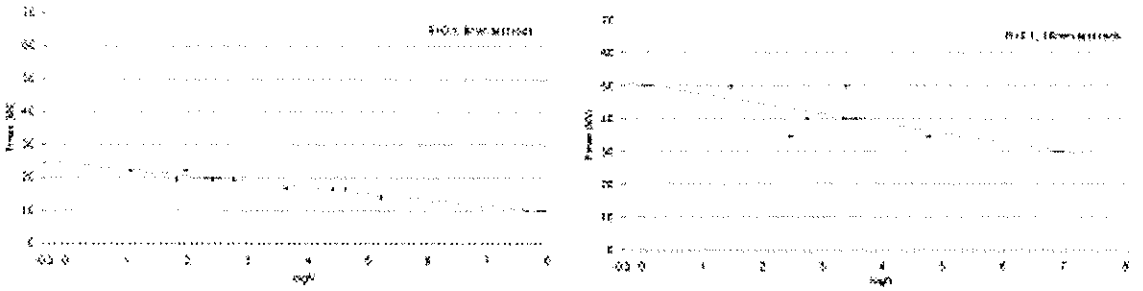

Figure 20 - Fatigue performance associated with adhesive failure modes in the PRF bonded GIROD fatigue series 6.2 (8mm ∅ bars) and series 6.1 (16mm ∅ bars) at R=0.1

It is of note that the sample set with 8mm rods (λ=20) is more consistent with the linear approximation of anticipated behaviour than the 16mm test set (λ=10). This indicates an influence of sample geometry upon fatigue behaviour, in addition to the basic fatigue resistance of the material acting as the critical component in the system.

Figure 21 presents the combined data set from all tests where the PRF adhesive is the critical fatigue failure mode.

The data has been compiled by comparing load levels in each test to the one-half cycle (logN = -0.3) value produced from the graph, i.e. the equivalent ramp load predicted ultimate strength at fatigue test load rate.

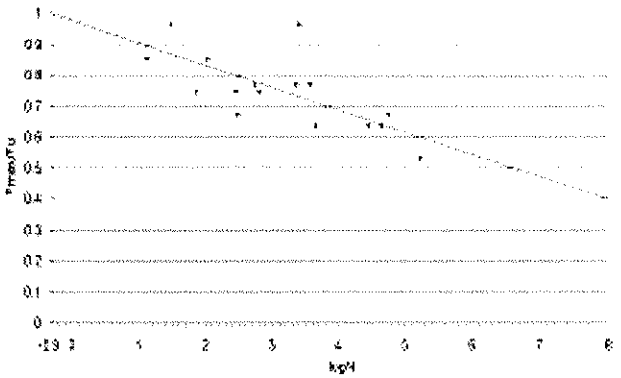

Figure 21 - Fatigue performance associated with adhesive failure modes in the PRF bonded GIROD fatigue specimens at R=0.1

4.2.4 Timber/Adhesive Interface Failure

Failures at the timber/adhesive interface were observed only in the PUR bonded samples. This is due to CO_2 bubble formation at the bond ("foaming" of the bond-line), causing a reduction in the effective cohesion area. This is the normal result of reaction of the adhesive components with moisture, in this case the moisture in the glulam material.

σ-logN relationships for these failures from series 6.1 and 6.2 are combined in Figure 22. It is of note that the scatter about the best-fit idealised linear relationship is greater than that observed in the other failure mode related test sets. This scatter is such that the validity of the linear extrapolation is in question.

This suggests that the fatigue resistance obtained in the PUR samples may be more a function of the variability in produced bond lines due to foaming rather than a product of material mechanical properties and specimen geometry.

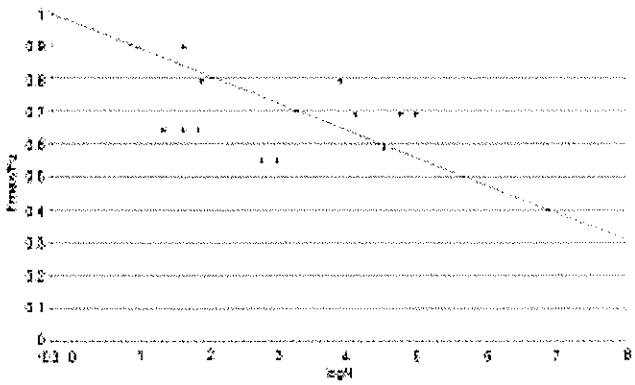

Figure 22 - Fatigue performance associated with adhesive/timber interface failure modes in the PUR bonded GIROD fatigue specimens at R=0.1

4.3 Relationship Between Experimental Results And Design Code Basis

4.3.1 Current Design Method For Bonded-In Rods

Owing to uncertainty about the behaviour of such connections and lack of reliable calculation methods, bonded-in rods have not yet been introduced in the main part of the draft standard and instead have been placed in an annex. CEN.TC250/SC5 has decided in principle to try to include bonded-in rods also in Eurocode 5 - Part 1: General rules and rules for buildings[12]. In 1992 it was agreed to put bonded-in rods in the programme of work and a working group was set up.

The group confirmed the need for standards in this field and a work programme including product, production and test standards was drafted. The group came to the conclusion that existing knowledge was insufficient to draft standards that would be acceptable to all European countries. To develop suitable test methods, the mechanical behaviour of bonded-in rod connections had to be understood to a greater extent. Durability, creep and creep-rupture behaviour of the adhesive bond were identified for study in more detail. The method presented in Annex A of Eurocode 5: Part 2 [2] presents four criteria for consideration in joints employing steel rods:

- Rod failure through yielding
- Shear failure in the adhesive
- Localised timber failure around the bond
- Failure of the host timber member

The yield failure of rods is identified as the preferred design mode. The yielding of the steel is a ductile failure mode, reserving capacity to transmit loads even after this limit state has been breached, albeit at excessive deformation levels. Parallels can be drawn here with the 'under-reinforcement' approach employed in design of concrete structures. This approach currently poses obstacles to utilising non-ferrous rods which have no yield point and subsequent plasticity (e.g. GFRP - glass fibre reinforced plastic), but again there is precedent of use that can be drawn from reinforced concrete to account for the absence of yield and subsequent plastic capacity. A partial coefficient approach for treatment of the full range of materials with potential application in bonded-in rod connections in timber structures has been considered [13], drawing in part upon design methods employed with other structural materials.

To date it has generally been considered that the requirements of adhesives in these cases were to achieve good adhesion to the timber, attain sufficient shear strength to maintain integrity across the adhesive layer and to provide anchorage to the rod through combined adhesion and mechanical interlock. Owing to the practicalities of surface preparation for steel rods in construction environments, it has become standard practice to employ textured or threaded rods in order to maximise mechanical interlock. Pressures of economy of production process versus the low cost of materials have commonly led to negation of specification of high levels of surface preparation.

In addition to the structural wood adhesives, which are rather brittle, ductile adhesives such as two-component polyurethane have been used in bonded-in rods. For the latter adhesive types, no standardised test procedures and requirements with respect to applications in timber structures and in metal-to-wood bonds exist.

4.3.2 Current Fatigue Design Basis

The basis for fatigue verification in EC5: Part 2 is through application of a fatigue coefficient (as summarised in Figure 23) and an appropriate fatigue safety factor. This form of assessment in relation to number of cycles to failure provides a common link between test data and design basis.

k_{fat} - log n relationship	Structural Situation	$k_{fat,\infty}$
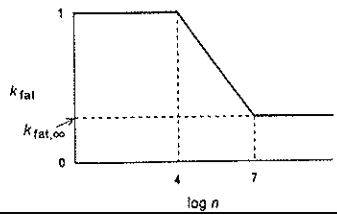	Timber members	
	• in compression perpendicular and parallel to the grain	[0,60]
	• bending, tension or reversed tension/compression	[0,30]
	• shear	[0,20]
	Joints with	
	• dowels	[0,25]
	• nails	[0,15]

Figure 23 - Relationship between k_{fat} and the number of cycle and values of $k_{fat,\infty}$ as presented in EC5: Part2

The value of k_{fat} is employed in the following equation:

$$f_{fat,d} = \frac{k_{fat} f_k}{\gamma_{M,fat}} \qquad (1)$$

where:
f_k = characteristic strength for static load
k_{fat} = fatigue coefficient obtained graphically (as in Figure 23)
$\gamma_{M,fat}$ = material safety factor for fatigue (drawn from EC1-Part1 [14])

4.3.3 Comparison Of Test Observations With Code Design Approach

The derivation of appropriate $\gamma_{M,fat}$ factor depends on the structure and its status with regard to damage tolerance. For structures that can be verified as damage tolerant, this safety factor can be taken as 1.00 (DDENV 1991-1:1996, Cl.B.5.(2)) [14]. Other cases require further consideration as to derivation of an appropriate factor.

Taking the case of a damage tolerant structure, this means that the end design result is determined as the product of a characteristic design value and the fatigue coefficient.

It must also be borne in mind that the tests performed relate to a variable tension cycle (R=0.1), employed for test practicality but which might not prove to be the most severe. For example, tests on timber have shown reversed loading (R=-1) to be the most severe, as illustrated in Figure 24.

Whilst it is not possible to construct curves from the data set of this limited study to derive characteristic values appropriate to definition of absolute values for k_{fat}, it is possible to benchmark observations against those proposed for general structural timber applications.

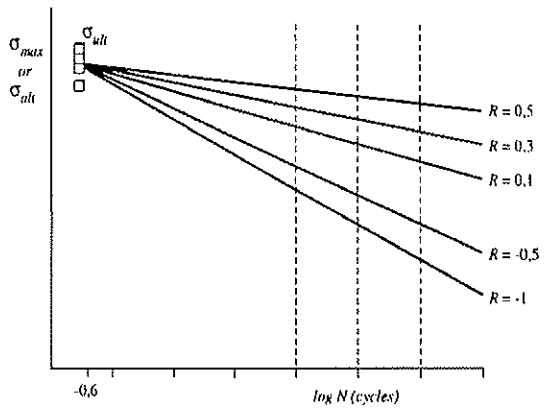

Figure 24 - Timber fatigue performance over a range of R ratios [1]

It is apparent from test observations that there is a deviation from suggested behaviour in the graph used to derive k_{fat}. The experimentally observed σ-logN relationship is linear from 0.5 to 10^7 cycles, whereas the k_{fat}-logN curve indicates no effect up to 10^4 cycles. From the data plots, the ratio of strengths at the key numbers of cycles can be summarised and compared as in Figure 25.

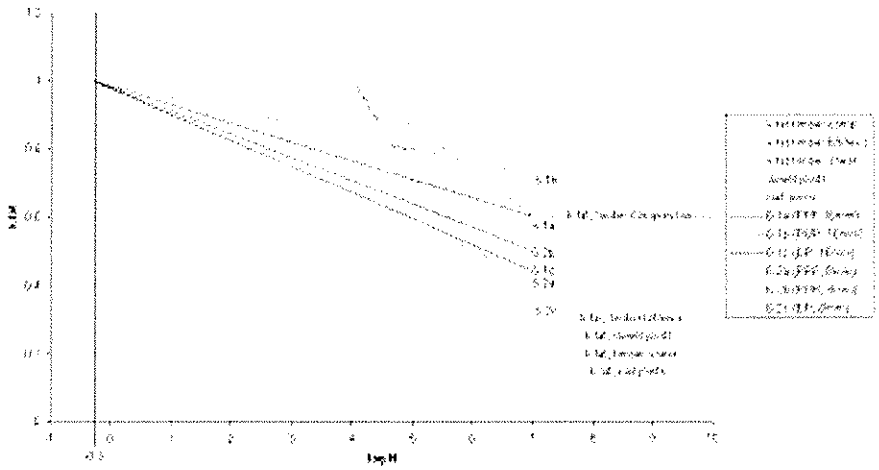

Figure 25 - Fatigue factors and logN relationship as defined in EC5: Part2 and translated directly from test observations across test set

Considering the results in relation to the specimen types, independent from the failure mode, there is a consistent trend in the ordering of fatigue effect upon the test specimens. The separation of the series 6.1 and 6.2 counterparts also indicates that there is not only a clear influence of adhesive type, but also of specimen geometry.

It is essential to note that these curves do not reflect the actual comparative performance of specimens, merely the degree to which fatigue effects a sample type. Hence the potential conclusion that could be drawn from this curve set that PUR is best, PRF second best and Epoxy least effective in fatigue resistance is not true. For example, consider the peak load data drawn from the test sets in Table 4. It is clear that at the half cycle point Epoxy has superior resistance, as is the case at 10^4 cycles. However the gradient of the projected log-linear relationships means that at the 10^7 cycle point, the difference is massively reduced, resulting in a reversal of order in the case of the 8mm test rods.

Sample		F@ 1/2 cycle (kN)	F@ 10^4 cycle (kN)	F@ 10^7 cycle (kN)
16mm rods	PRF	51	38	30
	PUR	67	47	33
	EP	72	50	33
8mm rods	PRF	25	17	12
	PUR	27	19	13
	EP	32	20	10

Table 4 - Selected fatigue resistance data from linear extrapolations of performance

It should also be noted that these performances are based upon approximated extrapolations from a limited test set and that there is no experimental data to validate the low-stress/high-cycle number performance. For example, it could be that at such low stress levels, fatigue limits might emerge in some cases, whereby fatigue failure does not manifest.

The data can also be similarly compared with the test curves on the basis of the critical failure modes, as shown in Figure 26. From these plots it is clear that in the specimens tested, the fatigue performance relationship for all modes appear to be very close.

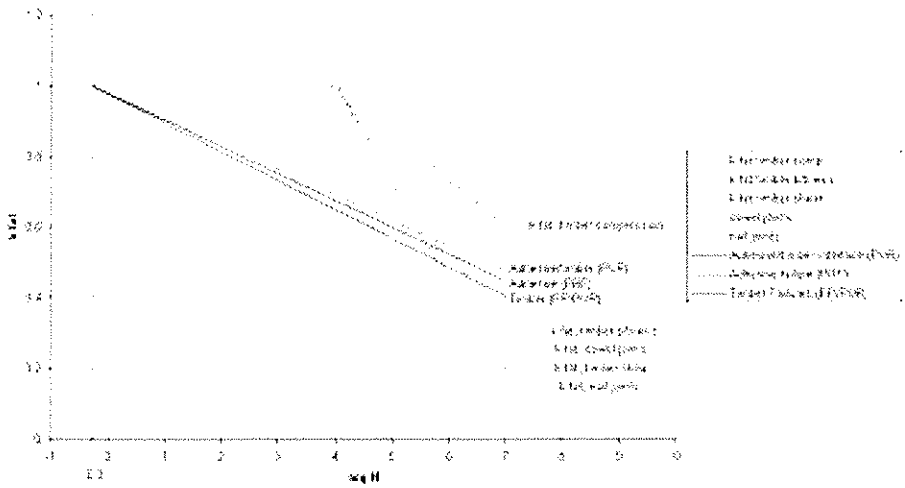

Figure 26 - Fatigue factors - logN relationship as defined in EC5: Part2 and translated directly from test observations of failure modes

Again, it is important to note that in the graphs, the curves do not directly represent the performance (i.e. capacity of the specimen), but the degree to which the specimen is affected by cyclic loading. Since the curves in EC5:Part 2 are also intended as a mechanism to relate 'static' load resistance to fatigue, there are a number of issues that require consideration in potential application of these curves in design.

4.3.4 Key Considerations in Inter-relation with 'Static Test' Data.

The relationships have been developed on the basis of equating a first half cycle of load with an equivalent static ramp load test. However, this is not strictly true, as the cycling of load through the remainder of the test does not incorporate a zero load condition.

A zero load / tension cycle would be defined as R=0, which would be marginally more severe on the specimens, but for which there are introduced a number of test practicality issues.

There is also a load cycle frequency affect. Frequency can have a profound effect upon the apparent fatigue behaviour, as illustrated in Figure 27. The number of load cycles to failure of wood, may decrease more than 100 times lowering the frequency from 1 cycle per 10 seconds to 1 cycle per 2 hours [15].

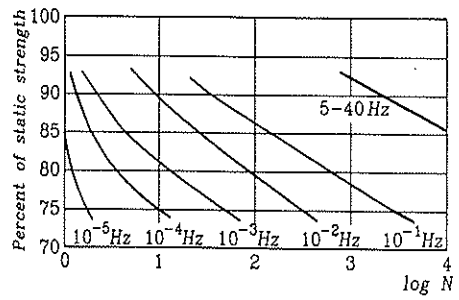

Figure 27 - σ - logN relationships for timber at different frequencies [9,16]

A static strength test performed in 5 minutes (the order of test duration for short term ramp load tests performed elsewhere in the GIROD project on specimens similar to the fatigue samples) results in a frequency at R=0.1 of $1.7x10^{-3}$. At low frequencies the fatigue cycle can also be seen to be an interaction with load duration effects. For example, a frequency of 10^{-5} Hz produces a single cycle time of approximately 28 hours. Recent studies have demonstrated that fatigue failure is dependant upon both the total time under load and the number of load cycles [17] (hence a frequency effect).

In the fatigue tests reported herein, load rate was held constant in order to achieve test frequencies around 1Hz. At higher frequencies, it is also possible to cause secondary effects which compromise the performance of the specimen in fatigue due to the build up of heat caused by high frequency strain alternation. Therefore, the number of cycles to failure alone is not an absolute descriptor of performance and must be considered in relation to frequency and stress rate.

Studies concerning the fatigue failure of clear specimens of timber have identified the influence of frequency upon the damage mechanisms in the timber, with creep effects and residual strain accumulation being identified as holding major importance[17]. Thus application of σ-logN based estimations independent of frequency should not be adopted. In terms of design methods related to a static test performance, this would therefore promote redefinition of k_{fat} to address frequency and R ratio as well as number of cycles to failure.

Fatigue frequency effects are also noted in steel. [18]. Marceau et al [19] also identified the dependency upon frequency of the fatigue fracture modes in thick bondline lap shear joints, creep-rupture being identified at low frequencies.

The actual excitation in a structure will be largely case specific in terms of magnitude of fluctuating actions, frequency and tension/compression balance. This will be a combination of permanent actions, variable imposed static actions and dynamic response to free or forced vibration. Whilst the static actions can be related to generally very low frequency cycling of load, dynamic effects will occur across a wide frequency range. The frequency of typical direct excitations can however be broadly classified in relation to source, as summarised in Table 5. It must be noted that these are excitation frequencies at source and that the dynamic load effects in the connection will be a function of these actions, other imposed loads and the reaction of the structure. Where vibration sources are remote, the excitation depends not only upon the nature of the source, but also the emission, transmission and immission via the intermediate material [20].

Load Source	Examples	Typical Dominant Excitation Frequency Range (Hz)
Human Activity	Walking, Running, Jumping, Dancing	1.5 - 3.5 Hz
Vehicular	Roads	1- 400 Hz
	Railways	8 - 20 Hz, 40 - 80 Hz
	Bridge / Traffic Interaction Effects	0 - 14 Hz
Machinery	Diesel Engines	5 - 22 Hz
	Electric Machines, Fans, Motors	3 - 16 Hz
Wind	Gusts, Buffeting, Vortex Effects, etc.	Variable, defined by dynamic interaction of wind and structure

Table 5 - Selected vibration sources and typical excitation frequency range [21-25]

It is apparent from the variation and wide range of the frequency of excitation developed from the sources identified that there is no clear preferable frequency to which any fatigue effect investigations should be linked.

4.3.5 Design Approaches With Other Materials

The issue of fatigue design is important in structural design, but the degree to which it has previously been addressed in timber design is far less substantial than in other materials, some of which provide pointers as to how a more complete verification method might be progressed.

For example, the EUROCOMP design guide for structural FRP materials [26] contains fatigue guidance specific to these materials. In terms of design, it adopts "Fail-safe" definitions to describe structural significance of components (see Section 5.2.2) and translates this to partial safety coefficients for fatigue strength, as detailed in Table 6.

Inspection and access	"Fail-safe" components	Non "Fail-safe" components
Component subject to periodic inspection and maintenance. Detail accessible	1.5	2.0
Component subject to periodic inspection and maintenance. Poor accessibility.	2.0	2.5
Component not subject to periodic inspection and maintenance	2.5	3.0

Table 6 - Partial safety coefficients for fatigue strength [26]

In concrete structure strengthening applications, recommendations for the adhesive and adhesive joint properties have been developed, based upon test definition for steel-to-steel test joints as summarised in Table 7 [27].

Property	Environmental condition for test	Recommended Value	Test Method
Shear Strength (fatigue)	20 °C	To survive 10^6 cycles of stress range between 0.4 and 4.0 N/mm^2	Double overlap joint

Table 7 - Application specific concrete strengthening fatigue test recommendation [27]

Both extracts illustrate alternatives to tackling the complex subject of full definition of the fatigue problem and verification of performance. Therefore, a fundamental choice in the scope of application will determine the appropriateness of further work in this field if specifically geared to development of timber design methods.

4.3.6 Items For Further Consideration In Bonded-In Rod Connections

Whilst the study reported herein draws upon only a limited number of experimental observations, it has highlighted a number of key issues for further consideration and future address. There is a massive scope of work that has not been covered by this investigation. A number of key points to direct possible expansion of this work are suggested, as follows.

The observations drawn are made upon a small sample group. The variability displayed in the sample group and the impact of variations in their fabrication upon refined prediction of fatigue failure mode is not possible from a test set of this size. It is not therefore possible to confirm whether the projected trends truly represent a reasonable mean performance or to directly link the values to characteristic properties which will be used in design.

The impact of varying cyclic load regimes (differing R and frequency) and alternative geometric configurations would also be necessary to fully develop appreciation of the fatigue performance. With this in mind, it might be necessary to refine the definition of fatigue factors with respect to the different influences (e.g. $k_{fat,n}$, $k_{fat,f}$, $k_{fat,R}$). Development of a fatigue safety factor specific to bonded-in rod connections might also be worthy of consideration.

5. Conclusions

A revised basis for design of bonded-in rods for structural timber connections is under preparation through the GIROD project. This draws heavily upon both existing knowledge and experimental investigation. The fatigue behaviour discussed herein is an area where experimental investigations are adding to the knowledge of these systems and expanding the scope of addressable issues in their design.

The structure of the Eurocodes provides opportunities to link-in test evidence to design methods in both of the instances discussed, primarily due to the explicit nature of the code formulation and the more fundamental link between limit states basis and material properties observed directly from tests.

Observations and projected fatigue lives presented herein must be taken in the context of extrapolations based upon a limited data set, lacking confirmatory data at high numbers of load cycle.

The majority of fatigue failure modes were common to those observed in static test counterparts to the fatigue test specimens. Significant incidents of alternative failure modes were however also recorded, especially failures in the steel rods.

It is apparent that different adhesive types behave in fundamentally different ways with respect to the fatigue performance and the eventual mode of failure at the fatigue ultimate limit state.

The geometry of the test specimens is at least as important under the conditions of this test as the adhesive type, but the general order of performance across the adhesive types was found to be consistent between specimen sets.

The scope for further work to enhance the knowledge and design methods employed is very large. A full description of failure mode-related fatigue performance basis of design would require further experimentation. To determine the full relationship with geometry and to verify the influence of R ratio and frequency upon the application of design methods based upon the observations drawn from the test set would be key to development of such development.

Acknowledgements

The project activities summarised in this paper were sponsored by the Commission of The European Communities DG XII, Science, Research and Development through SMT contract SMT4-CT97-2199.

Research activities detailed in this report were carried out on behalf of Moelven Toreboda Limtra AB (Sweden), Casco Products AB (Sweden), Studiengemeinschaft Holzleimbau e.V (Germany), GLTA (UK), Klebchemie M.G. Becker GmbH (Germany) and Wevo Chemie GmbH (Germany), by TRADA Technology in partnership with Swedish National Testing and Research Institute (Sweden), Lund Institute of Technology - Structural Mechanics (Sweden), Forschungs-und Materialprufungsanstalt, Baden-Wurtemberg (Germany) and Universitat Karlsruhe - Lehrstuhl fur Ingenieurholzbau und Baukonstruktionen (Germany).

References

1. ANSELL, M.P. (1995). Fatigue Design for Timber & Wood Based Materials. Step Lecture E22, Timber Engineering STEP 2, STEP, EUROFORTECH, Centrum Hout, Almere.
2. DD ENV 1995-2 (1997). Eurocode 5 Design of Timber Structures - Part 2: Bridges.
3. BAINBRIDGE, R.J. and METTEM, C.J. (1998). Moment Resistant Connections in Timber Structures: A Review of Existing and Innovative Systems. *Paper 11590,* Structures and Buildings Journal, The Institution of Civil Engineers,Thomas Telford Publishing Ltd., London.
4. JOHANSSON, C.J. (1995). Glued-in Bolts. STEP Lecture C14, Timber Engineering STEP 1, STEP, EUROFORTECH, Centrum Hout, Almere.
5. BAINBRIDGE, R.J., METTEM, C.J. and ANSELL, M.P., (1999). An Overview Of Research To Assess Fatigue Performance Of Bonded-In Rods For Timber Structures Using Three Adhesive Types. Cost Action E8 Workshop - Damage In Wood - Mechanical Performance Of Wood And Wood Products, Bordeaux, 27-28/5/99.
6. BAINBRIDGE, R.J. and METTEM, C.J. (1999). Bonded-In Rods For Timber Structures -A Versatile Method For Achievement Of Structural Connections. The Structural Engineer, 77, No.15, 1999, IStructE, London.
7. BONFIELD, P.W., ANSELL, M.P. and DINWOODIE, J.M. (1994). Fatigue Testing of Wood : A Detailed Guide For The Development of Life-Prediction Formulae From Fatigue Data. Proceedings of IUFRO S5.02 - Timber Engineering, Sydney, Australia, July 1994.
8. AMERICAN SOCIETY FOR METALS (1978). Metals Handbook, 9th Edition, Volume 1 - Properties and Selection: Iron and Steels. ASM, Metals Park, OH, USA
9. HANSEN, L.P. (1991). Experimental Investigation Of Fatigue Properties Of Laminated Wood Beams. Proceedings of the 1991 International Timber Engineering Conference Volume 4, (Sub-Conference 15), 4.203-4.210, London, UK.
10. BOYER, H.E. (1986). Atlas of Fatigue Curves, American Society For Metals.
11. HINGWE, A.K. (1982). Quality Control Source Book - Threaded Steel Fasteners, American Society for Metals, Metals Park, OH, USA.
12. DD ENV 1995-1-1 (1994). Eurocode 5 Design of Timber Structures - Part 1.1: General Rules and Rules for Buildings.
13. METTEM, C.J., BAINBRIDGE, R.J., ANSELL, M.P., HARVEY, K., HUTCHINSON, A. and BROUGHTON, J. (1999). Evaluation of Material Combinations for Bonded In Rods to Achieve Improved Timber Connections. CIB-W18/32-7-13, Proceedings of International Council For Building Research Studies And Documentation, Working Commission W18 - Timber Structures, Meeting Thirty-Two, Graz, Austria, August 1999.
14. DD ENV 1991-1 (1994). Eurocode 1 Basis of Design And Actions On Structures - Part 1: Basis Of Design.
15. NIELSEN, L.F. (1997) Lifetime and Residual Strength of Wood Subjected To Static And Variable Load. Proceedings of IUFRO S5.02, Timber Engineering, Copenhagen, Denmark.
16. BACH, L. (1979). Frequency Dependent Fracture Under Pulsating Loading. Report 68, Building Materials Laboratory, Technical University Of Denmark.
17. CLORIUS, C.O., UHRE PEDERSEN, M., HOFFMEYER, P. and DAMKILDE, L. (1996). Fatigue Damage in Wood. International COST 508 Wood Mechanics Conference, 14-16 May 1996, Stuttgart, Germany.
18. WEISER, P.F. (ed.) (1980) Steel Castings Handbook, 5th Edition, Steel Founders Society of America, Rocky River, OH, USA.
19. MARCEAU, J.A., McMILLAN, J.C. and SCARDINO, W.M. (1977). Adhesives Age, 21, No4, pp37.
20. KLEIN, G. and RAINER, J.H. (1995). Ground Transmitted Vibrations. Section 2.4, Vibration Problems In Structures, Birkhauser, Basel.
21. AMMANN, W., KLEIN, G, NATKE, H.G and NUSSBAUMER, H. (1995). Machine Foundations And Supports. Section 2.1, Vibration Problems In Structures, Birkhauser, Basel.
22. HIRSCH, G. and BACHMANN, H. (1995). Wind Induced Vibrations. Section 3, Vibration Problems In Structures, Birkhauser, Basel.
23. AMMANN, W. (1995). Vibration Induced By Traffic & Construction Activity - Roads. Section 4.1, Vibration Problems In Structures, Birkhauser, Basel.
24. BACHMANN, H., PRETLOVE, A.J. and RAINER, H. (1995). Dynamic Forces From Rhythmical Human Body Motions. Annex G, Vibration Problems In Structures, Birkhauser, Basel.
25. DEISCHL, F., EISENMANN, J. and STEINBEISSER, L. (1995). Vibration Induced By Traffic & Construction Activity - Railways. Section 4.2, Vibration Problems In Structures, Birkhauser, Basel
26. CLARKE, J.L. (Editor) , (1996). Structural Design of Polymer Composites - EUROCOMP Design Code and Handbook. E & F N Spon, London.
27. MAYS, G.C. and HUTCHINSON, A.R. (1992). Adhesives in Civil Engineering. Cambridge University Press, UK.

INTERNATIONAL COUNCIL FOR RESEARCH AND INNOVATION
IN BUILDING AND CONSTRUCTION

WORKING COMMISSION W18 - TIMBER STRUCTURES

INTERNAL STRESSES IN THE CROSS-GRAIN DIRECTION OF WOOD INDUCED BY CLIMATE VARIATION

by

J Jönsson
S Svensson
Department of Structural Engineering
Lund University
SWEDEN

MEETING THIRTY-THREE
DELFT
THE NETHERLANDS
AUGUST 2000

Presented by: S. Svensson

· A. Ranta-Maunus commented that the test results could be compared to numerical values from VTT.
· M. Ansell asked for more details on the image analysis techniques.
· S. Svensson responded that the University of Lund software was used to detect the mean intensity values of the markers to achieve a gray scale number. Photo image results and image analysis results were similar. Micro-strain resolution was approximately -4 to -5.
· R. Görlacher asked why 30% difference was found between dynamic and static E.
· S. Svensson stated that the reason was not known and wanted to use only the dynamic E results.
· R. Görlacher stated that dynamic E values should be more reliable because of geometry effect of the small specimens.

Internal stresses in the Cross-grain Direction of Wood Induced by Climate Variations

Johan Jönsson, Staffan Svensson
Dept. of Structural Engineering
Lund University, Lund, Sweden

Abstract

A method to determine the internal stress state across the grain of glue laminated wood (glulam) is described in this paper. An experimental equipment for cutting specimens and measuring released deformation is used. The internal stress state can be calculated from the observed released deformations. For evaluation purpose a small and well-defined test series was carried out for specimens with different climate treatment prior to testing. Results for seasoned specimens show that internal stresses exist in glulam without the presence of moisture gradients. Results for specimens with induced moisture gradient show that the stresses become larger when moistening from a specific climate A to another climate B than when drying from B to A. The largest mean stress level found in the test was about 0,7 MPa, which is higher than the characteristic value of tensile strength perpendicular to the grain!

1 Introduction

The weakest failure mode of solid wood is tension perpendicular to the grain direction. When failure occurs perpendicular to grain it is usually brittle with no indication prior to failure. In the literature one finds remarks like the following. "In any structural part tensile stresses perpendicular to the grain are carefully avoided since not only is the strength across the grain very low but checks or shakes due to shrinkage can completely destroy the tensile strength across the grain", Kollman and Côte (1968). In modern timber engineering, however elements and solutions are used in which tension perpendicular to the grain is a fact, e.g. arcs, frame corners, beams with variable cross-section, joints, etc. For such elements, design methods to determine stress across grain for elements of different geometry due to mechanical load, can be found in handbooks and sometimes in building codes.
The strength of wood is dependent on ambient climate condition (moisture state). This dependency is particular pronounced perpendicular to grain, Siimes (1967), The load carrying capacity for structural elements stressed perpendicular to the grain has in the recent past been addressed in a number of studies, Jensen and Hoffmeyer (1996), Gustafsson (1998), Aicher (1998), Morlier and Ranta-Maunus (1998). In these investigations the load carrying capacity is found to be not only dependent of moisture state but also on moisture history. The hygroscopic nature of wood and the internal constraint of shrinkage/swelling strains can explain this moisture history dependency. In a natural variable climate wood material will strive towards moisture equilibrium, hence moisture gradients will occur in solid wood. The moisture gradients induce internal stress. It has been shown that internal stresses in solid wood caused by a variation of ambient climate alone can reach high levels compared to the strength (Young and Norris (1959)). In extreme cases stress levels of 50% of the strength are possible (Svensson

and Toratti (1997)). Little research has been published in the area determining the internal stress in solid wood across the grain for natural climate. The present study will focus on how to measure internal stress in glued laminated wood since most structural elements enduring stresses perpendicular to the grain concerns glulam. Results showing the magnitude of internal stress will also be presented herein.

2 Material and method

2.1 Test specimen

All specimens used in the experiment were sawn from glulam beams with the standard size 90x270mm. The beams contain 6 lamellae of Norway Spruce. The glulam beams were manufactured by Moelven Töreboda Limträ AB, Sweden and taken directly from the production line. The thickness of the test specimens were chosen to 16mm, giving the specimens the dimensions h=270, b=90 and t=16mm. To succeed with the technique of cutting specimens, later described, only specimens more or less free from knots could be used. A total of 44 test specimens were used in the present test series see table 1.
To ensure that the test specimens were cut without uncontrolled formation of cracks, each specimen was provided with 10 elliptical holes as shown in figure 1. With this preparation each slice will become about 8mm wide. Markers, white dots on a black background were glued along each short side of the specimen see figure 1. These markers are measuring points and enable deformation measurement using a digital camera technique, described in next section. A test group contains of 4 specimens, each group was selected from the glulam beam with the aim to acquire the same material and physical properties.

2.2 Test program

The test sample of 44 specimens was divided into two groups, 24 reference and 20 gradient specimens. One half of the test sample, 12 reference specimens and 10 gradient specimens, was seasoned in RH 40%, 20°C and the other half was seasoned in RH 80 %, 20°C. When the specimens reached equilibrium the gradient specimens were moisture sealed on four sides. The sealing ensures one-dimensional moisture transport as shown in figure 1. After sealing the gradient specimens were put in the other climate i.e. the specimens seasoned in RH 40% were put in RH 80% and vice versa.

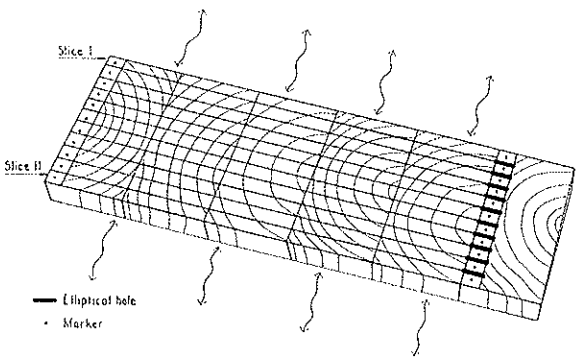

Figure 1. Test specimen.

The reference specimens were used to determine the existence of internal stresses in uniform moisture conditions and the variation of modulus of elasticity over the cross-section. The 20 gradient specimens were used to measure internal stresses caused by formation of a moisture gradient. The test schedule is given in table 1.To be able to evaluate the stresses the modulus of elasticity has to be determined. This was done on the reference group in RH 40% and RH 80%. In this study the dynamic modulus of elasticity was measured. These values were then converted to static modulus of elasticity according to figure 6. There were two reasons for using a dynamic measurement method, the ease and speed of testing and the fact that the thin slices are not suitable for a customary tensile test.

Table 1. Number of test specimens and day of test after climate change.

Test	FF40	FF80	FF40-80	FF80-40
Number of specimens	12	12	10	10

Test		FF40-80	FF80-40
Day of test	1	2st	2st
	3	2st	2st
	5	2st	2st
	7	2st	2st
	9	2st	2st

2.3 Test methods

2.3.1 Modulus of elasticity

A dynamic test method was used to determine the variation of the modulus of elasticity across the cross-section. It is based on finding the resonance frequency for a sample, in this case a thin slice, when excitated. A commercial equipment GrindoSonic Mk5® was used. By placing the thin slice on a foam rubber and hitting it at one end with a small hammer and receiving the wave at the other end, it is possible to determine the resonance frequency for the first axial mode. Using the measured frequency and equation (1) the dynamic modulus of elasticity can be calculated, see e.g. Spinner and Tefft (1961).

$$E_{dyn} = f^2 \frac{4ml}{hw} \qquad (1)$$

where f is measured frequency, m is the mass, l, h, w are the length, height and width of the specimen.

The correlation between the static and dynamic modulus was investigated on a test series consisting of 100 specimens. The specimens were seasoned in four different climates (RF 40, 60, 65 and 80%), and different specimens contain different amount of radial and tangential growth rings. The dimensions of the specimens were l=270, h=w=12 mm and contain 5 lamellae. The static modulus of elasticity is therefore an average value over the measuring length. The static tensile test was carried out in an MTS®-machine and the deformation in the loading direction was determined by extensometers. The slope in the $\sigma - \varepsilon$ diagram gave the

static modulus of elasticity. For all specimens the slope was determined between $\varepsilon = 6.7 \cdot 10^{-4}$ and $5.3 \cdot 10^{-3}$.

2.3.2 Deformation

Deformations were measured with a contact free technique, using a digital camera as measuring device. The specimen was first photographed when placed in the cutting apparatus, see figure 2, just before cutting and then just after cutting. The slicing technique is described in Svensson & Toratti (1997) and was modified in this study. The photographed images were then processed in a commercial computer program, Matlab® with an image process application (Heyden 1999). With this application the positions of the markers on the specimens are determined for both images. Deformations in each slice were calculated from the change of position for the two markers. Due to the chosen location of the markers, end effects on the internal stress field were included in the measured result. The stresses, later presented, were calculated directly from these measurements and are therefore the average stress (σ) in each slice presented in equation 2. The moisture content was measured in each slice
directly after cutting the specimen. This means that the modulus of elasticity for the gradient specimens was calculated according to figure 5.

$$\sigma = \varepsilon E(u) = \frac{\Delta l}{l} E(u) \qquad (2)$$

where ε is the strain, E the modulus of elasticity as a function of moisture content, Δl is the length change and l is the length between the two markers.
There must be force and moment equilibrium in the test specimen. This is not initially obtained because of several reasons: incorrectness in the measuring of the dynamic modulus of elasticity, incorrect translation from the dynamic modulus of elasticity to static modulus of elasticity, the difficult to measure the width in each thin slice, the camera lens (plan surfaces tendens to curve) and the fact that the camera was not perpendicular to test specimen. The presented stresses in figure 7 to 10 are adjusted, thus force and moment equilibrium are insured.
The problem with the camera can be excluded if using a different camera with replaceable lenses and using a copying easel when taking pictures. In further research this source of errors will be eliminated.

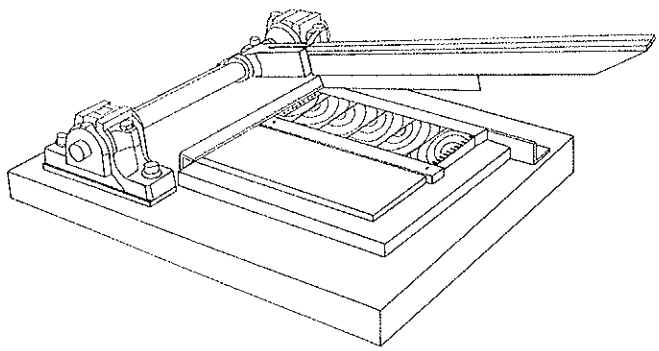

Figure 2. Slicing apparatus.

The distance between camera and specimen, the size of specimen and camera resolution determines the image resolution. The resolution of the camera used as measuring device is 1536x1024 pixels. In this specific test each millimetre contain seven pixels on the image. The image-processing program increases the image resolution, using the grey-scale resolution in the image. The images have 256 levels in the grey-scale including black and white. It is then theoretically possible to increase the image resolution 254 times but in practice, however, the image resolution is increased by 10-100 times (Heyden 1999). If the lower value is used the measuring accuracy of the present experiment is as least 1/70 mm. For the stress calculation this results in an accuracy of at least 0,02 MPa.

3. Results and discussions

The dynamic modulus of elasticity for each slice belonging to reference specimens seasoned in RH 40% and 80% are shown in figure 4. The results were taken as the average from 12 tested specimens.

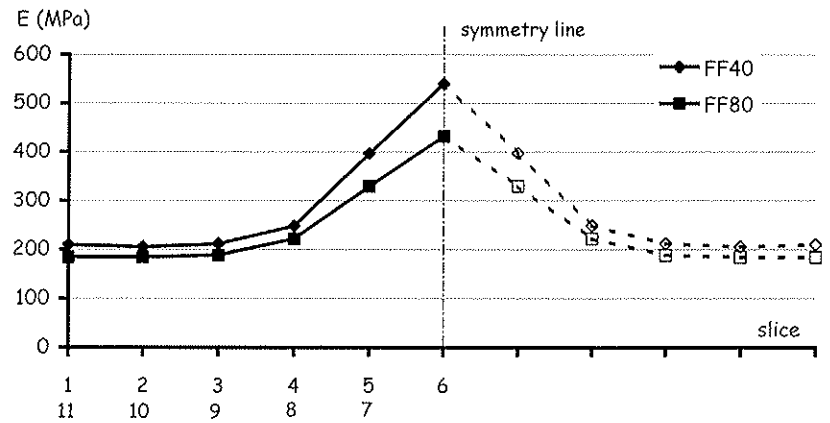

Figure 4. Dynamic modulus of elasticity for reference specimens seasoned in RH 40% (upper curve) and RH 80% (lower curve), corresponding to moisture content 9 and 16 %.

To explain figure 4 it is necessary to pay attention to the annual ring pattern i.e. the inclination of growth rings in relation to measuring direction. The modulus of elasticity has its greatest value in the radial direction. The value in tangential direction is approximately 60% of radial value. In an angle between radial and tangential direction the modulus of elasticity have its lowest value, only about 20% of the radial, Bodig & Jayne (1982). By observing the growth rings in the lamellae is it possible to establish that the four outermost slices have an orientation between radial and tangential. The modulus of elasticity in the middle slice (radial direction) is slightly lower than excepted see e.g. Kollman & Cote (1968). This depends on a number of factors e.g. high amount of juvenile wood and the fact that the pith between the different lamellae are displaced laterally. The displacement gives a deviation from pure radial wood.
The modulus of elasticity is dependent on moisture content. Lower moisture content increases modulus of elasticity. Figure 4 also shows that the modulus of elasticity in the four outermost slices is nearly constant, while the modulus of elasticity increases in the remaining slices with

increasing amount of radial wood. The measured relation between modulus of elasticity and moisture content is illustrated in figure 5.
The relation between static and dynamic modulus of elasticity is shown in figure 6. Dynamic modulus of elasticity is about 30% larger then the static one.

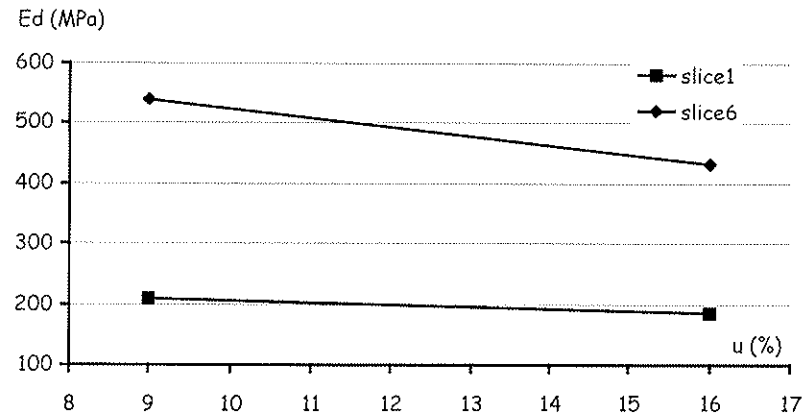

Figure 5. Dynamic modulus of elasticity versus moisture content.

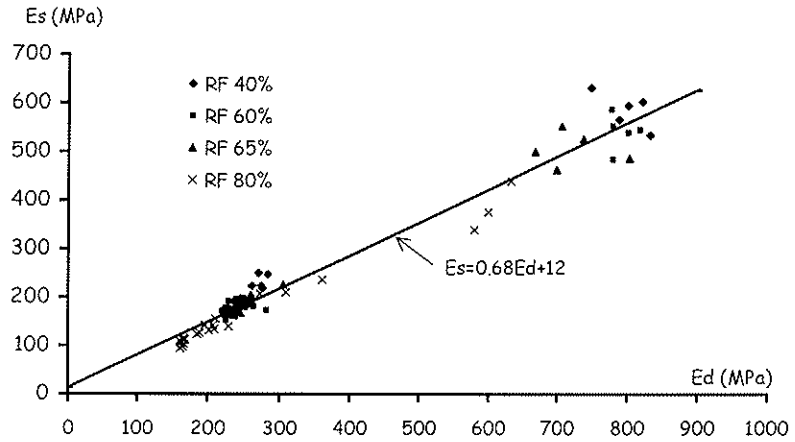

Figure 6. Static modulus of elasticity versus dynamic modulus of elasticity.

Figure 7 and 8 shows the internal stress distribution determined in specimen seasoned in RH 40% and 80%. When the glulam beams were delivered from the factory their moisture content were between 10-14%. When the test specimens were seasoned in RH 40% and RH 80% desorption and absorption, respectively, occurred. When wood dries/moistens the shrinkage/swelling is larger in the tangential direction than in the radial direction. This explains the stress state for the reference specimens. The middle slices in the specimen contain more radial material direction coinciding with measuring direction than the outermost slices, see figure 1. For the case with uniform drying (FF40) the outermost part of the specimens is constrained from shrinkage by the middle, this results in the internal stresses presented in figure 7. For the case with uniform moistening (FF80) the result will be the opposite as shown in figure 8. The largest tensile stress, approximately 0,2 MPa, was found in this case.
The stress was based on each specific slice width, height and modulus of elasticity.

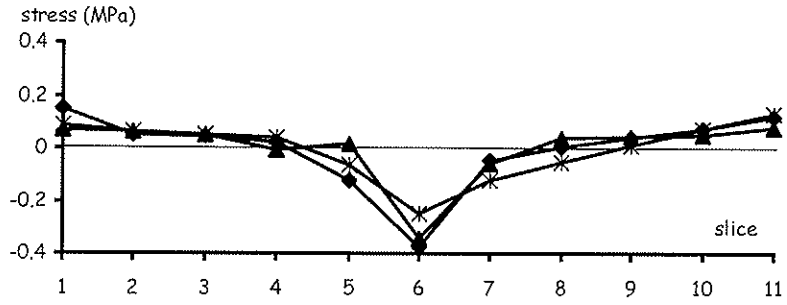

Figure 7. Internal stresses for three different test specimens seasoned in RH 40%.

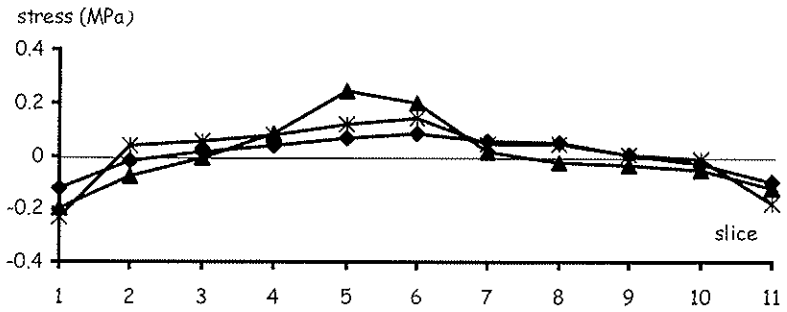

Figure 8. Internal stresses for three different gradient specimens seasoned in RH 80%.

Internal stresses are shown after 24, 120 and 216 hours for different gradient specimens, see figure 9 and 10. Different slices have different moisture content. The dynamic modulus of elasticity of each slice in gradient specimens, was directly taken from the corresponding slice in figure 4. These values were then corrected for moisture content, see figure 5. According to figure 6 the transformation from dynamic to static modulus of elasticity will be:

$$E_s=0,68E_d+12 \qquad (3)$$

where E_s is static modulus of elasticity and E_d dynamic modulus of elasticity. E_s was used to calculate the stresses shown in figure 7-10. In the future work the dynamic modulus of elasticity of each specific slice will be evaluated directly with the help of GrindoSonic Mk5®.
In the specimens, which changed from RH 40% to 80%, tensile stresses arise in the middle of the test specimen and increases with time. This phenomenon is more difficult to observe in the outermost slices. For the other test group (RH 80-40%), the internal stress distribution is the opposite and tensile stress arise in the outermost slices and in the middle compression stress occurs. The stress distribution seems to be more or less independent in time.
Drying specimens give lower stresses than moistening. The largest stresses in these two test groups differ by approximately a factor 2. Despite the steeper gradient of moisture content in FF80-40, it has a lower level of stress than FF40-80. The reason why the gradient of moisture content varies between these two test groups can be explained by the hysteresis effect. The

desorption isotherms gives a greater difference in moisture content than the corresponding adsorptions isotherms gives with given relative humidity, see e.g. Stamm (1964).

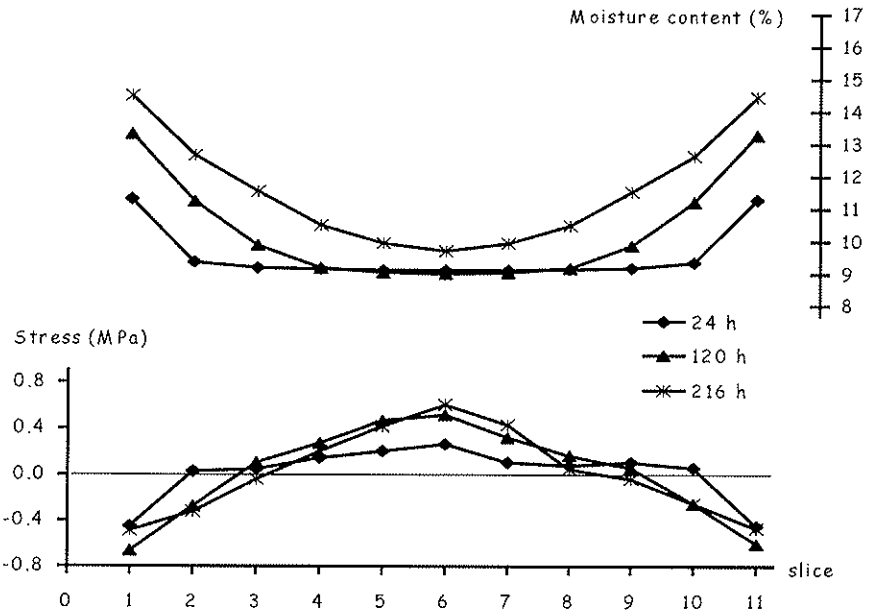

Figure 9. Internal stresses and moisture content after 24, 120 and 216 hours. Climate variation from RH 40% to RH 80%

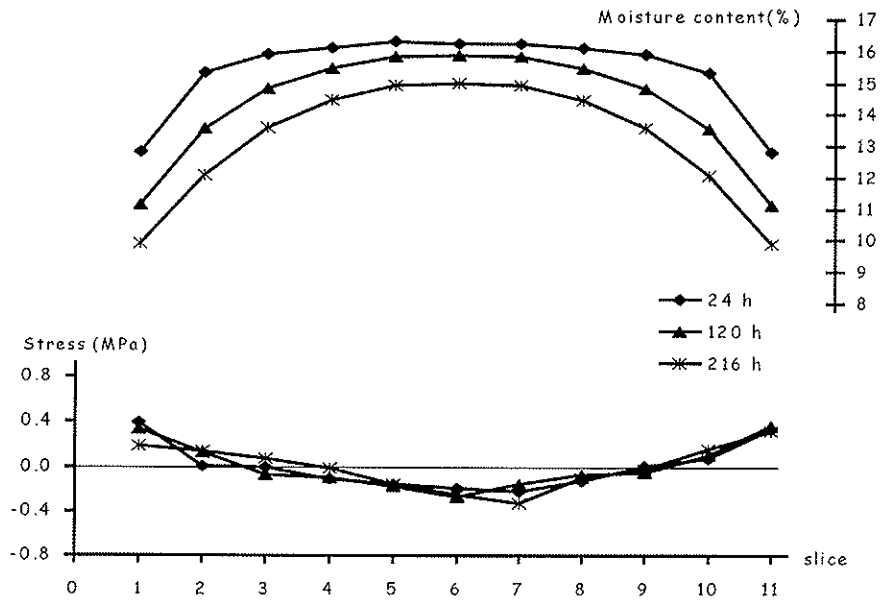

Figure 10. Internal stresses and moisture content after 24, 120 and 216 hours. Climate variation from RH 80% to RH 40%

4. Conclusions

In the experimental part of this study a contact free measuring technique was used. It turned out to be a fast and easy way measure the deformations. The speed of measuring is important since small test specimens are used, a change of moisture content is not tolerable. The accuracy is acceptable (1/70 mm), but can be improved by using a camera with a higher resolution. A dynamic test method was used to determine the modulus of elasticity, mainly for two reasons, the speed of measuring and the fact that the slices were not suitable for a customary tensile test. The relationship between E_s and E_d for different moisture content and varying annual ring pattern can be treated as linear.
The following conclusions can be drawn from this study.

- There is little difference between the value of modulus of elasticity for the four outermost slices. As expected the modulus of elasticity increases with increasing amount of radial wood.
- The influence of moisture content on the modulus of elasticity is most dominant on the slices in the middle part of the specimen.
- The modulus of elasticity for the middle part of the specimen is between 2-2,5 times the outermost part.
- In seasoned specimens i.e. uniform dried and moistened specimens, there were internal stresses!
- The maximum tension and compression stress for seasoned specimens was approximately 0,4 and 0,2 MPa.
- The stress level between the two groups of gradient specimens differs with approximately a factor 2.
- Results for specimens with induced moisture gradient shows that the stresses become larger for moistening from a specific climate RH 40% to another climate RH 80% than drying from RH 80% to RH 40%.
- The largest mean stress level was about 0,7 MPa, which is larger than the characteristic value of tensile strength perpendicular to the grain!

References

Aicher, S., Dill-Langer, G., Ranta-Maunus, A. 1998. Duration of load effect in tension perpendicular to grain of glulam in different climates. Holz als Roh- und Werkstoff 56, Springer-Verlag

Bodig, J., Jayne, B.A.. 1982. Mechanics of Wood and Wood Composites. Van Norstrand Reinhold Co. Ltd., New York

Gustafsson, P-J., Hoffmeyer, P.,Valentin, G. 1998. DOL effect on end-notched-beams. Holz als Roh- und Werkstoff 56, Springer-Verlag

Heyden, H. 1999. Matlab-file, bildmenu.m

Kollman, F.F.P., W.A. Cote 1968. Principles of Wood Science and Technology. Springer-Verlag, Berlin, Heidelberg

Morlier, P., Ranta-Maunus, A.1998. DOL effect of different sized timber beams. Holz als Roh- und Werkstoff 56, Springer-Verlag

S.K. Jensen, P. Hoffmeyer. 1996. Mechano sorptive behaviour of notched beams in bending. Technical ,University of Denmark

Siimes, F.E. 1967. The effects of specific gravity, moisture content, temperature and heating time on the tension and compression strength and elasticity properties perpendicular to the grain of Finnish pine, spruce and birch wood and the significance of these factors on the checking of timber at kiln drying. VTT Report 84, Helsinki

Svensson, S., Toratti, T. 1997.Mechanical Response of Wood Perpendicular to Grain when Subjected to Changes of Humidity. Structural Engineering, Lund Institute of technology

Youngs, R.L., Norris, C.B. 1959.Internal stress in wood. Forest Products Laborator, Forest Service U.S. Department of Agriculture

INTERNATIONAL COUNCIL FOR RESEARCH AND INNOVATION
IN BUILDING AND CONSTRUCTION

WORKING COMMISSION W18 - TIMBER STRUCTURES

MOMENT CAPACITY OF TIMBER BEAMS LOADED IN FOUR-POINT BENDING AND REINFORCED WITH PUNCHED METAL PLATE FASTENERS

by

J Nielsen
Department of Building Technology and Structural Engineering
Aalborg University

DENMARK

MEETING THIRTY-THREE
DELFT
THE NETHERLANDS
AUGUST 2000

Presented by: J. Nielsen

· M. Ansell suggested that using bonded plates (full depth) on both sides with adhesive as solution.
· J.Nielsen stated that economic might not allow for this solution.
· S. Thelandersson asked whether there was the economic thinking on what can be gained through impact analysis of more pay (value added) for high strength.
· J. Nielsen responded that intention was to decrease the required depth with reinforcement to arrive at a safe and efficient solution.
· L. Stehn stated that in Swedish analysis in economic gains would be available.
· S. Svensson suggested that the increase in stiffness via reinforcement might prove to be important for beam and joist applications.

Moment Capacity of Timber Beams Loaded in Four-Point Bending and Reinforced with Punched Metal Plate Fasteners

Jacob Nielsen
Department of Building Technology and Structural Engineering
Aalborg University, Sohngaardsholmsvej 57, DK-9000 Aalborg, Denmark
e-mail: jn@civil.auc.dk

1 Abstract

Tests on timber beams reinforced with punched metal fasteners are continued. The reinforced beams are loaded in four-point bending. The timber is Swedish spruce with cross sectional area of 45×120 mm and 45×170 mm. The reinforcement is from Gang-Nail Systems, types GNA20S and GNT150S. Beams with lateral reinforcement and beams with reinforcement located at the short edge are tested. The tests and the results are described.

2 Introduction

In 1999 some tests were made on timber beams reinforced with punched metal fasteners of type GNA20S. Beams with 120 and 170 mm cross-sectional depth were tested in 3-point bending to analyse the effect of reinforcement in areas with a moment peak. It was found that the reinforcement had an increasing effect on the bending strength and the stiffness for beams with 120 mm depth. For 170 mm beams no effect was found on the strength. The tests are described in Nielsen (1999) and Nielsen et al. (1999), where also the motivation for the work is given.

This year the work has been continued. In order to analyse the effect of a reinforcement the following has been performed:

- All tests are loaded in 4-point bending according to DS/EN 408.
- In order to obtain matching series the average stiffness for each series is sought to be equal.
- Beams in strength classes K18 and K24 and with cross-sectional depths of 120 mm and 170 mm are tested.

- The length of the reinforcement is the same as the span of the beam, see figure 1.
- Two types of plate location are used. One type with lateral reinforcement (one plate on each side) and one type with a reinforcement plate located at the small edge of the beam. All plates are located at the tensile edge.
- Two types of plate with different material thickness (1 and 1.5 mm) are tested.

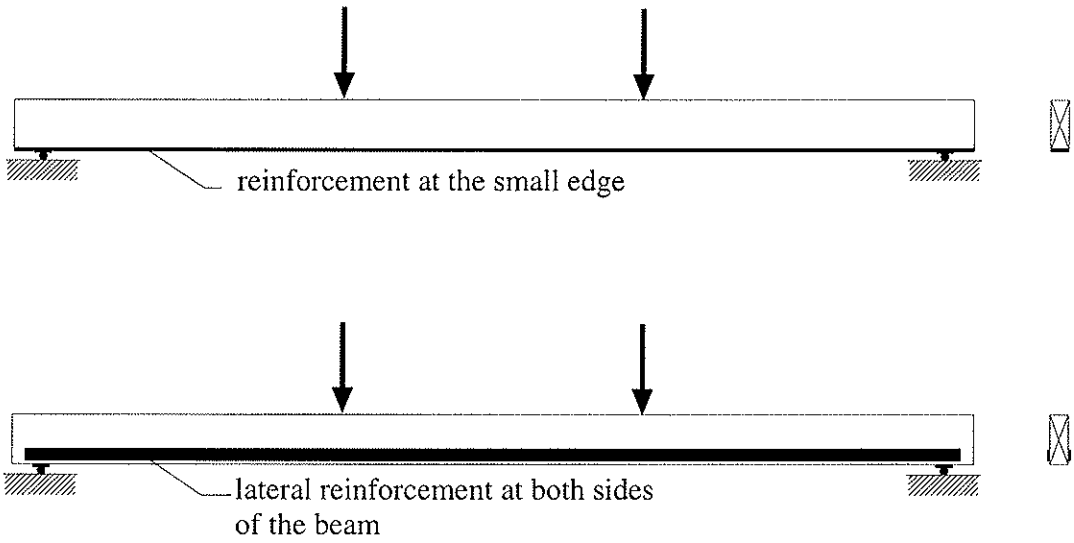

Figure 1: Location of reinforcement on beams in 4-point bending.

3 Test series

The applied timber is Swedish spruce with cross-sections of 45×120 and 45×170 mm. The dimensions of the beams and the test setup are shown in figure 2.

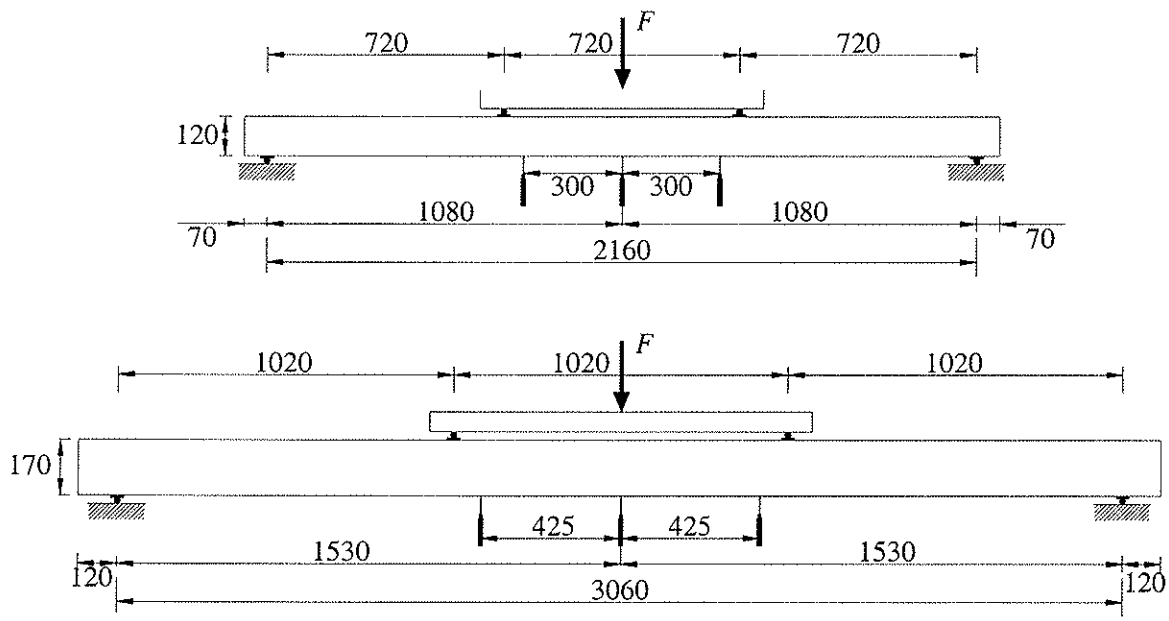

Figure 2: 120 and 170 mm beams in 4-point bending. Dimensions in mm.

The timber was selected and graded by a truss plant. When conditioned at 65% relative humidity and 21°C for some weeks the bending E-modulus of each beam was determined by measuring the displacements of the beams at load levels corresponding to 13% and 50% of the characteristic bending strength of K18 beams.

The E-modulus of a beam was defined as the average of two bending E-moduli found in four-point bending around the strong section.

When the E-modulus of each beam is known the beams are divided into two groups. All beams with a stiffness in the lower half are defined as beams of strength class K18 and all beams with a stiffness in the upper half are defined as beams of strength class K24. The beams for each series are then selected so the mean and standard deviation for the E-modulus are equal for each series within the same strength class.

The timber beams in series with reinforcement are then conditioned and manufactured according to prEN1075. During testing the moisture content of the timber is between 9-12%.

GNA20S or GNT150S plates from Gang-Nail Systems are used as reinforcements. The data of the plates are given in table 1.

Plate type		GNA20S	GNT150S
Plate (tooth) thickness	mm	1.0	1.5
Tooth length	mm	7.9	14.3
Tooth width	mm	2.9	3.1
Nail density	nails/cm^2	1.47	0.72
Tooth distance in main direction	mm	9/11	20.5
Tooth distance perp. to main direc.	mm	7	7.1
Characteristic tensile strength	N/mm	268	433

Table 1: Data of the reinforcing plates.

The plates were embedded at the truss plant with a hydraulic pressing tool. There were difficulties in embedding these plate sizes and embedding plates on the edge of the timber. When embedding lateral reinforcements in one step some of the timber tends to split parallel to the grain in a line close to the inner edge of the plate. To handle this problem the plates are embedded in smaller steps.

When embedding the reinforcement at the small side some beams tend to split in compression. This was mainly due to the control of the pressing tool. In many cases the plates were only partially embedded, since small gaps of 0-3 mm were found between the wood and the plate. As the number of teeth is high and they are located close to the timber edge, splitting cracks were observed in many cases.

Due to difficulties at the embedding process some of the tests were discarded.

12 different series with different cross sectional area, grade, plate type and plate location are made. There are planned 10 equal tests in each series. The test programme is shown in table 2. Only plates of type GNT150S are used in series with 170 mm beams.

Series no.	Timber		Plate		
	size mm × mm	strength class	size mm × mm	type	location
S1	45x120	K18	-		
S2	45x120	K24	-		
S3	45x120	K18	34x2200	GNA20S	lateral
S4	45x120	K24	34x2200	GNA20S	lateral
S5	45x120	K24	34x2200	GNA20S	edge
S6	45x120	K24	37x2200	GNT150S	edge
S7	45x170	K18	-		
S8	45x170	K24	-		
S9	45x170	K18	37x3100	GNT150S	lateral
S10	45x170	K24	37x3100	GNT150S	lateral
S11	45x170	K18	37x3100	GNT150S	edge
S12	45x170	K24	37x3100	GNT150S	edge

Table 2: Test program with 12 different series.

4 Results and discussion

The average failure loads are given in the tables 3 and 4. The failure load is given as a maximum measured value of the total load F, see figure 2. The mean value m and the coefficient of variation δ are calculated according to DS/EN 1058.

Series No.	Strength class	Plate		Number of tests	Failure load (F)	
		type	location		m [kN]	δ [%]
S1	K18	-	-	10	11.5	31
S3	K18	GNA20S	lateral	8	13.9	21
S2	K24	-	-	10	16.2	18
S4	K24	GNA20S	lateral	8	15.0	14
S5	K24	GNA20S	edge	7	14.4	14
S6	K24	GNT150S	edge	10	15.8	16

Table 3: Average failure load of series the with 120 mm beams.

Series No.	Strength class	Plate location	Number of tests	Failure load (F)	
				m [kN]	δ [%]
S7	K18	-	10	15.2	16
S9	K18	lateral	10	15.8	16
S11	K18	edge	10	14.9	16
S8	K24	-	10	20.4	22
S10	K24	lateral	7	20.2	17
S12	K24	edge	10	19.1	14

Table 4: Average failure load of the series with 170 mm beams.

In the tables 3 and 4 it is seen that the reinforcement only has a significant effect on 120 mm K18 beams (S3) which have a 20% higher average failure load than series S1. In other series the reinforcement has no effect on the average failure load. The above results apply the results in Nielsen (1999) and Nielsen et al. (1999).

In general the failure becomes more brittle in tests with a reinforcement. During loading the plates reduce the speed of a crack development, but at some stage the plate becomes plastic and in some cases plate failure will occur. The extent of the plastic zone is seen in figure 3. The locally increased plastic deformation in the plate at the knot causes the plate to buckle during unloading.

Figure 3: Extension of the plastic zone at a knot of an unloaded test in series S11.

The above fact indicates that both the strength and the stiffness of the plate types used are too small to have any reinforcing effect. As the plates are found to be weak in average it might be expected that the plate would have an effect on the beams with a low bearing capacity only. In the figures 4 and 5 the distribution of the failure load in each series is shown.

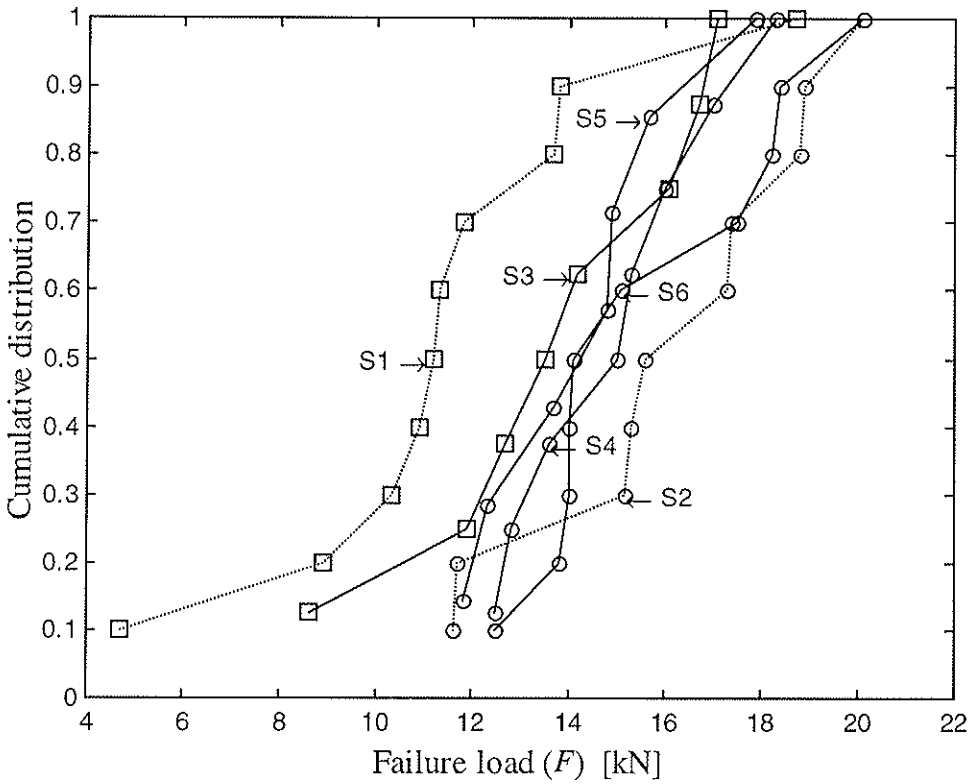

Figure 4: Distribution of the failure load of 120 mm beams.

Solid and dotted lines are used for beams with and without reinforcement, respectively. Squares and circles markers are used for K18 and K24 beams, respectively.

When comparing S1 and S3 in figure 4 the effect of the reinforcement is distinct. However, the distribution of failure loads of K24 beams with a reinforcement (S4, S5 and S6) is very much the same or even less than the beam without reinforcement (S2).

In figure 5 it is found that the reinforcement has no effect on the failure load for 170 mm beams. The difference between the two strength classes is clear.

In total it can be concluded that the reinforcement only has an increasing effect on 120 mm beams in strength class K18. In all other cases the reinforcement has no effect on the failure load – even in series with low capacity of the timber.

The tendency found in series S4, S5 and S6 raises the question: Does the reinforcement cause a weakness of the beam? GNA20S and GNT150S reinforcements located on the edge cut more than 30% of the fibres at the tensile edge. During loading there was found no withdrawal of the teeth in any plates. A solution might be to use a reinforcing plate with less teeth density. This will increase the strength and stiffness of the plate and, furthermore, the embedding problems will be minimal as the needed embedding force will be reduced.

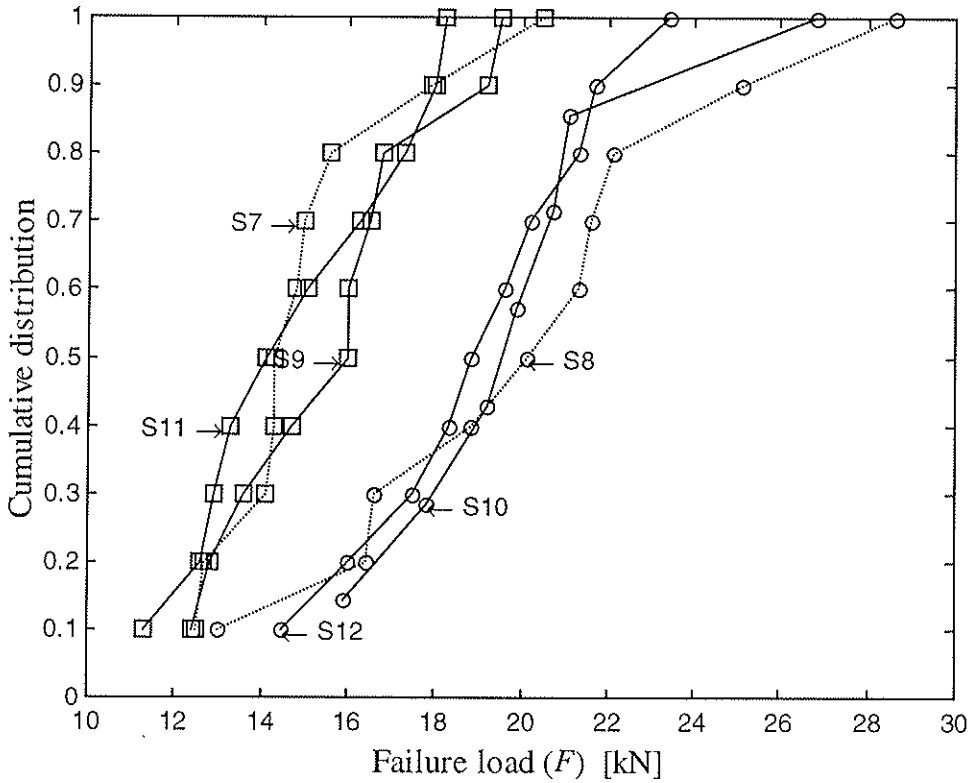

Figure 5: Distribution of the failure load of 170 mm beams.

Stiffness

In table 5 the average E-modulus of each series is given.

Series	E_{before} [MPa 10^{-3}]	E_{after} [MPa 10^{-3}]	Corr. [%]
S1	11.1	11.7	7
S3	10.4	14.5	62
S2	14.2	17.8	32
S4	14.2	18.2	62
S5	14.2	19.0	77
S6	14.0	21.8	20
S7	10.1	8.9	55
S9	8.9	11.0	-7
S11	9.5	10.7	36
S8	13.3	12.8	59
S10	13.7	12.9	37
S12	13.9	13.4	74

Table 5: Average E-modulus of each series.

E_{before} is calculated as described in section 3. E_{after} is based on linear regression of the straight-line portion of the deformation curve. The E-moduli are calculated for the same bending direction. The correlation coefficient between E_{before} and E_{after} in each series is also given in table 5.

No correlation is found in series S1, S2, S6, S7, S9, S10 and S11. There is found no explanation for this result.

The reinforcement increases the stiffness with more than 20% for 120 mm K18 beams. For 120 mm beams in strength class K24 the increasement is only 5-20%. The high stiffness values are found for the series with GNT150S on the edge.

For 170 mm K18 beams the stiffness increasement is ~20%. There is not found any significant effect on the stiffness for 170 mm beams in strength class K24.

In general the tests with a reinforcement become more brittle and the load displacement curves for these tests have distinct plastic path before failure. A failure in combination with compression failure of the wood is found in more than half of the tests with a reinforcement.

5 Conclusion

Based on the tests the following conclusions can be made:

- The reinforcement increases the strength and stiffness of 120 mm beams in strength class K18 by 20%.
- The reinforcement has no effect on the strength of 120 mm in strength class K24. However, the stiffness increases by 5-20%.
- The reinforcement has no effect on the strength of the 170 mm beams. . However, the stiffness increases by ~20% for 170 mm beams in strength class K18.

In further analysis is it recommended to use reinforcing plates with a less teeth density. This will increase the strength and stiffness of the reinforcement and it may also reduce the embedding difficulties as the needed embedding force is less.

6 References

- Nielsen (1999), Analysis of Timber Reinforced with Punched Metal Plate Fasteners, Proceedings of CIB-32, Graz, August 1999.
- Nielsen et al. (1999), Moment Capacity of Timber Reinforced with Punched Metal Plate Fasteners, Proceedings of the 1st RILEM Symposium on Timber Engineering, Stockholm, Sweden, September 13-15, 1999, pp 129-137, ISBN 2-912143-10-1.
- DS/EN 408 Timber Structures – Structural Timber and Glued Laminated Timber – Determination of some Physical and Mechanical Properties. European Standard, CEN January 1995.
- prEN 1075 Timber Structures – Test Methods – Joints made of Punched Metal Plate Fasteners. European Standard, CEN, May 1999.
- DS/EN 1058 Wood-Based Panels – Determination of Characteristic Values of Mechanical Properties and Density. European Standard, CEN, July 1995.

INTERNATIONAL COUNCIL FOR RESEARCH AND INNOVATION
IN BUILDING AND CONSTRUCTION

WORKING COMMISSION W18 - TIMBER STRUCTURES

LATERAL LOAD CAPACITIES OF HORIZONTALLY SHEATHED UNBLOCKED SHEAR WALLS

by

C Ni
E Karacabeyli
Forintek Canada Corp., Vancouver, British Columbia

CANADA

A Ceccotti
Universities of Florence and Venice

ITALY

MEETING THIRTY-THREE
DELFT
THE NETHERLANDS
AUGUST 2000

Presented by: E. Karacabeyli

· H. Blass asked about the rationale of horizontally sheathed shear walls and whether the same rationale for plywood would apply to OSB.
· E. Karacabeyli stated that 3-layer 9.5 mm OSB would be similar to plywood in terms of orientation; therefore, the same rationale would also apply. This is also important for industrial building with unblocked high walls in low seismic zones.
· M. Yasumura stated that from FEM analysis significant bending in the studs are observed in unblocked shear walls. Vertical loads will be more important for these walls.
· E. Karacabeyli responded that vertical loads would be important for cases without holddowns.
· M. Yasumura stated that large bending deformation of the studs would lead to second order effects from vertical loads.
· E. Karacabeyli responded that he would check whether vertical loads were applied in the tests.

Lateral Load Capacities of Horizontally Sheathed Unblocked Shear Walls

Chun Ni
Forintek Canada Corp., Vancouver, British Columbia, Canada

Erol Karacabeyli
Forintek Canada Corp., Vancouver, British Columbia, Canada

Ario Ceccotti
Universities of Florence and Venice, Italy

Abstract

Although design capacities for unblocked diaphragms are available in many design codes, capacities for unblocked shear walls are not. None the less, in applications such as exterior wall sheathing, the wood-based panels are, at times applied horizontally to the wall frame without blocking. There is a need, identified by the engineering community, for the determination of lateral load carrying capacities of unblocked shear walls. Full-scale tests were performed on unblocked shear walls. The results showed that typical failures occur along the unblocked horizontal joint where the nails either withdraw from the framing members or pull through the panel. Based on the test results, strength adjustment factors for unblocked shear walls are proposed. It was found that the factored design shear strengths for unblocked shear walls were reasonably conservative when compared to test results obtained in this study and also to the test results available in the literature.

1. Introduction

Platform-frame wood structures have generally performed well under seismic events (Rainer and Karacabeyli, 1999). This is primarily due the many shear walls present in the platform-frame wood structures which provide sufficient lateral load resistance against earthquakes.

The current Canadian Standard for Engineering Design in Wood (CSA, 1994) provides design values for shear walls sheathed with wood-based panels either oriented vertically, or horizontally with framing blocking. However, in British Columbia, Canada it is quite common to use shear walls sheathed horizontally with wood-based panels without blocking (Figure 1). Although there are design values for unblocked diaphragms, values for unblocked shear walls are not available.

In this study, full-scale shear walls were tested under static and reversed cyclic displacement schedules. Based on the test results, strength adjustment factors are proposed for unblocked shear walls.

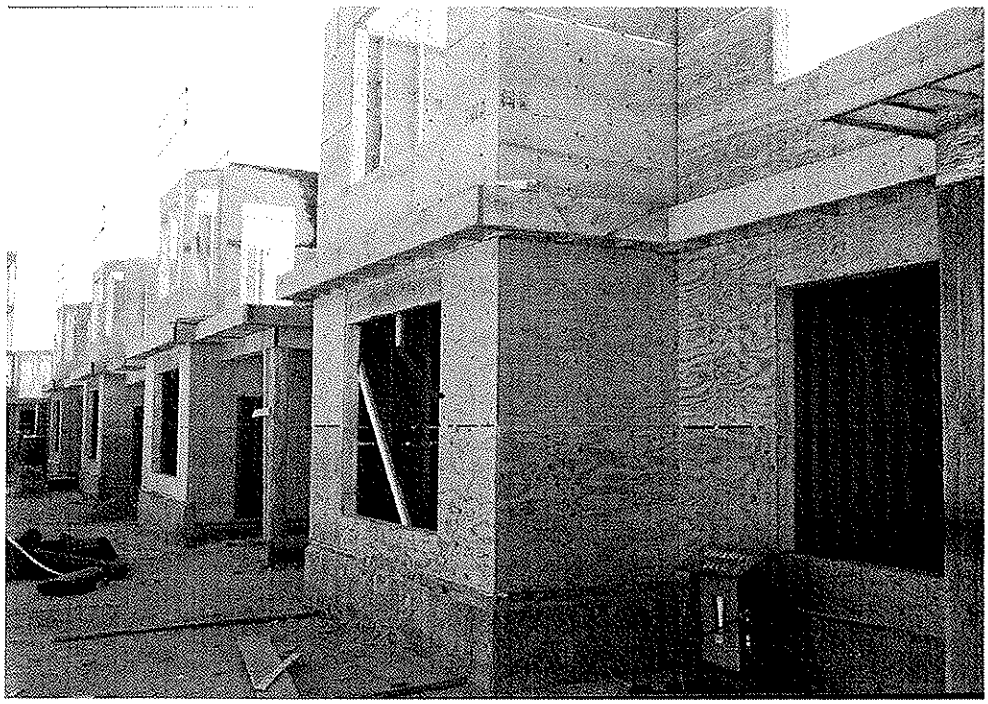

Figure 1. Unblocked shear walls.

2. Test Program

2.1. Test Wall Configuration

Three types of unblocked shear walls (2.44 m in height and 4.88 m in length) and reference blocked shear walls were tested under ramp and reversed cyclic tests. The configurations of the wall types are shown in Figure 2. Wall type 1 has a horizontal gap in the middle of the wall; wall type 2 has two horizontal gaps with a 305 mm wide panel strip in the middle of the wall; and wall type 3 has staggered horizontal gaps at a distance of 610 mm from each other. For all unblocked shear walls, the horizontal gap between panels is 12.5 mm.

All shear wall specimens were constructed using NLGA No. 2 and better grades of Spruce-Pine-Fir 38 mm × 89 mm lumber for the wall studs, and 1650f-1.5E MSR 38 mm × 89 mm lumber for the top and bottom plates. The top plate and the end studs consisted of double members, while the bottom plate and the interior studs consisted of single members. Canadian Softwood Plywood (CSP), 9.5 mm thick, was used as sheathing panels, and was connected to the framing members with type 8d smooth shank power nails. The detailed information about the shear wall test specimens is listed in Table 1.

For each wall configuration, two specimens were tested: one under static and another one under reversed cyclic displacement schedule. Although testing more replicates per wall configuration would be desirable, because of the low variability observed in previous tests, two specimens per configuration are considered to give acceptable mean values for lateral load resistances and displacements.

Conditioning and testing were performed at ambient laboratory conditions where average oven-dry moisture content of both lumber and the plywood were approximately 9 percent. The average oven-dry relative density of the lumber was approximately 0.44.

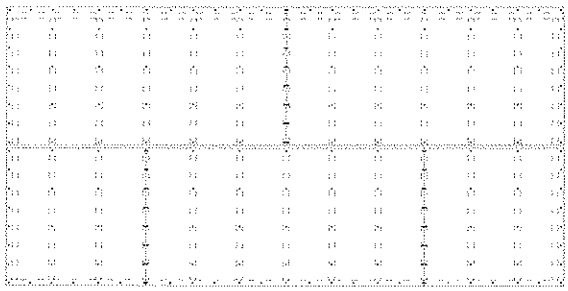

a) Type 1

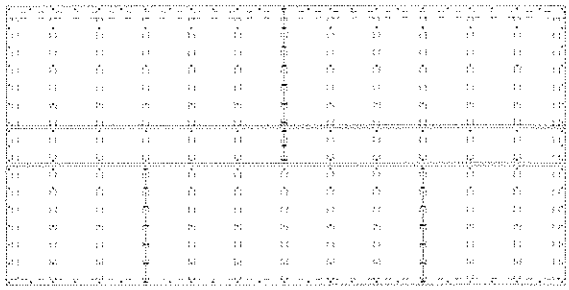

b) Type 2

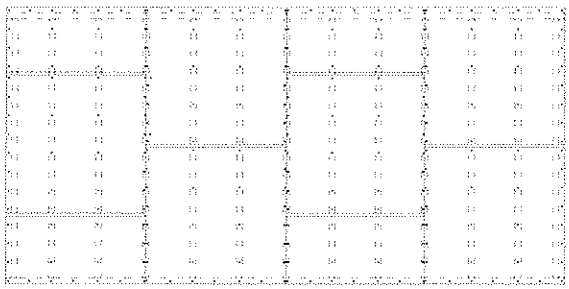

c) Type 3

Figure 2 Configurations of unblocked shear walls.

Table 1 Test matrix of blocked and unblocked shear walls.

Specimen	Load protocol	Type	Vertical load (kN/m)	Panel	Stud spacing (mm)	Nails size	Nail spacing (mm)	
							Supported edges	Intermediate studs
22-02	Ramp	Blocked	0	9.5mm CSP	406	Power 8d	150	300
22-03	FCC93	Blocked	0	9.5mm CSP	406	Power 8d	150	300
29-01	Ramp	1	0	9.5mm CSP	406	Power 8d	150	300
29-02	FCC93	1	0	9.5mm CSP	406	Power 8d	150	300
31-01	Ramp	Blocked	18.2	9.5mm CSP	406	Power 8d	150	300
31-02	FCC93	Blocked	18.2	9.5mm CSP	406	Power 8d	150	300
51-01	Ramp	1	18.2	9.5mm CSP	406	Power 8d	150	300
51-02	FCC93	1	18.2	9.5mm CSP	406	Power 8d	150	300
51-05	Ramp	1	18.2	9.5mm CSP	305	Power 8d	150	150
51-06	ISO98	1	18.2	9.5mm CSP	305	Power 8d	150	150
51-07	Ramp	1	18.2	9.5mm CSP	406	Power 8d	100	100
51-08	ISO98	1	18.2	9.5mm CSP	406	Power 8d	100	100
51-09	Ramp	1	18.2	9.5mm CSP	610	Power 8d	100	100
51-10	ISO98	1	18.2	9.5mm CSP	610	Power 8d	100	100
51-21	Ramp	2	18.2	9.5mm CSP	406	Power 8d	150	150
51-22	ISO98	2	18.2	9.5mm CSP	406	Power 8d	150	150
51-23	Ramp	3	18.2	9.5mm CSP	406	Power 8d	150	150
51-24	ISO98	3	18.2	9.5mm CSP	406	Power 8d	150	150

Note: Power 8d – D = 3.05 mm, L = 65 mm
FCC93, ISO98 – reversed cyclic displacement protocols, see Figure 3.

2.2. Load Protocol

Both ramp and reversed cyclic displacement protocols were used. The two reversed cyclic protocols are shown in Figure 3. FCC93 had a constant displacement frequency of 0.5 Hz. ISO98 had a constant displacement rate of 20 mm/sec. The ISO98 protocol has been proposed for the working draft of the ISO Standard "Timber structures – Joints made with mechanical fasteners – Quasi-static reversed-cyclic test method" (ISO, 1998).

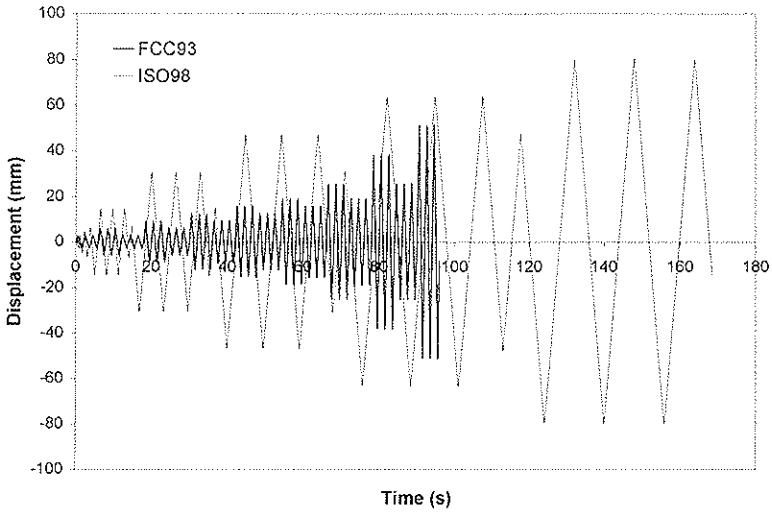

Figure 3 Reversed cyclic protocols.

2.3. Test Set-up

A schematic drawing of the test set-up is shown in Figure 4. This configuration is similar to that described in the ASTM Standard E564 (1991). A detailed description of the test set-up can be found in Karacabeyli and Ceccotti (1996).

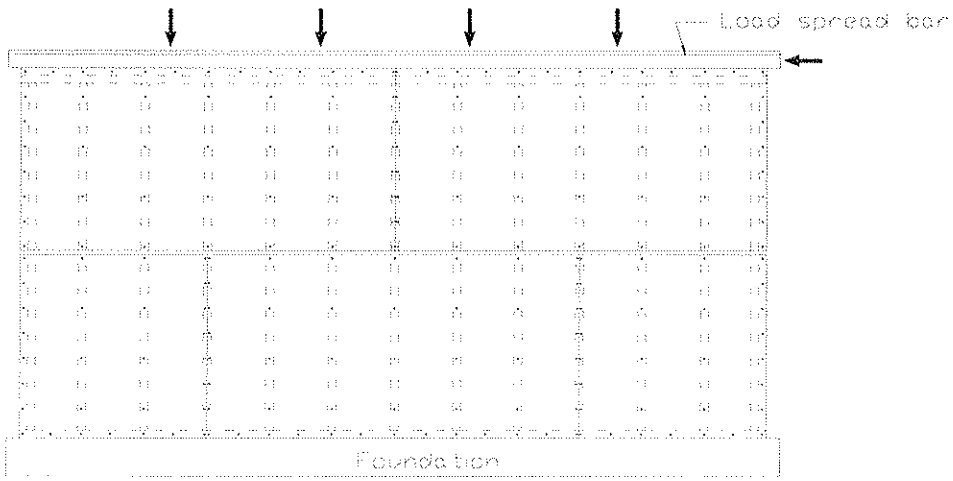

Figure 4 Test set-up.

3. Results and Analysis

Table 2 summarizes the maximum loads, ultimate displacements and secant stiffness of blocked and unblocked shear walls. The ratios of the maximum loads, ultimate displacements and secant stiffness between unblocked shear wall and blocked shear walls are also included in Table 2.

Table 2 Summary of Forintek's test results.

Specimen	Load protocol	Stud spacing (mm)	Nail spacing (mm)		Maximum load		Displacement		Stiffness	
			Supported edges	Intermediate studs	P (kN/m)	R_P	D (mm)	R_D	K (kN/m/mm)	R_K
22-02	Ramp	406	150	300	9.05		77		0.60	
29-01	Ramp	406	150	300	5.31	0.59	71	0.91	0.50	0.84
22-03	FCC93	406	150	300	7.98		50		0.91	
29-02	FCC93	406	150	300	5.23	0.66	43	0.86	0.71	0.78
31-01	Ramp	406	150	300	8.40		76		0.55	
51-01	Ramp	406	150	300	5.40	0.64	65	0.85	0.41	0.75
51-05	Ramp	305	150	150	9.36	1.11	80	1.06	0.58	1.06
51-07	Ramp	406	100	100	8.81	1.05	70	0.93	0.64	1.16
51-09	Ramp	610	100	100	5.89	0.70	68	0.90	0.57	1.04
51-21	Ramp	406	150	150	5.88	0.70	103	1.36	0.30	0.54
51-23	Ramp	406	150	150	7.53	0.90	78	1.02	0.45	0.82
31-02	FCC93	406	150	300	7.86		50		0.88	
51-02	FCC93	406	150	300	4.40	0.56	43	0.87	0.73	0.83
51-06	ISO98	305	150	150	9.18	1.17	58	1.17	0.62	0.70
51-08	ISO98	406	100	100	9.00	1.15	52	1.05	0.92	1.04
51-10	ISO98	610	100	100	5.73	0.73	49	0.99	0.60	0.69
51-22	ISO98	406	150	150	5.53	0.70	73	1.48	0.35	0.40
51-24	ISO98	406	150	150	8.58	1.09	65	1.31	0.53	0.60

Note:
Walls 22-02, 22-03, 31-01 and 31-02 are blocked shear walls.
D – the ultimate displacement, which is defined as the displacement at 80% of maximum load on the descending portion of the load-displacement curve.
K – the secant stiffness between 10% and 40% of the maximum load.
R_P – the ratio of maximum load of unblocked shear wall to maximum load of blocked shear wall with the same type of load protocol.
R_D – the ratio of maximum displacement of unblocked shear wall to maximum displacement of blocked shear wall with the same type of load protocol.
R_K – the ratio of secant stiffness of unblocked shear wall to secant stiffness of blocked shear wall with the same type of load protocol.

3.1. Wall configuration 1

Figure 5 shows the load-displacement responses of blocked and unblocked shear walls sheathed horizontally with nail spacing 150 mm at supported edges and 300 mm at intermediate studs under ramp and reversed cyclic tests. For framing member spaced 406 mm on center, the capacities of unblocked shear walls had approximately 60% of the capacities of the blocked shear walls at the same nail spacing and stud spacing. The ultimate displacements and secant stiffness of the unblocked shear walls were approximately 80% of that of the blocked shear walls. Unlike blocked shear walls where the nail joints along the perimeter of the panels reached their capacities, for unblocked shear walls, only nail joints along the unblocked horizontal joint reached their capacities. Figure 6 shows the deformed shape of the unblocked wall. The nail joints either withdrew from the studs or pulled through the panels.

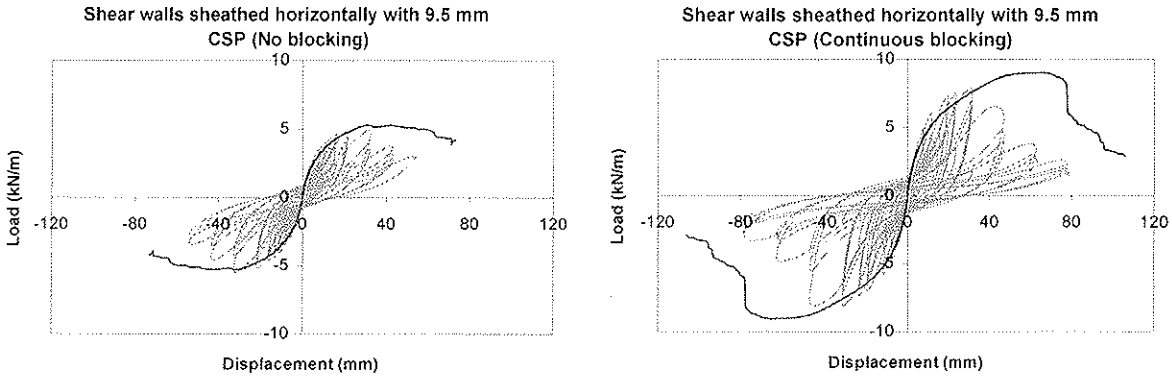

Figure 5 Load-displacements of blocked and unblocked shear walls.

Figure 6 Deformed shape of unblocked shear walls under wall configuration 1.

For framing members spaced 305 mm on center, the capacities of unblocked shear walls with nail spacing 150 mm both at supported edges and at intermediate studs had approximately 110% of the capacities of the blocked shear walls (406 mm stud spacing) with 150 mm perimeter and 300 mm intermediate nail spacing. The ultimate displacements and secant stiffness of these unblocked shear walls were approximately the same as those of the reference blocked shear walls.

The above conclusions can also be made for unblocked shear walls with nail spacing 100 mm both at supported edges and at intermediate studs. However, in these walls, a few studs split by nail joints along the unblocked horizontal joint, as shown in Figure 7. This indicated that at closer nail spacing, the capacities of the unblocked shear wall would be governed by the lumber tension strength perpendicular to grain, instead of the strengths of nail joints. Since this failure mode is not desirable, the use of nail spacing less than 100 mm should therefore not be encouraged in unblocked shear wall applications.

Figure 7 Studs split along the unblocked horizontal joint with 100 mm nail spacing.

3.2. Wall configuration 2

Configuration 2 of the unblocked shear wall had two unblocked horizontal gaps with a 305 mm wide panel strip at the middle of the wall. The unblocked shear walls with nail spacing 150 mm both at supported edges and at intermediate studs under wall configuration 2 had slightly higher capacities than unblocked shear walls with nail spacing 150 mm at supported edges and 300 mm at intermediate studs under wall configuration 1. The ultimate displacements of wall configuration 2 were approximately 50% larger than those of wall configuration 1. However, the secant stiffness of wall configuration 2 is only about 50% of the secant stiffness of wall configuration 1. The deformed shape of the unblocked wall under wall configuration 2 is shown in Figure 8.

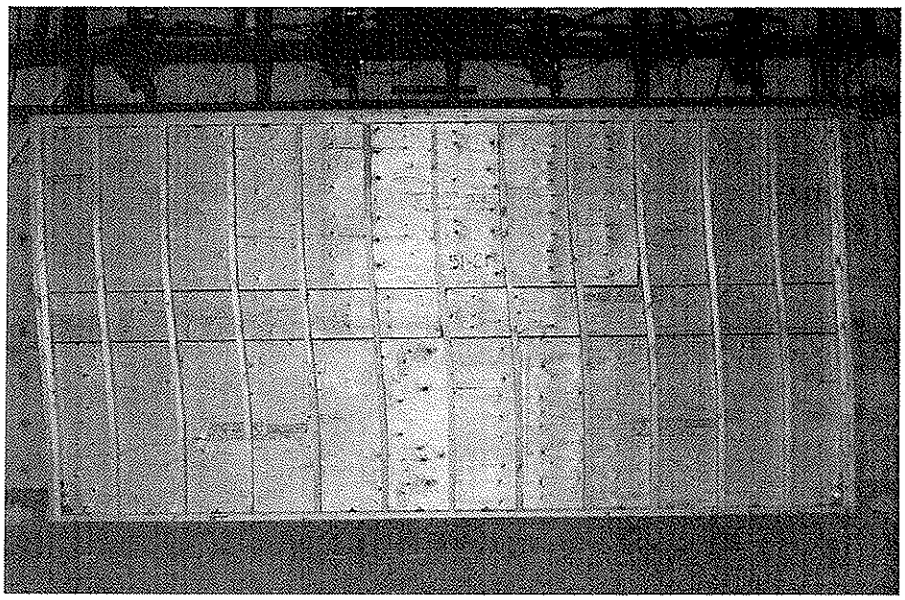

Figure 8 Deformed shape of unblocked shear walls under wall configuration 2.

3.3. Wall configuration 3

Configuration 3 of the unblocked shear wall had staggered unblocked horizontal gaps at a distance of 610 mm from each other. The unblocked shear walls with nail spacing 150 mm both at supported edges and at intermediate studs under wall configuration 3 had approximately 40% higher load capacities than those of unblocked shear walls with nail spacing 150 mm at supported edges and 300 mm at intermediate studs under wall configuration 1. The ultimate displacements of unblocked shear walls under wall configuration 3 were larger (up to 50%) than that of unblocked shear walls under wall configuration 1. The secant stiffness of wall configurations 1 and 3 were comparable. For wall configuration 3, a step failure pattern was observed, as shown in Figure 9.

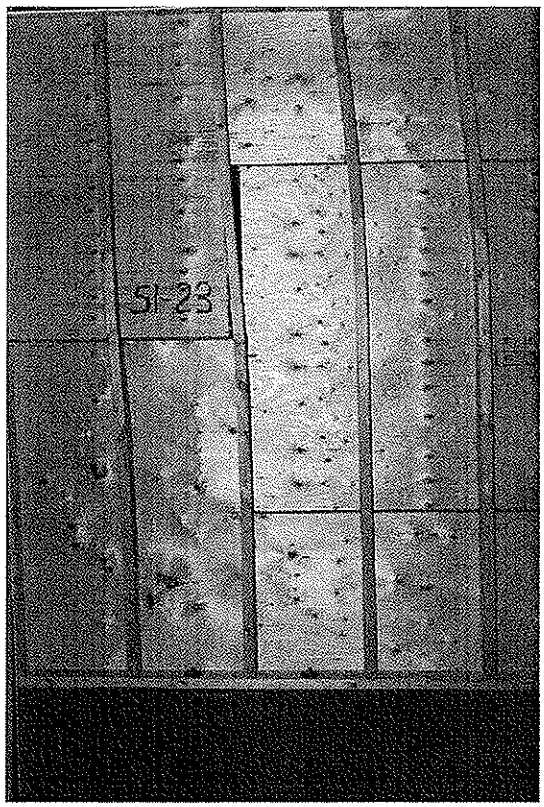

Figure 9 Step failure pattern of unblocked shear walls under wall configuration 3.

4. APA Tests

Tissell (1990) conducted tests at APA on unblocked shear walls with various nail and stud spacings. The walls, 2.44 m in length and height, were built with 38 mm x 89 mm kiln dried Douglas-fir lumber and 1220 mm x 2440 mm plywood panels, and tested in accordance with the provisions of ASTM E72 Standard.

The test results are summarized in Table 3. Typical failures of the unblocked walls occurred along the unblocked horizontal joint where the fasteners either withdrew from the framing members or pulled through the panel.

Table 3 Summary of APA's test results.

Type	Nail size	Nail spacing (mm) Supported edges	Intermediate studs	Panel thickness (mm)	Stud spacing (mm)	No. of tests	Ultimate load (kN/m) Min.	Max.	Avg.	Unblocked / Blocked
Blocked	6d	150	300	8.0	610	15	8.4	12.4	10.6	
Unblocked	6d	150	300	8.0	406	1			8	0.75
Unblocked	6d	150	150	8.0	406	2	9.5	10.9	10.2	0.96
Blocked	6d	150	300	9.5	610	5	7.8	15.7	10.8	
Unblocked	6d	150	300	9.5	610	1			4.4	0.41
Unblocked	6d	150	150	9.5	610	1			5.5	0.51

Tissell (1990) found that the strength of unblocked shear walls was a function of the nail spacing and framing spacing. Tests showed that for framing members spaced at 610 mm on center, the capacity of unblocked shear walls with nail spacing 150 mm at

supported edges and 300 mm at intermediate studs had about 40% of the capacity of blocked shear walls with 150 mm perimeter nail spacing. The capacity of unblocked shear walls with nail spacing 150 mm both at supported edges and at intermediate studs had about 50% of the capacity of the blocked shear walls.

For framing members spaced at 406 mm on center, the capacity of unblocked shear walls with nail spacing 150 mm at supported edges and 300 mm at intermediate studs had 75% of the capacity of the blocked shear walls (610 mm stud spacing) with 150 mm perimeter nail spacing. The capacity of unblocked shear walls with nail spacing 150 mm both at supported edges and at intermediate studs had 96% of the capacity of the blocked shear walls.

5. Recommended Design Values

The specified shear strength for an unblocked shear wall can be determined as a percentage of the specified shear strength of a reference blocked shear wall with 150 mm perimeter nail spacing and 610 mm stud spacing. A strength adjustment factor for unblocked shear walls, J_{ub}, is introduced. The strength adjustment factor J_{ub} is a function of the framing spacing and the nail spacing at supported edges and at intermediate studs.

Relative load capacities between unblocked shear walls in Table 4 were developed based on:

a) APA findings that for both 406 mm and 610 mm stud spacing, the average capacity of unblocked shear walls with 150 mm nail spacing at supported edges and 300 mm nail spacing at intermediate studs was approximately 80% of the average capacity of unblocked shear walls with 150 mm nail spacing both at supported edges and at intermediate studs, and

b) Forintek findings that for 100 mm nail spacing at supported edges and at intermediate studs, unblocked shear walls with 406 mm stud spacing had approximately 150% of the capacities of unblocked shear walls with 610 mm stud spacing. This indicates that the capacities of unblocked shear walls are inversely related to stud spacing.

Table 4 Relative load capacities of unblocked shear walls

Nail Spacing at	Nail Spacing at	Stud spacing (mm)			
Supported Edges (mm)	Intermediate Studs (mm)	305	406	508	610
150	150	2.50	1.88	1.50	1.25
150	300	2.00	1.50	1.20	1.00

The strength adjustment factors, J_{ub}, for unblocked shear walls in Table 5 were developed as follows:

- For 406 mm stud spacing, the average capacity of unblocked shear walls with 150 mm nail spacing at supported edges and 300 mm nail spacing at intermediate studs was approximately 60% the average capacity of blocked shear walls with 150 mm perimeter nail spacing and 406 mm stud spacing. It was found that the blocked shear walls with 406 mm stud spacing had approximately 5% higher capacities than blocked shear walls with 610 mm stud spacing (Tissell, 1990). Therefore, when compared to the blocked shear walls with 610 mm stud spacing, the average

capacity of those unblocked shear walls was still approximately 60%. This was used as the starting point in Table 5.

Table 5 Strength adjustment factor[1], J_{ub}, for unblocked shear walls[2]

Nail Spacing at Supported Edges (mm)	Nail Spacing at Intermediate Studs (mm)	Stud spacing (mm)			
		305	406	508	610
150	150	1.0	0.8	0.6	0.5
150	300	0.8	0.6	0.5	0.4

[1] Strength adjustment factor shall only be applicable to structural wood-based panels.

[2] Specified shear strength of unblocked shear wall shall be calculated by multiplying the strength adjustment factor and the specified shear strength of a reference blocked shear wall with 610 mm stud spacing and nails spaced at 150 mm on center around panel edges and 300 mm on center along intermediate framing members.

The rest of the strength adjustment factors were developed based on the relative load capacities of unblocked shear walls with a scaling factor of 0.4 (i.e. 0.6/1.5 = 0.4). The values of the strength adjustment factors reasonably match the APA and Forintek findings as follows:

1. APA test results

- For 610 mm stud spacing, the capacity of unblocked shear walls with 150 mm nail spacing at supported edges and 300 mm nail spacing at intermediate studs was about 40% of the capacity of blocked shear walls with 150 mm perimeter nail spacing. The capacity of unblocked shear walls with 150 mm nail spacing both at supported edges and spacing at intermediate studs was about 50% of the capacity of blocked shear walls with 150 mm perimeter nail spacing. These results agree well with the proposed strength adjustment factors in Table 5.

2. Forintek test results

- For 305 mm stud spacing, the average capacity of unblocked shear walls with 150 mm nail spacing at supported edges and 300 mm nail spacing at intermediate studs was approximately 110% of the average capacity of blocked shear walls with 150 mm perimeter nail spacing and 406 mm stud spacing. When compared to the blocked shear walls with 610 stud spacing, the average capacity of unblocked shear walls was approximately 120%, which suggest that the applicable strength adjust factor in Table 5 is conservative.

Stud splitting caused by nails loaded in tension perpendicular to grain is a brittle failure mode and it is not desired. For this reason, the strength adjustment factor J_{ub} was not developed for unblocked shear walls with 100 mm or smaller nail spacing at supported edges and at intermediate studs due to the potential splitting at the studs.

Unblocked shear walls under wall configuration 2 have lower capacities and secant stiffness than the corresponding unblocked shear walls under wall configuration 1. Unblocked shear walls with 150 mm nail spacing at supported edges and at intermediate studs under wall configuration 2 can be conservatively (with the exception of secant stiffness) treated as unblocked shear walls with nail spacing 150 mm at supported edges and 300 mm at intermediate studs.

In the next edition of CSA Standard O86.1 (1994), the unit factored design shear resistance is proposed be calculated as follows:

$$V_d = \phi v_d K_D K_{SF} J_{ub} J_{sp} J_{hd}$$

where
V_d –factored design shear resistance
ϕ - performance factor, 0.7 for shear wall
v_d – specified shear strength of blocked shear walls
K_D – load duration factor, 1.25 for static load and 1.15 for cyclic load
K_{SF} – service condition factor for fastenings, 1.0 for dry condition
J_{ub} – strength adjustment factor for unblocked shear walls (Table 5)
J_{sp} – species factor for framing material, 1.0 for Douglas-fir and 0.8 for Spruce-Pine-Fir
J_{hd} – hold-down effect factor, 1.0 for shear walls designed with hold-down connections

Comparisons of test results and factored design shear resistances are summarized in Tables 6 and 7. In general, the ratio of ultimate load and factored design resistance was found to be greater than 2.0. Because this ratio is slightly greater than the ratio found earlier for blocked shear walls, the proposed strength adjustment factors are judged to be acceptable.

Table 6 Unblocked shear walls[2] – APA[1]

Nail Spacing (mm)		Panel		No.	Ultimate Load (kN/m)			Factored Design	Load
Supported Edges	Intermediate Studs	Thickness (mm)		of Tests	Min.	Max.	Avg.	Resistance[3] (kN/m)	Factor[4]
150	300	7.5	406	2	8.0	8.6	8.3	2.6	3.2
150	150	7.5	406	2	9.5	10.9	10.2	3.4	3.0
150	300	9.5	610	1			4.4	1.9	2.3
150	150	9.5	610	1			5.5	2.4	2.3

[1] Table values were based on APA Research Report 154 (Tissell 1990).
[2] Shear walls were sheathed with rated sheathing panels connected with common nail 6d (d = 2.8 mm, L = 50 mm). Douglas-fir lumber were used as framing materials.
[3] ϕ = 0.7, J_{sp} = 1.0, K_D = 1.25 for static tests.
[4] Ratio of average ultimate load and factored design resistance according to CSA Standard O86.1.

Table 7 Unblocked shear walls[1] – Forintek

Specimen	Load protocol[5]	Stud spacing (mm)	Nail spacing (mm) Supported edge	Intermediate stud	Load capacity[2] (kN/m)	Factored design resistance[3] (kN/m)	Load factor[4]
29-01	Static	406	150	300	5.31	2.7	1.9
29-02	FCC93	406	150	300	5.23	2.5	2.1
51-01	Static	406	150	300	5.40	2.7	2.0
51-02	FCC93	406	150	300	4.40	2.5	1.8
51-05	Static	305	150	150	9.36	4.6	2.1
51-06	ISO98	305	150	150	9.18	4.2	2.2
51-21	Static	406	150	150	5.88	2.7 [6]	2.2
51-22	ISO98	406	150	150	5.53	2.5 [6]	2.2
51-23	Static	406	150	150	7.53	3.6	2.1
51-24	ISO98	406	150	150	8.34	3.4	2.6

[1] Shear walls were sheathed with 9.5 mm Canadian softwood plywood connected with power nail, 8d (d = 3 mm, L = 65 mm). SPF lumber were used as framing materials.
[2] Average ultimate load of tension and compression of first envelope curve in reversed cyclic tests.
[3] ϕ = 0.7, J_{sp} = 0.8, K_D = 1.25 for static tests, and 1.15 for cyclic tests.
[4] Ratio of average ultimate load and factored design resistance according to CSA Standard O86.1.
[5] FCC93, ISO98 – cyclic displacement schedules.
[6] Used strength adjustment factor J_{ub} for unblocked shear walls with nail spacing 150 mm at supported edges and 300 mm at intermediate studs.

6. Conclusion

Three types of unblocked shear walls were tested under ramp and reversed cyclic tests. A strength adjustment factor for unblocked shear walls, J_{ub}, is proposed to correlate the specified shear strength of an unblocked shear wall to the specified shear strength of a blocked shear wall of the same panel grade and thickness with 150 mm perimeter nail spacing. The strength adjustment factor J_{ub} is a function of the framing spacing and the nail spacing at supported edges and at intermediate studs. Comparisons of test results and factored design shear strengths show that the factored design shear strengths for unblocked shear walls are reasonably conservative.

7. Future Work

The strength adjustment factors for unblocked shear walls in this paper are applicable to walls with 2.44 m height. Work is in progress for extending the findings to walls with greater height, and to double-sided unblocked shear walls.

8. Reference

ASTM, 1991. Standard method of static load test for shear resistance of framed walls for buildings. ASTM E 564-76, ASTM, West Conshohocken, Pa.

CSA, 1994. Engineering Design in Wood (Limit States Design). Canadian Standards Association, 178 Rexdale Boulevard, Etobicoke, Ontario.

ISO, 1998. Timber structures – Joints made with mechanical fasteners – Quasi-static reversed-cyclic test method. ISO TC 165/WG 7.

Karacabeyli, E. and Ceccotti, A., 1996. Test results on the lateral resistance of nailed shear walls. Proceedings of the International Wood Engineering Conference, New Orleans, USA, Vol.2, p.179-186.

Rainer, J.H., Karacabeyli, E., 1999. Performance of wood-frame building construction in earthquakes. Special Publication No. Sp-40, Forintek Canada Corp., Vancouver, British Columbia, Canada.

Tissell, J.R., 1990. Structural panel shear walls. APA Research Report 154, P.O. Box 11700, Tacoma, Washington, USA.

INTERNATIONAL COUNCIL FOR RESEARCH AND INNOVATION
IN BUILDING AND CONSTRUCTION

WORKING COMMISSION W18 - TIMBER STRUCTURES

PREDICTION OF EARTHQUAKE RESPONSE OF TIMBER HOUSES CONSIDERING SHEAR DEFORMATION OF HORIZONTAL FRAMES

by

N Kawai
Building Research Institute

JAPAN

MEETING THIRTY-THREE
DELFT
THE NETHERLANDS
AUGUST 2000

Presented by: N. Kawai

· A. Ceccotti commented that it was a good paper combining the evaluation of diaphragm flexibility with torsional response. He questioned the rationale of adding 20% more forces for static calculations based on torsional moment.
· N. Kawai responded that the procedures give better solution.
· A. Ceccotti asked about the planned future work.
· N. Kawai responded that much work needed to be done. Some examples included multistory model, evaluation of force modification rules, more realistic houses with many vertical frames.
· M. Yasumura stated that the procedures that used heq_1 would depend on load protocol therefore, one would need to be careful with it.
· N. Kawai agreed and stated that ISO load protocol was used.
·E. Karacabeyli asked 0.8 heq_1 was used.
· N. Kawai responded that 100% heq_1 would under-predict the response and overestimate the performance.

Prediction of Earthquake Response of Timber Houses considering Shear Deformation of Horizontal Frames

Naohito Kawai

Building Research Institute, JAPAN

1 Summary

Related to the revision of Building Standard Law of Japan, the application of capacity spectrum method (CSM) is discussed as a convenient prediction method for the earthquake response of structures. For the application of CSM, there are some problems in the procedure to replace the structure to a single degree of freedom model, such as distribution of external forces, assumption of damping, and so on.

In this paper the predictions by CSM were compared with the results of time history analysis (THA) against ten artificial waves, using horizontally lumped mass system models, in which the shear deformation of horizontal frames are considered. The models of one-storied houses were used, which has 3 rows of shear walls in x-direction and 4 rows in y-direction, and the earthquake load is applied in y-direction. Vertical frames (rows of shear walls) and the parts of horizontal frames are modelled as shear panels, which have load-displacement hysteresis model based on the cyclic loading tests on a plywood sheathed shear wall.

As a whole, the predictions by CSM agreed well with the results of THA when the modified value of damping (h_{e1}) is used, which is calculated using 80 % of equivalent viscous damping corresponding to the first loop under the cyclic loading protocol of ISO/WD16670. And the CSM using damping calculated with 100 % of equivalent viscous damping corresponding to the stabilized loop seemed to give the upper limit of maximum displacement obtained by THA. However, CSM sometimes gives different distribution of response displacement from THA, in case the deformation by torsional behavior and horizontal shear deformation is relatively large. For a solution of this problem, modification of CSM is proposed to use the distribution of external force with adding torsional moment corresponding to the existing eccentric moment. When the distribution of external forces with 20 % of eccentric moment in CSM, correlation of the predicted maximum response displacement between THA and CSM was improved.

2 Introduction

In the seismic design or the evaluation of seismic performance of buildings, the prediction of maximum response displacement against strong ground motion is one of the most important problems. Time history analysis (THA) is one of the methods, which gives better predictions. However, as it needs high techniques and the results vary according to the

characteristics of the input waves, it is not suitable for a general seismic design procedure. While, as convenient prediction methods of non-linear response based on a linear response analysis, two methods are known, one is the application of property of energy conservation and another is the method called as equivalent linear response analysis or capacity spectrum method (CSM). Veletsos and Newmark first proposed the former (Veletsos et. al. 1960). Shibata and Sozen proposed the latter (Shibata et. al. 1976) and Freeman developed its sophisticated procedure (Freeman 1978).

In Japan, the Building Standard Law was revised and enforced on 1st of June 2000. The main purpose of the revision is to shift to a performance based standard, and one of the most important revisions in the area of structural performance is that Critical Strength Calculation was added as a method of directly calculating the stress and deformation. This calculation method can be applied for the building structures even if it does not conform to the prescriptive provisions. And the provisions of Critical Strength Calculation for seismic performance are based on CSM.

The author has confirmed the applicability of CSM for one-storied and two-storied timber structures with shear walls (Kawai 1999-1,2). CSM seems to give better predictions than the application of property of energy conservation. However, in the actual timber houses by Japanese conventional construction, the stiffness of horizontal frames such as floor and roof is not so high and they often have eccentricity of shear walls. Therefore, it is necessary to confirm the applicability of CSM and to discuss the details of the application method to timber houses with shear deformation of horizontal frames and eccentricity of shear walls.

In this paper, the results of earthquake response predictions by CSM are compared with the results of THA with using 12 types of horizontally lumped mass system models. In the models, the load-displacement hysteresis curves of shear walls and horizontal frames are modelled based on the results of static cyclic loading tests on shear walls. In the application of CSM, the assumption of damping for equivalent linear response is one of the important problems. In the preceding study on one-storied and two-storied houses (Kawai 1999-1,2), the author used 80% of equivalent viscous damping of first loop which can be obtained with applying the loading protocol proposed in ISO/TC165/WG7 to the hysteresis model of the shear wall. In this paper, 100 % of equivalent viscous damping for stabilised loop is also used to discuss the adequate procedure, which gives better predictions. And modification of distribution of external force used in CSM is also discussed for better agreement in the distribution of maximum displacement.

3 Vibration Models

Figure 1 shows the vibration model used in this study. In the actual houses, there are some rows of shear walls, and the floor or roof structure is divided by the rows of shear walls as shown in this figure. In this study, the model of one-storied house is used, which has 3 rows of shear walls in x-direction and 4 rows in y-direction, and the earthquake load is applied in y-direction. Masses are lumped at the intersection of the rows of shear walls in both directions. And vertical frames (rows of shear walls) and the parts of horizontal frames are modelled as shear panels as shown in figure 2. The number of freedom of this model is seven, which is same as the number of horizontal frames.

The load-displacement relationship of each shear panel is modelled based on the static cyclic test result on a plywood sheathed shear wall. The hysteresis is modelled with using the combination model of bi-linear and slip and the parameters in the model are determined to

trace the test result (Kawai 1998). In this study, the same model as the vertical frames is used for the horizontal frames with being modified from load-displacement relationship to the relationship between the shear force per unit length and shear deformation angle. Figure 3 and Table 1 shows the hysteresis model and parameters used for vertical and horizontal frames. In CSM, only the skeleton of the load-displacement relationship and the equivalent viscous damping ratio of the hysteresis model are used, and in THA, the whole of the hysteresis model is used.

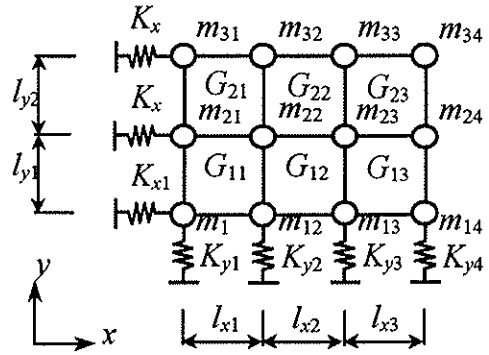

Figure 1: Horizontally lumped mass system model

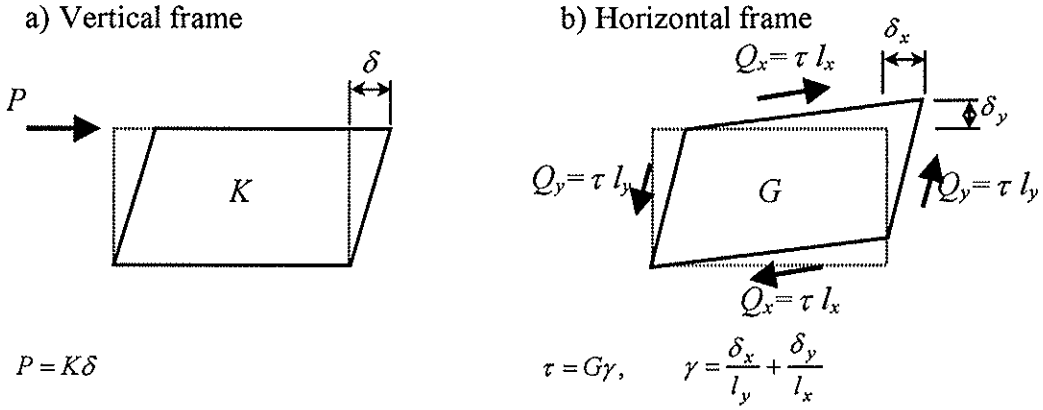

Figure 2: Shear panel models of vertical frame and horizontal frame

To discuss the applicability of CSM, 21 types of models are examined, in which the natural period, distribution of shear walls, stiffness and strength of horizontal frames are changed. Table 2 shows the difference of the 21 types of models. Models of type 1 to type 3 are symmetrical models without torsional behaviour, and others are asymmetrical models, which will reveal torsional vibration. Types 4 to 12 are models with eccentricity by asymmetrically arranged vertical frames and types 13 to 21 are models with eccentricity by asymmetrically arranged masses. The standard horizontal frame is assumed to have the same stiffness and strength with the shear wall sheathed with plywood (hardwood, thickness = 9 mm) nailed by JIS N50 with spacing of 150 mm. For types 5, 8, 11, 14, 17 and 20, the horizontal frame is assumed to have the standard stiffness and strength. For types 1, 2, 3, 6, 9, 12, 15, 18 and 21, stiffness and strength are reduced to 20 % of the standard, and for others, they are assumed to be 10 times of the standard which are near to be assumed as rigid frames.

Table 1: Parameters used in the model (unit: δ -mm, γ -10^{-3} rad.)

	Initial stiffness	δ_{B1} or γ_{B1}	K_{B1} or G_{B1}	K_{B2} or G_{B2}	δ_{S1} or γ_{S1}	δ_{S2} or γ_{S2}	K_{S1} or G_{S1}	K_{S2} or G_{S2}	K_{S3} or G_{S3}
Vertical Frame	K_0	4.5	0.53 K_0	0.03 K_0	18	90	0.47 K_0	0.07 K_0	−0.11K_0
Horizontal frame	G_0	1.67	0.53 G_0	0.03 G_0	6.67	33.3	0.47 G_0	0.07 G_0	−0.11G_0

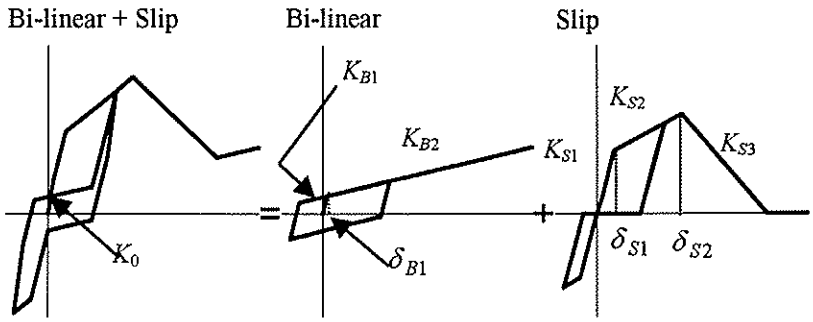

Figure 3: Hysteresis model for vertical and horizontal frames
For horizontal frames, G and γ are used instead of K and δ

Table 2: Types of models examined

Type	Proportion of K $K_{x1} - K_{y4}$	$m_{11} - m_{32}$ (kg)	$m_{13} - m_{34}$ (kg)	Initial period (sec) *1	G/G_S *2	l_{x1} - l_{x3} (m)	l_{y1} - l_{y2} (m)
1	3:3:3:3:1:1:3	1,000	1,000	0.3	0.2	3.64	3.64
2				0.4	0.2		
3				0.5	0.2		
4	3:3:3:3:3:1:1	1,000	1,000	0.3	10	3.64	3.64
5					1		
6					0.2		
7				0.4	10		
8					1		
9					0.2		
10				0.5	10		
11					1		
12					0.2		
13	3:3:3:2:2:2:2	500	1,500	0.3	10	3.64	3.64
14					1		
15					0.2		
16				0.4	10		
17					1		
18					0.2		
19				0.5	10		
20					1		
21					0.2		

*1: Initial period of this table is calculated using the summation of initial stiffness.
*2: G_S is the standard stiffness of horizontal frame used in this study. G_S = 1.291(kN/mm/rad.)

4 Prediction methods

4.1 Capacity Spectrum Method (CSM)

The procedure to apply CSM to the horizontally lumped mass system model is summarised as follows.

(1) Pushover analysis

Assuming proper distribution of external forces, calculation of one way loading with step by step method is executed. In this study, pushover analysis increasing displacement step by step was executed to obtain the load-displacement relationship over the maximum strength of the elements. In this analysis, the distribution of external force was assumed to be constant and proportional to the mass on each vertical frame, and only the skeleton of load-displacement relationship was used even when the deformation of the element decreases from the previous step.

(2) Calculation of Capacity Spectrum

Based on the result of pushover analysis, spectral acceleration ($_cS_a$) and spectral displacement ($_cS_d$) are calculated for each loading step using equations (1) and (2).

$$ {}_cS_a = \frac{\sum m_i \delta_i^{\,2}}{\left(\sum m_i \delta_i\right)^2} \cdot \sum P_i \tag{1} $$

$$ {}_cS_d = \frac{\sum m_i \delta_i^{\,2}}{\sum P_i \delta_i} \cdot {}_cS_a \tag{2} $$

where, m_i = mass on ith vertical frame, δ_i = displacement of ith vertical frame and P_i = external force to ith vertical frame. $_cS_a$ - $_cS_d$ curve corresponds to the load-displacement relationship of the equivalent single degree of freedom model.

(3) Calculation of equivalent period and equivalent damping ratio

For each point on the $_cS_a$ - $_cS_d$ curve, equivalent period (T_e) is calculated by the equation

$$ T_e = \frac{{}_cS_a}{{}_cS_d} \tag{3} $$

And also, for each point, equivalent damping ratio (h_e) is calculated using equivalent viscous damping ratio (h_{eq}) and original viscous damping ratio (h_v, 2% is assumed in this study) of the structure by the equation

$$ h_e = \alpha h_{eq} + \frac{T_e}{T_0} h_v \tag{4} $$

where, α = modification factor of damping, and T_0 = initial period. In equation (4), h_{eq} of the structure can be calculated as the weighted average value of equivalent viscous damping

ratio of each element ($h_{eq,i}$) weighted by the potential energy (W_i) at the displacement corresponding to the step.

$$h_{eq} = \frac{\sum(W_i h_{eq,i})}{\sum W_i} \tag{5}$$

According to the result of preceding study on one-storied and two-storied houses (Kawai 1999-1,2), it gives better predictions when the modification factor $\alpha = 0.8$ is used for the equivalent viscous damping ratio corresponding to the first loop of the model under the loading protocol proposed in ISO/WD16670. In this study, the equivalent viscous damping ratio corresponding to the stabilised (second or third) loop of the model was also used to discuss the proper procedure, which gives better prediction. Thus, h_{e1} and h_{e2} were calculated as h_e by following equations in this study.

$$h_{e1} = 0.8_1 h_{eq} + \frac{T_e}{T_0} h_v \tag{6}$$

$$h_{e2} = {}_2 h_{eq} + \frac{T_e}{T_0} h_v \tag{7}$$

where, ${}_1h_{eq} = h_{eq}$ corresponding to the first loop of the model under the loading protocol of ISO/WD16670, and ${}_2h_{eq} = h_{eq}$ of the stabilised loop.

(4) Calculation of Demand Spectrum

Using the equivalent period (T_e) and the equivalent damping ratio (h_e), acceleration and displacement of demand spectrum (${}_dS_a$ and ${}_dS_d$) are calculated. Demand spectrum is the response spectrum of input earthquake wave, and the response spectrum is usually given at the viscous damping ratio of 5%. Therefore, we have to calculate the spectral acceleration and spectral displacement corresponding to T_e and h_e of the equivalent linear response using some reduction factor of response spectrum. In this study, following response spectrum of input earthquake ($S_{a,5}$ (cm/s^2)) (Okawa 1998) and reduction factor F_h (Architectural Institute of Japan 1993) were applied. Figure 4 shows the response spectrum at the damping of 5% and the others calculated using F_h, which are drawn on the S_a-S_d co-ordinates.

$$S_{a,5} = \begin{cases} 480 & (T < 0.04) \\ 7250T + 190 & (0.04 \le T < 0.14) \\ 1205 & (0.14 \le T < 0.573) \\ 691/T & (T \ge 0.573) \end{cases} \tag{8}$$

$${}_dS_a = F_h S_{a,5} \tag{9}$$

$${}_dS_d = \frac{{}_dS_a}{\omega^2} \tag{10}$$

where, ω = circular frequency ($= 2\pi/T$).

$$F_h = \frac{1}{\sqrt{1 + 17(h - 0.05)\exp(-2.5T/T_e)}} \tag{11}$$

where, T_e = effective duration time (=30 sec. in this study).

(5) Prediction point

By the procedure 1 to 4, we can obtain Capacity Spectrum and Demand Spectrum. The prediction is given as the intersection of these two curves as shown in Figure 5.

(6) Deformation of each part of the structure

The deformation of each part of the structure corresponding to the prediction point can be obtained using the result of pushover analysis.

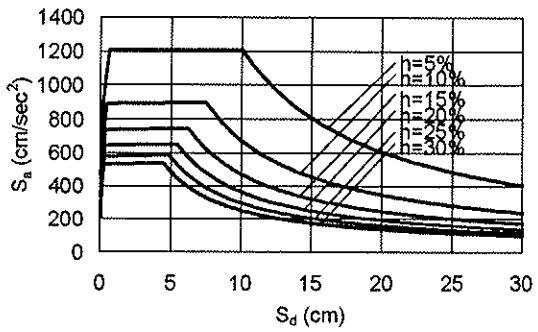

Figure 4: Response spectra of input earthquake

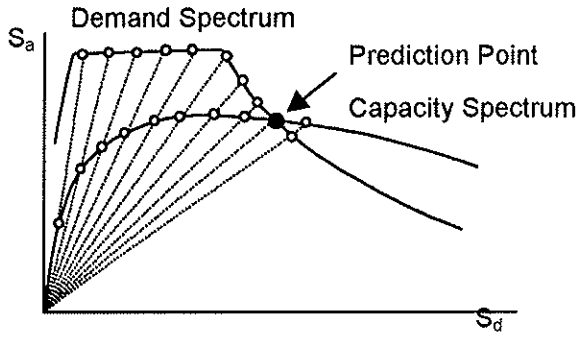

Figure 5: Prediction of response by CSM

4.2 Time history analysis (THA)

Time history analysis was executed using linear acceleration method (or Newmark's β method with β=1/6) on the horizontally lumped mass system models. Ten different artificial waves (Okawa 1998) were applied, which has the same target response spectrum as used in CSM and the same duration time of 120 seconds. Damping was assumed to be proportional to the initial stiffness, and the viscous damping ratio h_v was assumed to be constant and 2% for the initial period of primary mode. The load-displacement hysteresis model was the combination of bi-linear and slip as mentioned above, and the influence of damage in one side of displacement to the strength in the opposite side was considered by using the same value of experienced maximum displacement in both sides. This modification of hysteresis loop gives better agreement with the result of pseudo-dynamic tests on shear walls (Kawai 1998).

5 Results and discussion

5.1 Results

Figure 6 shows the comparison of maximum response relative displacement ($_rD_{max}$) between CSM and THA for types 1 to 12.

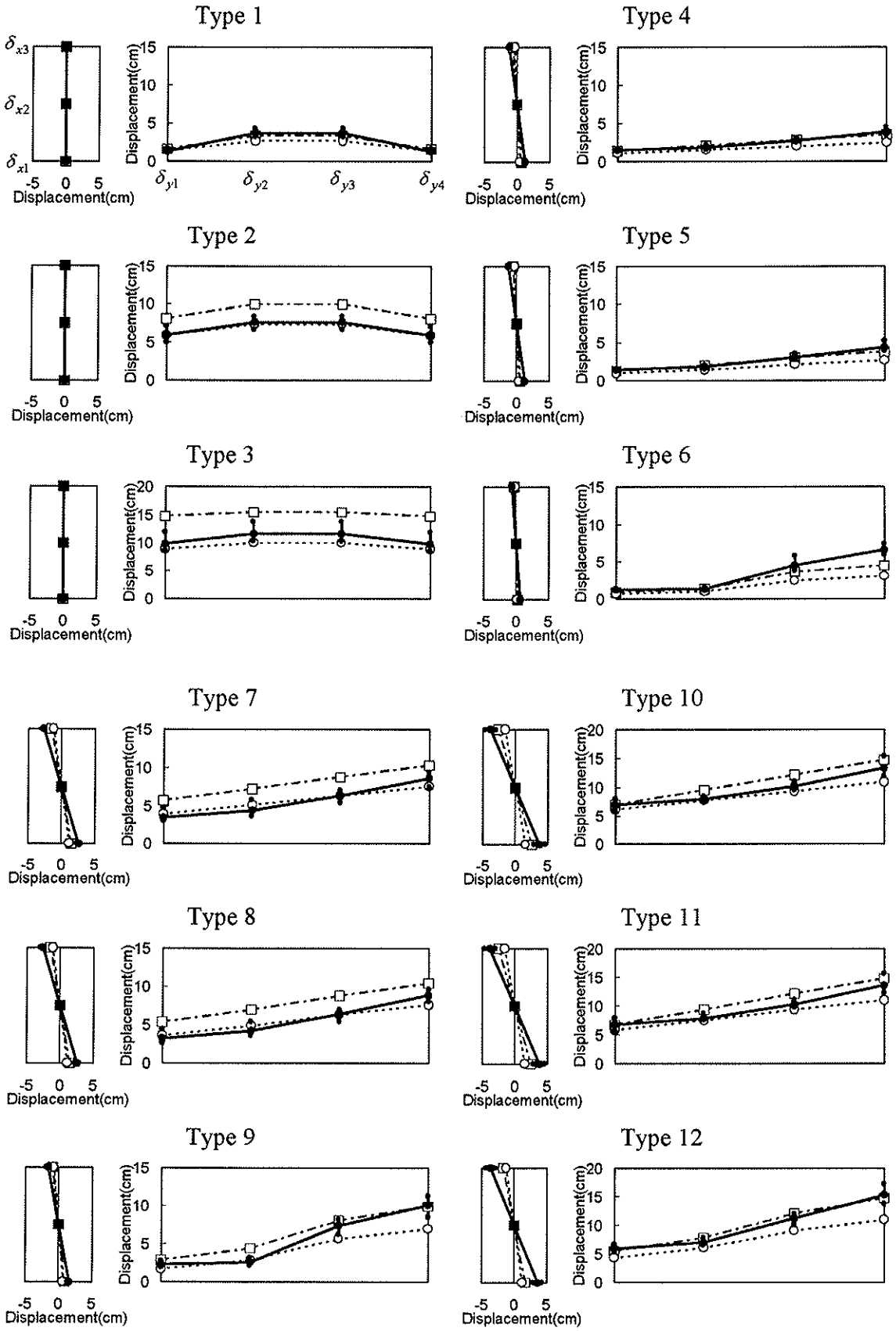

Figure 6: Comparison of predicted maximum response between CSM and THA

●—●: Average of THA, ┃: Max. and min. of THA,o---o: CSM with h_{e1},□···□: CSM with h_{e2}

As a whole, the prediction by CSM with h_{e1} (see equation (6)) agreed well with the result of THA except for some cases. In case when the deformation by torsion of the building and shear deformation of horizontal frame is relatively large, CSM with h_{e1} tends to give smaller predictions than THA (Types 6, 9 and 12). The prediction by CSM with h_{e2} (see equation (7)) often gives overestimate compared with the result of THA, but seems to give the upper limit with an exception of Type 6. The same tendencies were observed for types 13 to 21.

5.2 Modification on distribution external forces in CSM

To discuss the modification for better agreement, the modification of the distribution of external forces used in CSM was examined. The proposal of the modification is to use the distribution of external forces modified by adding the torsional moment corresponding to the eccentric moment, as shown in Figure 7. The proper ratio of the added moment to the existing eccentric moment was examined.

Figure 8 shows the examples of the correlation of predicted maximum response displacement between THA and CSM for types 13 to 21. Figure 8 (a) shows the correlation between THA and the original CSM using h_{e2} (see equation (7)) without adding torsional moment), (b) shows that between THA and the modified CSM using h_{e2} with 20 % of the eccentric moment added. When the distribution of external force with 20 % of eccentric moment is used instead of the distribution proportional to the masses, the coefficient of determination is improved from 0.945 to 0.962. It reveals that the torsional behaviour can be simulated well with this modification.

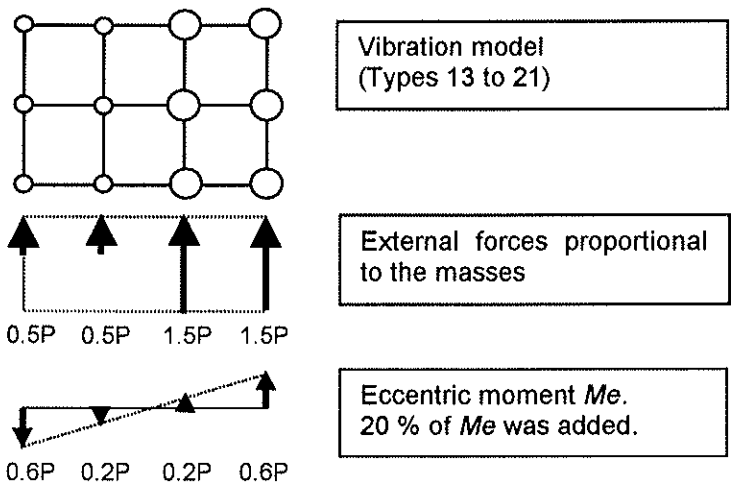

Figure 7: Proposed modification on distribution of external forces used in CSM

(a) CSM using h_{e2} vs. THA

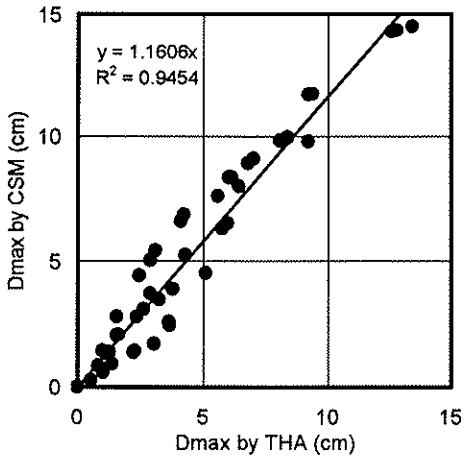

(b) Modified CSM vs. THA

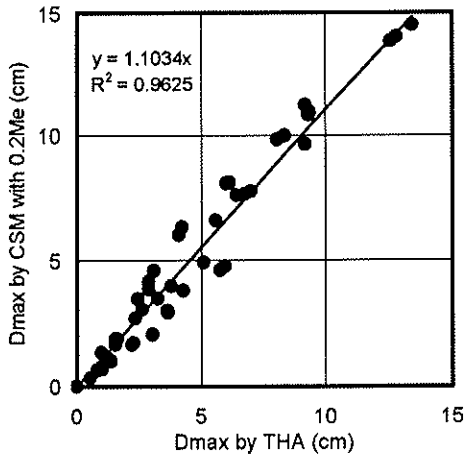

Figure 8: Correlation of predicted maximum displacement between THA and CSM

6 Conclusions

To confirm the applicability of Capacity Spectrum Method (CSM) to timber houses with shear deformation in horizontal frames, predictions of maximum response displacement by CSM were compared with the results of time history analysis (THA) using 21 types of horizontally lumped mass system models. The predictions by CSM agreed well with the results of THA when the modified value of damping is used, which is calculated using 80 % of equivalent viscous damping corresponding to the first loop under the cyclic loading protocol of ISO/WD16670. And the predictions by CSM using damping ratio corresponding to stabilized loop were near to the upper limit of predictions by THA. However, CSM sometimes gives different distribution of response displacement from THA, in case the deformation by torsional behavior and horizontal shear deformation is relatively large. For this problem, a modification to use external force to which torsional moment is added is proposed. When the 20% of existing eccentric moment is added for the models with eccentricity with asymmetrically distributed masses, the prediction by the modified CSM gives better agreement with THA in the distribution of maximum response displacement including torsional behavior.

7 Acknowledgement

The author thanks Dr. I. Okawa, Building Research Institute, for his kindness to provide the artificial earthquake waves for this study.

8 References

Architectural Institute of Japan, *Recommendations for Loads on Buildings*, 3rd Edition, Architectural Institute of Japan, 1993

Freeman, S. A., Prediction of response of concrete buildings to severe earthquake motion, *Douglas McHenry International Symposium on Concrete and Concrete Structures, SP-55, American Concrete Institute*, 1978, pp589-605

ISO/TC165/WG7, Timber structures – Joints made with mechanical fasteners – Quasi-static reversed-cyclic test method, 1998

Kawai, N., Pseudo-dynamic test on shear walls, *5th World Conference on Timber Engineering, Proceedings Volume 1*, 1998, pp412-419.

Kawai, N., Prediction methods for earthquake response of shear walls, *PTEC1999 Proceedings, Vol. 3*, 1999, pp317-324

Kawai, N., Application of Capacity Spectrum Method to timber houses, *CIB-W18 Proceedings Meeting Thirty-two*, 1999, 32-15-2, pp1-10

Shibata, A. and Sozen, M. A., Substitute-structure method for seismic design in R/C, *Proceedings of the ASCE, Journal of the Structural Division, Vol. 102*, ST 1-3, 1976, pp1-18

Shibata, A., *Seismic Analysis of Structures* (Japanese), Morikita Co. Ltd., 1981

Veletsos, A. S. and Newmark, N.M., Effect of inelastic behaviour on the response of simple systems to earthquake motions, *Proceedings of the Second World Conference on Earthquake Engineering, Vol. 2*, 1960, pp895-912

INTERNATIONAL COUNCIL FOR RESEARCH AND INNOVATION
IN BUILDING AND CONSTRUCTION

WORKING COMMISSION W18 - TIMBER STRUCTURES

EUROCODE 5 RULES FOR BRACING

by

H J Larsen
Danish Building Research Institute

DENMARK

MEETING THIRTY-THREE
DELFT
THE NETHERLANDS
AUGUST 2000

Presenter: H.J. Larsen

· H. Blass asked which MOE would one use in the design equation.
· H.J. Larsen said the MOE with the γ factor could be used although steel design used the unfactored MOE values.
· H. Blass commented that a factored MOE would lead to reduction in design requirements.
· H.J. Larsen agreed and will have to look into the details. Nevertheless, the design format has been formulated.

Eurocode 5 rules for bracing

H. J. Larsen
Danish Building Research Institute, Denmark

1 Background

The background for the rules for bracing in [Eurocode 5, 1993] was given in several CIB W18-papers e.g. [Brüninghof, 1983] and [Brüninghof, 1984]. The present paper summarises briefly the background of the rules and gives a proposal for a modification.

2 Single member in compression

2.1 Stiffness of supports

A simply supported, initially straight column with bending stiffness EI is considered, see figure 1. Its lateral deflection is prevented by $(m - 1)$ equidistant, intermediate elastic supports. The distance between them is a, i.e. the length of the column is $l = ma$. The intermediate supports are regarded as linear elastic springs with stiffness C.

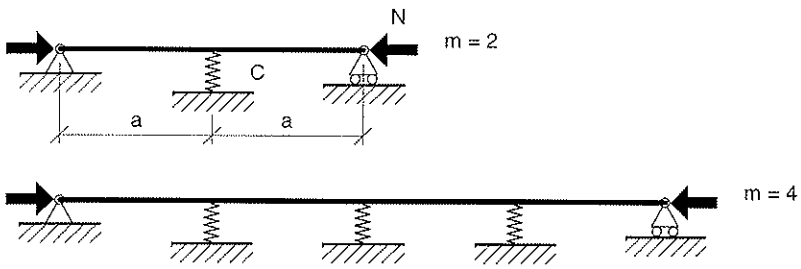

Figure 1 – Column with intermediate, elastic supports. The axial force is N.

An elastic analysis can be used to determine the minimum value of C that will ensure that the supports act as stiff supports, see e.g. [Timoshenko, & Gere 1961]. The underlying principle is illustrated for the case with one intermediate support, i.e. $m = 2$.

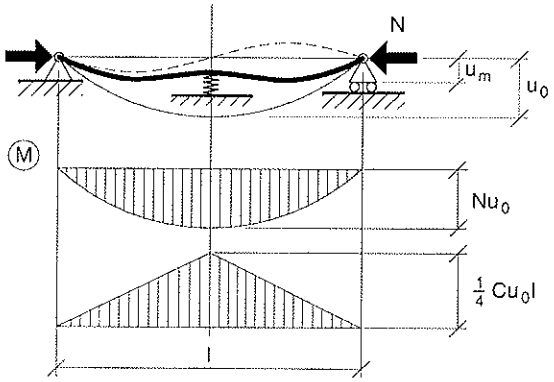

Figure 2 – Column with one intermediate, elastic support: Deflection curve and moment contributions.

It is assumed that the column is given an initial sinusoidal deflection with mid-span deflection u_0, see figure 2. The resulting moments in the column consist of a contribution from the axial force and a contribution from the reaction force Cu_0 from the spring. The moment causes a mid-span deflection:

$$u_m = \frac{Nu_0 l^2}{\pi^2 EI} - \frac{Cu_0 l^3}{48EI} = \frac{Nu_0}{N_E} - \frac{Cu_0 \pi^2 l}{48N_E} \tag{1}$$

where N_E is the Euler load-carrying capacity:

$$N_E = \pi^2 EI/l^2$$

The load-carrying capacity $N = N_{cr}$ is found by setting $u_m = u_0$:

$$N_{cr} = N_E + \frac{\pi^2}{48} Cl \le 4N_E \tag{2}$$

The maximum possible load-carrying capacity is limited to $4N_E$, corresponding to a completely stiff intermediate support. It is obtained for

$$C = \frac{144}{\pi^2} N_E / l = 14{,}6 N_E / l \tag{3}$$

The result is based on several simplifications, the most important being that the resulting deflection is also sinusoidal. The correct theoretical result for $m = 2$ is

$$C = 16 N_E / l \tag{4}$$

For an arbitrary value of m (≥ 2):

$$C = k_s m^2 N_E / a \tag{5}$$

$$k_s = 2\left(1 + \cos(\pi / m)\right) \tag{6}$$

Expression (5) corresponds to the situation where the axial force is $4N_E$ and leads to the unreasonable result that the bracing shall be stiffer if the sizes of the column are increased beyond what is needed. It is therefore proposed to replace (5) by:

$$C \ge k_s N_d / a \tag{7}$$

2.2 Strength of supports

To get an estimate of the reaction forces it is assumed that the column, see figure 3, has an initial sinusoidal deflection with the value e in the middle. Due to the axial force, N, e is increased to $u_m = eN_E/(N_E - N)$, where N_E is the Euler load-carrying capacity. The angle at the

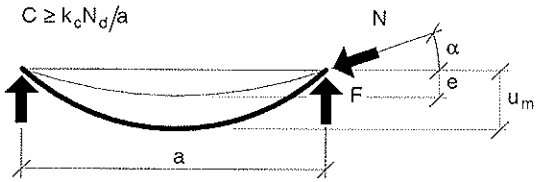

Figure 3 – Reaction in the deflected state

supports is $\alpha = \pi u_m/l$ and the reaction force $F = N\alpha$ If the intermediate support is sufficiently stiff, $a \leq 0.5l$, where l is the total length of the column. Then $N \leq 0.25N_E$, i.e.

$$F \leq 1.33\pi N_E/l \sim 4N_E/l \tag{8}$$

If it is required that $e/l \leq 1/300$ for structural timber and $e/l \leq 1/500$ for glulam, then the reaction forces become $N/75$ and $N/125$, respectively. [Eurocode 5, 1993] requires

$$F_d \geq N_d/80 \qquad \text{for structural timber} \tag{9}$$

$$F_d \geq N_d/100 \qquad \text{for glulam} \tag{10}$$

Bracing of the compression side of a beam

The compression side of a beam with moment M and depth h may be regarded as a column with an axial force $1.5N/h$. This is, however, rather much on the safe side: The bracing will normally be placed along the top of the beam, i.e. over the compression force, and the beam has a torsional stiffness. [Eurocode 5, 1993] therefore permits (9) and (10) to be used with

$$F_d = (1 - k_{cr})M_d/h \tag{11}$$

where k_{cr} is the factor for lateral instability of the beam.

3 Bracing of systems

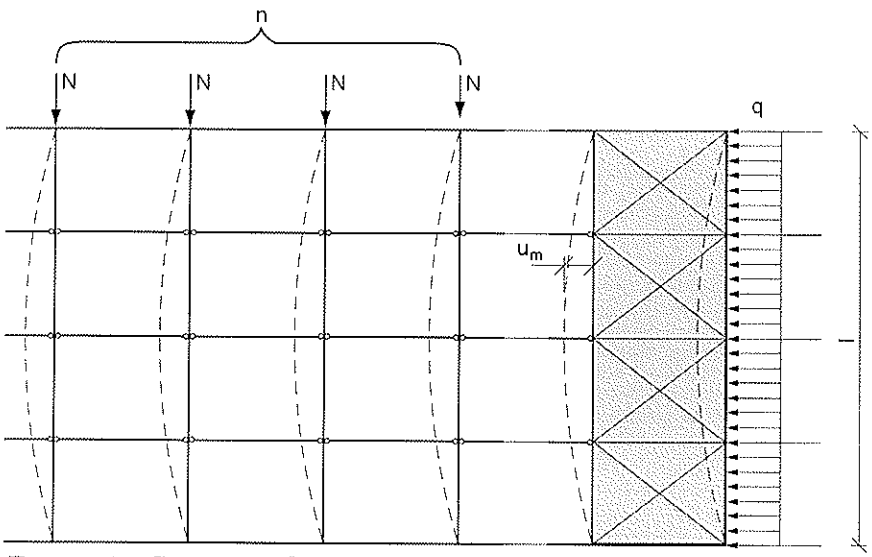

Figure 4 – System with n colums held in place by a bracing system

The system consists of n columns (e.g. the compression flanges of roof trusses) held in place by a bracing system (e.g. a wind bracing at the gables) loaded by a uniformly distributed action $q = q_0$, see figure 4. The columns may be part of the bracing. For simplicity, it is conservatively assumed that the axial forces in the columns, N, are equal and constant.

It is assumed that the resulting deflection in the middle of the bracing is u_m. u_m is due to an initial imperfection (conservatively assumed to be the same for all columns), the external action q_0 and the moment nNu_m from the axial forces. The moment is equivalent to an additional external load (for simplicity assumed to be uniformly and not sinusoidally distributed) of $q_1 = 8nNu_m/l^2$.

In [Eurocode5, 1993] it is required that the deflection from q_1 should not exceed $l/500$ i.e. $q_1 \leq 8nN/(500l) = nN/(63l)$. On the safe side, [Eurocode 5, 1993] requires that, in addition to the design value ($q_{0,d}$) of q_0, the bracing shall be designed for a uniformly distributed action:

$$q_{1,d} = k_l n N_d/(50l) \tag{11}$$

where k_l is a factor that allegedly takes into account that the workmanship should be higher for long spans:

$$k_l = min \begin{cases} 1 \\ \sqrt{15/l} \end{cases} \tag{12}$$

Furthermore, [Eurocode 5, 1999] limits the deflection for $q_{0,d}$ alone to $l/700$.

4 References

Brüninghoff, H., 1983: Determination of bracing structures for compression members and beams. Paper CIB – W18/176– 15 – 1.
Brüninghoff, H., 1984: Proposal for chapter 7.4, Bracing. Paper CIB – W18/17 – 15 – 1.
Eurocode 5, 1993: ENV 1995-1-1, Design of timber structures - Part 1-1: General rules and rules for buildings.
Timoshenko, S.P. & Gere, I.M., 1961. Theory of elastic stability.

INTERNATIONAL COUNCIL FOR RESEARCH AND INNOVATION
IN BUILDING AND CONSTRUCTION

WORKING COMMISSION W18 - TIMBER STRUCTURES

A DESIGN MODEL FOR LOAD-CARRYING TIMBER FRAME MEMBERS IN WALLS AND FLOORS EXPOSED TO FIRE

by

J König

Trätek - Swedish Institute for Wood Technology Research

SWEDEN

MEETING THIRTY-THREE
DELFT
THE NETHERLANDS
AUGUST 2000

Presented by: J. König

· H. Blass commented on the important influence of joints in gypsum boards on the charring rate and suggested that considering the joints be distributed everywhere would be easier. Load sharing of members during a fire was also discussed. H. Blass also asked whether gypsum boards would act as additional bracing for the wall.
· J. König answered that the gypsum on the fireside would not contribute.
· S. Thelandersson commented on the empirical based approach of the research in terms of what is the experimental background; how can the results be generalized; and how to handle the randomness and uncertainties of the parameters?
· J. König responded that information on material properties would be presented in another paper. Also no statistical data is currently available. He only used the average values; e.g., the average charring rate. In future additional factors might be introduced to take uncertainties into consideration.
· S. Thelandersson commented fire-rating information could be in the range of 65 minutes (+ or – 20 minutes); therefore, doubtful in principle that using average values would be appropriate. He also suggested that direct fire test on wall assembly should be considered.
· J. König responded that fire test results might also be doubtful. The current approach was to developed empirical model on the basis of testing of difference parameters; e.g., thermal properties. Model these properties and fit to model factors and perform critically analysis of the information. However, one could not really guarantee the outcome. Another example would be simplification with linearity of charring rate as a practical choice.
· S. Svensson questioned why design values could be given in the paper but not characteristic value information.
· J. König continued that too limited information is available to allow characteristic value information be given.
· S. Svensson asked about the factors used in the analysis.
· J. König responded that effect of temperature on strength and stiffness as material properties was determined.
· S. Svensson asked about where is the time term in Equation 15.
· J. König responded that in the Equation terms were related to engineering properties and heating. It is an indirect but easiest way.
· S. Svensson asked whether this approach gave good correspondence to strength reduction.
· J. König responded yes.
· E. Karacabeyli commented that the weight of gypsum on the ceiling would make a difference.
· J. König agreed but commented that data was not available therefore could not generalize. In these situation, code format should say failure time should be determined by testing.

A design model for load-carrying timber frame members in walls and floors exposed to fire

Jürgen König
Trätek - Swedish Institute for Wood Technology Research, Sweden

Summary

A design model is presented for the calculation of the load-bearing capacity of timber framed wall and floor assemblies exposed to standard fire exposure. It is implied that the cavities of the assemblies are filled with rock or glass fibre insulation, providing partial protection against charring of the wide sides of the timber members. The design model consists of a charring model giving a simplified rectangular residual cross section, and a mechanical model describing the strength and stiffness properties of the residual cross section. The charring model takes into account different charring rates that are dependent on the protection provided by the lining, and the conditions during the post-protection stage after complete failure of the lining. Criteria are given for the failure of linings including the length of fasteners. The reduction of strength and stiffness parameters is taken into account by multiplying cold values by modification factors. The model parameters were derived from test data, heat transfer calculations and mechanical modelling of the cross section using temperature dependent strain-stress relationships.

1 Introduction

Unlike heavy timber structures where the char-layer of fire exposed members performs as an effective protection of the remaining unburned residual cross section, the fire performance of light timber framed members is crucial to the protection provided by the linings and the cavity insulation. Also, in light timber members, strength and stiffness parameters are considerably more dependent on the effect of fire exposure than in heavy timber cross sections, since greater portions of the residual cross section are affected by elevated temperatures. During the recent decade, comprehensive experimental research was conducted on light timber frame assemblies, both on wall assemblies in full and medium scale, and on assemblies in bending in small-scale fire tests (König, J. 1995 and König et al. 1997) with standard fire exposure according to ISO 834 and natural fire using parametric fire curves. Following these investigations, as a first step, a design model was developed for standard fire exposure, with the main purpose to give the designer a tool that is easy to use, however sufficiently precise to describe the performance adequately, and to

take into account different failure modes (König et al. 2000). The model deals only with timber framed wall and floor assemblies with linings of gypsum plasterboard or gypsum plasterboard backed with wood-based boards, and cavities completely filled with rock or glass fibre insulation. In the following sections, a short general description of the design model is given. The model parameters were derived from test data, heat transfer calculations and mechanical modelling of the cross section using temperature dependent strain-stress relationships. Thermal and mechanical properties of materials are discussed by Källsner et al. (2000). Model parameters are published in a Nordic design manual by Östman et al. (1999) and in König et al. (2000).

2 General presentation of the design model

2.1 Charring phases

With respect to the performance of linings, König et al. (1997) identified the following protection and charring phases, see Figure 2.1 and 2.2:

- Charring phase 1 of initially unprotected wood (not shown in the figures)
- Protection phase before failure of boards, consisting of
  - Pre-charring phase (complete protection against charring)
  - Charring phase 2 (incomplete protection against charring)
- Post-protection phase after failure of the lining: charring phase 3

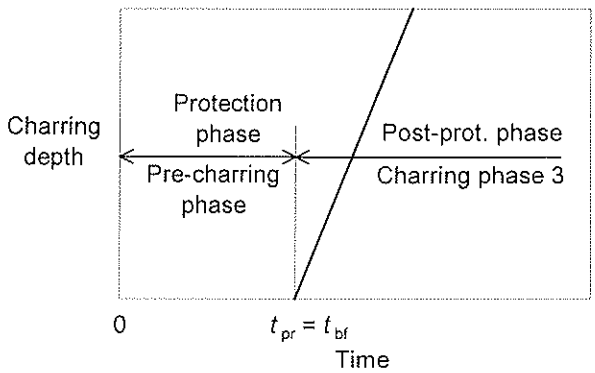

Figure 2.1: – Charring phases of timber members protected by wood-based boards

The protection phase is defined as the time period, during which the protection is attached to the timber member such that the member is not directly exposed to the fire, although there might be some charring during that phase. The protection phase ends at time t_{bf} (board failure). Where wood-based boards are used as protection, the start of charring t_{pr} coincides with the failure time t_{bf}. In the general case, e.g. when non-combustible boards are used, the protection phase consists of the pre-charring phase with complete protection against charring terminated at time t_{pr}, and charring phase 2. During charring phase 2, due to the insulation provided by the protection, the charring rate is normally smaller than it would have been without the protection (charring phase 1). Finally, after failure of the protection, during the post-protection phase the member is directly exposed to the fire. With respect to charring, this stage is called charring phase 3.

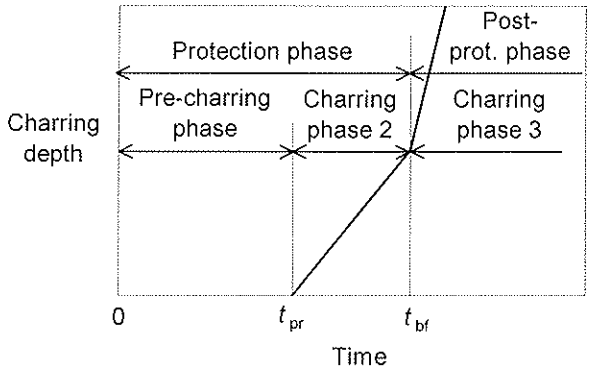

Figure 2.2 – Charring phases of timber members protected by non-combustible boards in general

2.2 Initially unprotected timber frame member

For timber frame members in wall and floor assemblies with cavities filled with insulating material, the residual cross section typically has a shape as shown in Figure 2 with pronounced corner roundings due to two-dimensional heat transfer in the wood and the insulation. The charring depth of the member is characterized by the charring depth in the middle of the width, given as

$$d_{\text{char}} = \kappa_s \, \beta_0 \, t \tag{1}$$

where

β_0 is the basic charring rate for one-dimensional charring of initially unprotected wood

κ_s is the cross section factor (see Table 2.1)

t is the time of fire exposure.

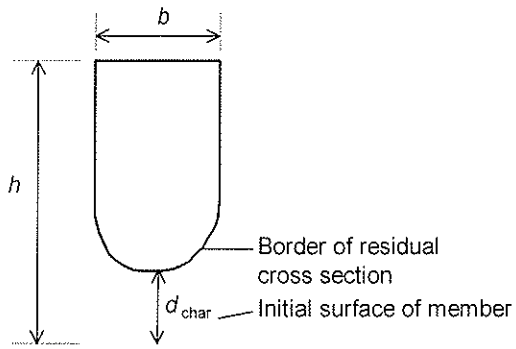

Figure 2.3 – Residual cross section of timber member in assemblies with insulated cavities

Table 2.1 – Cross section factors for different widths of member

b	κ_s
mm	–
38	1,4
45	1,3
60	1,1
90	1,0

2.3 Members protected by linings

Correspondingly to the schematic graphs of charring phases of Figure 2.1 and 2.2, simplified relationships of charring depth versus time rates are shown in Figure 2.4 and 2.5.

For members protected by wood-based boards, charring starts when the board is burned through at time t_{pr}. At this time the board, now consisting only of a char layer, is assumed to fall off the member, with the fire exposed side now being completely unprotected (post-protection phase or charring phase 3). When the cavity is filled with rock fibre insulation, the sides of the timber

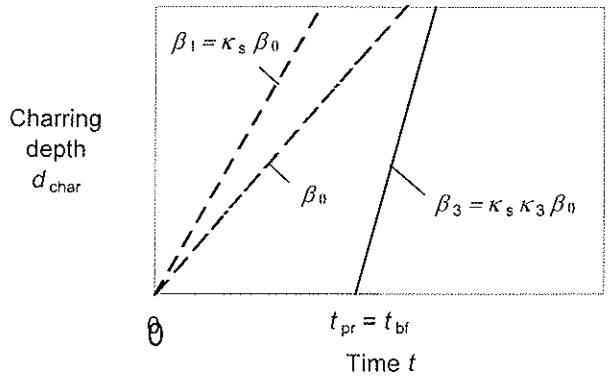

Figure 2.4 – Charring depths in timber frame member during charring phases 1 and 3

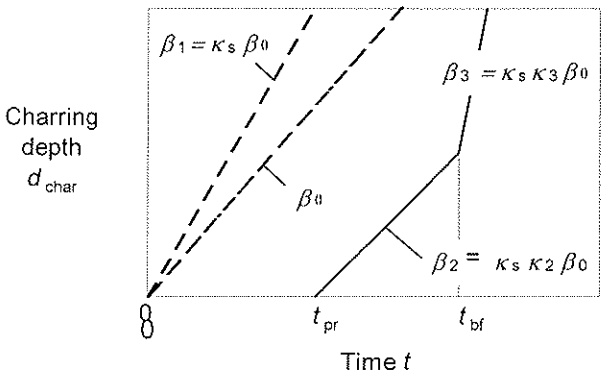

Figure 2.5 – Charring depths in timber frame members during charring phases 1, 2 and 3

members are still partially protected, provided that the insulation bats remain in place. Since the gas temperature now is considerably greater than in the beginning of the fire, the charring rate is much greater than given by equation (1):

$$\beta_3 = \kappa_s \kappa_3 \beta_0 \tag{2}$$

Where κ_3 is the post protection factor given as

$$\kappa_3 = 0{,}036\, t_{bf} + 1 \tag{3}$$

and t_{bf} is the failure time of the lining in minutes (see Figure 2.6). The charring depth is given by

$$d_{char,3} = \kappa_s \, \kappa_3 \, \beta_0 \, (t - t_{pr}) \tag{4}$$

where t_{pr} is the time of onset of charring (time of protection against charring).

Many non-combustible linings remain fixed to the timber frame during a period of time exceeding the time of onset of charring. During this stage – charring phase 2 – the charring rate is normally smaller than given by equation (1):

$$\beta_2 = \kappa_s \, \kappa_2 \, \beta_0 \tag{5}$$

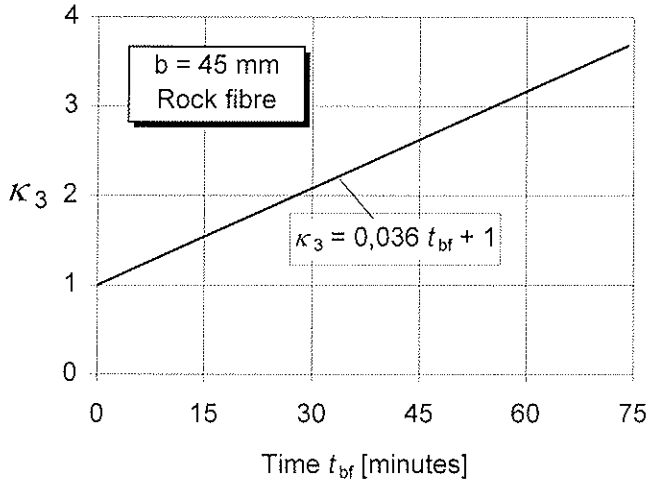

Figure 2.6 – Post-protection factor vs. failure time of lining

where κ_2 is the insulation factor of the lining. For charring phase 2 the charring depth is given as

$$d_{char,2} = \kappa_s \, \kappa_2 \, \beta_0 \, (t - t_{pr}) \tag{6}$$

and after failure of the lining for charring phase 3 as

$$d_{char,3} = \kappa_s \, \beta_0 \left[\kappa_2 \, (t_{bf} - t_{pr}) + \kappa_3 \, (t - t_{bf}) \right] \tag{7}$$

For linings made of gypsum plasterboard, for different joint configurations as shown in Figure 2.7, values of protection times t_{pr}, i.e. times when charring starts, and insulation factors κ_2 are shown in Figure 2.8 and 2.9 respectively.

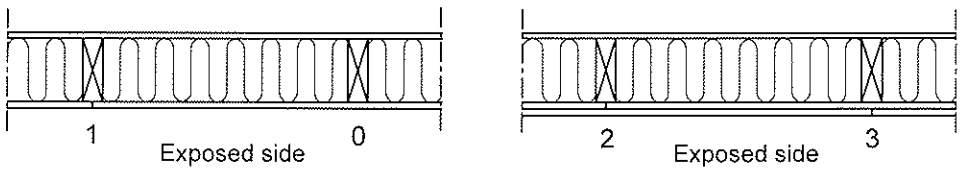

Figure 2.7 – Examples of joint configurations of single and double layered linings

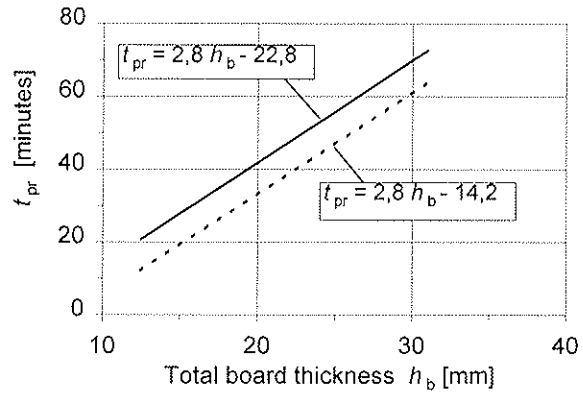

Figure 2.8 – Delay of start of charring provided by gypsum plasterboard

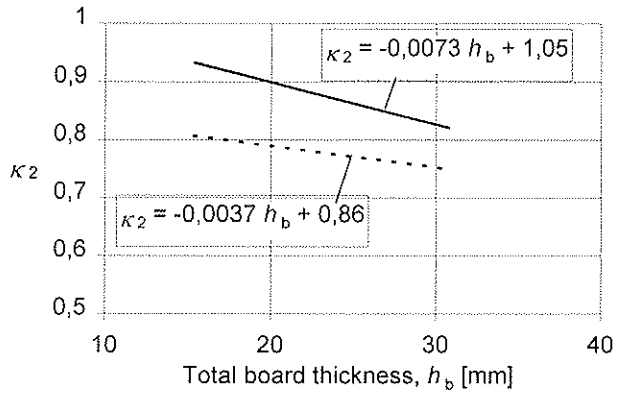

Figure 2.9 – Insulation factor versus total thickness of gypsum plasterboard

2.4 Failure criteria for linings

Failure times t_{bf} of the lining depend on the strength properties at elevated temperature. Since regular gypsum plasterboard (GA) falls off the timber frame in an early stage of the fire exposure – normally shortly after charring starts in the member behind the lining – charring phase 2 should not be taken into account for these boards. Therefore

$$t_{bf} = t_{pr} \tag{8}$$

For gypsum plasterboard with improved core cohesion (GF), the mechanical properties may vary dependent on, inter alia, density, glass fibre reinforcement and fillers.
The failure time of the lining depends on two failure modes:

- Failure due to mechanical degradation of the boards (including pull-through failure of connections)
- Failure of fixing to the timber frame (pull-out failure of fasteners).

For Nordic gypsum plasterboard of type F produced by Gyproc, test results show that the critical temperature reached on the non-exposed side of a board is approximately 600°C for ceiling linings and approximately 800°C for wall linings, although there exists a large scatter of test results. Based on these temperature criteria, failure times are shown in Table 2.2. For gypsum plasterboard type F of other origin, other temperature criteria may be relevant and failure times should be determined by testing.

Table 2.2 – Example of failure times of gypsum plasterboard linings due to mechanical degradation according to temperature criteria

Lining	t_{bf}	
	Walls	Ceilings
	min.	min.
1 layer GF (12,5 mm)	65	35
1 outer layer GF (15,4 mm) 1 inner layer GA (12,5 mm)	77	57
2 layers GF (2 ×15,4 mm)	> 90	> 60

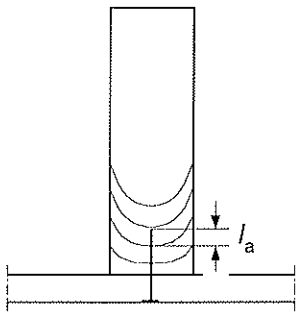

Figure 2.10 – Fixing of lining – Penetration length of fastener into unburned wood

When the strength properties of the lining is not seriously affected by elevated temperatures, the length of fasteners may be decisive, since the penetration into unburned wood may be insufficient causing withdrawal failure of the connection. Where the boards are screwed to the member in the middle (i.e. no joint), see Figure 2.10, the failure time is given as

$$t_{bf} = t_{pr} + \frac{l_f - l_{a,min} - h_{b,tot}}{\beta_0 \kappa_s \kappa_2} \tag{9}$$

where l_f is the length of the fastener, $l_{a,min}$ is the minimum length of penetration (anchorage) in the unburned wood and h_b is the total thickness of boards. For screws a penetration length of 10 mm is a reasonable assumption. For linings with joints and the boards fixed at the quarter points of the width, the failure time is given as

$$t_{bf} = t_{pr} + \frac{l_f - l_{a,min} - h_{b,tot}}{1{,}15\, \beta_0 \kappa_s \kappa_2} \tag{10}$$

since the charring depth is approximately 15 % greater at this location. Where resilient channels are used, their fixing to the timber frame members may be critical for the performance of the lining even though the boards remain fixed to the channels. Equation (9) should be used accordingly. After failure of the boards, resilient channels fixed to floor joists are still capable of keeping rock fibre bats in place, allowing charring phase 3 to be used in the design.

During this phase the failure time of the resilient channels is given as

$$t_{rf} = t_{bf} + \frac{l_f - l_{a,min} - \beta_0 \kappa_s \kappa_2 (t_{bf} - t_{pr})}{\beta_0 \kappa_s \kappa_3} \tag{11}$$

2.5 Simplified rectangular shape of residual cross section

In order to prevent an irregular shape of the residual cross section in the design, it is transformed to a rectangular shape by introducing a notional charring depth given as

$$d_{char,n} = \kappa_n \, d_{char} \tag{12}$$

with values of κ_n between 1,3 and 1,6. Unfortunately the transformation factor κ_n is dependent on the charring depth and the relevant cross section property (area, section modulus, second moment of area) that should be the same in both cases. A recommended value of 1,5 will give a reasonable approximation in most cases.

2.6 Reduction of strength and stiffness parameters

Using the same procedure as in cold design determining the load bearing capacity of a member, the strength and stiffness parameters have to be reduced due to the influence of elevated temperatures. Thus, following the format of ENV 1995-1-2 (1994)[1], the design strength and modulus of elasticity respectively are determined as

$$f_{fi,d} = k_{mod,fi,f} \frac{f_k}{\gamma_{M,fi}} \tag{13}$$

$$E_{fi,d} = k_{mod,fi,E} \frac{E_k}{\gamma_{M,k}} \tag{14}$$

where f_k and E_k are characteristic (cold) values of strength and modulus of elasticity and $\gamma_{M,fi}$ is a partial safety factor. Simplified linear expressions for the modification factors for fire are of the shape

$$k_{mod,fi} = a_0 - a_1 \frac{d_{char}}{h} \tag{15}$$

e.g. as shown in Figure 2.11 for cross sections with a width of 45 mm. In general, it is taken into account whether the fire exposed side of the cross section is in compression or tension. Modification factors are also derived for buckling about the weak axis of the original timber member which may occur where studs are not braced by panels on the unexposed side, e.g. in party walls.

2.7 Structural model for members in compression

For out-of-plane buckling, a considerable degree of rotational restraint of the stud ends can be taken into account, assuming pinned end supports and a buckling length l_{crit} given by

$$l_{crit} = 0{,}7\, l \tag{16}$$

where l is the length of the studs including the sole and head plate.

---

[1] For clearness, the coefficient k_{fi} is omitted here, taking into account that the 20 percentile is used instead of the 5 percentile as characteristic value for strength and stiffness parameters.

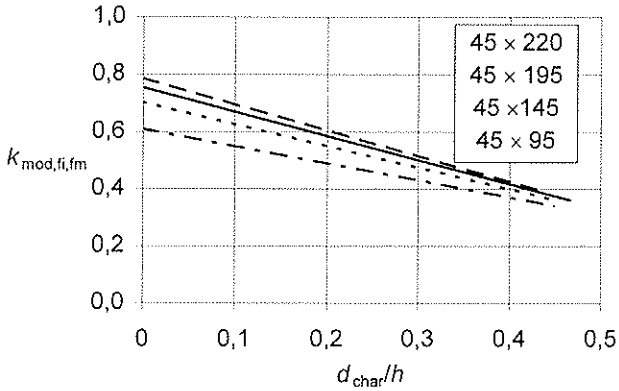

Figure 2.11 – Examples of modification factors for fire for reduction of bending strength (fire exposed side in tension, e.g. in single span floor joists)

3 Proposal for Eurocode 5

It is proposed to include the method described above in an informative annex to the revised Fire Part of Eurocode 5. Since the method, due to its complexity may be more adequate for a design manual, it is felt that it should be simplified further to be included in the code. Further simplifications are proposed:

- Only the notional charring rate β_n and charring depth $d_{char,n}$ are given to determine the notional residual cross section, see figure 3.1;
- modification factors are related to the notional charring depth ratio $d_{char,n}/h$ instead to d_{char}/h and are simplified further to reduce the number of expressions;
- Expressions (9) – (11) for the determination of failure times of linings are changed accordingly.

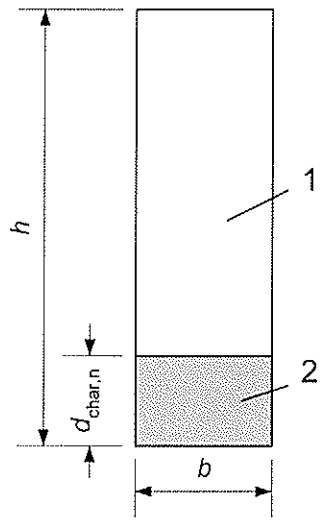

Key:
1 Notional residual cross section
2 Notional char layer

Figure 3.1 — Notional residual cross section of timber frame member protected by cavity insulation

4 References

ENV 1995-1-2 (1994). Eurocode 5 – Design of timber structures – Part 1-2 Structural fire design.

Källsner, B. and König, J., 2000. Thermal and mechanical properties of timber and some other materials used in light timber frame construction. CIB W18 Paper 33-16-3

König, J. 1995. Fire resistance of timber joists and load bearing wall frames. Swedish Inst. for Wood Technology Research. Report I 9412071.

König, J. and Walleij, L. 1999. One-dimensional charring of timber exposed to standard and parametric fires in initially unprotected and postprotection situations. Swedish Inst. for Wood Technology Research. Report I 9908029

König, J. and Walleij, L. 2000. Timber frame assemblies exposed to standard and parametric fires – Part 2: A design model for standard fire exposure. Swedish Inst. for Wood Technology Research. Report I 0001001.

König, J., Norén, J., Bolonius Olesen, F., and Toft Hansen, F. 1997. Timber frame assemblies exposed to standard and parametric fires – Part 1: Fire tests. Swedish Inst. for Wood Technology Research. Report I 9702015.

Östman, B., König, J., Mikkola, E., Stenstad, V., Karlsson, B., and Walleij, L. 1999. Brandsäkra trähus – Kunskapsöversikt och vägledning för lättbyggsystem i Norden. Swedish Inst. for Wood Technology Research. Publ. nr 9908034.

INTERNATIONAL COUNCIL FOR RESEARCH AND INNOVATION IN BUILDING AND CONSTRUCTION

WORKING COMMISSION W18 - TIMBER STRUCTURES

A REVIEW OF COMPONENT ADDITIVE METHODS USED FOR THE DETERMINATION OF FIRE RESISTANCE OF SEPARATING LIGHT TIMBER FRAME CONSTRUCTION

by

J König
Trätek - Swedish Institute for Wood Technology Research
SWEDEN

T Oksanen
VTT – Building Technology, Fire Technology
FINLAND

K Towler
Chiltern International Fire
UNITED KINGDOM

MEETING THIRTY-THREE
DELFT
THE NETHERLANDS
AUGUST 2000

Presented by: J. König

No discussion.

A review of Component Additive Methods used for the determination of fire resistance of separating light timber frame construction

Jürgen König
Trätek - Swedish Institute for Wood Technology Research, Sweden

Tuuli Oksanen
VTT – Building Technology, Fire Technology, Finland

Kevin Towler
Chiltern International Fire, United Kingdom

Summary

Verification of fire resistance of separating constructions is performed with respect to criteria I (insulation) and E (integrity). While fire testing is still the most common way of verification, design by calculation will be more common in the future. Several calculation methods called component additive methods have been in use since several years. All of them stipulate that in a construction built up of several layers or membranes, the total fire resistance is the sum of the contributions to fire resistance of each of the layers. This paper reviews and compares the design method given by ENV 1995-1-2 with methods being used in North America, the United Kingdom and Sweden. A proposal for the revised Fire Part of Eurocode 5 is presented.

1 Introduction

In most fire regulations, in order to facilitate safe egress of occupants and protect the lives of the fire brigade, an essential objective of the fire safety design is to limit the spread of fire from beyond the fire compartment of origin for an acceptable safe period of time. The required period of time is normally expressed in terms of the fire resistance test using a nominal time-temperature curve according to ISO 834, with required levels of fire resistance given by the building regulations or local authorities.

In buildings the boundaries of a fire compartment are the walls and floors that enclose the fire compartment. The separating function of the construction is provided by

- integrity (criterion E), i.e. to prevent the fire spread by passage of flames or hot gases, and
- insulation (criterion I), i.e. to limit the temperature on the unexposed side, thus preventing ignition of objects in the neighbouring compartment.

For separating constructions that are also load bearing, the collapse of the separating elements must be prevented during the required time of fire resistance (criterion R).
A complete design of fire resistance of compartment enclosures includes the verification of the above criteria E, I and R. In the following, several calculation methods are presented for the verification of the separating function of walls and floors. In two of them, the load bearing function is included. These methods are called component additive methods, since the fire resistance of a layered construction is obtained by adding the contribution to the fire resistance of the different layers.

Criterion I (insulation) is clearly defined as the stage at which the temperature increase on the unexposed side is limited to 140 K in average and 180 K at any location, and thus the verification could be made by heat transfer calculations instead of testing. A problem is that such calculations are a very complex problem and that material properties often are not known. It has also been argued that integrity (criterion E) cannot be determined by calculation, which is certainly true. Only the times of heat transfer through each layer can be added, while premature integrity failure may occur due to sudden failure of linings or opening of gaps, which often is dependent on the construction details such as fixings. However, design expressions or criteria can be given based on extensive experience of full-scale testing of wall and floor assemblies. Some rules will be proposed to be included in the redrafted version of EN 1995-1-2.

The requirement with regard to criterion I to limit the temperature rise on the unexposed side by the specified values 140 and 180 respectively, reflects the situation of standard fire tests, e.g. of load bearing walls according to EN 1365-1. Thermocouples are located evenly distributed over the surface in order to record the average temperature, and at specified locations where larger temperatures can be expected, e.g. near joints of panels.

2 ENV 1995-1-2

2.1 The method

For the verification of the load bearing function members exposed to fire, ENV 1995-1-2 gives values of protection times t_{pr} by which the onset of charring of timber elements is delayed by protection from fire of timber protecting claddings. In general, the protection time should be determined by testing; the test standard ENV 18361-7 is now subject to formal vote within CEN. For some materials such as wood-based panels, gypsum plasterboard and insulation material, expressions are given for the calculation of t_{pr}.

For the verification of the separating function, ENV 1995-1-2 uses the sum of protection times t_{pr} of each layer, however with a correction for the unexposed layer to take into account the time needed for the temperature rise from 160°C to 300°C. The temperature of 160°C corresponds to ambient temperature 20°C plus permitted temperature rise of 140 K, while the temperature of 300°C refers to level of onset of charring. With other words, the method gives the time for the exposed side to reach 300°C (this takes about 2 to 3 minutes)

plus the time needed for the 300-degree isotherm to move through all layers, with a correction for the unexposed side.

The requirements of ENV 1995-1-2 for a construction with different layers with respect to a 140 K increase of temperature are expressed as

$$\sum_i t_{pr,i} \geq t_{fi,req} + [15] \quad (1)$$

where

$t_{pr,i}$ is the protection time of layer i in minutes

$t_{fi,req}$ is the required time of fire resistance of the construction in minutes.

This should be applied to heat transfer path "a" as shown in Figure 2.1. The boxed value of 15 minutes includes both the time needed to increase from 160 to 300°C and a not specified extra safety margin.

In order to limit the temperature rise by 180 K at any location, the corresponding requirement is

$$\sum_i t_{pr,i} \geq t_{fi,req} + [5] \quad (2)$$

This requirement should be assessed to weak points or zones, e.g. where linings are jointed on the unexposed side, or where services lead to weak zones, see heat transfer paths "b", "c" and "d" shown in Figure 2.1. See also Table 2.1.

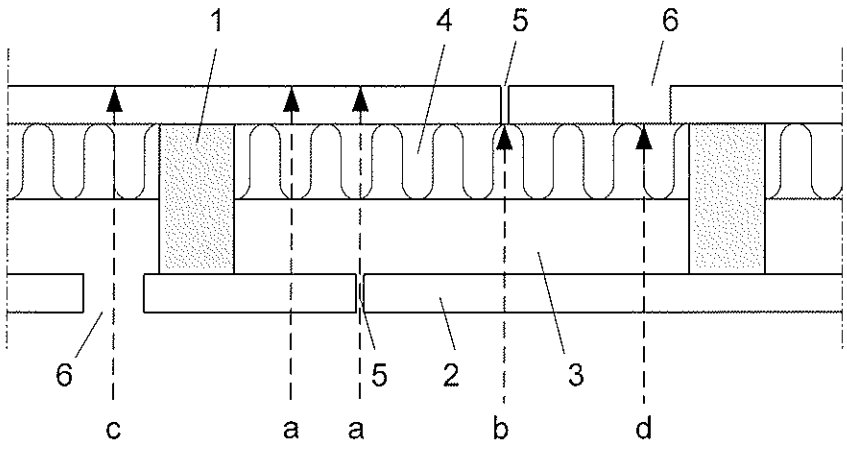

Key

1	timber frame member
2	panel
3	void cavity
4	cavity insulation
5	panel joint
6	position of services
a – d	heat transfer paths

Figure 2.1: Illustration of heat transfer paths through separating multiple layered construction

Table 2.1: Heat transfer path through layer to be taken into account

	Temperature rise on unexposed side °C	Heat transfer path according to Figure 2.1
General construction and joints on exposed side	140	a
Joints on unexposed side	180	b
Services	180	c, d

For panels wood-based and wood panels, the protection time t_{pr}, based on the assumption that such panel would fall off the construction four minutes before it is burnt through, gives values for t_{pr} considerably on the conservative side.

The effect of panel joints is taken into account by reducing the values of t_{pr} by a reduction coefficient ξ, but only for panels in horizontal position (floors), although this weakening effect also exists for panels in vertical position (walls).

2.2 Discussion

The method given by ENV 1995-1-2 is easy to use, however it is unable to reflect the real performance of multi-layered separating constructions. The main deviation from reality is that the methods gives equal weight to each layer, while it is known that the thermal performance of one layer is dependent on its position in the layered construction. The method simply assumes that each layer is exposed in the same way, even though layer 2, 3 and so on are preheated with a surface temperature of 300°C. In a test situation, the temperature in the furnace is increasing continuously, which would reduce the contribution of further layers due to greater heat attack. On the other hand, in many cases, a layer remains in place, even after its protection time t_{pr} is reached, providing further protection against direct fire exposure due to its insulation. This is the case for the inner layer of double layered linings on the fire exposed side, and for the contribution of panels on the unexposed side, where rock fibre insulation is used in the cavity and gypsum plasterboard is attached to the fire exposed side.

Even though the method in many cases gives acceptable results, it is not consistent. Especially the effect of joints is dealt with in a non-consistent way, by taking them into account for floors but not for walls. For the rest the method does not differentiate between floor and wall constructions. Some confusing elements are the boxed values (here in brackets) in expressions (1) and (2), consisting of physical data and safety factors.

3 United Kingdom

3.1 The method

In the UK, BS 5268: Part 4: Section 4.2 is used to evaluate the fire resistance of timber structures. The method contained within the standard is used to evaluate the performance of the structure when tested to BS 476 Part 8. This standard has been superceded within the UK by BS 476 Part 22. This method evaluates the stability, integrity and insulation of the structure being analysed. The term stability is no longer a criteria specified within BS 476 Part 22 or the new European test methods and the term "Loadbearing capacity" is used. The method considers only the following construction types:

- Internal walls 30 minute or stability, integrity and insulation (REI 30)
- Internal walls 60 minute for stability, integrity and insulation (REI 60)
- External walls 30 minutes for stability and integrity and 15 minutes for insulation (RE 30, I 15)
- External walls 30 minutes for stability and integrity and for insulation (REI 30)
- External walls 60 minutes for stability and integrity and 15 minutes for insulation (RE 60, I 15)
- External walls 60 minutes for stability and integrity and for insulation (REI 60)
- Timber floors 30 minutes for stability and 15 minutes for integrity and insulation (R 30, EI 15)
- External walls 30 minutes for stability and integrity and for insulation
- External walls 60 minutes for stability and integrity and for insulation

The analysis method is based on evaluating the contribution of the different parts of the construction to the overall fire resistance, namely the following elements:

- Flooring, or unexposed boarding system
- Size of studs and insulation within void
- Ceiling or exposed boarding system.

The contribution to the fire resistance for each of the different elements considers the following aspects :

- the material types, e.g. plasterboard (type A) plywood, hardboard, particleboard, tongued and grooved softwood flooring,
- thickness of material and whether an insulating material is present within the cavity.

The analysis considers all of the above factors, and the performance of the construction is evaluated by summing up the percentage contribution each element has in developing the required fire resistance. The contribution to stability, integrity and insulation is considered separately for each of the different elements within the construction. If the summation of percentages exceeds 100 % for each of the criteria R, E and I then the proposed design will achieve the required fire resistance.

3.2 Discussion

The UK method given above consists of tabulated data for a large number of materials/components. It gives results only for specified fire resistances 15, 30 and 60 minutes and cannot be used for other requirements that are specified in ID 2 (1994) and are used in the European classification for fire resistance. Contrary to the method given by

ENV 1995-1-2, the method also includes the loadbearing function, also the designer does not know about assumed load levels. For the designer the method is comprehensive, but a drawback is that it appears as a "black box".

4 North America

4.1 The method

The North American component additive calculation procedure (White, 1995, Richardson et al., 1997) is a method to determine conservatively the fire resistance of load-bearing light timber framed floor and roof assemblies and of loadbearing and non-loadbearing wall assemblies. The method uses principles described in Harmathy's "Ten Rules of Fire Endurance Rating" (White, 1995) to combine "assigned-time values" for each component of the assembly into a fire resistance time for the complete assembly. The method was developed by the National Research Council of Canada (NRCC) in the early 1960s, and has gained code approval in Canada (Supplement to the National Building Code of Canada, 1990) and in some U.S. building codes. The application of the method is generally limited to 60 or 90 min.

The fire resistance of the assembly is calculated by adding the time assigned for the protective membrane on the fire-exposed side of the assembly to the time assigned for the framing members plus the time assigned for any additional protective measures such as filling the cavities between the studs or joists with insulation. The assigned times are based on fire resistance tests of assemblies according to ASTM E 119. The criterion for the assigned time of the protective membrane is the membrane's ability to remain in place during fire resistance tests. The assigned times are defined for the boards commonly used in North American structures like Douglas fir plywood of different thicknesses, gypsum plasterboard of different types and thicknesses as well as different combinations of gypsum plasterboard, but not combinations of gypsum plasterboard and wood-based panels.

The times assigned to the framing members were based on the time between the failure of the protective membrane and the collapse of the assembly. Glass or rock fibre insulation protect timber studs from charring and thus delay the time of collapse. The times assigned for the insulation were based on their ability to further delay the collapse of the walls. The method includes also requirements for details of structures such as the minimum size and spacing of studs, wood joists and members of trusses, fastening the protective membranes to the frame as well as guidance how to install gypsum plasterboard to framing members.

The membrane on the side not exposed to fire makes no contribution to total fire resistance time. However, in order to ensure that the wall or floor/roof assembly does not fail because of fire penetration or heat transfer through the assembly, specified panel materials are accepted as the membrane on the unexposed side of the construction.

4.2 Discussion

The component additive method is extensively used by architects, fire-protection engineers and building officials in Canada and U.S.A. There are differences between the codes in what is accepted. There are individual items in the structures and the assigned time values

related to the structures that are not accepted by all the codes that otherwise accept the procedure. The method is simple and because of that it is also approximate e.g. same time value assigned to gypsum plasterboard is used for load-bearing and non-loadbearing walls. In Canada the method has been revisited in recent years by updating fire resistance times, most of which had not been changed since the method was originally published.

5 Sweden

5.1 The method

The Swedish components additive method is based on testing of non-loadbearing wall assemblies both in full and small scale (Norén, 1994). A short presentation of the method was included in Östman et al. (1994). The fire resistance of a wall assembly is the sum of contributions to fire resistance of the layers. Contrary to the method of ENV 1995-1-2 and the North American method, the contributions of the different layers are weighted, taking into account the thermal properties and performance of other layers building up the assembly. The following materials, apart from timber studs, were used:

- Wood-based panels (plywood, particleboard, fibreboard, bitumen impregnated fibreboard)
- Wood panels (tongued and grooved)
- Gypsum plasterboard (type A and F)
- Cement fibreboard
- Mineral wool of rock and glass fibre.

The tests showed, for example, the thinner panel is used on the fire exposed side, the more its performance depends on the backing layer. While a void cavity will have a cooling effect on the exposed panel, due to radiant heat transfer within the cavity, an insulated cavity will trap the heat, thus leading to faster increase of temperature and temperature dependent degradation and failure. In the same way, the insulating performance of the cavity insulation will be dependent on the performance of the exposed panel. If glass fibre is used as cavity insulation, it would melt shortly after failure of the exposed panel, now leaving the panel on the unexposed side unprotected. Here, the use of glass fibre has often a negative effect. An uninsulated construction would give a better fire resistance. The performance of rock fibre would give a dramatically improved fire resistance.

In the following the symbols deviate from those used in the above sources. The fire resistance according to criterion I, expressed as t_{ins}, is given as

$$t_{ins} = \sum_{i} t_{ins,0,i} \; k_{pos} \tag{3}$$

where

$t_{ins,0,i}$ is the basic value of layer "i"

k_{pos} is a coefficient of position.

The basic value of panel layers corresponds to the fire resistance of a single board without the influence of adjacent materials, i.e. the increase on its unexposed side by 140 K. Since the fire resistance of a single layer of glass fibre cannot be determined by testing, since it would melt almost immediately, for all insulation materials, the basic value is the additional contribution of the insulation layer derived from tests results. The coefficient of

position is defined to take into account the location of the layer in the construction. With other words: the method gives the time for the exposed side to reach 160°C (i.e. to increase by 140 K starting from normally 20°C) plus the time for the 160-degree isotherm to move through all layers.

The following characteristics can be noted:

- For the **exposed panel** the coefficient of position is dependent on the panel thickness and on the material of the second layer (void cavity, insulation or another panel)
- For the **unexposed panel** the coefficient of position is dependent on the type of insulation in the cavity; for rock fibre also on insulation thickness and for glass fibre also on the type of panel on the exposed side.
- For the **insulated or uninsulated cavities** the coefficient of position was put equal to one, except where gypsum plasterboard type F is used as exposed panel.

Basic values for panels and insulation materials are given in Figure 5.1 and 6.2. Coefficients of position are given in Table 5.1, 6.2 and 6.3. The basic values of glass fibre are only 50 percent of the values of rock fibre, since glass fibre melts within a few minutes after failure of the exposed panel. For insulation material combined with wood-based panels or gypsum plasterboard type A, the coefficient of position is one, where gypsum plasterboard type F is used on the fire exposed side, for glass fibre it is 2 and for rock fibre it is 1,5.

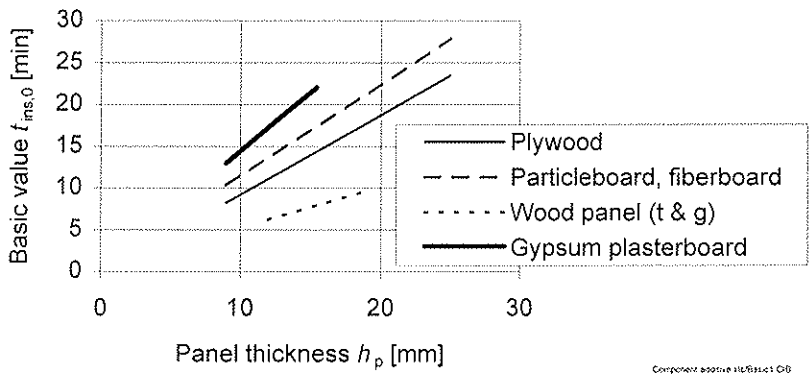

Figure 5.1: Basic values for some materials used as panels

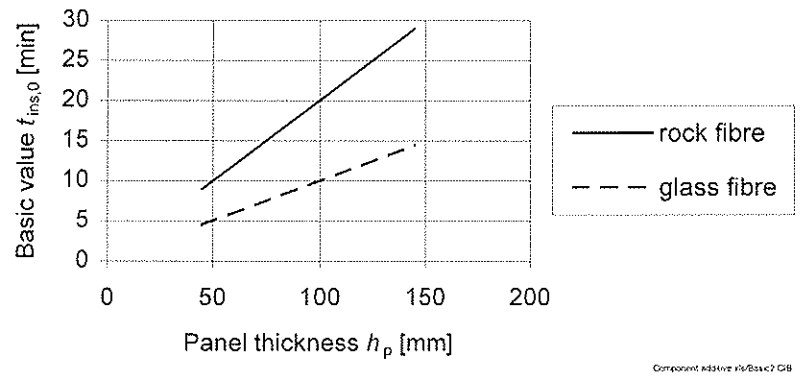

Figure 5.2: Basic values for rock fibre (26-30 kg/m^3) and glass fibre (20 kg/m^3); for other densities correction coefficients exist

Table 5.1: Position coefficients for single layered panels on the exposed side

Panel	Density kg/mm^2	Thickness mm	Position coefficient for panels backed by	
			rock or glass fibre	void
Plywood	450-590	9	0,72	
		12	0,78	
		15	0,84	0,8
		18	0,90	
		20	0,94	
		25	1,00	
Particleboard, fibreboard	600-800	9	0,72	
		12	0,78	
		16	0,86	
		19	0,92	0,8
		22	0,98	
		25	1,00	
Wood panels	≥ 400	15	0,84	0,8
		19	0,92	0,8
Gypsum plasterboard				
type H	≥ 740	9	0,72	
type A	≥ 680	12,5	0,80	0,8
type F	≥ 830	15	0,84	

Table 5.2: Position coefficients for single layered panels on the unexposed side

Panel	Density kg/mm^2	Thickness of panel on exposed side mm	Position coefficient for panels backed by				
			Glass fibre	Rock fibre of thickness			Void
				45	95	145	195	
Plywood	450-590	9	0,46	1,9	2,9	3,9	4,9	0,6
		12	0,67					
		15	0,88					
		18	1,09					
		20	1,23					
		25	1,58					
Particleboard, fibreboard	600-800	9	0,46	1,9	2,9	3,9	4,9	0,6
		12	0,67					
		16	0,95					
		19	1,16					
		22	1,37					
		25	1,58					
Wood panels	≥ 400	15	0,46	1,9	2,9	3,9	4,9	0,6
		19	0,67					
Gypsum plasterboard								
type H	≥ 740	9	0,46					
type A	≥ 680	12,5	0,74	1,9	2,9	3,9	4,9	0,7
type F	≥ 830	15	0,88					

Table 5.3: Position coefficients for walls with double layered panels with the layer numbers as defined in Figure 5.3

Construction: Layer number and material		Layer number				
		1	2	3	4	5
1, 2, 4, 5 3	Wood-based panel Void	1,0	0,6	1,0	0,5	0,7
1, 2, 4, 5 3	Gypsum plasterboard type A or H Void	1,0	1,0	1,0	1,0	0,7
1, 5 2, 4 3	Gypsum plasterboard type A or H Wood-based panel Void	1,0	1,0	1,0	0,8	0,7
1, 5 2, 4 3	Wood-based panel Gypsum plasterboard type A or H Void	1,0	0,6	1,0	1,0	0,7
1, 2, 4, 5 3	Wood-based panel Rock fibre bats	1,0	0,6	1,0	1,0	2,0
1, 2, 4, 5 3	Gypsum plasterboard type A or H Rock fibre bats	1,0	1,0	1,0	1,0	3,5
1, 5 2, 4 3	Gypsum plasterboard type A or H Wood-based panel Rock fibre bats	1,0	1,0	1,0	1,0	2,0
1, 5 2, 4 3	Wood-based panel Gypsum plasterboard type A or H Rock fibre bats	1,0	0,6	1,0	1,0	2,5

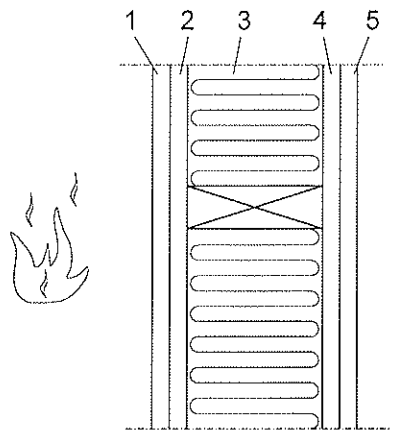

Figure 5.3: Definition of layer numbering

5.2 Discussion

The component additive method developed in Sweden prevents the drawbacks of the Eurocode method given in ENV 1995-1-2, however it is not as easy to use. An advantage is that it is more logic and gives the designer a better understanding of the performance, and a tool for improving the fire performance in the design. It was developed for walls, however with some modifications it should be able to use it for floors. Another parameter not covered by the method is the effect of panel joints without backing battens. For wood panels with tongued and grooved joints, this effect is included in the Swedish method.

The main advantage of the method is that it is general, and that it can be extended to other materials and combinations, both by testing or calculation. Since the method is based on limited test results, some modification of parameters is necessary.

6 Conclusions

The determination of the fire resistance of floor and wall assemblies by calculation is a complex task. In this paper four methods for the determination of the fire resistance with respect to the separating function of light timber framed assemblies are presented. Two of them include also the verification of the loadbearing function. All of them have advantages and drawbacks, due to conflicting goals: accuracy versus simplicity. The opinion of the Project Team redrafting the Fire Part of Eurocode 5 is that a design code should contain rational calculation methods, while tabulated data for constructions should be found in design manuals. This criterion would exclude the UK-method. The North American method is easy to use, however the logic behind is not obvious to the designer.

Since the Swedish method describes the real performance more adequately without being too complicated, it is proposed to adopt this method in the EN 1995-1-2 and to combine it with the existing ENV-method. Since the method is still incomplete, some corrections must be made to fit test results. It is also proposed to replace the tabulated data of coefficients of positions by simple equations. Since the method was developed only for wall constructions, it must be extended to include floor application, e.g by introducing a general reduction of coefficients of position. The effect of joints should be included as in ENV 1995-1-2. It is proposed to apply the method for the heat transfer paths given in the ENV with the exception of heat path b that should include all layers in order to take into account joints on the unexposed side. For that heat path b the value t_{ins} according to equation (3) should be increased by a few minutes, in order to adapt the time criterion to an temperature increase of 180 K instead of 140 K.

The main advantage of the proposed method is that it is more general and open for future extensions both by tests and general calculation methods.

Since integrity failure due to premature failure of linings may occur resulting from excessive deflections of loadbearing elements, a corresponding rule should be included. From fire tests can be seen that deflections of loadbearing constructions become excessive during the last 5 to 10 minutes prior to collapse. Therefore, equation (3) should not be used for times closer than, conservatively, 10 minutes from collapse.

7 References

ASTM E 119-88, 1988, Standard test methods for fire tests of building construction and materials. American Society for testing and Materials, Philadelphia

BS 5268, 1990, Structural use of timber, Part 4. Fire resistance of timber structures, Section 4.2. Recommendations for calculating fire resistance of timber stud walls and joisted floor constructions. British Standards Institution

EN 1365-1, Fire resistance tests for loadbearing elements, Part 1 Walls

ENV 1995-1-2:1994, Eurocode 5, Design of timber structures, Part 1-2 General rules – Structural fire design

ID 2, 1994, Interpretative document – Essential requirements No 2 – Safety in case of fire, Official Journal of the European Communities, No C 62/23, 28.2.94

Norén, J., 1994, Additionsmetoden – Beräkning av brandmotstånd hos avskiljande väggar (Addition method – Calculation of fire resistance for separating wood frame walls). Trätek – Swedish Institute for Wood Technology Research, Report I 9312070

Östman, B., König, J. and Norén, J.,1994, Contribution to fire resistance of timber frame assemblies by means of fire protective boards. Proceedings of the 3rd International Fire and Materials Conference, Washington D.C.

prENV 13381-7, Contribution to fire resistance of structural members - Part 7: Timber elements

Richardson, L. R. and Batista, M., 1997, Revisiting the Component Additive Method for Light-frame Walls Protected by Gypsum Board. Fire and Materials, vol. 21, 107-114

Supplement to the National Building Code of Canada, 1990, National Research Council of Canada, Ottawa

White, H. R., 1995, Analytical Methods for determining fire resistance of timber members. The SFPE Handbook of Fire Protection Engineering 2nd Edition 1995, Society of Fire Protection Engineers and National Fire Protection Association.

INTERNATIONAL COUNCIL FOR RESEARCH AND INNOVATION
IN BUILDING AND CONSTRUCTION

WORKING COMMISSION W18 - TIMBER STRUCTURES

THERMAL AND MECHANICAL PROPERTIES OF TIMBER AND SOME OTHER MATERIALS USED IN LIGHT TIMBER FRAME CONSTRUCTION

by

B Källsner
J König

Trätek - Swedish Institute for Wood Technology Research
SWEDEN

MEETING THIRTY-THREE
DELFT
THE NETHERLANDS
AUGUST 2000

Presented by: B. Källsner

· S. Thelandersson stated that the title was misleading and it was not clear where the properties came from. Also the thermal and mechanical properties should be measurable. In the paper some of these parameters were obtained via back calculations; therefore, one would need to be careful to put information in code as material properties.
· B. Källsner agreed. The information in the paper was apparent properties not test values and would make clear in code.
· S. Thelandersson stated that the scope of application should be limited.
· B. Källsner agreed that the scope should be limited to this type of walls that are normally used.
· J. Nielsen stated that the insulation and timber had perfect fit in the model. In reality 1 to 2 cm gap might exist. How would the results be influenced?
· B. Källsner answered the model used apparent values through calibration.
· S. Svensson commented that the influence on mechanical properties would be more sensitive to moisture rather than heat. In model, mass transfer was ignored. This type of information would be available from numerical results on wood drying.
· J. König agreed that moisture and temperature would have major influence. 100°c is a critical point below which moisture and temperature softening would be huge. Therefore, simplified approach with bi-linear relationship was adopted with the transition point at 100°c.
· S. Svensson commented that fire takes 1 hour and drying takes longer time.
· J. König agreed but said. Drying and burning are different. Moisture continuous change information with time is available. This may be supported via experiment of others.

Thermal and mechanical properties of timber and some other materials used in light timber frame construction

B. Källsner and J. König

Trätek – Swedish Institute for Wood Technology Research, Sweden

Summary

The Fire Part of Eurocode gives the option of applying simplified, more complex and general design rules. For assessment of general design rules, or the derivation of simplified design rules for thermal and mechanical analysis, material properties are needed such as thermal conductivity, specific heat capacity and reduced mechanical properties at elevated temperatures in combination with effects of moisture. Unfortunately there is a large variation of values given by different sources. This paper discusses different values and the dependence of calibrated properties on the applied model and gives the background of the values proposed to be adopted in the Fire Part of Eurocode 5.

1 Introduction

The Fire Part of Eurocode 5 contains rules for the design of timber structures exposed to fire. For normal design situations, design rules are simple and can be used by the structural engineer who normally does not need to have a deeper insight in the complex phenomena of wood and fire. Due to the move to performance based building regulations in many countries, alternative design methods, generally called fire safety engineering (FSE) – also including topics such as modelling of spread of fire and smoke, and the egress of occupants – are used to a larger extent. At the same time, we can see a large number of fire consultants appearing on the scene, with special competence of solving fire related problems. With other words, today building codes must move on two tracks, both giving simple rules for solving everyday problems and opening up for advanced solutions for special cases.

Consequently, ENV 1995-1-2 offers the option of using more advanced calculation methods. Regarding a general calculation method for the determination of the load-bearing capacity of a timber cross section, the ENV states that it should be based on explicitly given charring rates or general charring models, temperature and moisture content profiles in the residual cross section, and strength and stiffness properties dependent on temperature and moisture content. In an informative annex some information is given on thermal

properties of wood to be used in thermal analysis which might be used in a general charring model, however without defining a temperature criterion for the char-line. Regarding mechanical properties, the designer does not get any guidance. The designer who wishes to seek information in the literature will find plenty of information, unfortunately some of it being contradictory or even false. Many data are based on laboratory conditions rather than on the conditions that occur in a fire situation. Some of the data may be used in some applications, while they would give completely wrong answers in others.

A general problem when using models to calculate the heat transfer through structures is that, due to simplifications and deficiencies of the model, the thermal properties of the materials used as input parameters must be calibrated such that the results are fitted to those obtained by tests.

The load-carrying capacity of fire exposed wooden wall and floor assemblies are normally calculated in two steps. First, the temperature field in the structure is calculated. Based on the obtained temperature field in the wooden stud or beam, the capacity of the timber member is calculated.

The objective of this paper is to discuss the problem of giving material properties for thermal and mechanical analysis of timber structures in a design code, and to make proposals for the Fire Part of Eurocode 5, now being in the stage of redrafting for publication as EN 1995-1-2.

2 Properties for thermal analysis

2.1 General

In order to carry out a reasonably accurate calculation of the temperature field in a fire exposed timber member or a wall or a floor assembly, it is not sufficient just to give the thermal properties of the materials but also to set up the thermal model to be used in the structure. A general requirement on the thermal model is that it should be able to describe the transient heat transfer in the structure including properties as thermal conductivity, density and specific heat capacity for the used materials. The thermal properties of the materials should be varying with respect to the temperature.

In general, heat transfer can be explained by three modes: conduction, convection and radiation.

The fundamental equation for two dimensional conductive heat transfer is

$$\frac{\partial}{\partial x}\left(\lambda\frac{\partial T}{\partial x}\right)+\frac{\partial}{\partial y}\left(\lambda\frac{\partial T}{\partial y}\right)=\rho\, c\frac{\partial T}{\partial t} \qquad (1)$$

where

T Temperature [K]

λ thermal conductivity [W m^{-1} K^{-1}]

c specific heat [J kg^{-1} K^{-1}]

ρ density [kg m^{-3}]
x, y distances in direction of co-ordinates x and y [m]
t time [s].

The other two modes of heat transfer are

- convection, i.e. heat transfer due to random molecular motion and macroscopic fluid flow, mainly of interest calculating the heat transfer between surfaces and gas volumes, e.g. the outer surfaces of a wall or the lining surfaces in a void cavity.
- radiation, i.e. heat transfer by electromagnetic waves, e.g. between a heat source and a surface, or from a surface.

Commonly used models based on finite elements or finite differences take into account conduction in solids, convection between surfaces and gas volumes and radiation to and from surfaces. Parameters for convection and radiation at surfaces are given in the Fire Part of Eurocode 1 (ENV 1991-2-2). These are outside the scope of this paper. The models do normally not take into account the following:

- mass transfer of water and hot gases
- convection within porous materials
- degradation of materials e.g. the cracking of the char coal
- reaction energy released inside the wood due to pyrolysis
- abrupt change of structures, e.g. when fire protective claddings fall off,

which means that these effects must be taken into account in an indirect way by adopting modified material properties.

A more precise model, taking into account among other things mass transfer, was developed by Fredlund (1988), however due to its complexity, it is rather a tool for researchers than for design engineers.

In materials containing water, such as wood or gypsum plasterboard, the influence of mass transfer is most pronounced at temperatures around 100°C when water is evaporated and transported further into the wood where most of the vapour condenses into water again. To some extent, mass transfer can be taken into account by increasing the conductivity of the wood material around 100°C. In wood, pyrolysis gases move from the char front towards the fire where they meet oxygen and ignite. This mass transport counteracts heat transfer by conductivity through the char layer. The influence of convection within porous materials can be taken into account by increasing the conductivity. All these effects show that the properties to be used in thermal analysis are rather apparent or fictitious ones than "real" ones.

2.2 Used model

In the investigations reported here, a commercial computer software TCD (Temperature Calculation and Design), versions 3.0 and recently 5.0, were used for the thermal analysis of the fire exposed structures. This software includes the computer program TEMPCALC developed for the calculation of heat transfer using the Finite Element Method. The computer program solves the two-dimensional, transient, heat transfer differential equation incorporating thermal properties that vary with temperature. Mass transfer is not taken into account. Assemblies comprising several materials can be analysed and the heat absorbed by any existing void cavities in the assembly is taken into account.

The influence of element size on the calculated temperature field was studied for the wood and sheet materials. It was found that for a rectangular mesh the maximum element width and height should not be greater than 2,5 mm in order to obtain numerical stability. A proper step for the time setting was found to be in the range between 0,0001 and 0,002 h.

2.3 Wood

Annex E of ENV 1995-1-2 gives conductivity and specific heat values for wood and charcoal. The conductivity values for wood are taken from Kollmann (Kollmann1951, Kollmann et al. 1968), however, since they are valid between –50 and +100°C, of limited value. The heat capacity values of charcoal are according to Landolt-Börnstein (1961), but no information is given whether they should be used together with initial density values of wood or with temperature dependent density values. To conclude: the data given by ENV 1995-1-2 are incomplete and the designer has to search in other sources to find relevant input data for thermal analysis.

Thermal properties have been discussed thoroughly by other authors, see for example Thomas (1997) and recently Clancy (1999). Both sources contain a large number of references. König et al. (1999) conducted fire tests to determine charring of timber members of spruce exposed to fire with thermal conditions of one-dimensional heat transfer as in semi-infinite slabs. The results of the tests were used in order to determine the conductivity and specific heat of wood by calibrating them to the test results using the computer program TEMPCALC for calculation of heat transfer. The results, together with some curves from other sources are shown in figures 1 and 2.

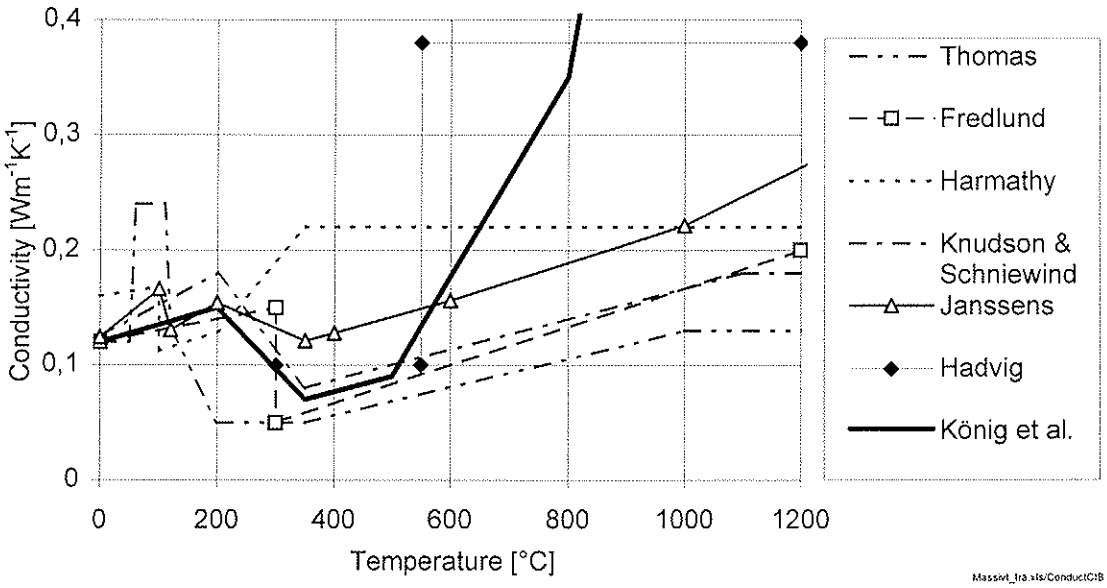

Figure 1: Conductivity vs. temperature of wood and charcoal

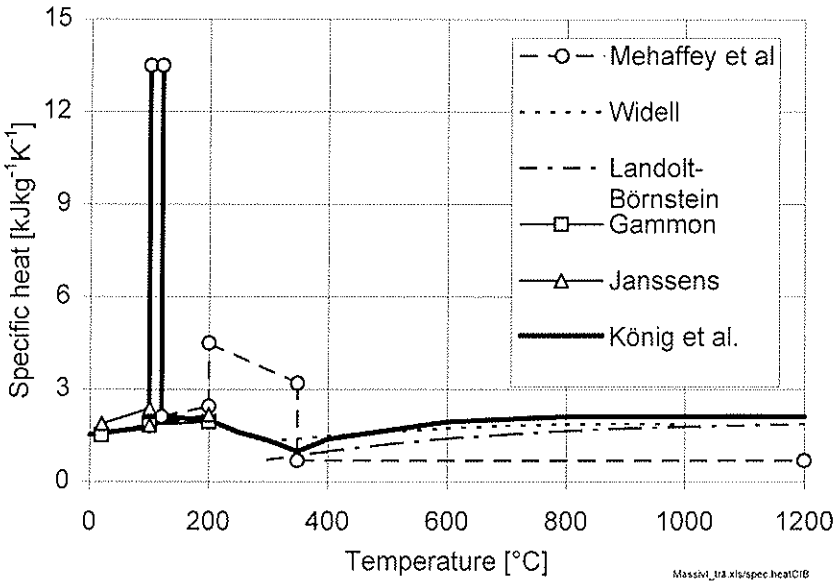

Figure 2: Specific heat vs. temperature of wood and charcoal

The graphs show considerable deviations between the values from different sources, especially for conductivity. While most conductivity values are situated in a narrow band over the entire temperature range, some of them deviate, which must be discussed further.

In commonly used heat transfer modelling mass transfer is not taken into account (one exception is the work done by Fredlund, 1988). Mass transfer takes place when the water in the wood vaporises and moves away from the char front into the wood and thereby increases the heat transfer, and when pyrolysis gases penetrate through the char layer, thus counteracting the heat transfer into the wood. In order to take into account these effects, conductivity values must be calibrated in order to include these effects. The values to be used are notional values rather than physically correct ones. Thomas (1997) simulated these conditions by increasing conductivity in a narrow temperature range where water vaporises. The large deviations at temperatures above 300°C, which is the temperature at the location of the char line, depend on whether the values refer to charcoal as a solid but porous material, or to the char layer that consists of charcoal with cracks. Due to the cracking, heat transfer is increased by radiation and convection. Both effects should be taken into account by increased notional conductivity values. This was, e.g. done by Hadvig calibrating conductivity values to test results, assuming that the transition to a cracking material takes places 6 mm away from the char line. At this location, the temperature is about 550°C, giving rise to a sudden increase of conductivity. The conductivity values by König et al. (1999) were obtained by calibration to test results, assuming a more smooth transition from an uncracked to a cracked char layer. Further, the consumption of the char layer taking place at about 1000°C and keeping the thickness of the char layer constant, is simulated by further increasing of the conductivity values above 800°C. Figure 3 shows, for comparison, the effect on charring of conductivity values used by König et al. (1999) and those given by Fredlund (1988), the latter being representative to the values of most sources.

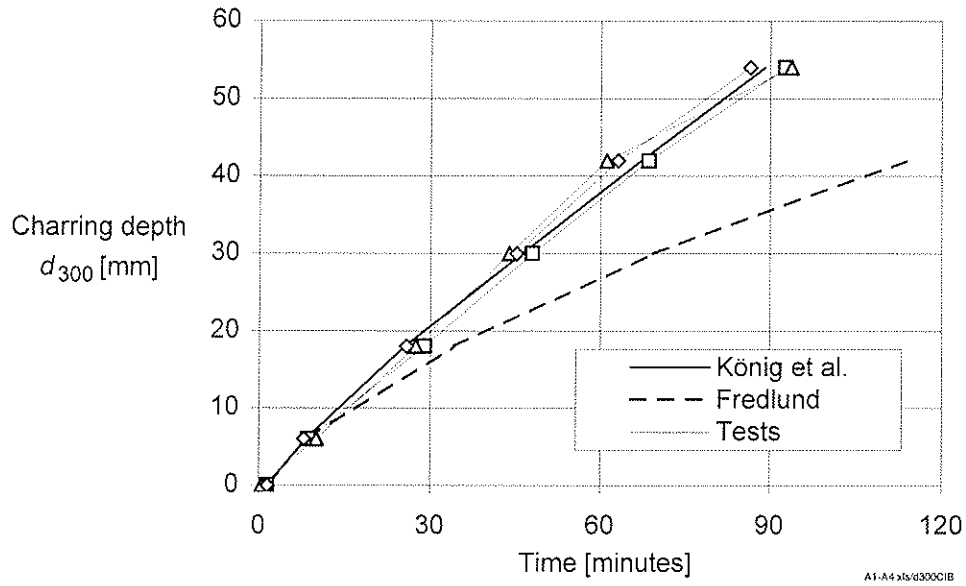

Figure 3: Comparison of calculated charring-depth time relationships – effect of conductivity values of the char layer.

The specific heat values shown in figure 2 are mainly of the same magnitude. The values obtained by König et al. (1999) were calibrated to test results and used together with density ratios according to Janssens (1994), however, in order to simulate the consumption of the char layer, the density was assumed to decrease linearly to zero between 800 and 1200°C.

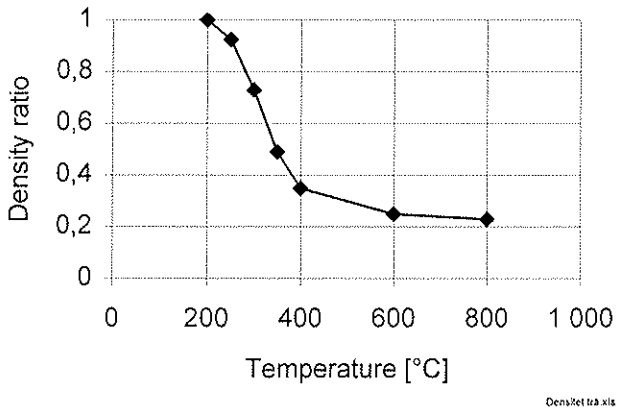

Figure 4: Density of wood vs. temperature according to Janssens (1994)

2.4 Mineral wool

In wall and floor assemblies with mineral wool filled cavities, the wide sides of the studs or joists are more or less efficiently protected against charring. Examples of conductivity values are shown in figure 5. The values given by Sterner et al. (1990) are for rock fibre of density 50 kg/m^3, recommended as input in TASEF, however no information is given regarding the source of the values. The values by Thomas (1997) were determined by calibrating them to test results by König (1995), using test specimens according to figure 6.

The calibration results by König et al. (2000a) are different since they used different properties for wood. Thomas (1997) used TASEF (Sterner et al., 1990) while König et al. (2000a) used TCD 3.0 (1990). Unfortunately, in this version of TCD the number of finite elements was limited, leading to compromises regarding optimum grid configuration and numeric precision. The calculation was repeated using TCD 5.0 (1999) with a much greater number of grid elements giving numerical stability. The results are shown in figure 6. The difference between this curve and the values obtained by Thomas (1997) are due to different conductivity values used for the char layer of the timber member. Thomas (1997) used smaller conductivity values and compensated this by greater conductivity values of the mineral wool in order to increase heat flux from the sides.

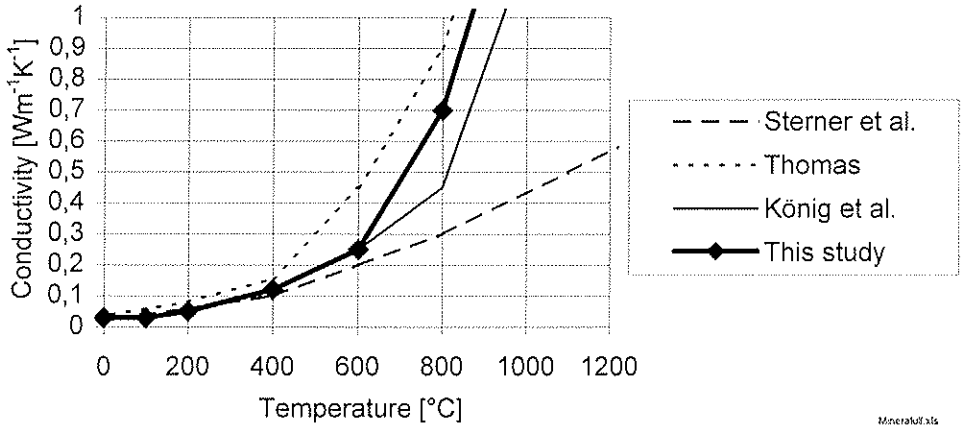

Figure 5: Thermal conductivity vs. temperature for mineral wool

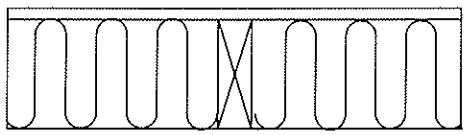

Figure 6: Example of section through assembly used in the calibration with fire exposure from below

2.5 Gypsum plasterboard

Gypsum plasterboard used as linings are widely used to improve fire resistance of wall and floor assemblies, mainly due to the large amount of water that is chemically bound as crystal water. Different values of thermal conductivity and specific heat of gypsum plasterboard found in literature are shown in figures 7 and 8. Reasons for the differences may be that gypsum plasterboard of different origin was used, or that some of the data relate to measured values, while others were calibrated. While regular gypsum plasterboard (type A according to prEN 520) contains a porous gypsum core to reduce the weight of the boards, improved qualities are obtained by adding other materials to the core such as glass fibre or fillers, e.g. vermiculite (type F according to prEN 520). One could expect a wide variation of thermal properties of different makes, since the fraction of gypsum varies (and with it the content of water and thus the amount of heat needed for calcination and vaporization), and the heat transfer is influenced by fillers and different cracking

behaviour. This would make it difficult to give general thermal properties in a design code. Tsantaridis et al. (1999) tested commonly used gypsum plasterboard from different countries (Canada, Japan, New Zealand, Sweden, USA) and found that board thickness is a relevant parameter to describe the fire protection by gypsum plasterboard. This supports the proposal to use – at least for application in design codes – the same thermal properties for different types of gypsum plasterboard.

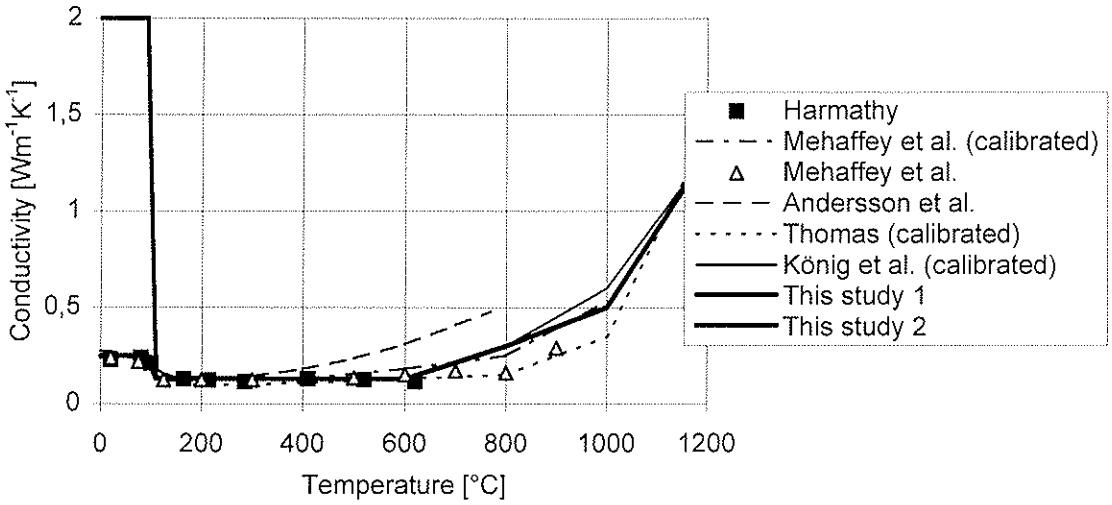

Figure 7: Thermal conductivity vs. temperature of gypsum plasterboard

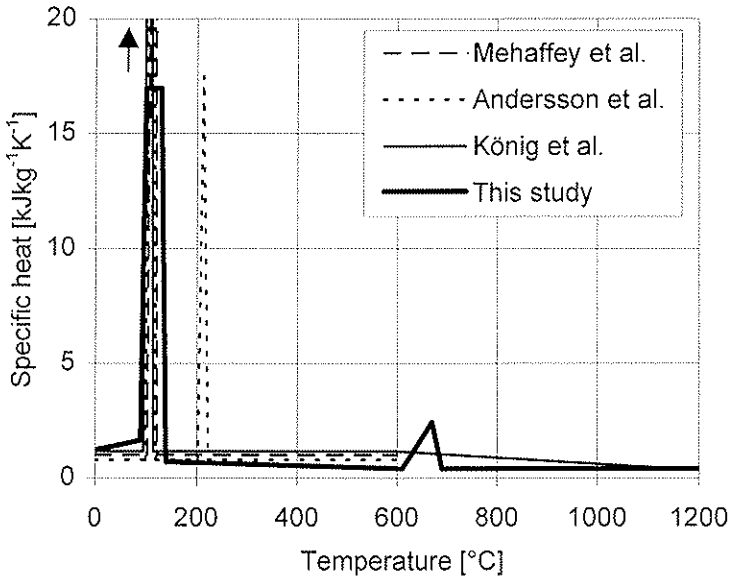

Figure 8: Specific heat vs. temperature of gypsum plasterboard

In order to calibrate the material parameters in this study, wall assemblies were investigated that were built up according to figure 6, however completed with one layer of gypsum plasterboard on the fire exposed side. The values marked as "this study 1" were calibrated by fitting the onset of charring and the charring depth in the timber member to test results by König et al. (1997). The specific heat values were related to a constant density of 825 kg/m^3. The difference with the values determined by König et al. (2000a) are due to different grid configuration and element sizes using different versions of TCD, see 2.4. Using the conductivity values "this study 1" shown in figure 7, the calculated

temperature history on the cavity side of the lining 150 mm from the centre of the stud is shown in figure 9. Considering the scatter of the test results, there is a good agreement between tests and calculation, except in the region of 100°C where calcination of gypsum takes place and water is vaporised. By assuming a considerably larger conductivity in that region, see the values "this study 2" of figure 7, the measured temperatures can be fitted much better. By this manipulation the mass transfer of the steam taking place is simulated, which increases the heat transfer considerably. This demonstrates that it is possible to find adequate input values of thermal properties to simulate phenomena that are not explicitly taken into account by the thermal model.

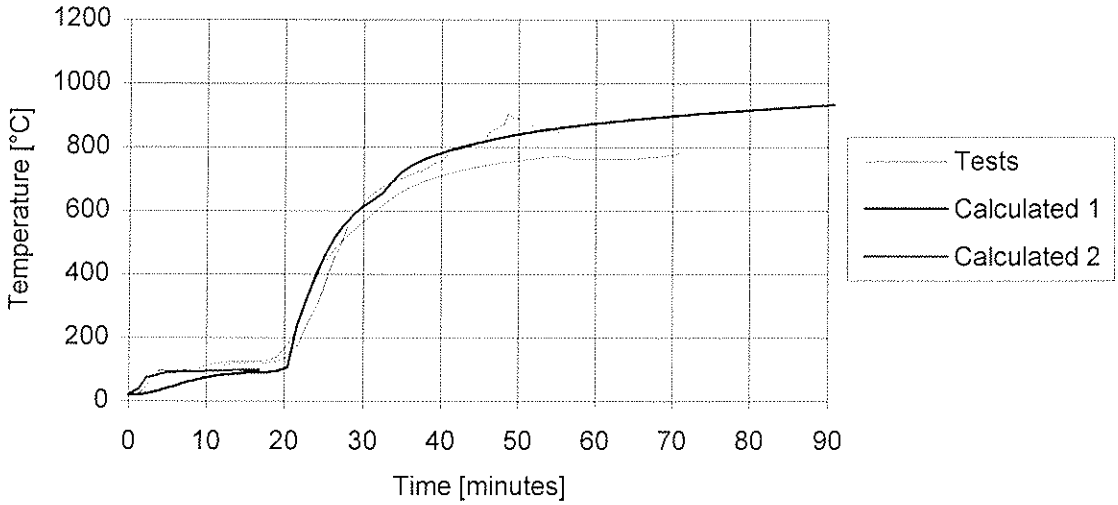

Figure 9: Comparison of calculated temperature histories on the cavity side of the lining (one layer of 15,4 mm gypsum plasterboard type F)

3 Properties for mechanical analysis of timber members

Efforts have been made to solve the problem of determining the strength of timber under the influence of elevated temperature and moisture. A solution was presented by Schaffer (1981) where the strength of the timber in the heat affected zone near the char line was reduced, taking into account both the temperature and moisture content profile in the timber member. For large cross sections this method gives reasonable results. Schaffer stated also that there was a considerable effect of creep that was not included in the model. Extensive fire testing by König (1995) and König et al. (1997) of light timber frame members showed that there occurred extensive plastic flow in the cross section. Thomas (1997) developed a model for timber studs, using test data by König (1995) to determine reductions of compressive strength, tensile strength and the modulus of elasticity in compression and tension. This approach was a shortcut in order to get reasonable input data for a finite element model of a wall stud. A similar approach was made by Clancy (1999). Both lacked from sufficient input from tests. Especially following to the work by König et al. (1997) essential results were available to overcome the shortcomings of other investigations. A design model was developed by König et al. (2000a), see also König et al. (2000b).

Using a spreadsheet program the strength and stiffness properties of the cross section were calculated, dividing the timber cross section into small elements and using local strain-stress relationships dependent on temperature, with temperatures obtained in the heat transfer calculations.
With the simplified bilinear stress-strain relationship shown in figure 10 as a starting point (Buchanan, 1990), relationships were determined of compressive strength, tensile strength and modulus of elasticity versus temperature. Taking into account that timber quality has only a very small influence on the reduction of strength (Norén 1988), high quality timber was assumed as in the tests. Assuming a dry density of 438 kg/m^3, the local compressive strength was taken as 44 N/mm^2 (Thunell, 1941, Kollmann, 1951a) and the local tensile strength derived from the bending tests at normal temperature using the relationship of figure 10. Since the fire tests were conducted with timber members in bending such that the fire exposed side of the member was either in compression or tension, it was possible to separate the effect of temperature on the strength and stiffness properties with respect to the state of stress. In the first step, calibrating the modulus of elasticity to measured deflections for the stage when charring was about to start, the relationships of figure 11 were obtained, adopting a simple bilinear model with a breakpoint at 100°C. The reduction obtained here is considerably larger than reported in other sources, but it is supported by tests made by Kollmann (1951b).

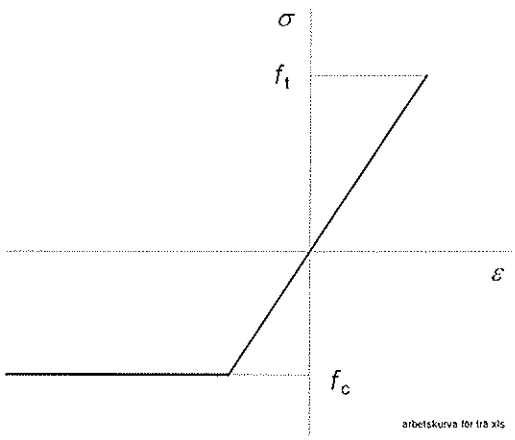

Figure 10: Simplified strain-stress relationship for wood

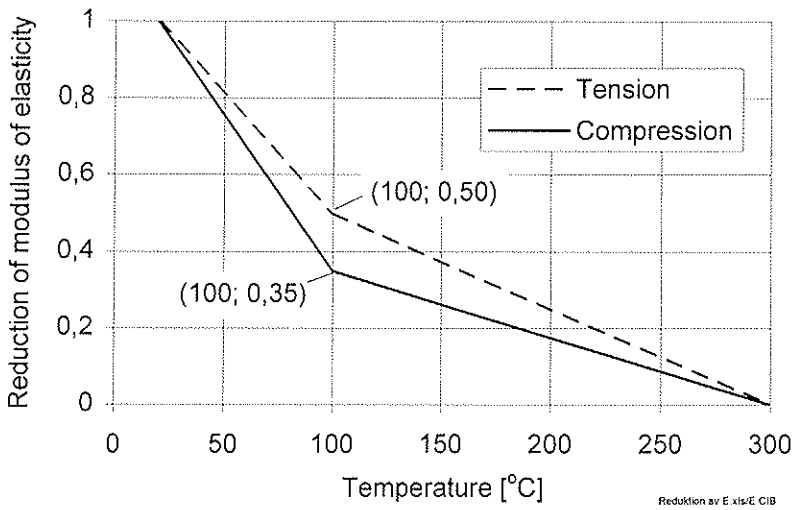

Figure 11: Effect of temperature on modulus of elasticity (König et al., 2000a)

Similarly, by using the reduction of modulus of elasticity obtained above, the temperature dependent tensile and compressive strength values were determined by calibrating them to the failure loads obtained in the fire tests, comparing them with predicted failure loads att normal temperature. The results are shown in figure 12 together with results reported in other sources (for detailed references see König et al. 2000a). Again, these values are considerably smaller than reported by other researchers. Reasons for this deviation may be that it is very difficult to obtain well-defined conditions in test specimens with respect to temperature and moisture content. Also the influence of the rate of loading can be expected to be important. Some researchers assume an increase of strength at temperatures above 100°C due to the drying of the wood. According to the results of this investigation, this effect is more than compensated due to local creep in the cross section.

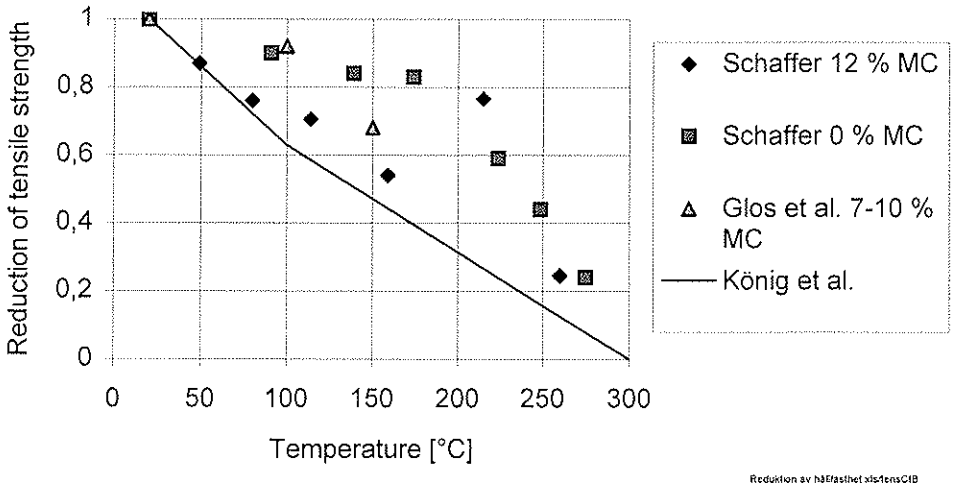

Figure 12: Effect of temperature on tensile strength

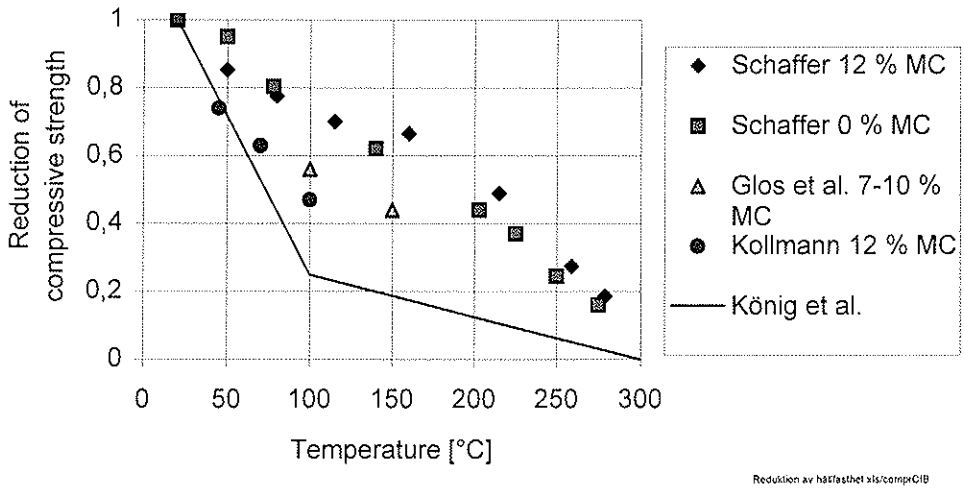

Figure 13: Effect of temperature on compressive strength

Using the temperature dependent relationships for strength and modulus of elasticity shown in figures 11 to 13, resultant strain-stress relationships are obtained as shown in figure 14. These were used by König et al. (2000a) to calculate modification factors for fire for the reduction of strength and stiffness parameters, e.g. the reduction of bending strength modulus of elasticity of light timber frame members, see also König (2000b).

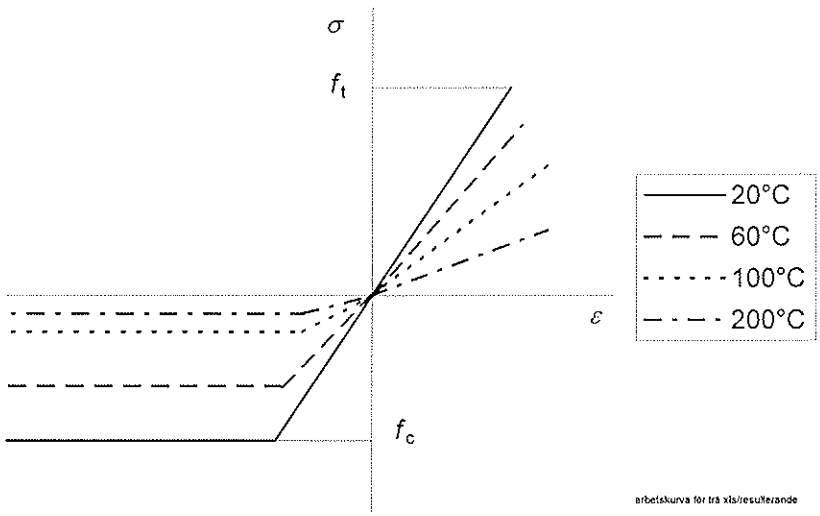

Figure 14: Resultant temperature-dependent strain-stress relationships

4 Conclusions

In the calibration procedure used, the main principle was to use thermal properties that could be found in the literature and to modify them, where necessary, in order to get results in agreement with results obtained from testing of fire exposed timber or wall and floor assemblies. The thermal properties should be calibrated such that they could be used independent of the physical arrangement of the materials in the structures. Thermal properties to be adopted in a design code cannot be true values as such; they are rather

apparent or fictitious values. They should reflect the physical properties and phenomena in an understandable way such that designers – who for this type of analysis should be specialists in the field of fire design – can use them in an appropriate way. The thermal and mechanical data presented here give safe results and should therefore be suitable for adoption in EN 1995-1-2.

5 References

Buchanan, A. H., 1990, Bending strength of lumber. Journal of Structural Engineering, Vol. 116, No. 5

Clancy, P., 1999. Time and probability of failure of timber framed walls in fire. PhD thesis, Victoria University of Technology, Australia

ENV 1991-2-2, 1994, Eurocode 1 – Basis of design and actions on structures, Part 2-2 – Actions on structures exposed to fire

ENV 1995-1-2: 1994, Eurocode 5 – Design of timber structures, Part 1-2 – Structural fire design

Gammon, B. W., 1987, Reliability analysis of wood-frame assemblies exposed to fire. Ph.D. Dissertation. University of California, Berkeley, U.M.I. Dissertation Services, USA

Fredlund, B., 1988, A model for heat and mass transfer in timber structures during fire. Lund University, Lund

Hadvig, S., 1981. Charring of wood in building fires. Technical University of Denmark, Lyngby

Harmathy, T. Z., 1995, Properties of building materials. The SFPE Handbook of Fire Protection Engineering, 2nd edition

Janssens, M., 1994, Thermo-physical properties for wood pyrolysis models. Pacific Timber Engineering Conference Gold Coast, Australia

Knudson, R. M., & Schniewind, A. P., 1975, Performance of structural wood members exposed to fire. Forest Products Journal, Vol. 25, No. 2

König J., Norén J., Bolonius Olesen F. & Toft Hansen F., 1997, Timber frame assemblies exposed to standard and parametric fires - Part 1: Fire tests. Swedish Institute for Wood Technology Research, Report No. I 9702015

König, J. and Walleij, L., 1999. One-dimensional charring of timber exposed to standard and parametric fires in initially unprotected and post-protection fire situations. Swedish Institute for Wood Technology Research, Report No. I 9908029

König, J. and Walleij, L., 2000a. Timber frame assemblies exposed to standard and parametric fires. Part 2: A design model for standard fire exposure. Swedish Institute for Wood Technology Research, Report No. I 0001001

König, J., 1995, Fire resistance of timber joists and load bearing wall frames. Swedish Institute for Wood Technology Research, Report No. I 9412071

König, J., 2000b, A design model for load-carrying timber frame members in walls and floors exposed to fire. CIB W18, Paper 33-16-2

Kollmann, F.,1951a, Technologie des Holzes und der Holzwerkstoffe. Zweite Auflage, erster

Band, pp. 737, 742

Kollmann, F., 1951b, Über das mechanische Verhalten von Kiefernholz bei Biegung und Temperaturen zwischen 20° und 100°. Svenska Träforskningsintitutet, Trätekniska Avdelningen, Meddelande 22, Stockholm

Kollmann, F. and Côté, W., 1968, Principles of wood science and technology, Vol 1 Solid wood. Springer Verlag, Berlin, Heidelberg, New York

Landolt-Börnstein, 1961, Zahlenwerte und Funktionen aus Physik, Chemie, Astronomie, Geophysik, Technik. Sechste Auflage, Band II, 4. Teil, Kalorische Zustandsgrössen, Springer Verlag, Berlin, Göttingen, Heidelberg

Mehaffey, J., R., Cuerrier, P., Carisse, G., 1994, A model for predicting heat transfer through gypsum board/wood stud walls exposed to fire. Fire and materials, Vol. 18.

Norén, J., 1988, Failure of structural timber when exposed to fire. Proceedings of 1988 Int. Conf. on Timber Engineering, Seattle

prEN 520, 1999, Gypsum plasterboards – Definitions, requirements, test methods, Draft European Standard

Schaffer, E. L., 1984, Structural fire design: Wood. Forest Products Laboratory, Research Paper FFL 450, Madison

Sterner, E. and Wickström, U., 1990, TASEF – Temperature analysis of structures exposed to fire – User's manual. Fire Technology, SP Report 1990:05, Borås, Sweden

TCD 3.0, 1990. User's Manual for TCD 3.0 with Tempcalc. Fire Safety Design, Lund

TCD 5.0, 1999, User's Manual for TCD 5.0 with Tempcalc. Fire Safety Design, Lund

Thomas, G. C., 1997, Fire resistance of light timber framed walls and floors. University of Canterbury, Canterbury, New Zealand

Tsantaridis, L. D., Östman, B. and König, J., 1999, Fire protection of wood by different gypsum plasterboards. Fire and Materials, Vol. 23, pp 45-48

INTERNATIONAL COUNCIL FOR RESEARCH AND INNOVATION
IN BUILDING AND CONSTRUCTION

WORKING COMMISSION W18 - TIMBER STRUCTURES

INTERNATIONAL STANDARDS FOR BAMBOO

by

J J A Janssen

University of Technology, Eindhoven
THE NETHERLANDS

MEETING THIRTY-THREE
DELFT
THE NETHERLANDS
AUGUST 2000

Presented by: J.J.A. Janssen

· H. Blass asked about the availability of the document for design, testing, etc.
· J.J.A. Janssen answered that ISO document would be available in 4 yrs. He will check with ISO TC 165 for permission to release the draft information.
· A. Jorissen asked about the connection and commented that a structure such as the Pavilion in Expo 2000 could not be designed from standards.
· J.J.A. Janssen agreed and it would take time. The standard deals with how to perform tests on joints with reference to other standards.
· Marsh asked about friction/bounded joints.
· J.J.A. Janssen answered that loss of strength of bamboo will result because friction/bound joints would be the weakness.
· E. Karacabeyli commented that the working drafts of ISO TC 165 could be obtained from representatives of individual countries.

International Standards for bamboo.

Dr. Jules J.A. Janssen,
European Co-ordinator of INBAR, the International Network of Bamboo And Rattan,
Based at Eindhoven University of technology, the Netherlands.
Address: P.O. box 513, 5600 MB Eindhoven, the Netherlands.
Phone + 31 40 247 29 48, fax + 31 40 243 85 75.
Email: J.J.A.Janssen@bwk.tue.nl
www.bwk.tue.nl/bko/research/Bamboo

1 Introduction

The need for international standards for bamboo firstly was felt during the International Bamboo Workshop in 1988 in Cochin, India. Next it has been discussed in CIB W18B meetings in Seattle (Boughton, 1989a and 1989b) and Kuala Lumpur (Janssen, 1992). This paper will highlight the reason for international standards for bamboo, and the progress, which has been made since 1992. Two standards are being prepared one about building codes and another about the determination of physical and mechanical properties.

2 Standards in general

A building code is a national regulation for the building industry, regarding materials, workmanship and structures. A more common name is "standards". Kaplinsky (1992) gives a good overview of the aspects of standards.
Unfortunately, many cases are known in which standards or regulations are based on middle class housing, and consequently working class housing is sub-standard and may be removed, because this does not meet "minimum acceptable standards".
On the contrary, good standards do not harm the lower income families, but they protect consumers, workers and the environment, and they promote economic growth. The issue is not whether standards should be implemented, but who defines them.
Standards sometimes protect the rich, and if they are meant to protect the poor (e.g. their safety at work) they are often not implemented. Standards are known as a part of the development problem, but they can play the role of a part of the development solution.
Good standards shall meet the following requirements.
-Protection of the consumer: sub-standard items are a loss of money for the client, and maybe even a danger for the consumer.
-Protection of the environment: effluent disposal and other forms of pollution are kept within acceptable limits.
-Reduction of cost of production: standards can eliminate most of the scrap, and improve quality, without rising production costs.
-Minimum standards of work: e.g. health, safety, and no child labour.
-Safety of the inhabitants: e.g. in earthquake areas high rise building built with sub-standard cement may not be safe; in hurricane areas houses built without adequate safety may be dangerous as well.
-Market requirements: a product made according to standards can more easily penetrate various markets, especially in the case of export.

We are living in an increasingly regulated world. This urges developing countries to work together in their efforts for standards, which meet their specific requirements. The

central issue is that standards regarding production and consumption recognise the environments in developing countries. Standards have to be defined in the South, by the South, for the needs of the South, and using the resources of the South.

Looking more specifically to housing, Schilderman (1992) has given a good summary. To start with, standards define a minimum level of quality of housing, mainly to prevent disasters or to reduce health risks. They have to be controlled. In the South however standards apply to urban areas only.
Standards should aim the following goals:
-They should be in line with local traditions,
-They should recognise that building is an incremental process,
-They should take into account the needs of the masses,
-They should recognise the upper class, and assist the lower class to improve their dwellings,
-They should take into account the lack of funds,
-They should take into account people's priorities,
-They should work with local materials,
One has to meet the basic needs of the masses, starting with an absolute minimum and showing the way for gradual improvement. The absolute minimum should ensure e.g. that houses do not collapse on the inhabitants. New standards should use the opportunities of bamboo to help people to solve their problems, starting at a low level and growing to a higher level.
One should not act in a prescriptive way ("walls should be 50 mm thick") but a standard should indicate a performance, e.g. being able to withstand a hurricane or an earthquake, and the like. We should show the way to reach this using bamboo, and we should give examples.
Such a bamboo standard can become a boost in stead of a burden. It can stimulate the use of bamboo, and provide recognition, by more and better use. A Unido-report (Unido 1991) says about wood: "In most developing countries, building legislation is inappropriate and does not recognise wood as a durable construction material. This has prevented banks and other financial institutions from supporting the use of wood in construction." The same remark is valid for bamboo. In the future we can think of a system of certification.
A considerable part of a bamboo standard should be based on observations: which type of housing did survive that disaster? Which houses are more durable or need less maintenance? A bamboo standard should teach valuable lessons.
After this lengthy introduction we have a clear overview of the good opportunities of standards. Our problem is, that bamboo does not appear in national building codes. This does not contribute to recognition, and sometimes even means "This material is forbidden". Anyhow it is a constraint for the progress of bamboo as engineering and building material for developing countries. A good national standard can open the way for engineers and designers.
If one leaves the development of national bamboo standards to the national authorities, one can foresee a wild diversity. If on the contrary we design an international model for national standards, we strengthen the position of bamboo considerably.
Look at the situation about timber: standards have been accepted by the US, by Europe and by Australia; they will never agree about a world standard any more. For us the opportunity for a world bamboo standard is open, and if we succeed we are half a century ahead of our colleagues in timber.

The International Organisation for Standardisation, the ISO, defines standards as "Technical specifications or rules, based on consensus, and approved by a recognised standardising body." The consensus is our task, and for approval we have to submit our proposal to the ISO, to give authority to our product.
Other arguments in favour of such an international model have been described by Boughton (1989a). Many countries are facing a huge shortage of housing. Therefore governments are willing to consider bamboo as a contribution to the solution. But bamboo still has the stigma of the poor man's timber, and it is not considered as a modern material. A building code would be the solution for this problem, and it would help to formalise the position of bamboo.
Advantages of codified design with bamboo can be summarised as follows.
-Engineering recognition: a code will stimulate engineers to use bamboo. "Engineers and architects prefer to work with the determinacy of a well-known system or material, supported by solid knowledge of its properties, backed by the existence of a minimum of code specifications on which they can base their judgement and design decisions". (Arce, 1993, page 2).
-Contractual advantages: a code makes any contract much easier.
-Trade advantages: quality control of products.
-Increased use of bamboo: socially better accepted, codification leads to innovation, specified more regularly in designs.

3 International Building code for bamboo

3.1 Introduction.

In the bamboo Congress and Workshop in Ubud, 1995, one of the recommendations was "INBAR is requested to organise a task force to discuss and finalise a building code for bamboo". Consequently a draft has been prepared under the full title: "An International model for national building codes, section bamboo". The target group is architects and builders, designers and engineers. These people are already familiar with national Building codes for timber, masonry, etc. but for bamboo a similar Code still is missing. This is a drawback for the recognition of bamboo as a building and engineering material. The draft (Janssen 2000a) has been submitted to the International Standard Organisation ISO. Once it has been accepted as an ISO-Standard, it can serve as the model or basis for developing National Building codes by countries, which grow and use bamboo in construction. The subjects are: philosophy, design concepts, structural design, beams, columns, joints, trusses, panels, durability, fire protection, grading, quality control.

3.2 Development

After the Ubud Congress and Workshop in 1995, we had a group of volunteers available, but needed some time to obtain the necessary funds. This time has been used for reflection: what will be the structure of an international model for bamboo-paragraphs in National Building Codes? And next, what documents and other information are already present? All these have been collected. Some examples are:
- standards for timber, like ISO- and ASTM-standards, and the Eurocode 5,
- articles about standards for developing countries,
- scientific documents with modern test results for bamboo.
Discussions have taken place about items, which are less common for standards, but

in our case very important, e.g. the use of observations and the place of these in a standard: which type of bamboo house did survive that disaster? A bamboo standard should teach such valuable lessons.

In the case of bamboo, the differences between the formal and the informal sector are very important. The purposes of regulations for the *commercial sector* are:
- to provide a healthy environment,
- to reduce the frequency of environmental, structural and other functional failures,
- to derive improvements in the quality and economy of construction, by setting up standards that form a reasonable and readily administered basis for contracts between builders and owners, and at the same time permitting innovation and development,
- to protect the interests of the neighbourhoods, and those of the community as a whole, from the irresponsible development of sites which may otherwise take place.

The purposes of regulations for the *non-commercial sector* are:
- to provide improvements in the standards of hygiene,
- to mitigate suffering and loss in the event of natural disasters such as earthquakes, winds, storms, floods and fires,
- to meet the needs of the owner or the occupier, rather than to serve the convenience of the regulating authority,
- to educate owners, occupiers and builders in the means with which to achieve the above at low cost.

3.3 Results

At this moment (June 2000), the result of all efforts is a draft for the said international model. A short summary of the content of this draft might be helpful to understand what the goal will become.

1. The document starts with a general philosophy about the purpose of this model, a description of the general requirements for the design of structures (mostly with regard to safety), a description of the scope, and assumptions and definitions. This stuff is just needed in any standard.

2. Design concepts, stating that for the commercial sector design concepts shall be based on calculations, but leaving open for the non-commercial sector the use of good tradition and of evaluation reports. This is exceptional for a building standard, but for bamboo we need such an approach. The use of good tradition is defined as follows:

Experience from previous generations, well preserved in a local tradition, and carefully transmitted to people living today, by means of a reliable system of oral transfer. This expertise can be considered as an informal, non-codified "standard".

Criteria for the reliability are:
- the content shall be generally known and accepted,
- it shall be considered as old and pure tradition, as general wisdom,
- the community shall be characterised by an undisturbed social structure, with a well-recognised social pattern.

Limitations are:
- the content cannot be transferred to other localities, to different botanical species, etc.
- after migration the presence of this tradition is no longer self-evident.

The evaluation reports are defined as follows.

Reports based on evaluations made after disasters like earthquakes and hurricanes. If these reports contain descriptions about structures, which did survive a quantitatively

described disaster, similar structures shall be considered as adequate for similar disasters in the future.
Criteria for the reliability are:
- the report shall be composed by acknowledged engineers, with adequate experience in the field,
- the report shall be accepted by the international technical community and/or proven by referees,
- the report shall give full details and full information, with which one can build similar buildings.
Limitations are:
- the report cannot be transferred to other localities, to different botanical species, etc.

3. Criteria for structural design, with paragraphs about limit states, serviceability, material properties, design requirements, allowable stresses, and all such topics needed in any building code or standard.

4. Schematisation: which is the process of "translating" the physical reality of a building structure towards a schematised system of symbols to be used during the calculation process. The schematisation is based on the theory of applied mechanics. Compared with materials like steel and timber, this process is for bamboo even more important, due to properties like the elastic behaviour of bamboo, the thin walls of bamboo culms, and the form of most bamboo culms: not perfectly straight, tapered, and with nodes at different intervals.

5. After this introduction we come to structural elements: beams and columns, for which paragraphs many elements from timber-standards could be applied, but with special emphasis on bamboo-properties.

6. The next subject is "joints", the most difficult item in bamboo-construction. In most examples of bamboo structures, the strength and stiffness of the bamboo culms are diminished in the weakness and deformation of the joint. This is a drawback for the safety and the economy of any bamboo structure. The text in this paragraph tries to describe a minimum level of safety, and to promote developments towards joints, which are both safer and more economical. The next paragraph, dealing with trusses, is merely an extrapolation of the text about joints.

7. Panels is the next item, with which we enter the modern industrial applications of bamboo. The production of panels from bamboo really is a good option for job creation in new industries in any region where bamboo is growing. It can also improve the position of the country on the world market, and it is an option to obtain hard currency by export to Western Europe and the U.S. Exactly for the international market a standard is essential.

8. Preservation and durability cover the weak spot of bamboo as a building material. Fortunately in the past years sufficient progress has been made, and based on these results it might be possible to write a draft-standard which shows also to way to a gradual improvement.

9. Grading and quality control are the last items and the most difficult ones also. These subjects are essential for the recognition of any building material, but personally the author feels we still are unable to describe these requirements in a draft standard.

4 International Standard for properties of Bamboo

4.1 Introduction

The goal is to raise an International Standard for the determination of mechanical and physical properties in the laboratory, because a standardisation of test methods is urgently needed. We need standards for tests on bamboo in a similar way like these are available for other building materials. The target group is laboratory-staff. The full name is "Determination of physical and mechanical properties of Bamboo" (Janssen 2000b). The subjects are: philosophy, general subjects, compression, static bending, shear, tension, moisture content, mass per volume, shrinkage. The document has been submitted to the International Standard organisation ISO.
The state of the art for the determination of the properties of bamboo is, that every laboratory is performing tests according to its own "standards". This is just a fact, it is certainly not a reproach! Bamboo researchers have done in the past, and still are doing, a good job in determining properties, in many cases even in difficult circumstances. But compared with timber research, the disadvantage of bamboo research is the lack of standards. This is a problem for the researcher: how to perform tests? And it is a problem for the reader of a report or article, in which the results are presented, since it is impossible to compare the results from one researcher with those from another. This really is a pity for the effort of both the researchers and the readers, and it is a drawback for the recognition of bamboo as an engineering material. Evidently, the absence of standards has not hindered the construction of bamboo houses at low-income levels, it has certainly impeded the wider acceptance of bamboo.

Arce (1993) has expressed this aspect as follows. "Engineers and architects prefer to work with the determinacy of a well known system or material, supported by solid knowledge of its properties, backed by the existence of a minimum code of specifications on which they can base their judgement and design decisions." A similar statement has been made by the Indian Standards Institution, in the preface to IS 6874 (1973), "Methods of tests for round bamboo's": " In order to ascertain the suitability of bamboo's for various structural purposes their physical properties are required to be tested. Standard methods of tests have been developed for the purpose and the same are described in this standard. The data obtained by these methods may be made use of with confidence where strength factors are involved."

4.2 Development

Between 1995 and 1997 a structure has been raised: it was agreed that the author should write a first draft, and a group of about fifteen referees from several bamboo-countries should give their comments. The first draft was ready in February 1998, and distributed to the said referees. Within a few months most of them have sent very valuable comments with which the draft could be improved considerably. One has to keep in mind that for the referees this is volunteer work! They have to do it in their own time.

The next step was a discussion to determine the text of this standard, in October and November 1998, in San José, Costa Rica. From that moment onwards this standard has already some authority within INBAR: no researcher will ignore this document when starting a new research programme. But for the recognition at the international level we need two more steps: recognition by National Standard Organisations of bamboo-countries, and recognition by ISO, the International Standard Organisation.

4.3 Results

At this moment (June 2000) the main result is the draft for the standard, the content of which will be discussed here. The philosophy has been to follow as much as possible the existing standards on timber (like some ISO-standards, and ASTM, and Eurocode 5), to further the acceptance of this new bamboo standard. Differences between timber and bamboo have been observed well. Much use has been made of the Indian Standard IS 6874 on testing of round bamboo's, and of some recent scientific publications on testing of bamboo, like Arce (1993). The content is like follows.

1. General items: foreword, with a general introduction; content and scope of this standard.

- Terminology, units, symbols, for which items the ISO-standards are used as far as possible.
- Organisation and use of this standard, including the determination of size and weight of specimens, temperature and moisture content, and the rate of loading in tests.
- Sampling and storage of specimens. This is a very important item: if the sampling has been done in an incorrect way, the test series is useless. An interesting difference can be observed whether the sample is for scientific research or for commercial purposes: if it is scientific, the selected culms have to be free of defects, but if it is for commercial purposes, the sample has to be representative for the total number of culms, with their defects. A good bookkeeping of all culms is prescribed as well, with much attention how to divide full culms into test pieces, and to keep a record from which culm each piece has been cut.

Paragraphs about tests on compression, static bending, shear, tension, moisture content, mass per volume (the modern name for density), and shrinkage. Much value has been obtained from the Indian Standard IS 6874 "Method of tests for round bamboo's". Results from publications on research results, and relevant ISO standards, have been taken into account as well. Each paragraph has the same structure: scope and field of application, references, principle, apparatus, preparation of test pieces, procedure, calculation and expression of results, and test report.
In the text on compression much attention has been given to a method to avoid strengthening of the test piece by friction between the bamboo and the steel platens at both ends; in timber testing this is never a problem but with bamboo it is. For bending tests a minimum free span has been prescribed, to avoid failure by transversal forces instead of by bending moments. For tests on tension special attention has to be given to a form of the test piece which will fail by tension and not by lateral compression in the grips.
Besides this Standard a manual (Janssen 2000c) also has been developed which gives practical solutions and explanations how to work with the official standard.
- The standard prescribes e.g. that culms should be marked clearly before felling; the manual gives a model for a form which can be used in the field, ideas about the use of paint and numbers, and how to make a sketch of each culm.
- The manual gives some elementary explanation about statistical background of prescriptions in the standard: why the number of test specimens should be not less than so and so.
- In the compression test, one is used to the use of steel platens to load the bamboo test piece till failure. The standard however prescribes the use of a friction-free intermediate layer, and the manual explains why it should be like this, and gives a practical solution.
- For the bending test it is made clear how to support and load the bamboo culm with

wooden saddles in order to create failure by bending stresses and not by forces perpendicular to the bamboo culm.
- For several tests examples are given for data-sheets which can be used for a report about the test.
- Some examples of calculations are given as well, with a special emphasis on the correct use of units.
In general, much use has been made from data in the Indian Standard IS 6874, and in the handbook published by Sotela (1990). Especially this last one contains valuable experience from practice in a good laboratory, in fact the Laboratory for Forest Products at the University of Costa Rica.

5 Progress since 1992

5.1 Bamboo Workshop Ubud 1995

As stated already, in the International Bamboo Congress and Workshop in Ubud, Indonesia, in 1995, one of the recommendations was " INBAR is requested to organise a task force to discuss and finalise a building code for bamboo". A group of volunteers was formed to discuss the purpose and content. One of the first conclusions was to divide this building code into two: the building code itself and the standard to determine material properties. We had to wait till November 1997 before we could make a real start: lack of funds was a problem for two years. This problem was solved when in November 1997 INBAR was raised as an intergovernmental agency, with funding from several donors, including a budget for the said work. During the year 1998 draft documents have been developed and distributed to the members of a committee of referees inside INBAR, for their comments.

5.2 Bamboo Workshop San José 1998

During two days before this International Bamboo Workshop, a meeting of two days was organised to discuss the said draft documents with the members of the committee. The result was a considerable improvement as well as a broad support, not only from the committee members but also from the audience, due to presentations during the Workshop itself. In the months after this meeting the texts have been adapted according to the discussions, and distributed to the members and also to the National Standardisation Institutes of 18 bamboo growing countries, to have their input as well. The goal of INBAR always has been to submit the draft documents to the ISO but also to have a broad support from National Standard Institutes. For this last reason, a meeting was called for October 19 to 22, 1999, in Los Baños, the Philippines. Al together we were with 27 people, and we discussed the draft documents during three days. It really was an exhausting exercise but the quality increased considerably as well as the understanding and the support of the National Standardisation Institutes.

5.3 Submission to the ISO

In 1999 the draft documents have been submitted to the ISO, resulting in an invitation to join the meeting of TC 165 in Harbin, China, in September 1999. At the end the meeting adopted a resolution: "ISO/TC 165 requests the secretariat to initiate the process necessary to establish, as preliminary work items: Determination of Physical

and Mechanical Properties of Bamboo, and Bamboo Structural Design, and seek the support of P members for this work". (Bamboo Structural Design is the new name for the Building Code). Normally one needs three years to reach this result! The next step is to participate in the July 2000 meeting of TC 165 in Seattle.

6. References.

Arce, O. 1993. Fundamentals of the design of bamboo structures. PhD. thesis Eindhoven University.

Boughton, G.N. 1989a. A proposal for a structural design code for bamboo. Paper presented at the CIB W18B meeting in Seattle.

Boughton, G.N. 1989b. Standardisation of connections for use with bamboo. Paper presented at the CIB W18B meeting in Seattle.

IS 6874. 1973. Indian Standard: Method of tests for round bamboos.

Janssen, J.J.A. 1992. Building with bamboo. Proceedings 2nd CIB W18B international conference on tropical and hardwood timber structures. Kuala Lumpur.

Janssen, J.J.A., editor. 2000a. Bamboo structural design. To be submitted to the meeting of ISO TC 165 in Seattle, July 2000.

Janssen, J.J.A., editor. 2000b. Determination of physical and mechanical properties of bamboo. To be submitted to the meeting of ISO TC 165 in Seattle, July 2000.

Janssen, J.J.A., editor. 2000c. Laboratory manual on testing methods for determination of physical and mechanical properties of bamboo. To be published by INBAR.

Kaplinsky, John. 1992. Whose standards are appropriate? In: Appropriate Technology, June 1992, vol. 19 no 1 pp 1-3.

Schilderman, Theo. 1992. Housing standards: can they be made appropriate? In: Appropriate Technology, June 1992, vol. 19 no 1 pp 5-8.

Sotela, J. 1990. Manual de ensayos fisico-mecanicos para especimenes de bambu. University of Costa Rica.

Unido 1991.Second consultation on the wood and wood products industry. Vienna, Austria. January 1991. Quoted are items 9g and 103.